Late Quaternary palaeolimnology and environmental change in the South Wollo Highlands, Ethiopia

by
Katie Loakes

A Doctoral thesis
Submitted in partial fulfilment of the requirements
for the award of

Doctor of Philosophy of Loughborough University

October 2015

Abstract.

Lake Hayq is a closed, freshwater basin on the eastern margin of the north-central highlands, Ethiopia. Using a sediment core extracted from the northern basin, this thesis aims to provide a high-resolution, detailed palaeolimnological reconstruction of changes to the environment and climate in the region since the late Pleistocene. A multi-proxy approach was applied, utilising diatoms, photosynthetic pigments and X-ray fluorescence (XRF) spectrometry. Lithological and chronological analyses were also performed, as well as the development of a transfer function to model diatom-inferred conductivity, and other quantitative analyses.

Between ~ 15.6 – 15.1 cal kyr BP, Lake Hayq experienced a lowstand, synchronous with the timing of Heinrich Event 1 and an intense drought across East Africa. At ~ 15.1 cal kyr BP a lake began to develop at the core site in response to wetter, more humid conditions, most likely caused by the reactivation of the African-Indian monsoonal circulation. This was abruptly ended however at ~ 14.7 cal kyr BP, as the climate shifted back towards aridity and Lake Hayq shallowed, in contrast to the majority of other East African lakes, which continued to refill. This most likely reflects changes to the Indian Ocean monsoon system caused by variability in the Atlantic Meridional Overturning Circulation at this time, in conjunction with site-specific mechanisms affecting the delivery of precipitation to Lake Hayq.

At ~ 12.3 cal kyr BP the African Humid Period resumed over Lake Hayq and the lake refilled, reaching maximum water depth between ~ 12.0 – 10.0 cal kyr BP. The lake was dominated by planktonic diatom taxa and photosynthetic pigments indicate it was meromictic. Lake level gradually declined throughout the Holocene, culminating in the termination of the African Humid Period. A high-resolution study of the period tentatively suggests that climate ‘flickering’, in the form of oscillations between dominant diatom taxa, occurred in the build up to the major climatic shift. The termination spanned ~ 600 cal years between ~ 5.2 – 4.6 cal kyr BP. A lowstand occurred between ~ 3.9 – 2.2 cal kyr BP, during which the lake became occasionally subsaline. In the late Holocene, ~ 2.2 – 1.3 cal kyr BP, Lake Hayq became deep and fresh again, although there is evidence of lake level variability.

The palaeo-record from Lake Hayq indicates that it broadly experienced the same high-latitude, glacial-interglacial dynamics and sub-millennial shifts in climate found in other palaeolimnological records from across East Africa. The precise timing and expression of these climatic events is not always synchronous between Lake Hayq and other East African waterbodies however, most likely caused by local, site-specific positive feedback mechanisms and variability in lake morphometry. This highlights the heterogeneous pattern of climate across the region and the significance of regional drivers.

This palaeo-record, spanning the late Quaternary, will help bridge gaps in current knowledge and understanding of the underrepresented, climatically sensitive and vulnerable north Ethiopian highlands. This is vital for future climate change modelling and regional downscaling, and may also inform ethnographic-archaeological research in a region considered to be the ‘cradle of humankind’.

Key words: Ethiopia, Lake Hayq, palaeolimnology, diatoms, photosynthetic pigments, conductivity, late Pleistocene, Holocene.

Acknowledgments.

Thank you first and foremost to Dr David Ryves for being my supervisor for the past three years; for always offering support, guidance, knowledge, encouragement, for putting up with my incessant questions and for always finding one more thing for me to do! Thank you also to Dr Keely Mills for stepping in as my second supervisor and offering all your East African knowledge and always going the extra mile to help.

Thank you to Professor Henry Lamb at Aberystwyth University for allowing me to use the sediment core on which my thesis is based (thank you to the team who collected it too) and for always offering your guidance, knowledge, advise and support. Thanks also to Catherine Martin-Jones for your help, sharing your data and bouncing a few ideas around. Thank you to Dr Helen Roberts for her continued work on this project, using optical luminescence dating to improve the cores chronology, and thank you to everyone else at Aberystwyth University who helped me in the lab and made my stays there all the more enjoyable!

At Nottingham University, thank you to Dr Suzanne McGowan and Julie Swales for allowing me to do my pigment analysis in your laboratory and also offering you technical help and support. A big thank you to Sarah Roberts and Mark Stevenson for showing me around the School of Geography, making me feel so welcome and including me in all the post-graduate activities, including the odd trip to the pub!

At Loughborough University, thank you to Dr Erika Hogan and Dr Jonathon Lewis for all your technical advice, help and support, and for making endless hours in the lab much easier and far more enjoyable! Thanks also to Stuart Ashby, Barry Kenny and Richard Harland for making my lab work easier. Thank you to all the other staff from the Department of Geography for your help and for making it a memorable experience!

Thank you also to Dr Michael Dee (University of Oxford), Professor Paula Reimer (Queens University Belfast) and the Quaternary Research Association (QRA) for dating the Lake Hayq sediment samples. Thank you to Dr Jonathan Tyler (University of Adelaide) for producing the age-depth model used in this thesis.

This work was made possible by funding from the QRA, the Loughborough University Graduate School and the Department of Geography, which allowed me to carry out analyses and travel around the world for conferences!

Thank you Dr Robert Marchant (University of York) and Drs John and Kathy Arthur (University of South Florida) for developing the original project for my thesis at Done Ella. It was truly a trip of a lifetime! Thank you to Dr Stephen Rucina for your friendship, kind words and generally looking after me on my first trip to Africa, and to Dr Aida Cuni-Sanchez, Dr Phil Platts and Dr Marion Pfeifer for making that long journey on rough roads all the more bearable. The trip would not have been possible without the British Institute in Eastern Africa (BIEA), who lent all the equipment, and the National Museums of Kenya. The trip was made all the more special by the kindness and hospitality of the people we met along the way.

Finally, a massive thank you to my parents, Claire and Richard, my brother James, and Tom, for getting me though the last three years (and the four years before that) and for all your support and encouragement... I'm sure you all still don't really understand what it is I do, what diatoms are, or what palaeolimnology is, but thank you all the same for always pushing me forward!

Table of Contents.

CHAPTER 3. ENVIRONMENTAL AND CLIMATIC VARIABILITY IN EAST AFRICA SINCE THE LAST GLACIAL MAXIMUM

CHAPTER 4. RESEARCH APPROACH AND METHODS

CHAPTER 6. RESULTS: THE PALAEOLIMNOLOGY OF LAKE HAYQ

CHAPTER 8. DISCUSSION

CHAPTER 9. CONCLUSION

APPENDICES AND DIATOM PLATES

List of Figures.

CHAPTER 2. THE AFRICAN MONSOONAL CLIMATE SYSTEM: THE PHYSICAL ENVIRONMENTAL & HUMAN INTERACTIONS

CHAPTER 3. ENVIRONMENTAL AND CLIMATIC VARIABILITY IN EAST AFRICA SINCE THE LAST GLACIAL MAXIMUM

CHAPTER 4. RESEARCH APPROACH AND METHODS

CHAPTER 5. A PLANNED STUDY OF HOLOCENE CLIMATE IN THE GAMO HIGHLANDS

CHAPTER 6. RESULTS: THE PALAEOLIMNOLOGY OF LAKE HAYQ

CHAPTER 7. RESULTS: A HIGH-RESOLUTION STUDY OF THE TERMINATION OF THE AFRICAN HUMID PERIOD

CHAPTER 8. DISCUSSION

List of Tables.

CHAPTER 3. ENVIRONMENTAL AND CLIMATIC VARIABILITY IN EAST AFRICA SINCE THE LAST GLACIAL MAXIMUM

CHAPTER 4. RESEARCH APPROACH AND METHODS

CHAPTER 5. A PLANNED STUDY OF HOLOCENE CLIMATE IN THE GAMO HIGHLANDS

CHAPTER 6. RESULTS: THE PALAEOLIMNOLOGY OF LAKE HAYQ

CHAPTER 7. RESULTS: A HIGH-RESOLUTION STUDY OF THE TERMINATION OF THE AFRICAN HUMID PERIOD

CHAPTER 8. DISCUSSION

Chapter 1

Introduction and Context.

1.1 Research Context

The Ethiopian climate system is a function of both global and regional climate-environmental dynamics. The annual climate is characterised by strong rainfall seasonality as a result of the annual migration of the Intertropical Convergence Zone (ITCZ) and its effect on the prevailing winds. This has resulted in three rainfall seasons across Ethiopia (*kiremt*, *bega* and the *belg*), driven by the convergence of various air masses and monsoon systems (Nicholson 1996; Umer et al. 2004; Chenug et al. 2008). When superimposed over the large changes in elevation over short distances, a patchwork of seasonal rainfall patterns and microclimates can be identified across Ethiopia (Friis et al. 2011). Local climate variability is influenced further by soils, vegetation, albedo, lakes and other water bodies, jet streams and in recent centuries, anthropogenic activities such as land use change, settlement patterns and population growth (Nicholson 1996; Gasse 2000; Friis et al. 2011).

Northern Ethiopia is perhaps the most climatically sensitive region of Ethiopia. Located at the northern most limit of the ITCZ, even a slight displacement in position, or weakening of the monsoon system, can cause the rains to fail. Numerous studies have demonstrated the relationship between East African rainfall variability, sea surface temperature (SST) anomalies in the Atlantic and Indian Oceans, the El Niño Southern Oscillation (ENSO) phenomenon and La Niña (Nicholson and Entekhabi 1986; Ogallo 1987; Ropelewski and Halpert 1987; Farmer 1988; Nicholson and Selato 2000). As such, the region has a long history of meteorological drought. The impact of droughts on the population is amplified by the vulnerability of the people to climatic variability. Poverty, agricultural dependence, gender and class inequality, rapid population increase in the last fifty years, lack of resources and technology, as well as local and regional conflicts, have all weakened the ability of local populations to predict, plan for, mitigate and respond to droughts effectively. Famine often ensues, which in recent decades (notably the 1980s) has received unprecedented international attention and an outpouring of aid relief given the severe, life-

threatening impact to the people affected (Clay and Holcomb 1986; BBC 2000; Meze-Hausken 2004; Hillier and Dempsey 2012).

In order to understanding such climate variability and sensitivity, knowledge of long-term changes in Ethiopia and East Africa on the millennial scale is necessary, with the use of palaeo-records. Archives from lake basins contain potentially excellent records of historical climatic and environmental change in the sediments accumulating at the bottom of them (Verschuren 2003). Continuous, high-resolution records can be found in climatically-sensitive lakes where the potential to respond to and record short-term fluctuations in climate is high and the signal is clear (Battarbee 2000; Umer et al. 2004). However, sedimentary records can be affected by issues such as identifying a suitable lake site, chronology, interrupted sedimentation and the uncertain relationship between sedimentary climate-proxy indicators and primary climate variables (Verschuren 2003). As such, multi-proxy approaches are often preferable in reconstructions of historical climatic and environmental conditions. Such studies provide more data and enable lake-catchment system responses to climate, and other external forces such as anthropogenic activities, to be more thoroughly identified, and quantitatively and qualitatively inferred (Battarbee 2000). Given the distribution of climatically sensitive lakes from across subtropical, tropical and arid areas of Africa, a comprehensive understanding of regional climatic and environmental dynamics is now possible, including how African climate sensitivity is affected by global teleconnections on a range of time scales.

On the millennial scale, the African climate is very sensitive to high-latitude glacial conditions and has been paced by Milankovitch cycles (~ 23.0 – 19.0 kyr) (Kutzbach and Street-Perrott 1985; Trauth et al. 2003; Gasse 2006). During the Last Glacial Maximum (~ 23.0 – 18.0 kyr BP), the most recent interval when Northern Hemisphere ice sheets were at their maximum extent, the majority of East African lakes were experiencing lowstands in response to reduced moisture and low temperatures (Gasse 2000; 2006; Ray and Adams 2001). During deglaciation (~ 20.0 – 11.5 kyr BP) East Africa experienced wetter and warmer conditions, punctuated by abrupt transitions from arid to humid, and humid to arid phases. The first major shift towards aridity occurred between ~ 18.0 – 15.0 kyr BP in response to Heinrich Event 1 (Stager et al. 2011). Lakes across the region experienced declining

water levels and some records suggest water bodies may have completely have dried out (Gasse 1977; Peck et al. 2004; Williams et al. 2006; Marshall et al. 2009; 2011; Stager et al. 2011).

At ~ 15.0 kyr BP the African Humid Period began, following a change in precession during a period of low eccentricity (Barker et al. 2004; Garcin et al. 2009). The African-Indian monsoon system was rejuvenated and lake basins across the region refilled (deMenocal et al. 2000; Garcin et al. 2012; Tierney and deMenocal 2013). This was abruptly interrupted between ~ 12.8 – 11.6 kyr BP by the Younger Dryas Stadial, a high-latitude event caused by the release of freshwater from disintegrating ice-sheets into the North Atlantic. Widespread drought and aridity occurred across East Africa and again, lake levels declined (Nicholson 1982). Monsoon circulation resumed at the start of the Holocene and lakes deepened, and in some cases, overflowed (Gasse and Van Campo 1994; Umer et al. 2004; Benvenuti et al. 2013). The African Humid Period terminated around 5.5 kyr BP as a result of declining summer insolation, which saw the monsoon and associated rain belts shift southwards. This culminated in a severe drought at 4.2 kyr BP, which is now recognised as being global in nature, and is believed to have contributed to the collapse of the Ancient Egyptian Old Kingdom and several other ancient civilisations (Bell 1971; Street and Grove 1979; Cullen et al. 2000; deMenocal 2001; Walker et al. 2012; Blanchet et al. 2013).

The late Holocene saw several brief periods of increased humidity and in the last millennium East Africa experienced a drier climate during Europe's Medieval Climatic Anomaly (~ 950 – 680 yr BP) and a relatively wet climate during the Little Ice Age (~ 680 – 100 yr BP) (Jones et al. 2001; Nicholson et al. 2013). Overall, aridity increased as the climate transitioned towards present day conditions.

The impact of long-term glacial-interglacial dynamics during the late Quaternary is therefore, relatively well understood. However, increasingly attention is being placed on examining short-term, sub-millennial shifts in climate (and sub-precessional cycles), as despite the breadth of high-quality, high-resolution data available, the nature of more abrupt shifts and changes to the palaeohydrology, cannot be adequately explained by orbital forcing alone (Verschuren et al. 2009). A series of

feedback mechanisms must have operated at various times and magnitudes in order to account for the non-linear climate sensitivity observed in some records. For example, the nature of the onset and termination of the African Humid Period are debated, with some records indicating a gradual transition and others an abrupt shift in climate (deMenocal et al. 2000; Fleitmann et al. 2003; Asrat et al. 2007; Kropelin et al. 2008). The extent to which local, non-linear mechanisms or ocean-atmosphere feedbacks affected the local expression of sub-millennial shifts is consequently unclear and in need of further research (deMenocal et al. 2000; Tierney and deMenocal 2013; deMenocal 2015; Shanahan et al. 2015). This is of critical importance for climate prediction, modelling and hindcasting under various scenarios, as increasingly public interest is on short-term, immediate changes in local climate within the next several decades, which may directly impact on them and their livelihoods. This will be particularly important for the climatically sensitive and vulnerable north of Ethiopia, which is often one of the first areas in the Horn of Africa to be affected by drought (Wolde-Mariam 1986). In addition, understanding abrupt shifts in climate and environment will also inform archaeological research (the study site, Lake Hayq, is approximately 540 km south of the ancient Kingdom of Aksum, an empire built on, and ultimately collapsing in response to changes in climate) and understanding of human evolution in this region, a possible location for the 'cradle of humankind', where some of the oldest hominid fossils have been found (Tattersall 2003; Gibbons 2009).

Palaeoclimatic and palaeoenvironmental research across Ethiopia has generally focused on the Rift Lakes in the Main Ethiopian Rift; the Ziway-Shala lakes basin (Grove et al. 1975; Gillespie et al. 1983; Benvenuti et al. 2002), Lakes Tilo (Telford and Lamb 1999; Lamb et al. 2000), Awassa (Telford et al. 1999) and Abhé in the Afar Depression (Gasse 1977), as well as peat records from the Bale Mountains, southern Ethiopia (Mohammed and Bonnefille 1998). It is only recently, in the last decade, that attention has been given to lake records from the northern highlands (the same is true of southern Ethiopian lake records such as Chew Bahir; Foerster et al. 2012). Near continuous sedimentary records have been collected from Lakes Ashenge (Marshall 2006; Marshall et al. 2009) and Tana (Lamb et al. 2007a; Marshall et al. 2011; Costa et al. 2014) and studied using multi-proxy approaches to assess climatic and environmental change and variability during the late Pleistocene

and Holocene. These records indicate that not only was the region affected by millennial scale variations in the monsoon system, in agreement with records from the Rift Lakes across East Africa, but that local, site-specific feedback mechanisms may have affected the nature and local expression of sub-millennial shifts in climate (Marshall 2006; Marshall et al. 2009; Costa et al. 2014).

The north Ethiopian highlands are therefore currently underrepresented in regional palaeo-records, creating a knowledge gap in the understanding of this climatically sensitivity and vulnerable area. The purpose of this research, conducted at Lake Hayq on the eastern margin of the north-central highlands, is to help to bridge that gap.

1.2 Research Aims

The aim of this research is to provide a high-resolution, detailed palaeolimnological reconstruction of changes to the environment and climate in the north-central Ethiopian highlands since the late Pleistocene, and to place these into a wider regional context. The sedimentary record from Lake Hayq is investigated using a multi-proxy approach, focussing on diatom, photosynthetic pigment and X-ray fluorescence (XRF) analyses. The combination of proxies will provide a quantitative assessment of changes to the both the lake and surrounding catchment during the time in question. From this, inferences can be made relating to changes in the local and regional climate and environment.

Specific research questions and hypotheses are:

1. Is there palaeolimnological evidence to suggest millennial scale hydrological changes during the glacial-interglacial period?
    - Hypothesis 1: Lake Hayq shows evidence of shifts towards aridity at the time of Heinrich Event 1 (~ 18.0 – 15.0 kyr BP) and the Younger Dryas Stadial (~ 12.8 – 11.6 kyr BP).
    - Hypothesis 2: Lake Hayq shows evidence of lake refilling at the time of the African Humid Period's onset (~ 15.0 kyr BP).
2. Is there palaeolimnological evidence to suggest hydrological changes during the Holocene?

- Hypothesis 3: Lake Hayq shows evidence of lake refilling following the Younger Dryas Stadial.
- Hypothesis 4: Lake Hayq shows evidence of sub-millennial drought events at ~ 8.2 kyr BP (8.2 event) and ~ 4.2 kyr BP (4.2 event).

3. How is the termination of the African Humid Period expressed in the palaeolimnological record?
    - Hypothesis 5: Lake Hayq shows evidence of lake level decline beginning around ~ 5.5 kyr BP in response to the termination of the African Humid Period.
    - Was the termination abrupt or gradual?
4. How do the findings from Lake Hayq compare to other records from Ethiopia, the Horn of Africa and subtropical Africa?
    - Hypothesis 6: The climate signal at Lake Hayq is expressed indirectly through changes in lake hydrology and associated catchment processes.
    - Hypothesis 7: Lake Hayq is in synchronicity with other palaeolake records from Ethiopia, the Horn of Africa and the wider region of subtropical Africa and further afield (the Mediterranean and Middle East).
    - What are the possible mechanisms controlling the expression of climatic events at Lake Hayq?
5. Is there palaeolimnological evidence of anthropogenic impacts to the lake catchment?
    - Hypothesis 8: Lake Hayq does not show any discernible evidence of anthropogenic activity in the catchment.

1.3 Thesis Outline

This thesis comprises nine chapters. Following this introduction to the research, Chapter 2 provides a regional overview of Ethiopia, discussing firstly how the African monsoonal climate system has shaped the environmental and climatic features of the country and the Horn of Africa. This is followed by an assessment of the current and historical pressures on the environment and natural resources. Chapter 3 then reviews recent progress, advances and challenges in the field of palaeolimnology, before moving on to an overview of current knowledge and understanding of the

palaeoclimate of tropical and subtropical Africa since the Last Glacial Maximum, utilising records from the continent and further afield.

Chapter 4 identifies the research approach and methods applied to this study. Chapter 5 is a stand-alone chapter, presenting the original plans for this thesis at Done Ella in the south-west Gamo-Gofa highlands. Despite major problems with the sedimentary record at this lake, which resulted in the change of site to Lake Hayq, this chapter has been included (1) as evidence of the authors' field work capabilities, (2) as an example of some of the pit-falls in palaeolimnological research, and (3) to publish the first limnological and palaeolimnological findings from a previously unstudied lake. The cultural history of the region is considered, followed by field work, methodology and results, which are then discussed.

The results of the study are then presented. Chapter 6 considers the complete sediment record, identifying changes in the lithology, geochemical, diatom and pigment data between ~ 15.6 – 1.3 cal kyr BP. Chapter 7 is a high-resolution study of a section of core pertaining to the termination of the African Humid Period. Both chapters discuss the results in terms of changes in the lake system, local climate and environment. Chapter 8 discusses the results from the study in the context of wider Ethiopia, the Horn of Africa and East Africa, identifying how the record from Lake Hayq compares to other records from the region. Thought is given to the impact the findings may have on predicting future climate change in the region, as well as methodological considerations. The research is concluded in Chapter 9.

Chapter 2

The African Monsoonal Climate System: The Physical Environment & Human Interactions.

2.1 Introduction

Ethiopia is currently at the forefront of an innovative research effort aimed at answering a key question on human evolution: how did hominins respond to the environment they lived in? The Hominin Sites and Paleolakes Drilling Project (http://hspdp.asu.edu/) is an international venture which will oversee drilling at six ancient lake beds across Ethiopia and Kenya with the aim of obtaining continuous climate records spanning the last 500,000 years in places where hominins lived and died. This research is crucial in pinning down exactly how and when climate variability affected human lineage and may help answer questions regarding the capacity of hominins to adapt to natural fluctuations in climate (Thomas et al. 2012; Gibbons 2013). Such interest in the Ethiopian and Kenyan rift as a possible candidate for the 'cradle of humankind' has existed since the discovery of older hominid fossils there, notably Lucy in 1974, the 3.6 Myr old *Australopithecus afarensis* discovered in Hadar, Ethiopia, and the 1.6 Myr old 'Turkana boy' in 1984, a near complete *Homo ergaster* skeleton who possessed an essentially modern body structure (Tattersall 2003). Most recently, Ardi, a 4.4 Myr old *Ardipithecus ramidus* was discovered in Aramis, Ethiopia, in 1992 (reconstructed by 2009) making her the earliest (partial) hominid skeleton found (Gibbons 2009). The Ethiopian environment and climate is therefore central in framing those early evolutionary steps.

In contrast to the study of past climate conditions, improved understanding of the current Ethiopian climate and environment is becoming more important as the effects of modern climate change become apparent. Already in Ethiopia minimum temperature is increasing considerably faster than maximum or mean temperatures, and changes in runoff and hydrology have been documented (Legesse et al. 2003; Conway et al. 2004). A 2011 report by the Institute for Environmental Security highlighted the increasing threat to human life in Ethiopia and the Horn of Africa from climate change as it amplifies other pressures such as environmental degradation and resource scarcity (Van de Giessen 2011). Food insecurity for example, may become more widespread as pressure from a rapidly rising population – 108.92

million people in 2012 (World Bank 2014) – burdens already strained resources and as a consequence, conflict between pastoralists, farmers and tribes may become more frequent (Brandt et al. 1997; Van de Giessen 2011). Access to fresh water is likewise a source of tension; plans to allocate more water to Ethiopia by building hydroelectric plants on the Blue Nile were met with threats of action from the Egyptian President Mohammed Morsi, which have continued to make headlines as recently as June 2013 (BBC 2013).

Comprehensive knowledge of Ethiopia's past climates and environments is therefore a topic of immense relevance and significance as two spectra of interest have emerged; one looking at the past and one looking at the future. In order to understand and quantify these changes, one must first look to the current state of the climate. This chapter considers the African monsoonal climate system and how it, along with other features, has shaped the modern physical environment of Ethiopia and the Horn of Africa, the wider study area of this research. The African monsoonal system is discussed and in Part I used to interpret the distribution of climatic zones, vegetation and environmental features in Ethiopia and the Horn of Africa. The distribution of lakes is then discussed, including a brief description of several lakes whose palaeo-records are discussed in further detail in the following chapter. This is followed in Part II by a review of current pressures on the environment and natural resources in the Horn of Africa, as well as current and historical human interactions with the environment.

2.2 African Monsoonal Circulation

The African climate is modulated by the pattern of upper air circulation and pressure that govern monsoon circulation (Fig. 2.1). Three major air streams flow over the continent: the north-east monsoon (Trade Winds) coming from the Arabian Desert, the south-east monsoon coming off the Indian Ocean, and the Congo Air with westerly, south-westerly flow, originating in the South Atlantic (Nicholson 1996; Kiage and Liu 2006). Both monsoons are thermally stable and associated with subsiding air, making them relatively dry. In contrast, the Congo Air is thermally unstable, convergent and humid, and therefore associated with rainfall. Two surface convergence zones separate these air flows: the Intertropical Convergence Zone

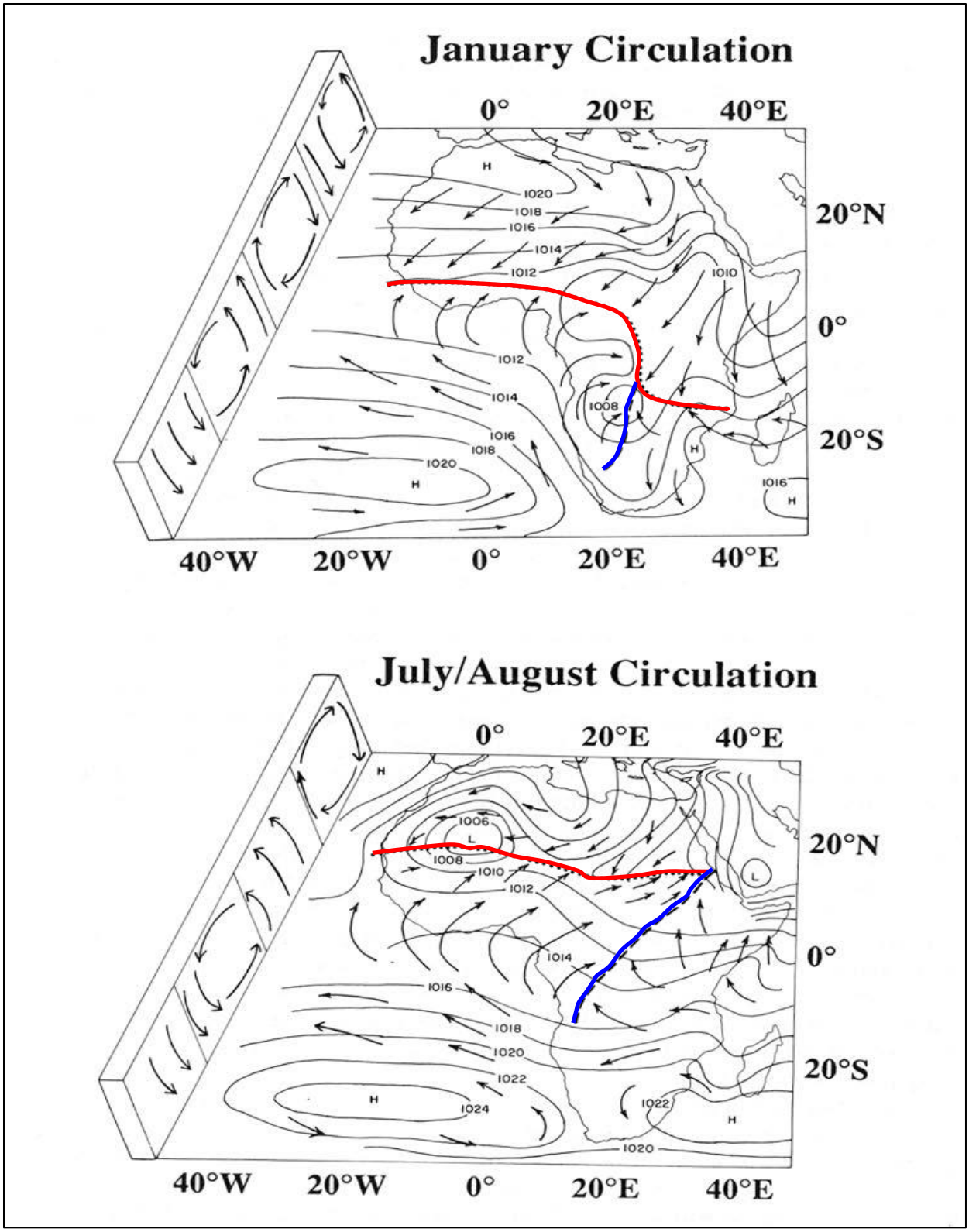

Figure 2.1. Schematic of the general annual pattern of winds and air pressure over Africa. The red line indicates the Intertropical Convergence Zone and the blue line indicates the Congo Air Boundary (adapted from Nicholson 1996).

(ITCZ), which separates the two monsoons, and the Congo Air Boundary (CAB), an area of north-east to south-west convergence which separates the easterlies and westerlies (Nicholson 1996; Trauth et al. 2003). A third convergence zone separates the dry, stable northerly flow from the Sahara and the humid southerly flow.

The northern and southern ends of the African continent experience a Mediterranean climate (dry summers and wet winters) due to the displacement of the mid-latitude westerlies towards the equator (Gasse 2000). These regions border subtropical deserts (the Sahara in the north and the Namib coastal desert in the south-west) dominated by subtropical anticyclones, which are separated by a wide belt of tropical climate (Gasse 2000). The tropical African climate is governed by the seasonal migration of the ITCZ between 10 º north and south as it responds to changes in maximum solar heating (Nicholson 1996; Gasse 2000; Nicholson 2000; Peyron et al. 2000; Gasse 2006). During the Northern Hemisphere winter, when the ITCZ lies to the south, high pressure builds up over the cold landmasses in the north and low pressure develops over the warm Southern Hemisphere. South-easterly winds flow from the high to low pressure. During the spring and summer as the Northern Hemisphere begins to warm in response to increasing insolation, the temperature difference between the land and ocean causes the ITCZ to migrate north. This causes the air above the land to rise and draw in humid air off the Indian Ocean. As this humid air rises, moisture is lost as monsoonal precipitation, resulting in northern and southern monsoonal climates with summer rains and winter dryness, and a humid equatorial zone with a bi-modal rainfall pattern (Gasse 2000; Gasse 2006).

Fluctuations in the intensity of interannual precipitation have been statistically linked with the El Niño Southern Oscillation (ENSO) (Nicholson 1996; Gasse 2000). However, these fluctuations may be a more direct response to sea surface temperature (SST) anomalies in the Atlantic and Indian Oceans, including the Indian Ocean Dipole (IOD) and strengthened/weakened monsoon systems and their interaction with the unstable CAB, which occur in the context of an ENSO event (Nicholson 1996; Gasse 2000; Gupta et al. 2010; Tierney et al. 2013). La Niña events have also been associated with African rainfall variability (Nicholson and Selato 2000).

On the orbital timescale, the African climate has been paced by variations in Earth's insolation as a result of orbital precession – the Milankovitch cycle (Trauth et al. 2003; Gasse 2006). Due to the geometry of precessional patterns, changes in summer solar radiation are in antiphase between the hemispheres. In North and Southern Africa, this results in monsoonal circulation and humid climates at 19.0 – 23.0 kyr intervals and in East Africa every 10.0 – 11.0 kyr following maximum equatorial insolation (Trauth et al. 2003; Verschuren et al. 2009). Clement et al. (2004) demonstrated the significance of precessional forcing on tropical moisture using climate modelling, which showed that a 180 ° shift in precession could alter annual precipitation in the tropics by at least 180 mm per year as well as induce shifts in seasonality. Other forcing factors influencing African climate on the glacial-interglacial timescale include Northern Hemisphere ice sheet volume, atmospheric transparency, surface boundary conditions, atmospheric gases, ocean properties and tectonic activity (Barker et al. 2004; Maslin and Christensen 2007). The African climate is thus sensitive to global teleconnections on a range of scales, from interannual variability to several millennia. Understanding these connections and how they are expressed in the climate is essential for interpreting palaeo-records and modelling future climate change.

2.3 Part I: The Physical Environment in the Horn of Africa

2.3.1 Defining the Horn of Africa

The East African region has been defined under various political and geographical guises. Based on the UN scheme of geographic sub-regions, East Africa can refer to the countries of Tanzania, Kenya, Uganda, Rwanda, Burundi (collectively known as the East African Community), Ethiopia, Djibouti, Eritrea, Somalia, Mozambique, Madagascar, Malawi, Zambia, Zimbabwe, South Sudan, Egypt and Sudan (the latter two also being considered part of North Africa) as well as several islands in the Indian Ocean. In the context of this research, 'East Africa' shall be used to refer to Tanzania, Kenya, Uganda, Rwanda, Burundi, Ethiopia, Djibouti, Eritrea and Somalia.

The Horn of Africa is a peninsula in East Africa projecting into the Arabian Sea. It comprises the countries of Ethiopia, Djibouti, Eritrea and Somalia (Stock 2004). The International Crisis Group also includes Sudan in the term, whilst The Horn of Africa Regional Environment Centre and Network includes Kenya. Political organisations

such as the European Commission and the Intergovernmental Authority on Development (IGAD) refer to the Horn of Africa as Ethiopia, Eritrea, Somalia, Djibouti, Sudan, Kenya and Uganda. In the context of this research, the 'Horn of Africa' shall be used to refer to Ethiopia, Djibouti, Eritrea and Somalia.

Ethiopia, officially known as the Federal Democratic Republic of Ethiopia, is a culturally rich and diverse nation. The Ethiopian government officially recognizes eighty-six ethnic groups and is divided into nine ethnically based states – Afar, Amhara, Benishangul-Gumuz, Gambella, Harari, Oromia, Somali, Southern Nations, Nationalities and Peoples' State, and Tigray – and two chartered cities – Addis Ababa and Dire Dawa (CSA 2007a).

2.3.2 Relief and Geology

Due to intensive volcanic and tectonic activity over the past 15 million years, the Horn of Africa is characterised by significant changes in elevation over short distances (Fig. 2.2 and 2.3). The Ethiopian highlands form an extensive uplift plateau exceeding 4000 m in altitude (the highest peak, Ras Dashan, is 4620 m above sea level) surrounded by peripheral lowlands to the east and west. The two largest and highest massifs in the highlands are the Semien Mountains in the north and the Bale Mountains in the south. In the north-east of Ethiopia and Djibouti lies the Afar Depression, an area formed by the triple (tectonic) junction where the spreading axes of the Gulf of Aden and the Red Sea meet the East African rift system on the continent. Most of the Afar region is < 1500 m in altitude and Lake Asal lies 155 m below sea level, making it the lowest depression in Africa. The south, south-eastern and western lowlands are also < 1500 m in altitude.

Such marked changes in altitude across Ethiopia and the Horn of Africa have created pronounced precipitation, temperature and evaporation gradients, resulting in various microclimates: (1) the *kolla*, a hot zone found in the Danakil Depression and the Blue Nile valley where elevations are < 1500 m; (2) the *weina dega*, a temperate area in the central plateau, with elevations between 1500 – 2400 m and daily temperatures of 16 – 30 ºC; (3) the *dega*, found in parts of the western and eastern areas of the north-western plateau. Elevations here are > 2400 m and daily

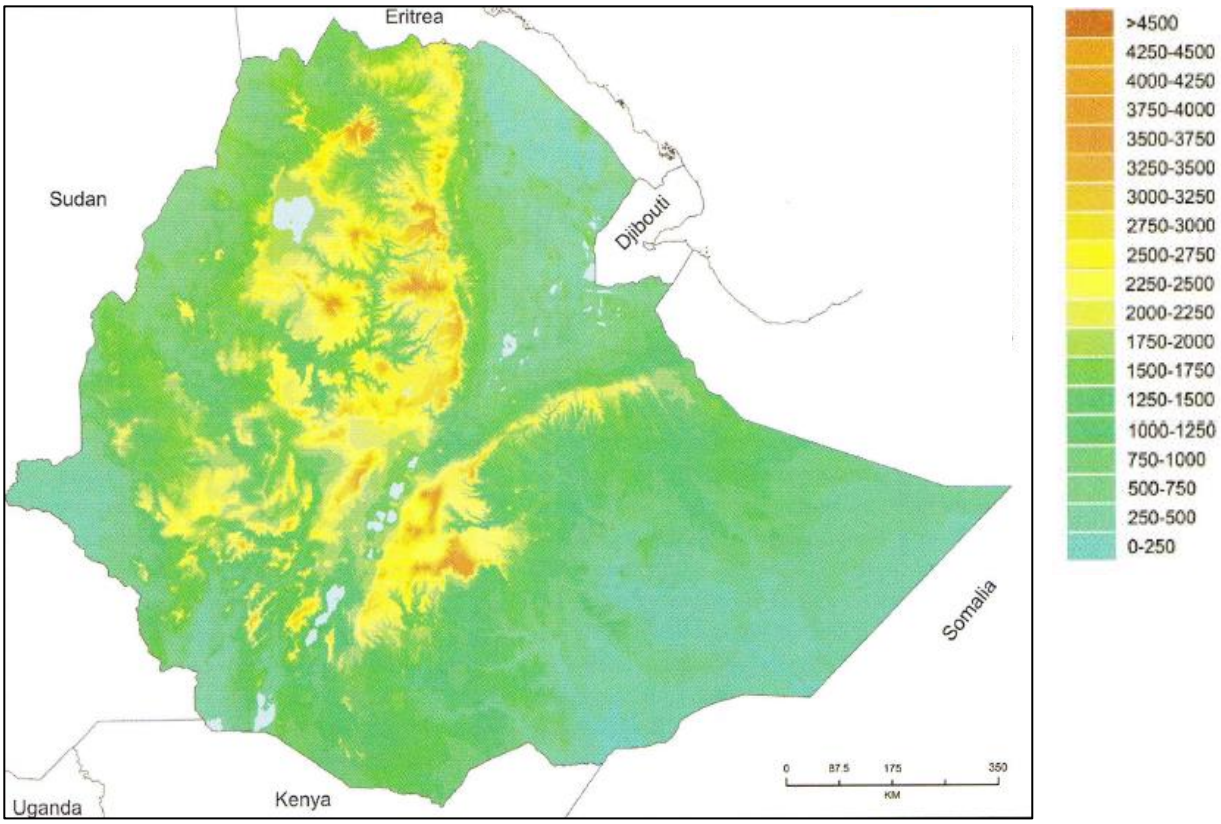

Figure 2.2. Schematic showing altitudes (metres above sea level) in Ethiopia (adapted from Friis et al. 2011).

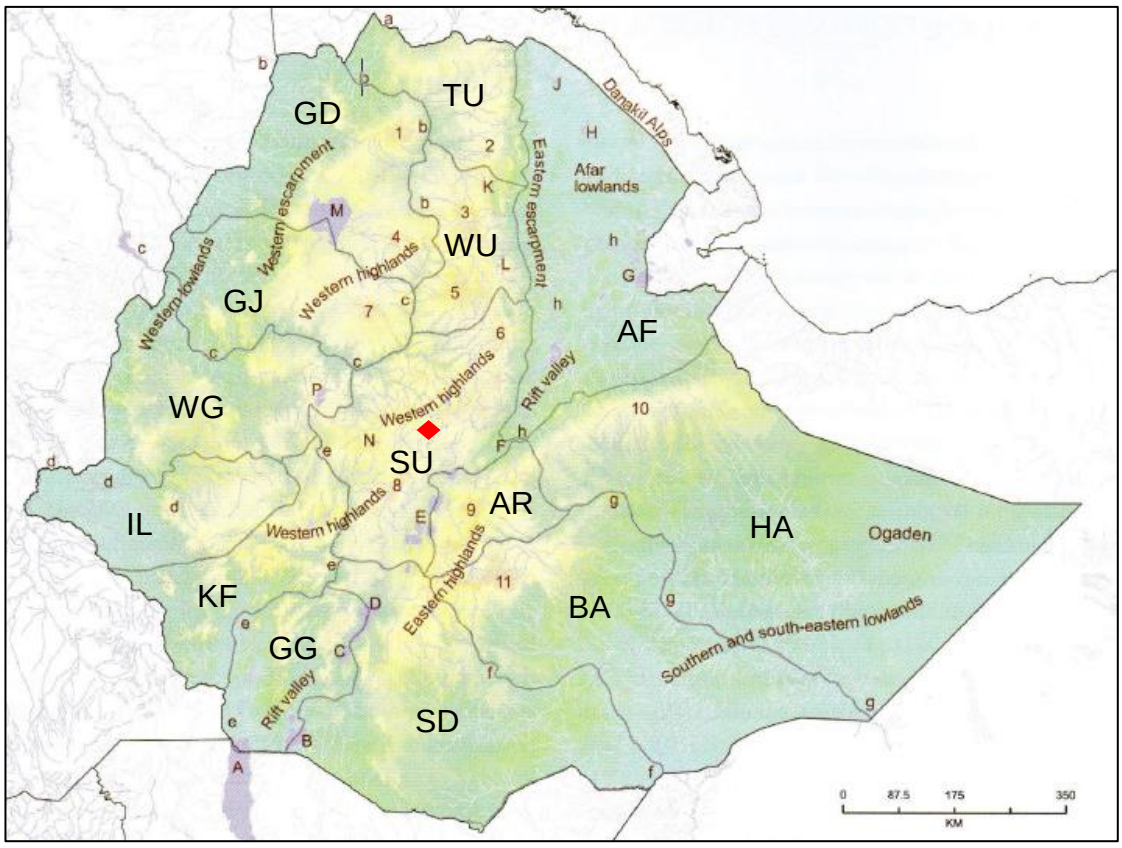

Figure 2.3. Schematic showing important topographical features of Ethiopia (adapted from Friis et al. 2011). Addis Ababa is indicated by the red diamond. Changes in colour indicate varying altitudes (see Fig. 2.2). Topographic features are indicated by numbers or letters. Mountain massifs: (1) Semien, including the peaks Ras Dashan and Bwahit, (2) Amba-Alage, (3) Abune Yosef, (4) Guna, (5) Amba Farit, (6) Abuye Meda, (7) Choke, (8) Gurage, (9) Mountains of Arussi, including Chilalo, Bada and Kaka, (10) Gara Muleta, (11) Bale Mountains, including Batu and Tulu Dimtu. Lakes and reservoirs: (A) Turkana, (B) Chew Bahir, (C) Chamo, (D) Abaya, (E) central group of Rift Valley lakes, including (from south to north) Awasa, Shala, Abijata, Langeno and Ziway, (F) Metahara, (G) cluster of desert lakes, including Afambo, Bario, Laitaf, Gamari and Abe, (H) Afrera, (J) cluster of desert lake in the Afar lowlands, including Asale, Karum and other unnamed lakes, (K) Ashenge, (L) Hayq and Hardibo, (M) Tana, (N) Wonchi, (P) Fincha and Chomen reservoirs. Rivers: (a) Mereb, (b) Tekeze, (c) Abay (Blue Nile), (d) Baro, with the southern tributaries Akobo and Gilo, (e) Omo, with the northern tributaries Gojeb and Gibe, (f) Genale, (g) Wabi Shebele, (h) Awash. Solid grey lines separate floristic regions (based on previous ethnic regions) used for recording distributions in the *Flora of Ethiopia and Eritrea*

project (Friis and Ryding 2001): (HA) Harerge, (BA) Bale, (SD) Sidamo, (GG) Gamo-Gofa, (KF) Kefa, (IL) Illubabor, (WG) Welega, (GJ) Gojam, (AR) Arussi, (SU) upland Shewa, (GJ) Gojam, (TU) upland Tigray, (WU) upland Welo, (AF) Afar.

temperatures are between 0 – 16 ºC (Chenug et al. 2008). As a result of such significant climatic and altitudinal variability, precipitation is spatially varied (Fig. 2.4).

During *kiremt* the wettest regions in the south-east of Ethiopia can receive > 350 mm of rainfall per month (McSweeney and Lizcano 2012), whilst the Afar Depression, one of the world's hottest and most arid deserts, receives < 300 mm from December to January (Lowenstern et al. 1999). Annually the western and central highlands receive the most rainfall (800 – > 2400 mm annually) whilst the Afar region, southern and eastern regions receive considerably less (0 – 400 mm annually) (Friis et al. 2011).

Friis et al. (2011) have reviewed the geology of Ethiopia (Fig. 2.5). The highlands are dominated by volcanic Tertiary extrusive and intrusive rocks, including agglomerates, basalts, ignimbrites, rhyolites, trachytes and tuffs. These rocks vary in thickness between 500 – 2500 m but reach a maximum of 3000 – 3500 m in the Semien Mountains. Northern Ethiopia is characterised by Palaeozoic and Mesozoic rocks and the east by a Mesozoic complex. The Mesozoic rocks consist of limestone and sandstone. Enticho sandstone, Adigrat sandstone, Antalo limestone and Angula shale are particularly prominent in central parts of the western highlands. Limestone is common in the eastern highlands. The Afar Depression contains Quaternary extrusive and intrusive formations whilst the Blue Nile gorge is characterised by Precambrian and Jurassic rocks. Precambrian rocks underlie all the other rock types in Ethiopia.

2.3.3 Modern Climate

Climate in the Horn of Africa is characterised by strong rainfall seasonality as a result of the annual migration of the ITCZ and its effect on the prevailing winds. Three seasons exist (Nicholson 1996; Umer et al. 2004; Chenug et al. 2008): (1) *Kiremt,* the longest rainy season, which lasts from June to September and delivers 50 – 70 % of rainfall. The rainfall is derived predominantly from south-westerly Congo Air converging with the south-east monsoon along the CAB. The rains cover all of Ethiopia except the far south and south-east, but during a strengthened Indian summer monsoon the CAB can bring the rains even further eastward; (2) *Bega*, the dry season, lasts from October to February when the ITCZ is most southerly and the

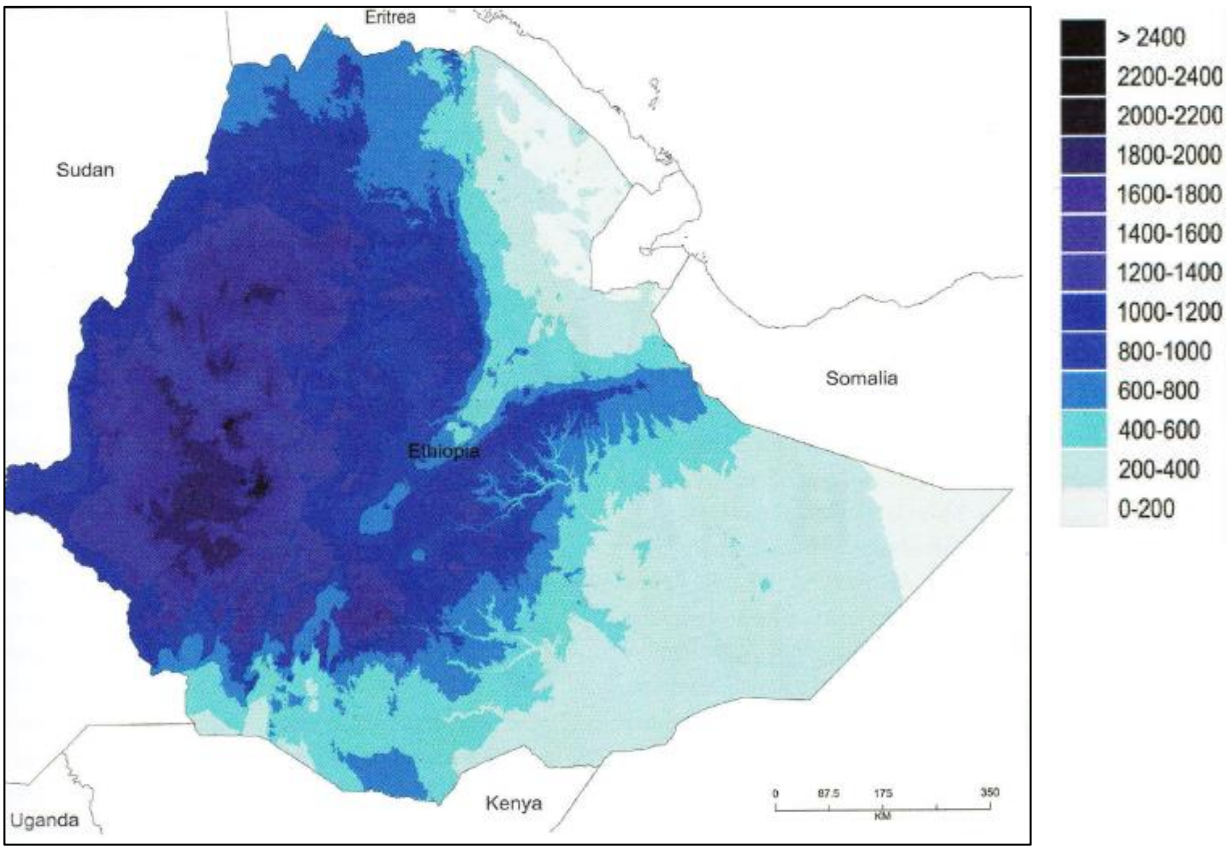

Figure 2.4. Mean annual rainfall (mm) across Ethiopia (adapted from Friis et al. 2011).

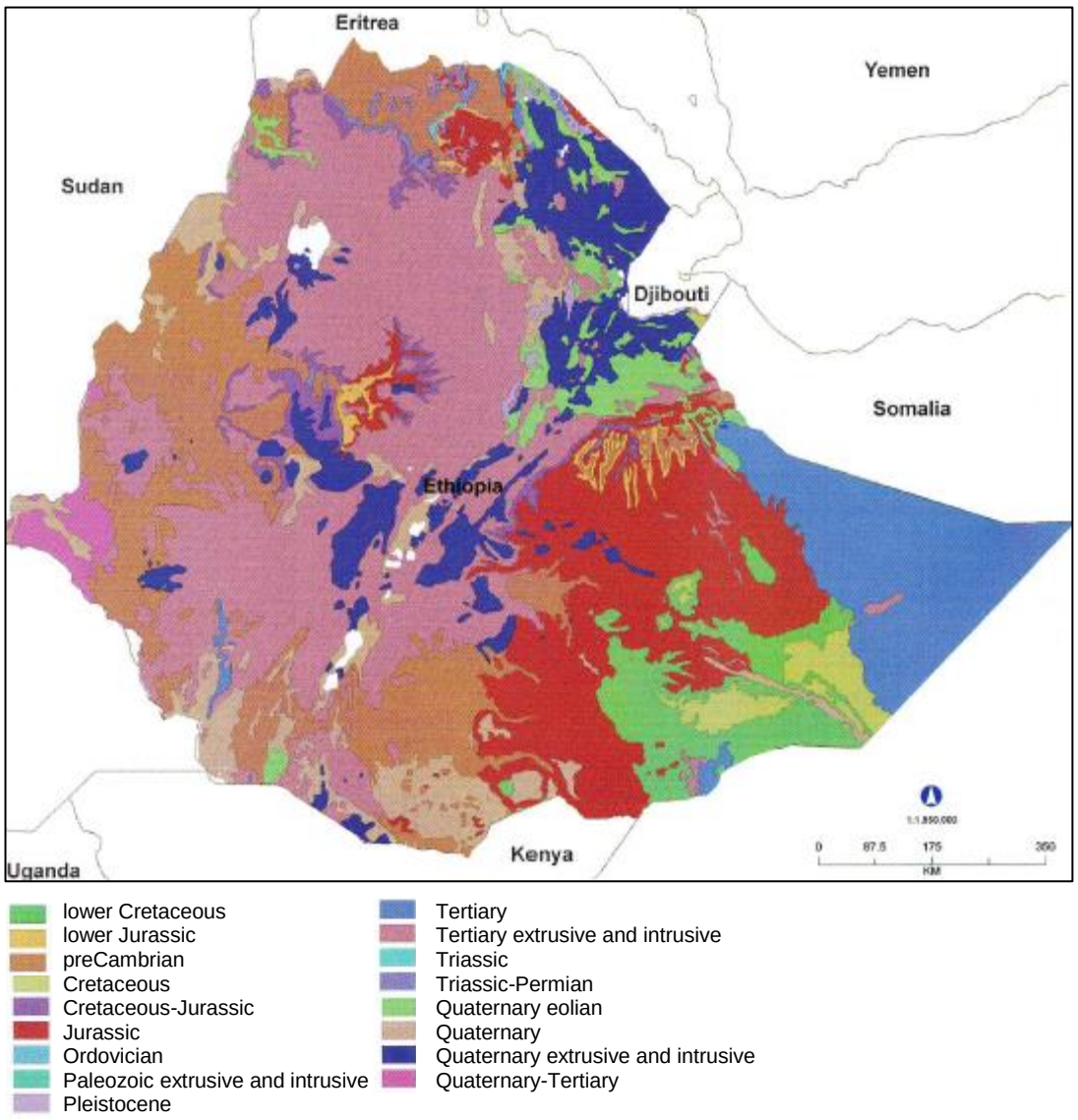

Figure 2.5. Schematic showing the geology of Ethiopia (adapted from Friis et al. 2011).

north-east monsoon over the Middle East dominates. Occasionally rain does fall in this season when Northern Hemisphere winter frontal systems interact with tropical systems and source depressions over the Indian Ocean; (3) *Belg*, the small rainy season occurs from March to May during which 20 – 30 % of annual rainfall occurs. It is the main source of rainfall for the south and south-east regions.

Generally the onset and duration of the rains follows a latitudinal pattern associated with the seasonal shift of the convergence zones. However, these seasons are not uniform across Ethiopia as a result of the position of the ITCZ superimposed over relief features. There are four major seasonal rainfall patterns across Ethiopia and Eritrea (Friis et al. 2011) (Fig. 2.6): (A) a bimodal rainfall pattern, as described above with a short dry season, found across central Ethiopia and flanking the Afar region; (B) a unimodal rainfall pattern with strong *kiremt* rains and rain during most of the year also, found in the western regions including Tigray and Wello; (C) a bimodal rainfall pattern with a long dry season, found in the southern and eastern regions; (D) an erratic rainfall pattern with a winter maximum, found in the Afar region.

Whilst the ITCZ is the dominant feature governing rainfall distribution across the Horn of Africa, altitudinal gradients play an important role in local climate variability. The Ethiopian highlands, for example, affect local climate by blocking unstable, moist, westerly Congo Air, preventing it from reaching the coastal areas in Ethiopia, Eritrea and Somalia, thus creating a coastal arid zone (Nicholson 1996; Umer et al. 2004). The highlands also result in leeward rain shadows, creating a complex patchwork of dry, subsiding air alternating with humid patches, causing rainfall variability over a few tens of kilometres (Nicholson 1996). Jet streams affect local climate; the Turkana jet, for example, enhances local aridity in northern Kenya and southern Ethiopia due to its descending air, as does the Somali jet stream which parallels the coast and increases frictional divergence (Nicholson 1996; Umer et al. 2004). The upwelling of cold water along the Somali coast supresses' rainfall further. Lakes and water bodies may further affect local climate; the larger East African Rift Lakes (or Great Lakes) can moderate regional hydrology and climate as they play a significant role in water recycling (Gasse 2000). Lakes Tanganyika, Malawi and Victoria in particular have been shown to modify diurnal cycles of cloudiness and convective activity and therefore the rainfall regime over their catchments (Nicholson

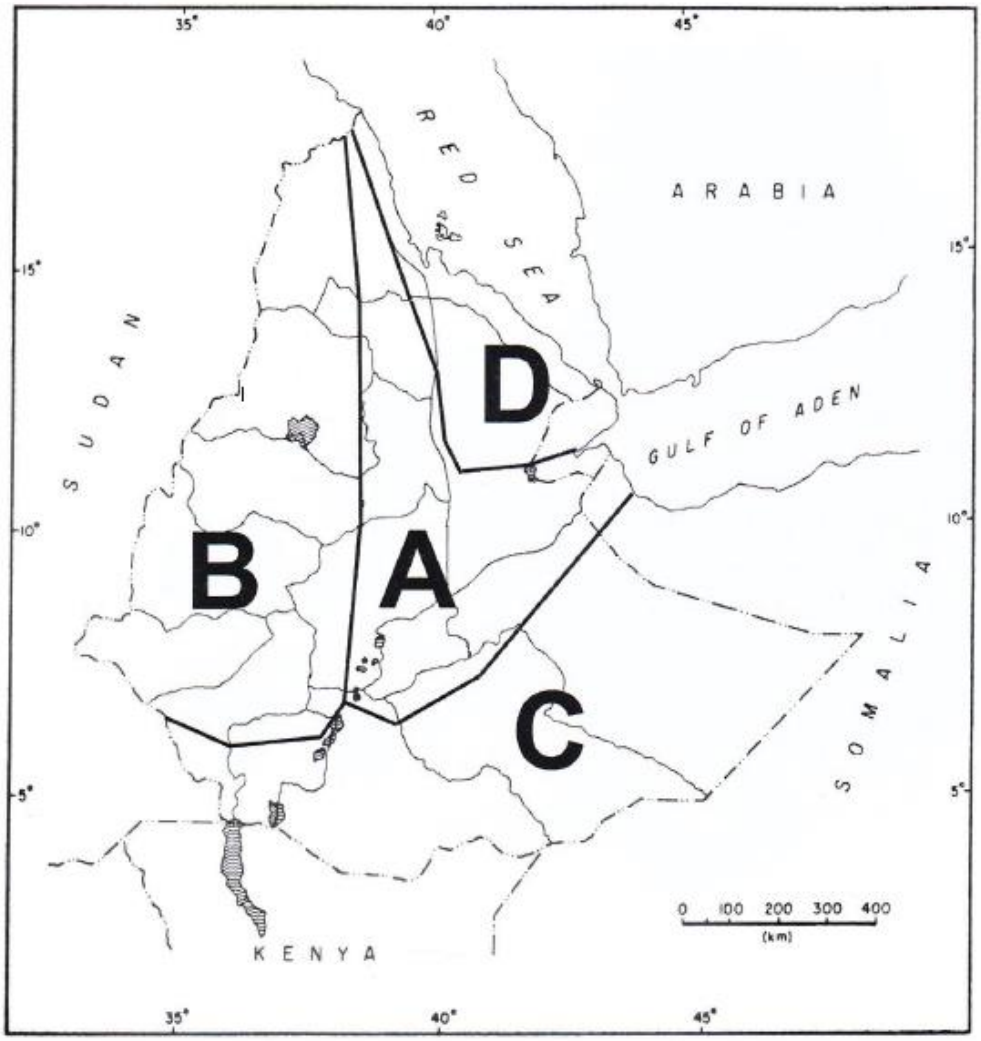

Figure 2.6. Schematic showing the major seasonal rainfall patterns in Ethiopia (Friis et al. 2011). See text for descriptions of regions A to D.

and Yin 2002). Lakes in the Horn of Africa therefore may affect local climate and environments by altering processes and mechanisms such as local soil moisture, runoff patterns, vegetation and forest cover (Trauth et al. 2010).

2.3.4 Soils

Friis et al. (2011) have reviewed the soil complexes of Ethiopia (Fig. 2.7). The soil types of Ethiopia form a complex mosaic. Last (2009) identified six broad soil groups based on region: (1) the plateau soil region, which is found in the highlands. Soils are derived from basaltic and other volcanic rocks and are mainly red lateritic or black vertisol soils. They are usually quite fertile; (2) the crystalline highlands soil, which is found at the edges of the highlands and are derived from metamorphosed, crystalline rocks. Soils are thin, acidic and not particularly fertile; (3) the desert soil region. In the Afar Depression, these soils are derived from recent lava or river deposits and so can be quite saline. In the Ogaden region the soils have been formed from sedimentary rocks and are rich in phosphorus; (4) the Ogaden dry steppe. These soils are derived from limestone and are rich in carbonates and are fertile; (5) the Rift Lakes region. Soils are derived from volcanic rocks and/or Quaternary sediments deposited by the larger lakes. The parent rocks vary in origin either coming from the flanks of the Rift Valley or the basaltic highlands; (6) the alluvial plains, which are found on the flood plains of larger rivers. These soils originate from material that has been transported from within the rivers catchment and so can be considerably fertile.

2.3.5 Modern Natural Vegetation

The distribution of vegetation in the Horn of Africa is governed by mean annual precipitation, topography, length of the dry season and, at high elevations, temperature (Peyron et al. 2000; Kiage and Liu 2006). Based on the work of White (1983), three vegetation zones have been identified in the plateau region: (1) Somalia-Massai vegetation types including deciduous savannah woodland and *Acacia* at low altitudes; (2) the Sudano-Zambezian zone with *Acacia-Commiphora* woodland at mid-altitudes; (3) Afro-montane vegetation in the highlands, including broad-leaf rainforest in the west, mixed humid forest on wet slopes to the south and coniferous forest with *Juniperus*, *Olea* and *Podocarpus* on dry slopes in the north and south. Friis et al. (2011) review and expand on White's (1983) classification (Fig.

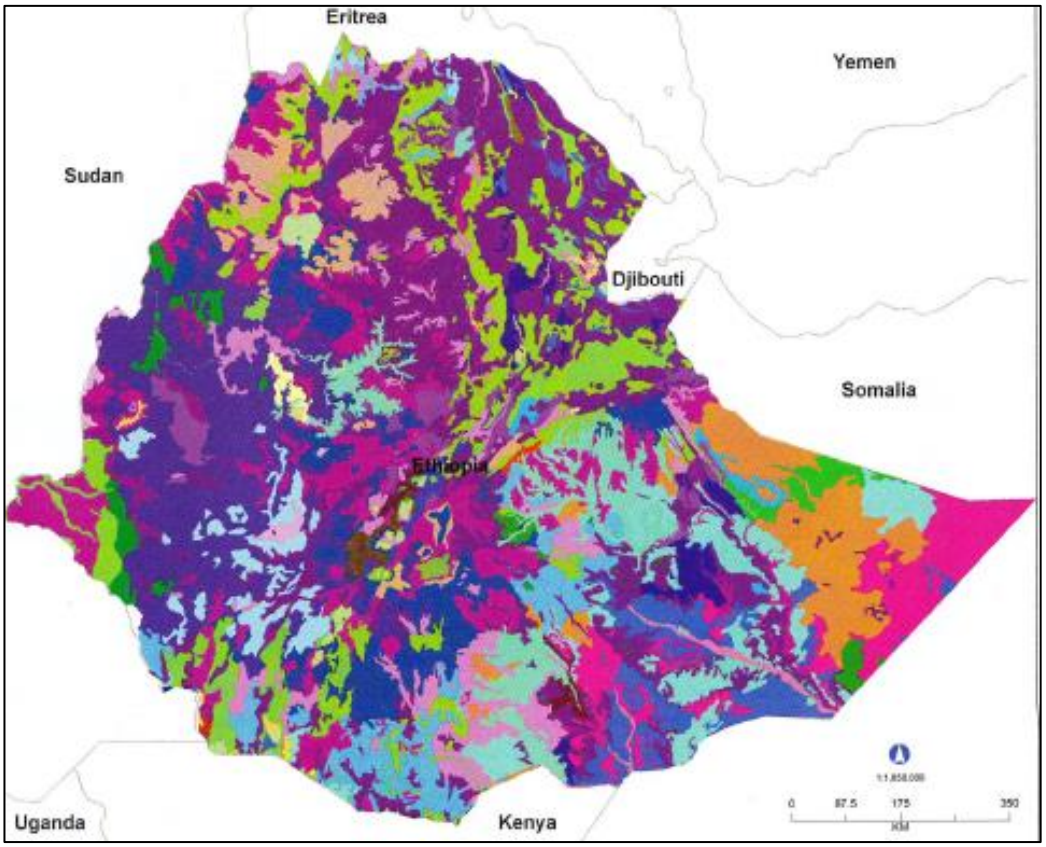

Calcaric Arensols
Calcaric Cambisols
Calcaric Fluvisols
Calcaric Regosols
Calcaric Chernozems
CalcaricVertisols
Calcaric Aernosols
Chromic Cambisols
Chromic Luvisols
Dystric Podzoluviso
Dystric Vertisols
Eutric Cambisols
Eutric Leptosols
Eutric Regosols
Eutric Vertisols
Eutric fluvisols
Gleyic Solonchaks
Haplic Alisols
Haplic Arenosols
Haplic Calcisols
Haplic Ferralsols
Haplic Gypsisols
Haplic Lixisols
Haplic Luvisols
Haplic Nitosols
Haplic Phaeozems
Haplic Solonchaks
Humic Ailsols
Humic Nitosols
Lithic Leptosols
Luvic Phaeozems
Mollic Andosols
No data
Petric Calcisols
Petric Gypsisols
Rendzic Leptosols
Rhodic Ferralsols
Salic Fluvisols
Sodic Solonchaks
Solonetz
Swamps
Vertic Cambisols
Vertic Luvisols
Vitric Andosols
Water bodies

Figure 2.7. Schematic showing the soil types of Ethiopia (adapted from Friis et al. 2011).

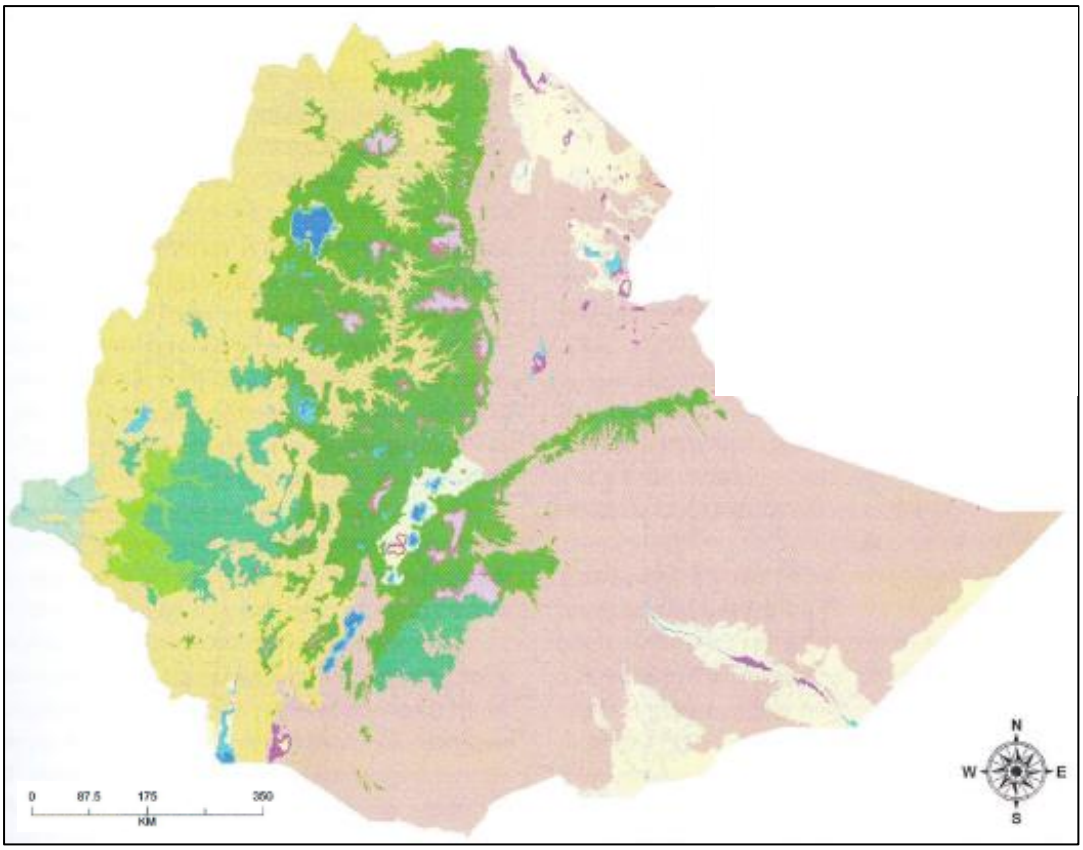

Desert and semi-desert scrubland
Acacia-Commiphora woodland and bushland proper
Acacia wooded grassland of the Rift Valley
Wooded grassland of the Western Gambela region
Combretum-Terminalia woodland and wooded grassland
Dry evergreen afromontane forest and grassland complex
Moist evergreen Afromontane forest
Transitional rainforest
Ericaceous belt
Afroalpine vegetation
Freshwater lakes- open water vegetation
Freshwater marshes and swamps, floodplains and lake shore vegetation
Salt lakes- open water vegetation
Salt pans, saline/brackish and intermittent wetlands and salt-lake shore

Figure 2.8. Schematic showing the natural vegetation types of Ethiopia (adapted from Friis et al. 2011).

2.8). The south, east and Afar Depression are dominated by *Acacia-Commiphora* woodland and bushland, with patches of desert and semi-desert containing salt pans and intermittent brackish wetlands, on the Eritrean and Somali borders. Western Ethiopia is characterised by *Combretum-Terminalia* woodland and wooded grasslands, with large areas of transitional rainforest and moist evergreen Afromontane forest in the south-west and wooded grassland in the western Gambela region. In the central highlands and along the Ethiopian Rift Valley, dry evergreen Afromontane forest and grassland dominate, with patches of Afroalpine and Ericaceous vegetation found throughout. An area of *Acacia* wooded grassland is found in the centre of the Ethiopian Rift Valley.

2.3.6 The Distribution of Lakes

Ethiopia is often referred to as the 'water tower of Africa' – of the 1.1 million km^2 that make up the country, 70,000 km^2 is covered by lakes, river and wetlands (Ayenew 2009). These inland water bodies are fundamental for the Ethiopian and wider East African ecosystems, as well as for the people who live around and work on them. Lakes in particular are important for the development of fisheries, irrigation and tourism, meaning that economic development in some locations is dependent on the sustainable use of these crucial water sources (Ayenew 2009).

The distribution of lakes in the Horn of Africa is governed by the geomorphology of physiographic regions shaped over tens of millions of years by volcanic-tectonic activity. Three main physiographic regions can be identified: the Rift Valley, highlands, escarpments and lowlands. Most lakes are confined to the Ethiopian Rift Valley (ERV) which extends from the Kenyan boarder in the south to the Afar Depression in the north (Fig. 2.3). The ERV comprises four systems: Lake Turkana, Chew Bahir, the Afar-Danakil Depression (the Afambo-Abhé lake group, Lake Afdera and Lake Asal) and the Main Ethiopian Rift (MER). The MER transects the highlands for 1000 km from the southern Afar in the north to the southern basin of Lake Chamo in the Gamo highlands. Lakes in the MER include Lakes Chamo, Abaya, Hawassa-Shallo, Chitu, Shala, Abijata, Langano and Ziwai[1]. There are several other small crater lakes scattered elsewhere in the ERV occupying small catchments. Rivers in

[1] 'Ziwai' is the Ethiopian spelling of the lake. It is more commonly referred to as Lake Ziway in academic literature and shall be referred to as such from here on in.

the highlands provide a sustained water supply to the Rift Lakes but water levels fluctuate with the amount and distribution of rainfall in the highlands (Street 1979a; Ayenew 1998).

Lake Tana, the largest lake in Ethiopia, is located in the north-western highlands. Other crater lakes in the northern highlands include Lakes Hayq[2] and Ardibo[3] in the South Wollo region, Lake Ashenge in the Tigray region and Dendi and Wonchi in the Shewa highlands. In the eastern highlands only a few lakes can be found close to the rift escarpment: Lakes Haromaya, Adele, Finkle and several small lakes in the Bale Mountains. Small crater lakes exist in the transitional escarpments; Lake Hare Seitan near the Guraghe Mountains, the Bishoftu lakes south of Addis Ababa and a small group of lakes in the Bilate River basin. The lowlands surrounding the Ethiopian plateau are largely devoid of lakes and swamps with the exception of the Gambela region, where wetlands and small ponds exist along the Baro and Akobo Rivers. Importantly, highland lakes and outflowing rivers feed the semi-arid and arid lowlands.

2.3.6.1 Lake Turkana Lake Turkana, formerly Lake Rudolph, straddles the Kenya-Ethiopia border and is the world's largest permanent desert lake and is a closed waterbody fed by three rivers – Kerio, Omo and Turkwel. There is no surface outflow and consequently the lake is highly sensitive to climatic fluctuations and depends on the balance between river and groundwater inflow and evaporation from the surface (annual evaporation is estimated to be 2335 mm [Ayenew 2009]). The River Omo accounts for 90 – 98 % of Turkana's hydrological input and originates in the central Ethiopian highlands (Beadle 1981). This inflow of water, sourced from the rain-fed highlands, maintains lake level in the desert. The Lake Turkana National Park in Kenya is a UNESCO World Heritage Site.

2.3.6.2 Chew Bahir Previously called Lake Stephanie, Chew Bahir means salt lake in Amharic. It is the most southerly and lowest (48 m above sea level) of a series of rift lakes in the north-easterly continuation of the Kenya Rift. It is an

[2] The study site for this research.
[3] 'Ardibo' is the Ethiopian spelling of the lake. It is more commonly referred to as Lake Hardibo in academic literature and shall be referred to as such from here on in.

ephemeral, saline lake in a wide, shallow basin approximately 64 by 24 km. It is fed by the Weyto River in the north and receives seasonal outflow from Lake Chamo. Today much of the area is a salt plain. Other habitats include marshes, mudflats, springs, bushland and mixed broadleaved scrub. When freshwater enters, this creates swamps and pools (Ayenew 2009).

2.3.6.3 The Ziway-Shala Basin The Ziway-Shala basin comprises four lakes – Lakes Ziway, Langano, Abijata and Shala – occupying volcano-tectonic depressions in the MER. A closed basin, the catchment covers 13,000 km^2, of which 1,433 km^2 is occupied by permanent water bodies. Lakes Ziway and Shala receive water from the western escarpment and Lake Langano from the eastern escarpment. Lake Abiyata is maintained by overflow from Lakes Ziway and Langano.

2.3.6.4 Lake Tana & the Blue Nile Lake Tana occupies a wide (66 by 84 km) lava-dammed depression, 1800 m above sea level. The lake has at least thirty-seven islands on it, twenty of which are home to churches and monasteries. Monks from the Ethiopian Orthodox Church have inhabited some of the islands for over 500 years (Ayenew 2009). Nowadays the lake is used for hydroelectric power generation, navigation, recreation, fishing and is a popular tourist destination.

The lake is fed by approximately forty rivers, the main ones being Gelda, Gilgel, Gumera, Infraz, Megech and Rib, which contribute 95 % of inflow (Ayenew 2009). The outflowing river is the Blue Nile, or Abay River, one of the two main tributaries of the River Nile (the other being the White Nile whose source is found in the headwaters of Lake Victoria). The Blue Nile provides the dominant contribution of peak flow (~ 68 %) and annual sediment load (~ 72 %) to the River Nile, especially in the spring floods when the river can rise by as much as 7 m (Williams 2009). As such, the Nile flood records, which date back to AD 622, when the record at the Roda Nilometer in Old Cairo began, can be used as a proxy for spring rainfall and drainage over northern Ethiopia. Approximately thirty kilometres downstream, the Blue Nile plunges down 45 m, forming the Blue Nile Falls, known locally as *Tiss Isat*, meaning smoke of fire. The river flows south from Lake Tana, then west across Ethiopia and then north-west into Sudan. The Blue Nile meets the White Nile at Khartoum, where it forms the River Nile. Approximately 300 million people live in the

River Nile's basin, spread across 10 countries (all of which are some of the poorest nations in the world), and 160 million people depend on the water for their livelihoods (Kameri-Mbote 2007).

2.3.6.5 Lake Ashenge Lake Ashenge is located 2440 m above sea level, covering an area of approximately 20 km^2. The catchment area is 129 km^2 and is used mainly for animal grazing. The level of the lake is believed to have dropped in the last 100 years due to neo-tectonic processes and to a lesser extent, the diversion of several tributaries for irrigation (Ayenew 2009).

2.4 Part II: Human Interactions with the Environment

2.4.1 A Climate Hazard: Drought

Drought is a complex natural hazard that differs from other natural hazards (for example, cyclones, earthquakes, floods) in several ways. Firstly, the effects of drought often accumulate slowly over a long period of time (one to several years) and can persist long after the event terminates. Due to this, droughts are sometimes referred to as a 'creeping phenomenon' as it is often difficult to identify the onset and end of a drought (Wilhite 1993). Secondly, there is no universally accepted definition of what a drought is, as its impacts vary with region and economic sector (Wilhite et al. 2013). The effects of a drought are superimposed onto a population's exposure to the hazard and their vulnerability to it. Meze-Hausken (2004) argues further that drought is defined by people's perceptions of it. For example, how does a population perceive changes in rainfall over a given time period, what are their rainfall needs for agricultural production and how does a population perceive one drought in contrast to another? These factors can make drought a difficult natural hazard to identify, respond to and mitigate.

Ethiopia has a long history of meteorological drought. Degefu (1987) compiled a long-term history of drought and famine in Ethiopia using data from the River Nile flood level records, historical archives and meteorological records. Twenty-seven events were identified from 253 – 242 BC to AD 1982, describing incidents of famine and crop failure, low River Nile flow, monsoon failures, social and political unrest, outbreaks of disease and plagues, high human mortality (resulting from starvation, suicide and murder) and high animal mortality (both domestic and wild).

2.4.1.1 ENSO, SST Anomalies & Rainfall Variability Multiple studies have demonstrated the existence of a relationship between East African rainfall variability, SST anomalies and the ENSO phenomenon (Nicholson and Entekhabi 1986; Ogallo 1987; Ropelewski and Halpert 1987; Farmer 1988). Periods of decreased rainfall in sub-Saharan Africa have been related to warmer SST in the equatorial Pacific, whilst other studies have identified a high degree of climate variability and monsoonal rainfall in ENSO affected areas (Nicholls 1988; Nicholls and Wong 1990; Comenetz and Caviedes 2002). Nicholson (1996) found that for the period 1901 – 1985, rainfall displayed an irregular periodic pattern with a dominant time scale of 5 – 6 years concurrent with ENSO events. Rainfall tended to be above average in East Africa during the ENSO year and was followed by drought the following year. A seasonal preference related to rainfall variability was also identified, with the positive anomaly tending to occur during the short *belg* rains of the ENSO year, and the drought occurring both in the *belg* rains the year prior to the ENSO event and during the long *kiremt* rains the year following the ENSO event (Nicholson 1996). Other studies have also statistically correlated reduced flows in the Blue Nile, River Nile and Atbara River with ENSO events (Eltahir 1996). Haile (1988) further identified that in Ethiopia the occurrence of droughts and famine corresponded to ENSO years. By evaluating the processes involved in drought causation, it appears that ENSO events and associated SST anomalies affect the distribution and intensity of rainfall across Ethiopia by disrupting and displacing the air masses responsible for producing rain (Haile 1988).

Through these assessments it has been shown that ENSO events and SST anomalies in the Atlantic and Indian Oceans can affect the intensity and delivery of rainfall to Ethiopia by displacing the ITCZ southwards and/or weakening the monsoon systems. Given the strong correlation between ENSO events and rainfall variability, successfully predicting when an ENSO event will occur could significantly assist with natural disaster preparation, including preparing for famine in vulnerable (often rural) areas. Additional drought monitoring and early warning systems could assist with this and inform policy makers regarding appropriate mitigation measures.

2.4.1.2 Historical Drought & Famine As previously discussed, Ethiopia is economically dependent on its agricultural sector, which is driven by the seasonal

occurrence of the rains across the country. The rains pace the pattern of planting, growth and harvesting around Ethiopia: 85 – 95 % of food production occurs during the *kiremt* rains and 5 – 15 % during the *belg* rains (Degefu 1987). The main harvest occurs during the *bega* season and the occasional rainfall that does fall in this season is usually sufficient to maintain grassland for livestock grazing. Ethiopia is also a financially vulnerable country, with limited capital, technology and resources available to adapt to and mitigate the effects of climate variability, including natural disasters. This combination of agricultural dependence and high vulnerability of its large population makes the country especially susceptible to famine, and so the occurrence of El Niño is potentially disastrous. If monsoon rains are weakened, late or fail, crop growth can be stunted or fail, resulting in shortages of food and fodder. This in turn may lead to livestock mortality and famine (Comenetz and Caviedes 2002). A spatial pattern of drought progression has been identified for Ethiopia based on drought occurrences from 1958 – 1977 (Wolde-Mariam 1986): droughts and the subsequent famine tend to be felt initially in the arid northern mountains of Eritrea and Tigray, before spreading south-east into the Awash Valley and then further south to the Harari and Bale regions. If the drought intensifies in severity, the central highland areas of Arsi, Omo, Shewa and Wello can become affected, followed by Gojam, Gonder, Ilubabor and Welega in the west.

Notable droughts and famines in Ethiopia include 'The Great Starvation' from 1835 – 1837. This drought affected Eritrea and the north and western provenances of Ethiopia after a failure of the rains. Historical records document that many people and livestock starved to death and there were outbreaks of cholera and cattle disease (Degefu 1987). From 1888 – 1892 one of the worst droughts in Ethiopian history occurred. Affecting the whole country, the drought became known historically as *kifu ken*, meaning the 'harsh days'. In 1888 both the *kiremt* and *belg* rains failed (meaning that agricultural and grazing land was not replenished following the dry *bega* season) and conditions were notably hot, causing a large proportion of the crops to fail. The effects of the famine were magnified by a rinderpest epidemic[4], which had decimated the Ethiopian cattle population and much of the rest of the

[4] An infectious viral disease affecting cattle and other ruminants. Symptoms include loss of appetite, fever, nasal and eye discharges, erosions in the mouth, nose and genitals, as well as diarrhoea followed by constipation. Animals die within 6 – 12 days of the onset of symptoms.

population across Africa by 1897, having been introduced accidentally through cattle trading by Italian colonists in 1885. To make matters worse, swarms of caterpillars, locust and rats annihilated what crops were left. Food prices soared as a result and there was widespread civil unrest (Pankhurt 1966). Given the high number of unburied human and animal corpses, sanitary conditions deteriorated rapidly and outbreaks of cholera, typhus, smallpox, dysentery, influenza and bronchitis added to the death rate (Pankhurt 1966). Additionally, there were reports of suicide, cannibalism and of animals attacking humans (Degefu 1987).

Another severe drought occurred in 1972 after an ENSO event which proved to be particularly disastrous for Africa. In Ethiopia the *belg* rains completely failed and the *kiremt* rains partially failed, which reduced the crop harvest, particularly in the north-east. Despite the suffering of the people, the government refused to acknowledge the situation and avert the impending disaster (Keller 1992). The government instead continued to focus on foreign exchange, exporting grain throughout the drought, including re-bagging grain that had entered the country as relief supplies (Wigger 1998). In 1973 the *kiremt* rains failed again and by 1974 the whole country was experiencing famine (Degefu 1987). A documentary was broadcast in Europe during this time depicting the scenes of extreme drought, hunger and poverty. This prompted some relief aid being sent to Ethiopia but due to political corruption and instability, it failed to reach the most drought stricken areas where it was most needed (Wigger 1998). The same documentary was broadcast across Ethiopia in 1974 with additional scenes showing the emperor, Haile Selassie, eating expensive food, drinking champagne and feeding his dogs from a silver tray. This sparked civil unrest and led to a military coup by the Derg.

In 1982 an ENSO event caused a two month delay of the *kiremt* rains and crop failure in northern Ethiopia. Below average rainfall followed in 1983 and the persistent drought caused rural populations to migrate in search of food and water. After initially denying how severe the situation was, the Ethiopian government reported in 1984 that only 6.2 million tonnes of food could be produced that year and 5 – 6 million people were at risk of starvation (BBC 2000). Pastoralist herders lost livestock due to lack of water and grazing grounds (Tiki et al. 2011). This drought in 1984 attracted an unprecedented amount of global interest and response from the

west, when images of emaciated, hunger stricken Ethiopians were broadcast around the world. The outpour of contributions from the west was phenomenal, raising US $1.2 billion in just over a year (Clay and Holcomb 1986). Western agencies became concerned however, by the lack of information and restrictions placed on them when attempting to deliver famine relief, and other aspects of the drought such as the war between government troops and liberation front forces were significantly downplayed; when food-aid arrived in the country it was often used to feed the army rather than famine affected areas (Keller 1992). Ethiopians fled the war and famine into neighbouring Sudan. In 1991, the EPRDM marched into Addis Ababa and ousted the Mengistu government and gradually conditions began to improve. This drought did result in the establishment of Early Warning Systems (EWS) by the international community; the Famine Early Warning Systems Network (FEWS NET) was put in place in the mid-1980s to ensure that vulnerability information was available (Kim and Guha-Sapir 2012).

The more recent drought in 2002 again attracted worldwide media coverage. In many parts of Ethiopia the *belg* rains failed completely and the *kiremt* rains were delayed by almost six weeks and were then considerably weaker than usual (Meze-Hausken 2004). The Afar, Oromiya and northern Somali regions were particularly hard hit and an estimated 11.5 – 15.0 million people were affected by food and water shortages across the country. The situation was worsened by a prolonged dry period between the *belg* and *kiremt* rains, which reduced the ability of people to prepare agricultural land for when the rains did eventually arrive. Sowing was delayed and the amount of seed available was reduced, pushing up food prices. Areas available for grazing and water for livestock were seriously reduced and weak animals succumbed to outbreaks of tuberculosis and scabies (Meze-Hausken 2004). Pastoralists were forced to herd their animals to grazing grounds up to 100 km away, but these grounds became overcrowded and overgrazed, resulting in violent conflict between some groups.

In 2011 a crisis erupted across Ethiopia and the rest of the Horn of Africa when, following the complete failure of the 2010 rains, the *belg* rains were significantly weakened. Malnutrition and hunger were widespread, affecting 10 – 13 million people and an estimated 50,000 – 100,000 people died (Hillier and Dempsey 2012;

Kim and Guha-Sapir 2012). The tragedy of the drought was that it has been predicted. EWS indicated an impending drought in August 2010 as changing weather conditions caused by La Niña were confirmed, and forecasts became more urgent in November 2010 when the rains failed (Hillier and Dempsey 2012). Between December 2010 and February 2011 multi-agency planning took place to begin contingency and response preparation and warnings were issued on the alarming situation. However, the window of opportunity to avert the impending crisis was missed and it was only in mid-2011 when a famine was declared that the humanitarian systems began to respond and aid arrived (Kim and Guha-Sapir 2012). By that time, global acute malnutrition levels exceeded 30 % in the affected regions (a level that the Integrated Food Security Phase Classification identifies as a catastrophe) and Crude Mortality Rates exceeded the emergency threshold of 1/10,000 per day (Kim and Guha-Sapir 2012). This disaster reflects both failings of the national governments in the Horn of Africa, as well as the international community, and highlights the need to manage the risk, rather than the crisis, by responding to early warnings effectively, rather than waiting until certainty is confirmed (Hillier and Dempsey 2012).

2.4.2 Environmental Pressures and Climate Change

Africa is the most vulnerable continent in the world to climate change and climate variability, a situation amplified by multiple ‘stresses’ operating across the continent: endemic poverty, complex and sometimes unstable governments and institutions, limited access to capital for economic growth (markets, infrastructure and technology), degrading ecosystems (deforestation, soil erosion and salinisation, desertification), natural disasters (meteorological droughts and floods), access to and management of safe drinking water, and internal conflicts. These factors complicate and reduce Africa’s capacity to mitigate the effects of climate change and adapt. The Intergovernmental Panel on Climate Change’s (IPCC) fourth (FAR) and fifth (AR5) assessment reports identified Africa’s current climatic sensitivity and vulnerable sectors, future climate projections, adaptation costs, constraints and opportunities (Boko et al. 2007; Niang et al. 2014). These reports consider continental Africa but identify specific climate variability and sensitivities in Ethiopia, the Horn of Africa and East Africa.

There is evidence (with “high confidence” in the Working Group I [WGI] AR5 terminology) of warming over land regions across Africa consistent with anthropogenic climate change, with decadal temperature analyses indicating significant warming over the last 50 – 100 years (Niang at al. 2014). In Ethiopia (and also South Africa), minimum temperatures have increased marginally faster than maximum and mean temperatures and in many parts of Kenya, South Sudan and Uganda the seasonal mean temperature has seen increases over the last 50 years (Conway et al. 2004; Kruger and Shongwe 2004; Funk et al. 2011; 2012). An increase in the frequency of extreme warm events has also been documented for countries bordering the western Indian Ocean between 1961– 2008 (Vincent et al. 2011). The warming trend is not uniform across the region however, and in East Africa an overall decrease in temperatures has been observed from weather stations along the coast and near to lakes (King’uyu et al. 2000). It is anticipated that under the A1B[5] and A2[6] scenarios, mean annual temperature rise over Africa (compared to the late 20th century mean annual temperature) will exceed 2 ºC by the end of this century (Niang et al. 2014).

Precipitation is also predicted to see changes in distribution and intensity by the end of the 21st century. East Africa has been experiencing an intensifying dipole rainfall pattern on the decadal time scale but this is spatially uneven with more rain falling in the northern sector and less in the south of the region (Schreck and Semazzi 2004). Overall, rainfall has decreased across the region over the last three decades between March and June (Funk et al. 2008; Williams and Funk 2011) and in the Horn of Africa, summer monsoonal rain has been decreasing for the last sixty years (Williams et al. 2012). However, areas of high or complex topography such as the Ethiopian highlands are likely to experience increases in rainfall and extreme events by the end of the century (Niang et al. 2014). Changes in runoff and hydrology have already been observed in Ethiopia, Kenya and Tanzania (Legesse et al. 2002; Eriksen et al. 2005).

[5] An emissions scenario describing a future world with rapid economic growth, a global population peaking mid-century and then declining, and a rapid introduction of efficient technologies. The technological emphasis is on a balance between fossil and non-fossil energy sources.
[6] An emissions scenario describing a heterogeneous future world, based on self-reliance.

Few regional and sub-regional climate change scenarios using regional climate models or empirical downscaling exist for Africa due to insufficient climate data, limited computational facilities and a lack of human resources (Boko et al. 2007). For 2080 – 2099 under a medium-high emissions scenario using twenty general circulation models (GCMs), annual mean surface temperature is expected to increase by 3 – 4 °C compared to 1980 – 1999, with the least warming occurring in equatorial and coastal areas (Christensen et al. 2007). Regional climate models tend to give smaller temperature increases but again this is complicated by predicted changes in vegetation and land use cover (Boko et al. 2007). For equatorial East Africa, maximum and minimum temperatures are projected to show an increase in the number of days warmer than 2 ºC above the 1981 – 2000 average by the mid- to late 21st century under A1B and A2 scenarios (Anyah and Qui 2012). Climate model projections for Ethiopia under the A2 and B1[7] scenarios show warming across all seasons, which may enhance evaporation as well as the frequency of heat waves (Conway and Schipper 2011). Temperatures over the upper Blue Nile are predicted to rise by 2 – 5 ºC by the end of this century under the A1B scenario compared to the 1961 – 1990 baselines (Elshamy et al. 2009).

Projected changes in precipitation are less consistent with models indicating significant differences in the range of seasonal mean rainfall. This is partly due to the inability of GCMs to successfully reproduce the mechanisms responsible for precipitation such as orography and the hydrological cycle, as well as global teleconnections, SST anomalies (which are particularly important for the Sahel), dust aerosol emissions, soil moisture and deforestation along the equator (Lebel et al. 2000). An assessment of twelve CMIP3 (the Coupled Model Intercomparison Project, phase 3) GCMs over East Africa suggests a wetter climate with more intense rainy seasons, including an increase in the number of extreme wet days, and less severe dry seasons by the end of this century due to recent cooling in the equatorial eastern Pacific (Moise and Hudson 2008; Shongwe et al. 2011; Vizy and Cook 2012). There are regional discrepancies however, as GCMs predict a wide range of spatial rainfall patterns over Ethiopia, whilst others indicate drying over

[7] An emissions scenario describing a future world with a global population peaking in the mid-century and then declining, a rapid change in economic structures toward a service and information economy, and the introduction of resource-efficient technologies.

large parts of Kenya, Uganda, Somalia, South Sudan and Tanzania. These inconsistencies have now been dubbed the ‘East African climate paradox’; whilst climate projections indicate future warming and increased rainfall, the East Africa long rains are actually declining. The inability of models to agree on the magnitude and direction of change as well as extremes will severely limit and hinder the ability of policy makers to manage water resources in the future. Discrepancies between models exist for the entirety of the African continent; for the western Sahel some models predict progressive drying, whilst others indicate wetter conditions with the expansion of vegetation (Hulme et al. 2001; Claussen et al. 2003).

Some models are also unable to simulate land use changes and extreme climate events including ENSO. This highlights the importance of resolving and improving the representation of regional atmospheric processes, alongside local climate effects, in climate models in order to improve the precision and reliability of simulations. Palaeoclimate simulations in conjunction with climate models may provide an important tool for resolving and assisting with constraining model parameters by supplementing the constraints of the instrumental record; they can distinguish between models which are overly sensitive and those which are not sensitive enough (Von Deimling et al. 2008). Palaeoclimate simulations may also be used to assign relative likelihood to different ensemble members and scenarios in probabilistic climate change prediction (Brown et al. 2008).

Despite the limitations and discrepancies, climate models do provide a useful baseline for identifying the likely impacts of climate change, within a likely envelope of behaviour. Water stress, for example, will become a greater risk to nations with climate change (“high confidence”). Six climate models show an increase in the number of people experiencing water stress in North and Southern Africa, whilst in East and West Africa people are likely to see a reduction in water stress (Boko et al. 2007). Even in the absence of climate change, present population trends and water use patterns suggest that many African countries will exceed their economically sustainable land-based water resources by 2025 (Ashton 2002). Under A2 and B1 scenarios, stream flow in the River Nile is expected to increase in the medium term (2010 – 2039) and then decline in the second half of this century due to a combination of declining rainfall and increasing evaporative demand (Beyene et al.

2010; Kingston and Taylor 2010). Changes in the Lake Tana basin, source of the Blue Nile, are inconclusive (Taye et al. 2011).

Lake systems are particularly at risk to changes in temperature, precipitation and changes in hydrology (Ayenew 2007). In Ethiopia for example, Lake Abiyata, the terminal lake in the Ziway-Shala basin, decreased by more than 50 % in size between 1973 and 2006 (Getnet et al. 2014). Although no significant changes have been documented in rainfall over the basin for the period 1975 – 2008, linear temperature increases have been observed in the surrounding Assela, Zeway and Butajira highlands. Land use in the basin has also seen substantial changes in recent decades. In 1990, 30.8 % of land was intensively cultivated which by 2007 had increased to 49.9 % (Getnet et al. 2014). Some land use types completely disappeared in this time period including bush-shrub grassland, dense woodland and wooded grassland. Associated with these changes, surface runoff increased in 35 % of the basins land area and decreased in 15 % of the land area. Irrigation and water abstraction have also increased across the basin in this time period. From 2002 – 2009 the area being irrigated for agriculture in two districts north and west of Lake Ziway increased from 1,435 ha to 16,510 ha. As a consequence of the increasing temperatures, land use change and pressure on resources, 207 Mm^3 of additional water has been lost through evaporation from the lakes and evapotranspiration from the land surface in 2007 compared to 1990 (Getnet et al. 2014). Given the magnitude of the changes observed over a relatively short time period, it is clear how current climate sensitivity coupled with additional anthropogenic pressures can severely reduce a system's ability to respond and essentially buffer the detrimental effects it incurs. This trend is likely to continue as long as resources are overexploited and climate patterns continue to change.

Climate change will also burden the health sector in Africa ("medium-high confidence") as it acts as a multiplier to existing health vulnerabilities such as insufficient access to safe drinking water and sanitation and food insecurity (Niang et al. 2014). Under various emission scenarios, the areas suitable for malaria transmission will expand and contract depending on location by 2020, 2050 and 2080 (though multiple drivers such as drug resistance, land use change, human migration will also affect transmission) (Thomas et al. 2004). East Africa in particular

is more likely to become suitable for malaria transmission (Hartmann et al. 2002). More rainfall falling in the warmer *kiremt* season could see previously malaria-free highland areas in Kenya, Ethiopia, Rwanda and Burundi experience modest increases in malaria by 2050 with even greater incursions by 2080. Siraj et al. (2014) estimate that a 1 ºC rise in temperature, without mitigation, would result in 410,000 additional infections per year in Ethiopia as malaria expands into new territories. This could be amplified by already compromised populations such as those afflicted with HIV and AIDS, or in conflict areas where access to health care and medical facilities is limited or restricted.

Agriculture is likely to be seriously, detrimentally affected in some regions by climate change ("high confidence"). South Africa and Zimbabwe could experience yield losses of up to 30 % as temperatures increase and precipitation decreases. Pest, weed and disease pressures on crop and livestock may also increase with climate change. However, in other areas the growing season is likely to be extended and benefit from warming; maize production in East Africa could expand to higher elevations (Thornton et al. 2009). Agriculture and food security will be significantly affected by additional forces though, such as access to capital and markets, technological innovation as well as the increasing trend of urbanisation across the continent and globalising food chains (Niang et al. 2014). Whilst some progress has been made in managing risks to food production from current climate variability, there is a "high confidence" that this will not be sufficient enough to address the long-term impacts of climate change (Niang et al. 2014).

Ecosystems will most likely see substantial changes due to climate variability, which alongside anthropogenic drivers such as land use change (in particular agricultural expansion) could be mostly detrimental. The ice cap of Mt. Kilimanjaro for example, could disappear between 2015 – 2020, having already seen an 80 % reduction in the areal extent of its' ice fields in the 20th century (Thompson et al .2002). The HadCM3 (Hadley Centre Coupled Model, version 3) GCM shows that under various emission scenarios, mixed rain-fed semi-arid systems will be affected in the Sahel, the Rift Lakes region and East Africa (Boko et al. 2007). Declines in fisheries in some of the East African Rift Lakes could potentially occur due to climate change; small variations in climate may affect thermal stratification, nutrient availability and water

inflow, all of which could destabilise plankton dynamics and therefore trophic interactions at higher levels (Verburg and Hecky 2009; Magadza 2010). The potential impact to fisheries is uncertain however, given the multitude of factors such as pollution, invasive species and overfishing, operating across the lakes, which themselves could be affected by climate change (Tumbare 2008). Coastal ecosystems will also be affected by climate change; episodes of coral bleaching and species invasions (including the outbreak of crown-of-thorns starfish) linked to climate variability have already been documented in Djibouti and Somalia (Boko et al. 2007). Sea-level rise is expected to adversely affect many African nations. Indian Ocean islands could see changes in the intensity, frequency and location of cyclones and the East African coast could similarly be affected by changes in the intensity and frequency of ENSO events. A 1 m rise in sea-level could cost Kenya US $500 million in crop losses based on current valuations, whilst in Eritrea the same amount of rise would cost US $250 million in damages to infrastructure (Boko et al. 2007).

Based on the multitude of potential climate change scenarios, forecast against a background of complex and multiple stresses, Africa clearly needs to adapt. However, limited availability of data and the uncertainty of climate modelling make it difficult to quantify where and how adaptation responses are most necessary, how much they will cost, and how much *not* adapting could cost (including the financial, social, environmental and cultural costs). These uncertainties are complicated and amplified by a multitude of factors such as extreme poverty, conflicts, lack of resources and technology, imperfect and sometimes corrupt governance systems, and economies dependent on the climatically-sensitive agricultural sector. In all regions of the African continent, national governments are attempting to implement adaptation systems but the evolving frameworks are not yet able to effectively coordinate the range of responses required due to under-resourced, incomplete and fragmented institutional planning (Niang et al. 2014). The best progress has been made at the individual or household level, without the support of governments, policy makers and stake holders (Berrang-Ford et al. 2011; Niang et al. 2014). Poverty and vulnerability are identified as the primary reason for overwhelming the adaptive capacity of African nations and as such, new policies need to strengthen the links between adaptation and development pathways with a focus on building resilience in order to increase adaptive capacity. Improved understanding of climate variability,

including better representation of the climate system and global teleconnections, using high-quality, high-resolution data (including palaeodata) will assist with this, and bring climate change to the forefront of African national planning.

2.4.3 Historical Interactions with Climate: The Kingdom of Aksum

It is clear that the people of the Horn of Africa are used to interacting with their climate, which has shaped their cultural, social and economic practices and will ultimately shape their future. Such interaction with climate is not a recent phenomenon and can be traced back to the establishment and decline of the Aksumite civilisation of late antiquity. The Kingdom of Aksum[8] rose to prominence in the Tigray region (approximately 960 km north of Addis Ababa and 540 km north of Lake Hayq) around 400 BC and became an international political and economic power before declining around AD 700. It has been hypothesised by Butzer (1981) that climate change was key in facilitating growth and development of the civilisation by allowing population growth. A subsequent climate shift, alongside political and economic instability, led to the decline and ultimate collapse of the kingdom by causing it to become increasingly inhospitable to the point it could no longer sustain its' population (Butzer 1981) (caution should be aired when interpreting Butzer's [1981] chronological framework given the various materials and techniques applied, as well as improvements in chronological analyses since the study was undertaken).

Archaeological evidence indicates that in the pre-Aksumite period (900/800 – 400 BC) a well-established, administrated society ruled by kings and queens existed on the northern Ethiopian plateau (Fattovich 2010). In the Tigray region, towns, villages, hamlets and ceremonial centres have been unearthed (Michels 2005). The two largest settlements were located at Yeha, where bronze and iron tools and weapons were found, and Matara. A large South Arabian influence was found in the architecture, ceramics, administrative devices, sculptures, inscriptions and writings (Anfray 1968; Ricci 1984; Fattovich 2010). Given the state of the current environment at Axum, it is apparent that for the civilisation to have established here, conditions and resources must have been significantly more productive and hospitable to allow a population to sustain itself. The environment around Axum

[8] 'Aksum' traditionally refers to the ancient Ethiopian city whilst 'Axum' refers to the modern city.

today has been degraded by years of intensive agriculture, unsustainable land use and deforestation. Much of the land is experiencing severe soil erosion; Ciampalini et al. (2012) calculated that erosion during the Aksumite reign was 2.8 t ha $^{-1}$ yr $^{-1}$ whereas more recently (1975 – 2006) this has increased to 65.8 t ha $^{-1}$ yr $^{-1}$ due to the conversion of terraces into grazing land without adequate soil conservation practices. This is enhanced by a lack of vegetation cover to protect and stabilise soils from the monsoon rains, which has caused them to thin considerably (Butzer 1981). Water is also scarce, and stream discharge and runoff are variable (Butzer 1981). These conditions could not have supported a population the size of Aksum's 2.8 kyr ago (10,000 – 20,000 people in AD 500; Butzer 1981). Evidence instead indicates that the land and climate were favourable enough to allow the developing civilisation to apply practices such as cattle ploughing, irrigation and terracing (Butzer 1981). It is important to consider that these practices during the pre-Aksumite period would have been applied during a single growing season of short, heavy *kiremt* rains, similar to what Axum receives at present, given its location in the far northern highlands.

By AD 50 the archaeological evidence supports the establishment of a kingdom at Aksum, indicated through architecture, settlement patterns, elite tombs and coinage (Phillips 1997; Finneran 2007; Fattovich 2008). Around this time a shift in climate has been hypothesised which would have increased the capacity of Aksum to grow food and therefore feed a larger population (Butzer 1981; Sulas et al. 2009). A northward extension of the ITCZ would have caused Aksum to receive the *belg* rains in the springtime in addition to the *kiremt* rains. Terwilliger et al. (2013) used stable hydrogen isotopic ratios (δ*D*) of land plant-derived fatty acids to confirm that the Aksumite Kingdom emerged during a short, moderate wet period following a stable climate. Machado et al. (1998) likewise found evidence of a wet period around this time from infilled valley deposits in the Tigray region, and Marshall et al. (2009) identified a wet period in the Lake Ashenge (approximately 220 km south-east of Axum) diatom record from 200 BC – AD 500, indicating a climate shift. This suggests that the increase in precipitation did not trigger an immediate rise in Aksum's prominence, but rather created suitable conditions to which the population gradually responded to and utilised (Marshall et al. 2009). Geo-archaeological evidence from Aksum itself, and the surrounding landscape, provides evidence of this climate shift

(Butzer 1981); sediments deposited in drainage channels between ~ AD 100 and AD 350 indicate seasonally abundant soil moisture, wet slope soils and strong periodic floods. This would have significantly lengthened the growing season for agriculture from five to seven, or even nine months, thus allowing two crops to be grown per year, as well as improving the supply of surface and subsurface water. Improved farming techniques, irrigation and terracing practices would have increased the area available for agriculture by expanding onto previously unworkable soils, as well as making farming more efficient and productive (Reader 1998; Sulas 2009). The effect of this climate shift would have substantially increased the capacity of the kingdom to grow food and feed its population, which in turn enabled the civilisation to concentrate on its territorial, economic and cultural expansion.

The international prominence of the kingdom as an economic and politically powerful trading centre developed around AD 100 when it began to utilise its proximity to the Red Sea port of Adulis (modern day Massawa) to funnel its import and export commodities. References to tropical timber, ivory, rhinoceros horn, hippopotamus hides, civet, slaves, gold dust and frankincense have been found in historical documents and archives (Butzer 1981; Casson 1989). The Roman and Byzantine empires were particularly important trading partners who paid with iron tools, cloth, glass beads and vessels. Other important trade links included Egypt, Gaul (western Europe during the Roman era), India, Nubia, Syria, Persia, China and the Black Sea region. By the 3rd century AD, the various kings of Aksum had progressively incorporated the surrounding regions into the kingdom, including all of modern day Tigray, Eritrea, the Sudan, the coastal plains and for a short time, Yemen (Anfray 1990; Fattovich 2008; 2010). In AD 330 King Ezana converted from worshipping the Greek deities to Christianity and so churches and monasteries were erected and by around AD 500 the kingdom had reached its maximum expansion (Phillips 1997; Fattovich 2010). The city covered an estimated 75 ha and supported a population of 10,000 – 20,000 people (Butzer 1981).

The kingdom began to decline however in the 7th and 8th centuries AD and finally collapsed at the end of the first millennium (Fattovich 2008). This collapse was driven by a combination of environmental and economic causes (Butzer 1981; Fattovich 2010). Conflict arose when the Beja nomads formed an independent polity

in the Eritrean highlands during the 7th – 9th centuries AD, cutting off Aksum's access to the coast (Fattovich 1987; 1990). Arab conquests and Muslim expansion along the Red Sea and in the Mediterranean in the 7th – 10th centuries compounded this further by replacing Aksum as the key trading authority in the region. The kingdom's economic prosperity began to fade as a result, leading to political instability.

This volatility was compounded further by progressive exhaustion of the landscape through intensive agriculture and deforestation. Timber was used for construction, manufacture, cooking and heating, and forest was additionally cleared to make room for agricultural expansion (Reader 1998). This scale of deforestation would have increased topsoil erosion and mobilisation by exposing the surface to the intensity of the monsoon rains, causing leaching of soil nutrients, thereby reducing soil fertility (Bard et al. 2000). Deposits in the sedimentological records from Aksum at this time contain cultural debris, rubble and evidence of saturated soils (Butzer 1981). This would imply there was widespread field abandonment in Aksum, most likely when land was no longer productive, and that the monsoon rains washed away rubble and debris in mudflows, covering abandoned buildings in the city. It is also hypothesised that at around AD 750, the climate reverted back to its previous (and present) state of one season of *kiremt* rains per year (a unimodal rainfall regime) (Butzer 1981). River Nile flood data support this change in climate (Williams 2009); Nile floods were high in AD 622 and continued to be high until AD 750 when they began fluctuating to slightly below average flow. From AD 930 – 1070 the flood records registered flow as abnormally low (Hassan 1981; 1997; 2007). This supports the hypothesis of reduced rains in northern Ethiopia at this time.

The diatom and stable isotope record from Lake Ashenge also supports a rapid shift back towards a drier climate and a unimodal rainfall regime, though some 250 years prior to that suggested by Butzer (1981) when Aksum was still the central economic and political power in the region (Marshall et al. 2009). This would suggest a more gradual decrease in rainfall, rather than an abrupt decline leading to catastrophic population decrease (Marshall et al. 2009). Whether abrupt or gradual however, the decrease in rainfall alongside environmental degradation would have meant only one harvest could be produced a year and so farming could no longer provide enough food to sustain the city's population. Consequently, droughts, famines and epidemics

may have become more frequent and widespread, as well as increasingly hostile attacks from neighbouring pastoralists. The population struggled to cope with the environmental changes and increasing isolation, causing them to migrate southwards (Pankhurst 1985; 1992; Bard et al. 2000). The city collapsed and was abandoned during the 8th century (Butzer 1981).

2.5 Conclusion

The African monsoonal system and its interaction with the ITCZ and CAB, is the driving force behind the climate, distribution of rainfall and seasonality in Ethiopia and the Horn of Africa. The expression of regional climate differences is amplified by variations in topography, the distribution of lakes and other hydrological features. Decadal climate variability may result from ENSO events and SST anomalies, which can be particularly hazardous to people through the occurrence of droughts. Perhaps most worrying is the potential impact of anthropogenic climate change on future climate variability in the Horn of Africa. Current GCMs and regional climate models are limited by a lack of regional data and by their ability to simulate the complex climate mechanisms, including the position and movement of the ITCZ and ENSO, operating across Africa. As a result it is difficult to identify how the Horn of Africa will be affected by climate change and how nations could begin to adapt and plan mitigation strategies now. Improved predictions and more robust climate models are essential for long-term plans as well as for hazard preparation. High-quality, high-resolution palaeo-records from across the region are essential for this, as they identify how the climate responded to previous climate perturbations, which is used in testing (hindcasting) and evaluating model sensitivity, as well as constraining model parameters.

Chapter 3

Environmental and Climatic Variability in East Africa Since the Last Glacial Maximum.

3.1 Introduction

This chapter aims to review current knowledge and understanding of the palaeoclimate of tropical and subtropical Africa in the late Quaternary. First, the application of palaeolimnology (the focus of this study) in East Africa is discussed, identifying recent progress and advances in the field, as well as key issues affecting research. Then, environmental and climatic variability during the late Quaternary is discussed. Three time-periods are identified based on the major climatic shifts: the Last Glacial Maximum, the last glacial-interglacial transition, and the Holocene. Consideration is given to a range of palaeo-records indicative of general climatic and environmental trends during these periods, identifying the high magnitude, sometimes abrupt events that shaped East African (and continental African) hydrology and the environment. For the benefit of the reader, events have been described in a chronological order. It is important to consider however that the events described did not occur during a definitive time period but were instead expressed at different magnitudes and frequencies across Africa at slightly different times, given the diversity of feedbacks operating across a patchwork of environmental conditions. Events have only been described in such a static fashion to help identify the cause and (cumulative) effect of climatic fluctuations in palaeo-records. Emphases is placed on hydrological and climate records from Ethiopia, the Horn of Africa and East Africa but terrestrial and marine records from elsewhere in the continent (West and Southern Africa, the Sahel) and further afield are also considered (Fig. 3.1).

3.2 Palaeolimnology in East Africa

Sedimentary sequences from tropical African lakes have been used to reconstruct climate and environmental changes at a range of time scales. The focus of these reconstructions has shifted from long-term glacial-interglacial dynamics during the Quaternary, to short-term (century to inter-annual scale), regional responses relevant to current issues of anthropogenic climate change and human societies. Previously, reconstructing such responses in East Africa had been hindered by a lack of

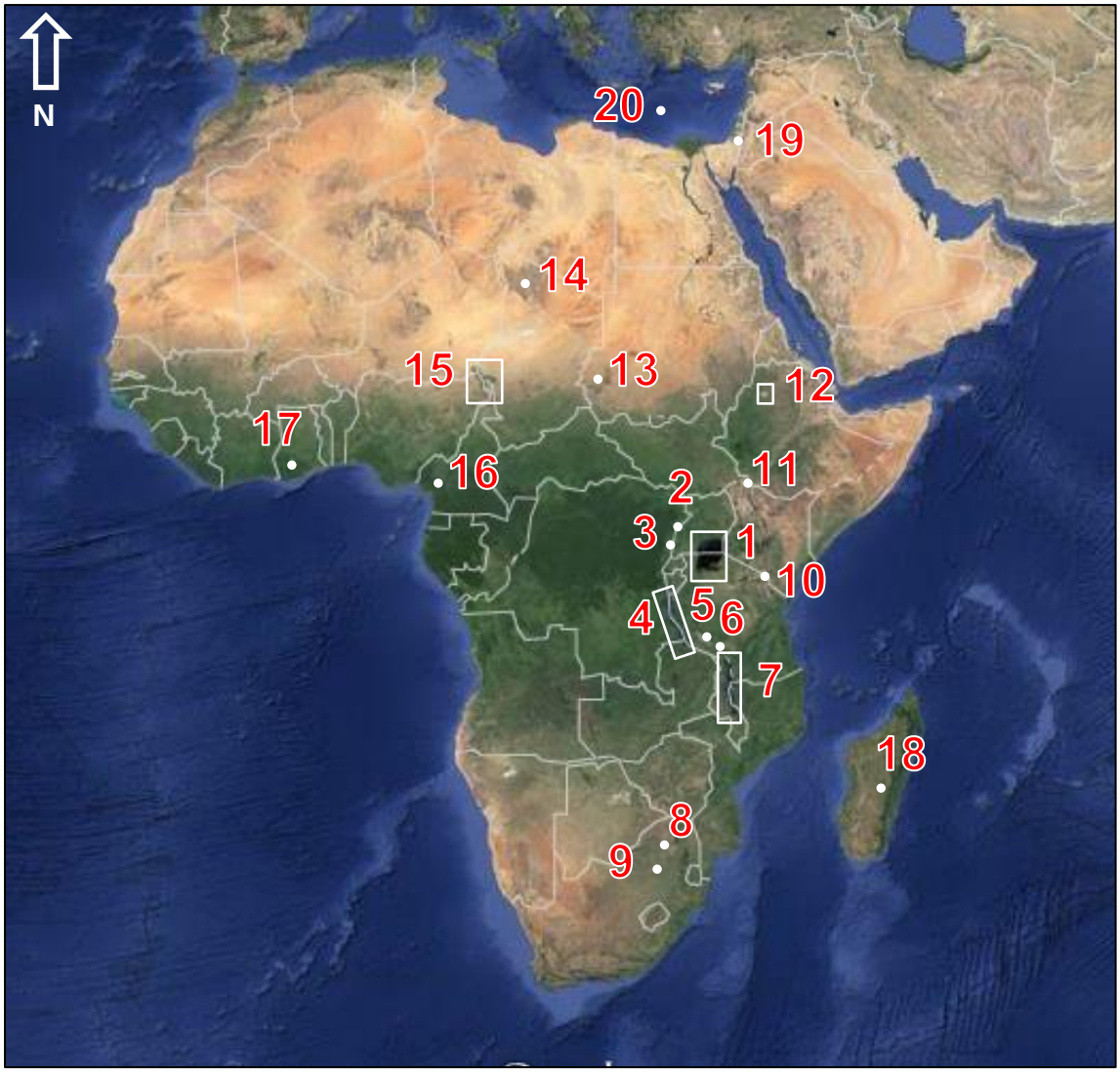

Figure 3.1 (a). Lakes and palaeo-record sites across Africa and the Mediterranean (Google Maps 2015): (1) Lake Victoria; (2) Lake Albert; (3) Lakes Edward, George, Kibengo, Kitagata, Kasenda and Wandakara; (4) Lake Tanganyika; (5) Lake Rukwa; (6) Lake Massoko; (7) Lake Malawi; (8) Wonderkrater spring mound; (9) Pretoria saltpan; (10) Lake Challa, Mt. Kilimanjaro; (11) Lake Turkana; (12) Lake Tana; (13) Jebel Marra, Marrah Mountains; (14) Tibesti Mountains; (15) Lake Chad; (16) Lake Barombi Mbo; (17) Lake Bosumtwi; (18) Lake Tritrivakely; (19) Soreq Cave; (20) eastern Mediterranean sapropels (multiple sites).

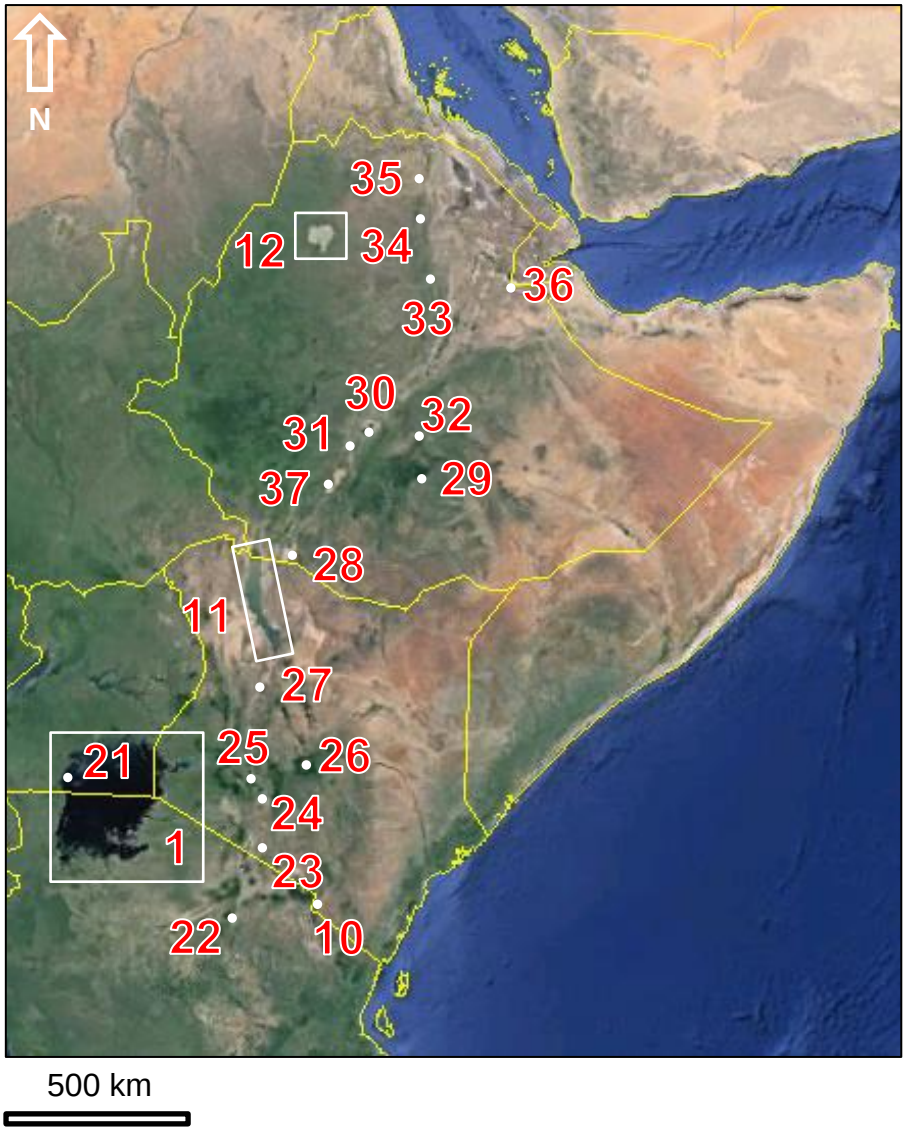

Figure 3.1 (b). Inset of Figure 9 (a), lakes and palaeo-record sites across the Horn of Africa (Google Earth 2013a): (1) Lake Victoria; (10) Lake Challa, Mt. Kilimanjaro; (11) Lake Turkana; (12) Lake Tana; (21) Lake Nabugabo; (22) Lake Manyara; (23) Lake Magadi; (24) Lake Naivasha; (25) Lakes Bogoria, Nakuru, Elementeita; (26) Sacred Lake, Mt. Kenya; (27) Lake Suguta; (28) Chew Bahir; (29) Lake Garba Guracha and the Tamsaa swamp, Bale Mountains; (30) Ziway-Shala basin (Lakes Ziway, Langano, Abijata and Shala); (31) Lake Tilo; (32) Mt. Bada, Arussi Mountains; (33) Lake Hayq; (34) Lake Ashenge; (35) Mekele outlier; (36) Lake Abhé; (37) Done Ella.

instrumental records prior to European colonisation, and by the limited potential of other high-resolution climate records such as ice cores, speleothems and tree rings (Verschuren 2003). Lakes therefore provide an excellent opportunity to reconstruct continental and regional climate variations using the sediments accumulating at the bottom of them.

Selecting a suitable lake and understanding the lake system is a crucial first step in obtaining a reliable sedimentary sequence and successfully interpreting it (Olaka et al. 2010). Continuous, high-resolution records needed for climate reconstructions are found in climatically sensitive lakes where the potential to respond to and record short-term fluctuations in climate is high, and the signal is preserved in an uninterrupted sequence (Battarbee 2000; Umer et al. 2004). Climatically sensitive lakes include hydrologically closed basins where evaporation dominates the water balance; hydrologically open lakes where surface/subsurface outflow is low in comparison to evaporation; and amplifier lakes where highly variable precipitation or river inflows override the stabilising effect of outflows, in a basin of unique, often tectonically formed morphology (Street 1980; Street-Perrott and Harrison 1985; Verschuren 2003; Olaka et al. 2010). Such lakes have been identified across the African tropics, subtropics and subtropical desert regions (Table 3.1). Continuous, long-term, climate-proxy records from across the African continent provide a spatial gradient of climatic and environmental variability, thus making investigations into regional hemispheric differences as well as inter-hemispheric symmetry (or asymmetry) possible.

Olaka et al. (2010) investigated the sensitivity of ten lake basins in the East African Rift Systems (EARS; Lakes Awassa, Manyara, Naivasha, Suguta, Turkana, Victoria and the Magadi-Natron, Nakuru-Elmenteita, Baringo-Bogoria and Ziway-Shala basins [Fig. 3.1]) and their potential for recording climate variability by assessing features such as lake form and hydrology. Tectonic control on basin geomorphology was demonstrated to affect the potential of a lake to yield good sedimentary sequences; graben-shaped lakes (Lakes Awassa, Naivasha, Suguta and the Nakuru-Elmenteita and Ziway-Shala basins, as well as the study site, Lake Hayq) show greater oscillations in lake level relative to surface area due to the steep sided catchments which constrain and protect them from wind-driven mixing. This

increases their potential to preserve sedimentary records. In contrast, pan-shaped lakes with gentle slopes (Lakes Manyara, Turkana and Victoria and the Baringo-Bogoria and Magadi-Natron basins) show greater oscillations in surface area to depth ratio, and sediment records tended to show greater evidence of erosion, reworking and drying out during Holocene arid-humid transitions.

Table 3.1. African lakes with continuous climate-proxy records.

Lake	Location	Length of record (kyr BP)	Authority
Naivasha	Kenya	175	Bergner et al. 2003; Trauth et al. 2003
Challa	Mt. Kilimajaro	140	Moernaut et al. 2010
Tanganyika	EARS	100	Scholz et al. 2003; Tierney et al. 2010
Malawi	EARS	79	Scholz and Finney 1994
Abhé	Ethiopia-Djibouti	70	Gasse 1977; Gasse et al. 1980
Massoko	Tanzania	50	Barker et al. 2003; Garcin et al. 2006
Chad	West Africa	50	Durand 1982
Tritrivakely	Madagascar	40	Gasse and Van Campo 1998
Albert	EARS	30	Beuning et al. 1997
Bosumtwi	Ghana	26	Maley 1992; Peck et al. 2004
Victoria	EARS	25	Stager et al. 1986
Rukwa	Tanzania	23	Vincens et al. 2005

Burrough and Thomas (2009) previously identified that lakes with a large catchment to surface area ratio tend to have a greater amplification factor and therefore do not require high inputs of water to maintain a positive hydrological balance. This would account for the magnitude of palaeolakes Suguta, Turkana, Naivasha, Awassa and the Ziway-Shala basin but not the Baringo-Bogoria and Magadi-Natron basins, which have large groundwater catchments (Olaka et al. 2010). This indicates that surface and subsurface flow must be considered when assessing amplification potential and climatic sensitivity of African lakes. The most sensitive lakes to local and regional climate fluctuations are the Rift Lakes with graben morphologies, humid conditions and a water balance dominated by rainfall and surface inflow (Lakes Awassa, Naivasha and the Ziway-Shala basin) (Olaka et al. 2010). Other lakes with similar morphology that receive low rainfall (Lake Suguta and the Nakuru-Elmenteita basin) do not record local signals of climate variability as they receive groundwater from neighbouring catchments (Olaka et al. 2010). They provide better evidence of

regional climate changes and explain why lake level fluctuations varied in magnitude across the region during the Holocene.

This demonstrates the complexity of lake sensitivity and amplification as well as highlighting how such sensitivity can affect the interpretation of sedimentary records in terms of local and regional climate events. However, even after giving due consideration to these variables, climatically sensitive lakes may still not guarantee continuous, high-resolution, sedimentary records. Hydrologically closed basins and shallow lakes are susceptible to drying out in response to short-term rainfall variability, which may truncate or destroy the climate record accumulating in their sediments (Verschuren 1999a). Given the magnitude of climatic fluctuations that occurred across the African continent since the Last Glacial Maximum, it is unsurprising that many lakes have at some point in time, dried up (Table 3.2). In the deeper lakes such as Lakes Tanganyika (maximum depth 1470 m) and Malawi (maximum depth 700 m) this is not an issue as they remained waterlogged during arid periods and sedimentation continued (Johnson 1996). On average, sedimentation rates across East Africa are about 1 mm yr^{-1} (although this is extremely variable) and so at lakes that remained wet during the late Pleistocene and Holocene, sub-sampling of palaeoclimatic data can occur at a century, decadal or even sub-decadal scale temporal resolution (Johnson 1996; Battarbee 2000). Site selection is thus crucial for accurately deciphering the complexity and magnitude of climate signals concealed in lake sediments (Verschuren 2003).

Table 3.2. African water bodies which show evidence of desiccation since the LGM.

Lake	Location	Authority
Victoria	EARS	Talbot and Livingstone 1989; Stager et al. 2002
Albert	EARS	Beuning et al. 1997; Williams et al. 2006
Challa	Mt. Kilimanjaro	Verschuren et al. 2009; Barker et al. 2013
Magadi	Kenya	Barker and Gasse 2003
Tana	Ethiopia	Lamb et al. 2007a
Abhé	Ethiopia-Djibouti	Gasse 1977; Gasse et al. 1980
Bosumtwi	Ghana	Talbot and Johannessen 1992; Peck et al. 2004; Brooks et al. 2005
Blue and White Nile headwaters	East Africa	Marshall et al. 2011

Chronology is a second important issue affecting lacustrine records in East Africa (Johnson 1996; Verschuren 2003). Finely laminated sediments with annual resolutions are the obvious preference for reconstructing climate variability at a century to decadal time scale but such records in intertropical Africa are very rare due to the complexity of the seasonal climate cycle and its preservation in sediments (Verschuren 2003). Exceptions where truly annual laminations have been found include Lake Malawi (Johnson et al. 2002) and Lake Hora in Ethiopia (Lamb et al. 2002b). With regard to obtaining radiocarbon dates (^{14}C), conventional methods and accelerator mass spectrometry (AMS) are both easily obtained on organic matter or carbonates but they are not always reliable (Johnson 1996). Sources of error include contamination by younger carbon though root penetration or bioturbation, contamination by minerogenic 'dead' carbon, the lake reservoir effect and the hard-water reservoir effect (Björck and Wohlfarth 2001; Lowe et al. 2004). These factors can hamper the accuracy of ^{14}C dating of bulk organic sediment samples, especially in organic lake sediments (Törnqvist et al. 1992). It is well recognised that the use of terrestrial macrofossils (twigs, leaves of deciduous trees, conifer needles, insect remains and charcoal) for ^{14}C dating improves results considerably since they are unlikely to be affected by such disturbances (Törnqvist et al. 1992). Therefore, macrofossils are the obvious preference for providing a reliable and accurate chronology but they cannot always be found in lake sediments.

Due to such discrepancies in the accuracy between chronological methods as well as multiple sources of error and issues of contamination, it has been necessary on several occasions to re-date a sediment sequence to confirm the reliability of the original chronology. For example, a reliable chronology was only obtained for core 64-2 from Pilkington Bay, Lake Victoria, after it was discovered the original dates were 330 years too old due to contamination with ancient carbon (Stager et al. 2003). Core LT84-8P from Lake Turkana was also re-dated after it was realised that the bulk carbonate dates were too old due to aeolian influxes of micrite and small ostracods from the east of the lake (Johnson 1996).

Given such complications in obtaining a reliable chronology, Verschuren (2003) recommends producing an accurate age model by (1) selecting a lake small enough to bury and preserve adequate quantities of terrestrial plant fossils; (2) obtaining ^{14}C

dates at intervals near to the two-sigma counting error of each date; (3) carefully selecting dates to be included in the age model; and (4) increasing the precision of the age model by wiggle-matching sediment ages against the atmospheric ^{14}C calibration curve.

A third complicating factor in East African lacustrine records is the often uncertain relationship between sedimentary climate-proxy indicators (physical, chemical or biological), and the primary climate variables of temperature, precipitation and wind (Verschuren 2003). In contrast to lakes in the northern temperate regions, where a range of climate proxies can be assumed to be directly controlled by variations in temperature, a reliable proxy of temperature change in Africa has not been established (Verschuren 2003). Recently, several African lake temperature records have been produced through the application of the TEX_{86} temperature proxy[9] but this may not be as reliable in small lakes where the signal may be compounded by substantial amounts of isoprenoid tetraether compounds derived from soil (Berke et al. 2012a).

Climate and environmental reconstructions therefore rely on inferring and calibrating the relationship between the sediment, water column and climate. Diatom-inferred conductivity for example, is used extensively across East Africa (L. Abiyata – Chalié and Gasse 2002a; L. Rukwa – Barker et al. 2002; L. Kasenda and Wandakara – Ryves et al. 2011; Munya wa Gicheru – Owen et al. 2012) either separately or in combination with other proxies. It has proved more difficult to calibrate diatom community assemblages with water depth. Where a significant relationship has been demonstrated, the robustness and sensitivity of calibrations and training sets remains disputed as the palaeolimnological model will be influenced by secondary variables (i.e. climate, human activity, catchment processes) not accounted for in the simulation (Battarbee 1991; Barker et al. 1994; Brugam et al. 1998; Juggins 2013). Likewise, a suitably robust training set has not been developed to calibrate diatom assemblages with water temperature despite several efforts (Pienitz et al. 1995; Lotter et al. 1997). Although some studies show evidence of apparent statistical

[9] TEX_{86} is based on the degree of formation of membrane lipids from aquatic Thaumarchaeota, specifically isoprenoid glycerol dialkyl glycerol tetraethers (GDGTs), which are often well preserved in lacustrine (as well as marine) sediments (Berke et al. 2012a).

significance, Anderson (2000) argues that quantitative reconstructions model a whole system, and so the effect of temperature will be shared amongst other variables (i.e. dissolved organic carbon, alkalinity, conductivity), which may exert a stronger influence on community assemblage than temperature, as well as secondary variables (Battarbee 2000; Juggins 2013).

Therefore, whilst some proxies can be used to reconstruct climate variables directly, most approaches are indirect and require a comprehensive understanding of processes occurring between the water column, the sediment record and the climate (Battarbee 2000). As a result, multi-proxy approaches are commonly used in palaeolimnology as not only do they provide more data, they enable lake-catchment system responses to climate, and other external forces such as anthropogenic activities (i.e. agricultural practices, clearing by burning), to be more thoroughly identified and inferred. Comparisons can then be made between responses and response rates to the external forcing, and the relationships between proxies, lake system and the forcing mechanism (Battarbee 2000).

3.3 The Last Glacial Maximum

The Last Glacial Maximum (LGM, ~ 23.0 – 18.0 kyr BP) is the most recent interval in global history when Northern Hemisphere ice sheets reached their maximum volume (Ray and Adams 2001). The combination of increased continental and sea ice volume, low sea surface temperatures (SST), heightened continental elevation in glaciated regions, intensified albedo and altered atmospheric and ocean circulation, caused global temperatures to decline (Clark and Mix 2002). In the tropical Atlantic the drop in air temperature and SST reduced moisture transport along the Congo Air Boundary (CAB), resulting in increasing aridity and cooler temperatures in central and tropical Africa (Kendall 1969; Street and Grove 1976; Hamilton and Taylor 1991; Jolly et al. 1998; Gasse 2000; Foerster et al. 2012).

The low temperatures and reduced moisture had significant impacts on hydrology in East Africa with the general effect of reducing regional lake levels and river flows (Hamilton and Taylor 1991). In the East African Rift System, Lake Tanganyika (Fig. 3.1 [a] site 4) was ~ 300 m lower than present at 21.0 kyr BP (Fig. 3.2; Gasse et al. 1989; Gasse 2000). Lake Victoria (Fig. 3.1 [a] site 1) was almost, if not completely,

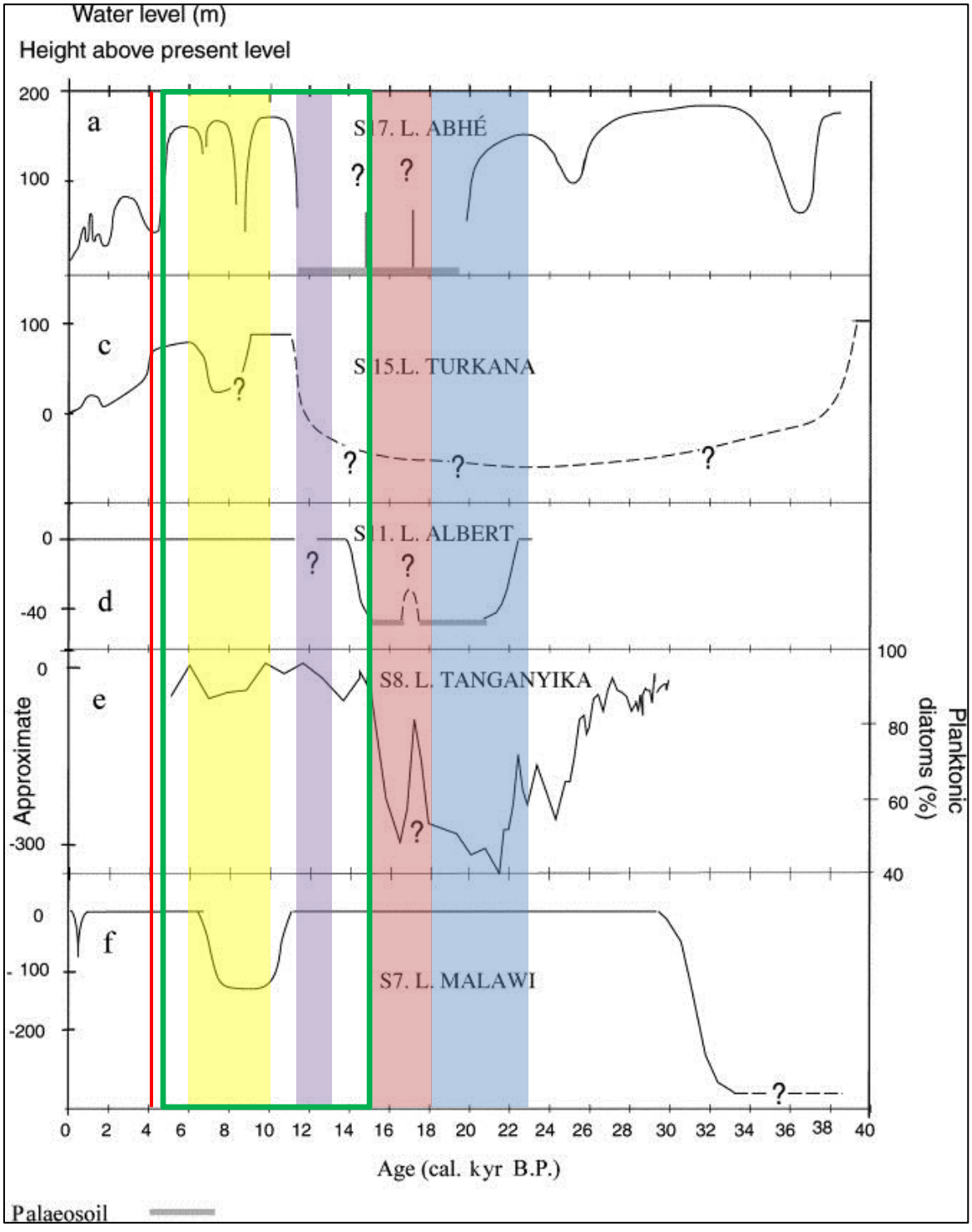

Figure 3.2. Water level fluctuations (height [meters] above present level) for Lakes Abhé (Gasse and Street 1978), Turkana (Johnson 1996), Albert (Talbot and Livingstone 1989), Tanganyika (Gasse et al. 1989) and Malawi (Finney et al. 1996; Johnson 1996). Key time periods are identified: LGM – blue, HE-1 – red, AHP – green box, YD – purple, HCO – yellow, and the 4.2 event – red line (adapted from Gasse 2000).

desiccated at 20.5 kyr BP (Talbot and Livingstone 1989) and Lake Albert (Fig. 3.1 [a] site 2) was 46 – 58 m lower than present from 20.2 – 18.0 kyr BP (Fig. 3.2; Beuning et al. 1997). At Lake Malawi (Fig. 3.1 [a] site 7) the concentration and percentage of periphytic diatoms in the fossil diatom record from the northern basin indicate a shallow lake was present during the LGM from 22.8 – 17.0 kyr BP (Gasse et al. 2002). Similarly in Tanzania, Lake Rukwa (Fig. 3.1 [a] site 5) was a shallow swamp-like waterbody divided into several sub-basins from 22.1 – 19.6 kyr BP (Barker et al. 2002; Barker and Gasse 2003). The Lake Massoko (Fig. 3.1 [a] site 6) fossil diatom record indicates an increase in the abundance of periphytic and aerophilous diatoms as well as maximum diatom-inferred conductivity at 20.0 kyr BP due to shallow water conditions (Barker and Gasse 2003). In Kenya a hiatus in sediment accumulation at Lake Magadi (Fig. 3.1 [b] site 23) occurred from 24.0 – 15.0 kyr BP, which has been attributed to a desiccation event (Barker and Gasse 2003). At Lake Challa (Fig. 3.1 [a] site 10) the precipitation-evaporation balance (P/E) began to drop at 23.0 kyr BP, indicating increasingly dry conditions and temperatures 3.5 – 6.0 °C lower than present (Barker et al. 2011; Sinninghe Damste et al. 2011; Barker et al. 2013). Seismic-reflection data also confirms the lake level declined at 20.5 kyr BP, although aridity was modest in comparison to previous Quaternary 'megadrought' events such as the period from ~ 114.0 – 97.0 kyr BP (Moernaut et al. 2010).

In Ethiopia a core from Chew Bahir (Fig. 3.1 [b] site 28) shows sharp increases in potassium (K) from 23.0 – 19.0 kyr BP indicating increasing aridity (Fig. 3.3); during dry environmental conditions and sparse vegetation cover, the K-rich gneisses in the lake catchment were easily eroded and washed into the basin via alluvial fans (Foerster et al. 2012). In the Main Ethiopian Rift (MER), the Ziway-Shala megalake (Fig. 3.1 [b] site 30), which was ~ 83 m above the present Lake Shala level (Shala Datum Level, AD 1972, 1558 m) from 30.0 – 25.0 kyr BP, declined significantly until 14.5 kyr BP, equating to a 9 – 32 % reduction in precipitation during the LGM, assuming temperatures 3.0 – 6.0 °C cooler than present (Street 1979a; Street 1979b). At Lake Abhé (Fig. 3.1 [b] site 36), the terminal lake for the Awash River in the Afar Depression, a stepwise fall in lake level occurred from 27.0 – 20.2 kyr BP and a palaeosol developed from 20.2 – 19.0 kyr BP, indicating the previously large (6000 km^2) and deep (170 m) freshwater lake was either desiccated, or very nearly so (Gasse 1977; Gasse et al. 1980). At Lake Tana (Fig. 3.1 [a] site 12), high-

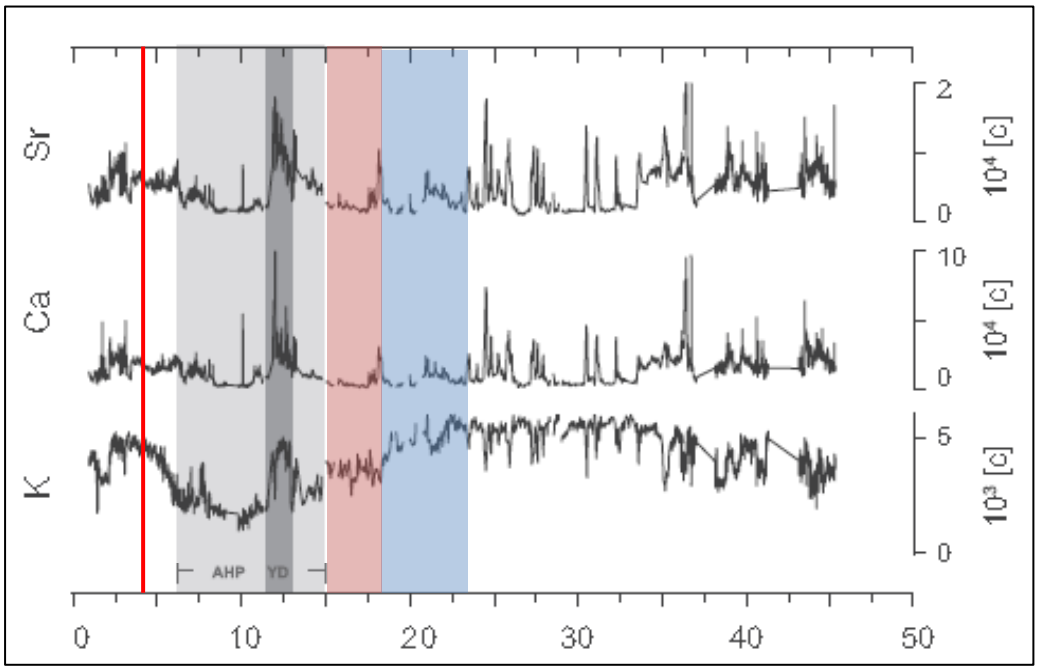

Figure 3.3. Element content (K – Potassium, Ca – Calcium, Sr – Strontium) of core CB-01-2009, recovered from Chew Bahir, Ethiopia, in 2009 from the now-dry western margin of the lake basin (N 04°50'6; E 36°46'8), against time. Key time periods are identified: LGM – blue, HE-1 – red, AHP – African Humid Period, YD – Younger Dryas Stadial, and the 4.2 event – red line (adapted from Foerster et al. 2012).

resolution seismic data suggest the lake may have been completely desiccated prior to 18.7 kyr BP (Lamb et al. 2007a). There is also evidence of reduced seasonal discharge from the Blue Nile during the LGM (Said 1993; Marshall 2006).

In contrast to the regionally low lake levels, there is evidence of glaciations on several mountain ranges in East Africa during the LGM. Dating of moraines, cirques and other glacial features indicate glaciers were present on the Simen and Bale Mountains and on Mt. Bada, Ethiopia (Fig. 3 and 9 [b] site 32) (Osmaston and Harrison 2005). Mounts Kilimanjaro, Kenya, Elgon and the Rwenzori and Aberdare Mountains were also glaciated during the LGM (Osmaston and Harrison 2005).

In the Madagascan highlands, terrestrial pollen records from Lake Tritrivakely (Fig. 3.1 [a] site 18) show evidence of low temperatures from 40.0 – 17.0 kyr BP, punctuated by short-term warm-dry periods, whilst diatom and sedimentary records show a positive P/E balance from 38.0 – 32.0 kyr BP followed by increasing aridity (Gasse and Van Campo 1998; Williamson et al. 1998). The lake was at least seasonally dry from 22.0 – 17.5 kyr BP (Gasse 2000). A SST alkenone-temperature record from an Indian Ocean core confirms glacial cooling (approximately – 2.5 °C) culminating around 20.0 – 19.5 kyr BP (Bard et al. 1997).

In the Sahel a cold (~ 6.0 °C cooler than present), wet period associated with the recharge of the confined “Middle aquifer of the Chad Formation” in Niger ended at 23.3 kyr BP (Edmunds et al. 1999). In the Sahara, dry season flow in the White Nile was low, if not absent, and parts of the channel became blocked behind dunes and mobile sand-bars, resulting in seasonal ponding of water (Williams and Adamson 1980; Said 1993; Williams et al. 2000). Studies from Morocco likewise show that mobile sand-bars migrated inland from west to east during the LGM, implying conditions were windier than present (Rognon and Coudé-Gaussen 1996). In Egypt River Nile flow was highly seasonal during the LGM and around the headwaters the channel became braided (Adamson et al. 1980), whilst the channels south of Khartoum (the Blue Nile and White Nile) were highly seasonal with low discharge (Maley 2000).

Certain locations in North Africa do appear to have retained wet conditions during this time. Radiocarbon ages of algal limestone in the caldera at Jebel Marra (Fig. 3.1 [a] site 13), indicate high lake levels from 23.5 – 16.5 kyr BP (Williams 2009). Lakes were also present in the Tibesti Mountains (Fig. 3.1 [a] site 14), from 24.0 – 18.7 kyr BP and 18.3 – 14.6 kyr BP, and in southern Egypt and in Sudanese Nubia the main River Nile is said to have had continuous flow (Maley 2000).

In West Africa, pollen records from Lakes Barombi Mbo and Bosumtwi (Fig. 3.1 [a] sites 16 and 17) indicate dry conditions during the LGM (Maley 1992; Maley and Brenac 1998; Gasse 2000). The period is characterised however by non-linear oscillations between dry and humid periods; at Lake Bosumtwi, $\delta^{18}O$ of calcite and $\delta^{15}N$ of organic matter indicate dry periods centred at 25.9 kyr BP, 21.9 kyr BP and 17.5 kyr BP, and a humid period from 21.0 – 18.5 kyr BP (Talbot and Johannessen 1992; Gasse 2000). In Southern Africa, the fossil pollen records from the Wonderkrater spring mound (Fig. 3.1 [a] site 8), indicates that summer temperatures during the LGM were ~ 4.0 °C cooler than present, whilst high-resolution stable isotope records from the Cold Air Cave speleothem, South Africa, imply it was less humid than the Holocene (Lee-Thorp et al. 2001; Holmgren et al. 2003; Truc et al. 2013). The stable isotope record from a stalagmite in Botswana likewise indicates glacial cooling of 2.0 – 3.0 °C (Holmgren et al. 1995; Gasse 2000) and the precipitation time series from the Pretoria saltpan (Fig. 3.1 [a] site 9), suggests 15 – 20 % less precipitation during the LGM than present (Partridge et al. 1997).

At the millennial scale, the rainfall deficit and cool temperatures observed in subtropical and tropical Africa may be accounted for by half-precessional intervals (Milankovitch cycles, ~ 11.5 kyr) in phase with orbitally-induced fluctuations in summer insolation (Fig. 3.4). Greater summer insolation during the LGM resulted in intensified monsoon circulation by enhancing the inter-hemispheric ocean-land pressure gradient which drew the monsoon winds inland (Kutzbach et al. 1993; Gasse 2006). This adequately explains the occurrence of dry conditions in the northern tropics. Given that the Southern Hemisphere is in antiphase with the Northern Hemisphere, the south would be expected to have experienced intensified monsoon rainfall during the LGM, which contradicts the findings presented (Nicholson 1986). This indicates that the hydrological budget of Africa during glacial

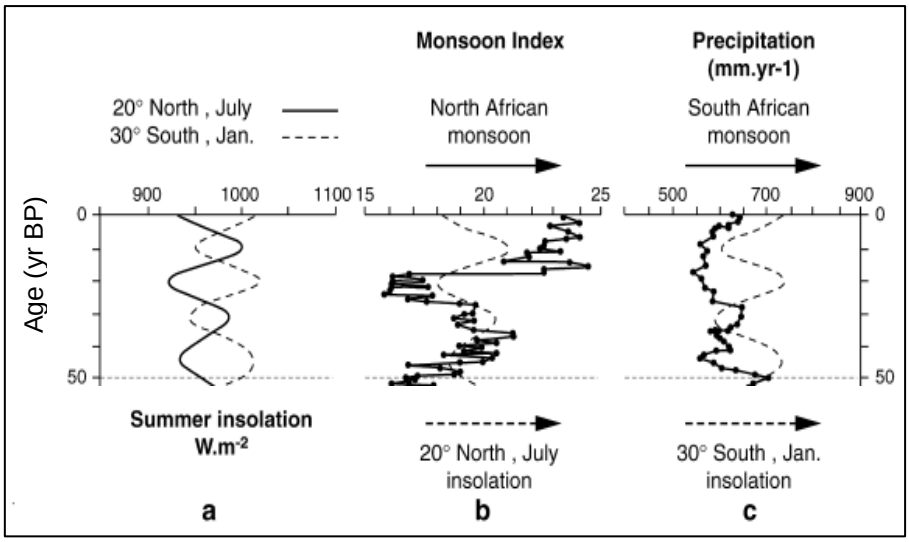

Figure 3.4 (a). Pleistocene variability in (a) summer solar radiation (watts per square meter, $W.m^{-2}$) in the northern and southern subtropics (Berger 1978), (b) the monsoonal precipitation index at 20 ° N based on fossil fauna assemblage variations in a deep-sea sediment core (RC24-07, equatorial Atlantic; McIntyre et al. 1989), and (c) South African monsoon precipitation reconstructed from a sedimentary record from the Pretoria Saltpan (Partridge et al. 1997) (adapted from Gasse 2000).

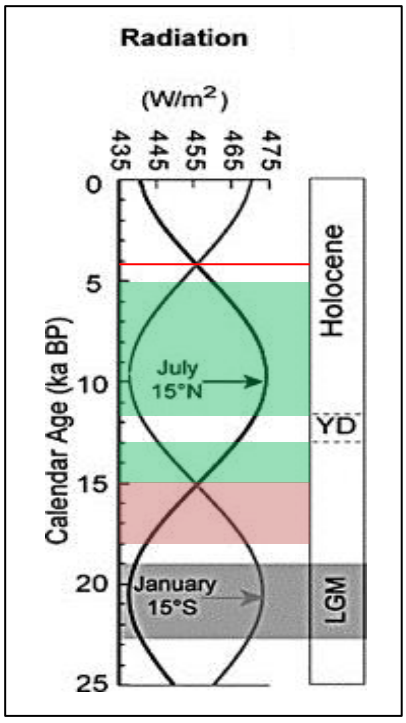

Figure 3.4 (b). Millennial changes in summer solar radiation (watts per square meter, W/m^2) over the past 25.0 kyr. Key time periods are identified: Last Glacial Maximum – LGM, HE-1 – red, AHP – green, Younger Dryas Stadial – YD, and the 4.2 event – red line (adapted from Gasse 2006).

periods was not solely paced by Milankovitch cycles. Coupled atmosphere-ocean General Circulation Models (GCMs) indicate that tropical aridity during the LGM was due to increased northward transport of oceanic heat away from the tropics. This was amplified by upwellings and zonal advection of cold water in the upper equatorial ocean which enhanced trade winds and consequently reduced Congo Air flow (Barker and Gasse 2003). GCMs therefore indicate the global hydrological cycle during the LGM was weaker than today (Bush and Philander 1998; Ganopolski et al. 1998).

3.4 The Last Glacial-Interglacial Transition

Palaeoclimatic reconstructions from East Africa during the last deglaciation (~ 20.0 – 11.5 kyr BP) indicate increasingly wetter and warmer conditions across the region, punctuated by abrupt transitions from arid to humid and humid to arid periods. Following on from a major desiccation event (Heinrich Event 1), the first arid-humid transition was centred at ~ 17.0 – 16.0 kyr BP, followed by additional events at 15.0 – 14.5 kyr BP and 11.5 – 11.0 kyr BP, the latter two being associated with the reactivation of the monsoon system (Fig. 3.4). The effect, relative strength and timing of these events varied with latitude and there is evidence of both an early end of full glacial conditions, as observed in both the Antarctic Byrd (21.0 kyr BP) and Vostok (18.5 kyr BP) ice records, and a stepped transition to interglacial conditions (14.6 kyr BP and 11.6 kyr BP), as found in records from Greenland (Johnsen et al. 1972; 1992; Jouzel et al. 1987; Blunier et al. 1998; Gasse 2000).

3.4.1 Heinrich Event 1

Heinrich Events occurred at approximately 7.0 kyr intervals throughout the last glaciation, during which massive influxes of freshwater were released into the North Atlantic, temporarily disrupting the northward transport of heat by the thermohaline circulation (THC) away from the tropics (Heinrich 1988; Vidal et al. 1997; Hemming 2004; Gherardi et al. 2005; Stager et al. 2011). Heinrich Event 1 (HE-1) was a mass iceberg discharge event that occurred between ~ 18.0 – 15.0 kyr BP and has been associated with reduced rainfall across tropical Africa (Bard et al. 2000; Waelbroeck et al. 2001). The release of freshwater during HE-1 would have caused SST's in the tropical Atlantic to rise, lessening the ocean-continent temperature-pressure ratio. Climate models suggest a southward shift of the Intertropical Convergence Zone

(ITCZ), a weakened Atlantic monsoon and reduced precipitation across the northern tropics as a result (Ruhlemann et al. 1999; Stager et al. 2002; Scholz et al. 2003; Brooks et al. 2005; Dahl et al. 2005). However, the intensity of the aridity and its extent (the signal has been detected in the Indian Ocean and western Pacific) suggests that severe, systemic weakening of the Afro-Asian rainfall systems also occurred, probably in response to cooler SST in the south-east Atlantic and Indian Oceans, which reduced the evaporative moisture content of the ITCZ (Stager et al. 2011). Therefore, the height of the HE-1 stadial likely coincided with an extreme and widespread drought, which resulted in many lakes becoming completely, or very nearly, desiccated.

At Lake Victoria, dating and re-examination of coring and seismic profiling data have confirmed lake level fell dramatically in the late Pleistocene; the physical properties of the cores Ibis 1 and 3 (taken from 32 m depth in the Damba Channel and from 66 – 68 m depth offshore) reveal at least two discontinuities corresponding to low lake levels and contain layers of littoral gastropods, which indicate oxidation and desiccation of sediments during lowstands, as well as rootlets or burrows, desiccation cracks and colour changes (Stager et al. 1986; Talbot and Livingstone 1989; Kiage and Liu 2006). New ^{14}C dates indicate the lake was desiccated from 17.0 – 16.0 kyr BP (Stager et al. 2011). A second desiccation event occurred at some point between 15.0 – 14.0 kyr BP and was not as widespread across equatorial East Africa (Stager et al. 2011). The first desiccation event from 17.0 – 16.0 kyr BP coincides with fluctuations in $\delta^{14}C$ and HE-1, pointing to casual links between North Atlantic ice-rafting events, solar variability and African aridity.

In the EARS, spikes in total organic carbon (TOC) and $\delta^{13}C$ values in core T97-52V (taken from 393 m depth between the Kavala Island Ridge and the Mahali peninsula) from Lake Tanganyika appear to coincide with Heinrich Events 1 – 6 (Scholz et al. 2003). Spectral analysis of key proxies indicate an 11.0 – 16.0 kyr cycle, most likely in response to water column productivity following mixing, increased nutrient availability and rapidly rising water levels after a lowstand event, such as the ice-rafting events in the North Atlantic (Scholz et al. 2003). At Lake Turkana (Fig. 3.1 [a] site 11), a lowstand is documented in the sediment record from ~ 19.0 – 18.0 kyr BP by high total inorganic carbon (TIC), high calcium (Ca) counts and the presence of

sand. The lake was at least 110 m lower than the current lake level and the South Basin was most likely desiccated (Morrissey and Scholz 2014). In Ethiopia a period of intense aridity at the time of HE-1 has been confirmed at Lake Tana through mineral magnetic, geochemical and seismic data, which has identified a distinctly aeolian, possibly Saharan, sediment component in a core from the centre of the lake, which currently has a maximum depth of 14 m (Marshall et al. 2011).

Elsewhere in East Africa, the timing of a desiccation event synchronous with HE-1 has been documented at Lakes Albert (Beuning et al. 1997; Williams et al. 2006), Challa (Verschuren et al. 2009), Ashenge (unconfirmed) (Fig. 3.1 [b] site 34; Marshall et al. 2009), Abhé (Gasse 1977) (Fig. 3.1 [b] site 36), Bosumtwi (Talbot and Johannessen 1992; Peck et al. 2004; Brooks et al. 2005), as well as the desiccation of the Blue and White Nile headwaters (Marshall et al. 2011). The nature of HE-1 was not static however, and many lakes (and other palaeo-sites) show a complex environmental response, especially in Southern Africa and the eastern Mediterranean, with some evidence of wetter conditions and lake highstands at this time (Thomas et al. 2012).

3.4.2 17.0 – 15.0 kyr BP Arid-Humid Transition

Despite the widespread aridity following the LGM, a transitional arid to humid period occurred around 17.0 – 15.0 kyr BP, marking the onset of more humid conditions across the African continent. During this time, precipitation began to increase in parts of East Africa and some lake levels began to rise.

In northern Ethiopia, Lake Tana saw a shallow water swamp develop in the centre of the lake from 16.7 – 15.7 kyr BP whilst the lake margins remained dry (Lamb et al. 2007a). An increase in periphytic and planktonic diatoms indicates initial lake infilling after the desiccation caused by HE-1. The shallow swamp was then succeeded by a shallow *Cyperus* swamp at the centre of the lake basin from 15.7 – 15.1 kyr BP. The water level is estimated to have been 24 m lower than present and most likely fed by seasonal stream flow, as evapotranspiration by the swamp vegetation would have exceeded inflow (Lamb et al. 2007a). Temperatures are estimated to have warmed by 3.7 ºC during this time (~ 16.0 ºC average), based on reconstructions using the branched glycerol dialkyl glycerol tetraether (brGDGT) paleotemperature proxy

(Loomis et al. 2015). At Lake Ashenge, an increase in effective moisture is documented at ~ 16.2 kyr BP by the diatom flora; from 17.2 – 16.2 kyr BP an abundance of lake-marginal and aerophilous species suggest the core site was partially exposed or close to the shore line (Fig. 3.5). An increase in the dominance of freshwater taxa after 16.2 kyr BP indicates lake level began to rise, resulting in a freshwater environment. In southern Ethiopia, Chew Bahir likewise saw an increase in more humid conditions slightly earlier than other lakes from 19.0 – 15.0 kyr BP (Fig. 3.6; Foerster et al. 2012). Lake Turkana also saw an increase in lake level from 18.0 – 17.5 kyr BP after which it decreased again, indicated by an increase in calcite preservation and a high amplitude reflection surface in the seismic data (Morrissey and Scholz 2014).

In the EARS, the Lake Tanganyika sedimentation rate increased from 6.0 mm century^{-1} at 20.5 kyr BP to 1.6 cm century^{-1} at 17.0 kyr BP, suggesting the establishment of wetter conditions (Fig. 3.2; Burnett et al. 2011). Pollen based reconstructions concur with this, indicating that temperature and precipitation increased from ~ 18.0 – 17.0 kyr BP, and the diatom record likewise indicates a positive lake water balance became established around 16.0 kyr BP (Chalié 1995; Gasse et al. 1989). Lake Malawi saw a 4 – 5 ‰ decrease in $\delta^{13}C$ values of TOC from 17.0 – 15.7 kyr BP indicating increased precipitation (Barker and Gasse 2003). At Lake Rukwa lake level began to rise at 16.2 kyr BP, evidenced by a planktonic diatom assemblage (Barker et al. 2002). The lake remained saline however, indicating water entered the lake from elsewhere, possibly as a result of the previously fragmented basin being reunited. Laminated diatomite and thick clay-stone deposits at Lake Suguta, a palaeo-lake in the northern Kenyan Rift (Fig. 3.1 [b] site 27), indicate the lake level was high from 16.5 – 15.0 kyr BP (Garcin et al. 2009). Lakes Victoria and Albert saw an early post-LGM humid period bracketed by two palaeosols indicating lowstands (Talbot and Livingstone 1989). A brief wet phase was recorded by the lake sediments between 16.0 – 15.0 kyr BP, pre-dating major lake refilling during the African Humid Period.

3.4.3 The Onset of the African Humid Period

The African Humid Period (AHP) is the most recent multi-millennial wet episode in East Africa, lasting from ~ 15.0 – 5.0 kyr BP, punctuated by the Younger Dryas

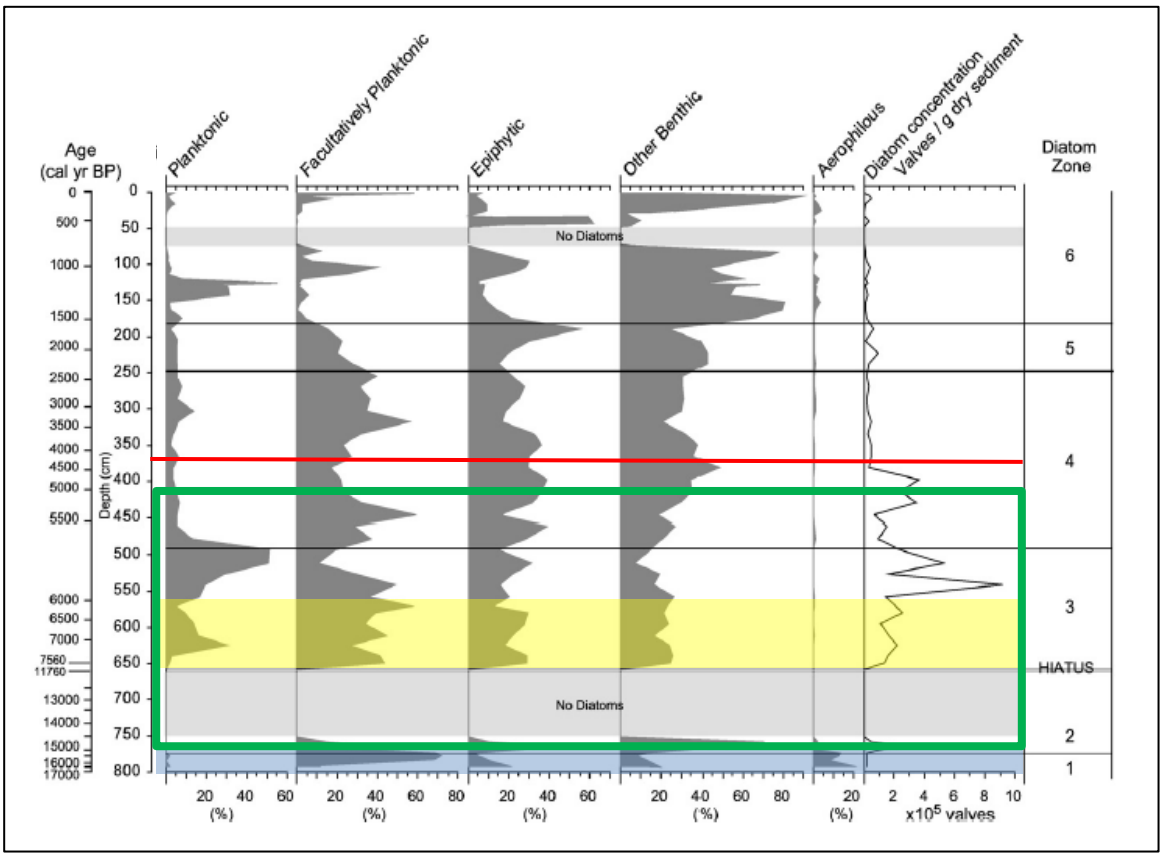

Figure 3.5. The diatom record (habitats and valve concentration) of Lake Ashenge against time and depth. Key time periods are identified: LGM – blue, AHP – green box, HCO – yellow, and the 4.2 event – red line (adapted from Marshall et al. 2009).

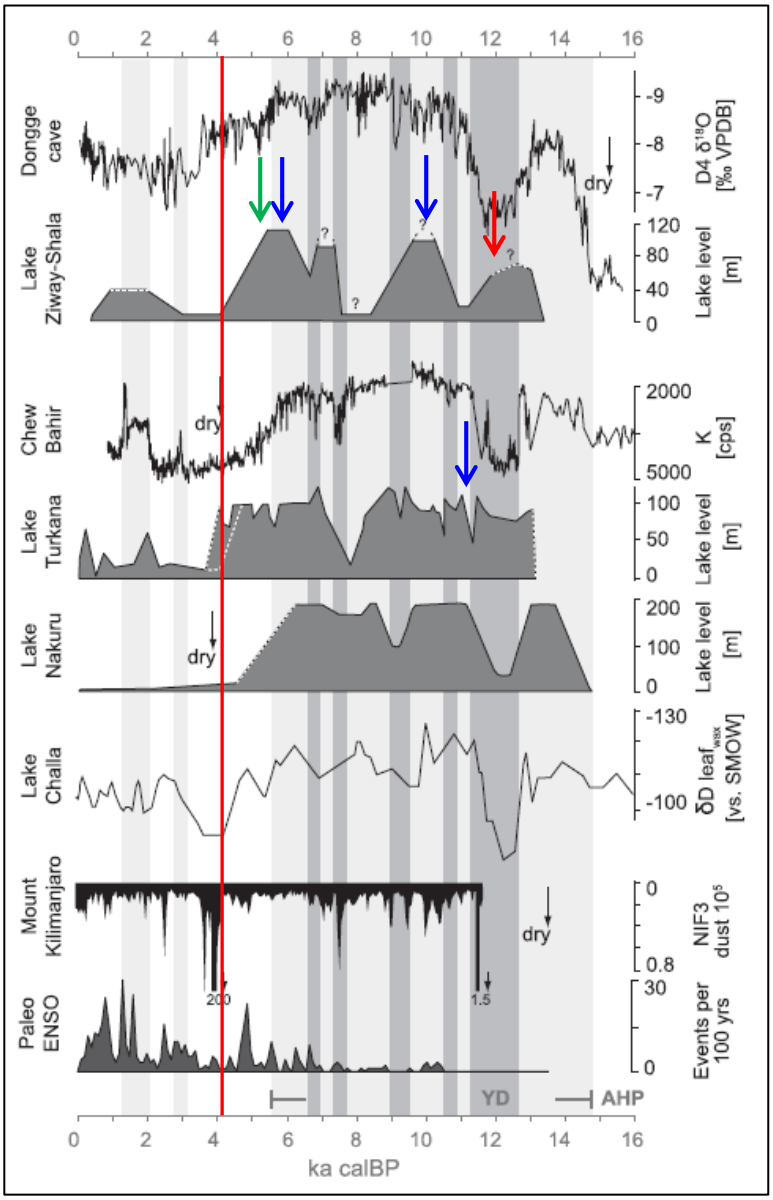

Figure 3.6. Comparison of the onset and termination of the African Humid Period (AHP) and Younger Dryas Stadial (YD) at Chew Bahir (potassium, K, record [note reverse scale]; Foerster et al. 2012), lake level records from Lakes Nakuru (Richardson and Dussinger 1986), Turkana (Johnson et al. 1991; Brown and Fuller 2008) and the Ziway-Shala basin (Gillespie et al. 1983), with the dust record from Mt. Kilimanjaro (Thompson et al. 2002), δD_{wax} records from Lake Challa (Tierney et al. 2011), the oxygen-isotope record from Dongge cave (China; Dykoski et al. 2005), and the paleo-ENSO record from Laguna Pallcacocha, southern Ecuador (Moy et al. 2002). Dark grey bars indicate dry episodes and light grey bars indicative humid episodes. The 4.2 event is shown by the red line. Potential overflow events are indicated by blue arrows, the Ziway-Shala macro-lake phase by the red arrow and

the Holocene separated lake phase by the green arrow (adapted from Foerster et al. 2012).

stadial (~ 12.8 – 11.6 kyr BP). The AHP is attributed to precessional changes during periods of low eccentricity, which saw an increase in Northern Hemisphere summer season insolation (approximately 8 % greater than today) (Fig. 3.4; Barker et al. 2004; Garcin et al. 2009). An eastward shift in the CAB, caused by deepening of the atmospheric low over India, enhanced the pressure gradient between India and Asia, which in combination with higher SSTs (~ 5.0 ºC rise in the Red Sea, Arabian Sea and eastern Mediterranean [Loomis et al. 2015]), resulted in significantly more humid conditions (Adkins et al. 2006). This rejuvenated the African-Indian monsoon circulation, bringing more moisture to Africa. Climate models indicate the strengthened summer insolation caused monsoon rainfall to increase by 35 – 45 % in northern tropical Africa (Prell and Kutzback 1987). The dramatic effect of this was to cause vegetation belts to migrate northwards resulting in the greening of the now hyper-arid Sahara (deMenocal et al. 2000; Gasse 2000; Garcin et al. 2012; Tierney and deMenocal 2013). A diversity of flora and fauna (hippos, crocodiles, elephants, giraffes and antelope) colonised the grasslands, and the landscape was incised by river networks and lakes (deMenocal 2015).

The AHP was still cool but effectively brought East African glaciation to an end (Hamilton and Taylor 1991; Hailemichael et al. 2002; Foerster et al. 2012). Pollen evidence from Tamsaa swamp and the small Lake Garba Guracha (Fig. 3.1 [b] site 29) suggest that deglaciation occurred between 16.7 – 15.0 kyr BP in conjunction with increased moisture availability (Mohammed and Bonneville 1998; Umer et al. 2007). A peat core from a cirque in the Arussi Mountains likewise indicates the ice cap on Mt. Bada had completely disappeared by 13.6 kyr BP (Street 1979a; Hamilton 1982). As a consequence spectacular lake basin refilling occurred across the region at this time. The onset (and termination) of the phase was not uniform across East Africa however, appearing to be abrupt at some lakes (Lakes Tanganyika and Tana) and gradual at others (Lakes Victoria and Challa) (Costa et al. 2014).

Lake Tana saw an increase in water depth between 15.9 – 15.3 kyr BP, fed by seasonal inflow from freshwater streams (Marshall et al. 2011). At 15.3 kyr BP, significant lake deepening occurred across the entire basin, evidenced by freshwater planktonic flora dominating the diatom assemblage. The lake rose to the overflow

level causing it to spill into the Blue Nile, which resulted in high flood levels from 13.9 – 13.2 kyr BP and in the main Nile River from 14.5 – 12.0 kyr BP (Williams 2009; Marshall et al. 2011). The hydrogen isotope composition of terrestrial leaf wax compounds (δD_{wax}) indicates however, that the onset of the AHP at Lake Tana did not fully occur until 13.0 kyr BP (Costa et al. 2014). The Ziway-Shala basin saw the reestablishment of wet conditions in two phases, the first being at 14.5 kyr BP and the second, more significant, at 11.5 kyr BP which saw the formation of a single giant lake (the macro-lake phase) (Fig. 3.6; Grove et al. 1975; Gillespie et al. 1983; Chalié and Gasse 2002a). Chew Bahir also documented a substantial increase in humidity from 14.5 –12.8 kyr BP, evidenced from the K record (Fig. 3.3; Foerster et al. 2012). At Lake Turkana a deep water environment developed rapidly at 14.0 kyr BP, evidenced by increased organic carbon and decreased TIC, as well as other significant changes in sediment type and the seismic character of the record (Morrissey and Scholz 2014). The seismic data during this highstand indicates the lake remained deep and undisturbed. Finely laminated sediments and extremely low inorganic carbon preservation provide further indication that water column stratification had developed and bottom waters were anoxic.

Geomorphological evidence in the Mekele outlier, an 8000 km^2 area on the western margin of the Ethiopian Rift (Fig. 3.1 [b] site 35), similarly indicates wetter conditions during the late Pleistocene. Seventeen individual landslides dated to this period provide evidence of peaking hydrostatic soil pressure due to perched water tables (arguments for the landslides being tectonic in origin were ruled out based on their length to width ratio and the occurrence of landslides in other areas in East Africa around this time) (Moeyersons et al. 2006). Eight tufa dams were also studied to determine the timing of the late Pleistocene wet period. The dams are a sedimentary response to karstic (limestone) system activity and are formed during relatively warm, wet environmental conditions when a near continuous flow of surface water and percolation occurs (Goudie et al. 1993). Two reliable dates were obtained from K'arano (15.8 kyr BP) and Tsigaba (14.1 kyr BP), providing evidence of increased moisture availability in the late Pleistocene (Moeyersons et al. 2006).

In East Africa, Lake Victoria saw major basin refilling from 15.0 – 14.0 kyr BP and at Lake Albert just prior to 13.8 kyr BP (Johnson et al. 1996; Beuning et al. 1997; Talbot

and Lærdal 2000). Studies of the White Nile using strontium isotope analysis as a water source tracer, indicate that flow from Lake Victoria via Lake Albert into the main River Nile reestablished between 14.7 – 14.5 kyr BP (Talbot and Lærdal 2000; Williams et al. 2006; Williams 2009; Box et al. 2011). The White Nile maintained high flood levels until 13.1 kyr BP (Williams 2009). Lake refilling also occurred at Lakes Magadi (Roberts et al. 1993), Manyara (Fig. 3.1 [b] site 22; Barker et al. 2004), Tanganyika (Gasse et al. 1989) and Malawi (Gasse et al. 2002; Johnson et al. 2004) between 15.5 – 15.0 kyr BP and Lake Rukwa reached its maximum water depth around 13.6 kyr BP (Barker et al. 2002). Lake Suguta began refilling at ~ 14.8 kyr BP and was overflowing into the Lake Turkana basin by at least 13.0 kyr BP (Garcin et al. 2009). Lake Suguta may have also received periodic overflow from the Baringo-Bogoria basin around this time, causing Lake Suguta to reach its highest shoreline by 13.8 kyr BP at the latest (Garcin et al. 2009). This created a hydrologically open system throughout the northern Kenyan Rift Valley, providing additional input for the Turkana-Nile River (Morrissey and Scholz 2014). The maximum highstand at Lake Suguta occurred at 12.8 kyr BP, with the mega-lake covering 2200 km^2 and being almost 300 m deep (Garcin et al. 2009; Borchardt and Trauth 2012; Junginger et al. 2013; Junginger and Trauth 2013).

In contrast, Lake Ashenge refilling preceded the AHP, lasting from 16.2 – 15.2 kyr BP, indicated by planktonic diatoms and low diatom-inferred conductivity (~ 1600 µS cm^{-1}) (Fig. 3.5; Marshall et al. 2009). However, actual diatom-inferred conductivity may have been even lower due to underrepresentation of key taxa in the modern training set (Marshall et al. 2009). The lake then became shallower from 15.2 – 14.2 kyr BP, presumably due to a localised shift towards low effective moisture and a more arid climate. Salinity at the lake became enhanced during this time, evidenced by the precipitation of calcite and the dominance of halophytic diatom taxa. The lake began to refill at 14.2 kyr BP but maximum $\delta^{18}O_{carbonate}$ values between 13.6 – 11.8 kyr BP indicate the lake became shallow again due to a period of prolonged aridity. The most positive $\delta^{18}O$ values occurred during this time along with enhanced carbonate precipitation and deposition of a shell horizon (Marshall et al. 2009). Lake Turkana also remained low at this time but the lake water level curve for this period remains poorly constrained (Garcin et al. 2012).

Other lakes across East Africa also experienced a return to cool, arid conditions following basin refilling and proceeding the Younger Dryas Stadial from ~ 14.0 – 11.5 kyr BP. Lake Albert appears to have responded most dramatically during this time, as temperatures dropped by ~ 3.0 ºC at 12.9 kyr BP. Considerable reductions in rainfall also occurred, indicated by a 40 ‰ enrichment in δD_{wax} (Berke et al. 2014). Cooling is further indicated by a pronounced increase in grass pollen as well as a reduction in semi-deciduous forest taxa (Berke et al. 2014). A slight recovery of *Moraceae* forest taxa indicates five wet centuries from 12.8 – 12.3 kyr BP, after which dry, cool conditions returned. Lakes Malawi and Tanganyika similarly experienced a 1 – 2 ºC cooling between 14.0 – 11.5 kyr BP (Powers et al. 2005; Tierney et al. 2008), and a hiatus in de-glacial warming occurred at Lake Victoria (Berke et al. 2012b) and the Congo Basin (Weijers et al. 2007).

3.4.4 The Younger Dryas Stadial

Lakes across East Africa exhibited an extreme shift back to arid conditions from ~ 12.8 – 11.6 kyr BP, which correlates with the high-latitude European Younger Dryas Stadial (YD) (Alley 2000). The YD occurred as a result of freshwater inputs from disintegrating ice-sheets weakening the North Atlantic Deep Water formation (NADW) causing anomalies in SST (Street-Perrott and Perrott 1990). Renssen et al. (2015) suggest that in addition to this, moderate negative radiative forcing and changes in atmospheric circulation may have occurred. The combined effect of these mechanisms on tropical Africa was to decrease precipitation, as it is thought the ITCZ was forced south of the equator during the event, causing widespread arid conditions (Nicholson 1982).

At Lake Tana, seismic reflector surfaces and reduced allochthonous inputs between ~ 13.0 – 11.5 kyr BP indicate a significantly lowered lake level and reduced precipitation and runoff in the catchment (Lamb et al. 2007a; Marshall et al. 2011). This lowstand led to exposure of the lake margins and declining sedimentation rates in the lake centre (Marshall et al. 2011). The Blue Nile and White Nile similarly do not indicate high flood events between ~ 13.0 – 9.7 kyr BP (Williams 2009). The Chew Bahir record is in agreement with this, showing a rapid shift towards arid conditions from 12.8 – 11.6 kyr BP. The K record shows a sharp increase in the lake basin at this time, likely caused by increasingly arid conditions and sparse vegetation cover

(Fig. 3.3; Foerster et al. 2012). The K record then indicates a short-term return to wet conditions at 11.8 kyr BP and then an abrupt, final return to full humid conditions at 11.6 kyr BP.

Lake Abiyata in the Ziway-Shala basin also shows evidence of lake regression from 12.6 – 12.0 kyr BP, indicated by increased calcium carbonate precipitation and a fine diatomaceous silt layer below a thick sand layer (Chalié and Gasse 2002a). The diatom assemblage however shows a mixture of taxa with various ecological tolerances, not indicative of a lowstand (Chalié and Gasse 2002a).

In equatorial East Africa, lake regression associated with the YD has been documented at Lakes Victoria (Johnson et al. 2000; Talbot and Lærdal 2000; Stager et al. 2002), Albert (Beuning et al. 1997; 1998), Tanganyika (Gasse et al. 1989), Suguta (Garcin et al. 2009), Challa (Barker et al. 2011), Massoko (Garcin et al. 2007) and Sacred Lake (Fig. 3.1 [b] site 26; Street-Perrott et al. 2007). Additional evidence of the YD can be identified in a shift to grassland pollen in the Burundi highlands (Bonnefille et al. 1995) and in variations of organic matter in a peat bog on Mt. Satima, Kenya (Street-Perrott and Perrott 1990). In West Africa, lake regressions coincident with the YD have also been reconstructed at Lakes Bosumtwi (Peck et al. 2004; Shanahan et al. 2006) and Barombi Mbo (Maley and Brenac 1998). The YD may have been multi-phasic in nature however, as palynological evidence from Lake Albert indicates a brief return to humid conditions from 10.9 – 10.4 kyr BP, interrupting the YD between 11.5 – 9.8 kyr BP (Beuning et al. 1998).

Lake Ashenge, in contrast, was at a lowstand 900 years before (13.6 – 11.8 kyr BP) the time period corresponding to the YD in other East African lakes and the Greenland ice cores (Alley 2000; Marshall et al. 2009). It appears therefore that the onset of the YD occurred earlier at Lake Ashenge compared to other lakes in East Africa. A degree of uncertainty in the timing of the event has been observed elsewhere in continental Africa; in the Sahel the drier conditions relating to the YD were observed from 14.5 – 11.5 kyr BP (Gasse 2000) and arid conditions at Lake Chad (Fig. 3.1 [a] site 15) occurred at 13.6 kyr BP (Marshall et al. 2009). Reduced lake levels at Lake Edward (Fig. 3.1 [a] site 3) began as early as 13.5 kyr BP and a lowstand at Lake Malawi preceded the YD by 200 years, as inferred from the diatom

record (Gasse et al. 2002; Lærdal et al. 2002). A core taken off the west coast of Africa similarly documents an arid event 800 years prior to the onset of the YD, but the offset can be explained by discrepancies in the marine ^{14}C reservoir (deMenocal et al. 2000). A core from the mouth of the Niger River documenting a premature onset to the YD by 700 years cannot be explained by such discrepancies (Lezine et al. 2005). Therefore the early onset of lake level response at Lake Ashenge may be the result of a progressive suppression of the ITCZ to the south, in conjunction with gradual cooling at high northerly latitudes prior to the start of the YD (Alley 2000; Marshall et al. 2009).

The trigger for the termination of the YD remains inconclusive; in Greenland, warming of 10 ºC (± 4 ºC) occurred within a decade and snow accumulation increased twofold in three years (Taylor et al. 1997; Grachev and Severinghaus 2005). The extremity and rapidity of the climate change in association with the termination of the YD indicates that atmospheric circulation was most likely the primary trigger, in conjunction with changes in oceanic circulation as well as feedback processes, such as albedo and vegetation cover (Garcin et al. 2007). Garcin et al. (2007) speculate that in the tropics, when the influence of the global cold surge weakened, a climatic threshold was crossed, probably driven in part by the orbital configuration affecting the Northern Hemisphere. This enhanced solar heating would have aided in recovery of the monsoon system and caused the ITCZ to shift northwards (Garcin et al. 2007).

3.5 The Holocene

The most recent geological epoch (11.7 kyr BP – to present) has seen significant changes in African (and global) hydrology and climate. The early to mid-Holocene saw the resumption of the AHP whilst conditions became cooler and more arid in the mid- to late Holocene. This time period was also punctuated by abrupt, high magnitude arid events, some of which are now known to have been global in nature, and saw the first major signs of human disturbance in the climatic and environmental record.

3.5.1 The Holocene Climatic Optimum

The transition from the YD to Holocene (12.0 – 11.3 kyr BP) saw a return of

increased seasonality in regional rainfall, indicating that monsoon circulation had recovered and the migration of the ITCZ became more pronounced following its suppression southwards (Garcin et al. 2007). This resumption of humid conditions was far more significant than those at the onset of the AHP, and had a more pronounced effect on East African hydrology; preserved snow accumulation on Mt. Kilimanjaro is dated at 11.7 kyr BP, indicating that the monsoon was once again active across Africa and promoting ice cap growth (Thompson et al. 2002). This period of 'optimum' climate (increased moisture and warmer temperatures) was most distinct between ~ 10.0 – 6.0 kyr BP (the Holocene Climatic Optimum, HCO), with evidence of the event found in both the Northern and Southern Hemispheres (Ciais et al. 1992). In East Africa the effect of the monsoon rejuvenation on lakes, was to cause most to deepen and in some cases, overflow.

In northern Ethiopia, Lake Tana's water level increased at the start of the Holocene and conditions appear to have remained stable for the duration of the HCO (Marshall et al. 2011). Temperatures gradually warmed (18.1 ºC at 13.0 kyr BP) throughout the Holocene (Loomis et al. 2015). The hydrogen isotope record of leaf waxes shows depleted δD_{wax} values in response to increased precipitation at Lake Tana; maximum humidity occurred at ~ 10.0 kyr BP (Costa et al. 2014). Magnetic and geochemical core data indicate a lowstand occurred from 8.4 – 7.5 kyr BP, as allochthonous inputs to the lake were reduced, signalling reduced precipitation and runoff in the catchment. The hydrogen isotope record likewise indicates an arid event from *D*-enriched waxes, though beginning slightly earlier at 8.5 kyr BP and lasting until 7.0 kyr BP (Costa et al. 2014). From ~ 7.2 – 6.8 kyr BP, lake level appears to have increased as allochthonous inputs from a destabilising catchment increased again, before the start of a long-term reduction in lake level at 6.8 kyr BP (Marshall et al. 2011). Temperatures by 6.6 kyr BP had reached 21.9 ºC, after which a steady cooling is observed (Loomis et al. 2015). At Lake Ashenge there is a hiatus in the sediment record from 11.8 – 7.6 kyr BP; sediments were most likely removed by aeolian deflation during a lowstand, and/or after rapid lake refilling following a lowstand (Marshall et al. 2009).

In the Ziway-Shala basin, diatom-inferred conductivity and chemistry at Lake Abiyata indicate conditions were significantly wetter than present from 12.0 kyr BP onwards

(Chalié and Gasse 2002a; Umer et al. 2004). As a result, the four separate lakes began to rise and a single macro-lake formed 74 – 122 m above the present level of Lake Shala (Nilsson 1940; Gillespie et al. 1983; Umer et al. 2004). Deposits above Lake Shala indicate the single, giant lake had a rich biodiversity as remains of fish species including an unknown *Barbus* resembling a North African species, were found in the sediments (Grove et al. 1975). This macro-lake reached an outlet and overflowed twice around 10.7 – 9.5 kyr BP and 6.3 – 5.1 kyr BP into the Awash River and subsequently into Lake Abhé (as well as other lakes along the river), causing it to reach its maximum extent (160 m deep) and dilution between 9.4 – 8.3 kyr BP (Butzer et al. 1972; Fontes et al. 1973; Gasse and Van Campo 1994; Umer et al. 2004; Benvenuti et al. 2013). During this time the sediment yield of the system reached a maximum, documented by high-relief incision surfaces in the Bulbula and Gademota areas, which provide evidence of flushing of huge volumes of late Pleistocene sediments (Roberts and Barker 1993; Thomas and Thorp 1995). The Tora geosol also appears to have formed at this time, indicating major chemical weathering and soil development in response to the humid conditions (Benvenuti et al. 2002). Lake level reconstructions from the MER and Lake Abhé indicate brief periods of aridity from 8.7 – 8.1 kyr BP and 7.8 – 7.2 kyr BP and a less severe drop in lake level at 6.7 kyr BP (Gasse and Street 1978; Street 1979a; Gillespie et al. 1983; Gasse 2000; Chalié and Gasse 2002a; Lamb et al. 2002a).

Elsewhere in the MER, Lake Tilo (Fig. 3.1 [b] site 31) shows evidence of stable, humid conditions in the early Holocene. Although Lake Tilo is fed by hydrothermal groundwater, the flow rate was relatively stable during the Holocene and thus climatically induced changes to the water budget can be inferred from variations in $\delta^{18}O$ and $\delta^{13}C$ ratios. The negative $\delta^{18}O_{calcite}$ record from ~ 8.8 – 8.0 kyr BP indicates a combination of higher precipitation, lower evaporation and greater spring-water inflow, as does the diatom assemblage from ~ 8.8 – 7.6 kyr BP (Telford and Lamb 1999; Lamb et al. 2000). As a result, the lake level at this time was 40 m higher than the present level (Leng et al. 1999) and fish bones deposited at the rim of this high lake level indicate there may have been overflow (Lamb et al. 2000). From 7.9 – 7.6 kyr BP a regional arid event is documented by a peak in $\delta^{18}O_{calcite}$, after which both $\delta^{18}O_{calcite}$ and $\delta^{18}O_{diatom}$ fall, before slowly increasing again at 6.0 kyr BP, reflecting less humid conditions (Lamb et al. 2005). A second peak in $\delta^{18}O_{diatom}$ and $\delta^{18}O_{calcite}$

then occurred at 5.9 kyr BP, indicating diminishing rainfall in the basin and increasing aridity (Lamb et al. 2005).

To the south, Chew Bahir documents an increase in K at 11.8 kyr BP indicating the return of humid conditions, and then another more substantial increase at 11.6 kyr BP, suggesting a rapid termination of the YD (Foerster et al. 2012). Having reached maximum humid conditions, fluctuations in K, Ca and strontium (Sr) indicate several brief arid episodes at 10.8 – 10.5 kyr BP and 9.8 – 9.1 kyr BP, a gradual increase in aridity from 8.0 – 7.5 kyr BP and a major drought event at 7.0 kyr BP (Fig. 3.3). Lake Turkana similarly saw rapid and significant lake level rise from 11.5 kyr BP, causing the lake to reach its overflow level (100 m higher than the present lake level, making the lake 460 m above sea level) and become connected to the White Nile basin via the now dry Turkana-Nile River (Garcin et al. 2012; Morrissey and Scholz 2014). There may have been a brief decrease in water level (~ 15 m) around 10.2 kyr BP, based on prehistoric near-shore settlements, but overall this highstand was relatively stable, and saw the formation of the highest and most distinctive shoreline in the basin until 8.5 kyr BP.

A substantial lake regression is then documented at Lake Turkana following this early Holocene highstand, which saw the water level decrease by 50 – 100 m. Evidence of the timing of the lowstand is conflicted however, with some records indicting drying between 9.0 – 8.5 kyr BP (Owen et al. 1982; Garcin et al. 2012) and others suggesting a later onset at 7.5 kyr BP (Forman et al. 2014). Between 7.5 – 7.0 kyr BP a highstand occurred at the lake, with evidence of relict beaches on the Mt. Porr strand plain indicating an 80 m increase in water level by 6.8 kyr BP (Garcin et al. 2012; Forman et al. 2014). The termination of this highstand is also debated, with evidence of a 60 m drop in lake level on the Mt. Porr strand plain from 6.4 – 6.0 kyr BP (Forman et al. 2014), and shoreline date from South Island suggesting an abrupt regression occurring from 5.3 kyr BP (Garcin et al. 2012).

Elsewhere in East Africa, early Holocene highstands were also documented at Lakes Edward and George (Fig. 3.1 [a] site 3) (Lærdal et al. 2002), Suguta (Garcin et al. 2009; Borchardt and Trauth 2012; Junginger et al. 2013), Challa (Damsté et al. 2011), Naivasha (Fig. 3.1 [b] site 24; Bergner et al. 2003), Victoria (Stager et al.

2003; Berke et al. 2012b), Albert (Barker et al. 2004), Rukwa (Barker et al. 2002) and Malawi (Gasse et al. 2002; Konecky et al. 2011). Lake Bosumtwi also documents a dramatic wetting event at 11.5 – 10.5 kyr BP (Talbot and Johannessen 1992). Records from many of these lakes indicate a major dry period centred at 8.2 kyr BP (the mechanisms for this climate event are discussed in section 3.4.2). At Lake Suguta the regression was especially dramatic as a 240 m drop in lake level occurred over 1000 years, beginning just after 8.5 kyr BP (Garcin et al. 2009). This marked the onset of Lake Suguta's disappearance. At Lake Victoria, the diatom records from Pilkington Bay and Damba Channel document a major reduction in the duration and/or intensity of water column mixing from 8.3 – 7.8 kyr BP (Stager et al. 2003). At Lake Malawi the regression occurred from 8.5 – 8.0 kyr BP (Fig. 3.2; Gasse et al. 2002). Pollen and micro-charcoal records from the Cederberg Mountains and the Tswaing crater, South Africa, likewise indicate a decrease in water availability from 9.4 – 7.2 kyr BP (Valsecchi et al. 2013; Metwally et al. 2014).

In North Africa, two wet periods can be identified in the Sahara from 10.5 – 8.5 kyr BP and from 7.5 – 5.0 kyr BP (Giraudi et al. 2012). Two arid phases have been identified from 8.5 – 8.0 kyr BP and 7.8 – 7.5 kyr BP, the latter of which caused the Sahara-Sahel vegetation to shift northwards (Giraudi et al. 2012). A more permanent shift towards arid conditions began in the eastern Sahara at 6.3 kyr BP and spread westwards (Damnati 2000; Mercuri et al. 2011). The River Nile similarly shows a gradual decline in river runoff beginning at 8.0 kyr BP, although prior to this a short-term decrease in Blue Nile contribution and sedimentation occurred from 8.5 – 7.3 kyr BP (Blanchet et al. 2013).

In the eastern Mediterranean Sea, the formation of sapropels provide additional evidence of orbital forcing inducing intensified (northern) summer monsoons during the HCO (Rossignol-Strick 1985). Sapropels are a distinct feature of the sediments in the eastern Mediterranean; a discrete, black, organic-rich layer containing an abundance of well-preserved planktonic microfossils and pollen (Bar-Matthews et al. 2000). The layers were deposited in dysoxic-anoxic bottom waters when deep water ventilation was reduced due to either, or a combination of, large fluxes of marine or continental organic matter (Rohling and Hilgen 1991). Low $\delta^{18}O$ values within sapropels indicate that surface water salinity was decreased at the time of

deposition, which may be attributed to increased River Nile runoff as well as increased precipitation and/or decreased evaporation over the eastern Mediterranean (Rholing and Hilgen 1991).

Although the exact ages of sapropels are debated, it is accepted that the S1 sapropel (Fig. 3.1 [a] site 20) was deposited between ~ 9.0 – 6.0 kyr BP when the AHP had resumed. Precipitation over the Ethiopian highlands had increased during this time as a result of the HCO and consequently, River Nile summer floods were high (Martinson et al. 1987; Rohling and Hilgen 1991; Fontugne et al. 1994). The $\delta^{18}O$ and $\delta^{13}C$ values from speleothems in the Soreq cave, Israel (Fig. 3.1 [a] site 19), similarly characterise a very wet period with annual precipitation almost double that of the present day from 8.5 – 7.0 kyr BP (Bar-Matthews and Ayalon 1997; Bar-Matthews et al. 2000). S1 formation was interrupted by a deteriorating climate following the optimum conditions during the AHP. The increasingly arid climate that marked the termination of the AHP significantly altered the freshwater balance in the Mediterranean by improving deep-water ventilation in relation to surface water cooling, thus ending sapropel formation (De Rijk et al. 1999).

3.5.2 The 8.2 Event

The regressions in lake level and river runoff documented in East and North Africa from ~ 8.5 – 7.5 kyr BP may equate to the abrupt 8.2 kyr BP cooling episode recorded in central Greenland ice cores (hereafter, the 8.2 event). From 8.4 – 8.2 kyr BP catastrophic melt water outburst from two North American proglacial lakes (Lakes Agassiz and Ojibway) released ~ 2×10^{14} m^3 of freshwater into the Labrador Sea (Barber et al. 1999). This discharge reduced salinity in the North Atlantic and subsequently weakened the NADW and slowed ocean circulation, causing anomalies in global SST (Rohling and Palike 2005). The event is clearly marked by a shift to low $^{18}O/^{16}O$ values in the oxygen isotope records from the Greenland ice sheet, as well as a decline in ice-core annual layer thickness, a minimum in atmospheric methane and subsequent increase in atmospheric CO_2, as well as a strong volcanic signal, most likely from an Icelandic volcano (Rasmussen et al. 2007; Walker et al. 2012). The event has been identified in numerous proxy records (pollen, lake sediments, chironomid and cladoceran assemblages, marine foraminiferal assemblages, cave speleothems) from around the world including the

Middle East, China, Brazil (Fleitmann et al. 2007; Cheng et al. 2009), the Mediterranean (Magri and Parra 2002; Peyron et al. 2011), the north-west Pacific (Hua et al. 2008), the South Atlantic (Broecker 1998), East Antarctica (Cremer et al. 2007), New Zealand (Augustinus et al. 2008), as well as Africa (Gasse 2000). As such, the 8.2 event has been suggested as a formal subdivision between the early and middle Holocene by a Working Group of INTIMATE (Integration of ice-core, marine and terrestrial records) and the Subcommision on Quaternary Stratigraphy (SQS) of the International Commission on Stratigraphy (ICS) (Walker et al. 2012)

Around Africa, SST anomalies in the monsoon moisture source region reduced precipitation across the tropical and subtropical regions, resulting in widespread aridity centred at 8.2 kyr BP. However, the Mt. Kilimanjaro ice core record identified a peak in wind-blown fluoride from dry lake basins at 8.4 kyr BP (Thompson et al. 2002) and evidence of an abrupt drought is found in Lake Bosumtwi at 8.6 kyr BP (Shanahan et al. 2006). These records indicate that the arid event occurred 200 – 400 years before the 8.2 event. Other climate proxy records from around the globe, such as the record of dust supply to Greenland, similarly indicate climatic change from 8.6 – 8.0 kyr BP, suggesting that the sharp changes observed around the 8.2 event may be superimposed on a long-term background climatic anomaly (Rohling and Palike 2005).

3.5.3 Termination of the African Humid Period

The AHP came to an end around 5.5 kyr BP as a result of declining summer insolation causing the African monsoon and associated rain belts to shift southwards (Street and Grove 1979; Gasse and Van Campo 1994; Blanchet et al. 2013). The magnitude and timing of the termination is debated as marine cores from the north-west coast indicate an abrupt onset and termination of the AHP (deMenocal et al. 2000), whilst lacustrine sediments from the Sahara and stalagmites from Ethiopia and Oman suggest a more gradual transition from as early as 7.8 kyr BP (Fleitmann et al. 2003; Asrat et al. 2007; Kropelin et al. 2008). A north to south progression of the AHP termination is suggested by deMenocal (2015), matching what would be expected from orbital forcing, interspersed with locally abrupt events due to additional nonlinear mechanisms. The overall effect of the end of the AHP was to

see a resumption of arid conditions across East Africa, causing lake and river systems to become desiccated and the Saharan grasslands to retreat.

Diatom and stable isotope evidence from Lake Ashenge indicate a shift at ~ 5.6 kyr BP towards aridity, which saw $\delta^{18}O_{carbonate}$ values increase by 10 ‰ in 200 years, followed by a stepped transition that lasted until 2.3 kyr BP (Fig. 3.5; Marshall et al. 2009). During this time $\delta^{13}C$ values increased, indicating enhanced evaporative concentration and a fall in lake level, further evidenced by a decline in the relative abundance of freshwater diatom taxa and diatom productivity. This is not interpreted by Marshall (2006) as an abrupt termination of the AHP. Lake Tana likewise saw a decline in allochthonous inputs, reflecting declining precipitation from as early as 6.8 kyr BP and lasting the following 2.5 kyr (Marshall et al. 2011). This period of increasing aridity culminated in a drought event at 4.2 kyr BP (Marshall et al. 2011). Reconstruction of the hydrogen isotope record from leaf waxes is in agreement with this, indicating a gradual termination of the AHP aided by vegetation feedbacks, until an abrupt drought event at 4.5 kyr BP (Costa et al. 2014). Lake Abhé also saw a declining lake level from 5.1 – 4.6 kyr BP (Fig. 3.2; Umer et al. 2004).

In the MER, the Ziway-Shala basin experienced declining lake levels from as early as 6.5 kyr BP in response to increasing aridity. The decline was amplified further by a south-eastern shift in the drainage network which saw the Awash and Mojo Rivers abandon the Ziway-Shala basin and instead flow towards the Afar Depression (Sagri et al. 2008). The loss of these rivers made the basin even more susceptible to fluctuations in climate and from 5.7 – 5.1 kyr BP a major decrease in lake level occurred, leading to the separation of Lake Ziway by 5.0 kyr BP and marking the beginning of the Holocene separated lake phase (Fig. 3.6; Grove et al. 1975; Benvenuti et al. 2002; Umer et al. 2004). Diatom-inferred conductivity from Lake Abiyata confirms a major decrease in precipitation and a water deficit from 5.7 – 3.8 kyr BP causing the lake to become shallow and saline (Umer et al. 2004). Brief wet periods were documented from 4.3 – 3.6 kyr BP and 2.9 – 2.6 kyr BP (Umer et al. 2004). Lake Tilo also experienced a substantial reduction in lake volume from 5.5 – 5.1 kyr BP, evidenced by a rapid increase in $\delta^{18}O$, a decline in mineral accumulation rates and increasing salinity in the mid-Holocene (Telford and Lamb 1999; Lamb et al. 2000; Lamb et al. 2005). Lake Awassa saw increasing $\delta^{18}O$ and $\delta^{13}O$ values,

indicating a shift towards aridity from 4.8 kyr BP, slightly later than in the MER (Lamb et al. 2002a). At 4.2 kyr BP, Lake Tilo records a further substantial increase in $\delta^{18}O$, marking a fall in lake level (Lamb et al. 2000). A wet period then occurred from 3.7 – 3.4 kyr BP, indicated by a switch to freshwater diatom species (Lamb et al. 2000).

In southern Ethiopia, the K record at Chew Bahir indicates the AHP began to end around 6.0 kyr and the transition took 1000 years for full aridity to be reached (Fig. 3.3; Foerster et al. 2012). At Lake Turkana, steady warming occurred from 5.7 kyr BP, based on reconstructed palaeo-temperatures using the TEX_{86} temperature proxy, culminating in the warmest, most arid conditions at 5.0 kyr BP (Berke et al. 2012a). Shoreline data from South Island shows that water level began falling abruptly from 5.3 kyr BP, and a sharp rise in the abundance of endogenic calcite in the southern basin at 5.0 kyr BP confirms that peak aridity occurred at this time (Halfman et al. 1994; Garcin et al. 2012). This also coincides with the youngest radiocarbon age of a raised beach terrace at the elevation of basin overflow into the River Nile, signifying a shift from an open to closed basin (Butzer 1980; Owen et al. 1982). Geomorphic evidence from the Mt. Porr strand plain indicates lake level was constrained to below 20 m by 4.5 kyr BP and remained below this level for the rest of the Holocene (Forman et al. 2014). At 4.2 kyr BP an abrupt and dramatic shift occurred in the diatom assemblage from one indicative of low conductivity to an assemblage associated with high conductivity and brackish waters (Halfman et al. 1992). This change signifies a substantial decrease in water depth in response to reduced precipitation in the basin which lasted until ~ 2.0 kyr BP (Ricketts and Johnson 1996; Garcin et al. 2012).

In Kenya, data from Lake Suguta is in agreement with the trends observed at Chew Bahir and Lake Turkana. Precipitation in the catchment began to decrease around 6.7 kyr BP, causing the lake level to drop by ~ 250 m over the following 1.7 kyr (Junginger et al. 2013). This indicates a gradual termination of the AHP. However, given the difference between the maximum and minimum shorelines of the palaeo-lake, it is possible the lake level remained high until 5.4 kyr BP for the onset of a gradual termination or until 5.2 kyr BP if followed by an abrupt reduction in precipitation (Junginger et al. 2013). Lake Rukwa also saw a regression beginning at 6.7 kyr BP which caused the lake to become saline by 5.5 kyr BP (Barker et al.

2002). Lake Victoria had been experiencing greater seasonal restriction of rainfall since ~ 7.8 kyr BP but it is not until 5.8 kyr BP that lake levels began to decline (though sediment accumulation and outlet down-cutting may also have contributed to the increasingly shallow lake trend) (Stager et al. 2003). Changes in vegetation around the basin further indicate the climate was becoming dryer as semi-deciduous forest declined and open grasslands established (Ssemmanda and Vincens 2002). The decline in lake level at Lake Victoria coincidently led to the formation of Lake Nabugabo (Fig. 3.1 [b] site 21). The lake was most likely a protected bay of Lake Victoria during the early Holocene but as the level of Lake Victoria declined, a longshore bar cut the bay off and formed a new isolated lake around 5.0 kyr BP (Stager et al. 2005). The lake is now renowned among evolutionary biologists for its five endemic species of haplochromine cichlid fish, a feat that would not have occurred without the termination of the AHP.

In contrast, δD_{wax} records and palynological data from Lake Malawi indicate that conditions at the lake were wet from 6.15 – 3.0 kyr BP (Konecky et al. 2011). Biogenic silica profiles likewise indicate a shift to wetter conditions around 4.5 kyr BP, which culminated in a highstand shortly after (Johnson et al. 2004). This is most likely a result of the southern location of the lake in relation to the position of the ITCZ during the mid-Holocene. This ‘climatic hinge’ is a lateral boundary which divides tropical and subtropical Africa (Konecky et al. 2011).

The demographic response in North Africa to the termination of the AHP was a major, unreversed population collapse (deMenocal 2015). Radiocarbon dating of ~ 1000 archaeological sites from the western, central, eastern and northern (Atlas Mountain range) Sahara indicate a 1.8 % population loss per generation at the end of the AHP, and a 55.0 % loss from 6.3 – 5.2 kyr BP (Manning and Timpson 2014). Ultimately, this led to the emergence of Egypt’s Pharaonic civilisation in the Nile Valley as populations were forced to mobilise in order to survive (Kuper and Kröpelin 2006).

3.5.4 The 4.2 Event

The termination of the AHP culminated in a severe and abrupt drought event centred at 4.2 kyr BP (hereafter, the 4.2 event) in response to temporary weakening of the

monsoon system. Whilst the forcing mechanism for the 4.2 event is less clear than for the 8.2 event (i.e. there is no evidence of a major release of freshwater into the North Atlantic or of significant ice growth in the Northern Hemisphere), a southwards migration of the ITCZ would be consistent with the documented low-latitude aridity. This would also account for the increase in strength of westerlies over the North Atlantic and a cooling of the oceans' surface waters (1 – 2 ºC), increased precipitation and subsequent glacial advances in North America (Mayewski et al. 2004; Walker et al. 2012). It is also suggested that Pacific tropical deep waters cooled enough at this time to trigger the start of the modern El Niño Southern Oscillation (ENSO) regime, which subsequently became more pronounced in the mid-latitude regions (Fig. 3.6; Sun 2000).

The 4.2 event is now recognised as being global with evidence of it found throughout tropical and North Africa (Gasse 2000; Thompson et al. 2002; Williams 2009), the Middle East and Gulf of Oman (Bar Matthews and Ayalon 1997; Cullen et al. 2000; Gupta et al. 2003), Asia (Gasse and Van Campo 1994; Prasad and Enzel 2006), China (Wang et al. 2005; Huang et al. 2007; 2011), Europe (Hughes et al. 2000; Drysdale et al. 2006), North America (Dean 1997; Booth et al. 2005) and Peru (Davis and Thompson 2006).

In East Africa, evidence of this drought event has been found in the Ziway-Shala basin (Gillespie et al. 1983; Chalié and Gasse 2002a), Lakes Tana (Marshall et al. 2011), Awassa (Telford et al. 1999; Lamb et al. 2002a), Tilo (Telford and Lamb 1999; Lamb et al. 2000), Abhé (Gasse 1977), Turkana (Owen et al. 1982; Johnson et al. 1996; Marshall et al. 2011), Victoria (Stanley et al. 2003), Edward and George (Lærdal et al. 2002), the Bahr-el-Ghazal depression in South Sudan (Gasse and Van Campo 1994), as well as the Mt. Kilimanjaro ice core record (Fig. 3.6; Thompson et al. 2002). However, the 4.2 event can be difficult to identify in lacustrine records as it occurs when the climate was more arid than at any other time since the LGM (Marshall et al. 2011).

In North Africa evidence of the 4.2 event has been found in River Nile flow records and geoarchaeological evidence. A sediment core from the Nile deep-sea fan indicates a highly arid period from 4.3 – 3.7 kyr BP in the River Nile drainage area,

characterised by an increase in the contribution of aeolian dust, a decrease in the intensity of Blue Nile discharge and a decrease in the proportion of sediment derived from the White Nile (Williams 2009; Blanchet et al. 2013). In contrast, oxygen isotope compositions from the teeth and bones of ancient Egyptian mummies indicate aridification occurred more gradually from 5.5 kyr BP onwards (Touzeau et al. 2013). Geological and geoarchaeological data from an excavation at the Saqqara necropolis supports both records, identifying a gradually drying climate from 5.0 – 4.5 kyr BP, culminating in an extreme shift towards a very dry climate at 4.2 kyr BP (Welc and Marks 2014).

It is believed that the arid event was so severe it had a dramatic impact on human population dynamics in North Africa. In Egypt, a failure of the annual flood of the River Nile occurred due to a drastically reduced summer monsoon in the Blue Nile basin (at present, the Blue Nile contributes ~ 68 % of the River Nile's summer flood [Lamb et al. 2007a]). Ancient texts from this time describe the desert spreading across the land and the Nile Delta being so low it was crossed on foot (Bell 1971). This proved to be disastrous and plunged the Old Kingdom into the First Dark Age; widespread drought and famine resulted in extreme social, political and economic instability across the land, which is thought to have contributed significantly to the collapse of the Egyptian Old Kingdom (~ 4600 – 4100 yr BP) (Bell 1971). The associated desertification to the east and west of the River Nile has also been connected with the movement of people from the Libyan dessert into the Nile Valley and southwards, following the shifting rain belts (Welc and Marks 2014). Other civilisations and cities in the eastern Mediterranean also began to disintegrate around this time, including the Akkadian Empire in Mesopotamia (Cullen et al. 2000; deMenocal 2001), the city of Byblos (Lebanon) as well as several others in Syria and Palestine (Bell 1971). As such, the 4.2 event appears to be one of the most significant climatic events of the Holocene in terms of its widespread (mostly detrimental) impact on humans and has been proposed as a formal boundary between the middle and late Holocene by a Working Group of INTIMATE and SQS of ICS (Walker et al. 2012).

3.5.5 The Late Holocene

The late Holocene saw several brief periods of increased humidity following the 4.2 event centred at ~ 3.0 – 2.0 kyr BP, ~ 1.6 kyr BP and ~ 1.3 kyr BP. It has been suggested that enhanced, higher frequency ENSO events during this time caused these periods of stable humid conditions, which saw brief increases in regional lake levels (Fig. 3.6; Foerster et al. 2012). In the last millennium, East Africa experienced a drier climate during Europe's Medieval Climatic Anomaly (MCA, ~ 950 – 680 yr BP) and a relatively wet climate during the Little Ice Age (LIA, ~ 680 – 100 yr BP) which was interrupted by three prolonged arid periods (Jones et al. 2001). Overall however, aridity increased as the climate transitioned towards present day conditions. The period also began to see more significant alterations to the environment by human activity as populations grew and agricultural practices and cultivation became more intensive and widespread.

In northern Ethiopia, Lake Ashenge recorded an overall low lake level and gradually intensifying aridity during the late Holocene. Magnetic susceptibility data show an increase in allochthonous inputs from 3.9 kyr BP culminating at 2.9 – 2.7 kyr BP (Marshall et al. 2009). Whilst this may indicate increased rainfall in the catchment, no lake water dilution is inferred from the diatom assemblage. Therefore it is more likely that anthropogenic activity from agricultural and cultivation caused the excessive soil erosion documented in the lake, although the first signs of intensive cultivation at Lake Tana are documented much later around 1.7 kyr BP (Marshall et al. 2011). From 2.2 – 1.5 kyr BP a wet episode occurred, shown by an increase in freshwater diatom taxa and slightly reduced conductivity (Marshall et al. 2009). Evidence of this wet period was also found in the Tigray deposits, which resulted in increased soil formation, and at Lake Hayq[10] (Fig. 3.1 [b] site 33), where $\delta^{18}O$ values show slightly wetter conditions (Machado et al. 1998; Lamb et al. 2007b).

From 1.5 – 1.0 kyr BP the climate in the Lake Ashenge basin became increasing dry again. An abrupt increase in the dominance of benthic and aerophilous diatom taxa and a minor positive shift in the isotope values, indicate the water level at Lake Ashenge had decreased in response to the enhanced evaporative concentration

[10] The study site for this research.

(Fig. 3.5; Marshall et al. 2009). Amplified allochthonous inputs indicate that the rate of erosion was high during this period, implying the catchment was becoming increasingly unstable. The deposits from Tigray likewise show a period of soil degradation at this time (Machado et al. 1998). This catchment instability was most likely driven by intensive agricultural practices in the catchment and a short, but intensive, wet season enhancing sediment supply to the lake. From 1.0 kyr BP to present, the Lake Ashenge diatom assemblage indicates a shallow, saline lake interrupted only by a brief wet spell from 500 – 300 yr BP. The Tigray valley deposits confirm this shift towards aridity (Machado et al. 1998).

At Lake Tilo, stable $\delta^{18}O_{carbonate}$ values indicate low precipitation in the basin until ~ 3.7 kyr BP when a brief wet episode occurred, lasting for approximately 300 years (Lamb et al. 2000). Following this, lake level dropped and became increasing saline in response to the increasing aridity, reaching its present condition around 2.0 kyr BP (Telford and Lamb 1999; Lamb et al. 2005). The last period of lake level rise in the Ziway-Shala basin occurred later, from 2.5 – 2.0 kyr BP, in response to increased humidity beginning at ~ 4.0 kyr BP, which may have seen Lakes Shala, Langano and Abijata briefly reunite before establishing the boundaries they occupy today (Fig. 3.6; Benvenuti et al. 2002; Chalié and Gasse 2002a; Lamb et al. 2002a; Mohammed et al. 2002).

Chew Bahir continued to experience arid conditions until 2.0 kyr BP, interrupted only by a brief humid period at 3.0 kyr BP. At 2.0 kyr BP a longer humid period occurred, lasting until 1.3 kyr BP when it terminated abruptly (Fig. 3.3; Foerster et al. 2012). The Lake Turkana water level also continued to decline after the 4.2 event, falling below its modern level between 2.6 – 1.5 kyr BP (Fig. 3.6; Umer et al. 2004). A humid phase at 1.5 kyr BP caused lake level to rise above its modern level, after which it declined again, reaching its present day water level. Despite these major fluctuations, Lake Turkana has always been a permanent waterbody in an otherwise inhospitable desert, and therefore a refuge for people. Following the mid-Holocene fall in water level, Lake Turkana saw the emergence and/or expansion of pastoral herders into the basin, seeking sufficient water and pasture for livestock, alongside the hunter-gatherers who relied on fishing (Robbins 1972; Ashley et al. 2011; Ndiema et al. 2011). This transition and amalgamation of different people and

lifestyles led to new social, cultural and economic practices in the Turkana basin (Wright 2011).

In the last millennium, aridity and warming synchronous with the MCA is evident across East and Southern Africa at Lakes Victoria (Stager et al. 2003), Bogoria, Nakuru, Elementeita (Fig 9. [b] site 25; De Cort et al. 2013), Sacred Lake (Konecky et al. 2014) and Tanganyika (Tierney et al. 2008), the Ethiopian highlands (Bonnefille and Umer 1994), the Kuiseb River (Namibia; Scott 1996), the Cango Cave system (South Africa; Talma and Vogel 1992) and the Wonderkrater records (Scott and Thackeray 1987; Scott 1999). The onset of MCA conditions was not synchronous across Africa however, with parts of Southern Africa experiencing greater warming in the early MCA and central and North Africa experiencing greater warming in the later MCA (Nicholson et al. 2013).

LIA cooling is documented in pollen records from Ethiopia and Southern Africa (Bonnefille and Umer 1994; Scott 1996; Scott et al. 2003) as well as Lakes Victoria (Stager et al. 2003), Naivasha (Verschuren et al. 2000), Bogoria, Nakuru, Elementeita (De Cort et al. 2013), Malawi (Powers et al. 2011), Chilwa (Malawi; Owen and Crossley 1989) and glaciers in the Rwenzori Mountains (Russell et al. 2009). In contrast, the western Ugandan crater lakes Kibengo, Kitagata, Kasenda and Wandakara and Lake Edward (Fig. 3.1 [a] site 3) suggest century-scale droughts during the height of the LIA (Russell and Johnson 2005; Russell et al. 2003; 2007; Ryves et al. 2011). Russell et al. (2007) therefore suggest a rainfall gradient across East Africa during the LIA with the most western regions being dry and eastern regions being wet. Lake Tanganyika and Lake Sibaya (South Africa) also document relatively dry conditions during the LIA but this is most likely driven by their southerly locations on the ‘climatic hinge’ between the wet equatorial regions and the dry south (Stager et al. 2009; 2013).

Most recently general warming has occurred over Africa since the 1880s, punctuated by a cool spell in the mid-20th century (19th – 21st century Ethiopian climate events are discussed in Chapter 2) (Nicholson et al. 2013; Nicholson 2014).

3.6 Conclusion

It is clear that global teleconnections have played a role in both general climate variability and abrupt climatic shifts in tropical and subtropical Africa. The expression of these changes has been different locally and regionally, complicated by the effects of orography on monsoon system variability, the distribution of lakes and more recently by anthropogenic activities altering the hydrology and water balance of lake basins. This review therefore provides a regional framework against which new findings may be compared and contrasted.

Based on the breadth of palaeoclimatic evidence from across the region, there are two issues arising which need addressing. First, it is evident from the records that the availability of high quality data across Ethiopia and the Horn of Africa is spatially uneven. High-resolution palaeo-records come predominantly from lakes in the MER (the Ziway-Shala basin, Lake Turkana and Chew Bahir) and, despite recent findings from Lakes Tana and Ashenge in the north, the highlands and escarpments are sparsely represented.

Secondly, despite the numerous climate archives from across East Africa, there are discrepancies between records regarding regional climatic events such as the termination of the AHP. Uncertainty remains regarding the timing (due to errors in dating methods) and expression of these high-magnitude transitional periods based on the diverging response of biotic and hydrological systems not only between sites but also within the same site. Lake Turkana is a prime example of this, where palaeo-shoreline and relict beach evidence conflict when identifying the timing of Holocene high- and lowstand periods (Garcin et al. 2012; Forman et al. 2014). Isotope composition of terrestrial leaf wax compounds and biogenic silica profiles from Lake Malawi, likewise fail to agree on the timing and duration of mid-Holocene wet periods (Johnson et al. 2004; Konecky et al. 2011), whilst palaeo-shorelines and hydrological modelling at Lake Suguta provide contrasting evidence of both a gradual and abrupt termination of the AHP (Junginger et al. 2013).

Therefore, the apparent response of a system to a climatic event may be biased by the sensitivity of the climatic proxy, chronological restraints and resolution, and model assumptions. Additional records from across East Africa are necessary in

addressing this issue, as by providing further high quality, high-resolution evidence of climatic and environmental change since the LGM, our understanding of the complex mechanisms that govern the East African climate will be improved. Providing these data is essential for accurate and robust reconstructions of past climate fluctuations, which can be utilised in future climate and environmental modelling under varying scenarios, including adaptation and mitigation responses by the population of this vulnerable region.

Chapter 4
Research Approach and Methods.

4.1 Introduction

This chapter describes the palaeolimnological approaches used in this study. A detailed description of the study site, Lake Hayq, is presented first. Field sampling is then described, followed by laboratory procedures and sampling methods. Emphasis is placed on diatom and photosynthetic pigment analyses as these are the two main proxies used in this research for inferring environmental and climatic variability at the site. Finally, the numerical analyses applied in the study are discussed.

4.2 Study Site: Lake Hayq

Lake Hayq is located on the eastern margin of the north-central highlands in the South Wollo province of the Amhara region, northern Ethiopia (11º20'53''N, 39º42'32''E; 1950 m altitude) (Fig. 3.1 [b] site 33). The lake sits in a graben formed within Tertiary volcanic bedrock. The lake is within the Awash River basin, 30 km north of the town Dessie and close to the Ambasel Mountains (Lamb et al. 2007b; Ayenew 2009). The Ethiopian Rift lies 25 – 30 km to the east where it widens into the Afar Depression.

4.2.1 Geology

The geology of northern Ethiopia has been described in detail in Chapter 2. The basin sits on Termaber basalt that formed during the Miocene to early Pliocene. The basalt consists of lenticular basalts, tuffs and rhyolitic lava flows. Diatomaceous deposits and thick palaeosols also occur at different levels in the bedrock indicating periods of volcanic quiescence when soils developed and the lake formed (Ghinassi et al. 2012). Three units were identified by Ghinassi et al. (2012) in the basalt: Unit I, a 450 m thick layer of basalts containing basaltic breccias and red palaeosols; Unit II, a layer consisting of ignimbritic flow deposits and basaltic layers approximately 250 m thick; and Unit III, a deeply weathered 300 m thick basalt layer with paleosol and lacustrine diatomaceous deposits.

4.2.2 Climate

The climate of northern Ethiopia has been described in detail in Chapter 2. The

Lake Hayq basin climate can be defined as subhumid, with a mean annual temperature of 18 ºC with a diurnal range of 8 – 23 ºC. Climate data from four stations within 50 km of the lake record the influence of the south-east monsoon and high-elevation westerlies on the distribution of precipitation; total annual rainfall is 1000 – 1100 mm yr^{-1}, with 79 % of rainfall occurring between April and September (Demelie 2000; Darbyshire et al. 2003).

4.2.3 Land Cover

The surrounding lowlands and lake shores are intensively cultivated. Common crops include tef, wheat, millet, maize, coffee, chickpeas, *Citrus* species and *Eucalyptus* plantations (Darbyshire et al. 2003). Terracing permits agriculture on steeper slopes as well. Natural vegetation only occurs in small pockets at elevations below 2400 m. This includes savannah woodland and evergreen bushland (*Acacia* spp., *Dodonaea angustifolia*, *Euclea schimperi*, *Euphorbia candelabrum*, *Ficus* spp., *Teclea simplicifolia*, *Ziziphus mucronata*), ruderal herbs, (*Rumex* spp., *Solanum incanum*, *Tribulus terrestris*) and grasses (*Hyparrhenia hirta, Pennisetum sphacelatum*) (Darybshire et al. 2003). The natural montane vegetation of the region is the dry *Juniperus procera* forest but very little remains. Around the lake the forest is largely restricted to isolated shrubby pockets on steep, inaccessible slopes. Other scattered stands of forest on slopes over 2400 m contain *J. procera* together with *Acacia abyssinica*, *Celtis africana*, *Cordia africana*, *Olea europaea*, and in particularly sheltered valleys, *Podocarpus falcatus*.

4.2.4 Drainage Basin and Hydrology

Lake Hayq is 6.7 km long and 6.0 km wide, with a surface area of 23.2 km² and a catchment of 65.0 km² (Lamb et al. 2007b). It is a deeply shelving lake with a mean depth of 37.4 m (Fig. 4.1 and 4.2). In 1938 the maximum lake depth was 88.8 m but in 2000 this had decreased to 81.0 m, indicating a 7.8 m fall over 60 years (Lamb et al. 2007b). The main input to the lake comes from the Ankwarka River (Demlie et al. 2007). The lake has no visible outlet. An apparent palaeochannel indicates that the nearby Lake Hardibo overflowed into Lake Hayq at some point in history (overflow ceased most recently in 1962 [Yesuf et al. 2013]). Ghinassi et al. (2012) suggest that during these historical overflow events, Lake Hayq's surface area expanded up to three times. The palaeochannel is now permanently dry and would require a 16 –

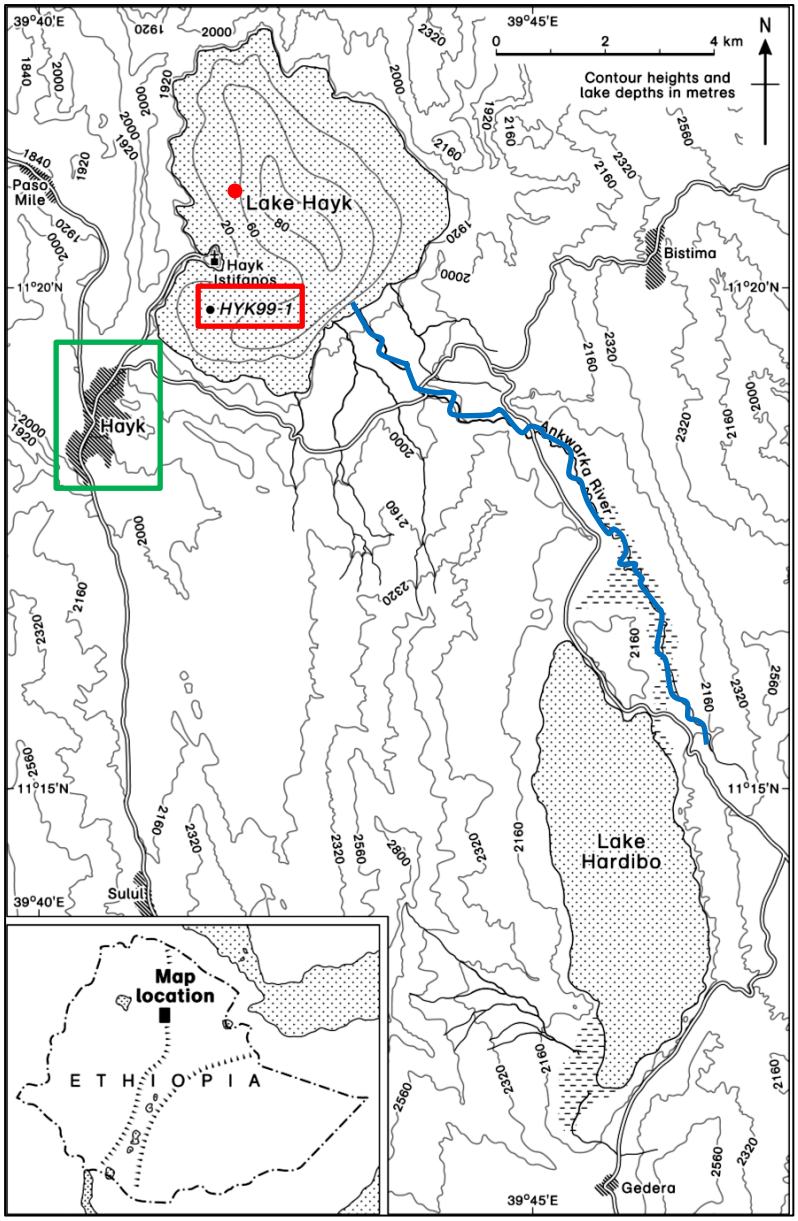

Figure 4.1. Map of Lake Hayq showing bathymetry and the surrounding catchment. Inset shows location of Lake Hayq in Ethiopia (adapted from Lamb et al. 2007b). The red box indicates the location of core HYK99-1 extracted in 1999 and used by Lamb et al. (2007b) and Darbyshire et al. (2003). The approximate location of core Hayk-01-2010 is indicated by the red circle. The Ankwarka River is indicated in blue and the town of Hayq by the green box.

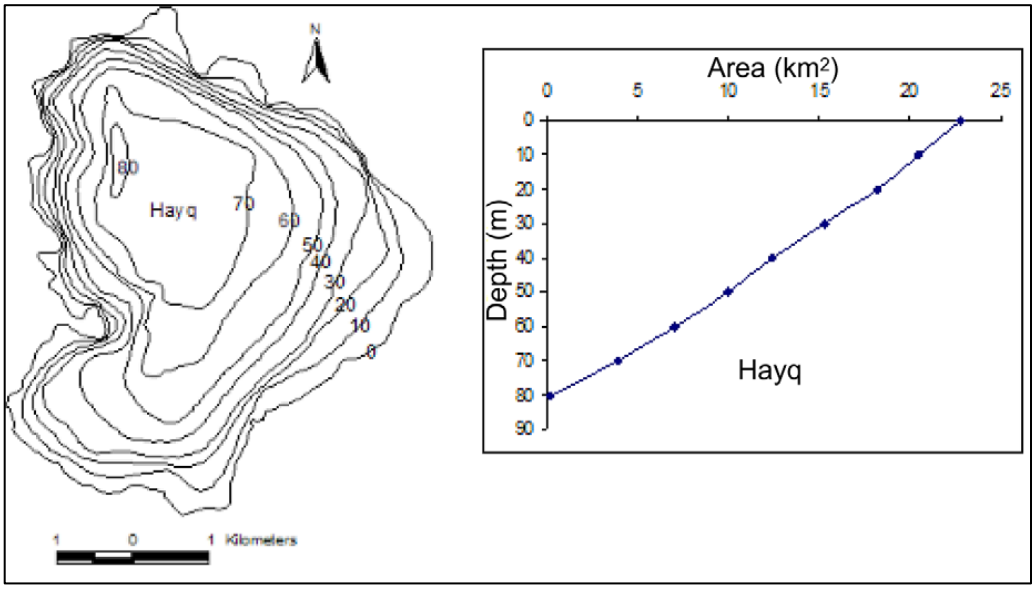

Figure 4.2 (a). Bathymetric map and depth-area relation of Lake Hayq (adapted from Demlie et al. 2007).

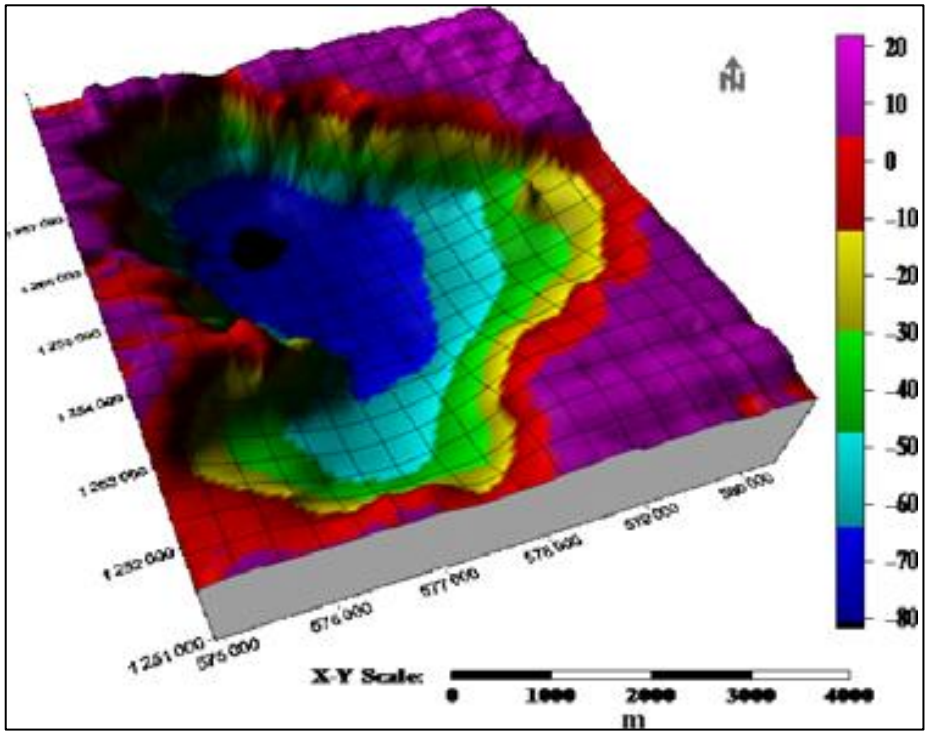

Figure 4.2 (b). A three-dimensional meshed, shaded-rendering surface map of Lake Hayq. Changes in depth are indicated by colour; red shows the lake surface (0), whilst black indicates the deepest layers of the lake (- 800), close the location of Hayk-01-2010. The map was created to inform long-term management of the lake, as well as for fishing and recreational purposes (adapted from Yesuf et al. 2013).

18 m rise in water level at Lake Hardibo to cause overflow again. Occasional water flow now occurs between the lakes through an artificial irrigation canal. A second palaeochannel indicates that Lake Hayq overflowed during highstands into the Wazi River, a tributary of the Mille River which ultimately joins the Awash River in the south of the Afar Depression (Ayenew 2009). It is estimated a rise of ~ 40 m would be required to make Lake Hayq overflow again (Lamb et al. 2007b). More recent lake level changes have been documented through the transformation of an island near the western margin of the lake into a peninsula; in 1938 the 9th century Istifanos monastery was located on the island but by 1969 lake level had dropped causing the island to become attached to the mainland (Lamb et al. 2007b). Further declines in lake level have been documented during the 1970s and 1980s and more recently, caused by inappropriate farming practises, removal of vegetation and poor land management, which have reduced discharge from the upstream watersheds (Fig. 4.3; Yesuf et al. 2013).

4.2.5 Limnology

The limnology of Lake Hayq was described by Baxter and Golobitsch (1970) who concluded that based on Talling and Talling's (1965) classification of African lakes, Lake Hayq is a fairly typical class II[11], oligotrophic tropical lake. Conductivity was 920 µS cm^{-1} making it a freshwater lake. Chemical stratification was not pronounced although there was some accumulation of ammonia, phosphate and silica at greater depths. The predominant cation is magnesium and the predominant anions are bicarbonate and carbonate. Baxter and Golobitsch (1970) further state that the thermal stratification is similar to that of other Ethiopian lakes of comparable depth but the oxygenated layer was relatively deeper compared to others (around 40 m). The lake was also notable for its unusual water clarity (transparency measured with a Secchi disk was 9 m) and its low plankton density (chlorophyll *a* was < 1 µg l^{-1}) at the time of observation.

Since then, phytoplankton biomass has increased significantly (chlorophyll *a* was ~ 12.5 – 22.9 µg l^{-1} in the early 1990s) which has reduced water clarity (transparency

[11] A lake with high total ion concentrations (alkalinity of 6 – 60 meq/l) arising from accumulation and evaporation in closed basins, or by inflow rich in solutes (carbonate, bicarbonate, sodium). Conductivity is between 600 – 6000 µS. Typical lakes include Lakes Albert, Edward, Kivu, Rukwa Tanganyika and Turkana.

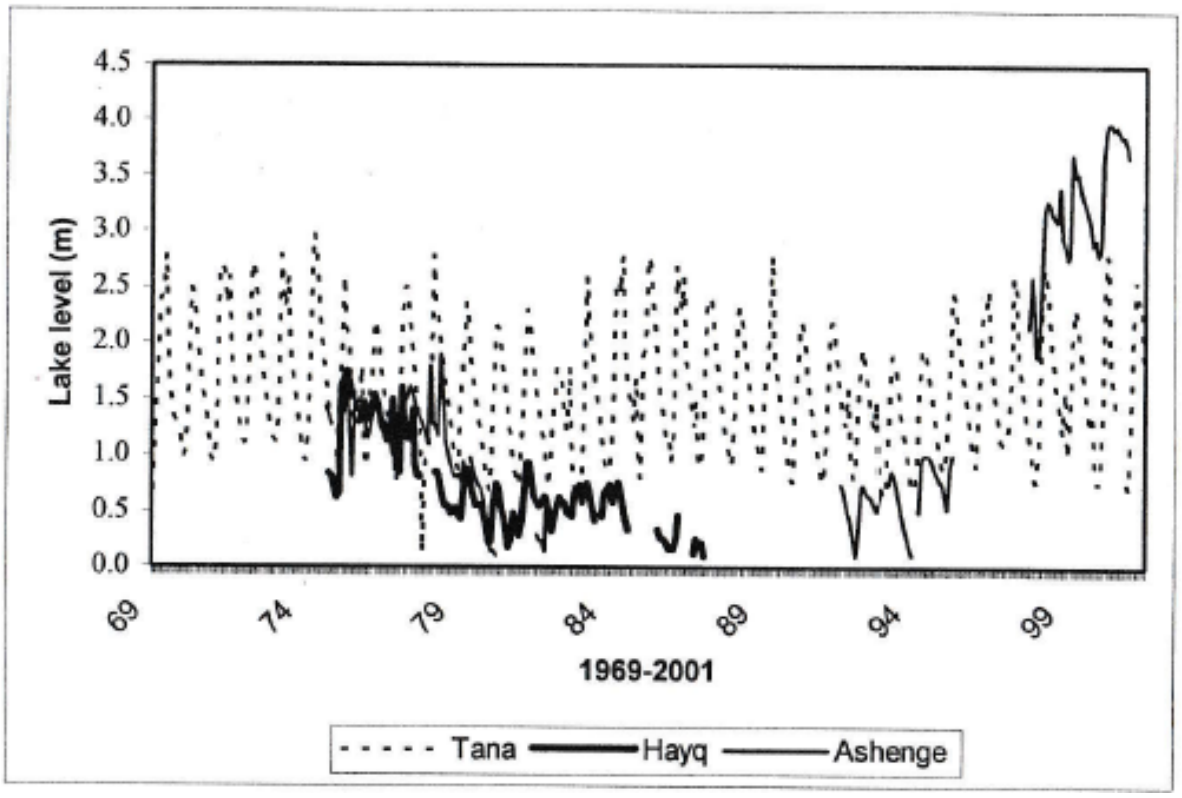

Figure 4.3. Lake level (m) records for Lakes Tana, Hayq and Ashenge from 1969 – 2001 (Ayenew 2009).

measured with a Secchi disk was 1.24 m) (Elizabeth et al. 1992). The oxygenated layer had also decreased to 10 m. These changes in limnology have been attributed to the introduction of planktivorous fish in 1978, which released phytoplankton from grazer control. Other factors that may have contributed to these changes include an increase in cultural eutrophication and a decrease in water level. A spate of fish kills in the lake have most likely been driven by these changes also; given the depth of the lake, the instability of the water column and the shallow oxygenated layer, anoxia is common following mixing in the lake, resulting in high fish mortality (Elizabeth et al. 1992). Fetahi et al. (2011a; 2011b) further identify that episodic mixing may have driven changes in zooplankton community structure.

The water balance of Lake Hayq is relatively well understood given the availability of hydrometeorological data, field hydrogeological investigations and groundwater modelling (Ayenew and Demlie 2004; Asmare 2005; Demelie et al. 2007). Total annual inflow from precipitation, catchment runoff and rivers into Lake Hayq is 45.2 million m^3 (Table 4.1). Evaporation is the main outflow from the lake (65 % of losses), which combined with abstraction for irrigation has an annual loss of 34.6 x 10^6 m^3. Groundwater inflow (5.9 x 10^6 m^3 yr^{-1}, 11 %) and outflow (1.4 x 10^6 m^3 yr^{-1}, 3 %) also play a significant role in the lake's hydrology (Lamb et al. 2007b). Additionally, the net unmeasured groundwater flux suggests a further 15 x 10^6 m^3 yr^{-1} (29 %) groundwater outflow. Stable isotope composition from the lake has $\delta^{18}O$ values from + 7.1 – + 9.1 ‰ between 1975 and 2001, indicating evaporative enrichment in comparison to the mean annual precipitation value of - 1.2 ‰ (Lamb et al. 2007b).

4.3 Field Sampling

Lake Hayq was cored in January 2010 by Henry Lamb, Michael Marshall, Helene Ducrotoy (Aberystwyth University) and Oliver Langkamp (University of Cologne). Coring was carried out from an anchored raft in the northern basin of the lake at the GPS recorded point N 11°20'46.4"; E 39°42'23.2", 1905 m elevation and 78.2 m water depth (Fig. 4.4). The sediment core was taken from the raft using a UWITEC hammered piston corer, with a 5.8 cm diameter and 210 cm barrel with a plastic liner, which was manually hammered into the lake bed (Aaby and Digerfeldt 1986).

Coring began 89 cm below the sediment surface and the core, Hayk-01-2010[12], was extracted in nine drives, labelled 1 – 9, totalling ~ 1200 cm. One known repeat drive was extracted (drives 2 and 3). Plant arrangers' oasis was used to stabilise the sediment-water interface and the cores were cut into two sections (with the exception of drives 6 and 9, which were shorter in comparison to the other cores), labelled A and B, for packing and transport (Table 4.2).

Table 4.1. Water balance estimates for Lake Hayq (Lamb et al. 2007b). Inflows are estimated from field measurements of the Ankwarka River and spring flows in February and March 2000, average rainfall from 1966 – 1999, and a runoff coefficient of 0.3 (estimated using area weighting of six land-use, five slope and two soil type units of the lake catchment [Tripathi and Singh 1993]). Evaporation is based on Penman estimates combined with a seven year Colorado Class-A pan evaporation record (1985 – 1991) measured at the town of Hayq.

Source	Water balance estimate ($m^3 \times 10^6\ yr^{-1}$)	(%)
Precipitation on lake	+ 26.0	+ 52.0
Catchment runoff	+ 19.0	+ 37.0
Groundwater inflow	+ 5.9	+ 11.0
Groundwater outflow	- 1.4	- 3.0
Evaporation	- 33.0	- 65.0
Abstraction	- 1.6	- 3.0
Net unmeasured ground water flux (outflow)	- 15.0	- 29.0

4.4 Laboratory Methods

On return to the laboratory at Aberystwyth University the core was refrigerated at 4 °C. In February 2013 the core was made available for the purpose of this research. Each core section was cut in half lengthways using a steel wire and each half was covered in cling film, resealed in plastic casing and labelled. One half of each core was kept refrigerated at Aberystwyth University for archiving and the other 'working' half was transported to Loughborough University to undergo analyses. When not being sub-sampled, working halves were kept sealed in cling film and refrigerated.

[12] 'Hayk' is an alternative spelling for L. Hayq and shall only be used in reference to the core Hayk-01-2010.

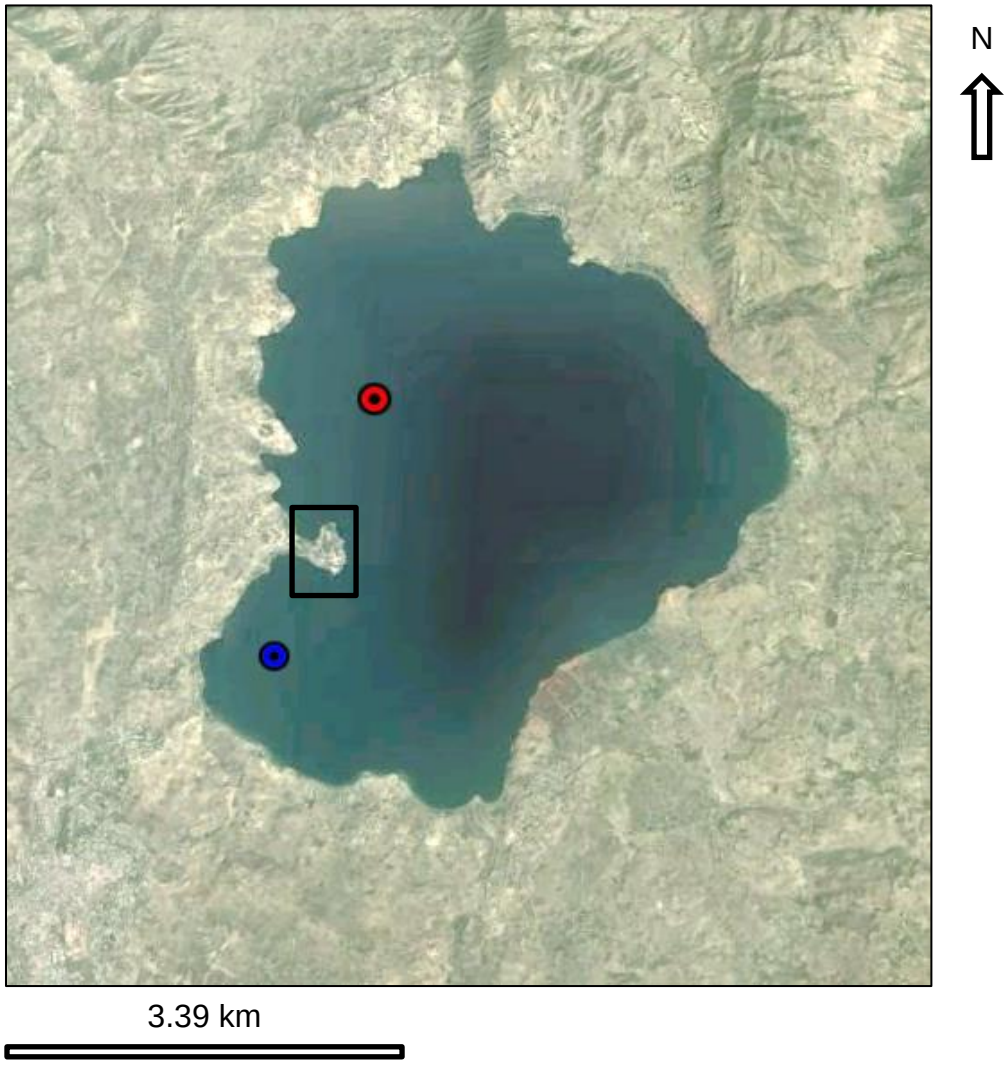

Figure 4.4. Aerial view of Lake Hayq (Google Earth 2013b). The red circle shows the location of core Hayk-01-2010. The blue circle indicates the approximate location of core HYK99-1 extracted in 1999 and used by Lamb et al. (2007b) and Darbyshire et al. (2003). The black box indicates the position of the Istifanos monastery, located on an island in the 9th century, which has since become attached to the mainland as the water level has dropped.

Table 4.2. Drive details of core Hayk-01-2010.

Drive	Subdrive	Core length (cm)	Depth below sediment surface (cm)	Sampling interval (cm)	
				Diatoms	Pigments
1	A	95.5	89.0 – 184.5	2	2
	B	87.0	184.5 – 271.5	2	2
2	A	93.5	247.5 – 341.0	2	Not sampled
	B	47.0	341.0 – 388.0	2	Not sampled
3	A	83.5	236.5 – 320.0	2	Not sampled
	B	50.5	320.0 – 370.5	2	Not sampled
4	A	89.0	226.5 – 315.5	0.5 cm between 269.0 – 301.0, remainder at 2 cm	0.5 cm between 269.0 – 301.0, remainder at 2 cm
	B	90.0	315.5 – 405.5	2	2
5	A	84.5	369.0 – 453.5	0.5 cm between 387.0 – 412.5 cm, remainder at 2 cm	0.5 cm between 387.0 – 412.5 cm, remainder at 2 cm
	B	67.0	453.5 – 520.5	2	2
6		90.0	522.5 – 612.5	0.5 cm between 523.0 – 531.0 cm, remainder at 2 cm	0.5 cm between 523.0 – 531.0 cm, remainder at 2 cm
7	A	93.0	572.5 – 665.5	2	14
	B	81.5	665.5 – 747.0	2	14
8	A	21.5	723.5 – 745.0	2	14
	B	77.0	745.0 – 828.0	2	14
9		47.0	773.0 – 820.0	2	Not sampled

4.4.1 Troels-Smith Sediment Classification

Each core half was cleaned and photographed in preparation for sediment description. The sedimentary sequence was then divided into lithostratigraphic units based on sediment type and colour. The Troels-Smith sediment classification scheme was applied to characterise and define the units accurately (Aaby and Berglund 1986; Schnurrenberger et al. 2003). Changes in colour were identified using a Munsell colour chart.

4.4.2 Organic, Carbonate and Water Content

Loss-on-ignition (LOI) was used to estimate the organic (C_{org}) and carbonate content (CO_3) of the sediment. Methodology followed standard techniques (Dean 1974). At least 1 cm^3 of sediment (typically weighing 1 – 2 g) was extracted from the core at 2 cm intervals. The samples were placed in pre-weighed crucibles, re-weighed and dried overnight at 105 °C. After cooling in a dry desiccator, samples were weighed again. The loss in mass is taken as an estimate of water content. The samples were

then placed in a furnace at 550 °C for two hours. After cooling, samples were weighed. The resulting weight loss is attributed to the combustion of organic matter and is a measure of LOI. The final heating was for four hours at 925 °C, after which samples cooled and were weighed. The amount of carbon dioxide lost in the process is a result of carbonates being converted to oxides and so is used to determine carbonate content.

In order to identify any depth discrepancies as a result of the coring process, organic, carbonate and water content profiles were compared between cores. This served as the main tool for identifying overlap or gaps between core sections and was used in conjunction with diatom and elemental profile data, as well original field notes.

4.4.3 Diatoms

4.4.3.1 Ecology, Morphology and Distribution

Diatoms are a microscopic, unicellular group of photosynthesising algae belonging to the Division Chrysophyta, Class Bacillariophyceae (Battarbee et al. 2001). Two main forms of diatoms have been identified: centrics (Centrales) and pennates (araphid and raphid) (Pennales) (Julius and Theriot 2010). These forms vary in cell size (typically 20 – 200 μm), frustule shape, striae and punctae/areolae density and pattern and form of raphe ends (Mann and Droop 1996). It is the arrangement of these skeletal features which are used to describe and identify diatoms to variety, species or sub-species level in palaeoenvironmental research, without the need to extract DNA.

Diatoms serve as powerful ecological indicators in limnological environments due to several unique characteristics. Firstly, diatoms are ecologically sensitive to the environment in which they are present. There are currently > 24,000 identified diatom species (though there could be as many as 100,000 – 200,000 taxa; Julius and Theriot 2010), which have adapted to a variety of aquatic conditions (Guillard and Kilham 1977; Mann and Droop 1996). Physical conditions include factors such as temperature, light, turbulence and ice-cover, whilst chemical conditions include nutrient availability, pH, dissolved organic carbon and salinity (Battarbee et al. 2001). The many combinations of environmental conditions have created a diversity of

niches enabling diatoms to be found in almost every aquatic (even simply moist) environment, including fresh and marine waters, as well as soil. Consequently, many diatom species are cosmopolitan, having a wide geographical distribution, whilst others are more restricted and some are endemic to a particular region. Given the diversity of habitat combinations and the abundance of diatoms, discovery of a new species occurs frequently (Julius and Theriot 2010; You et al. 2015; Kopalova et al. 2015). Secondly, diatoms respond rapidly to environmental fluctuations, so should the environmental conditions change to beyond the tolerance threshold of a certain taxon, the diatom assemblage will respond rapidly to reflect the new environmental conditions. The frequent species turnover exhibited by diatoms makes them preferable to other palaeoenvironmental proxies such as chironomids, which respond slower to environmental changes (Verschuren 2003). Finally, diatoms have a silica wall which preserves them in sediments. They are often found preserved in multi-millennial sediment records.

Being mostly autotrophic, diatoms are restricted to the photic zone but can occupy a diversity of habitats found within that region where there is sufficient light. In general, the species found in different habitats within a lake are characteristic of each particular habitat, although species can be found in more than one habitat (Battarbee et al. 2001; Julius and Theriot 2010). Planktonic diatoms are those which spend their entire life cycle suspended in the water column. In general, centric diatoms are considered planktonic. Benthic diatoms live attached to some form of substrate around the margins of lakes. Diatoms found on stones are referred to as epilithic, on aquatic vegetation as epiphytic, on mud as epipelic and on sand as epipsammic. Substrate disturbance frequency and magnitude is also a factor affecting species distribution. In general, pennate diatoms are benthic. Facultatively planktonic diatoms may include centric and pennate taxa, which spend part of their life cycle both floating free in the water column and attached to substrates. Tychoplanktonic diatoms are those that have been swept into the plankton through a disturbance, such as turbulence, in their benthic habitat. Aerophilous species are found in subaerial environments such as soils, bogs and marshes. However, the ecology of many species is not known in detail, and so continued monitoring and research is necessary to inform understanding of species' 'optimum' conditions. Within habitats, both centric and pennate diatoms can be found as single, individual cells or in large

colonies attached to one another by mucous filaments (Battarbee et al. 2001). In large enough numbers, diatoms can form sediment comprised entirely of frustules: diatomite.

4.4.3.2 Diatom Based Studies in East Africa

Extensive diatom based studies have been carried out across lakes in East Africa since the early 20th century. The first intensive diatom studies were carried out in central East African lakes by Müller (1903; 1904; 1905; 1910), Forti (1909 – 1910), Hustedt (1922) and Zanon (1941). This was followed by Hustedt (1949) who was the first to characterise East African waters according to their diatom flora. Cholnoky (1964) was the first to publish quantitative studies from the Ruwenzori Mountains as well as Mount Kenya and the Bangweulu swamps (Zambia) (Gasse 1986). Hustedt's (1949) work was later expanded on by Richardson (1968; 1969), Hecky and Kilham (1973) and Richardson et al. (1978). Other work in the 20th century considered diatom resource requirements; Kilham (1971) studied ambient silica concentrations and the conditions leading to dominance of the major planktonic diatom groups. Kilham et al. (1986) expanded on this, investigating resource relationships (phosphorus, silica and light requirements) among planktonic diatoms, and Kilham and Kilham (1990) related diatom occurrence, specifically *Stephanodiscus* species, to elemental and nutrient loading in African lakes. Work on diatom flora in desert regions has been less extensive but publications have been made by Bastow (1960) who studied the diatom flora of drainage ditches near Khartoum, and Karim (1975) at Jebel Marra. Gasse (1975; 1980) has published diatom studies from Ethiopia and Djibouti.

Research in the late 20th century and early 21st century has built upon these relatively descriptive studies by using diatoms as palaeo-indicators to infer long-term (millennial to sub-millennial scale) changes in lake level and hydrochemical composition associated with climate variability during the Quaternary. Such studies have been conducted at Lakes Victoria (Stager 1998; Stager et al. 2003), Malawi (Gasse et al. 2002), Tanganyika (Cocquyt 1998; Stager et al. 2009), Abhé (Gasse 1977), Abiyata (Chalié and Gasse 2002a), Challa (Barker et al. 2011), Munya wa Gicheru (Owen et al. 2012), Rukwa (Barker et al. 2002), Tilo (Telford and Lamb 1999), several small lakes on Mt. Kenya (Barker et al. 2001; Street-Perrott et al.

2007) and on deposits on the Baringo basin (Kingston et al. 2007). More recently, the focus has shifted to short-term (century to decadal scale) investigations of abrupt regional climate shifts, as well as environmental changes associated with anthropogenic activity, during the late Pleistocene and Holocene. Such studies have been conducted at Lakes Tana (Marshall 2006; Lamb et al. 2007a), Ashenge (Marshall 2006; Marshall et al. 2009), Abijata (Legesse et al. 2002), Duluti (Öberg et al. 2012), Nabugabo (Stager et al. 2005) and the Ugandan crater lakes (Mills 2009; Ryves et al. 2011).

4.4.3.3 Diatom Analysis

4.4.3.3.1 Preparation Diatom and microscope slide preparation followed standard methodology (Battarbee 1986; Renberg 1990). Approximately 0.1 g of wet weight sediment per sample was used for analysis. Five millilitres of 30 % H_2O_2 was added to each sample before being placed in a water bath in a fume cupboard and slowly heated to 80 °C. Samples were observed frequently to ensure they did not dry out and remained in the water bath for 5 – 8 hours until the reaction had stopped. Then 1 – 2 drops of 50 % HCI were added to each sample to eliminate any remaining H_2O_2 and carbonates. Samples were topped up with distilled water and left to settle overnight. The supernatant liquid was decanted off the following morning and samples were topped up again with distilled water. This washing process was repeated four times. Two drops of weak ammonia was added to samples with the final wash to keeps any clays in suspension. Once washed, samples were diluted and placed on coverslips and allowed to dry. The coverslips were then mounted in Naphrax and heated on a hot plate in a fume cupboard at 130 °C.

4.4.3.3.2 Counting Strategy In general 300 valves were counted per sample under oil-immersion phase-contrast light microscope (LM) at x 1000 magnification on a Leica DMRA research microscope. In certain sections of the core it was necessary to modify the counting procedure due to variability in valve abundance or a sample being dominated by a single taxon. In samples where valve abundance was low the count was reduced to a seemingly more practical target count. This was done by performing a transect across a section of a microscope slide and then based on the occurrence of valves in that space, scaling the target count down. In some instances the target was revised to as few as 50 valves when diatom abundance was very low.

In other samples it was not deemed worthwhile to continue counting and taxa were simply identified as being present in the sample. Ultimately this scaling down approach was judged based on the practicality of counting a representative number of identifiable valves in a given time period. Advice and guidance from colleagues was sought when making such decisions (Ryves; Lewis; Hogan 2013 pers. comm.).

In instances where a single taxon dominated the assemblage (accounting for > 33.3 % of valves) counts were increased by 200 valves (500 valves in total) and the dominant taxon no longer included, following the DARES (2004) protocol. This method was time consuming however, given the dominance of a single taxon in some samples and so was not performed on every sample. Instead it was considered more practical to revert back to standard counts of 300 valves. Before doing so however, it was deemed necessary to ensure that species diversity and relative species abundance (how common or rare a species is relative to other species in a defined community) would not be significantly affected by counting fewer valves than recommended by DARES (2004). To do this, twenty-one samples dominated by a single taxon, were randomly selected (with the exception of three which had already been counted according to the DARES [2004] protocol) and counted to 500 valves, recording the cumulative number of species after every twenty valves. The results indicate that in 90.5 % of samples, the number of species plateaued before 500 valves were counted. Of these, 21.1 % saw no change in the number of species between 300 and 500 valves. In 26.3 % just one additional taxon was identified and in 47.4 % two additional taxa were identified. These increases in the number of taxa however, only accounted for 0.2 – 0.8 % of valves in a count of 500. A comparison of the three samples counted using the standard method (300 valves) and the DARES (2004) protocol found that the relative species abundance was not significantly different between the two methods (Fig. 4.5). It was concluded that relative species abundance was not significantly affected by standard counts of 300 valves, rather than the additional valves recommended by DARES (2004), and so would be sufficiently accurate for samples dominated by a single taxon.

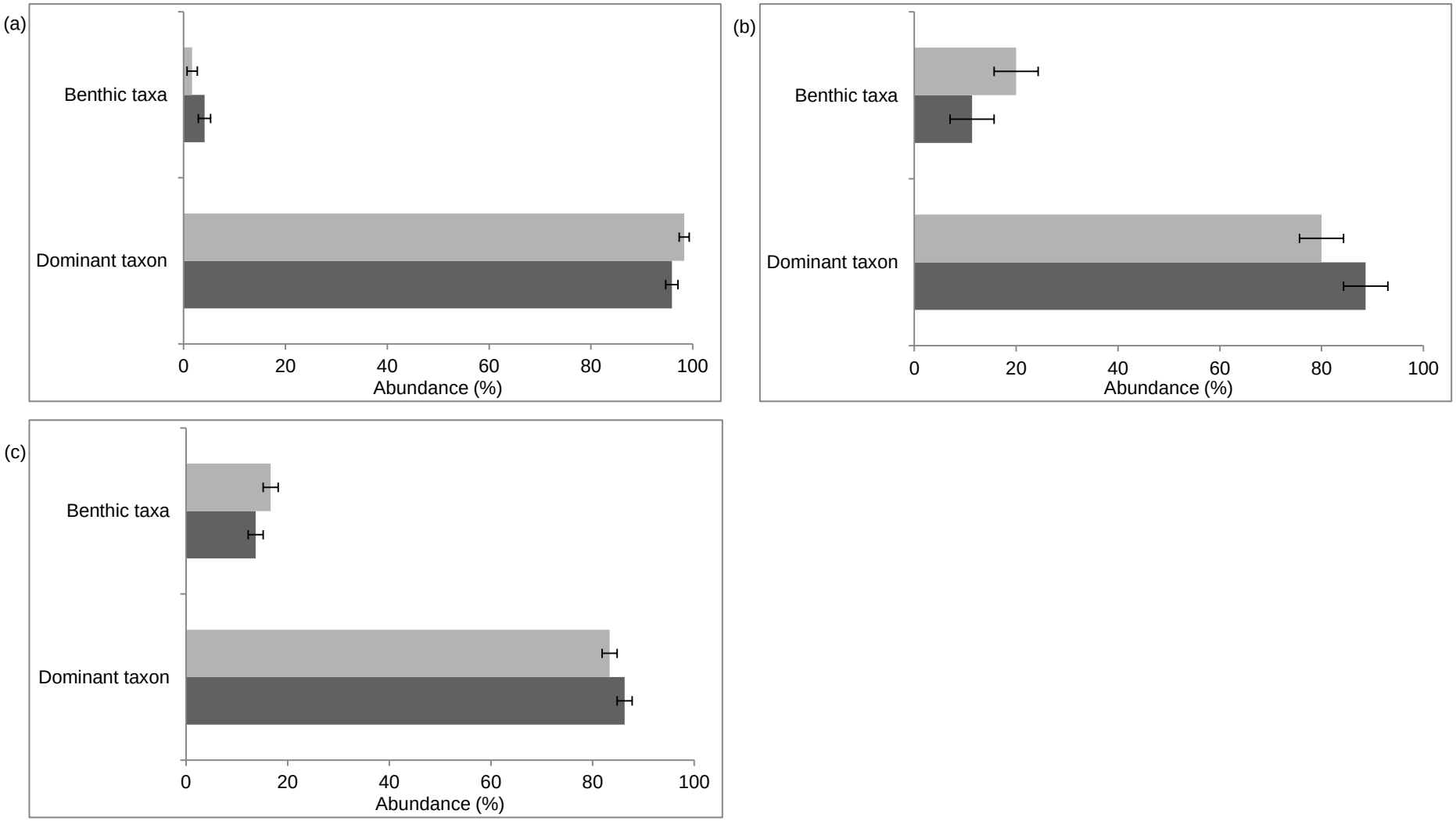

Figure 4.5. Comparison of three samples (a – 1A 36.5 cm, b – 4B, 118.0 cm, c – 5B, 12.5 cm) counted using the standard method (300 valves) (light grey) and the DARES (2004) protocol (dark grey) showing percentage differences between the dominant taxon and benthic taxa. Error bars are indicated.

In sections of the core sampled at a high-resolution (drives 4A, 42.5 – 74.5 cm; 5A, 18.0 – 43.5 cm; 6, 0.5 – 8.5 cm at 0.5 cm resolution) replicate counts were performed in order to separate the diatom signal from external variables. In each high-resolution section, a representative (> 10 %) number of evenly spaced intervals were selected and for each one, three samples made from the same diatom solution. Three-hundred valves were counted for each sample. The standard deviation of the relative abundance of the dominant taxa identified in replicate samples was used to calculate within sample variability (Fig. 4.6). It was found that generally, species with a larger average abundance had a greater standard deviation but this did vary within samples (Table 4.3). The average standard deviation across all samples was calculated as 2.82 % which may be applied to all diatom samples in order to estimate within sample variability. Changes in the relative abundance of dominant taxa between samples within this variability are considered to be the diatom signal and therefore accepted error of the method. Variability beyond this estimate is considered significant.

Table 4.3. Dominant taxa found in replicate samples and their standard deviation which serves as an estimate of within sample variability.

Taxa	Number of replicate samples	Average abundance (%)	Average standard deviation (%)
Stephanodiscus parvus	3	56.01	12.03
Aulacoseira granulata var. *angustissima*	39	51.39	7.00
Fragilaria radians	18	44.92	2.59
Gomphonema parvulum	18	8.62	1.69
Ulnaria ulna var. *ulna*	36	5.67	1.37
Nitzschia subcommunis	18	7.25	0.91
Ulnaria delicatissima	36	3.29	0.76
Gomphonema pumilum	18	3.27	0.90
All taxa combined	186	-	2.82

4.4.3.3.3 Taxonomy, Concentration and Dissolution Diatom taxonomy follows Krammer and Lange-Bertalot (1988; 1991a; 1991b; 1999), Gasse (1986), Hustedt (1949) and Patrick and Reimer (1966). Currently accepted names were verified against recent publications (Williams 2011) and authoritative databases (AlgaeBase 2015; DiatCode 2015). Valves were identified to species level where possible. Diatom concentration was estimated by adding a known number of

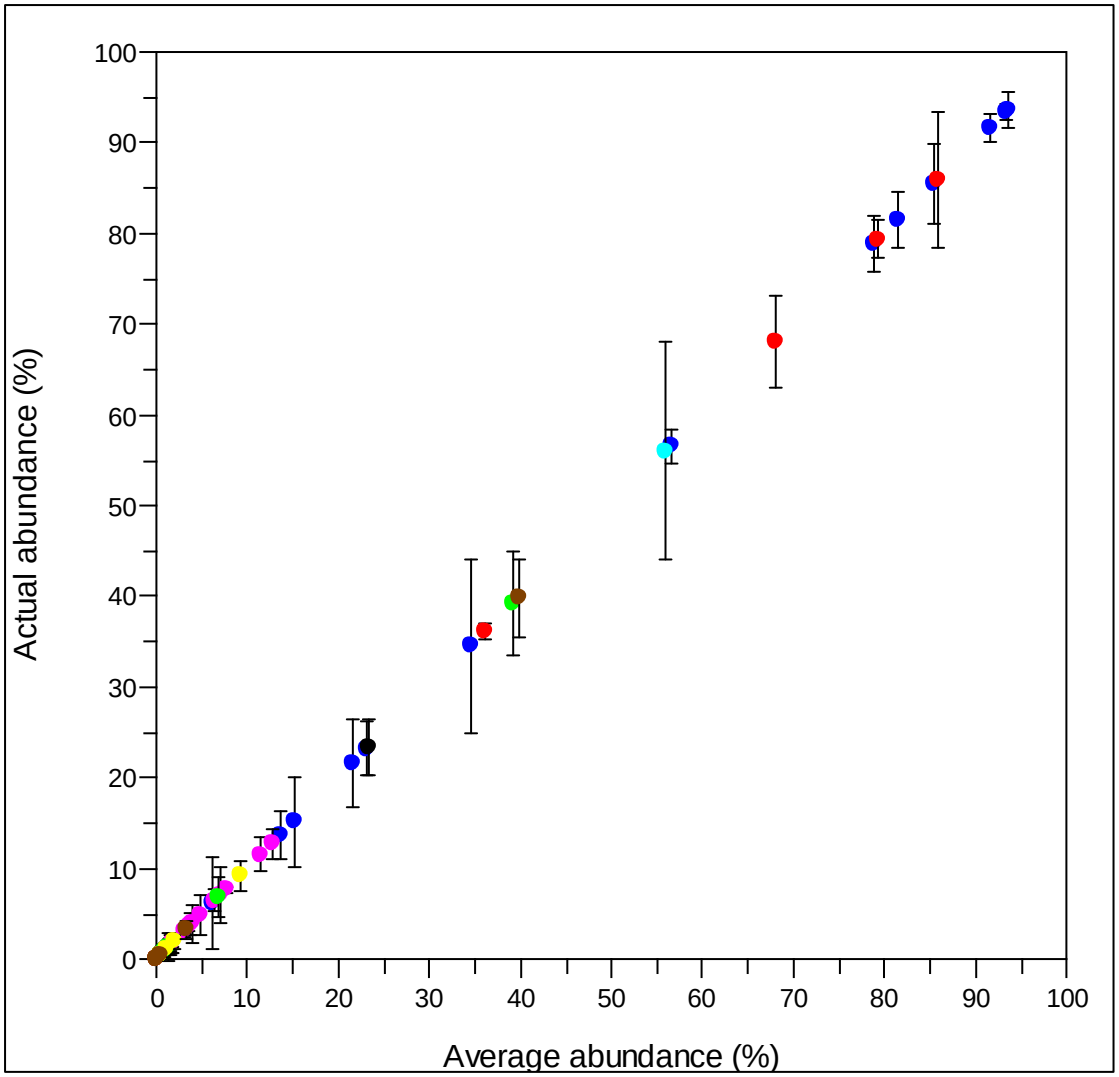

Figure 4.6. Mean abundance of dominant taxa identified in replicate counts and their within sample variability (error bars) calculated using the standard deviation: *Stephanodiscus parvus* (cyan), *Aulacoseira granulata* var. *angustissima* (blue), *Fragilaria radians* (red), *Gomphonema parvulum* (green), *Ulnaria ulna* var. *ulna* (purple), *Nitzschia subcommunis* (brown), *Ulnaria delicatissima* (black) and *Gomphonema pumilum* (yellow).

microspheres to the samples (Battarbee and Kneen 1982). Valve dissolution was assessed during counting using a binary system with valves marked as either '0' for visibly dissolved or '1' being non-dissolved or 'pristine'. This strategy was used to calculate the proportion of pristine to all classifiable valves within a species or assemblage (Flower and Likhoshway 1993; Ryves et al. 2001; 2006):

$$F_i = \frac{\sum_{j}^{m} n_{ij}}{\sum_{j}^{m} N_{ij}} \quad (1)$$

In this fractional dissolution index (or *F* index), *nij* is the number of pristine valves of species *j* (of *m*) counted in a sample *i*, compared to *Nij*, the total number of classifiable valves of species *j*. *F* varies between 0 (all valves visibly dissolved) and 1 (perfect preservation).

4.4.3.3.4 Nitzschia subcommunis There is a high degree of morphological similarity between many of the smaller, slender *Nitzschia* species found in East Africa as well as diversity of form within species (Gasse 1986). As such, identifying a single taxon amongst a variety of similar species can be problematic. Such an issue was encountered when trying to identify the species recognised in this research as *Nitzschia subcommunis* (Hustedt) (15 – 50 µm long, 2.5 – 3.5 µm wide; Fig. 4.7). In order to establish the taxonomy of the species, 105 valves were measured in length from a randomly selected sample dominated by the taxon (5A, 71.5 cm, 56 % dominance). Valves varied from 24 – 66 µm in length. The majority of valves (44.6 %) were between 42 – 50 µm in length and 81.6 % were ≤ 50 µm (Fig. 4.7). Based on these results and the morphological structure of the valves, as well as seeking advice from colleagues, it was concluded that the species in question was *Nitzschia subcommunis* as identified by Hustedt (1949) at Lake Albert (see Plate VI).

4.4.3.3.5 Separating Fragilaria-Ulnaria taxa Several varieties of the longer, slender *Fragilaria-Ulnaria* taxa have been amalgamated by taxonomists due to difficulties distinguishing between the sub-species in sample material. Gasse (1986) and Cocquyt (1998) use *Synedra acus* to refer collectively to the varieties *radians*, *angustissima* and *delicatissima*. Patrick and Reimer (1966) in contrast, distinguish

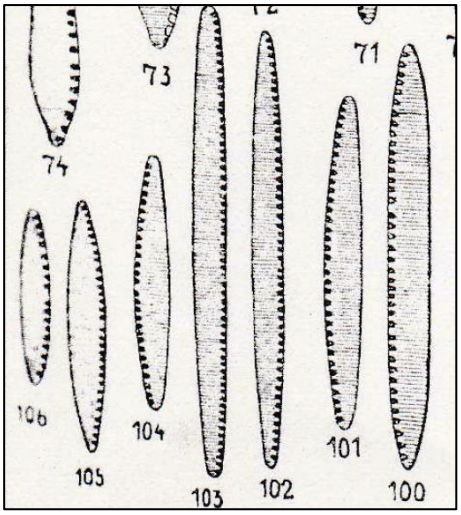

Figure 4.7 (a). Hustedt's (1949) classification of *Nitzschia subcommunis* (specimens 100 – 106) (adapted from Hustedt 1949, Plate XIII).

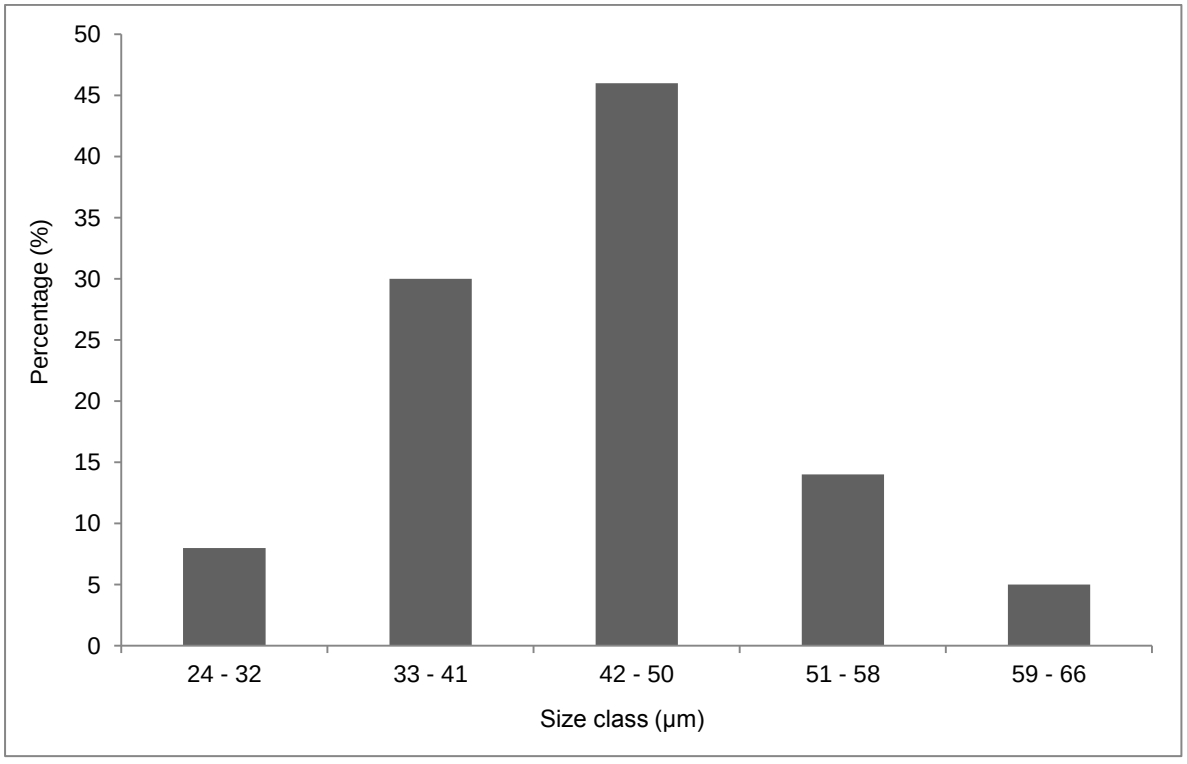

Figure 4.7 (b). Size class distribution of 105 *Nitzschia subcommunis* valves (15 – 50 µm based on Hustedt's [1949] classification), used to aid its identification.

between *Synedra acus*, *Synedra delicatissima* and *Synedra radians* (referred to as *Ulnaria acus*, *Ulnaria delicatissima* and *Fragilaria radians* in this research) (Fig. 4.8). Given the distinguishable morphological differences between *Fragilaria-Ulnaria* taxa in this study, it was decided by the author to base their classification on the varieties identified by Patrick and Reimer (1966), rather than amalgamate the valves and potentially loose palaeolimnological data (see Plates III and IV for photographs).

4.4.4 Photosynthetic Pigments

4.4.4.1 Ecology, Morphology and Distribution

Photosynthetic pigments are found in phototrophs for the purpose of light harvesting for photosynthesis, or for protection against damaging levels of light. In aquatic environments the pigments of photosynthetic organisms include chlorophylls (Chl), carotenoids (carotenes and xanthophylls), photoprotective compounds and their derivatives (isomers, allomers, epimers, pyrolysis products as well as pigment-specific structural modifications) (Leavitt and Hodgson 2001). Chlorophylls are magnesium coordination complexes made up of four pyrrole units cyclically arranged with an isocyclic ring (McGowan 2013). Carotenoids are larger compounds characterised by an aliphatic polyene chain comprised of eight isoprene (C_5H_8) units (McGowan 2013). They are produced by benthic and planktonic algal communities (Chl *a*, *b* and *c*), phototrophic bacteria (bacteriochlorophylls, Bchls), aquatic plants and macrophytes, and may also be present in detrital material which may become re-suspended or transported (Brown 1969; McGowan 2013).

The majority of pigments degrade rapidly in the water column (> 95 % of compounds, half-life of days) before reaching the sediment due to processes such as microbial oxidation, grazing by invertebrates, bacterial degradation, cell lysis and enzymatic metabolism during senescence (Leavitt and Hodgson 2001). Water column properties may cause additional degradation through variability in oxygen, light and heat concentration (as such, care should be taken during pigment handling and storage during analysis) (Leavitt 1993; Cuddington and Leavitt 1999). Pigment degradation is slower once in sediments, especially under anoxic conditions, but can be affected by light variability and invertebrate burrowing (Leavitt and Carpenter 1989). Degradation among pigments varies. Chlorophylls are easily broken down but

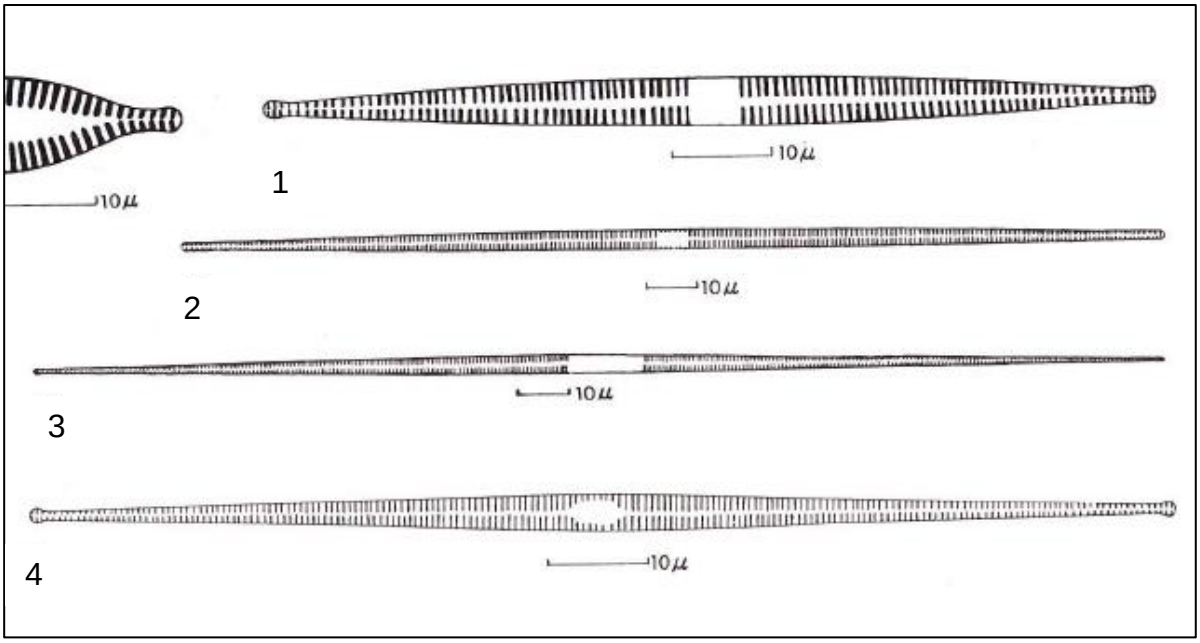

Figure 4.8. Patrick and Reimer's (1966) classification of (1) *Synedra acus* (*Ulnaria acus*), (2) *Synedra delicatissima* (*Ulnaria delicatissima*), (3) *Synedra delicatissima* var. *angustissima* and (4) *Synedra radians* (*Fragilaria radians*) (adapted from Patrick and Reimer 1966, Plate 5, pg. 172).

as they produce detectable breakdown products, they can be easily identified in sediment. Carotenoids in general are more stable. As a result, whilst pigments will record changes in the dominant algal groups, fossil records may be biased due to preferential deposition and differential degradation of certain pigments (additional bias is caused by standard algal monitoring techniques which rarely sample the entire water column) (McGowan 2013). The most favourable conditions for pigment preservation are those in a shallow, non-turbid lake, where pigments are buried rapidly (due to a smaller sinking depth), and removed from exposure to heat, light and oxygen.

If pigments can pass through these initial stages of deposition and once the morphological structures of the source photosynthetic organisms have disintegrated, the lipid-soluble chlorophylls, carotenoids and derivatives provide a signature of historical aquatic environments preserved in the sediment (water-soluble phycobilins are less commonly used due to poor preservation) (Leavitt and Hodgson 2001; McGowan 2013). As such, pigments make excellent biomarkers as they are: (1) widely distributed, due to being a fundamental component of all photosynthetic organisms; (2) being taxonomically affiliated with specific groupings of photosynthetic organisms (Table 4.4); (3) relatively simple to isolate and quantify using a variety of analytical techniques; and (4) persistent in the sedimentary environment under favourable conditions (McGowan 2013).

Since the identification and isolation of pigments in sediments during the early to mid-20th century, pigments have been used as a tool in palaeolimnological research (Fox 1944; Cook 1945; Vallentyne 1954). Early studies used pigments as a biomarker for former populations of phototrophic prokaryotes and as a measure for estimating historical changes in lake productivity (Fogg and Belcher 1961; Brown and Coleman 1963; Brown 1968). As analytical techniques, chemical identification methods, pigment taphonomy and determinations of compound distribution improved, the range for palaeolimnological applications expanded (Leavitt and Hodgson 2001). Fossil pigments are now used to quantify historical changes in algal and photosynthetic bacterial community composition (Yacobi et al. 1990), food-web interactions (Leavitt et al. 1994a; 1994b), lake acidification (Guilizzoni et al. 1992),

Table 4.4. Pigments commonly found in lake sediments and their taxonomic affinities, source (listed in order of quantitative importance, P: planktonic, L: littoral, T: terrestrial, S: sedimentary) and stability (1: most stable to 4: least stable) (adapted from Leavitt and Hodgson 2001; McGowan 2013).

Pigment	Affinity	Source	Stability
Chl *a*	All photosynthetic algae, higher plants	P, L	3
Chl *b*	Green algae, euglenophytes, higher plants	P, L	2
Chl *c*	Dinoflagellates, diatoms, chrysophytes	P, L	4
Bchls *a* and *b*	Purple sulfur and nonsulfur bacteria	-	-
Bchls *c*, *d* and *e*	Green sulfur bacteria	-	-
Pheophytin *a*	Chl *a* derivative	P, L, T, S	1
Pheophytin *b*	Chl *b* derivative	P, L, T, S	2
Pheophorbide *a*	Grazing, senescent diatoms	P, L, S	3
Pyro-pheo (pigments)	Derivatives of *a* and *b* phorbins	L, S	2
Steryl chlorin esters	Chlorophyll derivatives from grazing	-	-
β-carotene	Most algae and plants	P, L, S	1
α-carotene	Cryptophytes, prochlorophytes and rhodophytes	P, L	2
Alloxanthin	Cryptophytes	P	1
Fucoxanthin	Diatoms, prymnesiophytes,chrysophytes, raphidophytes, several dinoflagellates	P, L	2
Diadinoxanthin	Diatoms, dinoflagellates, prymnesiophytes, chrysophytes, raphidophytes, euglenophytes and cryptophytes	P, L, S	3
Diatoxanthin	Diatoms, dinoflagellates, chrysophytes	P, L, S	2
Peridinin	Dinoflagellates	P	4
Canthaxanthin	Colonial cyanobacteria, herbivore tissues	P, L	1
Echinenone	Colonial cyanobacteria	P, L	1
Myxoxanthophyll	Colonial cyanobacteria	P, L	2
Oscillaxanthin	Cyanobacteria (Oscillatoriaceae)	P, L	2
Scytonemin	Colonial cyanobacteria	L, P	-
Zeaxanthin	Cyanobacteria	P, L	1
Lutein	Green algae, euglenophytes, higher plants	P, L, T, S	1
Neoxanthin	Green algae, euglenophytes, higher plants	L	4
Violaxanthin	Green algae, euglenophytes, higher plants	L	4
Isorenieratene	Green sulfur bacteria	P	1
Okenone	Purple sulfur bacteria	P	1
Rhodopinal	Purple sulfur bacteria	-	-
Astaxanthin	Herbivore tissue, N-limited green algae	P, L	4

variation in salinity (Vinebrooke et al. 1998), changes in physical lake structure (Hodgson et al. 1998), mass fluxes within lakes (Ostrovsky and Yacobi 1999), UV radiation records (Leavitt et al. 1997; 1999), as well as primary productivity (Leavitt and Hodgson 2001; McGowan 2013). Pigments can also be used as indicators of

anthropogenic activities such as eutrophication (Lami et al. 1991; Bunting et al. 2007), fisheries management, land use practices, atmospheric deposition of contaminants (Guilizzoni et al. 1992; Vinebrooke et al. 2002) and climate change (Leavitt et al. 1994c; Hall et al. 1999; Leavitt and Hodgson 2001). The reliability of historical pigment reconstructions has likewise improved as understanding of pigment production, deposition and biogeochemistry has developed. Increasingly pigments are being used (independently or alongside additional proxies) for environmental reconstructions during the Holocene and the Pleistocene.

4.4.4.2 Pigment Based Studies in East Africa

The first intensive studies of pigments in East Africa were conducted by Talling (1965; 1966) who used short-term field experiments over varying time scales to study photosynthetic behaviour at Lakes Victoria, Albert, Edward, George, Bunyoni and Mulche (Uganda). Since then, pigments have been used extensively in lake monitoring across East Africa, either as an independent biomarker or in conjunction with other proxies in order to address phytoplankton composition and dynamics as well as improve understanding of the role and ecological significance pelagic algal communities play in limnetic systems and communities. Many of these studies have used algal pigments to measure contemporary changes in lake productivity.

Melack (1981) for example, conducted a survey of photosynthetic activity in four Kenyan soda lakes (Lakes Bogoria, Elmenteita, Simbi and Sonachi) over an 18 month period with the purpose of comparing and contrasting diurnal and monthly variability in photosynthetic activity, rates and phytoplankton abundance. Overall, it was found that the highest and most efficient photosynthetic rates in African soda lakes occur during blooms of cyanophytes (Melack 1981). Lake Sonachi was investigated again by Verschuren et al. (1999) in order to ascertain long-term controls on algal and invertebrate communities over the past 175 years in conjunction with documented lake level fluctuations and changes in the lake mixing regime (Verschuren 1999b). It was found that long-term changes in nutrient supply associated with vegetation succession in the catchment were responsible for successive phases in the ecological community (Verschuren et al. 1999).

At Lake Tanganyika, Descy et al. (2005) conducted a two year study (2002 – 2003) of chlorophyll and carotenoid pigments from several on- and off-shore stations to measure primary productivity as well as degradation processes over relatively short time periods (months, seasons, years). Whilst broadly similar to previous findings from the lake (Hecky and Kling 1981), Descy et al. (2005) concluded that high interannual variation and spatial heterogeneity of the phytoplankton may render it difficult to assess long-term changes in phytoplankton driven by climate change, in particular, warming lake temperatures. A parallel study was conducted at Lake Kivu by Sarmento et al. (2006) from 2002 – 2004. Wind patterns and water column stability were found to cause substantial interannual variability in algal biomass and assemblage composition, and it was concluded that based on the dominant phytoplankton functional groups, Lake Kivu was in an intermediate trophic position between the oligotrophic Lakes Tanganyika and Malawi and the eutrophic Lake Victoria (Sarmento et al. 2006).

At Lake Zeekoevlei in South Africa, pigments were used alongside stable isotopes ($\delta^{13}C$ and $\delta^{15}N$), rates of primary palaeo-productivity and total inorganic carbon (TIC) to investigate changes in plankton and macrophyte communities in response to anthropogenic activity (Das et al. 2009). The lake was transformed during the 20th century as it became a popular yachting destination and dams were established to maintain water level, causing it to become hyper-eutrophic. Cyanobacteria have since declined, though the hyper-eutrophic conditions continue. The lake is currently characterised by chlorophyll *a*, β-carotene, echinenone, fucoxanthin and zeaxanthin with seasonal blooms of cyanobacteria and diatoms (Das et al. 2009).

As well as contemporary studies, pigments have been used as a palaeo-tool for reconstructing past limnetic environments. At Lake Malawi, Castañeda et al. (2009) used algae and compound-specific carbon isotopes to examine past variations in algal community composition and primary productivity since the LGM. Mohammed et al. (2002) similarly used pigment analysis to assess primary productivity at three Ethiopian lakes (Lakes Langano, Abijata and Shala) during the late Holocene. However, the application of pigments as a palaeo-tool is limited and little is known regarding the effect of major hydrological fluctuations, such as those during the Quaternary, on algal ecosystems in East African lakes. It is not clear how lake

primary productivity was affected by changes in lake level, whether there were shifts in the dominant algal groups or what the effect was of changing surface temperatures or wind regimes on algal groups (Castañeda et al. 2009).

Understanding these dynamics in East African lake systems is important given the potential implications for organisms high in the food chain (i.e. fish and people). By assessing how the aquatic ecosystems were affected by historical periods of climate variability it may be possible to predict how lakes may respond to future episodes of climate change and therefore planning, mitigation and adaptation policies can be implemented.

4.4.4.3 Pigment Analysis

4.4.4.3.1 Pigment Extraction Pigments were extracted at the University of Nottingham, following standard methodology (Leavitt and Hodgson 2001; McGowan 2013). Approximately 200 mg of freeze-dried sediment were used per sample for analysis, to which 5 ml of extraction solvent was added. Samples were stored overnight in a freezer to extract. Samples were then filtered using a 0.22 µm lock-on syringe filter and dried with nitrogen. Dried samples were immediately capped and stored in a freezer in order to preserve pigments in an inert atmosphere. In preparation for high performance liquid chromatography (HPLC) analysis, a known measure of injection solvent was added to each dried sample and the dissolved extract transferred to the associated autosampler vial. Lighting was subdued at all times during the extraction process.

4.4.4.3.2 HPLC Analysis HPLC analysis was conducted at the University of Nottingham using the method prescribed by Chen et al. (2001) and an Agilent 1200 Series separation module with quaternary pump. Carotenoids and chlorophyll concentrations are quantified using reversed-phase HPLC (RP-HPLC) (Pfander and Riesen 1995; Jeffrey et al. 1999). Pigments are separated in a column of fine particles (< 10 µm) based on their differential attraction to the packing material (the non-polar stationary phase) and the solvents moving at high pressure (> 2000 kPa) through the column (the polar mobile phase) (Leavitt and Hodgson 2001; McGowan 2013). In RP-HPLC the stationary phase consists of a Thermo Scientific ODS Hypersil column (205 x 4.6 mm; 5 µm particle size) and the mobile phase of three

solvents: solvent A (80: 20, methanol: 0.5 M ammonium acetate), solvent B (9: 1, acetonitrile: water) and solvent C (ethyl acetate), modified from Chen et al. (2001). As the pigment mixture is introduced through the column, polar pigments will be more strongly attracted to the polar solvents and so pass through the HPLC column rapidly. They are the first compounds to be identified by the photo-diode array detector, which detects UV-visible spectral data every two seconds. Inversely, non-polar pigments are attracted to the non-polar packing and so are not re-dissolved in the mobile phase until its polarity is decreased by gradually altering the solvent composition, until their affinity for the mobile phase exceeds that of the stationary phase. Polarity is the prime driver in elution order as pigment compounds are released from the stationary phase (the retention time) (McGowan 2013). Once pigments have been eluted from the HPLC column, the compounds are scanned with a spectrophotometer at a wavelength of maximal pigment absorbance to produce a chromatogram (McGowan 2013). Some reversals in the chromatographic sequence may occur as a result of pigments co-eluting.

Whilst the criteria for HPLC at the University of Nottingham are stated above, there are a multitude of methods (e.g. saponification, phase partitioning), hardware, software, gradient systems and solvent mixes available for separating pigments. Methods will be optimised depending on the type of material from which pigments are to be extracted, the ultimate goal of the study, as well as investigator experience using a specific HPLC system (Leavitt and Hodgson 2001; McGowan 2013).

4.4.4.3.3 Pigment Identification Pigments were identified according to Jeffrey et al. (1997) and Roy et al. (2011) by comparing retention times and the absorption spectra of the chromatogram with an authentic standard under the same separation conditions.

4.4.5 X-ray Fluorescence (XRF) Spectrometry

X-ray fluorescence (XRF) analysis was performed on the sediment core at Aberystwyth University by Catherine Martin-Jones using the Itrax® core scanner. The method focuses an intense micro x-ray beam through a flat capillary waveguide onto the sedimentary surface. This irradiates the surface, causing it to emit secondary x-rays due to the photoelectric effect (Boyle 2001; Croudace et al. 2006);

the incoming x-rays eject electrons from inner atomic shells. This creates gaps which are filled by electrons falling back from the outer shells and the energy released is emitted as a secondary pulse of x-radiation (Weltje and Tjallingii 2008). The wavelength spectra are characteristic of the elements involved and are used to estimate their relative abundances (Boyle 2001). The rate of emission varies with the concentration of the elements present and the absorption of the outgoing x-rays by the sample. The Itrax® core scanner collects high-resolution, near continuous elemental profiles as well as optical and x-radiographic images. The advantage of the method is that continuous, high-resolution data can be obtained very rapidly in a non-destructive manner.

Following the standard procedure described by Croudace et al. (2006), the sub-drives were loaded into the horizontal cradle (< 1.8 m per scan). The Core Scanner Navigator programme was then used to define the analytical parameters of the scan. This included setting the length of the core to be scanned, the voltage and current to the x-ray tube (30 mA and 30 kv with a 10 second exposure time) and measuring the topographic surface scan of the core to ensure that no contact between the XRF detector and sediment surface occurs. The Q-Spec programme was used to define the likely elements in the core sample and then refine the elemental peak area to get the best spectral fit. The Core Scanner Navigator programme was used to calibrate the x-ray line camera diode and record a reference response for the x-ray detector before finally setting the x-ray and XRF exposure time. All the sub-cores were scanned at 200 µm intervals. After scanning samples were re-sealed and returned the refrigerator for storage.

4.5 Chronological Analysis

4.5.1 Dating Macrofossils

Prior to bulk samples being sent for analysis, sediment was sampled for planned dating using terrestrial macrofossils (e.g. twigs, leaves of deciduous trees, conifer needles, insect remains) or macrocharcoal. Multiple 1 cm thick sediment samples were taken from varying depths in one of the repeat drives and sieved through a 250 µm, 125 µm and 63 µm mesh size with deionised water. The residues were transferred to petri-dishes and observed under a Leica dissecting microscope (x 10 – 50 magnification) with the intention of picking out samples to be used for obtaining

dates. However, upon observation none of the residues contained appropriate samples and so it was concluded that bulk dates would suffice.

4.5.2 AMS ^{14}C Analyses

Fourteen bulk sediment samples were extracted from core Hayk-01-2010 for accelerator mass spectrometry (AMS) ^{14}C dates. Nine were sent to the ^{14}CHRONO Centres' radiocarbon dating laboratory at Queens University Belfast, and five to the Oxford Radiocarbon Accelerator Unit (ORAU) at the University of Oxford.

Samples were treated following standard techniques (Reimer 2014 pers. comm.); bulk sediment sample were treated with hydrochloric acid (HCl, 4 %) and digested (two hours at 80 ºC) to remove any carbonates, before being washed with deionized water. Samples were dried overnight (60 ºC), weighed into a pre-combusted quartz tube with an excess of copper oxide (CuO), sealed and combusted to carbon dioxide (CO_2). Samples were converted to graphite on an iron catalyst using the zinc reduction method (graphitization reaction) (Slota et al. 1987) and the $^{14}C/^{12}C$ and $^{13}C/^{12}C$ ratios then measured by AMS. The sample $^{14}C/^{12}C$ ratio was corrected and normalised to the HOXII standard (SRM-4990C; National Institute of Standards and Technology). The radiocarbon ages were corrected for isotope fractionation using the $\delta^{13}C$ measured by AMS, which accounts for both natural and machine fractionation. The radiocarbon age and one standard deviation were calculated using the Libby half-life of 5568 years (Stuiver and Polach 1977).

Results were reported as conventional radiocarbon years before present (yr BP) relative to AD 1950 and calibrated using the CALIB Rev 7.0.2 programme (Stuiver and Polach 1977; Stuiver and Reimer 1986; 1993). In order to provide the maximum degree of model flexibility, an age-depth model was constructed by J. Tyler (University of Adelaide) based on a 0.4 span smooth spline interpolation using the programme CLAM for R (Blaauw 2010; Tyler 2015 pers. comm.).

4.6 Numerical Analyses

4.6.1 Statistical Zonation of Diatom and Pigment Datasets

Assemblage zones reflecting distinctive natural groupings were determined for the stratigraphical diatom data using the optimal sum of squares partitioning method

(Birks and Gordon 1985) in the programme PsimPoll 4.27 (Bennett 1995 – 2007). Statistically significant splits were identified using a broken-stick model (Bennett 1996). Pigment abundances were zoned using the same method after being normalised using a log (x + 1) transformation. Optional splits (i.e. those not deemed statistically significant by the broken-stick model) have been included in some diagrams as additional sub-zones in order to ease interpretation.

4.6.2 Ordination Analyses

Exploratory analysis of the diatom and pigment data was carried out in the programme CANOCO version 4.5 (ter Braak and Šmilauer 2002). The ordination technique, detrended correspondence analysis (DCA), was applied to reveal the major patterns between diatom species (percentage data) and depths (hereafter, samples) (Correspondence Analysis [CA] revealed an arch in the data and so was deemed inappropriate for use). Detrending was by segments and species data was log transformed in order to reduce high species abundance values skewing the ordination distribution. Rare species were down-weighted and samples with < 50 valves were omitted. The gradient length of axis one was used to determine whether unimodal or linear ordination techniques were most appropriate; DCA was deemed the most appropriate method as the gradient length of axis 1 exceeded 2 standard deviations (SD) and so no other ordination techniques were applied. The linear ordination technique, principle components analysis (PCA), was applied to the pigment data. Species (pigment concentration data) and samples were centred and species data were log transformed. Ordination plots of axes one and two were produced in CanoDraw (ter Braak and Šmilauer 2002).

4.6.3 Quantitative Reconstructions

Diatoms analysis is one of the most successfully applied and powerful tools used in palaeolimnology for understanding climatic and environmental change recorded in lake sediments. By calibrating the modern day distribution of diatom species (found in surface sediment samples representing the most recent years of sediment accumulation) against a known environmental variable/gradient, it is possible to infer palaeoenvironmental changes in fossil diatom assemblages (Gasse et al. 1995; Battarbee et al. 2001; Mills and Ryves 2012; Juggins 2013). Clear correlations have been made between diatom species composition and a range of physical variables,

including water temperature (Weckström et al. 1997a; 1997b) and water depth (Brugam et al. 1998; Stone and Fritz 2004; Wolin and Stone 2010), as well as hydrochemical variables, such as pH (Gasse and Tekaia 1983; Birks et al. 1990), salinity (Cumming and Smol 1993; Reed 1998a; Davies et al. 2002), ionic composition (Gasse et al. 1983; Fritz et al. 1993) and nutrient content (Bradshaw et al. 2002), in a range of lake types around the world. However, the relationship between diatoms and some environmental variables is better understood than others (Chapter 3, 3.2) and so the robustness and sensitivity of reconstructions can vary (Verschuren 2003). Telford and Birks (2011) for example, identified that uneven sampling of an environment gradient can bias transfer function performance as the part of the gradient with more observations will have precise estimates of species optimal conditions, as well as more analogues, in contrast to the part of the gradient with fewer samples. Conductivity (salinity) is a particularly robust variable and is widely use in transfer functions. The relationship between diatoms and conductivity is well understood, as is the response by lakes to climate variability, expressed through changes in water volume and salt concentration (Gasse et al. 1995; Gasse et al. 1997; Battarbee 2000; Mills and Ryves 2012). As such, conductivity can be successfully used in a transfer function in climatically sensitive lakes. Lake Hayq is a closed basin (although it may have been an open system at times during the late Quaternary given the presence of palaeochannels between the waterbody and Lake Hardibo) known to have experienced historical changes in water depth and lake volume in response to climate variability, evidenced recently by the connection of the Istifanos monastrey island to the shore. It is likely therefore that a conductivity transfer function may be successfully applied to the fossil diatom record from Hayk-01-2010 in order to infer palaeoclimatic variability.

Modern calibration (training) sets for Africa (and Europe) have been established on the European Diatom Database (EDDI; http://craticula.ncl.ac.uk/Eddi/jsp/) by combining and harmonising data from a series of smaller datasets to create a database of diatom training sets and transfer functions. The African dataset is a merger of the harmonised North African and East African datasets. It comprises 284 samples, which were collected from 1960 – 1986 (EDDI 2015a). Countries sampled include Algeria, Tunisia, Morocco and Niger in North Africa, and Djibouti, Ethiopia, Kenya, Malawi, Niger, Rwanda, Tanzania, Uganda and Zaire in East Africa. Sites

vary from hypersaline lakes located below sea level to afro-alpine bogs at 4000 m altitude, hydrothermal springs to small artificial ponds. Site conductivities range from 40 – 400,000 µS cm^{-1} and pH from 5.5 – 10.9. Diatoms were counted and described by Ben Khelifa (1989) and Gasse (1986). A total of 604 taxa were identified. Environmental data include alkalinity, calcium, chloride, conductivity, magnesium, pH, potassium, salinity, silica, sodium, sulphate and total phosphorus.

The East African conductivity transfer function and model has been applied to diatom sequences to reconstruct hydrological histories (Barker et al. 2002; Chalié and Gasse 2002a; Stager et al. 2009; 2011). A regional training set has also been developed for west Ugandan crater lakes by Mills and Ryves (2012) to improve the accuracy of palaeo-conductivity reconstructions compared to the larger East African training sets. In total, 64 surface sediment samples were collected (although only 58 samples contained diatoms) from 56 crater lakes in western Uganda along with water chemistry data. In order to bridge the gap between fresh and hypersaline lakes and improve the representation of key diatom taxa found in fossil assemblages, eighteen additional lake sites (with salinities of 1,050 – 16,300 µS cm^{-1}) were integrated into the dataset from the EDDI East African training set.

Inferred changes in climate and environment using modern training sets and fossil diatom assemblages are based on several assumptions: (1) the diatom taxa in the modern training set are connected in some way to the environment they live in; (2) the environmental variable to be reconstructed is an important ecological determinant in the system of interest; (3) the diatom taxa is the same biologically in the modern calibration set as it is in the fossil assemblage, and its ecological response to the environmental variable of interest has not changed over time; (4) the mathematical methods applied, sufficiently model the biological response of the diatom taxa to the environmental variable of interest and allow for unbiased, accurate reconstructions; (5) other environmental variables that are not of interest have a insignificant influence on reconstructions (Juggins 2013). Therefore, where a diatom assemblage demonstrates a strong response to an environmental gradient (e.g. freshwater to saline, alkaline to acidic transitions), a transfer function can be created (Birks 1998). This requires regression (where modern diatom assemblage response to the variable of interest are modelled) and calibration (where modelled

responses are used to infer past variable levels from the fossil assemblage composition). The training set should encompass a range of sites from the geographical region of interest, which span the limnological gradient of the variable in question. Based on the distribution of taxa preserved in the surface sediments of the training set lakes, regression techniques can be applied in order to quantify the response of each diatom taxa to the environmental variable of interest (Gasse et al. 1995; Fritz et al. 2010).

The development of numerical techniques has allowed the relationship between diatom assemblages and environmental variables to be successfully quantified and resolved. However, limitations have been identified in reconstructing particular variables, such as temperature (Anderson 2000; Battarbee et al. 2002), in application to certain systems such as shallow lakes (Sayer 2001), or with particular training set design or other spatially dependent calibrations (Cwynar et al. 2012). Juggins (2013) argues that whilst such quantitative reconstructions are useful for simplifying the complex, multivariate relationships between taxa and their environment, the fundamental assumption on which reconstructions are based (that the relationships between taxa and their environment which are embodied in the model coefficients do not vary in time and space) are often violated, which may result in confounding effects in some variables and possibly hidden or misleading reconstructions. To limit such problems, Juggins (2013) recommends: (1) better understanding of the causal relationship between the environmental variable and the taxa of interest, and avoid reconstructing variables that are acting as surrogates for other underlying aspects; (2) stating the relative explanatory power of a variable in the training set and avoid using variables with low values; (3) avoid using automated procedures for identifying which variables can be reconstructed; (4) recognise that reconstructions of variables that account for only a small fraction of the variance in the diatom assemblage are problematic and are most likely affected by secondary variables; (5) collaborate, use and compare training sets from different provinces. When given due attention, such issues can be resolved effectively and quantitative reconstructions performed successfully to interpret the ecological signal in lake sediments.

4.6.4 Quantitative Reconstructions of Salinity using a Transfer Function

Transfer function development was carried out in the programme C2 version 1.7.2 (Juggins 2007) by merging the EDDI combined African dataset with selected European sites from the combined TP (total phosphorus) dataset. This was done in order to ensure the validity of the model by including all taxa, including *Cyclotella ocellata*. This taxon was found to dominate (41.5 – 100.0 %) the fossil assemblage at certain intervals but is poorly represented in the combined African training set, being present in only 10.9 % of samples (Gasse et al. 1995). The taxon does not exceed 2.6 % abundance in 93.5 % of these samples. The two samples where it reaches its greatest abundances are a plankton sample from the Medjerda Channel, Tunisia (8.5 %, 1,574.0 µS cm^{-1}) and a rock-scrap sample from Lake Aguelmane Azigza, Morocco (8.3 %, 410.0 µS cm^{-1}). Few of the samples originate from freshwater (minimum of 115.0 µS cm^{-1}, Diffa, Niger) and most are from high-salinity lakes (maximum of 47,680.0 µS cm^{-1}, Bara, Niger).

As such, the optimum and tolerance of *Cyclotella ocellata* is known to bias transfer functions reconstructing African water conductivity as the modern samples it is present in are mostly from high-salinity lakes (mean of 11,865.0 µS cm^{-1}) (Chalié and Gasse 2002b; Marshall et al. 2009). In contrast, the European samples where it reaches its optimum development (maximum of 68.4 % at Dittligsee, Switzerland) have significantly lower conductivities (mean of 286.1 µS cm^{-1}, optimum of ~ 390.0 µS cm^{-1}) (Fig. 4.9). Therefore, where quantitative interpretations of fossil assemblages in which *Cyclotella ocellata* is present are made, caution should be aired (Chalié and Gasse 2002b; Marshall et al. 2009).

In order to compensate for this inherent bias in the African training set, a new training set was developed that would increase the coverage of the conductivity gradient for *Cyclotella ocellata*, reducing the ecological gap in the training set, and therefore improving the modelled response. This involved identifying the closest modern analogues for *Cyclotella ocellata* and combining them with the African training set. Prior to the transfer function development, the complete (733.0 – 0.5 cm) fossil dataset (as percentages) was verified against the combined African training set and the *Cyclotella ocellata* dominated interval (678.0 – 429.0 cm) against the combined TP training set to check for miscoding, mismatching and possible no

analogue situations. The Modern Analogue Technique (MAT) was then applied to identify the mean or weighted mean of the closest five analogues for each fossil sample. For the complete fossil dataset, 76.26 % of the closest analogues were derived from the East African training set and 18.49 % from the North African training set. As such it was decided to use the combined African training set. For the *Cyclotella ocellata* interval, sites occurring as the nearest analogue ten or more times were selected for inclusion in the transfer function. In total, twelve European sites were selected as the closest analogues, accounting for 68.78 % of the nearest analogues (Table 4.5). Not all analogues contained *Cyclotella ocellata* due to the presence of other diatom species in the section of interest, but the taxon retained high abundances in those that it did. It was deemed that the analogues selected for inclusion appropriately represented the diversity of taxa found in the *Cyclotella ocellata* interval (678.0 – 429.0 cm).

A new training set ('Combined Africa & Europe') was created by combining species and environmental (conductivity) data from the African training set with the twelve European sites, as well as deleting thirty-one samples from the African training set that contained *Cyclotella ocellata*; the new training set comprised 251 sites and 852 species. Two models were created in order to compare and evaluate their performance; one using Weighted Averaging Partial Least Squares (WA-PLS) and one using Weighted Averaging (WA). Both were cross validated using the bootstrapping technique (10,000 cycles). The predictive power of the WA-PLS model was evaluated by assessing the root mean squared error of prediction (RMSEP) scores for components 1 – 5. RMSEP did not improve with increasing complexity and so the model was not used. Both classical and inverse deshrinking were performed using WA (Table 4.6). A comparison of the RMSEP scores found that WA inverse deshrinking performed best (RMSEP – 0.466). The model was assessed further based on reconstruction diagnostics; minimum distance to the closest modern analogue, the sample sum in fossil data and the sample standard error of conductivity bootstrap estimates by WA inverse deshrinking. The minimum distance to the closest modern analogue averaged 47.7, whilst the mean sample sum in fossil data was 96.6 indicating a very high degree of matching between the fossil and training set data. Sample standard error was generally low, ranging from 1.1 – 2.4

Table 4.5. The twelve closest analogue matches from the combined TP training set for fossil samples within the *Cyclotella ocellata* interval (678.0 – 429.0 cm).

Site name	Country	Site code	Occurrences in MAT	Max. depth (m)	Conductivity (µS cm^{-1})	*C. ocellata* presence (%)
Dittligsee	Switzerland	CH019	42 (10.42 %)	16.5	564.8	68.4
Lago di Endine	Switzerland	CH021	42 (10.42 %)	8.0	353.7	66.2
Gerzensee	Switzerland	CH026	40 (9.76 %)	10.0	448.0	57.4
Lac de Bret	Switzerland	CH014	42 (10.24 %)	18.0	356.8	54.2
Unterer Chatzensee	Switzerland	CH017	42 (10.24 %)	7.8	318.0	53.8
Öschlesee	Germany	CEUR056	12 (2.93 %)	15.0	435.0	0.2
Lac de l'Esclauze	France	FRO12	10 (2.44 %)	4.0	57.0	0.2
Wannisbordsee	Switzerland	CH076	12 (2.93 %)	14.0	20.5	-
Lago di Annone (east)	Italy	CEUR006	10 (2.44 %)	11.3	344.0	-
Niedersonthofener See	Germany	CEUR054	10 (2.44 %)	21.0	315.0	-
Lac Tanay	Switzerland	CH070	10 (2.44 %)	31.0	170.0	-
Tullybrick Lough	UK	NI029	10 (2.44 %)	11.2	454.3	-

µS cm^{-1}. It was concluded that this newly developed training set would therefore be appropriate for use on all fossil samples identified in Hayk-01-2010.

4.7 Conclusion

The range of proxies and laboratory methods used in this research will provide a quantitative and qualitative reconstruction of palaeolimnological variability in Lake Hayq during the late Pleistocene and Holocene, from which local climatic and environmental changes can be made. By using a combination of biological, geochemical and elemental proxies, inferences can be independently made and verified, giving strength to the overall interpretation of the record. Consideration has been given to the use of numerical analyses and quantitative reconstructions, in order to maintain accuracy and produce precise, unbiased data. The information

obtained will be used not only to indicate changes in the Lake Hayq basin, but also to allow for comparison to other palaeolimnological records at a range of temporal scales from Ethiopia and the wider region of East Africa.

Table 4.6. Performance statistics for Weighted Averaging showing, (a) codes and names, (b) performance statistics.

(a)

Code	Name
WA_Inv	Weighted averaging model (inverse deshrinking) for Cond
WA_Cla	Weighted averaging model (classical deshrinking) for Cond
WATOL_Inv	Weighted averaging model (tolerance downweighted, inverse deshrinking) for Cond
WATOL_Cla	Weighted averaging model (tolerance downweighted, classical deshrinking) for Cond
RMSE	Root mean squared error for the training set (apparent RMSE)
R2	Squared correlation between inferred and observed values
Ave_Bias	Average bias in residuals
Max_Bias	Maximum bias in residuals
Boot_R2	Squared correlation between bootstrap predicted and observed values
Boot_Ave_Bias	Average bias in bootstrap residuals
Boot_Max_Bias	Maximum bias in bootstrap residuals
RMSE_s1	Root mean squared error of prediction s1(bootstrap RMSEP)
RMSE_s2	Root mean squared error of prediction s2 (bootstrap RMSEP)
RMSEP	Root mean squared error of prediction (s1 + s2) (bootstrap RMSEP)
%Change	% Reduction in RMSEP
Rand. t-test	Randomisation t-test significance

(b)

Code	RMSE	R2	Ave_Bias	Max_Bias	Boot_R2	Boot_Ave_Bias	Boot_Max_Bias	RMSE_s1	RMSE_s2	RMSEP	%Change	Rand. t-test
WA_Inv	0.35441	0.842619	1.57E-15	0.47717	0.753859	0.025772	1.31888	0.135622	0.445923	0.466091		
WA_Cla	0.386092	0.842619	8.06E-16	0.295902	0.754579	0.029753	1.11323	0.156394	0.449966	0.47637	-2.20544	0.729
WATOL_Inv	0.288975	0.895369	1.35E-15	0.453019	0.768461	0.052249	1.45284	0.228946	0.435889	0.492357		
WATOL_Cla	0.305393	0.895369	1.16E-15	0.336785	0.768879	0.056559	1.3541	0.248143	0.433403	0.499413	-1.43297	0.245

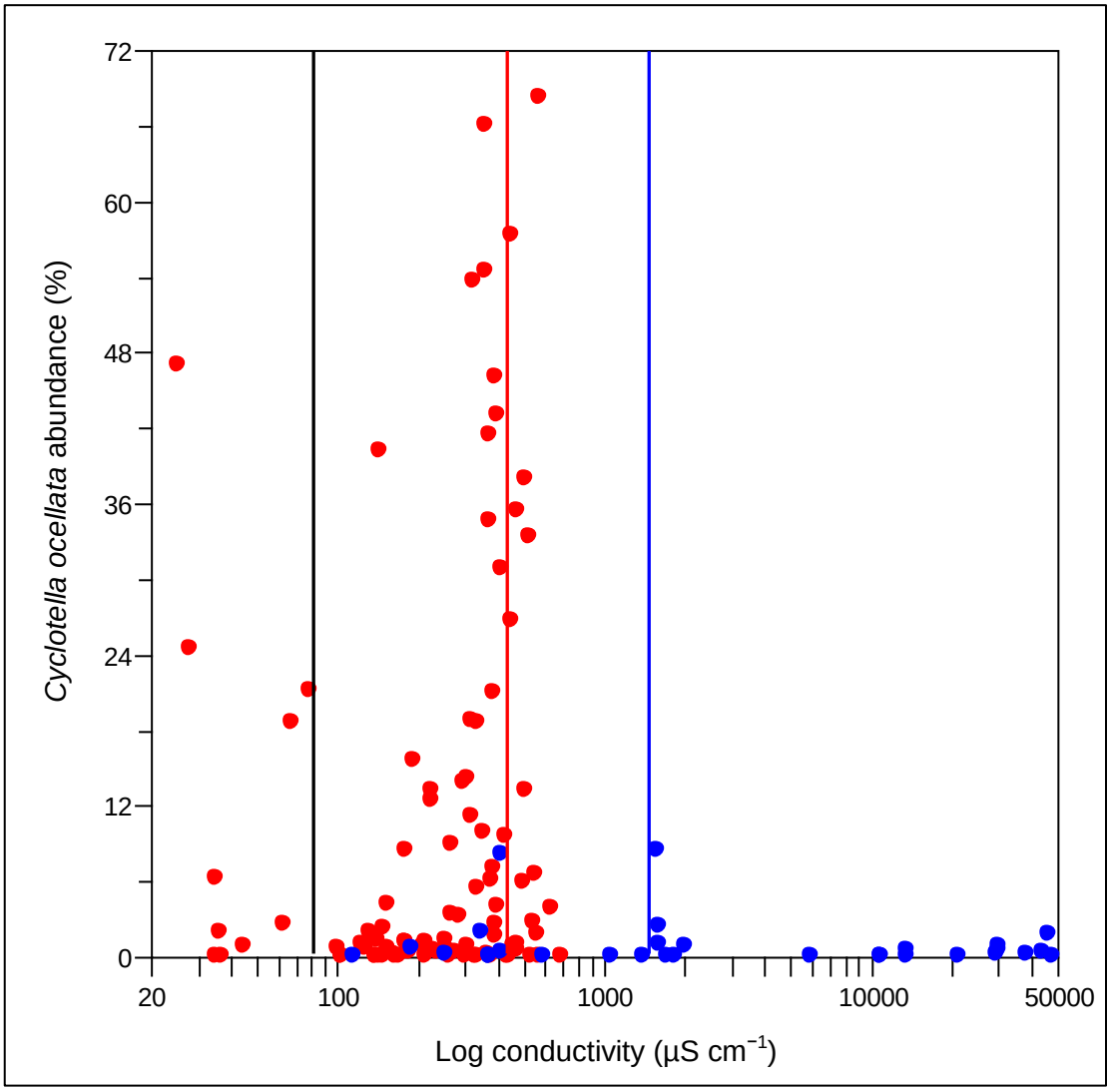

Figure 4.9. *Cyclotella ocellata* abundance (%) and log conductivity (µS cm^{-1}) of the thirty-one samples from the combined African training set (blue circles) and ninety-eight samples from the combined TP training set (red circles) containing the taxon. Optimum conductivity values are indicated for the African training set (blue line), the 12 European analogue sites (red line) and for the combined training set (black line).

Chapter 5

A Planned Study of Holocene Climate in the Gamo-Gofa Highlands.

5.1 Introduction

Originally this PhD project planned to reconstruct Holocene climate and environmental change in the south-west Gamo-Gofa[13] highlands of Ethiopia. The region has been the focus of ethnographic and archaeological research investigating the evolution of the caste system among the indigenous Gamo people during the mid- to late Holocene and is currently the focus of a NSF funded project. Several lakes, including Lakes Chamo and Abaya, lie within close proximity to important archaeological sites under investigation in the area. The intention of the project was to collect new core material from a lake in the region and employ palaeolimnological techniques (physical analysis, chronological methods and diatom analysis) to provide an environmental context for the archaeological research being conducted. The project was in collaboration with Dr Robert Marchant (Department of Environment, University of York) and Drs John and Kathy Arthur (Department of Anthropology, Interdisciplinary Studies and Criminology, University of South Florida).

Field work was undertaken in the summer of 2012 at a small lake, Done Ella[14], approximately 19 km west of Lake Abaya, and a 7 m sediment sequence recovered. Preliminary diatom analysis the following October at Loughborough University found that diatoms were irregularly present in the top ~ 30 cm of sediment only and absent below this depth. As a result it was decided to abandon the project for the purpose of this PhD research (though chronological and XRF analyses continued at other institutions). Despite no longer being the focus of research, this short chapter has been included detailing the work that was carried out at Done Ella, as despite the sparseness of diatoms, this in itself is a finding and is worthy of documenting for future research efforts in the region. The cultural history of the Gamo-Gofa province shall be considered first, followed by a description of the lake based on field observations. The methods employed and findings are then discussed.

[13] The Gamo-Gofa province is now, with some boundary changes, known as the North Omo Zone. It is still referred to as Gamo-Gofa in much of the literature and as such it shall be referred to as so in this chapter.

[14] 'Done Ella' is the local name for the lake. It is also known as Lake Abysaa but shall be referred to as Done Ella from here on in.

5.2 Cultural History and Ethnoarchaeology

Excavations at the Mochena Borago Rockshelter indicate the south-west highlands have been occupied by hunter-gatherers since ~ 53.0 – 38.0 kyr BP (Brandt et al. 2012). Since then the hunter-gatherers have developed to become the Gamo (meaning lion); a complex and dynamic mix of ~ 1,104,400 people living in approximately forty societies across the southern highlands of Ethiopia (CSA 2007a). The Gamo live by a complex caste system used to ensure the survival of their community by upholding the wishes of their ancestors' wills. The Gamo divide themselves into groups based on occupation which is determined at birth by patrilineal kinship; a child will belong to the same caste as their father and shall only marry within the same caste (Asante 2009). Birth into a caste is therefore considered destiny. Occupations include *mala* (farmers, smiths and weavers), *tsoma chinasha* (potters and ironsmiths), *tsoma mana* (potters) and *tsoma degala* (hide workers, smiths, ground-stone makers) (Weedman Arthur et al. 2009). The *mala* are considered the most prestigious and powerful in terms of hierarchal status as their occupation is considered sacred, pure (as they work with, and produce, raw products such as grain and milk) and fundamental to life. The artisans in contrast are less pure than the *mala* and therefore not considered full members of Gamo society. As such they do not participate in community assemblies, have no political rights and cannot be elected to positions of authority (Weedman 2006). They are still perceived as important members of Gamo society however and often have mediating roles such as messengers and healers. Communication and interactions between the *mala* and artisans is often restricted due to perceptions of impurity and pollution (Weedman Arthur et al. 2009). This system is used to orchestrate Gamo society, determining wealth, status and access to materials and resources.

Access to agricultural land serves as an extension of the caste system used to determine wealth, position within the tribe, ability to perform cultural practices and role in political and economic matters. Common crops in the Gamo region include maize, the tree cabbage, sorghum, barley, potatoes, chickpeas, horse beans and the 'false banana' plant, *enset*. Animal husbandry is also a crucial aspect of agricultural practices. Access to land is based on six historical characteristics (Olmstead 1973): (1) Land is restricted to males only. Females are reliant on males (their father, husband or brothers) for their economic and ritual needs; (2) Access is only

permitted to Gamo citizens. This has changed during the course of the 20th century due to the Ethiopian political system which now allows non-citizens, women and ex-slaves to access land; (3) Sharecropping is permitted on a temporary basis; (4) Permanent transfers of land are legal; (5) Land is unambiguously assigned to an individual and that individual shall have the right to that land throughout their lifetime unless they decide to relinquish it. Ownership of the land also encompasses a ritual connection which allows the owner to make sacrifices, place curses and engage in sexual relationships on his land only. To do so on another mans' land would breach the rules of taboo; (6) Inheritance of land may be divided among heirs. These rigid rules maintain division between the *mala* and artisans, citizens and non-citizens.

The religion of the Gamo is based on the philosophy of their ancestors (Asante 2009). The head of the village or village elder is known as the *cbima* and it is he who guides the village (*kebele*) along the path of order, harmony and balance that equate to the good behaviour (*woga*) prescribed by their ancestors. When behaviour prohibited by the moral and cultural rules occurs (*goma*) it is believed to bring suffering to the *kebele* by breaching the rules of taboo (*gome*). The *cbima* will perform sacrifices in the spirit house (*tsosa'ketsa*) to appease the ancestors for the sake of the villagers. Only someone belonging to the *mala* can perform this ritual, not an artisan. The artisans can only perform rites of passage on an individual level, for example, healing rites or circumcisions.

Understanding this caste system is essential for interpreting archaeological findings as the *mala* and artisans will have separate housing locations, material artefacts and burial grounds. It will also inform research as to how long such a system has been in place in Gamo culture, including when social divisions occurred and structures were put in place. As such, excavations of sites and successfully identifying to which caste an archaeological artefact belongs can reveal details of socioeconomic status, marital status, cultural beliefs, traditions, ceremonies and practices in historical Gamo societies.

Recent ethnoarchaeological studies in the Gamo highlands have tended to focus on craft specialisms such as middle Palaeolithic (100,000 – 40,000 years BP) stone tool hafting and ceramics (Weedman 2006). For example, the morphology and

distribution of hide worker tools act as a useful indicator of social status in Gamo culture (Weedman 2006). The type and material of a tool handle and its decoration may reflect political and economic change, ethnic relationships, marriages, friendships, ethnic identify, language and ties to other Gamo regions. For example, the Gamo use *zucano* and *tutuma* type handles. Both are known currently and historically to other central and southern Ethiopian cultures and their presence in Gamo society is an indication of past social networks, geographical positions, migrations and regional identity. Political affiliations have also been evidenced through tool handle type. When the regional capital moved from the central Gamo highlands to the south at the end of the 20th century, the *tutuma* handle became more widespread, signalling the change in political and economic affiliation. Only those with strong ties to the north continued to use the *zucano* handle type. Therefore tools and their morphology can be seen as a material manifestation of changing social, cultural, political and economic boundaries (Weedman 2006). They are not just a product of the environment and available resources, but are markers of social identify, twinned with cultural, social and geographic divisions (Weedman 2000).

Pottery, beer fermentation and food in Gamo society is another example of how archaeologists have been able to document and interpret past social and economic status through material culture (Arthur 2002; 2003). Only wealthier households could afford to grow additional grains to make beer and purchase the large beer jars to store it. In addition to beer, wealthier households also owned more land and cattle enabling them to produce and eat luxury foods containing grain and animal by-products such as milk and butter, which require larger, more expensive jars for storage. The vessels used for beer and luxury food storage also contain a higher degree of attrition in their surfaces than those of poorer households due to the cultural practice of not washing the vessel after food preparation. Poor households would not be able to afford beer, luxury foods or the jars for storage. Pottery assemblages and their surface attrition is therefore an exceptional indicator of household socioeconomic status, allowing archaeologists to interpret Gamo wealth variations (Arthur 2002; 2003).

Gamo society and culture are therefore complex and dynamic institutions based on historical concepts of patrilineal-endogamous ancestry. These concepts, alongside religious beliefs, are used to orchestrate and divide the Gamo into a very specific hierarchy which governs every aspect of Gamo life. Ethnoarchaeology is a useful tool for understanding and interpreting archaeological findings in the region by inferring that ancient societies used the same techniques as their modern counterparts. As such, historical understandings of the Gamo people are continually being improved upon and new archaeological findings are being made.

5.3 Study Site: Done Ella

Done Ella is located in the Main Ethiopian Rift, ~ 19 km west of Lake Abaya in the Gamo-Gofa highlands (~ 3000 m altitude) in the Southern Nations, Nationalities and People's Region (SNNPR) administrative province (6°15'32.93"N, 37°39'48.05"E, 2005 m altitude) (Fig. 3.1 [b], site 37 and Fig. 5.1). The lake is approximately 200 km south of the Ziway-Shala basin, 340 km south of Addis Ababa and 28 km north-west of Arba Minch, the provincial capital of the region. No literature has been published on the lake at present so all of the following observations were made in the field.

5.3.1 Climate

The climate of southern Ethiopia has been described in detail in Chapter 2. Based on the assessment made by Friis et al. (2011), Done Ella sits in a complex area where the boundaries of the biomodal and unimodal rainfall patterns meet. Climate data are available from a meteorological station at Arba Minch (National Meteorology Agency 2014). The region has a single rainy season from April to September. Most rainfall occurs in July and August, reaching around 240 mm per month. From November to March less than 25 mm may fall per month. The mean minimum temperature does not fluctuate substantially during the year (14 – 16 °C). Mean maximum temperature in contrast shows greater seasonal fluctuations, ranging from 24 – 25 °C from June to September and 28 – 32 °C from November to March.

5.3.2 Land Cover

The lake shores and surrounding highlands are intensively cultivated and include terracing and ploughing. Common crops in the Gamo-Gofa highlands include maize, sorghum, peas, beans, potatoes and cabbage. *Enset* is also an important crop

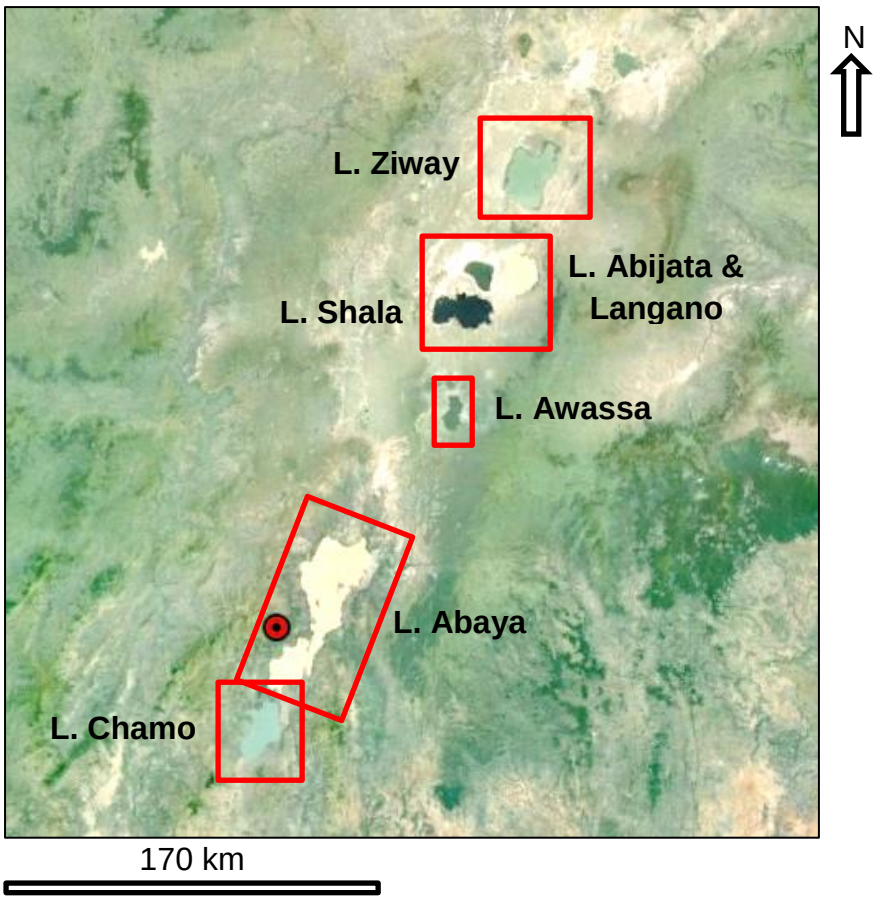

Figure 5.1. Location of Done Ella (red circle) in the Main Ethiopian Rift (Google Earth 2013d). Nearby lakes are indicated.

grown in the region. There were no large herds of grazing livestock around the lake. Natural vegetation occurs in pockets on steeper slopes in the Done Ella basin. This includes *Acacia-Commiphora* woodland and bushland and *Combretum-Terminalia* woodland and wooded grassland (Friis et al. 2011).

5.3.3 Hydrology and Limnology

Done Ella sits in a steep sided basin formed in Quaternary extrusive and intrusive rock formations (Fig. 5.2). Inflow comes from one small stream and outflow from another small stream at the northern end of the lake. It is a shallow lake with an average depth (based on multiple GPS echo sounder measurements from around the lake) of 5.0 m. The maximum lake depth recorded was 5.7 m using a GPS echo sounder. At the centre of the lake, the photic-pelagic zone is very shallow, < 0.5 m deep, due to a dense mat of a species of *Myriophyllum*. An area of open water encircles the area of *Myriophyllum* species. The littoral zone is characterised by the water lily, *Nymphaea* species, tall grasses and *Cyperus* reeds (Fig. 5.3). A marsh area exists around the lake margin.

The lake has experienced historical fluctuations in water level. A palaeo-shoreline is evident in the slopes around the lake indicating the water level was significantly higher and considerably deeper (estimated as > 10 m deeper) than present at some point in history (Fig. 5.4). Anecdotal evidence of higher lake levels was also obtained; around the edge of the lake several buildings were abandoned when the water level began to rise. All that remains now of the buildings are the impression of the foundations in the ground (Fig. 5.5). Whilst it was not clear exactly when this event happened, it did occur during the lifetime of the tribal elders in the village, so potentially within the last 60 – 70 years. It was believed by the villagers that the rise in lake level, which caused the buildings to be abandoned, was punishment for prohibited behaviour. The lake level has since declined and the foundations now lay in a marsh area.

The lake is not used recreationally or for fishing by the local people living in the small village around the lake. As a result it was difficult to establish what animal species, if any, lived in and around the lake. No fish were observed during field sampling and only a few water birds such as stalk and ibis were seen.

(a)

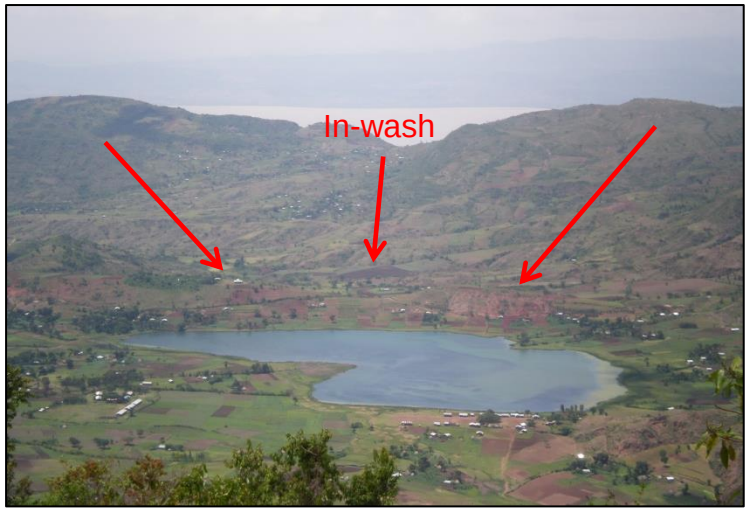

(b)

(c)

(d)

Figure 5.2. Photographs of Done Ella. In (a) Lake Abaya can be seen in the background. Photographs by Katie Loakes.

(a)

(b)

(c)

(d)

Figure 5.3. Photographs of Done Ella macrophytes: (a) – (c) the water lily, *Nymphaea*, and *Cyperus* reeds; (d) the littoral marsh area. Photographs by Katie Loakes.

Figure 5.4. Palaeo-shoreline (indicated by the red line) around Done Ella. Photograph by Katie Loakes.

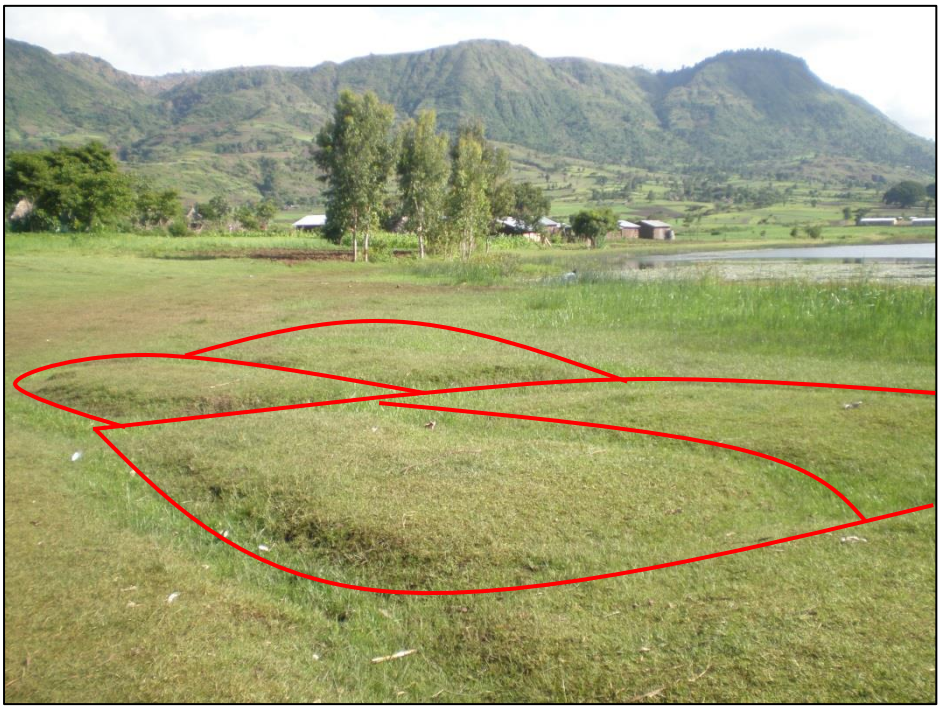

Figure 5.5. Foundations (indicated by the red line) of four buildings around Done Ella, flooded by rising waters. Photograph by Katie Loakes.

5.4 Field Sampling

Field work took place in June and July 2012. Bathymetry was measured using a GPS echo sounder to establish the lakes' depth profile and identify sites appropriate for coring. Four short cores (labelled HON-Kajak 1 – 4 and varying in length from 29 – 67 cm) containing unconsolidated surface sediments were extracted from around the lake using a HON-Kajak sediment corer with a 1 m tube from an anchored inflatable boat (Fig. 5.6). The cores were divided into 1 cm sections in the field and sealed in labelled plastic sample bags. A long sediment core (DE-2012) was taken from the centre of the lake (6°15'36.4"N, 37°39'51.8"E, 5.3 m water depth) from an anchored raft using a Russian peat corer, 5 cm diameter and 50 cm chamber (Aaby and Digerfeldt 1986). The corer was pressed 40 cm into the sediment and through the process of adding consecutive rods and rotating the core chamber, used to core 7 m into the sediment, extracted as fourteen 50 cm drives, labelled 1 – 14. Each drive was wrapped in cling film, tinfoil and placed in PVC tubes cut in half which were wrapped in more tinfoil and labelled for packaging and transport. A YSI probe was used to record depth (m), temperature (°C), conductivity (µS cm^{-1}), dissolved oxygen (percentage and mg l^{-1}) and pH through the water column at the core site.

Additional measurements using the YSI probe were taken from a small inflatable boat at three locations within the littoral zone to compare spatial variability according to vegetation density (locations were identified as within the area of *Myriophyllum*, open water and within the area of *Nymphaea*). Six macrophytes were identified in the lake and two samples of each were collected and sealed in plastic sample bags. One sample of each macrophyte was sent to the National Museums of Kenya for identification by Dr Stephen Ruccina and the other was transported back to Loughborough University for diatom analysis.

5.5 Laboratory Methods

On return to the laboratory at Loughborough University the four HON-Kajak cores and DE-2012 were refrigerated at 4 °C. The macrophytes samples were frozen.

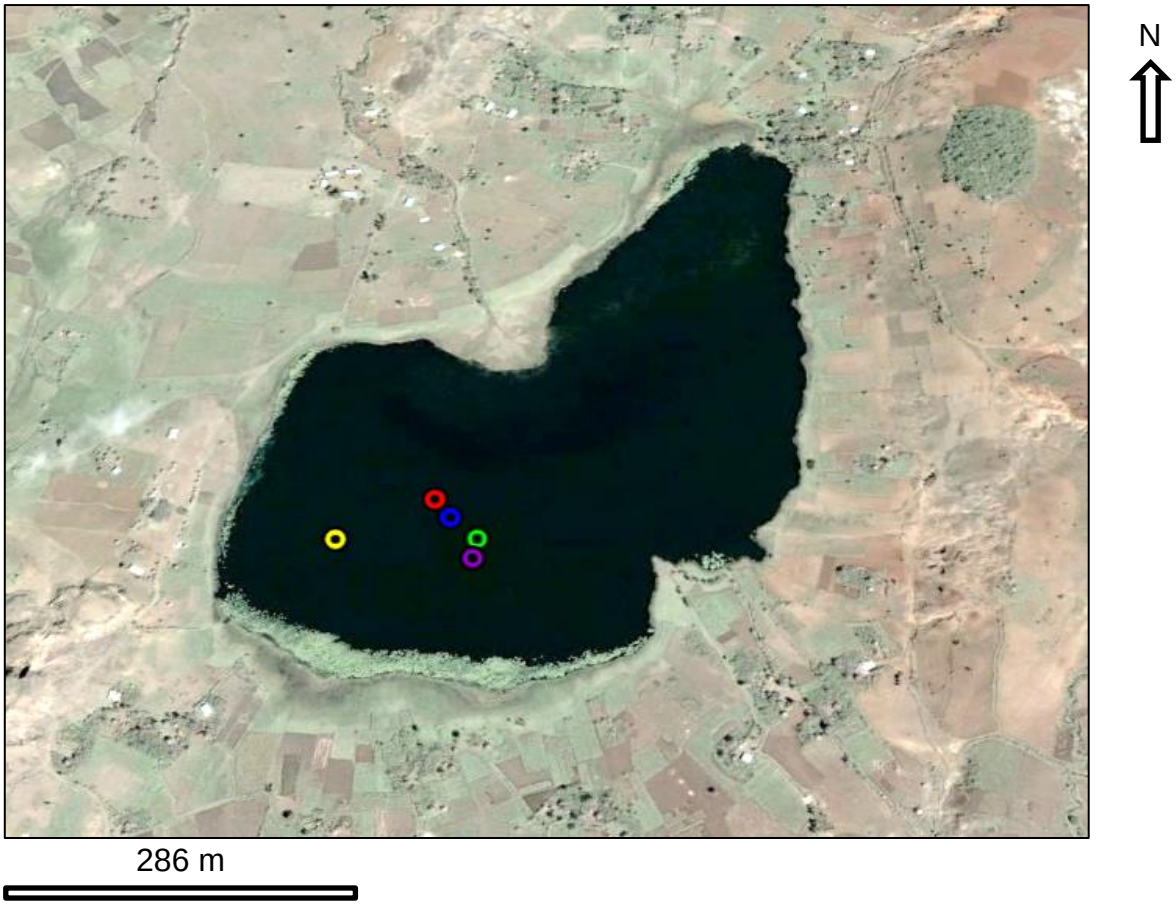

Figure 5.6. Aerial view of Done Ella (Google Earth 2013c). Locations of the HON-Kajak cores and DE-2012 are indicated by the coloured circles. Cores extracted using the HON-Kajak sediment corer are represented by the red (HON-Kajak core 1), blue (HON-Kajak core 2), yellow (HON-Kajak core 3) and green (HON-Kajak core 4) circles and DE-2012 by the purple circle.

5.5.1 Diatom Analysis

Diatom and microscope slide preparation followed the standard methodology described in detail in Chapter 4. Taxonomy follows Krammer and Lange-Bertalot (1988; 1991a; 1991b; 1999), Gasse (1986) and Hustedt (1949). Currently accepted names were verified against recent publications, literature and authoritative databases (AlgaeBase 2015; DiatCode 2015). Valves were identified to species level where possible. For the majority of samples it was necessary to lower the count from 300 valves to a more practical target due to very low valve concentrations. This was done after firstly scanning each sample for ten minutes and then based on the occurrence of valves in that time, scaling the target count down. For most samples the target was revised to 50 valves. Valve dissolution was assessed using a binary system with 0 being visibly dissolved and 1 being pristine (*F* index; Ryves et al. 2001). Diatom concentration was estimated by adding a known number of microspheres to the samples (Battarbee and Kneen 1982). Preliminary diatom analysis was conducted at approximately 5 cm intervals in the four HON-Kajak cores and 20 – 30 cm intervals in DE-2012.

5.5.2 X-ray Fluorescence (XRF) Spectrometry

XRF analysis was performed on DE-2012 by the author at Aberystwyth University using the Itrax® core scanner. The methodology is described in detail in Chapter 4. The fourteen cores were scanned at 700 µm intervals for 10 seconds. After scanning the cores were re-sealed and returned the refrigerator for storage. In additional to elemental data, a digital image was taken of each core.

5.6 Chronological Analysis

Five bulk sediment samples of 1 cm thickness, weighing between 2.8 – 6.5 g, were taken at 30 cm, 250 cm, 300 cm, 400 cm and 700 cm depth from DE-2012 for accelerator mass spectrometry (AMS) ^{14}C dating at the Beta Analytic laboratory in London.

Samples were treated following standard techniques; each sample was dispersed in deionized water and then sieved through a < 180 µm mesh size to check for rootlets and other plant macrofossil materials. The < 180 µm fraction was treated with hydrochloric acid (HCl) and digested (several hours at 70 ºC) to remove any

carbonates, before being washed with deionized water. Samples were dried overnight (90 ºC). Prior to combustion, the sample material was examined under at x 45 magnification on a binocular scope to inspect for any remaining physical contamination. A small sub-sample from each sediment sample was placed into concentrated HCl to verify that no acid resistance carbonates such as dolomite had survived the pretreatment. Upon verification, the remaining sample was combusted to carbon dioxide (CO_2), graphitized and the $^{14}C/^{12}C$ and $^{13}C/^{12}C$ ratios measured by AMS. The $^{13}C/^{12}C$ ratio was measured directly from the sample combustion in an Isotope Ratio Mass Spectrometer (IRMS).

5.7 Results

5.7.1 Chronology

The AMS ^{14}C dates obtained from DE-2012 ranged in age from 1490 to 3640 cal yr BP, based on the median estimate of the age range at the two-sigma calibration (Table 5.1). However, the calibrated ages did not occur in sequential order. Instead, the youngest sediments were located in the shallowest and deepest sediments, sandwiching the oldest sediments in the middle of the core. Consequently, the ages measured for this core cannot be used to produce a reliable chronology.

Table 5.1. AMS radiocarbon chronology of Done Ella, core DE-2012.

Beta Analytic laboratory number	Depth from sediment surface (cm)	Conventional age, ^{14}C yrs BP	Calibrated age, cal yr BP, weighted average, 2 sigma calibration (relative area under probability distribution)	Calibrated age, cal yr BP, median estimate (to the nearest 10 yrs)
376434	70.0	1610 ± 30	1560 - 1410	1490
376435	290.0	3400 ± 30	3700 - 3575	3640
376436	340.0	3370 ± 30	3690 - 3660 and 3650 to 3560	3630
376437	440.0	2800 ± 30	2965 - 2845	2910
376438	740.0	1650 ± 30	1610 - 1525	1570

5.7.2 XRF Geochemistry

Selected geochemical elemental concentrations for DE-2012 are shown in Fig. 5.7. Peak area profiles for calcium (Ca), iron (Fe), potassium (K), silicon (Si) and titanium (Ti) have been normalised by incoherent scatter (inc) to minimise the effect of

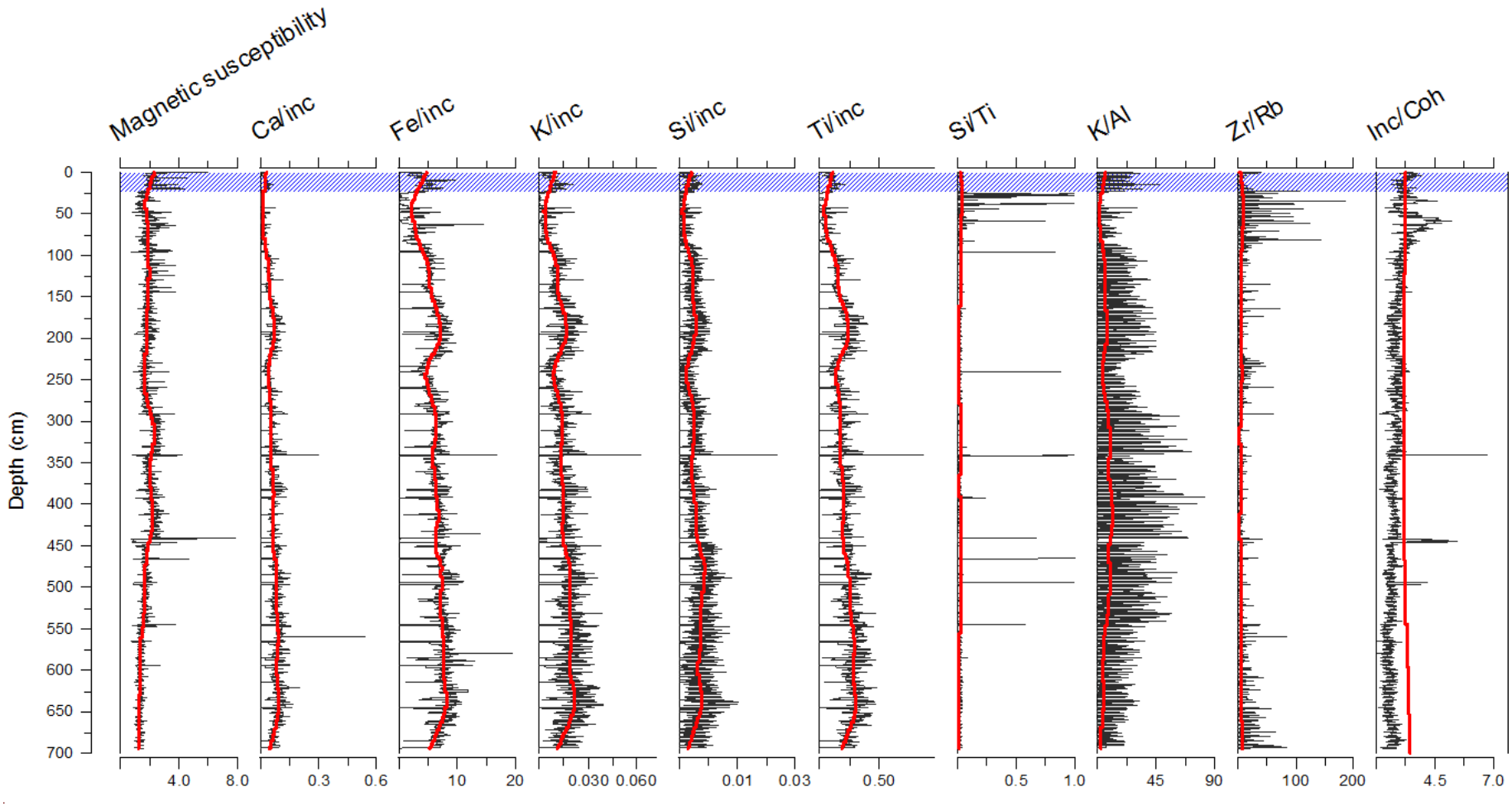

Figure 5.7. XRF results for DE-2012. Elemental data is given as peak area units with element X-ray fluorescence values divided by incoherent scatter (inc). Magnetic susceptibility is given as κ, SI units. The average trend is indicated in red. The blue zone indicates where diatoms were found in the sediment.

organic matter and water content variability, unrelated to sediment geochemistry (Marshall et al. 2011). Ratios of potassium: aluminium (K/Al), silicon: titanium (Si/Ti) and zirconium: rubidium (Zr/Rb) are shown, as well as the incoherent: coherent backscatter intensity ratio (inc/coh).

The lithogenic elementals Ca, Fe, K, Si and Ti increase from the base of the core, reaching maximum values early in the sequence at 639.9 cm. After peaking, the elements follow the same trend, simultaneously increasing and decreasing in value up to 456.2 cm. At 442.0 cm all elements experience a sharp drop in value but recover and return to the pattern of regular increases and decreases. K/Al similarly experiences frequent rises and declines in concentration with large peaks at 661.2 cm, 569.2 cm, 371.3 cm, 314.7 cm, 265.2 cm, 222.8 cm and 180.4 cm. Si/Ti (an estimate of biogenic silica, particularly the abundance of siliceous microfossils [Conley 1988]) experiences a more gradual increase in concentration up to 456.2 cm after which it declines reaching a minimum value at 350.1 cm. A second period of increase is then observed, followed by a second decrease. In contrast, Zr/Rb and inc/coh remain constant in value with minor peaks at 548.0 cm and 236.9 cm for Zr/Rb and a single peak at 442.0 cm for Inc/Coh.

At 236.9 cm Ca, Fe, K, Si and Ti simultaneously dip in value, after which values increase – Fe and Si gradually, Ca, K and Ti sharply – and peak at 180.4 cm. Elements then decline in a pattern of smaller rises and declines, reaching minimum values at 31.9 cm followed by a sharp increase at 17.7 cm. After a peak at 180.4 cm, K/Al demonstrates the same trend, reaching a minimum value at 31.9 cm before an increase at 17.7 cm. After a gradual increase in value up to 95.5 cm, Si/Ti experiences a pattern of sharp increases and decreases centred at 67.2 cm, 53.0 cm and 31.9 cm. Zr/Rb similarly demonstrates significant increases centred at 81.3 cm, 60.1 cm and 31.9 cm. Inc/Coh reaches a maximum value at 60.1 cm after which values return to those previously observed.

Magnetic susceptibility (a proxy of allochthonous inputs) remains stable throughout the record, showing very little overall variability.

5.7.3 Water Column Profiles

At the site of DE-2012, measurements using the YSI probe were taken at 0.1 – 0.5 m intervals from the surface to 5.5 m depth (Fig. 5.8). Temperature declined slightly with water depth, as did pH from 8.27 at the surface to 6.58 at 5.5 m. Conductivity increased steadily from the surface to 5.0 m water depth where it increased from 197.0 µS cm^{-1} to 240.0 µS cm^{-1} at 5.5 m water depth. Dissolved oxygen showed the greatest variability in measurement, which ranged between 9.46 (105.5 %) – 10.46 mg l^{-1} (112.7 %) from the surface to 3.6 m depth before decreasing to 1.57 mg l^{-1} (15.8 %) at 5.5 m depth.

In the littoral zone, measurements from within the area dominated by *Myriophyllum* were taken at 10 cm intervals to a depth of 3.5 m (Fig. 5.9). Temperature ranged between 20.88 ºC at the surface to 19.13 ºC at 3.5 m. Conductivity showed little variation through the water column. From the surface to 1.75 m depth, conductivity was consistently measured as 161 µS cm^{-1}. From 2.0 – 3.5 m conductivity varied slightly between 159 – 162 µS cm^{-1}. The pH of the water varied between 8.03 at the surface to 7.57 at 3.5 m depth. Dissolved oxygen ranged between 10.77 mg l^{-1} (117.4 %) at the surface to 10.23 mg l^{-1} (111.8 %) at 1.25 m depth. At 1.5 m dissolved oxygen dropped to 9.16 mg l^{-1} (101.1%) and continued to decline to 2.42 mg l^{-1} (28.2 %) at 3.5 m depth.

In the area of open water within the littoral zone, measurements were taken at 10 cm intervals to 90 cm (Fig. 5.9). Temperature varied between 20.1 – 22.0 ºC through the water column. Conductivity showed very little variability (159 – 160 µS cm^{-1}). The pH of the water also showed little variability declining linearly from 8.64 at the surface to 8.01 at 90 cm. Dissolved oxygen varied through the water column; at 10 cm depth dissolved oxygen was measured as 8.28 mg l^{-1} (94.3 %). At 20 cm this dropped to 6.93 mg l^{-1} (81.0 %) but then increased to 7.43 mg l^{-1} (82.9 %) after which it continued to rise to 9.22 mg l^{-1} (101.5 %) at 90 cm.

In the area closest to the shore, which was dominated by the lily *Nymphaea,* measurements were taken at 25 cm intervals to 2.0 m water depth (Fig. 5.9). Temperatures varied slightly from 20.05 ºC at the surface to 19.42 ºC at 2.0 m.

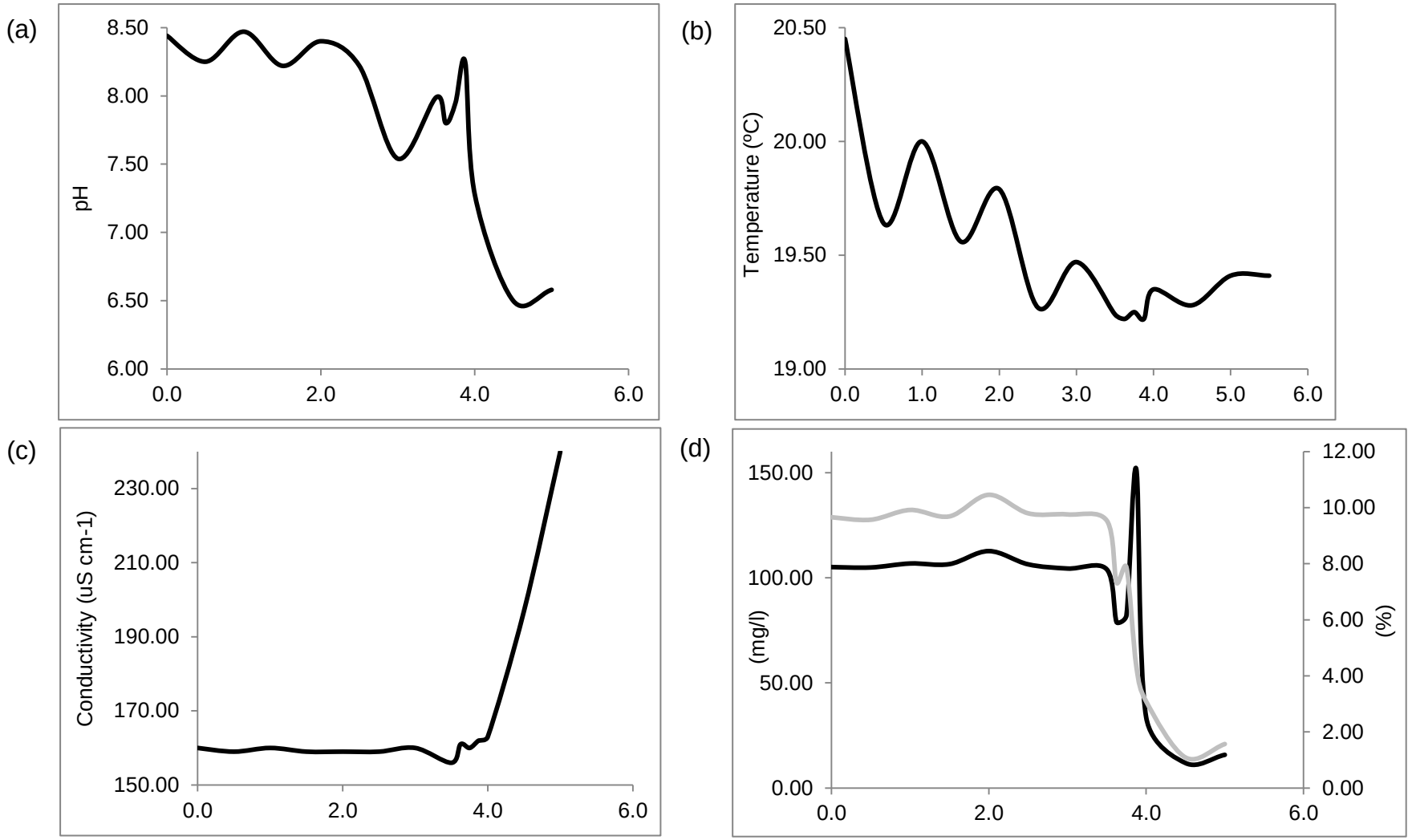

Figure 5.8. Water column properties at the site of core DE-2012, showing (a) pH, (b) temperature (ºC), (c) conductivity (µS cm^{-1}), and (d) dissolved oxygen as mg/l (grey) and percentage (%, black) against depth (m).

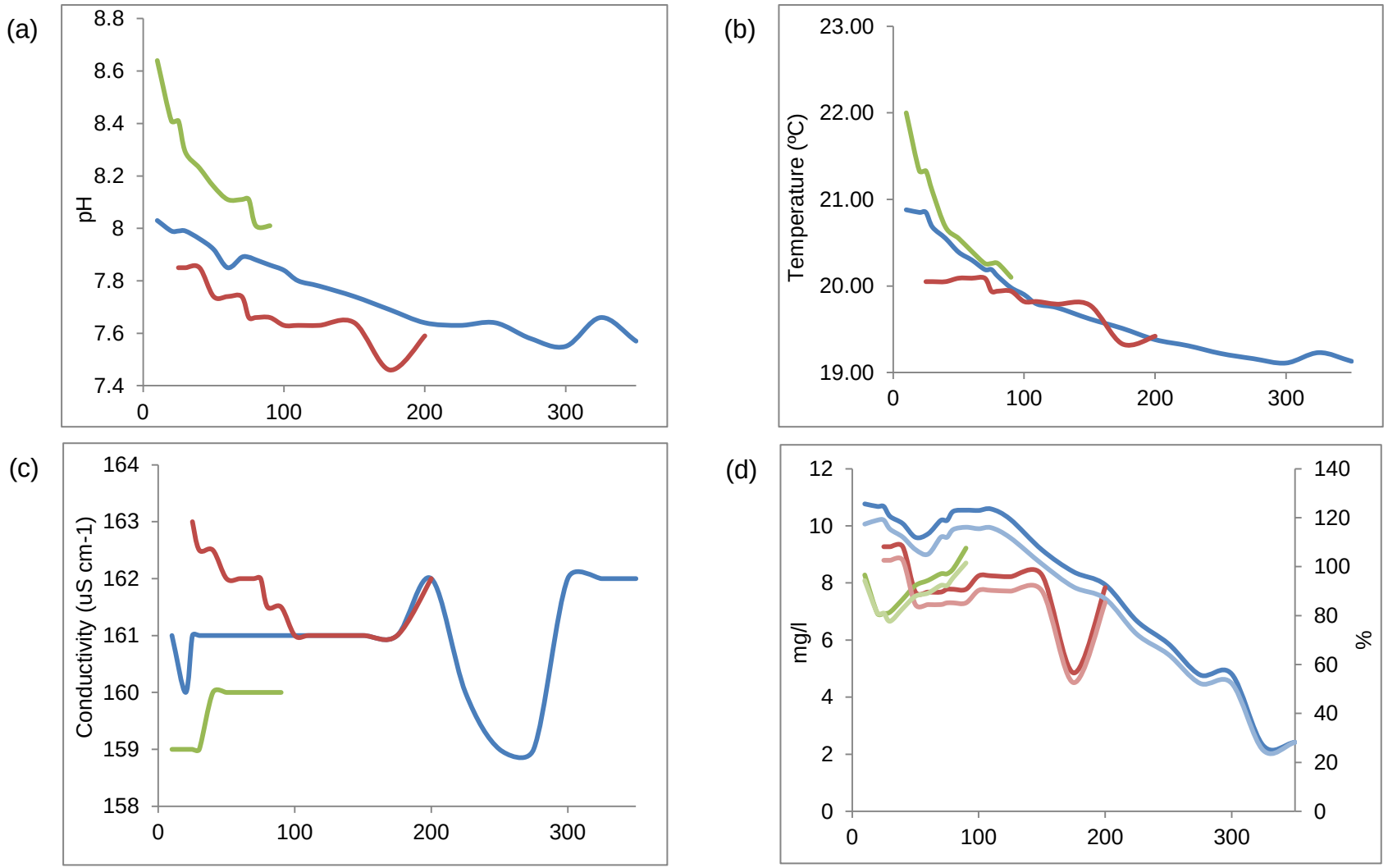

Figure 5.9. Water column properties at the littoral site (blue), the area of open water within the littoral zone (red) and the area closest to the shore (green), showing (a) pH, (b) temperature (ºC), (c) conductivity (µS cm^{-1}), and (d) dissolved oxygen as mg/l (dark lines) and percentage (%, light lines) against depth (m).

Conductivity ranged between 161 µS cm^{-1} and 163 µS cm^{-1} and pH between 7.46 and 7.85. Dissolved oxygen declined with depth from 9.27 mg l^{-1} (102.6 %) at the surface to 7.84 mg l^{-1} (85.3 %) at 2.0 m. An anomalous measurement occurred at 1.75 m where dissolved oxygen was measured as 4.85 mg l^{-1} (52.6 %).

5.7.4 Diatoms

Neither the HON-Kajak cores or DE-2012 contained an abundance of diatoms. The macrophyte samples were not used for diatom analysis based on the results from the sediment cores.

HON-Kajak core 1 was 29 cm long. Diatoms were found at irregular intervals through the core (Fig. 5.10 [a]). Of the five samples, valves were found at a countable concentration in three (1.5 cm, 9.5 cm, 19.5 cm). Common taxa included *Aulacoseira granulata*, *Ulnaria delicatissima*, *Gomphonema parvulum*, *Gomphonema pumilum*, *Cocconeis placentula* var. *lineata*, *Cocconeis placentula* var. *placentula*, *Navicula cryptotenella*, *Nitzschia subacicularis* and *Rhopalodia gibba*. Of these, 64.7 – 91.8 % of valves were in pristine condition. Valve concentration was low, ranging between 7.9 – 19.5 x 10^5 g^{-1} wet sediment.

HON-Kajak core 2 was 52 cm long. Diatoms at a countable concentration were only found in three of eight samples (9.5 cm, 29.5 cm and 39.5 cm; Fig. 5.10 [b]). Seventeen species were identified in the samples from this core. Common taxa included *A*. *granulata*, *U. delicatissima*, *C*. *placentula* var. *lineata*, *G*. *parvulum*, *G*. *pumilum*, *N*. *cryptotenella*, *Luticola mutica* and *N*. *subacicularis*. Valve concentration was very low and ranged between 0.95 – 7.19 x 10^5 g^{-1} wet sediment. The majority (76 – 100 %) of diatoms were in pristine condition.

HON-Kajak core 3 was 65 cm long. Diatoms were not present in samples below 50 cm and were only found at countable concentrations in three samples above 30 cm (9.5 cm, 19.5 cm and 29.5 cm; Fig. 5.10 [c]). Common taxa included *A*. *granulata*, *U. delicatissima*, *Fragilaria radians*, *Ulnaria ulna* var. *ulna*, *G*. *parvulum*, *G*. *pumilum*, *C*. *placentula* var. *lineata* and *C. placentula* var. *placentula*. Diatom preservation was high, with 77.3 – 100.0 % of valves being in pristine condition. Valve concentration ranged between 0.56 – 48.14 x 10^5 g^{-1} wet sediment.

(a)

(b)

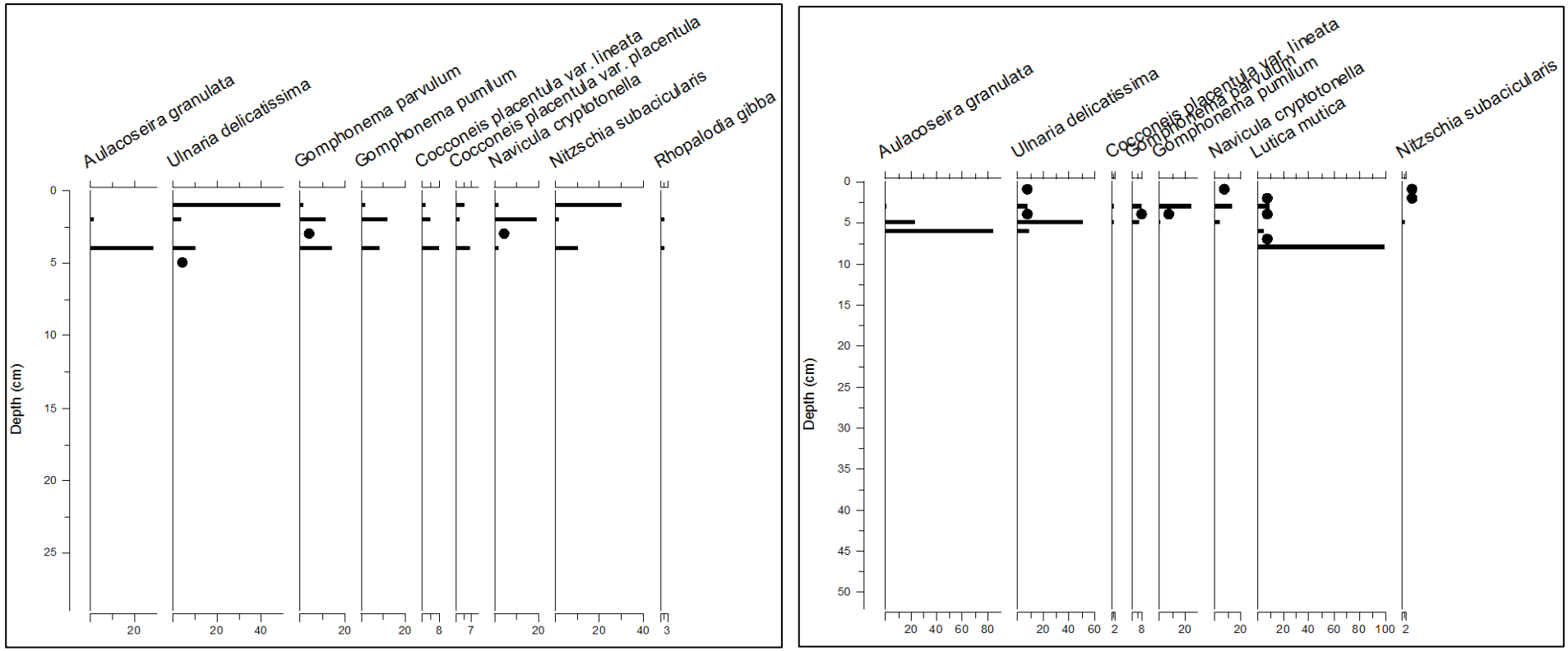

Figure 5.10. Diatom data, shown as percentages (%), for (a) HON-Kajak core 1 and (b) HON-Kajak core 2. Circles represent depths at which a taxon is present in low abundances (< 0.5 %).

(c)

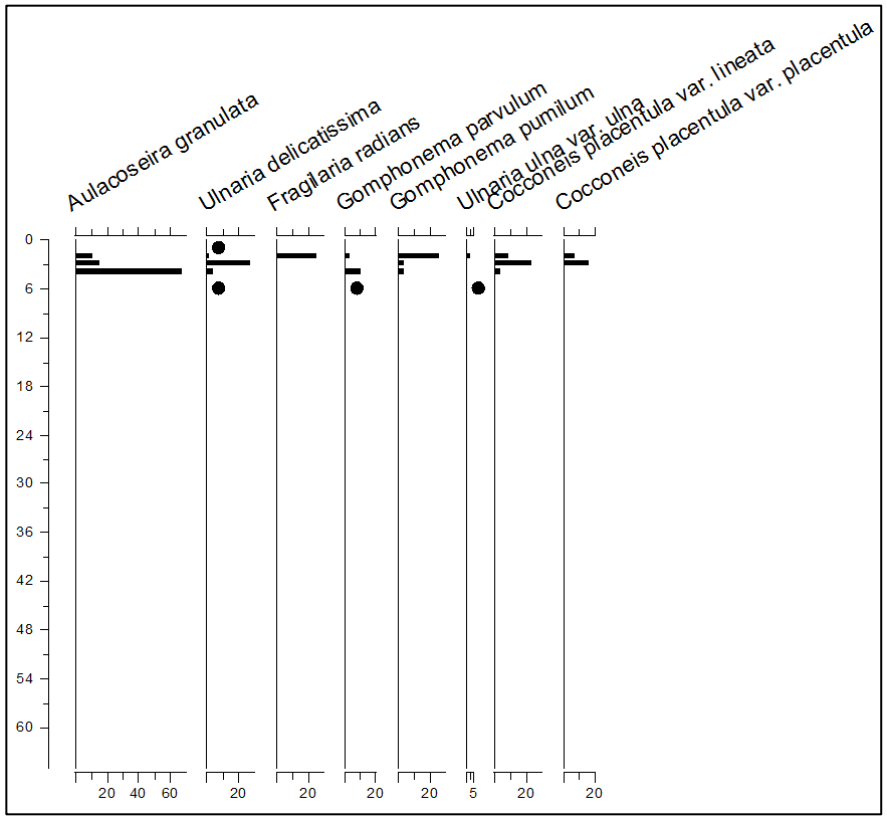

(d)

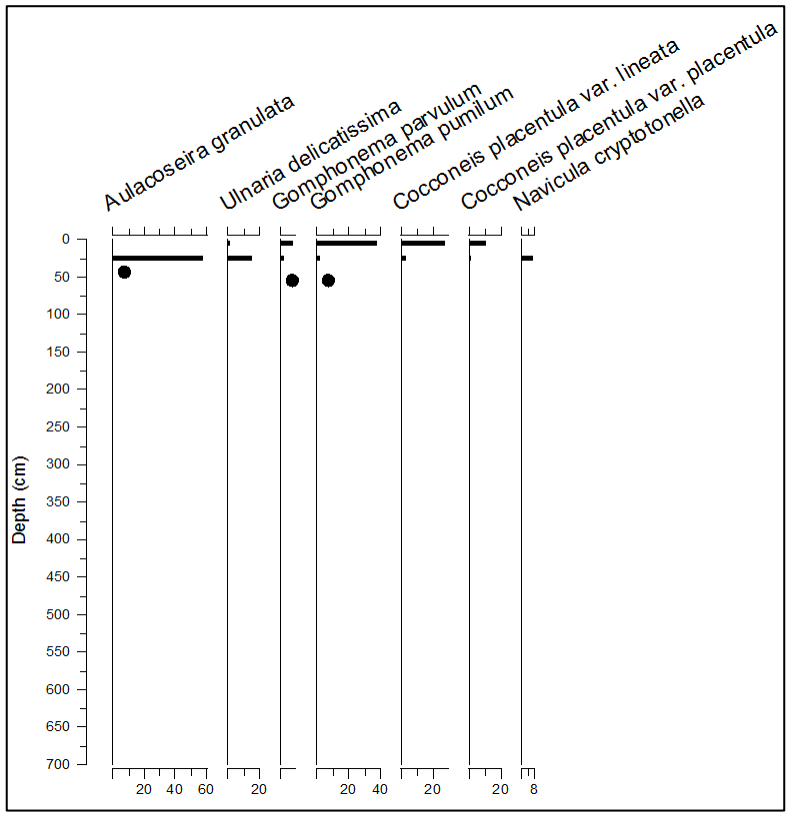

Figure 5.10. Diatom data, shown as percentages (%), for (c) HON-Kajak core 3, and (d) DE-2012. Circles represent depths at which a taxon is present in low abundances (< 0.5 %).

HON-Kajak core 4 was 67 cm long. Diatoms were only found in the surface sediment (0.5 cm). Diatoms present were *Achnanthes minutissima* var. *scotica*, *U. delicatissima*, *U. ulna* var. *ulna*, *N*. *subacicularis* and *Synedra familiaris*. Of these 89.8 % were in pristine condition.

In DE-2012 diatoms were only observed in the top 25 cm (Fig. 5.10 [d]). Fourteen species were identified in the samples extracted above this depth. Dominant taxa included *A. granulata*, *C. placentula* var. *lineata*, *C. placentula* var. *placentula*, *U. delicatissima*, *G. parvulum*, *G. pumilum* and *N .cryptotenella.* Of these valves 60 – 84 % were in pristine condition and valve concentration varied between 22.7 – 45.6 x 10^5 g^{-1} wet sediment. Below 25 cm, valves were found sporadically (0 – 3 valves per sample) with concentrations varying from 1.9 – 8.4 x 10^5 g^{-1}.

5.8 Discussion

5.8.1 Diatom Preservation and Dissolution

Given the sparseness of diatoms in the sediment it was not possible to perform reliable statistical analyses on the data to produce a climatic and environmental record. Understanding this loss of information is nevertheless important for assessing the quality of the palaeoenvironmental inferences that can be made from this record. Without additional data from the lake it is difficult to establish definitively why diatom concentration was low and why preservation was poor. It would seem likely that either the physical and/or chemical properties of the lake were inhospitable for diatoms and prevented a community from establishing, or the properties of the lake led to silica dissolution and valve fragmentation, which biased the assemblage to more resistant taxa (Ryves et al. 2001; Battarbee et al. 2001; 2005).

Diatom preservation in lake sediments has been linked to multiple aspects of physical limnology, water chemistry and biological interactions (see Chapter 6 for further discussion) (Lewin 1961; Haberyan 1985; 1990; Flower 1993; Barker et al. 1994; McMinn 1995; Reed 1998a; 1998b; Bidle and Azam 1999; Gibson et al. 2000; Ryves et al. 2001; 2006; Bidle et al. 2002; 2003). Whilst it is not possible to state categorically which limnological variables, if any, may have contributed to the low diatom concentration (through destruction and/or fragmentation) observed at Done Ella, the limnetic conditions may have produced inhospitable conditions for diatom

community development and/or preservation in the sediments. For example, the shallowness of Done Ella may result in turbulent mixing of the uppermost sediments, promoting dissolution through initial valve breakage and re-suspension of valves into silica under-saturated waters. In-wash of sediment from the steep, agriculturally intensive catchment may likewise encourage turbulence and promote physical valve breakage (Fig. 5.2). In-wash is certainly an issue affecting the neighbouring Lake Abaya, whose water is clearly sediment laden in contrast to Lake Chamo (Fig. 5.1).

Water pH may also be a potentially contributing factor at Done Ella to valve dissolution. In general, lakes with a low pH tend to preserve valves better than those with a high pH as silica dissolution increases above pH 9.0 (Lewin 1961; Round 1964; Flower 1993; Ryves et al. 2006). Barker (1992) for example, found poor diatom preservation at Lake Manyara (Tanzania) which has a pH of close to 10. At Done Ella, the highest pH was recorded as 8.47 at 1.5 m water depth. This pH may encourage valve dissolution with it being on the cusp of the threshold value needed to dissolve silica. However, well preserved diatom records have been extracted from alkaline lakes also and pH has not be a significant factor affecting valve preservation in data sets from Spanish and other East African lakes (Hecky and Kilham 1973; Flower 1993; Reed 1998b).

Without additional data from Done Ella regarding factors such as salinity, silica concentration, sedimentation rate and biological interactions, it is not possible to state why diatom concentration was low. There are numerous factors which may have discouraged diatom growth or increased valve dissolution but their significance at Done Ella cannot be determined.

5.8.2 Geochemical Interpretation

Calcium, iron, potassium, silicon and titanium indicate allochthonous inputs from varying mineral hosts (Boës et al. 2011). However, as there is little variability in the elemental geochemistry, it is difficult to assess whether the nature of detrital material entering the lake is a result of varying hydrological activity.

As diatoms are largely absent from Done Ella, variability in biogenic silica is likely due to catchment supply; catchment soils containing silicon may be washed into the

lake during periods of wetter climate (Burnett et al. 2011). As such, the geochemical data indicates a gradual shift to a drier climate between 700.0 – ~ 100.0 cm after which the climate appears to experience more abrupt, short-lived, wet periods (81.3 – 24.7 cm). This is in agreement with increased kaolinite concentrations signalling chemical weathering under humid conditions (Burnett et al. 2011). Increased mechanical weathering between 700.0 – ~ 100.0 cm suggests a drier climate punctuated by frequent wet spells, until chemical weathering increases again between 81.3 – 31.8 cm, suggesting a wetter climate. The incoherent: coherent backscatter intensity ratio provides further evidence of a drier climate transitioning to a wetter one given the peak at 60.1 cm, indicating higher productivity and preservation within the lake (Burnett et al. 2011). Grain size becomes coarser during this wet period which indicates a greater proportion of clastic sediment (Kylander et al. 2011).

However, whilst the XFR data may suggest a climatic change, the effect of human impact through settlement, land use change, deforestation and agricultural practices cannot be ruled out. Human activity in the basin may destabilise catchment processes resulting in a false climate signal being exhibited in the data. In order to determine whether the signal is indeed a result of climate or due to human activity, a reliable age-depth model is required so that the results may be put into the chronological context of human development and activity in the region.

5.8.3 Chronology

As the chronology of the sediment record is unreliable, it is very difficult to determine when changes in the catchment occurred and why. It is likewise difficult to state the reason for the unreliable chronology at Done Ella. Although pre-treatment before radiocarbon measurement is undertaken very carefully at laboratory facilities, there are still a large number of unknown factors which may result in a sample being ascribed a false age, especially if obtained from bulk sediment samples (Björk and Wohlfarth 2001). An important source of error in lake sediments is contamination by younger or older organic material. Such contamination may occur as a result of root penetration, percolation by younger humic acids or bioturbation (Karland et al. 1984; Olsson 1991; Björk and Wohlfarth 2001). Björk et al. (1998) for example found that late-glacial bulk sediment ages were 200 – 600 years older than the corresponding

ages of plant macrofossils in a study in south-west Sweden. This was attributed to sediment reworking during periods of increased soil erosion, which led to incorporation of older organic material (Björk et al. 1998).

A second known source of error may arise from the 'reservoir effect', when the $^{14}C/^{12}C$ ratio in the lake is lower than the atmospheric ratio (Olsson 1986; Wang and Amundson 1996; Reimer et al. 2013). For example, if submerged plants in the lake contribute to the sediment then the ^{14}C determination will indicate an earlier event than the actual date (Olsson 1986). A low $^{14}C/^{12}C$ ratio may also be derived from dissolved old carbonate (the hard-water effect), the lake being sealed off from the atmosphere by perennial ice cover (although this does not apply to Done Ella), or the lake being fed by water or groundwater containing old carbon (Björk and Wohlfarth 2001). Other source of error include lake water composition, which may limit the accuracy of radiocarbon ages on bulk sediment, aquatic plant and animal samples (Olsson 1986; 1991) and contamination by bacteria, fungi or dust during sample storage (Björk and Wohlfarth 2001).

Dating error has also been shown to result in some African lake records from sediment being periodically (once in several decades) eroded, re-deposited or slumping due to wave turbulence during severe storms (wave theory) (Verschuren 2003). Verschuren et al. (1998) for example, found using ^{210}Pb-dating that deep-water sediments in the central basin of Lake Victoria had been subjected to a widespread sediment erosion event, which effectively limited the time resolution of the study to centuries rather than decades. Poor correlation between inferred climatic events in fossil diatom records has also been found between sites in the middle of Lake Victoria (Stager and Johnson 2000) and a 30 m deep channel between offshore islands (Stager et al. 1997), highlighting variability of site-specific sedimentation conditions (Verschuren 2003). This shows how high-frequency 'signals' in proxy climate records may be a result of re-suspension and deposition of surface sediments rather than ecological or climatic variability (Verschuren 2003). Selecting a suitable lake is therefore imperative. Crater lakes may appear to be a suitable choice as crater rims tend to protect them from wind driven turbulence. However, steep bottom slopes in these lakes may promote sediment slumping (Hilton 1985; Verschuren 2003). By assessing basin topography, lake morphometry

and mean and annual peak wind speeds and directions it can be determined whether wave theory may be applied to determine the dominant process of sediment distribution (Håkanson and Jansson 1983; Hilton 1985). These variables can then be used to evaluate whether or not local sedimentation conditions within a lake are likely to allow for continuous, undisturbed accumulation of sediment and climate proxies (Verschuren 2003).

An alternative reason for the unreliable chronology may result from the methodology used in the field. Whilst Russian peat corers are designed to minimise disturbance to the sediment profile (Aaby and Digerfeldt 1986), it is possible that some may have occurred during sediment extraction in the field, affecting the linear chronology of the sediment cores as they were collected.

Clearly there is a complex range of factors operating within lake systems, which may affect AMS ^{14}C dating and result in sediment samples being ascribed a false age. The unreliable chronology at Done Ella may be a result of one or several of these sources of error. Given the discontinuities in the chronology, it is difficult to determine where the error has originated from and whether the entire sequence or just a single date has been affected. As a result, the chronology cannot be credited as being an undisturbed, continuous record and as such is not reliable.

5.9 Conclusion

Originally this PhD project planned to reconstruct Holocene climate and environmental change in the south-west Gamo-Gofa highlands of Ethiopia, in order to provide a climatic context for ethnographic and archaeological research being conducted in the region. Field work was carried out successfully at the small lake Done Ella in 2012, a site where no research had previously been conducted. Unfortunately, the sediment cores collected from the lake yielded very limited diatom data from which no interpretations can be made. The chronology of the sediment core is likewise unreliable, which further taints the accuracy of the elemental profiles. Whilst it is not possible to state categorically how these records have been affected so as to produce such unreliably archives, speculation can be made based on current understanding of lake processes, sources of error and contamination issues. It was decided that given the scarcity and unreliability of data, the project could not

be continued for the purpose of the authors' PhD research. Despite this, the findings from Done Ella are still significant as being the first research carried out at the lake and may act as a precautionary warning to other researchers considering work at the site. Pollen analysis is ongoing at the National Museums of Kenya and options to improve the chronology are being considered at the University of York.

Chapter 6

Results: The Palaeolimnology of Lake Hayq.

6.1 Introduction

This chapter presents the palaeolimnological results from Lake Hayq. The chronological framework of the core, Hayk-01-2010, is presented first, followed by a lithological overview and the geochemistry. A detailed description of the diatom and photosynthetic pigment records is then presented. The combined data provide a detailed body of evidence for the palaeolimnological changes that occurred in the Lake Hayq basin during the late Pleistocene and Holocene, against which interpretations of the environmental and climate can be made.

6.2 Chronology

The Lake Hayq chronology is based on fourteen AMS ^{14}C dates derived from bulk sediment samples extracted from Hayk-01-2010 (Table 6.1). Figure 6.1 shows the age-depth model constructed using a 0.4 span smooth spline interpolation. The stratigraphic dates indicate the core covers the period 15,600 – 1,350 cal yr BP. Sedimentation rates vary over five main periods (Fig. 6.3); (1) Between 15,600 – 15,450 cal yr BP (822.0 – 789.0 cm) the sediment accumulation rate is relatively stable and high, averaging 0.2 cm yr^{-1}, (2) from 15,450 – 12,200 cal yr BP (789.0 – 541.0 cm) sedimentation decreases, reaching a low of 0.05 cm yr^{-1} (14,100 – 13,400 cal yr BP, 670.0 – 626.0 cm), before steadily increasing again, (3) between 12,200 – 11,800 cal yr BP (541.0 – 474.0 cm) accumulation is stable again, averaging 0.2 cm yr^{-1}, (4) at 11,800 cal yr BP, sedimentation declines again to a minimum of 0.01 cm yr^{-1} (296.25 cm) before increasing, and (5) from 2,500 – 1,350 cal yr BP (200.0 – 89.5 cm) sedimentation averages 0.1 cm yr^{-1}. These rates are generally comparable to average sedimentation across the larger East African Rift Lakes, such as Lakes Malawi and Tanganyika, during the Holocene (0.1 cm yr^{-1}; Johnson 1996).

6.3 Lithology

Three main lithostratigraphical units are identified in Hayk-01-2010 based on variations in composition and physical properties of the sediment layers (Figs. 6.2 and 6.3, see Appendix 1 and 2 for full details). Water, organic and carbonate content, and other physical properties, are described for each unit.

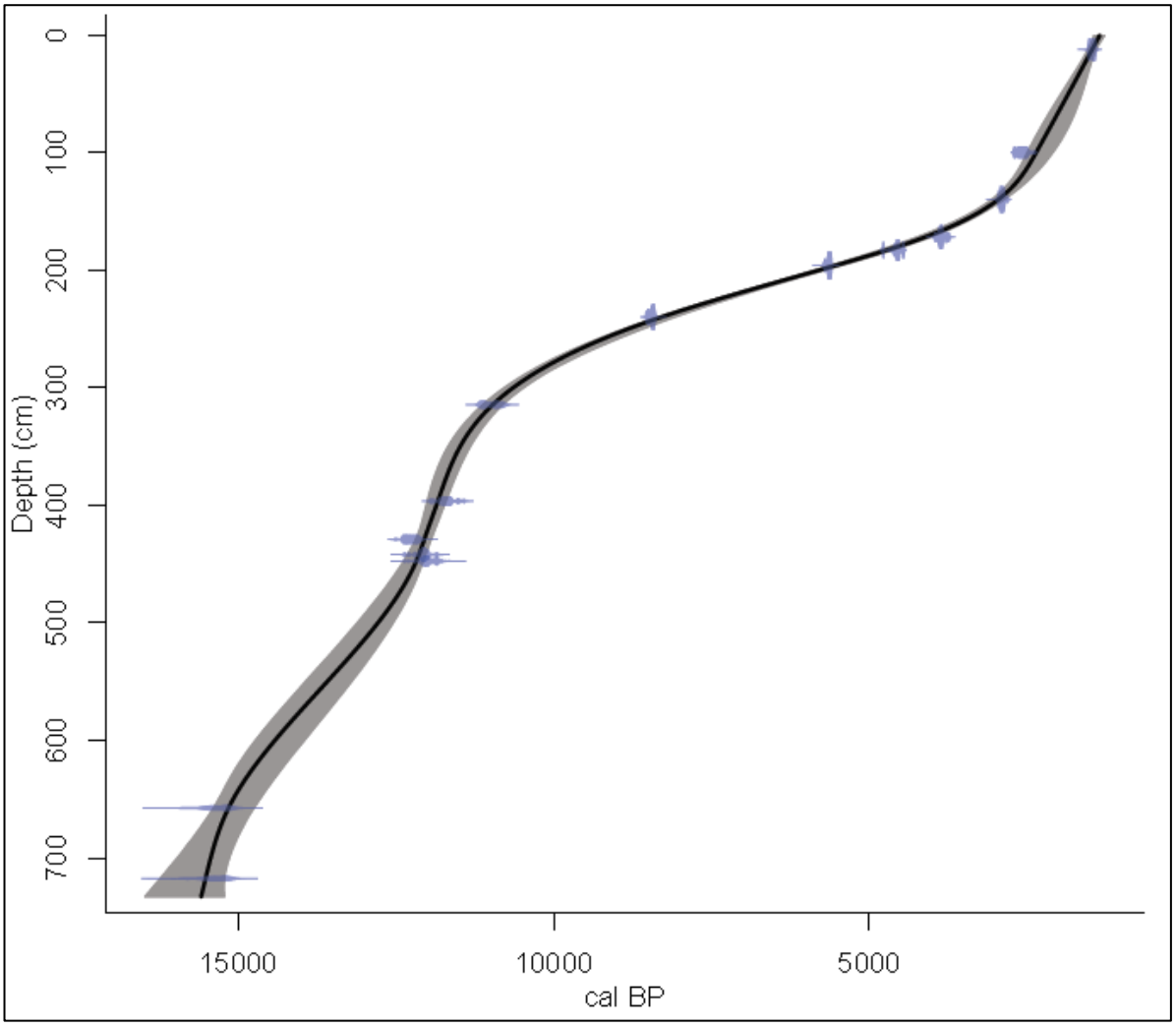

Figure 6.1. Age-depth model of fourteen bulk AMS ^{14}C dates from core Hayk-01-2010, constructed by J. Tyler using the program CLAM for R. Depth refers to depth below the top of the sediment core. The individual age distribution for each date, as relative area under probability distribution, is shown in blue. The black line indicates the most likely age-depth distribution, whilst the grey envelope represents the models chronological uncertainty.

Table 6.1. AMS radiocarbon chronology of Lake Hayq, core Hayk-01-2010.

Laboratory	Laboratory reference	Depth below top of sediment sequence (cm)	Conventional age, ^{14}C yrs BP	Calibrated age, cal yr BP, weighted average, 2 sigma calibration (relative area under probability distribution)	Calibrated age, cal yr BP, median probability (to nearest 10 yrs)
^{14}CHRONO Centre	UBA-27072	12.5	1583 ± 32	1404 - 1545 (1.00)	1470
ORAU	OxA-30960	100	2485 ± 32	2432 - 2728 (0.99)	2580
ORAU	OxA-30883	140	2795 ± 31	2837 - 2965 (0.93)	2900
^{14}CHRONO Centre	UBA-25092	172	3563 ± 36	3816 - 3934 (0.74)	3860
ORAU	OxA-30885	183	4068 ± 33	4496 - 4645 (0.68)	4560
ORAU	OxA-30886	196	4914 ± 35	5592 - 5715 (1.00)	5640
ORAU	OxA-30887	240	7650 ± 45	8386 - 8540 (1.00)	8440
^{14}CHRONO Centre	UBA-27073	314.5	9643 ± 79	10749 - 11204 (1.00)	10970
^{14}CHRONO Centre	UBA-27074	396.5	10102 ± 44	11587 - 11840 (0.69)	11710
^{14}CHRONO Centre	UBA-25093	429	10393 ± 45	12061 - 12423 (0.98)	12270
^{14}CHRONO Centre	UBA-25094	442	10287 ± 46	11926 - 12241 (0.85)	12060
^{14}CHRONO Centre	UBA-27075	447.5	10254 ± 62	11756 - 12239 (0.96)	12000
^{14}CHRONO Centre	UBA-27076	657.5	12846 ± 67	15120 - 15596 (1.00)	15320
^{14}CHRONO Centre	UBA-25095	717.5	12873 ± 60	15157 - 15614 (1.00)	15360

The basal, and smallest, unit (L-I, 822.0 – 797.0 cm) consists of stiff black clay (grain size < 0.002 mm) with some fine sand (grain size 0.2 – 0.6 mm) intermixed. Organic matter (6.5 – 7.1 %), carbonate (4.8 – 6.5 %) and water content (36.2 – 38.3 %) are all low in this unit. Dry mass, organic and minerogenic accumulation rates are at their maximum. The overlying unit (L-II, 797.0 – 595.0 cm) is characterised by grey gyttja – common lake mud comprised of organic matter – intermixed with silt (grain size 0.06 – 0.02 mm). The shade of colour varies in this unit (light to dark grey) and is

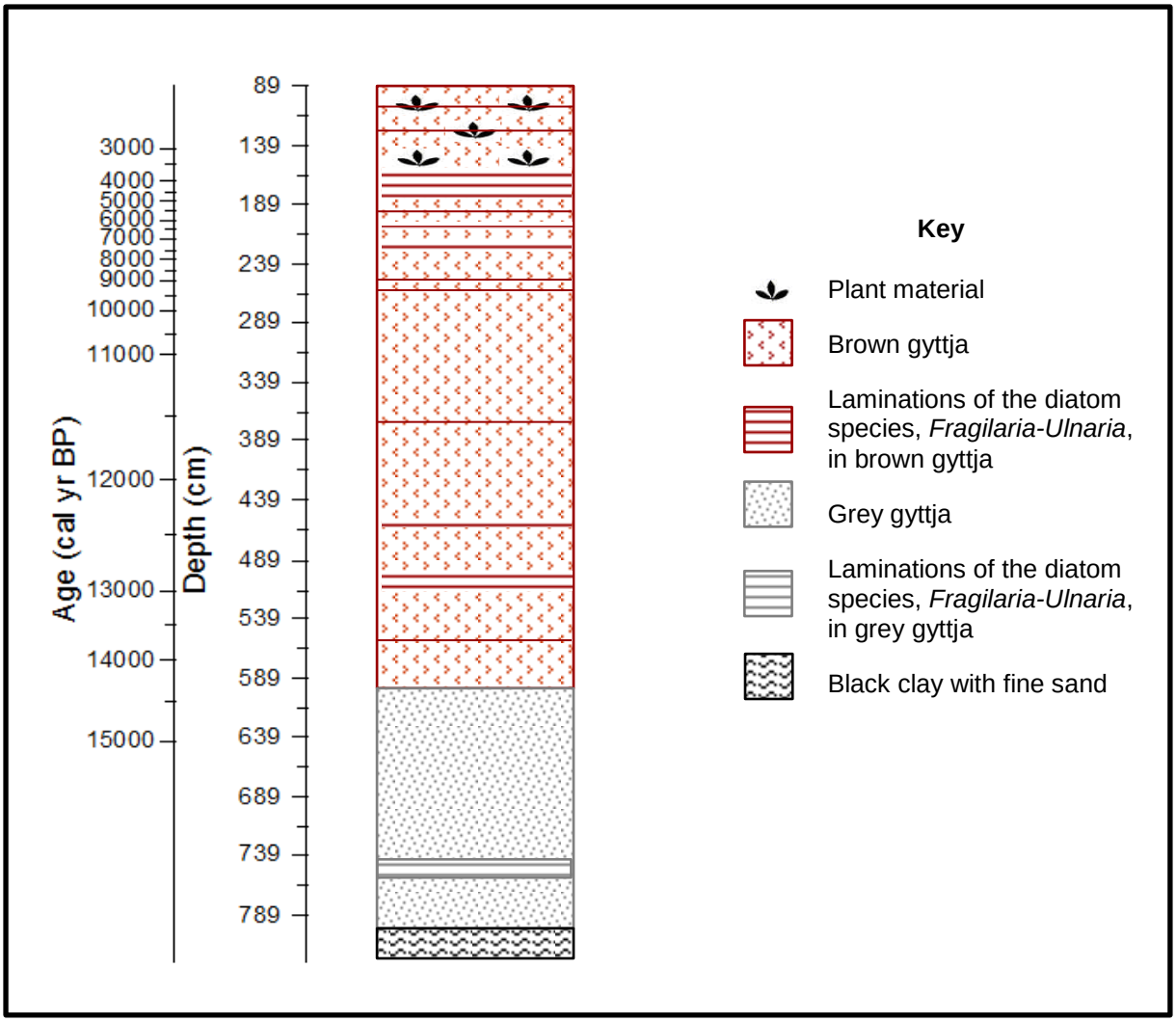

Figure 6.2. Lithological profile of Hayk-01-2010.

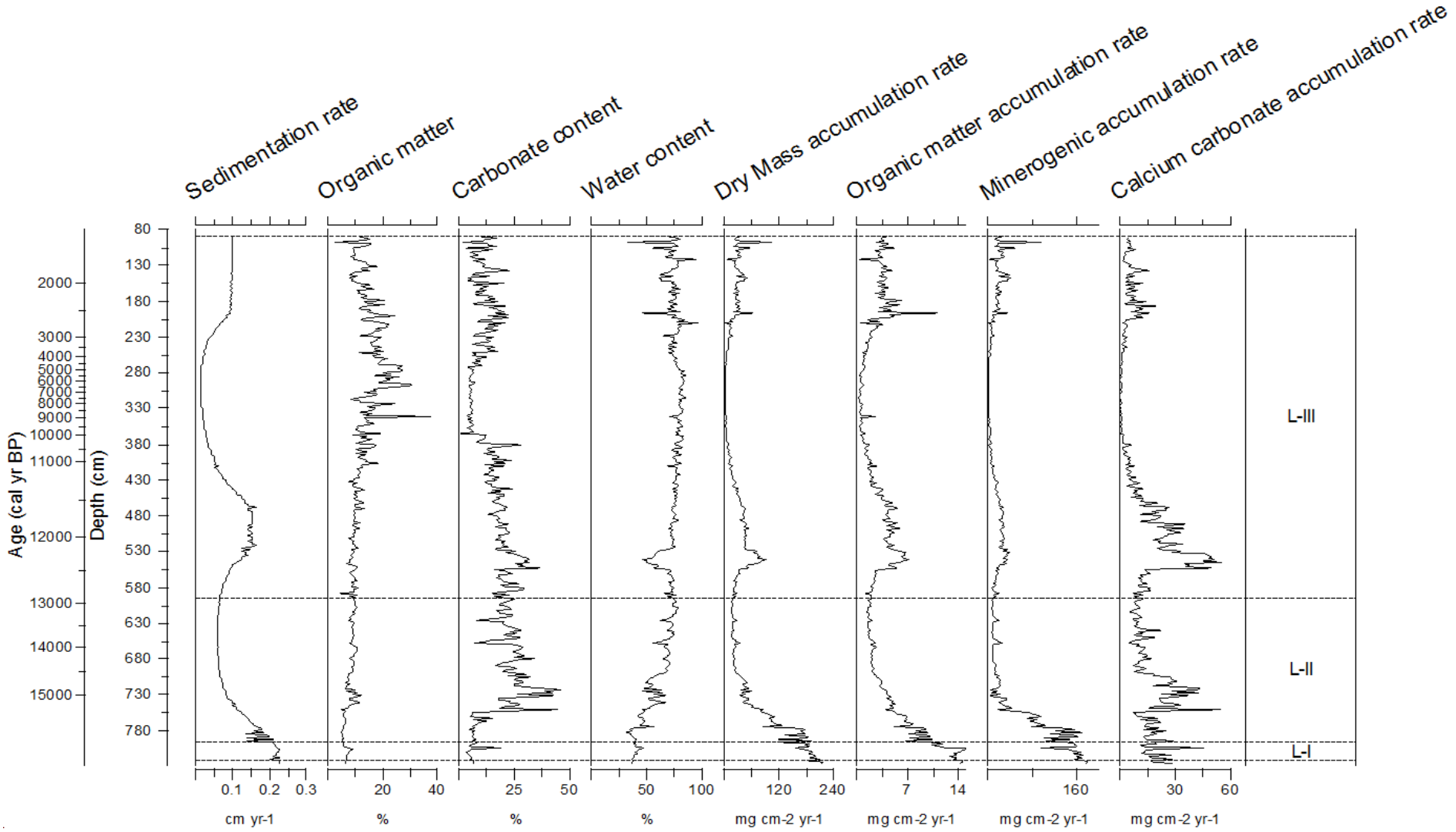

Figure 6.3. The three main lithostratigraphical units (L-I – III) identified in Hayk-01-2010. Organic, carbonate and water content are expressed as percentages of the total wet weight of the sediment, sedimentation accumulation rate as cm yr^{-1}, dry mass, organic matter, calcium carbonate ($CaCO_3$) and minerogenic accumulation rates as mg cm^{-2} yr^{-1}.

occasionally marbled with brown gyttja. Between 739.0 – 754.5 cm faint marl laminations are identifiable at irregular intervals. Organic matter remains low and relatively constant (4.7 – 10.8 %) throughout the unit. Carbonate content varies significantly (3.0 – 44.7 %) in a series of peaks and troughs, whilst water content shows an overall increase from 37.6 – 75.8 %. Dry mass, organic matter and minerogenic accumulation rates all decline in this unit and then plateau, whilst calcium carbonate increases in the mid-zone (750.0 – 710.5 cm) and then declines. The largest unit (L-III, 595.0 – 89.0 cm) consists of brown gyttja (varying from dark brown-grey to brown in colour) intermixed with silt. Traces of plant material (> 0.1 – < 2.0 mm in size) are found in the top 70.0 cm. This unit is reasonably well stratified throughout. A feature of interest is the irregularly spaced, thick (> 1.0 – 7.0 mm) matrix of laminations consisting of a pulp-like dark yellow deposit. Smear slides of this deposit show that it contains dense mats of the long, slender diatom taxa, *Fragilaria* and *Ulnaria*. Organic matter increases steadily from 595.0 cm (9.3 %), reaching maximum values between 340.0 – 298.0 cm (38.0 – 30.7 %) after which it declines (11.2 %). Carbonate content gradually declines between 595.0 – 388.0 cm (21.8 – 13.7 %) before peaking at 380.0 cm (54.2 %). A steady low ($\bar{x}$ = 5.8 %) is then observed between 376.0 – 272.0 cm, after which it increases (11.8 %) between 380.0 – 89.0 cm. Water content is highest in this unit, remaining relatively constant ($\bar{x}$ = 74.8 %). Dry mass, organic matter, minerogenic and calcium carbonate accumulation rates increase from the base of the unit up to ~ 544.5 – 536.0 cm. Rates then steadily decline and reach minimum values between ~ 334.0 – 320.0 cm. Values increase again and remain relatively stable between ~ 196.0 – 89.0 cm.

6.4 X-ray Fluorescence (XRF) Geochemistry

Selected geochemical elemental concentrations for Hayk-01-2010 are shown in Figure 6.4. Peak area profiles for calcium (Ca), potassium (K), silicon (Si) and titanium (Ti) have been normalised by incoherent scatter (inc) to minimise the effect of organic matter and water content variability, unrelated to sediment geochemistry (Marshall et al. 2011). Ratios of potassium: aluminium (K/Al, an approximation of chemical over mechanical weathering; Burnett et al. 2011), silicon: titanium (Si/Ti, a proxy for biogenic silica productivity) and zirconium: rubidium (Zr/Rb, a proxy for grain size of allochthonous material found in lake sediments) are shown. Magnetic susceptibility (κ) is used as a proxy of allochthonous inputs, whilst the incoherent:

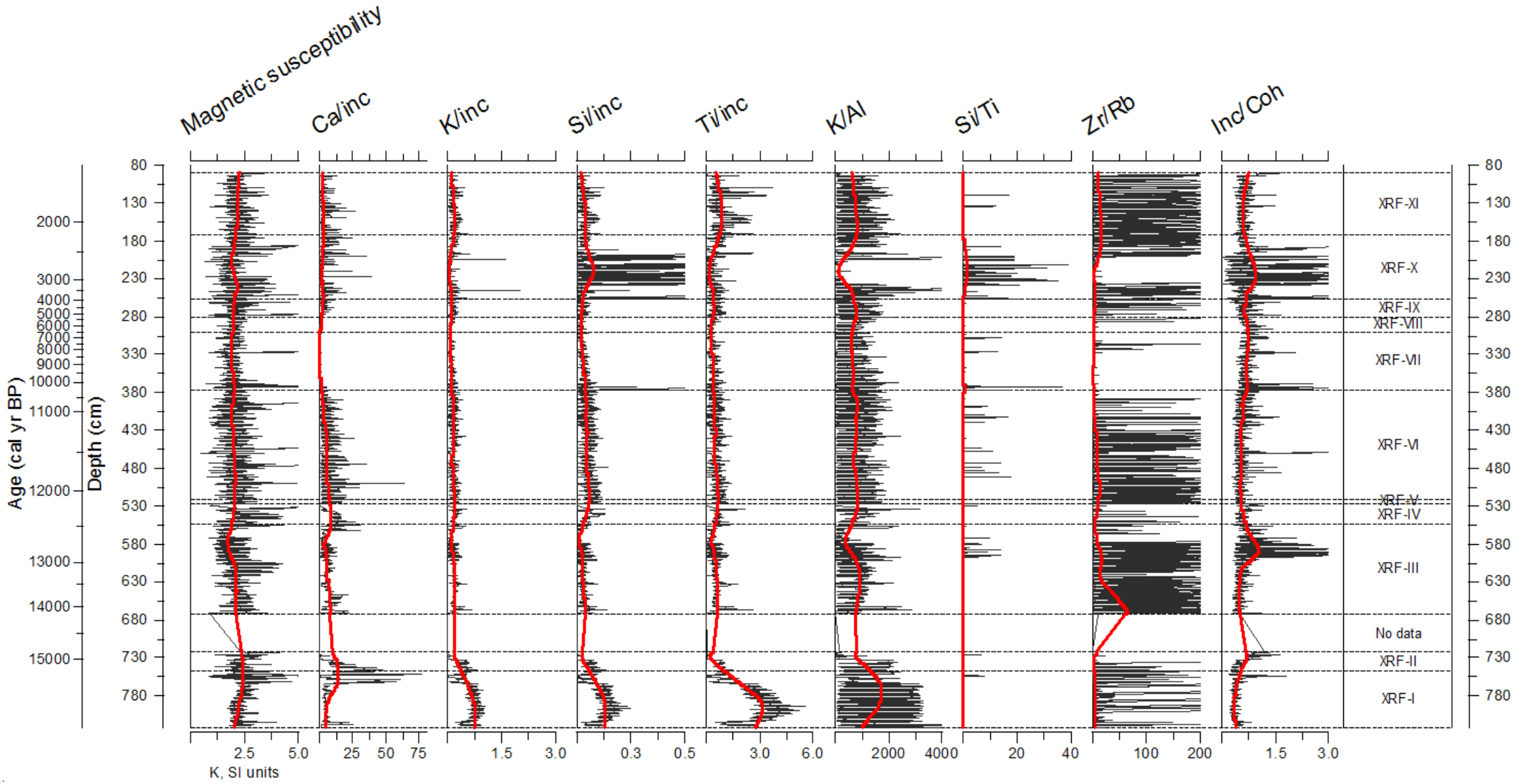

Figure 6.4. XRF results for Hayk-01-2010. Elemental data is given as peak area units with element X-ray fluorescence values divided by incoherent scatter (inc). Magnetic susceptibility is given as κ, SI units. The mean trend is indicated in red.

coherent (inc/coh) backscatter intensity ratio serves as a qualitative proxy of organic matter content. The ratio is dependent on the average atomic number of material in the sediment; organic carbon has a lower average atomic mass than carbonates, aluminosilicates, or silica. The ratio therefore increases with greater organic carbon concentration (Burnett et al. 2011). Ratios are dimensionless. Unfortunately, the Itrax® core scanner became inoperable and required mechanical maintenance before core 7B could be scanned. As such, geochemical data are not available between 722.83 – 673.14 cm.

The lithogenic elements, K, Si and Ti are at their maximum values at the base of the sediment record and immediately decline, plateauing at ~ 743.5 cm. Ca values, representing authigenic carbonate minerals or biogenic calcium carbonates, in contrast, show a slight increase from ~ 822.0 – 799.0 cm, which then become more rapid and peak at ~ 759.0 cm before declining. Similar to Ca, inc/coh increases from the base of the sediment, peaking at ~ 735.5 cm. The K/Al ratio also increases early in the sediment record, reaching maximum values between ~ 793.5 – 769.0 cm and then declining. Si/Ti and Zr/Rb show little overall variability from the base of the sediment record to 722.8 cm.

Between ~ 673.1 – 249.0 cm, most of the elemental profiles show moderate fluctuations but are stable overall. K, Si and Ti show a slight decline, as does Ca, though the decrease is more pronounced and minimum values are reached earlier than other elements between ~ 367.0 – 305.5 cm. In all these profiles, a minor decrease occurs at ~ 588.0 cm but elemental values recover and maintain their steady trends. This same decrease is also evident in the Si/Ti ratio after which values maintain a relatively stable trend. In the inc/coh ratio, an increase is evident at ~ 588.0 cm, as well as in the Si/Ti ratio, though the increase is less substantial. After this fluctuation, all elemental ratios maintain stable values. In contrast to the other profiles, Zr/Rb reaches maximum values at ~ 671.5 cm, after which it declines sharply until ~ 629.0 cm and then demonstrates an overall, slight decrease.

All profile values vary between ~ 249.0 – 189.0 cm. K, Ti, K/Al and Zr/Rb experience a decrease centred at ~ 231.0 – 227.0 cm. Ca shows a very minor decline centred at ~ 229.0 cm but it is less pronounced that the other elemental profiles. Si, Si/Ti and

inc/coh demonstrate an increase between ~ 249.0 – 189.0 cm. Upon recovery, elemental profiles are relatively stable again. K, Ti and K/Al show slight declines from ~ 165.0 cm to the top of the sediment record, whilst inc/coh shows a steady increase. Magnetic susceptibility remains stable throughout the record, showing very little overall variability.

6.5 The Diatom Record

The diatom record for Hayk-01-2010 is shown in Figure 6.5. In addition, habitat groups, valve concentration (valves x 10^5 g^1 dry sediment, hereafter x 10^5 g^{-1}), accumulation rate (x 10^6 valves cm^{-2} yr^{-1}), dissolution index (*F* index), Hill's N2 species diversity index, which measures the number of species in each sediment interval where each taxon is weighted by its abundance (Hill 1973), as well as DCA axis 1 and 2 values are displayed in Figure 6.6. Diatom-inferred (DI) conductivity is shown in Figure 6.7. The stratigraphic diagrams have been divided into ten statistically significant zones (D-I – D-X).

6.5.1 Zone D-I (822.0 – 748.0 cm, 15,600 – 15,200 cal yr BP) Diatoms were not preserved in sufficient quantities in this zone to count and so have been simply identified as being present (Fig. 6.8). Diatoms identified include *Cyclotella cyclopuncta*, *Cyclotella ocellata* and *Hantzschia amphioxys*. Diatom-inferred conductivity reaches a maximum in this zone (~ 9,000 µS cm^{-1}) but then declines significantly towards the top of the zone (< ~ 800 µS cm^{-1}).

6.5.2 Zone D-II (748.0 – 716.0 cm, 15,200 – 14,800 cal yr BP) This zone is characterised by the dominance of the planktonic *C. ocellata*, which ranges between 41.5 – 100.0 % abundance (Fig. 6.8). In the upper zone (730.5 – 711.0 cm), less common species include the planktonic *C*. c*yclopuncta* ($\bar{x}$ = 3.2 %) and the facultatively planktonic *Pseudostaurosira brevistriata* ($\bar{x}$ = 1.5 %) and *Staurosirella pinnata* ($\bar{x}$ = 2.6 %). The benthic *Encyonema muelleri* ($\bar{x}$ = 9.8 %) and *Epithemia sorex* ($\bar{x}$ = 5.1 %) are rare. Valve concentration is low ($\bar{x}$ = 100 x 10^5 g^{-1}), and preservation is poor (maximum *F* index value of 0.3). Diatom-inferred conductivity averages ~ 300 µS cm^{-1}.

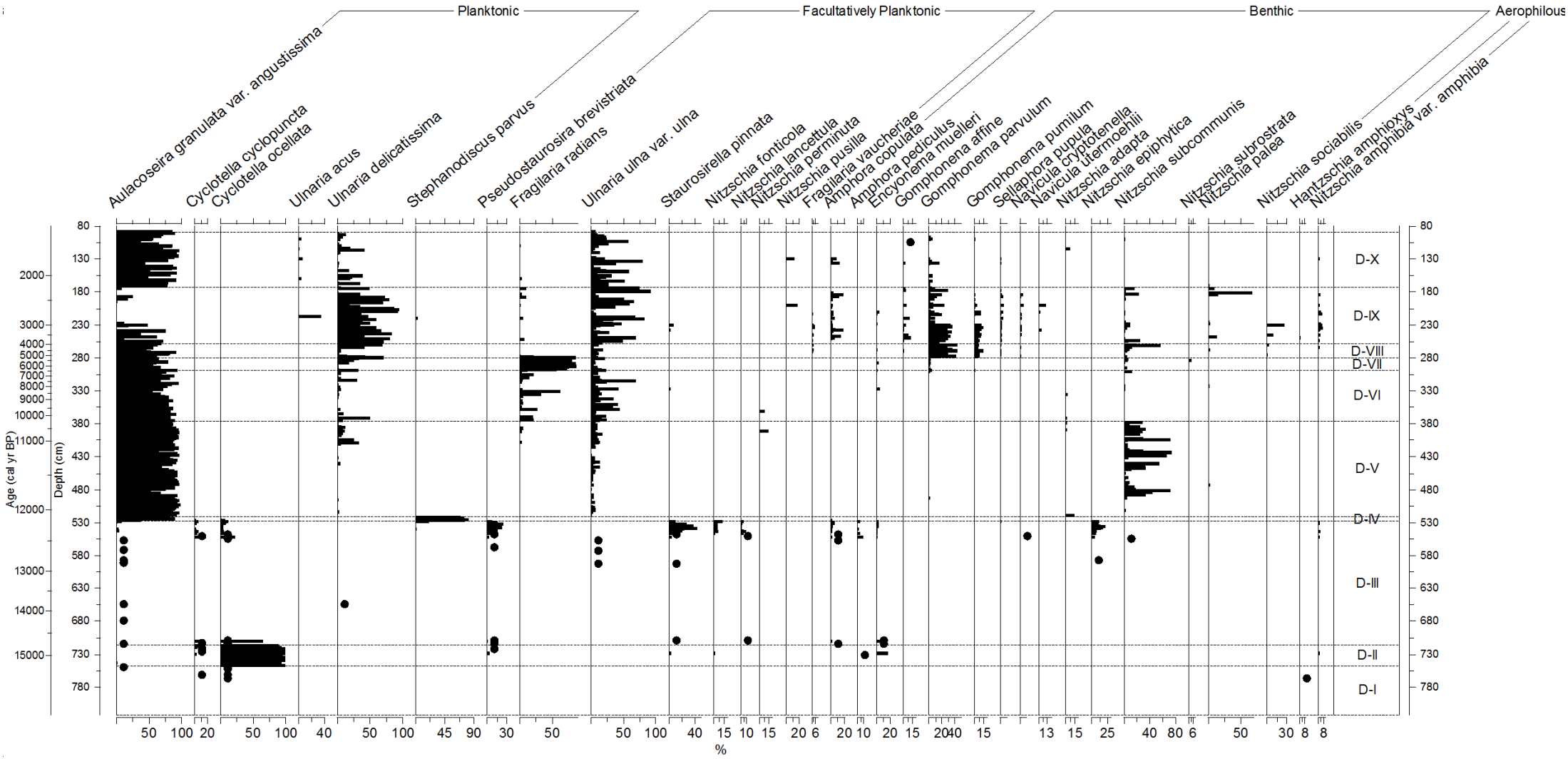

Figure 6.5 (a). Diatom data, shown as percentages (%), for core Hayk-01-2010, against depth (cm), arranged according to habitat preference. Circles represent depths at which a taxon is present in low abundances (< 0.5 %). Average sample standard deviation is 2.82 %.

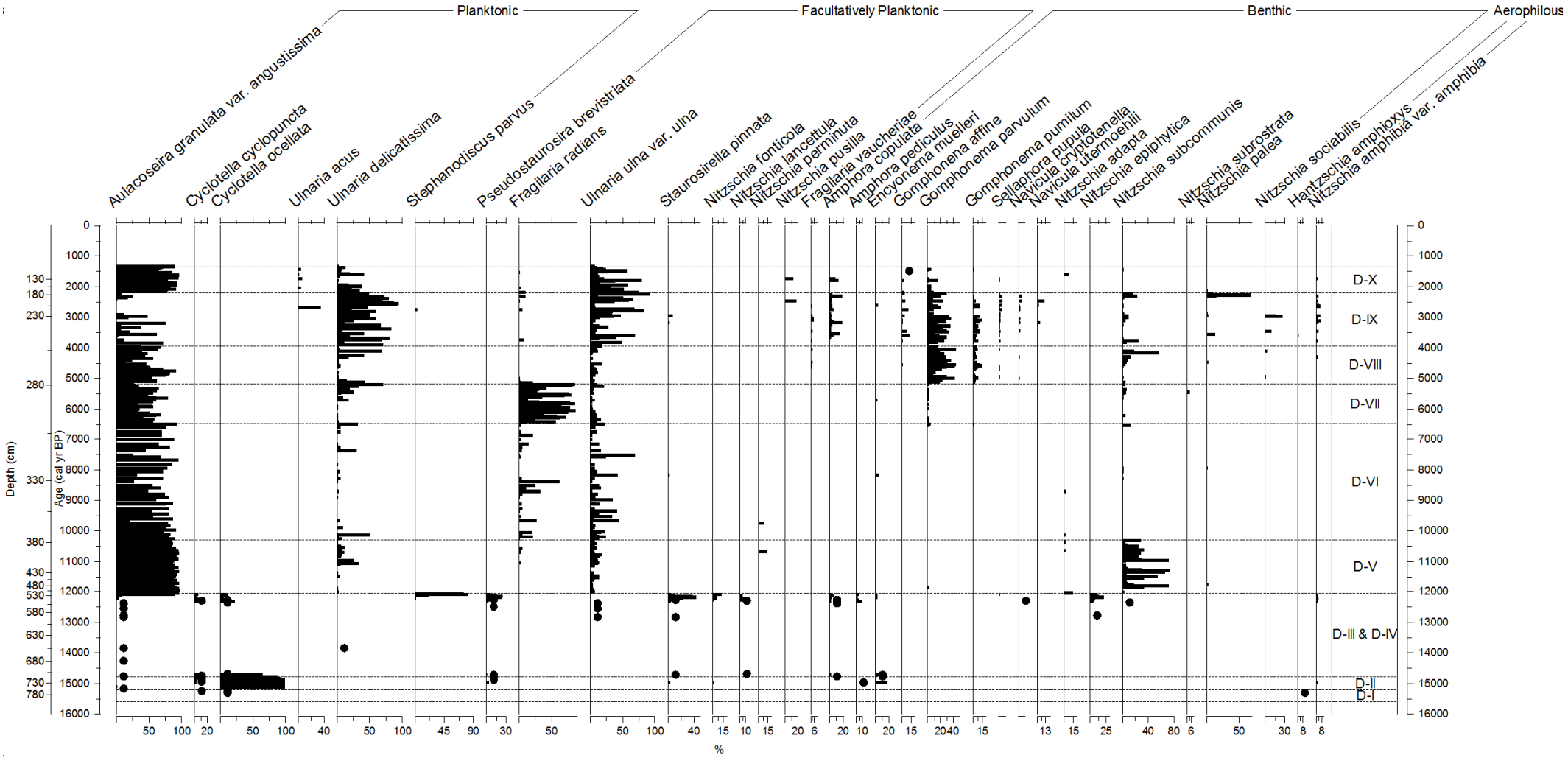

Figure 6.5 (b). Diatom data, shown as percentages (%), for core Hayk-01-2010, against age (cal yr BP), arranged according to habitat preference. Circles represent depths at which a taxon is present in low abundances (< 0.5 %). Average sample standard deviation is 2.82 %.

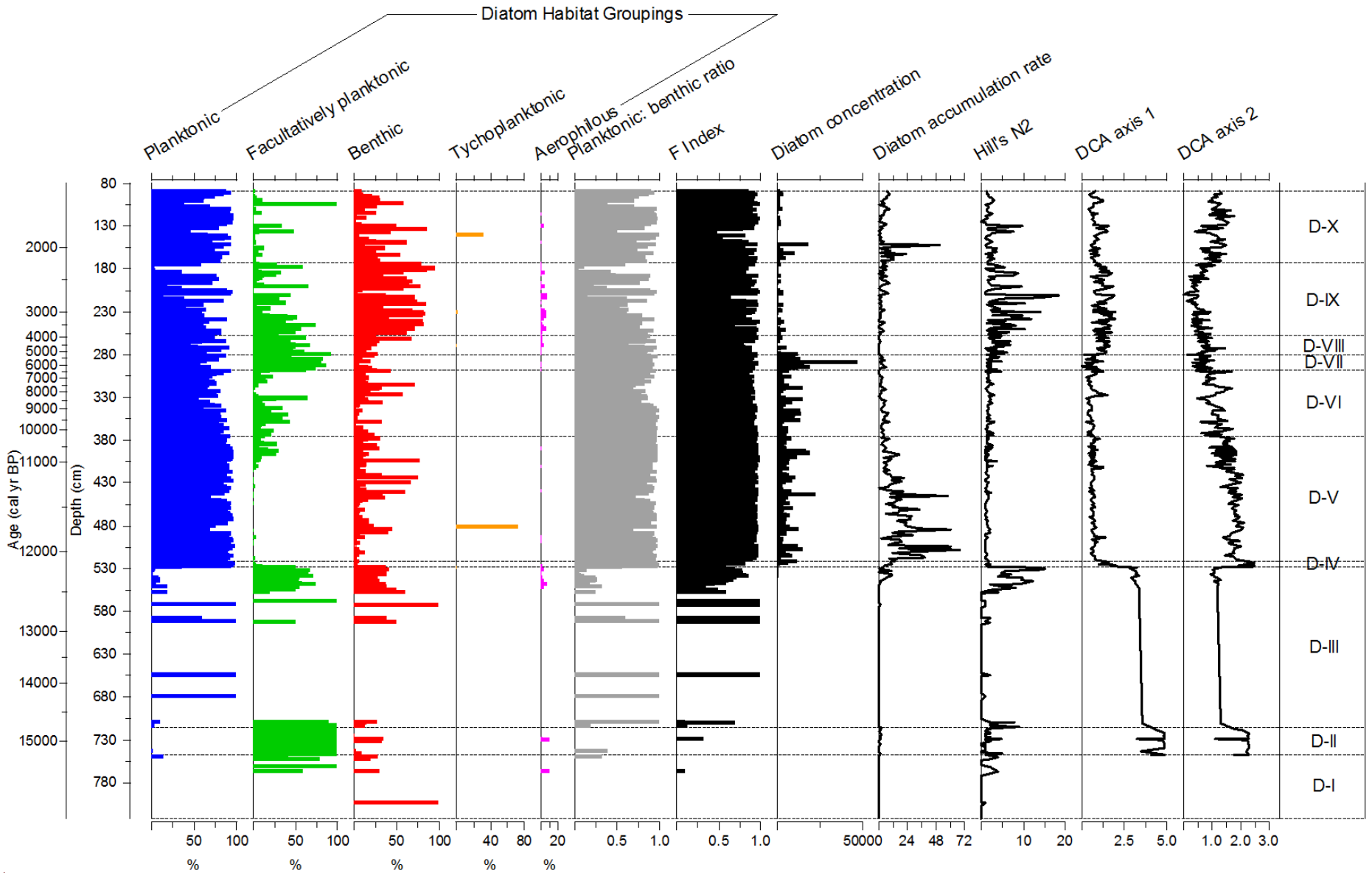

Figure 6.6. Associated diatom metrics. Habitats are shown as percentage of total diatom assemblage (%), concentration as valves x 10^5 g^{-1} dry sediment and accumulation rate as x 10^6 valves cm^{-2} yr^{-1}.

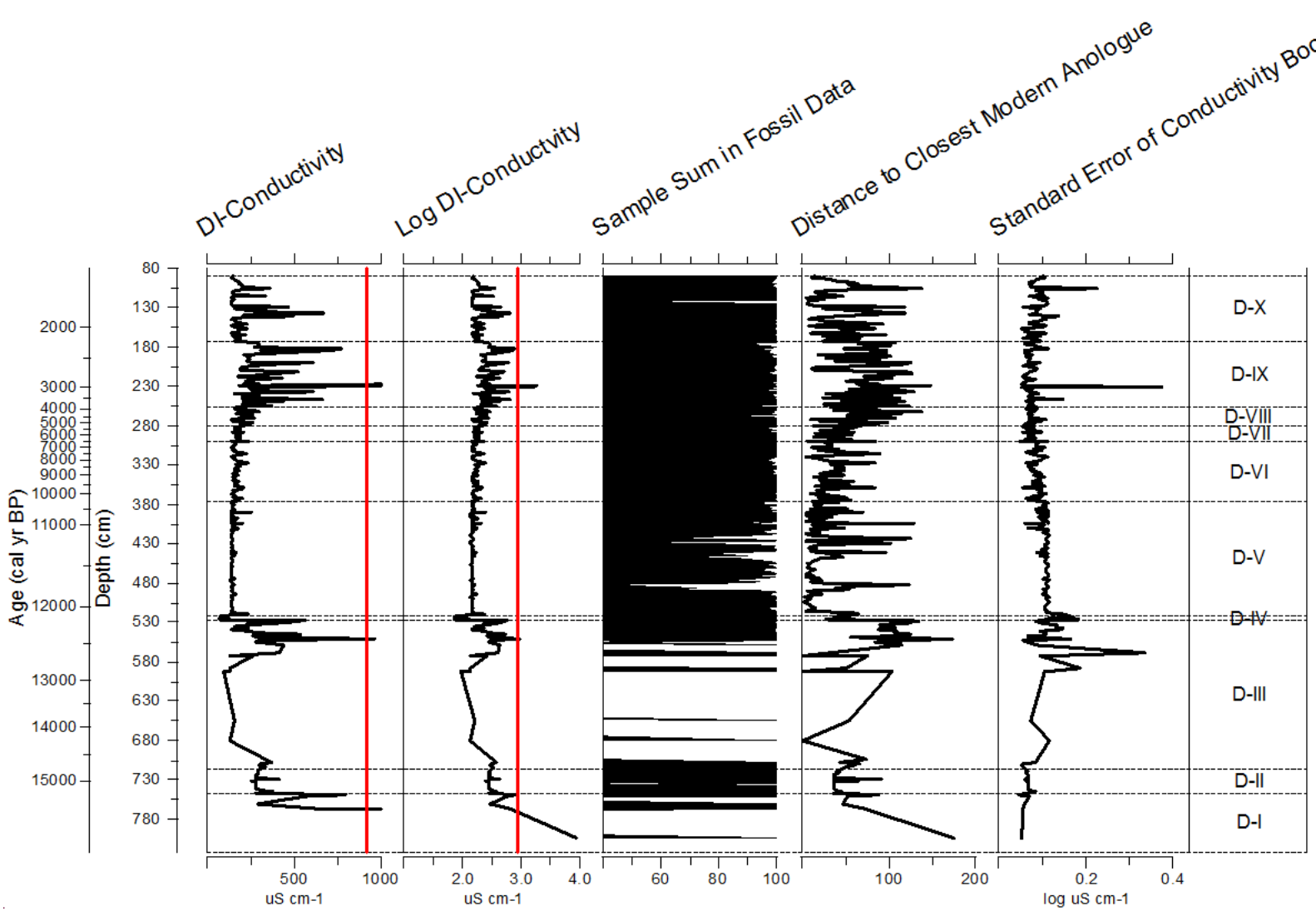

Figure 6.7. Diatom-inferred (DI) conductivity created using weighted averaging inverse deshrinking. Conductivity is given as µS cm^{-1}. Conductivity recorded in 1969 (920 µS cm^{-1}) is indicated by the red line (Baxter and Golobitsh 1970). Reconstruction diagnostics are used to evaluate model performance. Diatom preservation is poor in zones D-I – D-III (see Fig. 6.6), hence the intermittently low sample sum in fossil data.

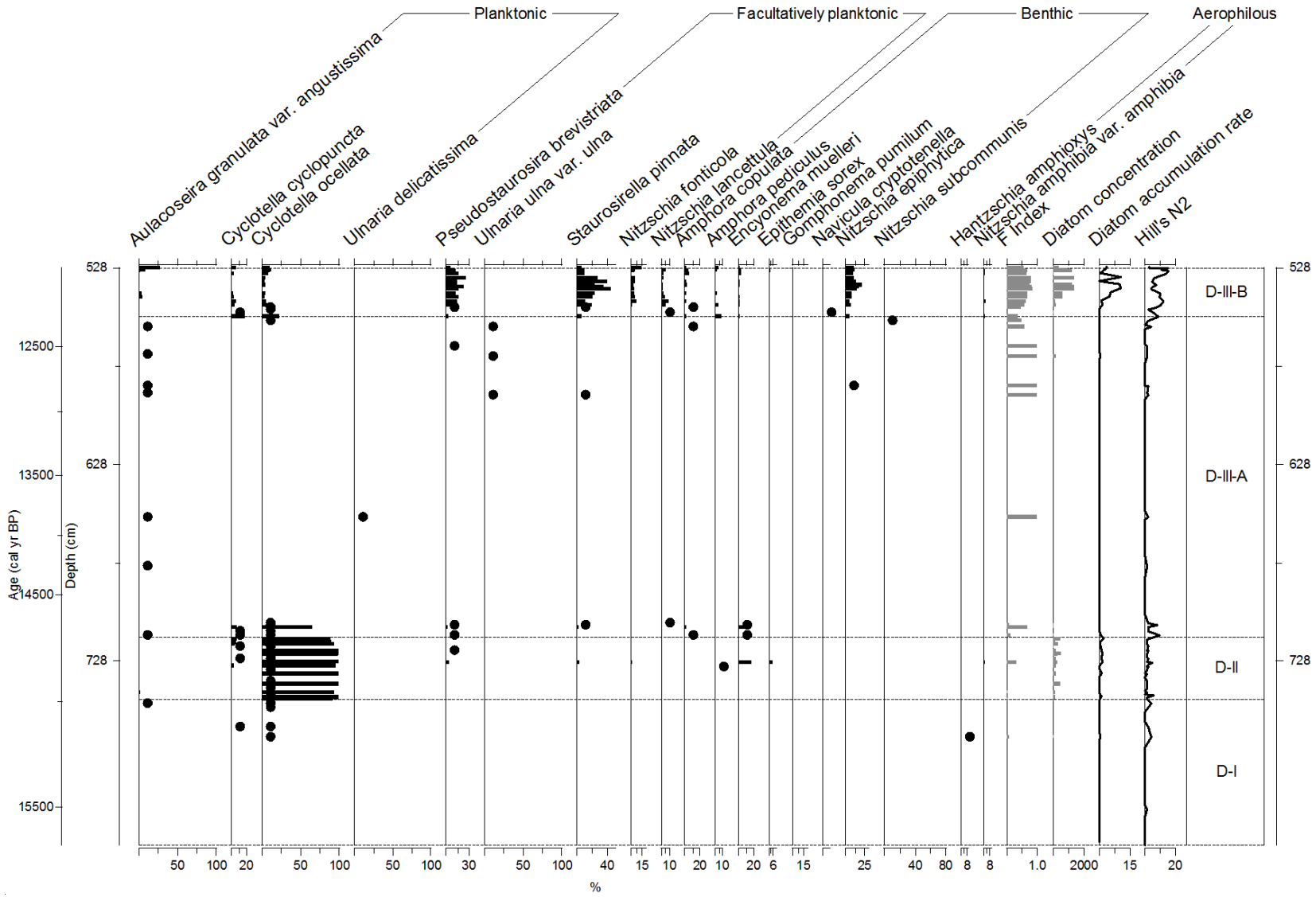

Figure 6.8. Diatom data, shown as percentages (%), for zones D-I to D-III, arranged according to habitat preference. Circles represent depths at which a taxon is present in low abundances (< 0.5 %). Diatom concentration is shown as valves x 10^5 g^{-1} dry sediment and accumulation rate as x 10^6 valves cm^{-2} yr^{-1}. Average sample standard deviation is 2.82 %.

6.5.3 Zone D-III (716.0 – 528.13 cm, 14,800 – 12,100 cal yr BP) This zone can be divided into two sub-zones; the first being mostly devoid of diatoms, and the second which acts as a transition between depths where diatoms are largely absent and the overlying zones where valve concentration increases dramatically (Fig. 6.8). Sub-zone D-III-A (716.0 – 553.0 cm, 14,800 – 12,300 cal yr BP) is the largest sub-zone but diatoms were not preserved in sufficient quantities and so have been simply identified as being present. Diatoms identified include *Aulacoseira granulata* var. *angustissima*, *P. brevistriata*, *S. pinnata*, *Ulnaria ulna* var. *ulna* and *Nitzschia epiphytica*. Diatom-inferred conductivity is low ($\bar{x}$ = ~ 260 µS cm^{-1}), however it is important to note there are few samples to reconstruct conductivity from in this sub-zone, which will have disproportionately biased the model.

Sub-zone D-III-B (553.0 – 528.13 cm, 12,300 - 12,100 cal yr BP) is characterised by the establishment of a diverse diatom assemblage featuring planktonic, facultatively planktonic and benthic taxa. *Cyclotella cyclopuncta* and *C. ocellata* simultaneously peak at the start of the sub-zone (18.0 % and 24.0 % respectively, 553.5 cm) and then maintain low abundances (< 5.4 %). The facultatively planktonic *P. brevistriata* and *S. pinnata* begin to increase at 547.0 cm and reach moderate abundances (26.0 % and 44.7 % respectively) between 539.0 – 533.0 cm, before declining (both 1.3 %). *Nitzschia epiphytica* likewise increases at 547.0 cm and maintains an average abundance of 11.2 %. The aerophilous, *H. amphioxys* and *Nitzschia amphibia* var. *amphibia* are also present (2.0 % and 4.0 % respectively). Hill's N2 diversity values indicate that species diversity increased considerably in this sub-zone. Diatom-inferred conductivity demonstrates considerably variability in this sub-zone, ranging from ~ 150 – 1000 µS cm^{-1}.

6.5.4 Zone D-IV (528.13 – 521.13 cm, 12,100 – 12,050 cal yr BP) This zone is dominated by the planktonic taxon, *Stephanodiscus parvus* (Fig. 6.9). With the exception of a single, isolated occurrence in Zone IX (4.4 %, 219.5 cm), this is the only zone in the diatom record where *S. parvus* is present. The taxon increases rapidly from 56.0 % to 81.5 % (528.0 – 526.25 cm), and with the exception of a short-lived decrease towards the mid-zone (8.0 %, 525.0 cm), maintains high abundances throughout ($\bar{x}$ = 60.0 %). *Aulacoseira granulata* var. *angustissima*

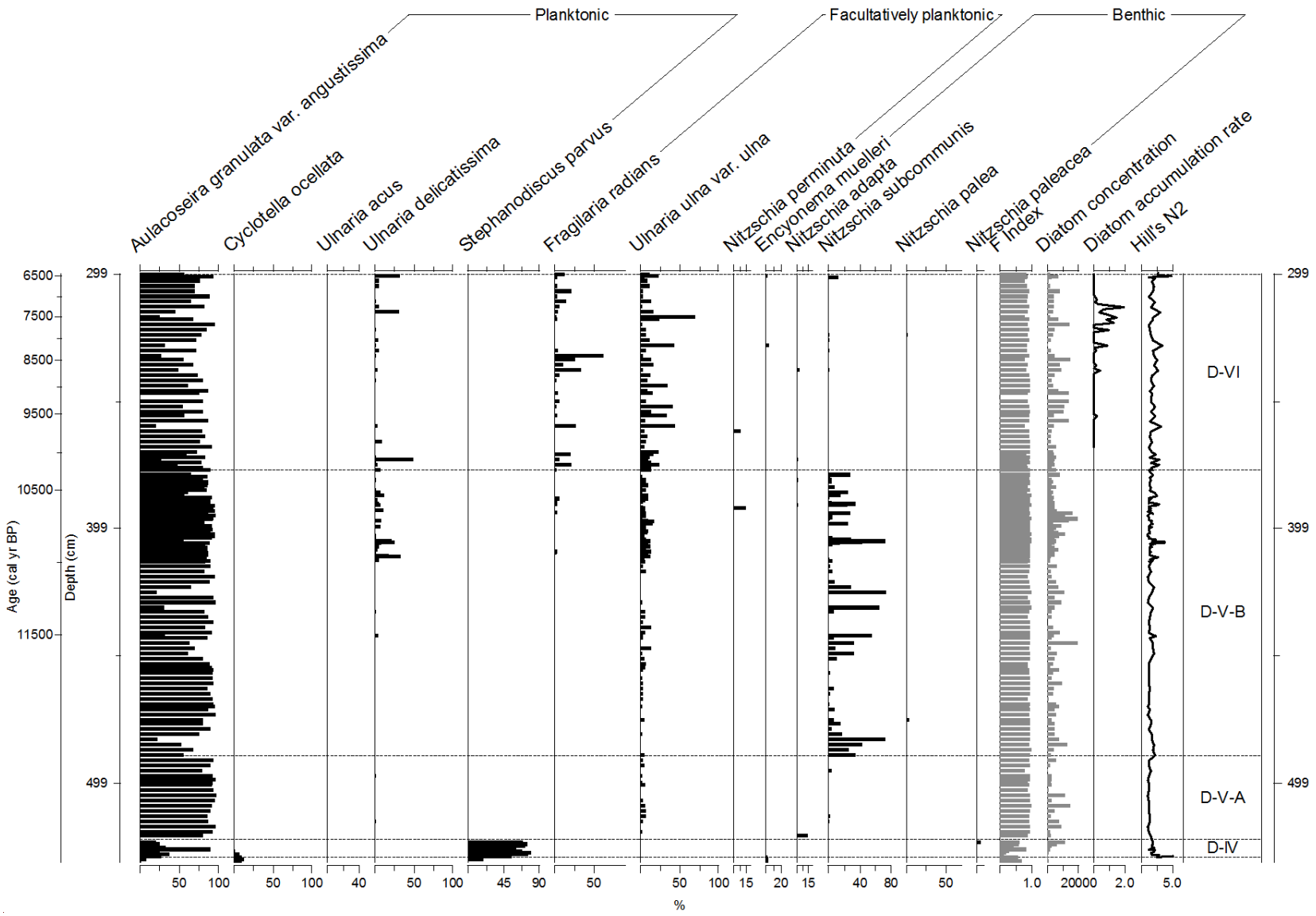

Figure 6.9. Diatom data, shown as percentages (%), for zones D-IV to D-VI, arranged according to habitat preference. Circles represent depths at which a taxon is present in low abundances (< 0.5 %). Diatom concentration is shown as valves x 10^5 g^{-1} dry sediment and accumulation rate as x 10^6 valves cm^{-2} yr^{-1}. Average sample standard deviation is 2.82 %.

demonstrates a dramatic increase in abundance from 27.3 % to 91.0 % (528.0 – 525.0 cm), coinciding with the drop in *S. parvus*, after which it maintains a steady occurrence ($\bar{x}$ = 24.5 %). *Hantzschia amphioxys* and *N. amphibia* var. *amphibia* continue to be rare. Valve preservation is poor at the base of the zone but improves significantly (*F* index values of 0.36 – 0.92). Valve concentration averages ~ 1,700 x 10^5 g^{-1}. Diatom-inferred conductivity is very low, averaging ~ 90 µS cm^{-1}. A minimum of 70 µS cm^{-1} is observed at 526.25 cm.

6.5.5 Zone D-V (521.13 – 376.05 cm, 12,050 – 10,300 cal yr BP) This zone is characterised by the dominance of the planktonic *A. granulata* var. *angustissima*, which has an average abundance of 81.8 % (Fig. 6.9). Due to the dominance of *A. granulata* var. *angustissima*, Hill's N2 diversity values indicate that species diversity is low throughout this zone. Valves are very well preserved (*F* index values of 0.79 – 0.99) and concentration averages ~ 4,000 x 10^5 g^{-1}. Accumulation rate is greatest in this zone, reaching a maximum of 67.91 x 10^6 valves cm^2 yr^{-1}. Diatom-inferred conductivity is generally stable, ranging from ~ 140 – 250 µS cm^{-1}.

Sub-zone D-V-A (521.13 – 488.0 cm, 12,050 – 11,850 cal yr BP) is characterised by the overwhelming dominance of *A. granulata* var. *angustissima*, which accounts for 81.0 – 99.0 % of all diatoms present. The facultatively planktonic *U. ulna* var. *ulna* is present intermittently in low abundances (< 8.5 %). *Nitzschia adapta* is present at 520.0 cm (14.7 %), whilst the planktonic *Ulnaria delicatissima* and benthic *Nitzschia subcommunis* occur at several depths in very low abundances (2.0 % and 5.3 % respectively).

Sub-zone D-V-B (488.0 – 376.05 cm, 11,850 – 10,300 cal yr BP) continues to be dominated by *A. granulata* var. *angustissima* ($\bar{x}$ = 80.5 %). Several periods of decline are evident however. The first is between 488.0 – 480.0 cm, where *A. granulata* var. *angustissima* declines to an average of 55.7 %. This occurs simultaneously with the appearance of *N. subcommunis*, which increases rapidly from 35.1 – 73.0 % between 488.0 – 482.0 cm. The second period of *A. granulata* var. *angustissima* decline is found from 448.0 – 444.0 cm where it decreases to 66.1 %, and the third at 430.0 cm and 424.0 cm where the taxon declines to 27.3 %, sandwiching a period of higher abundance (95.8 %, 428.0 – 426.0 cm). Several other short-lived

decreases occur at 404.4 cm (25.3 %), 390.0 cm (57.8 %) and 386.0 cm (58.2 %). Also present in this sub-zone is *N. subcommunis*, which exhibits a series of peaks and troughs. Following low abundances ($\bar{x}$ = 5.1 %), *N. subcommunis* experiences a substantial increase (33.6 – 55.8 %) between 448.0 – 441.0 cm. A decline occurs, after which the taxon exhibits several peaks (66.0 % and 74.8 %) from 430.0 – 424.0 cm. Following a second decline, *N. subcommunis* peaks at 404.0 cm (73.7 %) and then ranges between 4.3 – 35.2 %. *Ulnaria delicatissima* increases dramatically at 410.3 cm (34.7 %), after which it decreases slightly (26.7 %, 315.4 cm) and then maintains low abundances (< 12.7 %). *Ulnaria ulna* var. *ulna* continues to occur in low abundances ($\bar{x}$ = 5.8 %).

6.5.6 Zone D-VI (376.05 – 299.0 cm, 10,300 – 6,500 cal yr BP) This zone continues to be dominated by *A. granulata* var. *angustissima*, though in slightly lower abundances than the underlying zone ($\bar{x}$ = 67.5 %) (Fig. 6.9). A series of declines occur at 359.0 cm (20.6 %), 331.0 cm (27.6 %), 327.0 cm (33.3 %) and 316.0 cm (25.8 %). The facultatively planktonic *U. ulna* var. *ulna* experiences large increases in abundance throughout the zone (35.5 – 70.6 %) in a series of peaks isolated by lower abundances ($\bar{x}$ = 10.8 %). *Ulnaria delicatissima* peaks at 372.0 cm (50.7 %) after which it declines dramatically, exhibiting only two moderate increases at 314.0 cm (31.3 %) and 300.0 cm (33.3 %). *Fragilaria radians* likewise exhibits a series of peaks in abundance (27.0 – 63.5 %) at 359.0 cm, 337.0 cm and 331.0 cm. It is notable that several of the peaks in *Fragilaria* and *Ulnaria* taxa occur simultaneously with declines in *A. granulata* var. *angustissima*. Rare taxa include *S. pinnata*, *Nitzschia perminuta* and the benthic *E. muelleri*, *Nitzschia adapta*, *Tryblionella gracilis* and *N. subcommunis*. Valve concentration increases to an average of ~ 4,400 x 10^5 g^{-1}, whilst accumulation rate declines (< 8.2 x 10^6 valves cm^2 yr^{-1}). Preservation is excellent (average *F* index value of 0.91). Diatom-inferred conductivity continues to remain stable, averaging ~ 170 µS cm^{-1}.

6.5.7 Zone D-VII (299.0 – 280.13 cm, 6,500 – 5,200 cal yr BP) This zone sees large increases in the abundance of the facultatively planktonic *F. radians* ($\bar{x}$ = 46.5 %), which reaches a maximum of 88.4 % at 293.25 cm (Fig. 6.10). By 281.25 cm abundance has declined rapidly to 3.0 %. *Ulnaria delicatissima* is very low at the base of the zone (< 2.8 %) until 288.0 cm when it rises to 17.9 % and then steadily

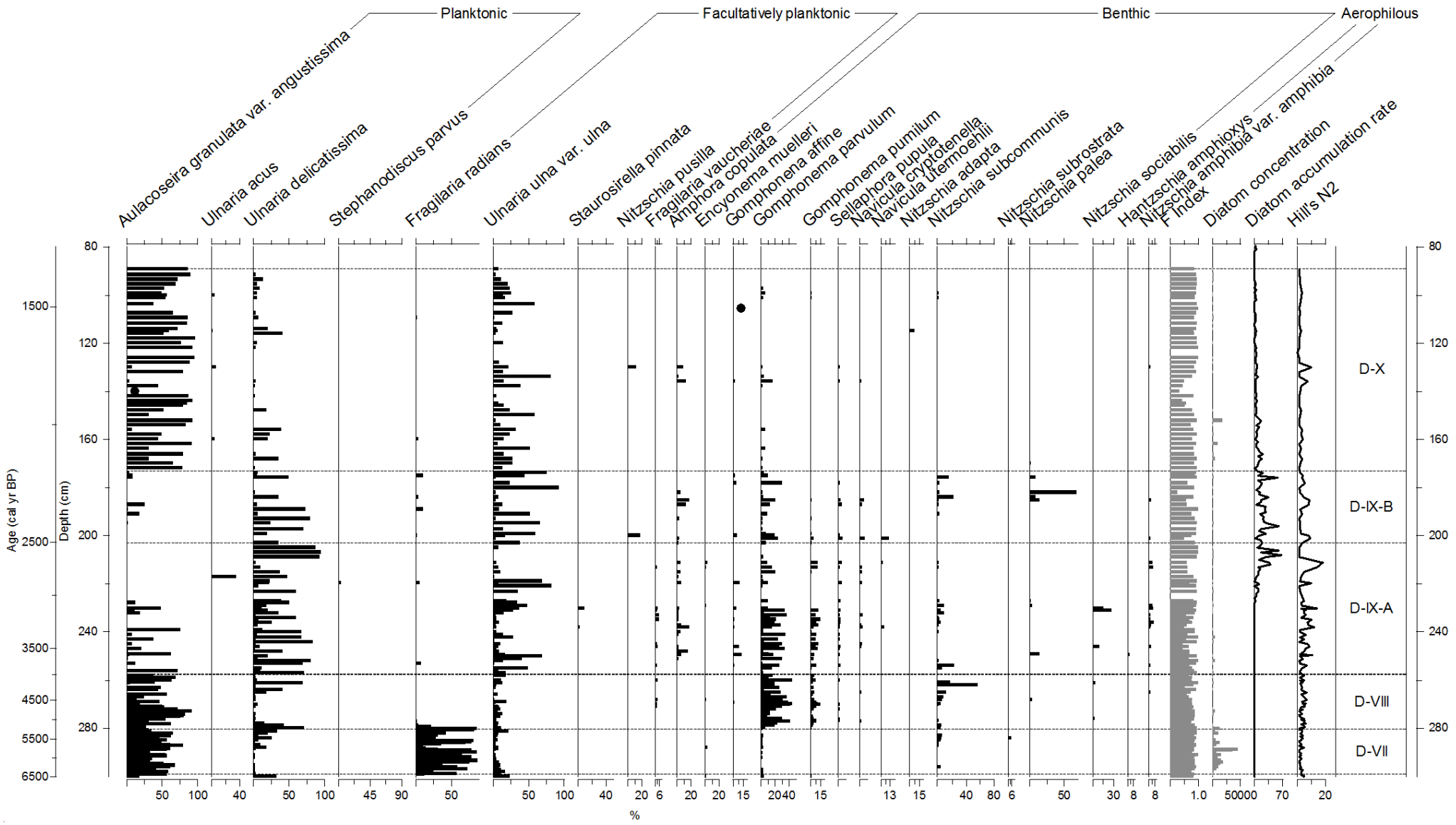

Figure 6.10. Diatom data, shown as percentages (%), for zones D-VII to D-X, arranged according to habitat preference. Circles represent depths at which a taxon is present in low abundances (< 0.5 %). Diatom concentration is shown as valves x 10^5 g^{-1} dry sediment and accumulation rate as x 10^6 valves cm^{-2} yr^{-1}. Average sample standard deviation is 2.82 %.

increases, peaking at 72.0 % (280.0 cm) before a moderate decline (43.4 %, 278.8 cm). *Ulnaria ulna* var. *ulna* maintains a steady abundance ($\bar{x}$ = 5.2 %). *Aulacoseira granulata* var. *angustissima* declines in this zone, averaging 36.6 %, though a peak occurs at 287.25 cm (79.7 %). *Gomphonema parvulum* occurs sporadically (< 4.3 %). *Nitzschia subcommunis* likewise appears intermittently (< 8.2 %). Maximum valve concentration in the diatom record occurs at 288.75 cm, reaching ~ 47,100 x 10^5 g^{-1} and preservation is excellent (average *F* index value of 0.85). Diatom-inferred conductivity increases marginally, averaging ~ 180 µS cm^{-1}.

6.5.8 Zone D-VIII (280.13 – 257.5 cm, 5,200 – 3,950 cal yr BP) This zone is characterised by the establishment of the benthic taxon, *G. parvulum*, which maintains a relatively stable abundance ($\bar{x}$ = 19.5 %) (Fig. 6.10). *Gomphonema pumilum* similarly established itself, though at lower abundances ($\bar{x}$ = 4.8 %). The benthic *N. subcommunis* continues to appear occasionally, varying significantly between 0.33 – 57.1 %. *Ulnaria ulna* var. *ulna* continues to maintain a steady abundance ($\bar{x}$ = 6.0 %). The planktonic *U. delicatissima* reaches a maximum at the base of the zone (72.0 %) before declining to lower abundances (< 6.9 %). A second peak of 70.0 % occurs at 261.0 cm, before declining again. *Aulacoseira granulata* var. *angustissima* similarly continues a pattern of rising and declining, ranging between 0.33 – 91.7 %. *Fragilaria radians* is mostly absent from this zone (< 3.3 %) except at the base (22.2 %, 279.3 cm). Other rare taxa include the benthic *E. muelleri*, *Fragilaria vaucheria*, *Sellaphora pupula*, *Navicula cryptotenella*, *Nitzschia palea* and *Nitzschia sociabilis*. Valve concentration declines significantly in this zone to an average of ~ 1,270 x 10^5 g^{-1} and accumulation rate reaches a minimum (< 0.3 x 10^6 valves cm^2 yr^{-1}). Preservation overall remains very good, but is occasionally poor (*F* index value range of 0.53 – 0.98). Diatom-inferred conductivity increases in this zone from ~ 200 µS cm^{-1} at 279.25 cm, to ~ 300 µS cm^{-1} at 262.0 cm.

6.5.9 Zone D-IX (257.5 – 173.0 cm, 3,950 – 2,200 cal yr BP) This zone is defined by the rapid decline, disappearance and recovery of *A. granulata* var. *angustissima* in conjunction with an increase in the diversity of facultatively planktonic and benthic taxa (Fig. 6.10). Hill's N2 diversity values indicate this is the most species diverse zone in the sediment record. Valves continue to be well

preserved (average *F* index values of 0.79), whilst concentration ranges considerably from ~ 30 – 5,300 x 10^5 g^{-1}.

Sub-zone D-IX-A (257.5 – 203.0 cm, 3,950 – 2,500 cal yr BP) sees *A. granulata* var. *angustissima* fluctuate between 4.0 – 76.1 % up to 228.0 cm, after which it almost completely disappears from the diatom record (< 0.3 %). *Ulnaria delicatissima* maintains a relatively steady abundance, averaging 31.1 %. The planktonic *Ulnaria acus* appears once at 217.0 cm (35.9 %). *Gomphonema parvulum* continues to average 16.6 % abundance until 231.0 cm when it drops to 6.2 %. *Gomphonema pumilum* similarly declines to an average abundance of 1.8 %. *Ulnaria ulna* var. *ulna* increases steadily, reaching a maximum of 83.3 % (221.0 cm) after which is declines substantially (< 9.9 %). The facultatively planktonic *F. radians*, *S. pinnata* and the benthic *Gomphonema acuminatum*, *Gomphonema affine* are present in low abundances, as are the benthic taxa *Amphora copulata*, *E. muelleri*, *F. vaucheria*, *S. pupula*, *N. cryptotenella*, *Navicula utermoehlii* and *N. sociabilis*. The aerophilous *H. amphioxys* and *N. amphibia* var. *amphibia* appear intermittently (< 7.3 %). Diatom-inferred conductivity increases significantly throughout this zone from ~ 170 µS cm^{-1} (256.0 cm) to 1,800 µS cm^{-1} (230.0 cm).

Sub-zone D-IX-B (203.0 – 173.0 cm, 2,500 – 2,200 cal yr BP) is characterised by the rejuvenation of *A. granulata* var. *angustissima*. Two small peaks are observed at 191.0 cm (18.9 %) and 187.0 cm (26.0 %), after which the taxon declines again. Abundance then increases and reaches 78.9 % at 172.0 cm. *Ulnaria delicatissima* maintains high abundances, reaching 79.9 % (193.0 cm) before declining. *Gomphonema parvulum* averages 8.9 %, whereas *G. pumilum* appears infrequently in low abundances (< 5.6 %). *Ulnaria ulna* var. *ulna* continues to increase, reaching a maximum of 93.7 % (180.0 cm). *Fragilaria radians*, *G. affine* and *Nitzschia pusilla* are present in low abundances, as are the benthic taxa *S. pupula*, *N. cryptotenella*, *N. utermoehlii* and *N. palea*, which reaches a maximum of 68.7 % at 182.0 cm. The aerophilous *N. amphibia* var. *amphibia* is also present (4.3 %). Diatom-inferred conductivity continues to fluctuate, ranging from ~ 200 – 800 µS cm^{-1}.

6.5.10 Zone X (173.0 – 89.0 cm, 2,200 – 1,350 cal yr BP) This zone is characterised by the recovery of *A. granulata* var. *angustissima*; the taxon exhibits a

pattern of rising and declining, ranging between 1.6 – 97.0 % (Fig. 6.10). Declines at 164.0 cm, 150.0 cm, 134.0 cm and 103.5 cm are met with increases in *U. ulna* var. *ulna* (82.0 % at 134.0 cm). Overall, *U. ulna* var. *ulna* declines, reaching 8.0 % at 89.5 cm. *Ulnaria delicatissima* appears sporadically towards the base and top of the zone, averaging 9.0 %. Other facultatively planktonic and benthic taxa decline in this zone; *G. parvulum* averages 1.8 %, whilst *N. pusilla*, *A. copulata* and *N. adapta* appear intermittently. Hill's N2 values indicate species diversity declined in comparison to Zone IX, but remains high overall. Valves are very well preserved, and on occasion in pristine condition (*F* index values of 0.7 – 1.0), with the exception of a period from 146.0 – 136.0 cm where valves were more highly dissolved (*F* index values of 0.3 – 0.8). Valve concentration increases in comparison to the underlying zone, averaging ~ 1,900 x 10^5 g^{-1}. Accumulation rate also increases, peaking at 51.1 x 10^6 valves cm^2 yr^{-1} (152.5 cm). Diatom-inferred conductivity declines in comparison to the previous zone ($\overline{x}$ = ~ 200 µS cm^{-1}) but large peaks are evident at 136.0 cm (~ 670 µS cm^{-1}) and 105.5 cm (~ 360 µS cm^{-1}).

6.6 Unimodal Ordination: Detrended Correspondence Analysis (DCA)

For the complete diatom dataset, DCA was deemed the most appropriate ordination technique as the axis 1 gradient length was 4.875 SD (standard deviation of species turnover) units (Table 6.2). The first and second axes account for 26.2 % of variation in the dataset, with the addition of axes 3 and 4 accounting for very little cumulative variance (33.7 %). A DCA plot of the diatom species and samples, split into the major zones identified in section 6.5 is shown in Figure 6.11. Axis 1 provides a summary of the major compositional shifts in the diatom record. The highest DCA scores reflect the oldest zones, D-II – D-IV, characterised by the planktonic *C. ocellata* and *C. cyclopuncta* as well as other associated benthic taxa such as *P. brevistriata* (Chalié and Gasse 2002b). The lower DCA scores correspond to the younger zones, D-V – D-X, which are largely dominated by *A. granulata* var. *angustissima*, as well other significant taxa such as *F. radians* and *U. ulna* var. *ulna*. This reflects various stages of lake development from the late Pleistocene through to the Holocene, from initial colonisation to deep water formation. This can be broadly interpreted as an indication of water permanence and depth at the core site. Axis 2 appears to be driven by diatom habitat preferences, with lower DCA scores corresponding to zones characterised by facultatively planktonic and benthic taxa (*G.*

Table 6.2. Summary of DCA results for the Lake Hayq diatom dataset.

Dataset	No. of samples	No. of species	Total inertia	Axis	1	2	3	4
All diatoms	423	281	2.824	Eigen values	0.543	0.195	0.123	0.091
				Length of gradient	4.875	2.503	2.232	1.967
				Cumulative % variance of species data	19.2	26.2	30.5	33.7
Diatom samples 522.0 – 89.0 cm	379	256	1.772	Eigen values	0.358	0.156	0.091	0.085
				Length of gradient	2.641	2.264	1.899	1.735
				Cumulative % variance of species data	20.2	29.0	34.1	38.9

acuminatum and *N. sociabilis*, zones D-VII, D-VIII and D-IX), and higher DCA scores to zones dominated by planktonic taxa (*A. granulata* var. *angustissima* and *S. parvus*, zones D-V, D-VI and D-X), which can be interpreted as an indicator of lake depth and habitat availability.

The repeated DCA technique on the condensed dataset (including only samples between 522.0 – 89.0 cm) again produced an axis 1 gradient length exceeding 2 SD units (2.641), making it the most suitable technique (Table 6.2). The first and second axes account for slightly more cumulative variation than for the complete dataset at 29.0 %, as do the first four axes (38.9 %). A DCA plot of the diatom species and samples, split into the major zones identified in section 6.5 is shown in Figure 6.12. Axis 1 is driven by diatom habitat preferences with lower DCA scores corresponding to zones characterised by facultatively planktonic and benthic taxa (*G. acuminatum* and *N. utermoehlii*, zones D-VIII and D-IX) and higher scores to zones dominated by planktonic taxa (*A. granulata* var. *angustissima* and *C. cyclopuncta*, zones D-V, D-VI, D-VII and D-X), which can be interpreted as an indicator of lake depth and habitat availability. The dissimilarity in axis 2 is more subtle; there are no extreme ecological differences in tolerance thresholds for the taxa present (i.e. pH, salinity). Similar to axis 1, it seems axis 2 may be driven by diatom habitat preferences, with lower scores corresponding to zones characterised by facultatively planktonic and benthic taxa during shallow water periods (*Gomphonema minutum*, *G. acuminatum*, *N.*

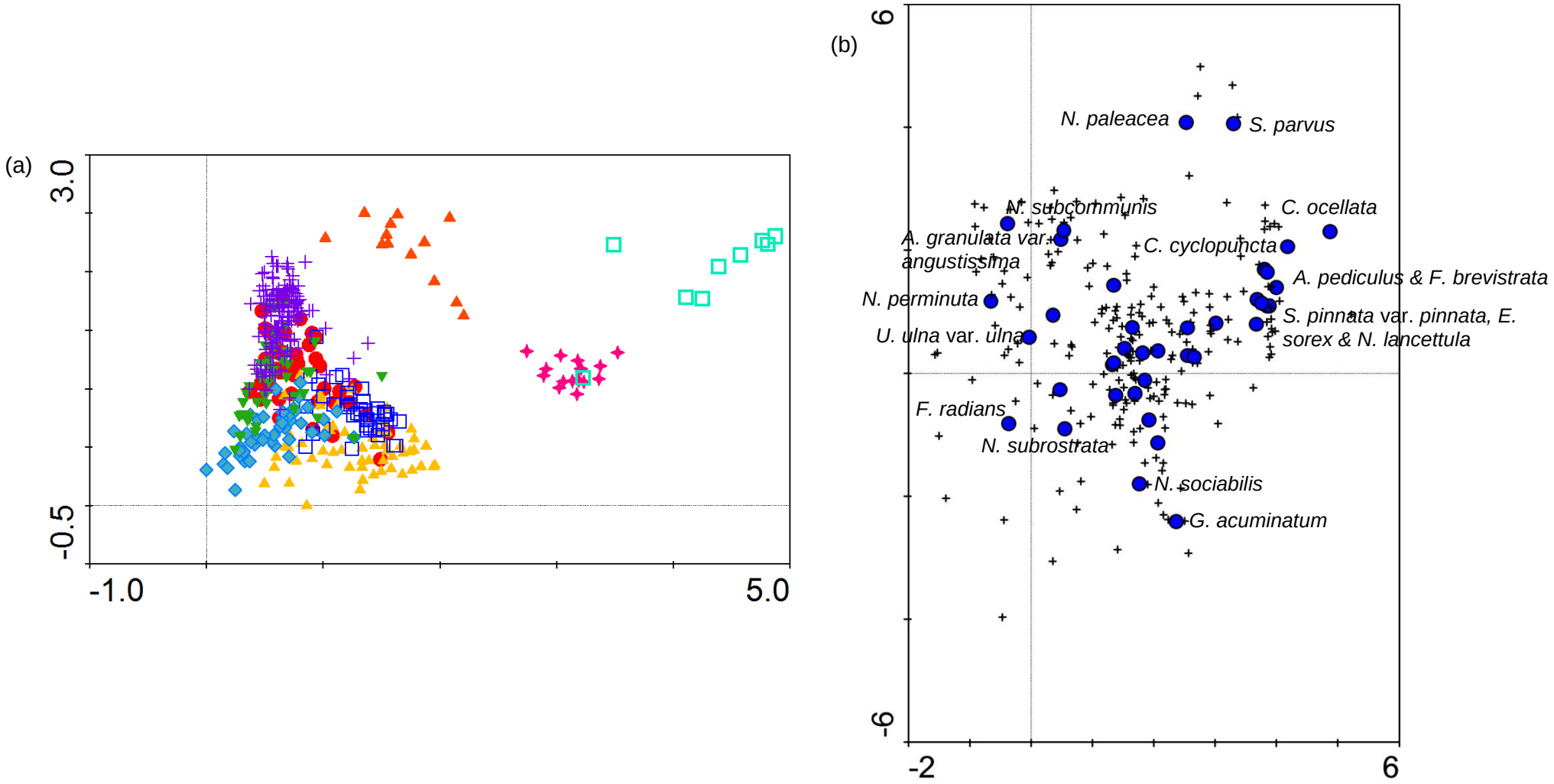

Figure 6.11. DCA results for the complete diatom dataset showing (a) samples according to zone (D-II – cyan square, D-III – pink star, D-IV – orange triangle, D-V – purple cross, D-VI – green triangle, D-VII – blue diamond, D-VIII – blue square, D-IX – yellow triangle, D-X – red circle), and (b) species (taxa > 5.0 % shown as blue circles, all other taxa as a black cross). Taxa located at the extremities of axes have been identified.

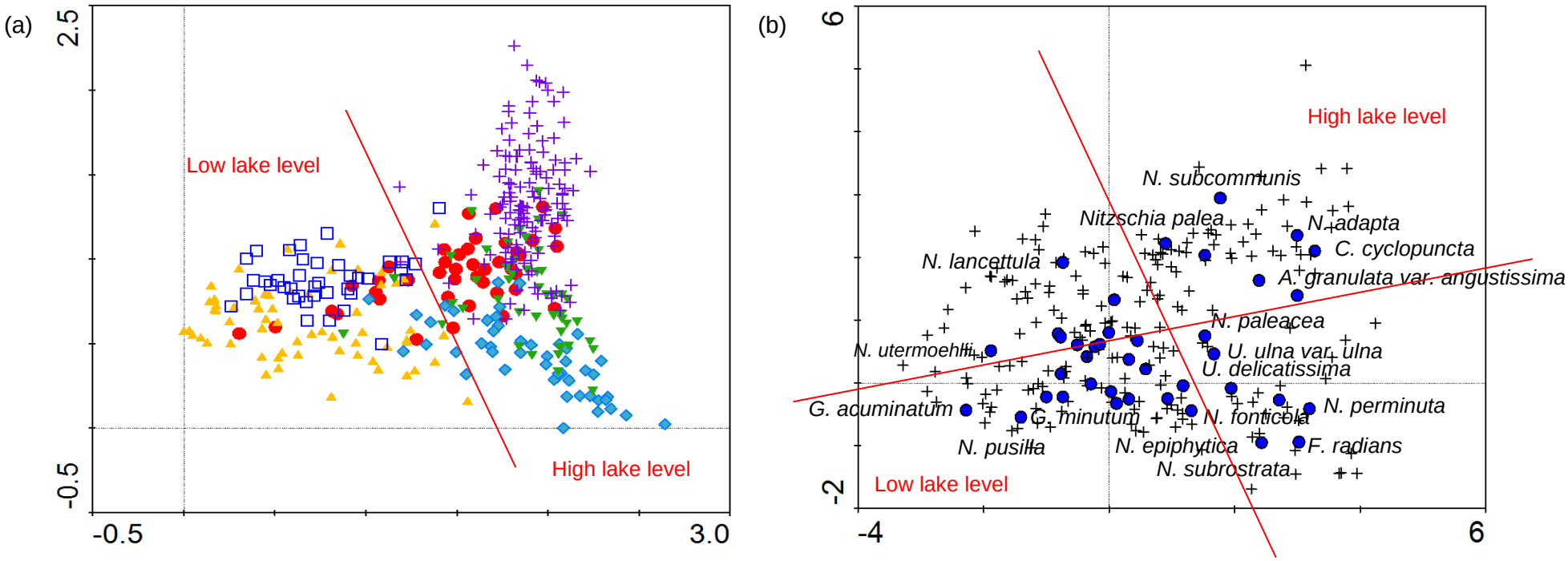

Figure 6.12. DCA results of the condensed dataset (including only samples between 522.0 – 89.0 cm) showing (a) samples according to zone (D-V – purple cross, D-VI – green triangle, D-VII – blue diamond, D-VIII – blue square, D-IX – yellow triangle, D-X – red circle), and (b) species (taxa > 5.0 % shown as blue circles, all other taxa as a black cross). Taxa located at the extremities of axes have been identified. The red lines illustrate the *approximate* divide between planktonic and benthic taxa on axis 1, and benthic and facultatively planktonic taxa on axis 2, reflecting diatom habitat availability during high and low lake levels.

fonticola and *F. radians*, zones D-VII and D-IX) and higher DCA scores corresponding to benthic taxa present during periods of deep water (*N. subcommunis*, *N. adapta* and *N. palea*, zone D-V). This may reflect changing availability of habitats in the littoral zone with variations in water level; benthic habitat areas may increase or decrease with water level rise depending on basin morphology (Stone and Fritz 2004).

6.7 The Pigment Record

The pigment record for Hayk-01-2010 is shown in Figure 6.13. Fourteen pigments (six chlorophylls/chlorophyll degradation products and eight carotenoids) have been identified and are presented in concentration (nmol pigments g^{-1} organic matter, hereafter nmol pigments g^{-1} OM). Affinities of pigments are based on those identified by Leavitt and Hodgson (2001) and McGowan (2013). The stratigraphic diagram has been divided into ten statistically significant zones (P-I – P-X).

6.7.1 Zone P-I (822.0 – 763.0 cm, 15,600 – 15,300 cal yr BP) The only pigment present in this zone is isorenieratene (green sulfur bacteria) in low concentrations (2.2 – 3.4 nmol pigments g^{-1} OM).

6.7.2 Zone P-II (763.0 – 749.0 cm, 15,300 – 15,200 cal yr BP) Present in this zone are lutein-zeaxanthin (green algae, euglenophytes, higher plants and cyanobacteria), canthaxanthin (colonial cyanobacteria and herbivore tissues), isorenieratene, chlorobactene (green sulfur bacteria), β-carotene (most plants and algae), the chlorophyll degradation product pheophorbide *a* (grazing and senescent diatoms) and bacteriochlorophyll *e* (green sulfur bacteria). All are found in low concentrations (1.9 – 30.0 nmol pigments g^{-1} OM). Total pigment concentration is 83.5 nmol pigments g^{-1} OM.

6.7.3 Zone P-III (749.0 – 736.0 cm, 15,200 – 15,050 cal yr BP) The only pigment present in this zone is isorenieratene (3.3 nmol pigments g^{-1} OM).

6.7.4 Zone P-IV (736.0 – 656.5 cm, 15,050 – 13,900 cal yr BP) This zone is dominated by carotenoid pigments. Alloxanthin (cryptophytes), diatoxanthin (diatoms, dinoflagellates, chrysophytes), lutein-zeaxanthin, canthaxanthin,

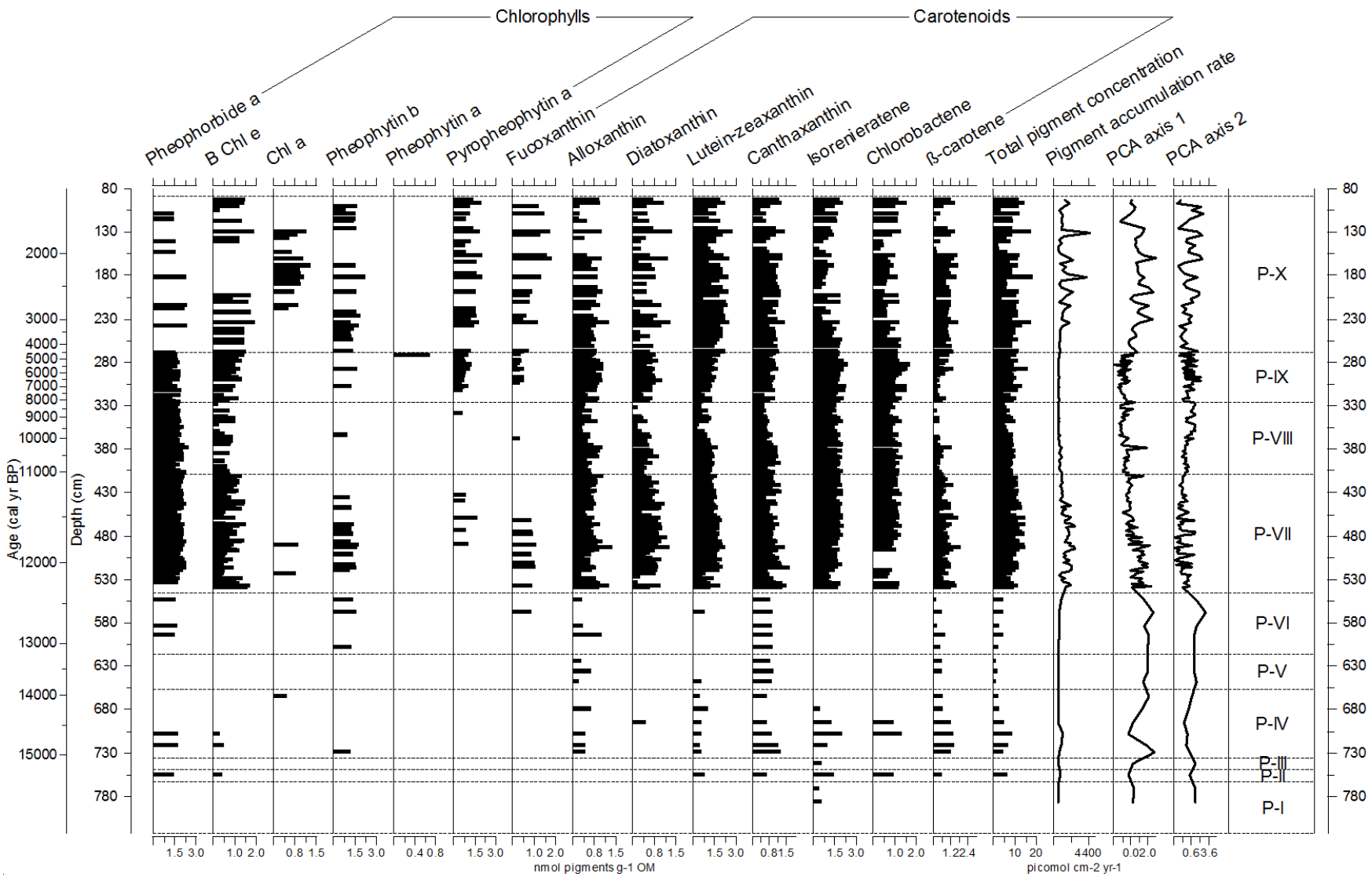

Figure 6.13 (a). Pigment concentration (nmol pigments g^{-1} OM) for core Hayk-01-2010 and associated metrics, against depth (cm). Pigment accumulation rate is shown as picomol cm^{-2} yr^{-1}. PCA scores refer to carotenoid pigments only.

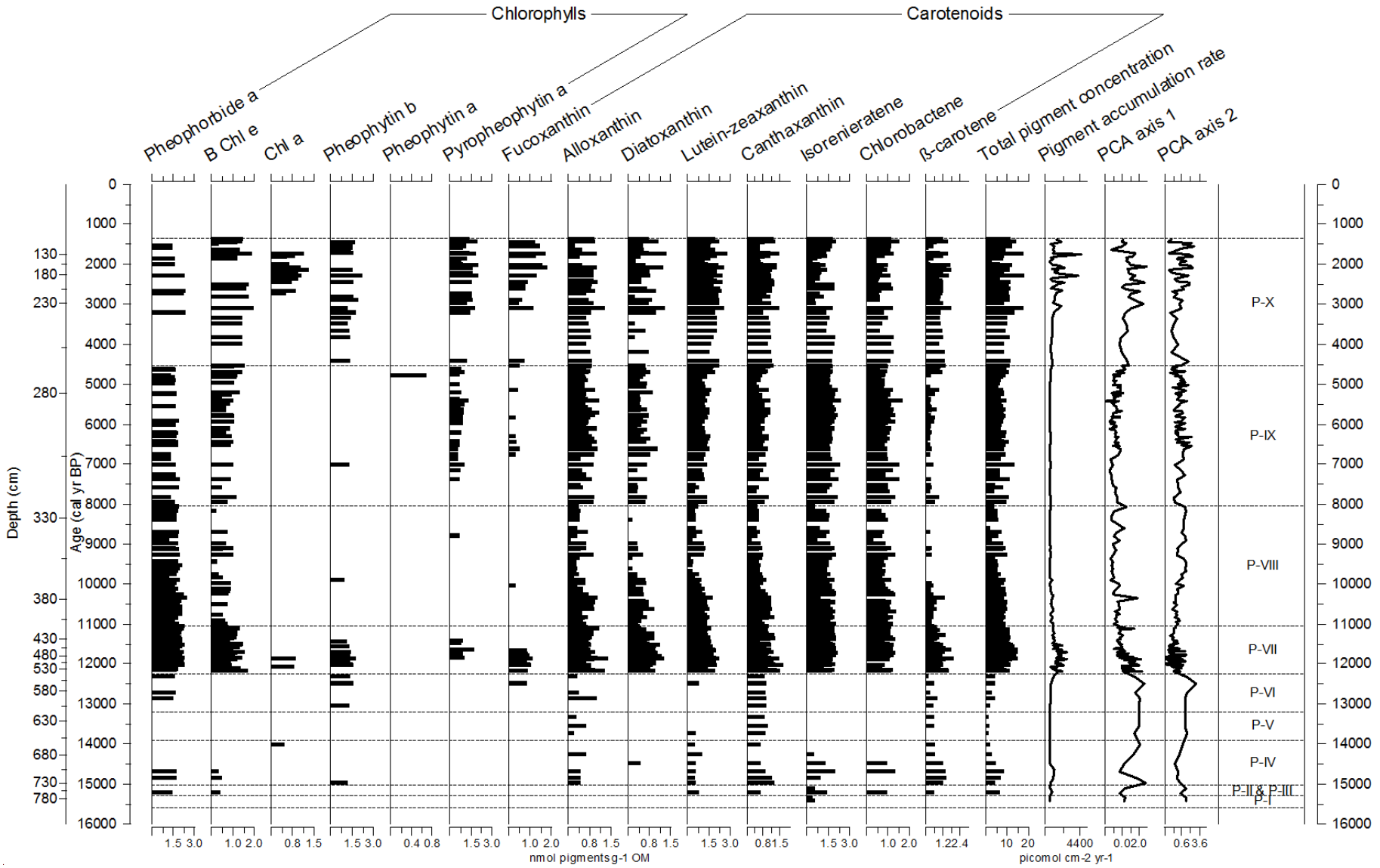

Figure 6.13 (b). Pigment concentration (nmol pigments g^{-1} OM) for core Hayk-01-2010 and associated metrics, against age (cal yr BP). Pigment accumulation rate is shown as picomol cm^{-2} yr^{-1}. PCA scores refer to carotenoid pigments only.

isorenieratene, chlorobactene and β-carotene are intermittently present in varying concentration. Pheophorbide *a*, bacteriochlorophyll *e*, chlorophyll *a* (all photosynthetic algae and higher plants) and pheophytin *b* (derivative of chlorophyll *b*) are also present. Total pigment concentration is greatest at 707.5 cm and then declines considerably (225.0 – 12.5 nmol pigments g^{-1} OM).

6.7.5 Zone P-V (656.5 – 616.5 cm, 13,900 – 13,200 cal yr BP) Total pigment concentration is low in this zone (10.4 – 16.4 nmol pigments g^{-1} OM). Alloxanthin, lutein-zeaxanthin, canthaxanthin and β-carotene are present in moderate concentrations. Chlorophylls and associated degradation products are absent.

6.7.6 Zone P-VI (616.5 – 546.5 cm, 13,200 – 12,250 cal yr BP) Total pigment concentration increases in this zone reaching 81.6 nmol pigments g^{-1} OM at 553.5 cm. Canthaxanthin and β-carotene are present throughout, whilst alloxanthin and lutein-zeaxanthin appear sporadically. Fucoxanthin (diatoms, prymnesiophytes, chrysophytes, raphidophytes and several dinoflagellates) occurs for the first time in the pigment record at 567.5 cm (7.2 nmol pigments g^{-1} OM). Pheophorbide *a* and pheophytin *b* are also present intermittently.

6.7.7 Zone P-VII (546.5 – 408.5 cm, 12,250 – 11,050 cal yr BP) This zone sees a gradual increase in total pigment concentration as carotenoids become more abundant in the record. Accumulation rate mirrors total pigment concertation and ranges between 290.2 – 2,455.2 pmol cm^2 yr^{-1}. Carotenoids concentrations at the base of this zone are generally high (243.8 nmol pigments g^{-1} OM) but decline significantly (27.0 nmol pigments g^{-1} OM, 531.0 cm) before rising again at ~ 515.5 cm (263.5 nmol pigments g^{-1} OM). Chlorobactene disappears from the record between 519.5 – 495.5 cm but recovers and maintains a generally stable concentration. Other carotenoids also maintain high concentrations, though a decline is evident at 453.5 cm, which is most pronounced in diatoxanthin as it decreases from 3.8 to 0.8 nmol pigments g^{-1} OM. Fucoxanthin appears intermittently from 537.5 – 461.5 cm and then disappears from the pigment record. Pheophorbide *a* is present from 533.5 cm onwards in high concentrations ($\overline{x}$ = 122.9 nmol pigments g^{-1} OM). Bacteriochlorophyll *e* likewise become more established in this zone but fluctuates significantly in concentration, ranging from 1.8 – 51.8 nmol pigments g^{-1} OM.

Pheophytin *b* is found between 519.5 – 435.5 cm only, and pyropheophytin *a* (derivative of *a* and *b* phorbins) between 489.5 – 433.5 cm.

6.7.8 Zone P-VIII (408.5 – 325.5 cm, 11,050 – 8,050 cal yr BP) Total pigment concentration decreases in this zone from a range of 24.2 – 455.5 nmol pigments g^{-1} OM between 408.5 – 354.5 cm, to a minimum of 13.2 nmol pigments g^{-1} OM at 352.5 cm. The carotenoids show the same general trend of declining towards the top of the zone, with β-carotene disappearing from the record at 366.5 cm and reappearing at 348.5 cm. Isorenieratene and chlorobactene maintain the most stable concentrations (54.2 and 10.5 nmol pigments g^{-1} OM respectively). Pheophorbide *a* is also stable ($\overline{x}$ = 82.5 nmol pigments g^{-1} OM), whereas bacteriochlorophyll *e* fluctuates considerably and disappears from the record at certain depths. Accumulation rate declines then remains stable (< 552.2 pmol cm^2 yr^{-1}).

6.7.9 Zone P-IX (325.5 – 268.89 cm, 8,050 – 4,550 cal yr BP) This zone is characterised by stable total pigment concentrations ($\overline{x}$ = 138.0 nmol pigments g^{-1} OM) with a maximum of 453.2 nmol pigments g^{-1} OM at 287.5 cm. The base of the zone sees small declines in the concentration of several carotenoids (alloxanthin, diatoxanthin, lutein-zeaxanthin and canthaxanthin) after which they increase and maintain steady concentrations. Diatoxanthin and β-carotene disappear occasionally, whilst fucoxanthin is found intermittently from 303.5 cm onward in low concentrations (< 2.9 nmol pigments g^{-1} OM). Several increases are evident in the carotenoids at 287.5 cm, 283.0 cm, 278.5 cm and 269.5 cm. Pheophorbide *a* and bacteriochlorophyll *e* maintain steady concentrations ($\overline{x}$ = 40.7 and 8.9 nmol pigments g^{-1} OM respectively) though occasionally disappear. Pyropheophytin *a* is also present intermittently from 313.5 cm onwards in moderate concentrations. Accumulation rate continues to remain stable (< 273.3 pmol cm^2 yr^{-1}).

6.7.10 Zone P-X (268.89 – 89.0 cm, 4,550 – 1,350 cal yr BP) Total pigment concentration reaches greatest values in this zone with peaks of 861.7, 1044.0 and 1068.0 nmol pigments g^{-1} OM (234.5 cm, 181.5 cm and 129.5 cm). These peaks are matched by significant decreases however, and a minimum of 21.0 nmol pigments g^{-1} OM is observed at 145.5 cm. Accumulation rate fluctuates considerably throughout this zone, ranging between 86.3 – 4,537.3 pmol cm^2 yr^{-1}, but generally mirror total

pigment concentration. The carotenoids display a similar trend of rising and declining. Alloxanthin and β-carotene in particular, decline significantly between 153.5 – 133.5 cm and 125.5 – 115.5 cm, sandwiching higher concentrations at 129.5 cm. Fucoxanthin appears intermittently at moderate concentrations ($\overline{x}$ = 19.2 nmol pigments g^{-1} OM). Pheophorbide *a* becomes scarce, occurring sporadically in high concentrations ($\overline{x}$ = 105.2 nmol pigments g^{-1} OM). Bacteriochlorophyll *e* is found in high concentrations ($\overline{x}$ = 97.2 nmol pigments g^{-1} OM) up to 202.5 cm, after which it disappears from the record until 141.5 cm where it returns to similar concentrations as before. Pheophytin *b* likewise appears less frequently in the mid-zone (218.5 – 129.5 cm). The decline of bacteriochlorophyll *e* and pheophytin *b* coincides with the establishment of chlorophyll *a* in the sediment between 218.5 – 133.5 cm where it averages 6.5 nmol pigments g^{-1} OM. Pyropheophytin *a* occurs frequently from 238.5 cm onwards and maintains an average of 38.9 nmol pigments g^{-1} OM.

6.8 Linear Ordination: Principal Components Analysis (PCA)

Following PCA analysis of the pigment dataset, the first axis accounts for 30.8 % of variance and the second axis for 16.2 % (Table 6.3). The cumulative variance explained by the four axes is 70.0 %. A PCA plot of the sedimentary pigments identified and samples split into the major zones identified in section 6.7 is shown in Figure 6.14. Axis 1 shows a clear division between sedimentary pigments derived from macrofaunal grazing and those derived directly from the breakdown of phytoplankton groups, which may be interpreted as an indication of the zooplankton population size in Lake Hayq. Low PCA axis 1 scores correspond to zones containing an abundance of the grazing indicator, pheophorbide *a* (zones P-VII and P-VIII), suggesting a larger zooplankton population, whilst high scores reflect zones containing higher concentrations of pigments derived from the degradation of cyanobacteria and other algae, indicating a small or absent zooplankton population (zones P-IV, P-VI and P-X).

Axis 2 separates green sulfur bacteria from general indicators of total algal abundance (β-carotene, chlorophyll *a* and canthaxanthin), which may be interpreted as a gauge for lake depth, mixing regime and light intensity. Low PCA axis 2 scores correspond to zones dominated by green sulfur bacteria (zones P-VII, P-VIII and P-

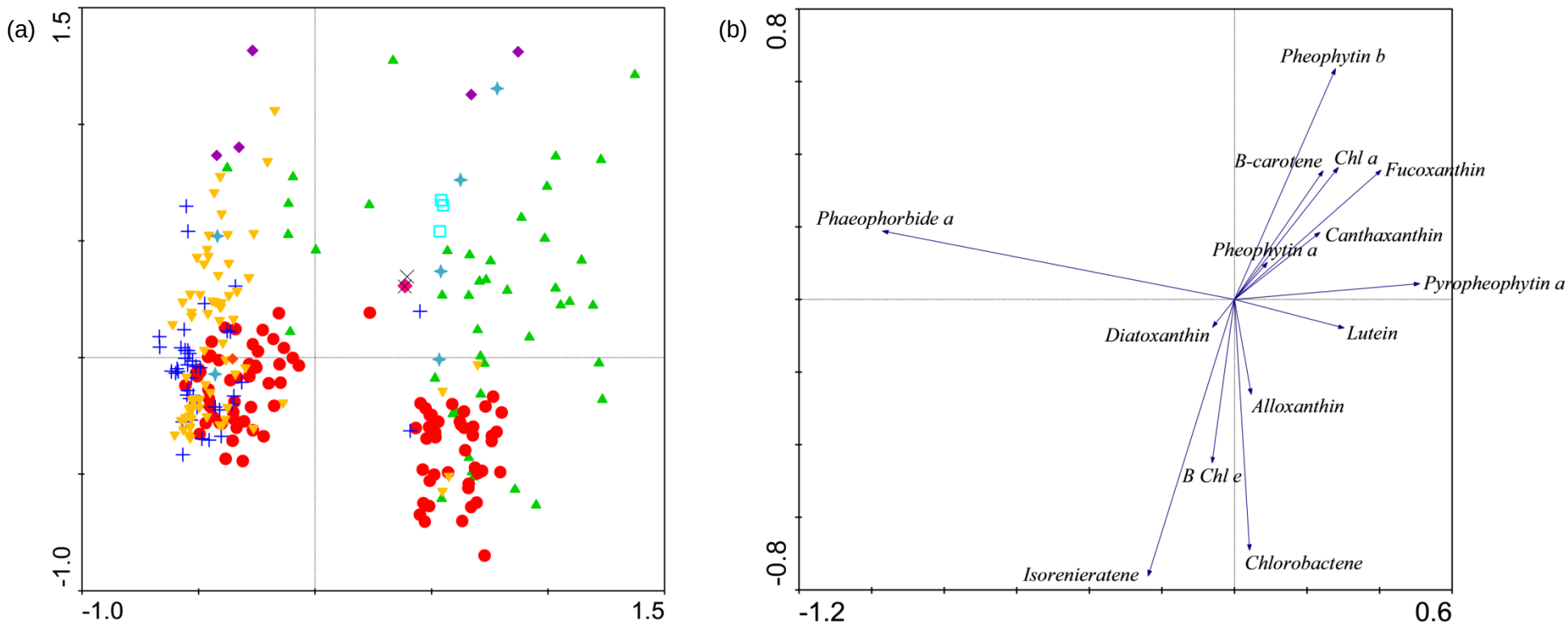

Figure 6.14. PCA results for the complete sedimentary pigment dataset showing (a) samples according to zone (P-I – X symbol, P-II – orange diamond, P-III – pink diamond, P-IV – blue star, P-V - cyan square, P-VI – purple diamond, P-VII - yellow triangle, P-VIII – blue cross, P-IX – red circle, P-X – green triangle), and (b) sedimentary pigments.

Table 6.3. Summary of PCA results for the Lake Hayq pigment dataset.

Dataset	No. of samples	No. of species	Total variance	Axis	1	2	3	4
All pigments	263	14	1	Eigen values	0.308	0.162	0.143	0.088
				Cumulative % variance of species data	30.8	47.0	61.2	70.0
Carotenoids only	263	8	1	Eigen values	0.406	0.166	0.122	0.1
				Cumulative % variance of species data	40.6	57.2	69.4	79.3

IX), which indicates meromixis in a deep lake with some light penetrating the anoxic zone. Higher scores correspond to zones with an availability of benthic habitats, signalling a low lake level, and reduced light in the water column due to the abundance of phytoplankton (zones P-VI and P-X).

PCA analysis was repeated to include only carotenoid pigments, as chlorophylls have been intermittently preserved at times throughout the sediment record, evidenced by the presence of chlorophyll degradation products. Axis 1 and 2 account for 57.2 % of variance, whilst the addition of axis 3 and 4 increase cumulative variance to 79.3 % (Table 6.3). A PCA plot of the pigment species and samples split into the major zones identified in section 6.7 is shown in Figure 6.15. Axis 1 shows a division between zones dominated by green sulfur bacteria and more common pigments found in most plants and algae. Low PCA correspond to zones dominated by isorenieratene and chlorobactene (zones P-VIII and P-IX), whilst higher PCA scores are associated with zones containing a greater concentration of β-carotene and canthaxanthin (zones P-IV, P-VI and P-X), similar to axis 2 of the complete pigment record. This generally reflects changes in lake depth (and by association, availability of benthic habitats), mixing regime and light intensity.

Axis 2 separates fucoxanthin and diatoxanthin. High PCA scores correspond to zone P-X, which contains the highest concentrations of fucoxanthin and low, intermittent

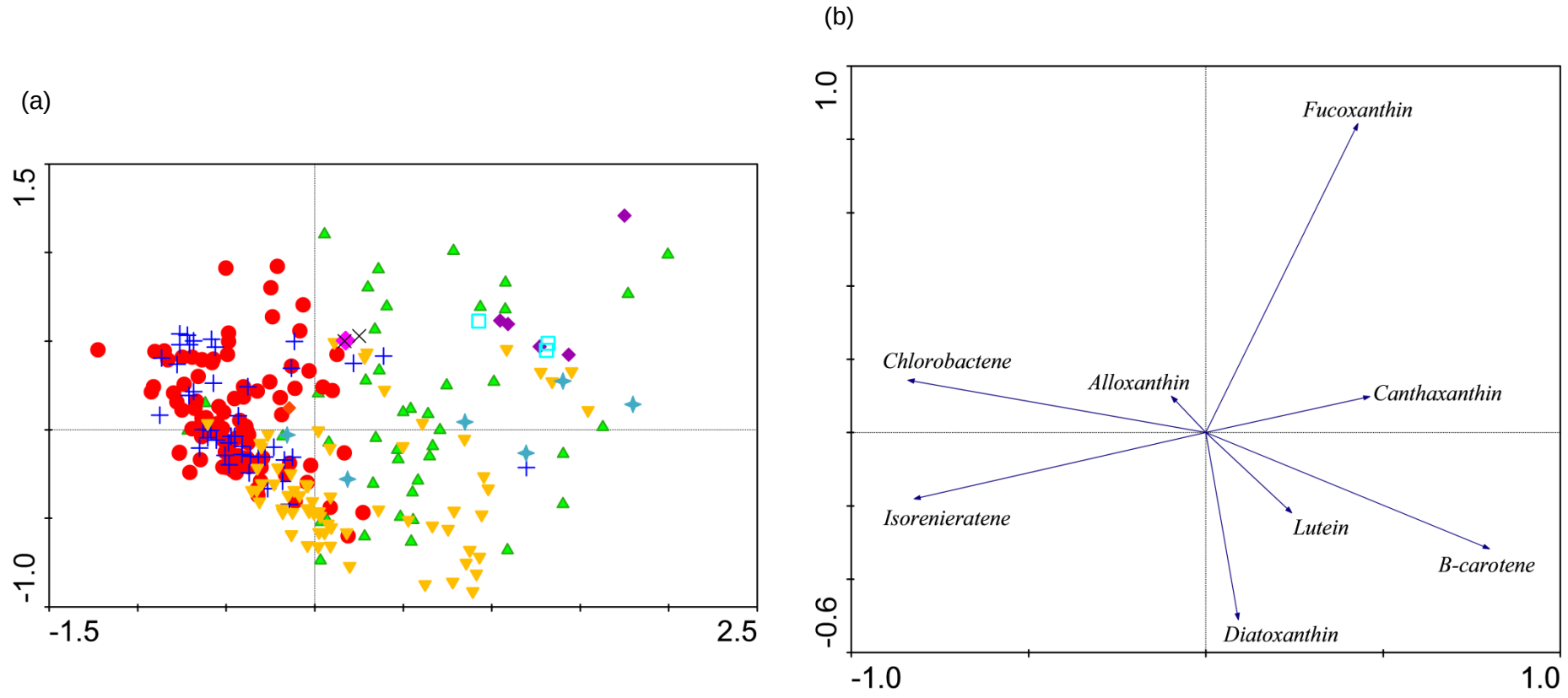

Figure 6.15. PCA results for carotenoid pigments only, showing (a) samples according to zone (P-I – X symbol, P-II – orange diamond, P-III – pink diamond, P-IV – blue star, P-V - cyan square, P-VI – purple diamond, P-VII - yellow triangle, P-VIII – blue cross, P-IX – red circle, P-X – green triangle), and (b) sedimentary pigments.

concentrations of diatoxanthin, whilst lower PCA scores correspond to zone P-VII, which shows the opposite trend (low, intermittent concentrations of fucoxanthin and higher concentrations of diatoxanthin). Both carotenoids are derived from similar phytoplankton groups (diatoms, dinoflagellates, chrysophytes) and so the division most likely reflects the lability of fucoxanthin. As such, the pigment is often only found in the uppermost sections of sediment records (McGowan 2013).

6.9 Interpretation and Synthesis of the Lake Hayq Record

All available data from the independent proxy records analysed from core Hayk-01-2010 are now interpreted in terms of limnetic and environmental changes that have taken place in the Lake Hayq basin over the past ~ 15.6 – 1.3 cal kyr BP. Figures 6.16 and 6.17 provide a summary of the major shifts in the proxy records; the records are divided into eleven major zones (Hayq-I – Hayq-XI). Zones are based on significant shifts in the diatom data, which is the primary proxy in this research. Figure 6.18 is a simplified lake level curve based on the collective interpretation of the available proxies, indictaing changes in the lake system, including connectivity.

6.9.1 Hayq-I (822.0 – 748.0 cm, 15,600 – 15,200 cal yr BP) Geochemical data indicates that the Lake Hayq basin was experiencing extremely arid conditions during this time period. High values of lithogenic potassium and titanium are indicative of allochthonous inputs to the core site and therefore catchment erosion. Under generally dry conditions with low vegetation cover, Foerster et al. (2012) argues that lithogenic material is more easily eroded and transported to the basin. This is in agreement with grain size values, which indicate coarser material at the core site and therefore a greater proportion of clastic sediment (Burnett et al. 2011). Evidence of this was found physically in the core as sand particles were identified. The authigenic calcium component shows a delayed response in comparison to the lithogenic elements but likewise indicates dry environmental conditions; precipitation of lacustrine calcium occurs when calcium become supersaturated in the water column as a result of increased temperatures and the removal of carbon dioxide (Tucker and Wright 1990; Brown 2011).

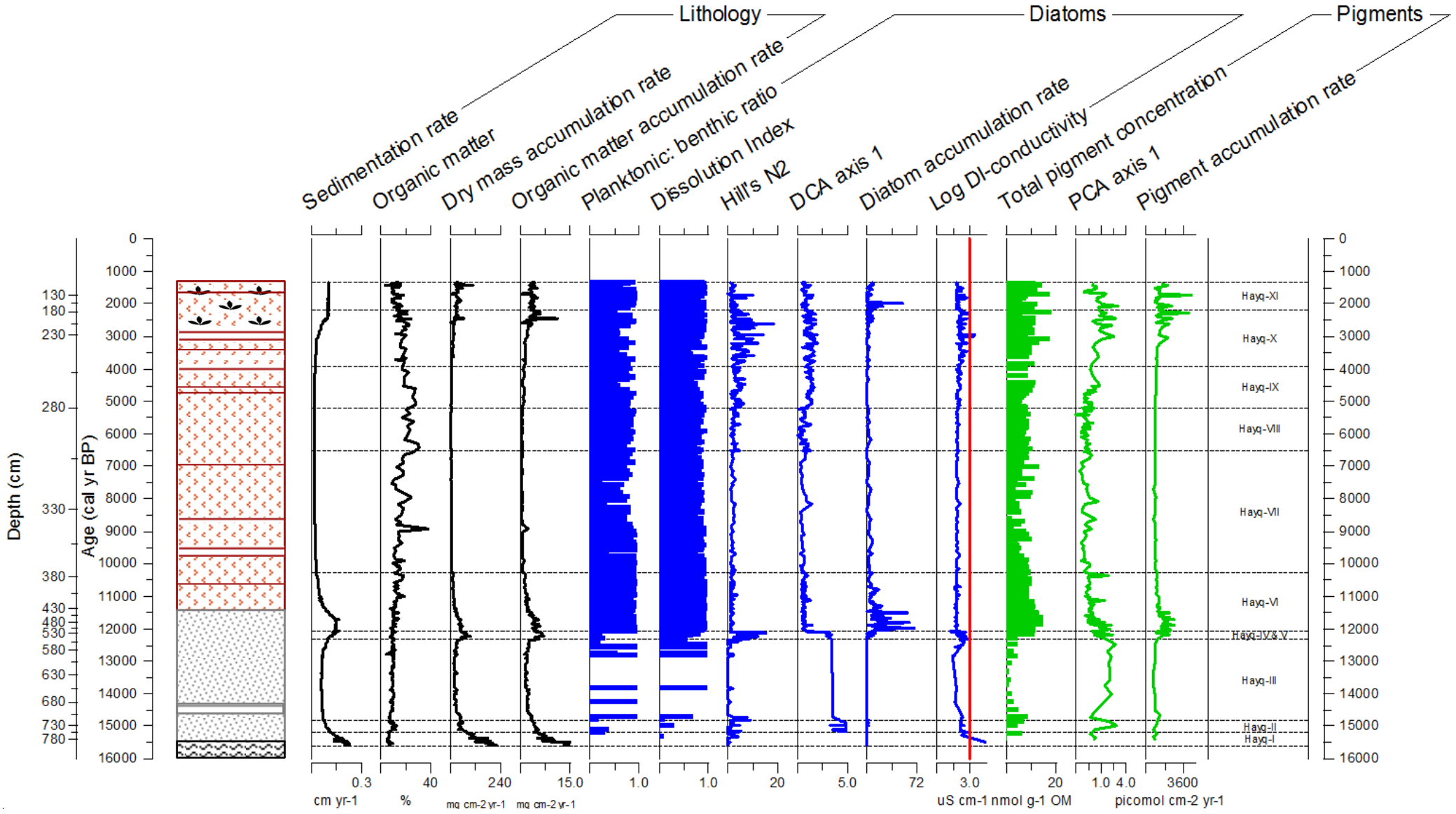

Figure 6.16. Summary proxy records showing major compositional changes. Sedimentation accumulation rate is expressed as cm yr^{-1}, organic matter content as a percentage of the total wet weight of the sediment, and dry mass and organic matter accumulation

rates as mg cm^{-2} yr^{-1}. Diatom accumulation rate is expressed as x 10^6 valves cm^{-2} yr^{-1} and diatom-inferred (DI) conductivity as µS cm^{-1}. Conductivity recorded in 1969 (920 µS cm^{-1}) is indicated by the red line (Baxter and Golobitsh 1970). Pigment concentration is shown as nmol pigments g^{-1} OM and accumulation rate as picomol cm^{-2} yr^{-1}. PCA scores refer to carotenoid pigments only. See Figure 6.2 for lithological profile key.

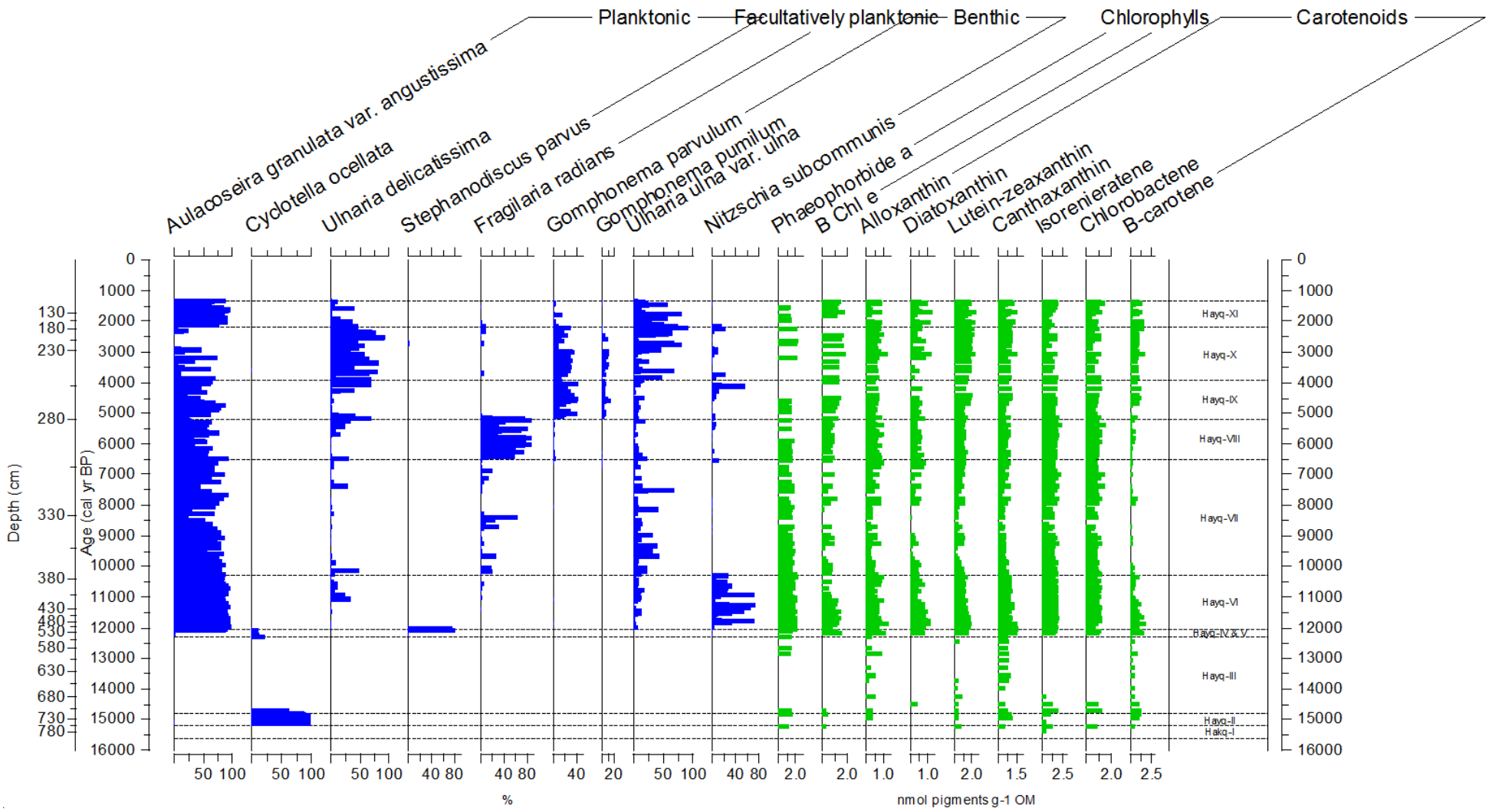

Figure 6.17. Summary diagram of key diatoms and pigments, showing major compositional changes. Diatoms are shown as percentage presence (%). Average sample standard deviation is 2.82 %. Pigments are shown as concentration (nmol pigments g^{-1} OM).

Table 6.4. Conductivity classifications based on schemes devised by Williams (1967) and Hammer (1986), and Gasse (1986).

Authority	Classification	Conductivity (µS cm^{-1})
Williams (1967) and Hammer (1986)	Freshwater	< 670
	Subsaline	670 - 5,500
	Saline	> 5,500
	o Hyposaline	5,500 - 30,000
	o Mesosaline	30,000 - 70,000
	o Hypersaline	> 70,000
Gasse (1986)	Very low	< 300
	Low	300 - < 1,000
	Medium	1,000 - 3,000
	High	3,000 - 10,000
	Very high	> 10,000

The diatom record concurs with the geochemical data, which indicates the lake was at a lowstand, expressed by the negligible concentrations of diatoms and traces of benthic and aerophilous taxa. The occurrence of *Hantzschia amphioxys* in this zone provides further evidence of a shallow lake environment and indicates sediment reworking from marginal or exposed areas in the catchment. This is in agreement with the compacted nature of the sediment as well as the low water content, which suggests the core site may have been exposed at times, possibly alternating between longer periods of dry, saline conditions and short wet episodes, when runoff in the catchment would have been channelled down the steep-sided lake basin to the core site. Diatom-inferred conductivity and the variable preservation indicate the core site was saline-hyposaline when it did contain water (which may have prevented vegetation and soils from developing) but it most likely repeatedly dried out during this time (Table 6.4). Water residence time at the core site would have been quite short, given the extremity of this environment.

Pigment concentration was similarly low during this period, indicating poor preservation conditions. Over exposure to light, oxygen rich (causing photo-oxidation) and high temperature conditions in a very shallow lake habitat, as well as physical reworking of the sediments (as evidenced by the diatom record) may have degraded pigments in the water column and in the uppermost sediments, preventing them from being incorporated into the fossil record.

6.9.2 Hayq-II (748.0 – 716.0 cm, 15,200 – 14,800 cal yr BP) This zone is characterised by the dominance of *Cyclotella ocellata* in the diatom record, signalling an increase in lake depth and (for the time being) water permanence. *Cyclotella ocellata* is considered a pioneer taxon in lake colonisation and has a wide ecological tolerance in terms of tropic state, being present in ultra-oligotrophic to eutrophic lakes (Servant-Vildary 1978; Servant and Servant-Vildary 1980; Cremer and Wagner 2003). Optimum pH is 8.5 indicating the lake was most likely alkaline (Gasse et al. 1995; EDDI 2015b). The taxon is able to maintain itself in both deep water and littoral environments (Stoermer and Yang 1970; Gasse et al. 1989). Based on data from the EDDI (2015b) combined TP training set, *Cyclotella ocellata* reaches optimum development in European (particularly Swiss) lakes, of ~ 8 m depth, although it is present in lakes up to 370 m deep (Lago Maggiore, Italy, 0.2 % abundance). Average depth of lakes where *Cyclotella ocellata* accounts for < 10.0 % is 29 m (EDDI 2015b). In European lakes where the taxon accounts for > 10.0 % abundance, conductivity averages 322.3 µS cm^{-1}, indicating a preference for freshwater and total phosphorus averages ~ 45.2 µg/l, suggesting eutrophic conditions (EDDI 2015b). The presence of other facultatively planktonic and benthic taxa, including *Pseudostaurosira brevistriata*, which is commonly found in association with *Cyclotella ocellata*, indicates the core site was still fairly close to the littoral zone at this time (Chalié and Gasse 2002b).

This increase in lake depth and area, from an essentially dry core site in the previous zone, to a permanent waterbody approximately ~ 8 m deep, with an area of < 4 km^2, is supported by the geochemical data, as declines in calcium and potassium indicate increasingly humid, wetter conditions (Demlie et al. 2007; Brown 2011; Burnett et al. 2011). Grain size at the core site became smaller, signalling a greater distance between the shoreline and core site and therefore a deeper lake (Burnett et al. 2011). The abruptness of both the diatom and geochemical response would suggest the shift from arid to wet conditions was relatively quick, spanning three to four decades (~ 15,200 – 15,170 cal yr BP). The effect of the wetter conditions subsequently diluted the water at Lake Hayq, signalling a positive water balance. Diatom-inferred conductivity confirms the lake was fresh.

However, as valve preservation is poor in this zone, it is possible that the assemblage has been biased towards the robust, more silicified *Cyclotella* taxon over finer forms (*Cyclotella ocellata* is clearly identifiable even when dissolved; see Plate II). Diatom preservation in lake sediments has been linked to multiple aspects of physical limnology, water chemistry and biological interactions: temperature (Lewin 1961; Bidle et al. 2002), pH (Lewin 1961; Barker et al. 1994; McMinn 1995), salinity (Lewin 1961; Barker et al. 1994; Reed 1998a; Ryves et al. 2006), ionic strength (Lewin 1961), organic, carbonate and silica content (Flower 1993; Ryves et al. 2001), stratification and meromixis (McMinn 1995; Ryves et al. 2006), water depth (Flower 1993), water permanence (Reed 1998b), sedimentation processes (Haberyan 1990), bioturbation (Gibson et al. 2000), bacterial dissolution (Bidle and Azam 1999; Bidle et al. 2003) and grazing and faecal pelletisation by zooplankton (Haberyan 1985). Potentially other diatom taxa have been removed from the sediment record as a result of such factors, especially those linked to water depth and permanence, leaving only the robust *Cyclotella* taxon. This may have a disproportionate effect on assemblage-based inferences, such as the conductivity model, and interpretations (Ryves et al. 2001; 2006). Despite this, Ryves et al. (2001) found that reconstructions of salinity at Devils Lake, North Dakota, still performed well with significant dissolution and up to 50 % valve loss (*F* index value of < 0.3). Furthermore, *Cyclotella ocellata* has been identified as a dominant taxa in late Quaternary sediments from lakes across East Africa, including the nearby Lake Ashenge (~ 200 km north of Lake Hayq) from 16.2 – 15.2 cal kyr BP where it colonised the core site following exposure (Marshall et al. 2009), and Lake Abiyata from ~ 12.0 – 7.0 kyr BP (Chalié and Gasse 2002b). This lends support to the (above) interpretation of the core site.

Sedimentary pigments are similarly affected by preservation during this time. There is a greater diversity of carotenoids as they are generally more stable than labile chlorophylls (McGowan 2013). β-carotene in particular is a common pigment found in almost all algae groups and is a very stable carotenoid, as is canthaxanthin, which is indicative of colonial cyanobacteria, signaling the core site may have experienced nutrient enrichment at this time (Reuss et al. 2005). However, limited preservation favoring stable carotenoids precludes any evaluation of phytoplankton community changes at this time.

6.9.3 Hayq-III (716.0 – 553.0 cm, 14,800 – 12,300 cal yr BP) The diatom record indicates an equally sudden end to the wet conditions (~ 14,740 – 14,720 cal yr BP) and a return to very shallow lake conditions at the start of this zone, evidenced by the sudden decline and disappearance of *Cyclotella ocellata*. The intermittent variety of planktonic, facultatively planktonic and benthic taxa found in only trace amounts suggests a fluctuating lake level; at times the core site may have been occasionally wet and fresh (confirmed by diatom-inferred conductivity, although as previously mentioned in 6.5.3, model reliability may be biased in this zone due to the lack of diatoms present) but at other periods, lake level would have been very low, repeatedly drying out, which would have prevented the preservation of diatom taxa at the core site. The sedimentary pigment data likewise indicates a poor preservation environment, based on the irregular pattern in which pigments have been incorporated into the fossil record. β-carotene and canthaxanthin are the only pigments to appear consistently throughout this zone, most likely due to their stable chemical structure, although both are in lower concentrations than the previous zone (as is total pigment concentration) indicating productivity at the core sight was very much reduced, signally drier conditions and a shallow lake.

As the geochemical data is fragmented for this zone, it is difficult to identify the nature of change in the climate and environment at this time. There is some indication of an arid climate; grain size increased, suggesting a closer proximity of the shoreline to the core site, and the authigenic calcium component indicates evaporative conditions. However, the disjointed nature of the data inhibits definitive conclusions from being made. Sedimentation declines in this zone, similar to rates identified at Lake Ashenge during this time (0.22 mm yr^{-1}; Marshall 2006).

6.9.4 Hayq-IV (553.0 – 528.13 cm, 12,300 – 12,100 cal yr BP) This zone may be considered as a transitional period between a shallow waterbody and a deeper, stable lake system. The diatom assemblage is again characterised by *Cyclotella ocellata*, as well as *Cyclotella cyclopuncta*. *Cyclotella cyclopuncta* is often found in lakes across Europe and, like *Cyclotella ocellata*, may be considered a pioneer species in lake colonisation or recovery following an arid period (Marciniak and Khursevich 2002; Scussolini et al. 2011). The two have been found as dominant taxa in assemblages together and indicate a moderately deep (~ 8 m), oligotrophic to

mesotrophic lake in the first stages of existence (Scussolini et al. 2011). Water permanence would have become longer as the lake became established and depth increased.

Pseudostaurosira brevistriata continues to be present, given its association with *Cyclotella ocellata*. *Nitzschia epiphytica*, a tropical African species, has also been found to be associated with *Cyclotella* taxa (Barker et al. 2002). This benthic and facultatively planktonic assemblage indicates that whilst a deeper lake was certainly developing in the basin, the core site was still fairly close to the littoral zone at this time (Chalié and Gasse 2002b). This is further evidence by the aerophilous taxa, *Hantzschia amphioxys* and *Nitzschia amphibia* var. *amphibia*, which suggest sediment reworking from other exposed sections of the basin. The assemblage is indicative of freshwater and includes less saline tolerant taxa such as *Epithemia sorex*. Diatom-inferred conductivity confirms the lake was generally fresh but may have become subsaline at times. The water remained alkaline, with pH ranging from 7.8 – 8.5 (Gasse et al. 1995).

The increased diversity of sedimentary pigments (carotenoids and chlorophyll degradation products) indicates that preservation conditions at the core site improved substantially in order to allow incorporation into the fossil record. There is a delayed response in the pigment record compared to the diatoms (pigments do not become well established until ~ 539.0 cm, ~ 12,200 cal yr BP). This may suggest that preservation conditions improved as a result of primary production by diatoms, which, upon settling and decomposing at depth, reduced oxygen concentration in the bottom waters, although this phenomenon is difficult to identify (Leavitt 1993). Alternatively, the establishment of colonial blue-green algae and cryptophyte algae may instead reflect a shift from benthic to pelagic habitat availability as a result of lake deepening (McGowan et al. 2005).

Dinoflagellate, chrysophyte and green sulfur bacteria assemblages begin establishing themselves in the lake at this time, indicating an availability of fresh, benthic conditions. The large increase in colonial blue-green algae was likely to have been important in supporting diatom taxa in the developing lake. The facultatively planktonic *Nitzschia fonticola* is defined as a nitrogen heterotroph, which obtains

nitrogen solely from amino acids (*Pseudostaurosira brevistriata* is another nitrogen heterotroph) (Kilham et al. 1986). The defining feature of this taxon's ecology is its symbiotic relationship with non-nitrogen fixing colonial blue-green algae; the taxon lives on colonies of the algae which reduces *Nitzschia fonticola* losses through sinking and grazing as well as providing it with a source of organic nitrogen compounds (Kilham et al. 1986). Together, this combination indicates relatively stable, warm, stratified waters. Nutrients (phosphorus in particular) may have been limiting, although not so severe as to eliminate the colonial blue-green algae from the waterbody.

Short-term fluctuations in the geochemical data provide an indication of wetter, more humid conditions in the Lake Hayq basin, which would have caused the lake to deepen. The decline of calcium suggests less evaporative conditions, and therefore increased humidity, which prevented preservation. Grain size similarly decreases and the incoherent: coherent backscatter intensity ratio indicates improved preservation and higher productivity as a result of a wetter climate (Burnett et al. 2011). Increasing accumulation rates, caused by the steep basin focusing the sediments in this developing lake stage, also indicate enhanced productivity in the lake, which would suggest a positive water balance (Balis and Kalff 1995).

6.9.5 Hayq-V (528.13 – 521.13 cm, 12,100 – 12,050 cal yr) The alternating dominance between *Stephanodiscus parvus* and *Aulacoseira granulata* var. *angustissima* in this zone may represent decadal fluctuations (~ 20 cal years) in nutrient availability in the lake, expressed as dominant seasonal blooms. Both are planktonic taxa, indicating a deep, fresh (in agreement with diatom-inferred conductivity), alkaline lake with low light conditions, but the taxa favour different silicon: phosphorus (Si: P) ratios.

Stephanodiscus parvus is a good competitor for silicon (Si) and a poor competitor for phosphorus (P). The taxon therefore requires a high supply rate of phosphorus to the epilimnion in order to become dominant. Its' optimal molar Si: P ratio is ~ 1.0 (Kilham et al. 1986). Therefore, when *Stephanodiscus parvus* dominates at Lake Hayq, this indicates a low Si: P ratio. The competitive nature of the taxon for nutrients is further evidenced by its increase in abundance following blooms of *Nitzschia fonticola* and

Nitzschia epiphytica in the previous zone, which has been documented at Lakes Malawi and Tanganyika (Kilham et al. 1986).

Aulacoseira granulata var. *angustissima* in contrast is a poor competitor for silicon and so requires a high Si: P ratio (Kilham et al. 1986). The short-lived dominance of the taxon in the mid-zone suggests a favourable, temporary change in nutrient upwelling (Gasse et al. 2002). This may have been caused by catchment or in-lake processes. However, as diatom species diversity is low and geochemical data do not indicate any significant climatic shift in this zone, it is not possible to identify what processes may have caused this temporary shift in the Si: P ratio.

Given the high supply rate of phosphorus to Lake Hayq at this time, it may be expected that sedimentary pigment concentration would have increased with the availability of nutrients. However, the majority of sedimentary pigments decline. This is likely to have been driven by in-lake processes that regulate silicon and phosphorus loading rates to the epilimnion of tropical lakes. Kilham and Kilham (1990) have proposed a series of processes that could have produced low Si: P ratios in the epilimnion of African lakes in the early Holocene when water levels were at a maximum and *Stephanodiscus* taxa dominated. The major hypothesis presented is that there is a positive relationship between lake depth and increased phosphorus loading to the epilimnion. In some lakes this may be a result of strong physical mixing of the water column due to fetch length. The wind energy could cause large quantities of phosphorus to be transferred from below the mixed layer. This is evidenced at Lake Albert, which became dominated by *Stephanodiscus* taxa at 12.0 kyr BP and continues to be so today (Harvey 1976). The lake has very low silicon (< 16 µM Si) and relatively high phosphorus (> 4 µM P) concentrations, giving it a low Si: P ratio of 0.5 – 4.0 (Talling 1963). Lake Albert is generally well mixed and oxygenated to the bottom (58 m). In contrast, lakes that are shallow or meromictic, such as Lake Kivu, are dominated by other planktonic diatoms (Kilham et al. 1986). This positive lake depth and phosphorus loading relationship would account for the dominance of *Stephanodiscus parvus* at Lake Hayq alongside low sedimentary pigments as the hypoxic conditions required for pigment preservation would not be present.

6.9.6 Hayq-VI (521.13 – 376.05 cm, 12,050 – 10,300 cal yr BP) Geochemical data indicates the Lake Hayq basin experienced increasingly humid, wet conditions during this period. Increased chemical weathering, biogenic silica and smaller grain sizes are indicative of a wetter, humid environment as a result of enhanced precipitation (Brown 2011). Lacustrine carbonate content also declines marginally, indicating lower water column temperatures and dilution (freshening) of the lake. Increasing water content similarly indicates the core site was submerged. Allochthonous inputs remain fairly constant indicating catchment stability.
As a result of the wetter climate, Lake Hayq experienced water level rise and lake deepening, whilst continuing to remain fresh (confirmed by diatom-inferred conductivity). This is evidenced by the dominance of freshwater, planktonic taxa. *Aulacoseira granulata* var. *angustissima* is one of the most widely distributed species of the genus in Africa (Kilham et al. 1986). The species has the lowest light requirements of common *Aulacoseira* taxa in Africa and signals that Lake Hayq was fairly deep and well mixed (a necessity to keep the heavily silicified valves in suspension), driven by intense wind mixing in a cooler, enhanced rainfall regime (Kilham et al. 1986; Gómez et al. 1995; Marshall et al. 2009). Optimum pH is around 8.0 – 8.5, indicating the water was alkaline (Gasse 1986).

As previously discussed, *Aulacoseira granulata* var. *angustissima* flourishes in lakes where silicon is not limiting, and in comparison to other *Aulacoseira* taxa has high phosphorus requirements; it is an indicator of carbonate-rich, moderately alkaline, eutrophic conditions (Kilham 1971; Kilham et al. 1986). Its increase in abundance in conjunction with the abrupt decline and disappearance of *Stephanodiscus parvus* in the previous zone (Hayq-V) indicates a greater availability of silicon in the lake. Gasse et al. (2002) used up-core changes in the ratio *Aulacoseira*/*Cyclostephanos* + *Stephanodiscus* (A/C+S), to infer changes in nutrient upwelling at Lake Malawi. Increases in *Aulacoseira* taxa (a high A/C+S ratio) implied a deep mixed layer with a strong nutrient flux from the hypolimnion, resulting in high Si: P ratios in the euphotic zone (Gasse et al. 2002). However, whilst Gasse et al. (2002) interpret a low A/C+S ratio as a more stratified lake, it is evident in the previous zone that Lake Hayq must have been well mixed in the deeper water. Therefore, the rapid increase in *Aulacoseira granulata* var. *angustissima* dominance over *Stephanodiscus parvus* is potentially a result of a critical threshold in lake depth being crossed, caused by a

major rise in water level and lake opening in response to a wetter climate, as documented at Lake Tanganyika around 15.0 kyr BP (Gasse et al. 1989).

The most likely cause of this threshold being crossed at this time is that Lake Hayq may have become connected to Lake Hardibo and received its overflow, assuming that given their proximity to one another, Lake Hardibo was also experiencing a highstand in response to the wetter, humid conditions. Ghinassi et al. (2012) estimate that Lake Hardibo would require a 16 – 18 m rise in water level in order to overflow into Lake Hayq. The overflow would have caused Lake Hayq to increase in depth and volume, inundating the surrounding shoreline. The wide coastal plain on the southern margin of the lake would have flooded first, as the Ankwarka River channel was backfilled, followed by the slopes around the eastern and northern lake margins. Given the steepness of the slopes around the west of the lake, there would have been little area available to accommodate water level rise. Overall, the rise in lake level would have increased the surface area of Lake Hayq by up to three times, covering a maximum of ~ 70 km² (Ghinassi et al. 2012). Lake Hayq may have subsequently overflowed itself into the Wazi River, creating a hydrologically open system, which Lamb et al. (2007b) estimate would require Lake Hayq to have been ~ 40 m higher than present (Ayenew 2009). This period may be identified as a highstand at Lake Hayq, reaching maximum water level (potentially ~ 120 m deep) during the Holocene (Fig. 6.18). Water residence would have decreased in response to the combination of inflow and outflow, promoting the flushing of many nutrients, organic matter, potential contaminants and other particles, preventing them from becoming incorporated into the sediments.

Wind driven mixing would have continued to prevail at Lake Hayq, but depth increased to a threshold level whereby the bottom water become impenetrable to wind energy and was no longer mixed. This deeper mixed layer resulted in higher silicon availability, which favoured *Aulacoseira granulata* var. *angustissima*. This *Aulacoseira* dominated period therefore represents water level maximum at Lake Hayq. This contrasts to Kilham and Kilham's (1990) argument that *Stephanodiscus* indicates maximum water level; the *Stephanodiscus parvus* dominated period at Lake Hayq is too brief (~ 50 years) and early (12,100 – 12,050 cal yr BP, Hayq-V) in comparison to other Ethiopian lake highstands to be considered as representing

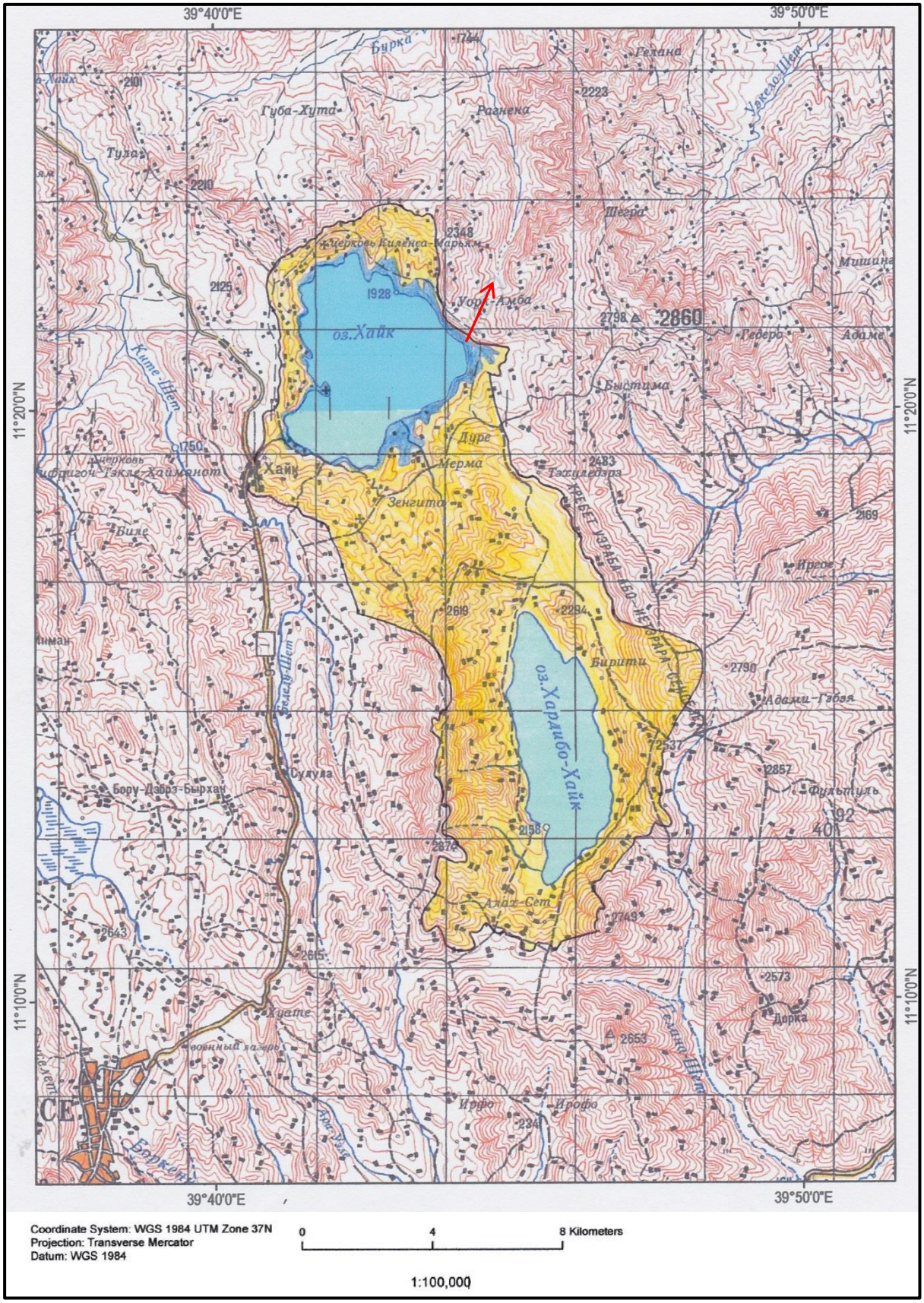

Figure 6.18. Annotated map of Lake Hayq and the surrounding area. The lake catchment is indicated in yellow (with black outline) and lake level maximum (~ 120 m) in dark blue. The direction of overflow into the Wazi River is shown by the red arrow (Soviet military 1984).

maximum lake depth. Most Ethiopian and East African lakes experienced highstands and overflowed for several centuries to millennia during the Holocene Climatic Optimum (~ 10.0 – 6.0 kyr BP; Chapter 3, 3.5.1), a period that corresponds to *Aulacoseira granulata* var. *angustissima* dominance at Lake Hayq.

This deep, stratified lake system is in agreement with the sedimentary pigment record. The dominance of green sulfur bacteria provides evidence of strong stratification. Lake Hayq would have been well-mixed in the upper lake stratum (the mixolimnion), where *Aulacoseira granulata* var. *angustissima* dominated, but a chemocline developed in the bottom waters, which wind energy could not penetrate. This chemocline separated the upper water layers from a dense layer of anoxic conditions in the monimolimnion. Green sulfur bacteria are a characteristic pigment of these meromictic lake conditions, as they photo-oxidize hydrogen sulfide produced in the anoxic sediments (Parkin and Brock 1981; Hodgson et al. 1996; McGowan 2013). The presence of green sulfur bacteria provides additional evidence of the turbulent conditions in the upper waters as they are able to tolerate low light intensity of poor quality (Parkin and Brock 1980; Chen et al. 2001).

Ulnaria ulna var. *ulna* was also present in low abundances in the zone and similar to *Aulacoseira granulata* var. *angustissima*, is a poor competitor for silicon, making it a high Si: P species. It does however, have somewhat higher phosphorus requirements than other *Ulnaria* taxa (Kilham 1986). Its presence indicates submerged macrophytes in the littoral area (Gasse 1987).

Nitzschia subcommunis has not been widely identified in African lakes and may have been amalgamated with other taxa at times. Haberyan (1987) for example, collectively referred to *Nitzschia subcommunis* and several other *Nitzschia* taxa at Lake Rukwa as *Nitzschia* cf. *spiculum*. Its presence at Lake Hayq is indicative of fresh, alkaline water and it may live in an epiphytic or epipelic form. Hustedt (1949) identified it as a benthic taxa found in association with algae. *Nitzschia subcommunis* is therefore likely to be an obligate nitrogen heterotroph, similar to *Nitzschia fonticola* (Kilham et al. 1986), indicated by is greatest abundances during stable periods of profuse colonial cyanobacteria. The manner in which *Nitzschia subcommunis* appears in greatest abundances, synchronous with declines in *Aulacoseira granulata*

var. *angustissima* may indicate brief, temporary declines in water level in response to short-lived arid spells, or alternatively, periods of reduced wind driven mixing.

The phytoplankton community is relatively stable in this zone with evidence of green algae and higher plants, cryptophytes, dinoflagellates (further indicting Lake Hayq was stratified and eutrophic) and chrysophytes (McGowan 2013). The high concentrations of pheophorbide *a* alongside low chlorophyll *a* concentrations, signal that zooplankton populations became well established at Lake Hayq (Hurley and Armstrong 1990). Both the diatom and pigment records indicate this was the first significant period of biological productivity in Lake Hayq, evidenced by the sudden increases in diatom and total pigment concentration and accumulation rates (as well as organic matter and minerogenic accumulation rates), and improved preservation in comparison to the previous zones. The increase in diatom accumulation rate and concentration at the start of this zone (~ 480.0 cm) may also account for an increase in biogenic silica, which may represent diatom productivity (as well as contributions from chrysophytes and sponges) as silica frustules are preserved in the lake sediment (Fig. 6.19). However, after this initial synchronous peak, biogenic silica productivity does not appear to reflect diatom accumulation rate and they become asynchronous. This is most likely a result of increased dust deposition or due to improved preservation caused by higher temperatures, which may indicate a gradually shifting climate towards the end of this time period (Burnett et al. 2011).

6.9.7 Hayq-VII (376.05 – 299.0 cm, 10,300 – 6,500 cal yr BP) This zone may be characterised as the start of gradual water level and lake area decline at Lake Hayq. The decline would have been most evident firstly in the steep northern margins of the lake. *Aulacoseira granulata* var. *angustissima* continues to dominate the diatom assemblage but abundance declines in conjunction with increases in facultatively planktonic and benthic taxa. The increase in epiphytic *Ulnaria ulna* var. *ulna* indicates greater availability of benthic vegetation. Increases in the planktonic *Ulnaria delicatissima* and facultatively planktonic *Fragilaria radians* may also be indicative of lake level decline; Gasse (1986) identifies these varieties as important components of the plankton and bottom mud in small, shallow lakes such as Lakes Naivasha (7.3 m) and Chibwera (Uganda) (12.5 m), though it is also present in deeper lakes such as Lake Luhondo (Rwanda) (68.0 m). This assemblage indicates

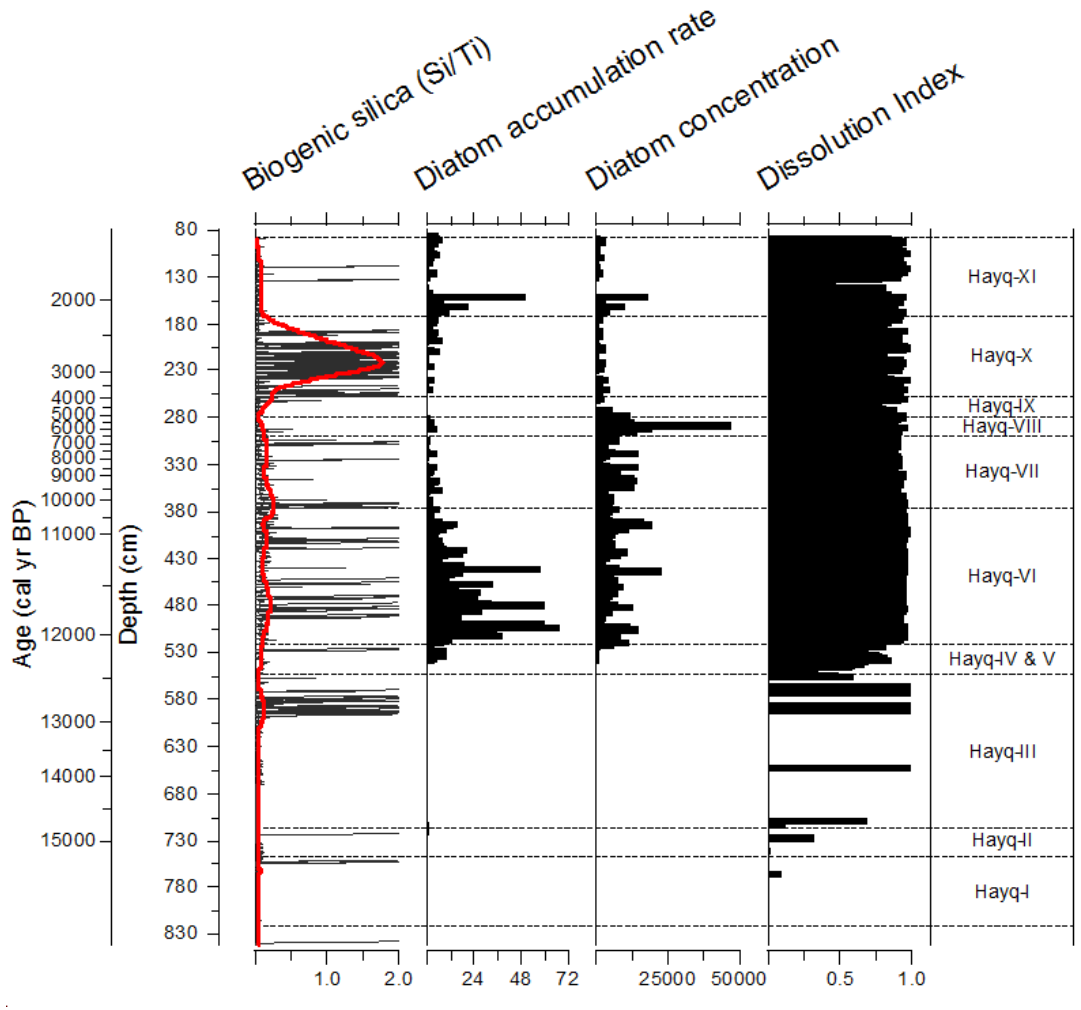

Figure 6.19. Biogenic silica production (shown as peak area units with element X-ray fluorescence values divided by incoherent scatter. The mean trend is indicated in red) and diatom accumulation rate (x 10^6 valves cm^{-2} yr^{-1}) and concertation (valves x 10^5 g^{-1} dry sediment).

that water level was beginning to decline (which would have consequently reduced lake surface area and volume) but the lake remained alkaline and fresh (confirmed by diatom-inferred conductivity). The long, slender species *Ulnaria delicatissima* and *Fragilaria radians* are poor competitors for silicon, similar to *Aulacoseira granulata* var. *angustissima*, but they are highly competitive for phosphorus. They have marginally greater silicon and lower phosphorus requirements than *Ulnaria ulna* var. *ulna* and so indicate that phosphorus availability was beginning to decline with lake level (Kilham et al. 1986). This is supported by the decrease in colonial cyanobacteria towards the centre of this zone. Water pH remained alkaline, ranging from 7.6 – 8.6 (Gasse et al. 1995).

Green sulfur bacteria continued to dominate the pigment record, confirming that the lake remained meromictic. Pheophorbide *a* indicates that zooplankton maintained a steady population at the lake. Cryptophytes, chrysophytes and dinoflagellates decline in this zone but total algal abundance remains relatively stable indicating productivity did not decline. Diatom accumulation rate and valve concentration does not suggest a decline in productivity either; similarly high concentrations of valves have been identified in records from Lakes Ashenge, Tana and the Ziway-Shala basin around this early to mid-Holocene stage, indicating a period of regionally high productivity (Chalié and Gasse 2002b; Marshall 2006; Marshall et al. 2009).

Geochemical data do not indicate any significant, abrupt change in climate at this time, although allochthonous elements and authigenic calcium do show a gradual decline, which may indicate of a steady shift towards aridity. The diatom record does indicate a declining lake level however, which may be attributed to a reduction in effective moisture. Sediment accumulation rates also decline, reaching a minimum of 0.1 mm yr^{-1}, which is significantly lower than other Ethiopian lakes at this time (Lakes Tana [0.98 mm yr^{-1}], Ashenge [0.92 mm yr^{-1}] and the Ziway-Shala basin [0.70 mm yr^{-1}]; Chalié and Gasse 2002b; Marshall 2006). It is important to emphasise however, that whilst there is evidence of water level decline, Lake Hayq remained overall, a relatively deep lake system and this zone is only the start of a gradual shallowing process that would span the following 2.4 cal kyr. The lake most likely closed during this time as water level declined, but it may have continued to receive overflow from Lake Hardibo.

6.9.8 Hayq-VIII (299.0 – 280.13 cm, 6,500 – 5,200 cal yr BP) The diatom assemblage in the zone suggests that water level continued to fall during this time, evidenced by further declines of *Aulacoseira granulata* var. *angustissima*. Green sulfur bacteria indicates that Lake Hayq was still meromictic however, suggesting that lake depth had not declined to such an extent that the waterbody was completely mixed. The increase and subsequent maximum abundance of *Fragilaria radians* may be a result of two processes; the first being a decline in the availability of phosphorus in the water, increasing the Si: P ratio, but this is not supported by the cyanobacteria, which is more stable and abundant than the previous zone, or by the decline of *Aulacoseira granulata* var. *angustissima*. Alternatively, a decline in wind-driven mixing, or short-term fluctuations in effective moisture which caused changes in lake depth, may have favoured *Fragilaria radians* over *Aulacoseira granulata* var. *angustissima*. The lake remained fresh (evidenced by diatom-inferred conductivity), alkaline (pH 7.4 – 7.8) and lake chemistry did not change significantly (Gasse 1986).

Similar to the previous zone (Hayq-VII), no significant climate shift is evident from the geochemical data at this time, and despite evidence of gradual water level decline, Lake Hayq was still a relatively deep waterbody. Diatom and total pigment accumulation rates indicate that productivity was lower at this time in comparison to the early Holocene. Sedimentation and other accumulation rates also reach their minimum value, which would suggest a change in productivity. Cryptophytes, dinoflagellates and chrysophytes, as well as zooplankton populations, remain relatively stable.

6.9.9 Hayq-IX (280.13 – 257.5 cm, 5,200 – 3,950 cal yr BP) This zone shows evidence of the first significant water level decline at Lake Hayq, potentially as a critical threshold in depth is crossed following gradual decline since the early Holocene. Overflow most likely ceased to and from Lake Hayq during this time period, creating a climatically sensitive, hydrologically closed system (Battarbee 2000; Umer et al. 2004). The lake would have most likely been shallower than its' modern state (maximum depth of ~ 80 – 90 m), which at this depth, has been dominated by *Aulacoseira* taxa in recent centuries and receives no overflow from Lake Hardibo and does not overflow itself (Lamb et al. 2007b).

The periphytic *Gomphonema parvulum* and *Gomphonema pumilum* rapidly increase in abundance, alongside an increase in the diversity of other benthic taxa, as well as further declines of *Aulacoseira granulata* var. *angustissima* and *Fragilaria radians*. This indicates an upsurge in the availability of macrophyte habitat in a shallow benthic area (Cocquyt 1998; Barker et al. 2003). *Gomphonema* taxa are commonly found in epilithon samples as well as on floating mats of swamp vegetation (Barker et al. 2003) and indicate Lake Hayq was still dilute (diatom-inferred conductivity does increase in this zone but is still within the boundaries of being fresh [Table 6.4]). This would suggest that as lake level declined, shallow near-shore sections of the lake basin were exposed and colonised. Alternatively, or in addition to, if Lake Hayq had been receiving overflow from Lake Hardibo (or overflowing itself), and this gradually declined, this would have left swamp-like, marsh areas in the wide coastal plain in the southern margin if the lake, abundant with macrophytes, suitable for *Gomphonema* taxa and other benthic diatoms. The collection of benthic taxa present suggests Lake Hayq may have increased slightly in alkalinity (*Sellaphora pupula* has an optimum pH of 8.0).

Despite the decline in water level, Lake Hayq was still meromictic, evidenced by the presence of green sulfur bacteria. Green algae, cryptophyte, dinoflagellate and chrysophyte populations remain relatively stable. Total pigment concentration does not indicate a significant change in phytoplankton production.

6.9.10 Hayq-X (257.5 – 173.0 cm, 3,950 – 2,200 cal yr BP) Lake Hayq reaches a Holocene lowstand in this zone. Diatom-inferred conductivity indicates the lake was subsaline at times and the abundance and diversity of benthic diatom taxa signals that lake level had declined and was at its shallowest of the Holocene period. The Lake Hayq system would have been closed, as overflow to and from the waterbody ceased. This would have significantly reduced the lake surface area and volume in the steep sided lake basin. Potentially Lake Hayq may have declined to ~ 30 m or less, where the deeply shelving morphometry gives way to a larger, shallow expanse on the lake bottom (Fig. 6.20). Lake surface area would have subsequently been reduced to < ~ 16 km² (Demlie et al. 2007).

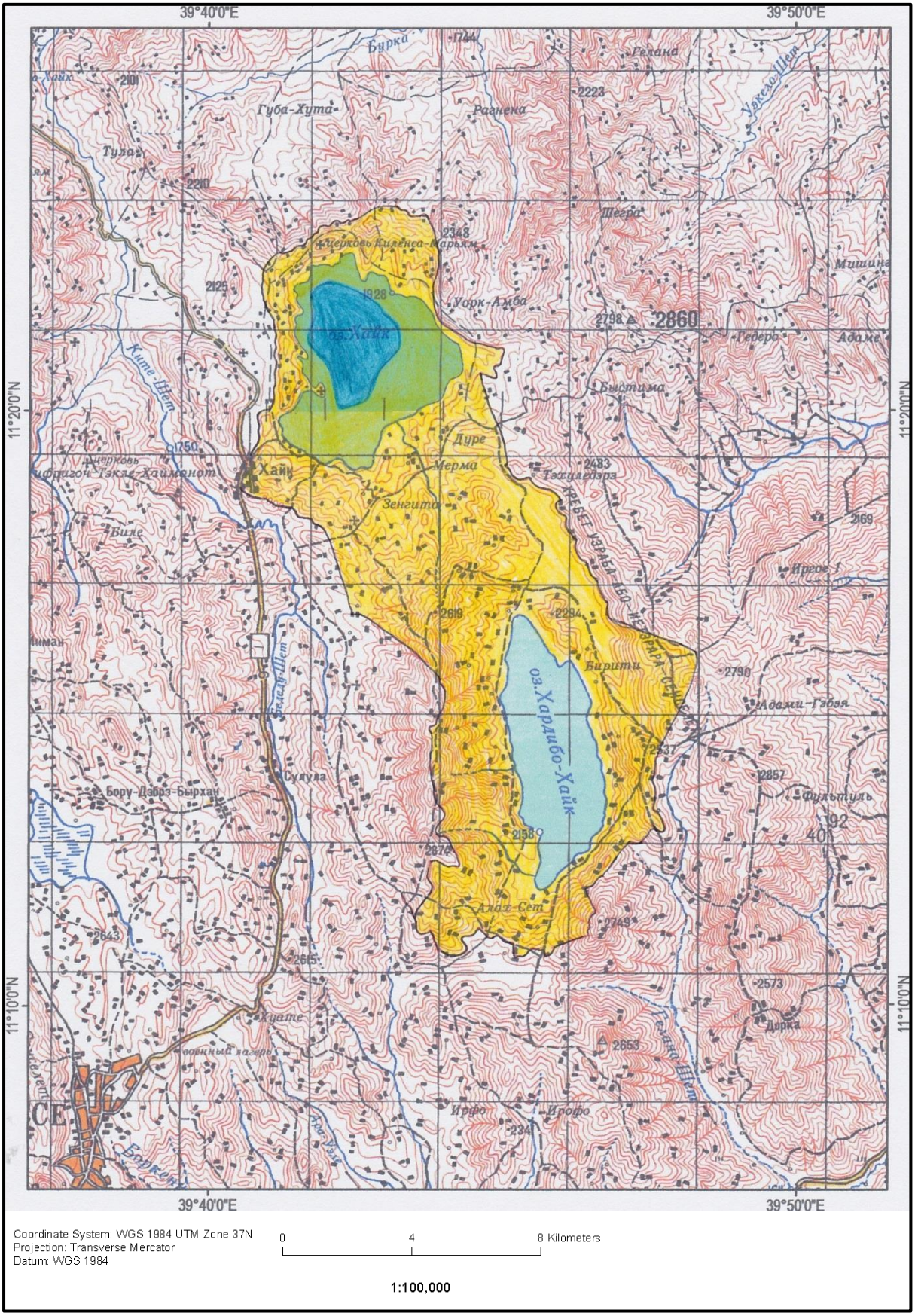

Figure 6.20. Annotated map of Lake Hayq and the surrounding area. The lake catchment is indicated in yellow (with black outline) and the Holocene lake level minimum (~ 30 m) in dark blue (Soviet military 1984).

Water residence time at Lake Hayq would have most likely increased during this time period as inflow and outflow ceased. This would have promoted water transparency at the lake, given the low supply rate of dissolved (and coloured) organic matter from the catchment, which would have been photo-oxidised and bleached by ultraviolet radiation (Kalff 2003). Assuming Lake Hayq experienced the same remarkable water clarity as found in the mid- to late 20th century prior to anthropogenic activity (evidenced by generally low chlorophyll *a* concentrations and a 9 m Secchi disk depth [Baxter and Golobitsch 1970]), light may have penetrated to approximately 22.5 m depth (based on Cole's [1975] premise of light penetration equating to two and a half times the Secchi disk depth), providing a large expanse of suitable habitats for benthic diatom species to colonise.

The zone is largely dominated by *Ulnaria* taxa; the epiphyte *Ulnaria ulna* var. *ulna* indicates shallow water conditions and abundant macrophytes, whilst *Ulnaria delicatissima*, generally considered a planktonic taxon, is also indicative of low water levels, having been associated with several shallow lakes across East Africa (Gasse 1986). The increase of dense mats of *Ulnaria delicatissima*, resulting in laminations in the sediment, is likely a result of short-lived turbulent periods mixing the shallow water in the littoral zone. In these wind penetrable areas, most likely on the lake shelves, frustules are re-suspended and rapidly deposited into the sediment, forming the mass of intertwined valves (Gasse 1986; Verschuren 2001).

The switch from an assemblage dominated by *Aulacoseira granulata* var. *angustissima* to one dominated by *Ulnaria* taxa signals a drop in lake level rather than a change in the availability of nutrients; a negative shift in the Si: P ratio would favour *Ulnaria* over *Aulacoseira* taxa, causing a switch between dominance, but this would also trigger a decline in cyanobacteria (Barker et al. 2000; Barker et al. 2003). No decrease in colonial cyanobacteria is evident at Lake Hayq at this time. In contrast, canthaxanthin concentrations are relatively high in this zone, signalling an availability of phosphorus. Colonial cyanobacteria predominate among the benthic algae of many lakes, providing further support for lake level decline, and its abundance in this zone also accounts for the increase in the obligate nitrogen heterotroph, *Nitzschia subcommunis (*Kalff 2003).

Although low in concertation in comparison to other pigments at this time, the appearance of chlorophyll *a* may also be indicative of increased availability of phosphorus at Lake Hayq, as well as a decrease in lake depth; the diversity of benthic substrates would have encouraged growth of algae in the shallow, protected regions of the lake, which also improved preservation by reducing sinking depth (Moss 1968; Cyr 1998; McGowan 2013). Fucoxanthin may similarly indicate improved preservation as it is particularly labile (McGowan 2013). Many chlorophyll degradation products are still present however, indicating how easily chlorophyll *a* is broken down, with the exception of pheophorbide *a*, which declines, signalling a reduction in macrofauna (Leavitt and Brown 1988).

The abundance of colonial cyanobacteria, euglenophytes as well as benthic and green algae may have caused the decline of green sulfur bacteria during this time. These groups are commonly found co-dominating and are often found in abundance in littoral habitats of shallow, saline lakes (Kalff 2003). The abundance of phytoplankton due to nutrient enrichment in the upper water column would have caused water transparency to decline to such a degree that light could no longer penetrate the anoxic bottom waters, causing green sulfur bacteria to decline as it could not photo-oxidize hydrogen sulfide (McGowan 2013). This decline in light availability may have also contributed to the decline of *Aulacoseira granulata* var. *angustissima*. Alternatively and more likely, the decrease in lake level may have enabled wind energy to penetrate the thermocline and mix the water column, weakening meromixis (other pigments continue to be present, indicating meromixis did not completely break down) and green sulfur bacteria to deteriorate. However, the disappearance of *Aulacoseira granulata* var. *angustissima* from this zone may also indicate a decline in wind driven mixing, which would have maintained the meromictic conditions. Chrysophytes and cryptophytes also demonstrate peaks in this zone, though they are more common in oligotrophic-mesotrophic waters.

Overall, the diatom and phytoplankton assemblage is typical of shallow (~ 30 m deep), fresh-subsaline, mesotrophic-eutrophic East African lakes with an availability of epiphytic and epilithic habitats, and indicates Lake Hayq had a low to medium alkalinity and pH of 7.0 – 8.0 (Gasse 1986). The aerophilous *Hantzschia amphioxys*

and *Nitzschia amphibia* var. *amphibia* increase in abundance in this zone which may also indicate sediment reworking from exposed sections of the basin.

The geochemical data show significant variability during this time period and the overall trend, in contrast to the diatom and phytoplankton assemblage, is indicative of wetter conditions in the mid-zone (~ 237.0 – 204.0 cm, 3,150 – 2,500 cal yr BP). However, the fluctuations exhibited by elemental profiles may instead be interpreted as climate instability rather than a direct climatic transition from dry to humid conditions. The weathering proxy (potassium: aluminium ratio) indicates increased chemical weathering towards the mid-zone, which suggests wetter conditions. However, two peaks sandwiching this apparent wet period signal greater mechanical weathering and extreme aridity of equal measure to zone Hayq-I, which was interpreted as a late Pleistocene lowstand at the lake basin. Calcium, potassium and grain size profiles follow this same trend of low values in the mid-zone indicating enhanced precipitation, bracketed by extreme aridity and enhanced evaporitic conditions, causing the core site to become closer to the shoreline (Brown 2011; Burentt et al. 2011; Foerster et al. 2012). The incoherent: coherent backscatter intensity ratio, although high towards the centre of the zone, reaches minimum values which may be interpreted as low productivity and poor preservation due to a drier climate. It seems therefore that the climate may have experienced a shift to aridity between ~ 3,850 – 2,900 cal yr BP. This aridity was interrupted however by a wet period (~ 2,900 – 2,550 cal yr BP), but the extremity of aridity was great enough to supress lake level recovery and prevent water level from rising, evidenced by the abundance of benthic diatoms and algae as well as low lake productivity. This aridity was later reinforced from ~ 2,450 – 2,400 cal yr BP, which maintained the shallow lake conditions.

6.9.11 Hayq-XI (173.0 – 89.0 cm, 2,200 – 1,350 cal yr BP) The geochemical data in this zone sees a return in values to those observed earlier in the sediment core in zone Hayq-V to Hayq-VI. This indicates that following aridity from ~ 3,850 – 2,400 (Hayq-X), the climate became wetter, cooler and windier again, as experienced during the early to mid-Holocene (12,100 – 6,500 cal yr BP). Sedimentation, and other accumulation rates, increased in this zone, becoming comparable to average rates found in lakes in the East African Rift Valley and Lake

Victoria during the Holocene (0.1 cm yr^{-1}; Johnson 1996; Stager et al. 1997), as well as Lakes Ashenge and the Ziway-Shala basin (0.8 mm yr^{-1} and 1.4 mm yr^{-1} respectively; Chalié and Gasse 2002b; Marshall 2006).

The enhanced precipitation regime led to the recovery of lake level; diatom-inferred conductivity shows that Lake Hayq was fresh again, although values are on the cusp of being subsaline at the start of this zone and gradually decrease, indicating a steady recovery rather than abrupt transition. *Aulacoseira granulata* var. *angustissima* in contrast does rapidly return and dominate the diatom record. This indicates that Lake Hayq was once again deep and relatively well mixed (Gasse 1986). Potentially, the lake may have reached a similar depth, as well as volume and area, as its' modern state; the diatom assemblage over the past 100 years has also been dominated by *Aulacoseira* taxa, and records of maximum lake level range from 81.0 – 88.2 m between 1938 – 2001 (Baxter and Golobitsch 1970; Lamb et al. 2007b). It is possible therefore that during this late Holocene period, Lake Hayq was at a maximum depth of approximately 80 – 90 m, with a surface area of > ~ 23 km^2.

Benthic taxa and species diversity decline as *Aulacoseira granulata* var. *angustissima* becomes reestablished. *Ulnaria ulna* var. *ulna* and *Ulnaria delicatissima* continue to feature in this zone suggesting that submerged macrophytes were present in the littoral zone. The decline and disappearance of chlorophyll *a* also indicates an increase in lake depth, which in conjunction with the reestablishment of green sulfur bacteria in the anoxic zone, suggests that phosphorus availability became more limiting.

Lake level was not stable however and short-term drops in water level are evidenced by decreases in *Aulacoseira granulata* var. *angustissima* in conjunction with increases in *Ulnaria ulna* var. *ulna* and other benthic and facultatively planktonic taxa such as *Gomphonema parvulum*, *Amphora copulata* and *Nitzschia adapta*. The phytoplankton assemblage is also indicative of short-term fluctuations in lake level as peaks in dinoflagellates, chrysophytes, euglenophytes and colonial cyanobacteria occur synchronous with peaks in *Ulnaria ulna* var. *ulna*. These short-term fluctuations may potentially equate to the 7.8 m drop over 60 years during the 20th century (Lamb et al. 2007b).

Overall, this zone is characterised by a return of early to mid-Holocene climatic conditions which triggered a recovery in lake level and reestablishment of an *Aulacoseira granulata* var. *angustissima* dominated diatom assemblage. Sedimentation and accumulation rates likewise recover in this zone and maintain values similar to those found in zone Hayq-VI.

6.10 Summary of the Palaeolimnological Record of Lake Hayq

The interpretation of these limnetic and environmental changes inferred from the available data are summarised below.

Hayq-I (822.0 – 748.0 cm, 15,600 – 15,200 cal yr BP)

- Lake lowstand and hyposaline conditions in response to alternating periods of longer, dry conditions and short, wet episodes.
- Hydrologically closed and no connection with Lake Hardibo.
- Low diatom and pigment concentrations indicate negligible lake productivity and poor preservation.
- Aerophilous taxa indicate sediment reworking from exposed areas of the catchment.

Hayq-II (748.0 – 716.0 cm, 15,200 – 14,800 cal yr BP)

- Increased lake depth (~ 8 m deep, < 4 km² surface area), fresh water and increased water permanence.
- Colonisation by pioneer taxa.

Hayq-III (716.0 – 553.0 cm, 14,800 – 12,300 cal yr BP)

- Climatic shift back to arid conditions.
- Lake level decline and an intermittent mix of planktonic, facultatively planktonic diatoms.

Hayq-IV (553.0 – 528.13 cm, 12,300 – 12,100 cal yr BP)

- Transitional period of lake colonisation dominated by pioneer data, due to a wetter climate.

- A moderately deep (~ 8 m depth), oligotrophic-mesotrophic, fresh-subsaline lake.
- Evidence of symbiotic relationships between diatoms and pigments and improved preservation.

Hayq-V (528.13 – 521.13 cm, 12,100 – 12,050 cal yr BP)

- A deep, fresh, well mixed lake, with phosphorus being transferred from below the mixed layer.
- Short-term fluctuations in nutrient availability causing shifts in diatom taxa dominance.

Hayq-VI (521.13 – 376.05 cm, 12,050 – 10,300 cal yr BP)

- Major water level rise and lake potentially hydrologically open in response to increasing precipitation and humidity in the region, which may have triggered overflow from Lake Hardibo and caused Lake Hayq overflow itself.
- A deep (maximum of ~ 120 m, ~ 70 km² surface area), fresh, turbid (wind driven mixing) lake, with carbonate rich, alkaline waters and an availability of silicon.
- Meromictic conditions allowing for green sulfur bacteria to establish in the anoxic bottom waters.
- Further evidence of symbiotic relationships between obligate nitrogen heterotroph diatoms and pigments.
- Presence of green algae, cryptophytes, dinoflagellates, chrysophytes and zooplankton.
- First period of significant lake productivity and improved preservation.

Hayq-VII (376.05 – 299.0, 10,300 – 6,500 cal yr BP)

- Some indication of a shift towards aridity which triggered the start of gradual lake level decline due to reduced effective moisture.
- Lake becomes hydrologically closed (no outflow) but was still connected to Lake Hardibo via overflow.
- Increased availability of benthic habitats and declining phosphorus concentrations.

Hayq-VIII (299.0 – 280.13 cm, 6,500 – 5,200 cal yr BP)

- Lake level declining with shallow areas in the littoral zone.
- Gradual decline of overflow from Lake Hardibo.
- Still relatively productive.

Hayq-IX (280.13 – 257.5 cm, 5,200 – 3,950 cal yr BP)

- First period of significant lake level decline and greater availability of benthic habitats and submerged macrophytes.
- Hydrologically closed and no longer connected to Lake Hardibo.
- Presence of green algae, cryptophytes, dinoflagellates, chrysophytes and zooplankton.

Hayq-X (257.5 – 173.0 cm, 3,950 – 2,200 cal yr BP)

- Holocene lowstand (~ 30 m deep, < ~ 16 km². surface area), causing the lake to become subsaline.
- A closed system.
- Abundance of macrophytes and presence of benthic algae.
- Decreased lake level enabled wind energy to penetrate the thermocline, mixing the water column and weakening meromixis.

Hayq-XI (173.0 – 89.0 cm, 2,200 – 1,350 cal yr BP)

- Climate returned to conditions similar to those of Hayq-V and Hayq-VI; wetter, cooler and windier.
- Recovery of lake level (potentially a similar depth and area as the modern lake state), causing it to freshen.
- Short-term fluctuations in lake level, though still a closed system.

Chapter 7

Results: A High-Resolution Study of the Termination of the African Humid Period.

7.1 Introduction

This chapter presents high-resolution palaeolimnological results from a section of core Hayk-01-2010 attributed to the termination of the African Humid Period (AHP). As previously discussed in Chapter 3, the timing and abruptness of the termination of the AHP is subject to an ongoing debate as to whether the termination occurred gradually over several millennia as a linear response to orbital changes, or whether non-linear climate feedback dynamics (i.e. vegetation feedbacks) caused abrupt shifts within just a few centuries (deMenocal 2015). Conflicting evidence and unresolved discrepancies between proxy records and sites across Africa intensify the debate and consequently, current understanding of the nature and impact of abrupt climate transitions in Africa remains limited, as well as the impact this had on palaeoenvironments and human development.

The Horn of Africa remains underrepresented in the study of the termination of the AHP, despite being a key area in terms of climatic variability, sensitivity and vulnerability (Chapter 2). Tierney and deMenocal (2013) used hydrogen isotopic composition of leaf waxes (δD_{wax}) from a marine core record (P178-15P) from the Gulf of Aden to reconstruct regional shifts in the hydrological cycle during the late Quaternary. The δD_{wax} record indicates an abrupt transition at the end of AHP around 5.0 kyr BP, synchronous with other δD_{wax} records from Lakes Tanganyika and Challa. The average timing of the termination at these sites is 4,960 ± 70 yr BP (similar to West Africa which is estimated to have begun at 4,900 ± 400 yr BP) and lasted between 280 – 490 years, indicating an abrupt end to the AHP (Tierney and deMenocal 2013). Whilst this study provides a reference point for characterising the nature of the AHP's termination, additional evidence from multiple proxies and sites across the Horn of Africa is required in order to definitively identify the mechanisms driving the climatic shift, as well as the regional impact on the palaeoclimate and palaeoenvironment.

A section of Hayk-01-2010 (302.0 – 267.0 cm) has been sampled for diatoms and pigments at 0.5 cm resolution (average sediment accumulation rate of 0.02 cm yr^{-1})

in order to provide a high-resolution, continuous record detailing the palaeolimnology of Lake Hayq between ~ 6,650 – 4,450 cal yr BP, the period during which the AHP is believed to have terminated. Geochemical data are provided first, followed by a detailed description of the diatom and pigment record. The interpretation of this high-resolution palaeolimnological data will provide a detailed record of the environmental and climatic changes that occurred in the Lake Hayq basin in response to the termination of the AHP, identifying when the AHP ended and over what time scale.

7.2 X-ray Fluorescence (XRF) Geochemistry

Selected geochemical elemental concentrations for the high-resolution section of Hayk-01-2010 (302.0 – 267.0 cm) are shown in Figure 7.1. Peak area profiles for calcium (Ca), potassium (K), silicon (Si), titanium (Ti) have been normalised by incoherent scatter (inc) to minimise the effect of organic matter and water content variability, unrelated to sediment geochemistry (Marshall et al. 2011). Ratios of potassium: aluminium (K/Al) and silicon: titanium and (Si/Ti) are shown as well as the incoherent: coherent (inc/coh) backscatter intensity ratio. Ratios are dimensionless.

The lithogenic elements, K, Si and Ti are low in concentration from 302.0 – 290.5 cm, showing very little overall variability. Between 291.0 – 288.5 cm these elements all demonstrate an increase, which peaks at ~ 286.0 cm. A minor decrease occurs but elements remain relatively stable and in higher concentrations than before the peak. A second increase is documented at ~ 279.0 cm, peaking at 277.3 cm when K, Si and Ti reach their maximum concentration. It is at this depth that Ca (a proxy for authigenic carbonate minerals or biogenic calcium carbonates) begins its stepped increase, having been exceptionally low in concentration up until ~ 279.0 cm. K, Si and Ti once again decline, returning to concentrations similar to those before the second peak by ~ 274.5 cm. Ca experiences a second increase at this depth. A third increase in K, Si and Ti occurs at ~ 270.5 cm and concentrations remain high. Ca also increases at 270.0 cm but declines after reaching its maximum concentration.

The K/Al ratio (an approximation of chemical over mechanical weathering) follows the same overall pattern as K, Si and Ti. Two small peaks centred at ~ 297.5 cm and ~ 294.5 cm are evident in the K/Al record, which are less apparent in the lithogenic

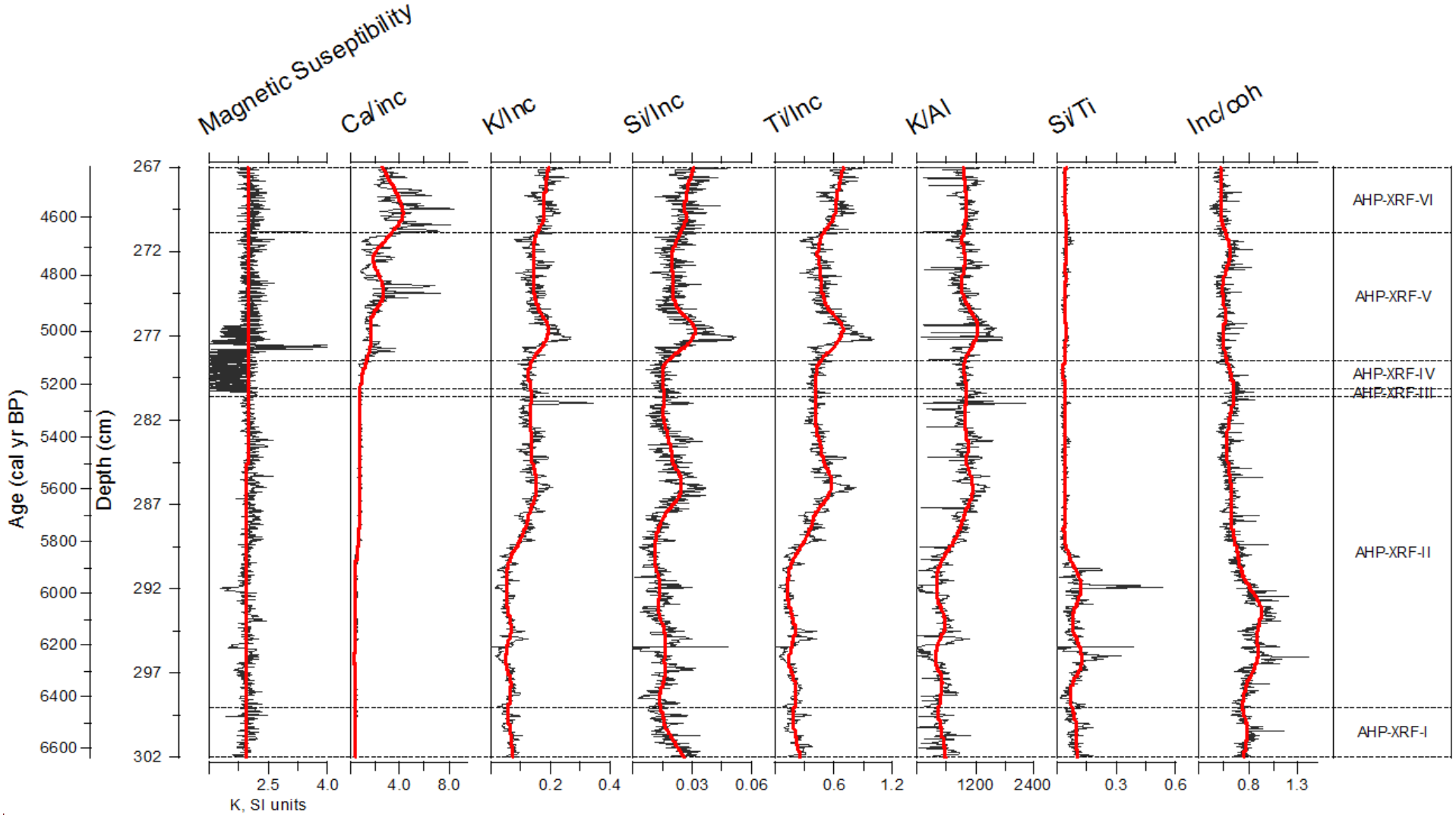

Figure 7.1. XRF results for the high-resolution section (302.0 – 267.0 cm) of Hayk-01-2010. Elemental data is given as peak area units with element X-ray fluorescence values divided by incoherent scatter (inc). Magnetic susceptibility is given as κ, SI units. The mean trend is indicated in red.

element profiles. The Si/Ti ratio (a proxy for biogenic silica productivity) declines slightly between 302.0 – 297.9 cm, before increasing and peaking at ~ 296.5 cm. Si/Ti declines again before a second rise centred at ~ 292.0 cm. After this second peak, Si/Ti declines to a relatively stable, low concentration between ~ 289.0 – 267.0 cm. The inc/coh ratio (a proxy for organic content) demonstrates a more stepped increase between 302.0 – 293.5 cm; a small peak occurs at ~ 300.5 cm, followed by a second rise from 298.5 – 296.5 cm and a final peak centred at ~ 293.5 cm. The inc/coh ratio then declines to values similar to those at the start of the profile and then continues to decrease, demonstrating small fluctuations around ~ 280.5 cm and ~ 272.5 cm. Magnetic susceptibility remains relatively stable; fluctuation does occur between ~ 280.5 – 276.5 cm but the overall trend shows very little variability.

7.3 The High-Resolution Diatom Record

The high-resolution diatom record for 302.0 – 267.0 cm is shown in Figure 7.2. In addition, habitat groups, valve concentration (valves x 10^5 g^1 dry sediment, hereafter x 10^5 g^{-1}), accumulation rate (x 10^6 valves cm^{-2} yr^{-1}), dissolution index (*F* index), Hill's N2 species diversity index, DCA axis 1 and 2 values, as well as diatom-inferred conductivity are displayed in Figure 7.3. This high-resolution section falls across zones D-VI, D-VII, D-VII of those identified in the complete diatom record (822.0 – 89.0 cm) (Chapter 6, 6.5). In order to identify the natural groupings in the high-resolution diatom record, which may be less apparent amongst the complete record, the section has been zoned again separately using the same method (Chapter 4, 4.6.1). The stratigraphic diagrams have been divided into six statistically significant zones (AHP-D-I – AHP-D-VI).

7.3.1 Zone AHP-D-I (302.0 – 299.0 cm, 6,650 – 6,450 cal yr BP) This zone is dominated by *Aulacoseira granulata* var. *angustissima*, which reaches a maximum abundance of 94.8 %. *Ulnaria delicatissima* is found at 300.0 cm where it accounts for 33.3 %. *Fragilaria radians* and *Gomphonema parvulum* occur in low abundances ($\bar{x}$ = 4.8 % and 3.4 % respectively). *Ulnaria ulna* var. *ulna* increases from 8.7 % (302.0 cm) to 23.3 % (300.0 cm), whilst *Nitzschia subcommunis* is found at 300.8 cm (13.8 %). Valve preservation is very good (average *F* index value of 0.8) and concentration is low, averaging ~ 2,900 x 10^5 g^{-1}. Diatom-inferred conductivity ranges between ~ 150 – 240 µS cm^{-1}.

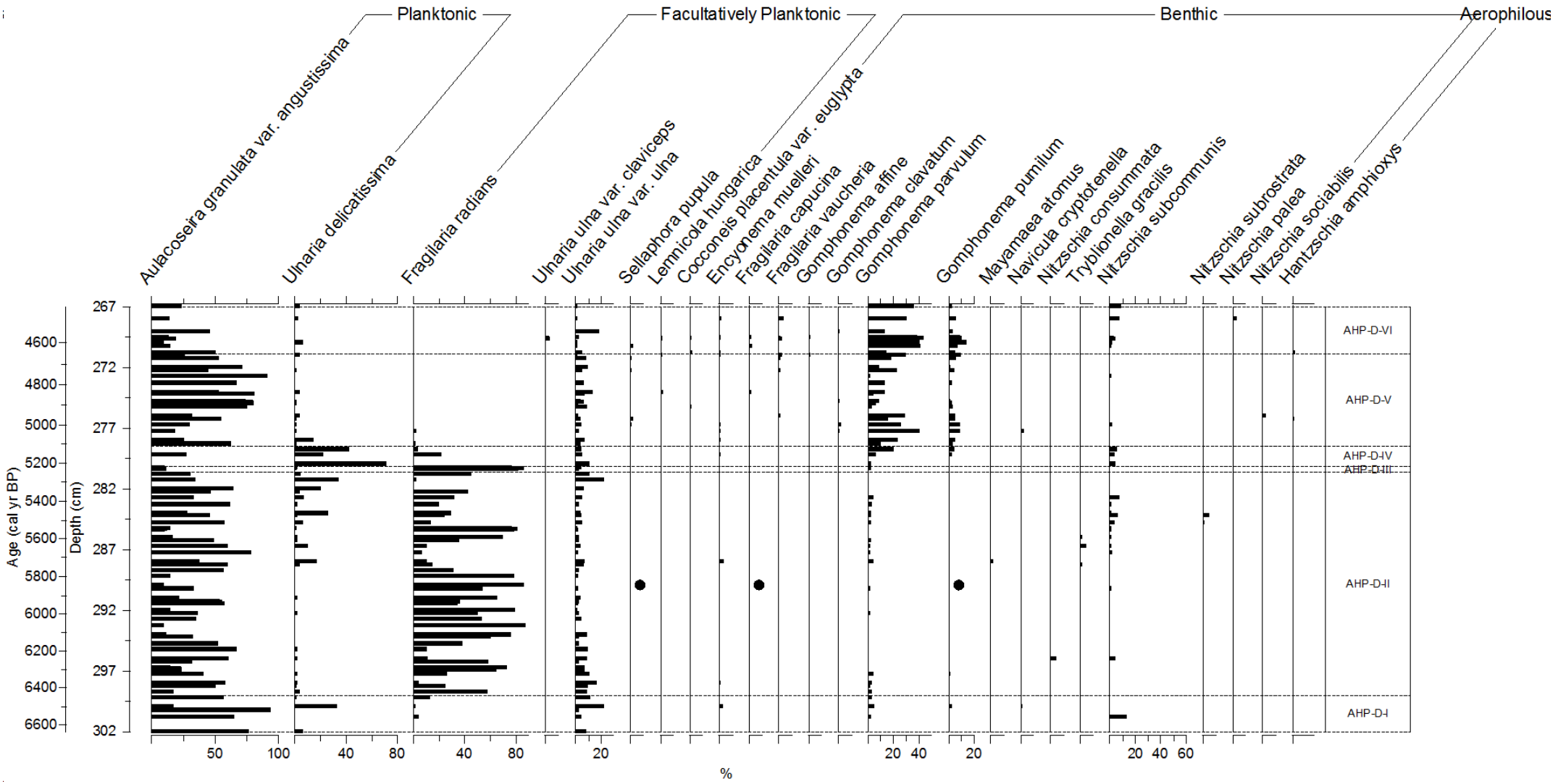

Figure 7.2 (a). Diatom data, shown as percentages (%), for the high-resolution section (302.0 – 267.0 cm) of Hayk-01-2010, against depth (cm), arranged according to habitat preference. Circles represent depths at which a taxon is present in low abundances (< 0.5 %). Average sample standard deviation is 2.82 %.

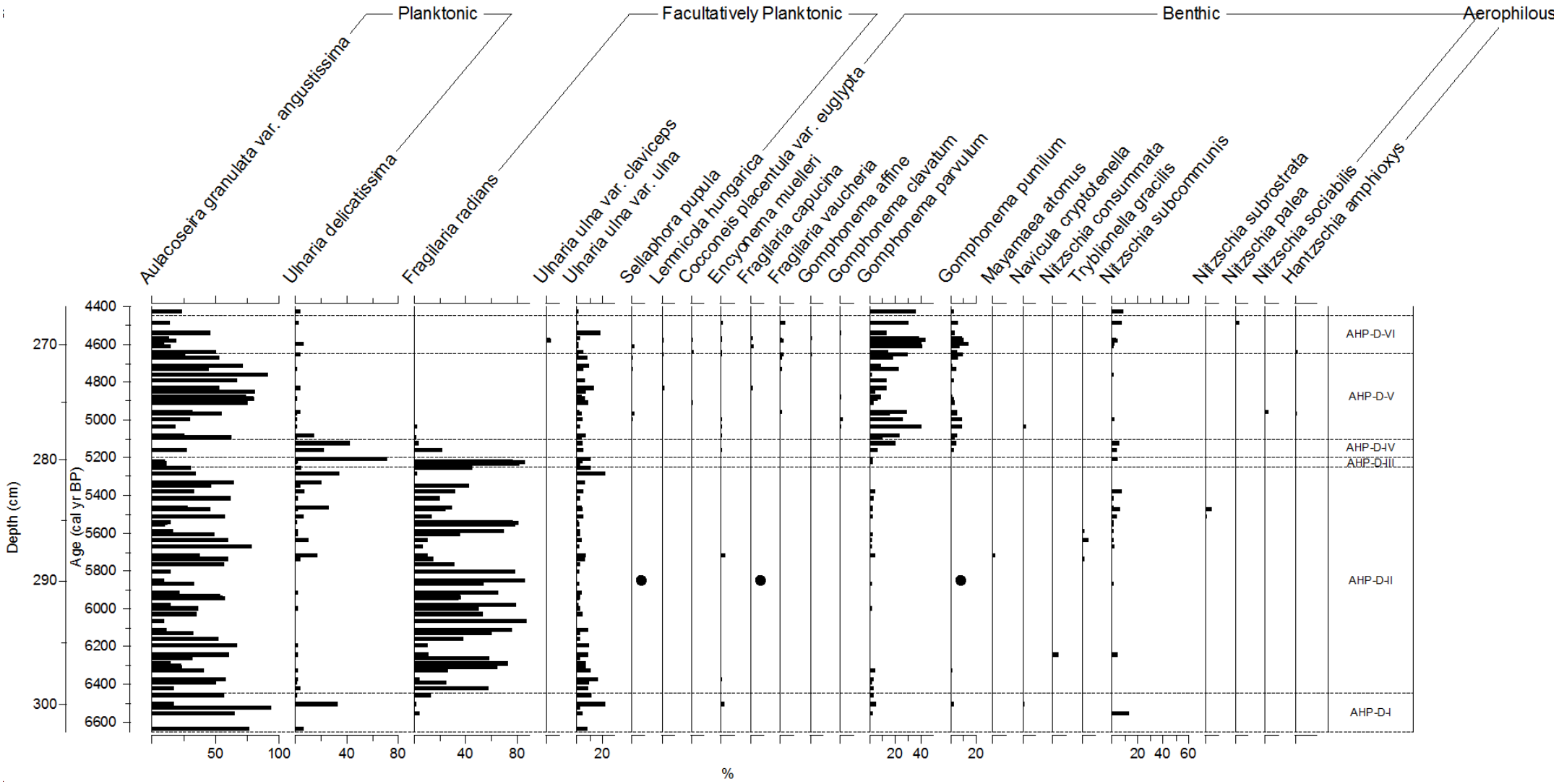

Figure 7.2 (b). Diatom data, shown as percentages (%), for the high-resolution section (302.0 – 267.0 cm) of Hayk-01-2010, against age (cal yr BP), arranged according to habitat preference. Circles represent depths at which a taxon is present in low abundances (< 0.5 %). Average sample standard deviation is 2.82 %.

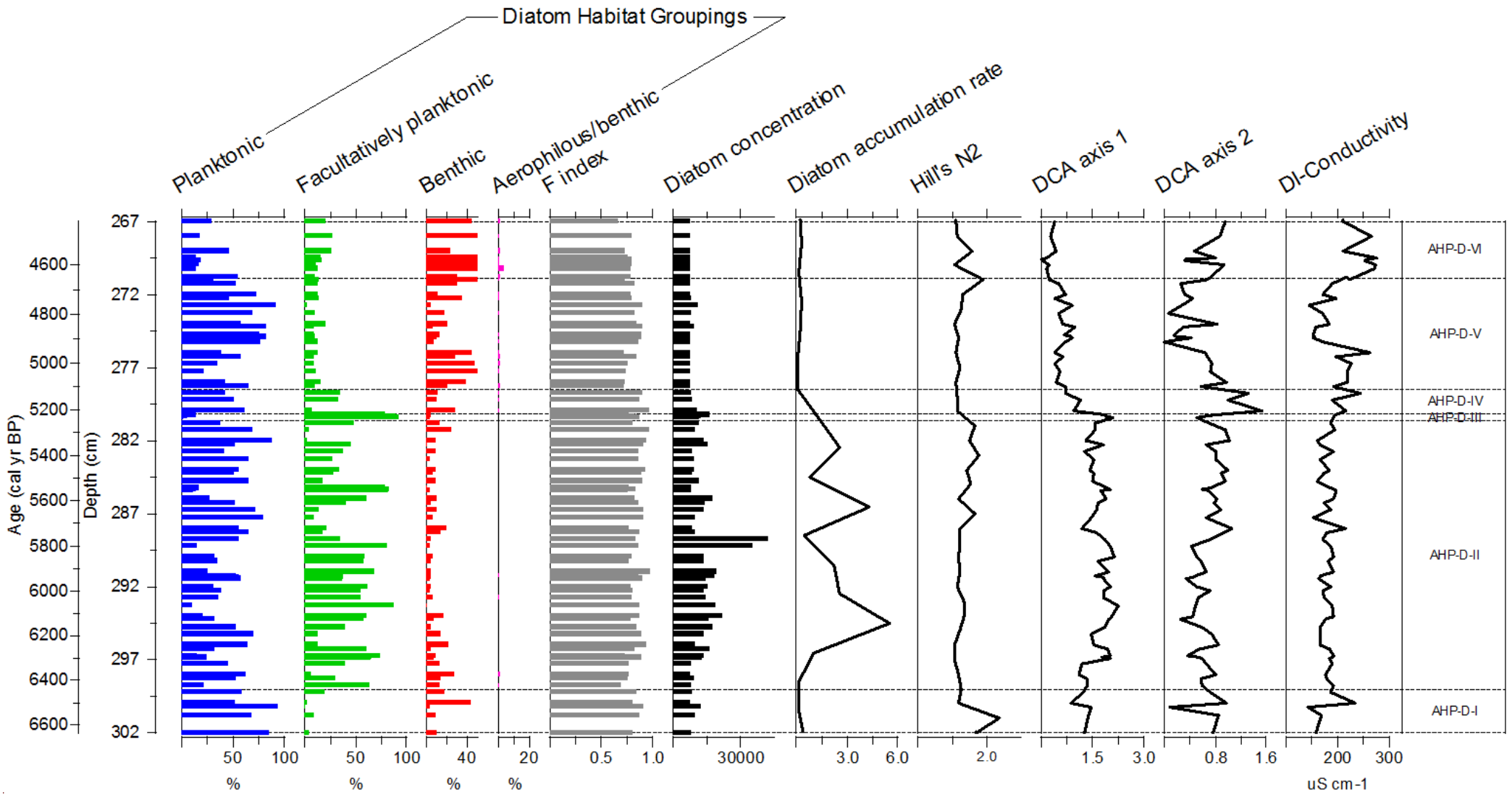

Figure 7.3. Associated diatom metrics for the high-resolution section (302.0 – 267.0 cm). Habitats are shown as percentage of total diatom assemblage (%), concentration as valves x 10^5 g^{-1} dry sediment, accumulation rate as x 10^6 valves cm^{-2} yr^{-1} and diatom-inferred conductivity as µS cm^{-1}.

7.3.2 Zone AHP-D-II (299.0 – 280.6 cm, 6,450 – 5,250 cal yr BP) This zone is characterised by an increase in the abundance of *F. radians a*nd a pattern of peaks and troughs by *A. granulata* var. *angustissima*. *Fragilaria radians* increases significantly at the base of the zone (58.6 %, 298.8 cm) after which the taxon demonstrates a pattern of rising and declining. Peaks are centred at 296.9 cm (74.0 %), 293.3 cm (88.1 %), 290.0 cm (87.0 %) and 185.4 cm (79.1 %), separated by lower concentrations (4.3 – 54.0 %). The rises and declines exhibited by *F. radians* alternate with *A. granulata* var. *angustissima* in dominance. The highest concentrations of *A. granulata* var. *angustissima* occur at 295.3 cm (68.4 %), 291.4 cm (58.5 %), 287.3 cm (79.7 %), 283.3 cm (63.0 %) and 282.0 cm (65.6 %). These increases in *A. granulata* var. *angustissima* occur simultaneously with the declines exhibited by *F. radians*.

Ulnaria delicatissima occurs in low abundances from 299.0 – 288.3 cm (< 4.0 %) until 288.0 cm when it increases to 17.9 %. After a decline (3.0 %, 284.3 cm), the taxon increases in a series of peaks to 34.9 % (281.3 cm). *Ulnaria ulna* var. *ulna* appears in low abundances ($\overline{x}$ = 5.9 %), demonstrating a decline from the base towards the centre of the zone (0.7 %, 285.35 cm) before increasing. Other taxa present include *G. parvulum*, which occurs intermittently (< 4.3 %) at the base and towards the top of the zone, and *N. subcommunis*, which is found between 287.3 – 282.8 cm in low abundances (< 8.2 %). Rare benthic taxa include *Encyonema muelleri*, *Mayamaea atomus*, *Nitzschia consummata*, *Tryblionella gracilis* and *Nitzschia subrostrata*.

Valve preservation remains very good (*F* index value of 0.7 – 1.0), whilst concentration increases steadily from the base to the mid-zone (~ 1,250 – 47,100 x 10^5 g^{-1}, 299.0 – 288.75 cm) and then decreases. Accumulation rate increases from the base of the zone, reaching a maximum of 5.5 x 10^6 valves cm^{-2} yr^{-1} (294.5 cm), before declining. Two smaller peaks of 4.3 and 2.6 x 10^6 valves cm^{-2} yr^{-1} occur at 286.5 cm and 282.5 cm. Hill's N2 diversity values indicate that species diversity remains relatively stable throughout the zone. Diatom-inferred conductivity is low between 299.0 – 288.0 cm (< ~ 175 µS cm^{-1}) with the exception of a peak at 297.0 cm when it increases to ~ 230 µS cm^{-1}. After a second peak at 287.0 cm (~ 240 µS

cm^{-1}), diatom-inferred conductivity increases slightly, ranging between ~ 175 – 200 µS cm^{-1}.

7.3.3 Zone AHP-D-III (280.6 – 280.13 cm, 5,250 – 5,200 cal yr BP) This is the smallest zone in the high-resolution diatom record and sees a major peak in *F. radians* as it reaches 82.6 % abundance. This occurs simultaneously with a drop in *A. granulata* var. *angustissima* ($\bar{x}$ = 7.5 %). *Ulnaria ulna* var. *ulna* and *G. parvulum* maintain low abundances ($\bar{x}$ = 5.5 % and 2.5 % respectively).

7.3.4 Zone AHP-D-IV (280.13 – 278.5 cm, 5,200 – 5,100 cal yr BP) This zone sees a significant decline in *F. radians* as it drops to 22.2 % (279.3 cm). *Ulnaria delicatissima* also decreases in several stages from 72.0 % (280.0 cm) to 43.4 % (278.8 cm) and then 1.3 % at the top of the zone. *Aulacoseira granulata* var. *angustissima* is only present at 279.25 cm (28.2 %). *Ulnaria ulna* var. *ulna* continues to occur in low abundances ($\bar{x}$ = 6.7 %), whilst *G. parvulum* sees a steady increase, reaching 20.2 % (278.8 cm). *Gomphonema pumilum* also occurs in low abundances, as does *N. subcommunis* ($\bar{x}$ = 2.8 % and 5.0 % respectively). Preservation is excellent (average *F* index value of 0.9) and Hill's N2 diversity values indicate species diversity increases slightly. Diatom-inferred conductivity averages ~ 200 µS cm^{-1}.

7.3.5 Zone AHP-D-V (278.5 – 270.9 cm, 5,100 – 4,650 cal yr BP) This zone is defined by the alternating dominance of benthic and planktonic taxa. Between 278.25 – 275.25 cm, a substantial increase in the abundance of *G. parvulum* occurs ($\bar{x}$ = 24.9 %) and, to a lesser extent, *G. pumilum*, ($\bar{x}$ = 6.4 %). These taxa then decline from 275.25 – 272.25 cm. *Gomphonema parvulum* decreases to an average of 5.7 % before increasing slightly to 13.1 % and *G. pumilum* declines to a steady average of 2.0 %. This decline in benthic taxa occurs simultaneously with a substantial increase in the abundance of *A. granulata* var. *angustissima*, from 19.0 % to 91.7 % (277.3 – 272.75 cm). *Aulacoseira granulata* var. *angustissima* then declines slightly, simultaneous with increases in both *G. parvulum* and *G. pumilum* ($\bar{x}$ = 19.3 % and 5.7 % respectively). *Ulnaria ulna* var. *ulna* maintains a steady abundance ($\bar{x}$ = 6.0 %). Other taxa present in this zone in low abundances include

Sellaphora pupula, *Cocconeis placentula* var. *lineata*, *Navicula cryptotenella*, *Nitzschia sociabilis*, *N. subcommunis* and the aerophilous *Hantzschia amphioxys*.

Valve preservation is varied but generally good (*F* index values of 0.7 – 0.9). Concentration is minor, averaging ~ 1,000 x 10^5 g^{-1}, and accumulation rate also remains low (< 0.3 x 10^6 valves cm^{-2} yr^{-1}). Hill's N2 diversity values indicate that species diversity is greatest towards the base of the zone. Diatom-inferred conductivity is low, ranging between ~ 170 – 200 µS cm^{-1}.

7.3.6 Zone AHP-D-VI (270.9 – 267.0 cm, 4,650 – 4,450 cal yr BP) This zone is defined by a reappearance of facultatively planktonic and benthic taxa. *Gomphonema parvulum* increases substantially, reaching a maximum of 44.6 % (269.6 cm). *Gomphonema pumilum* also increases and maintains an average of 8.1 %. Other facultatively planktonic and benthic taxa occurring in this zone include *Gomphonema affine* and *S. pupula*. *Ulnaria ulna* var. *ulna* is found in low abundances ($\bar{x}$ = 1.5 %) until 269.0 cm when it increases substantially to 19.6 % before declining again. The diversity of taxa increases in this zone; *Lemnicola hungarica*, *C. placentula* var. *lineata*, *Cocconeis placentula* var. *euglypta*, *E. muelleri*, *Fragilaria capucina*, *Fragilaria vaucheriae*, *N. cryptotenella*, *N. subcommunis*, *Nitzschia palea* and the aerophilous *H. amphioxys* are all found in low abundances. Consequently, Hill's N2 diversity values indicate species diversity is greatest in this zone. *Aulacoseira granulata* var. *angustissima* fluctuates between 10.3 – 47.1 %. Valve preservation reaches a minimum in this zone but is still good overall (average *F* index value of 0.7). Valve concentration is likewise very low ($\bar{x}$ = 470 x 10^5 g^{-1}), as is accumulation rate (< 0.3 x 10^6 cm^{-2} yr^{-1}). Diatom-inferred conductivity is low, ranging between ~ 160 – 190 µS cm^{-1}.

7.4 Unimodal Ordination: Detrended Correspondence Analysis (DCA)

For the high-resolution diatom dataset, DCA was deemed the most appropriate ordination technique as the axis 1 gradient length was 2.257 SD (standard deviation of species turnover) units (Table 7.1). The first and second axes cumulatively account for 32.2 % of variation in the dataset, with axes 3 and 4 accounting for very little additional cumulative variance (38.8%). A DCA plot of the diatom species and samples is shown in Figure 7.4, which has been divided into the zones identified in

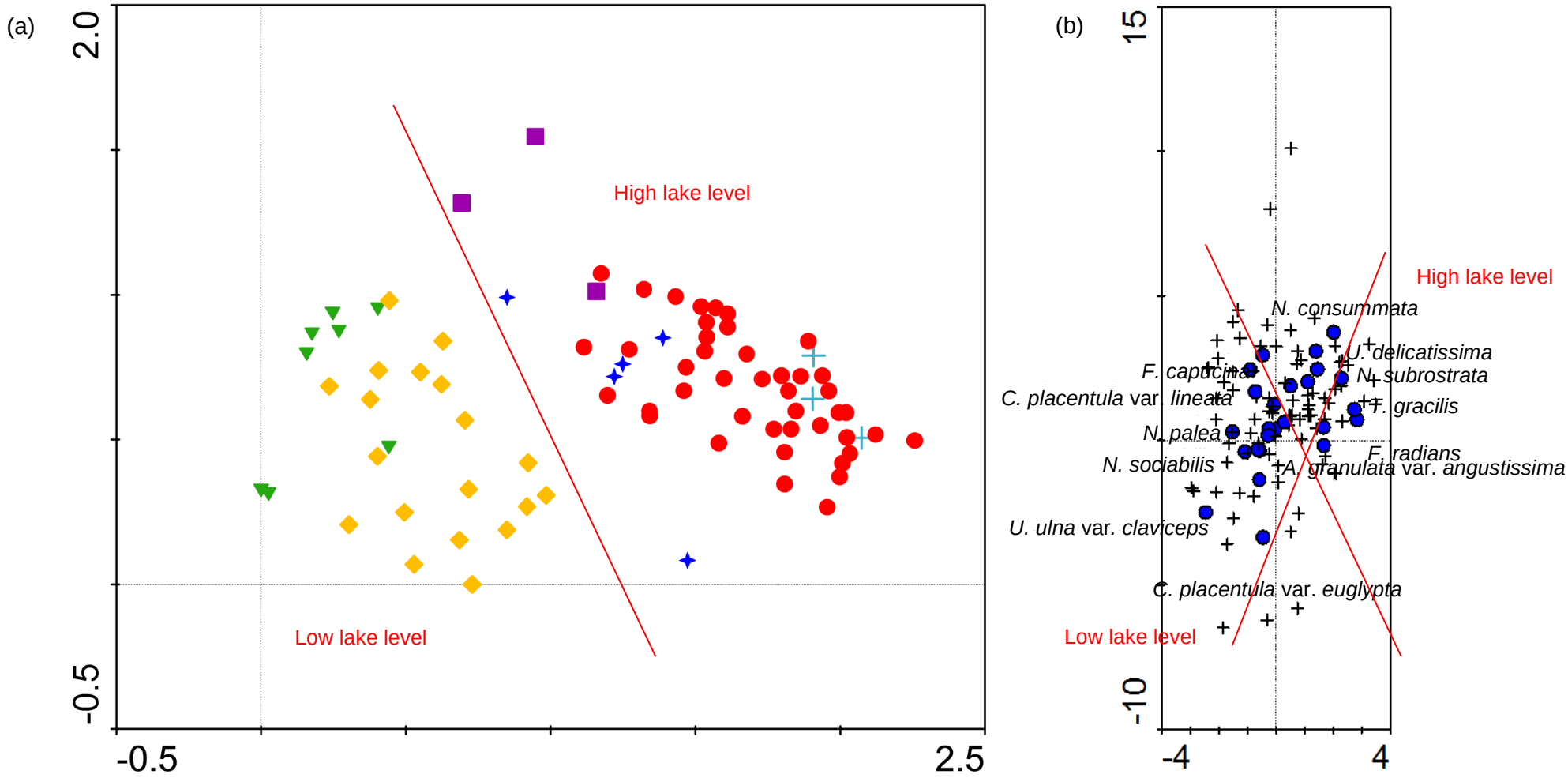

Figure 7.4. DCA results for the high-resolution diatom dataset showing (a) samples according to zone (AHP-D-I – dark blue star, AHP-D-II – red circle, AHP-D-III – light blue cross, AHP-D-IV – purple square, AHP-D-V – yellow diamond, AHP-D-VI – green triangle), and (b) species (taxa > 5.0 % shown as blue circles, all other taxa as black cross). Taxa located at the extremities of axes have been identified. The red lines illustrate the *approximate* divide between periods of high lake level and low lake level.

Table 7.1. Summary of DCA results for the high-resolution Lake Hayq diatom dataset (302.0 – 267.0 cm).

Dataset	No. of samples	No. of species	Total inertia	Axis	1	2	3	4
High-resolution diatoms	81	135	1.232	Eigen values	0.322	0.075	0.043	0.038
				Length of gradient	2.257	1.546	1.401	1.007
				Cumulative % variance of species data	26.2	32.2	35.7	38.8

section 7.3. Axis 1 provides a summary of the major compositional shifts in the high-resolution diatom record. The lowest scores correlate to the youngest zones dominated by benthic taxa (*C. placentula* var. *lineata* and *F. capucina*, zones AHP-D-V and AHP-D-VI) and higher scores correspond to the oldest zones dominated by planktonic taxa (A. *granulata* var. *angustissima* and *U. delicatissima*, zone AHP-D-II). This reflects changes in diatom habitat availability, which can be used as an indication of changes in lake depth. Dissimilarity between axis 2 DCA scores represents the transitional period between a deeper and shallower lake; low scores correspond to zones dominated by benthic taxa (*C. placentula* var. *euglypta* and *F. vaucheriae*, zone AHP-D-V), whilst higher scores reflect zone AHP-D-IV, a period when abrupt declines in planktonic taxa occur simultaneously with the establishment of benthic and facultatively planktonic taxa. Collectively, axis 1 and 2 summarise the mid-Holocene changes in water level at Lake Hayq.

7.5 The High-Resolution Pigment Record

The high-resolution pigment record for 302.0 – 267.0 cm is shown in Figure 7.5. Thirteen pigments have been identified and are presented in concentration (nmol pigments g^{-1} organic matter, hereafter nmol pigments g^{-1} OM). This high-resolution section falls across zones P-XI and P-X of the complete pigment record (Chapter 6, 6.7) but has been zoned again separately to identify natural groupings using the same method (Chapter 4, 4.6.1). The stratigraphic diagram has been divided into seven statistically significant zones (AHP-P-I – AHP-P-VII).

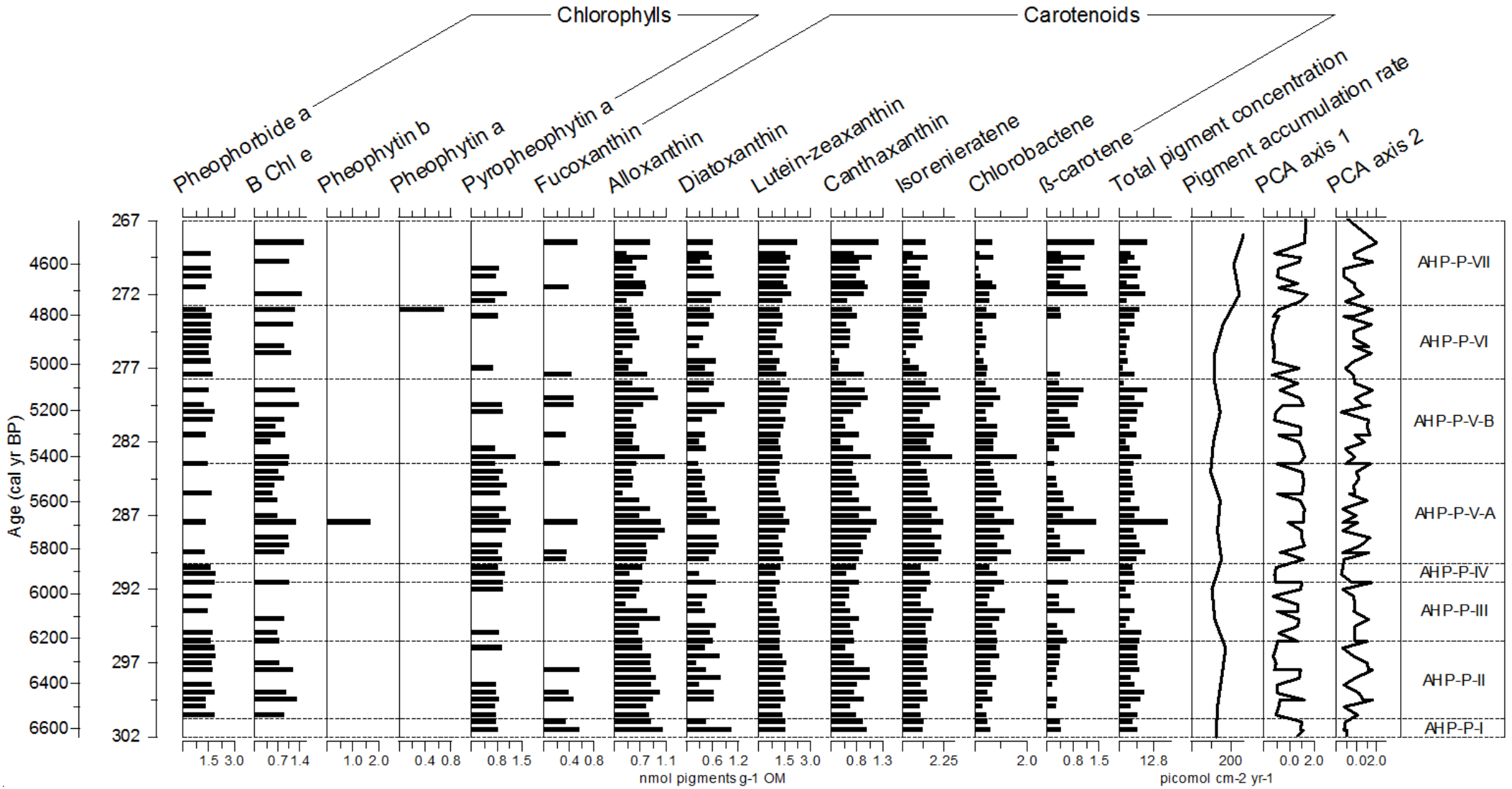

Figure 7.5 (a). Pigment concentration (nmol pigments g^{-1} OM) for the high-resolution section (302.0 – 267.0 cm) and associated metrics, arranged according to depth (cm). Pigment accumulation rate is shown as picomol cm^{-2} yr^{-1}.

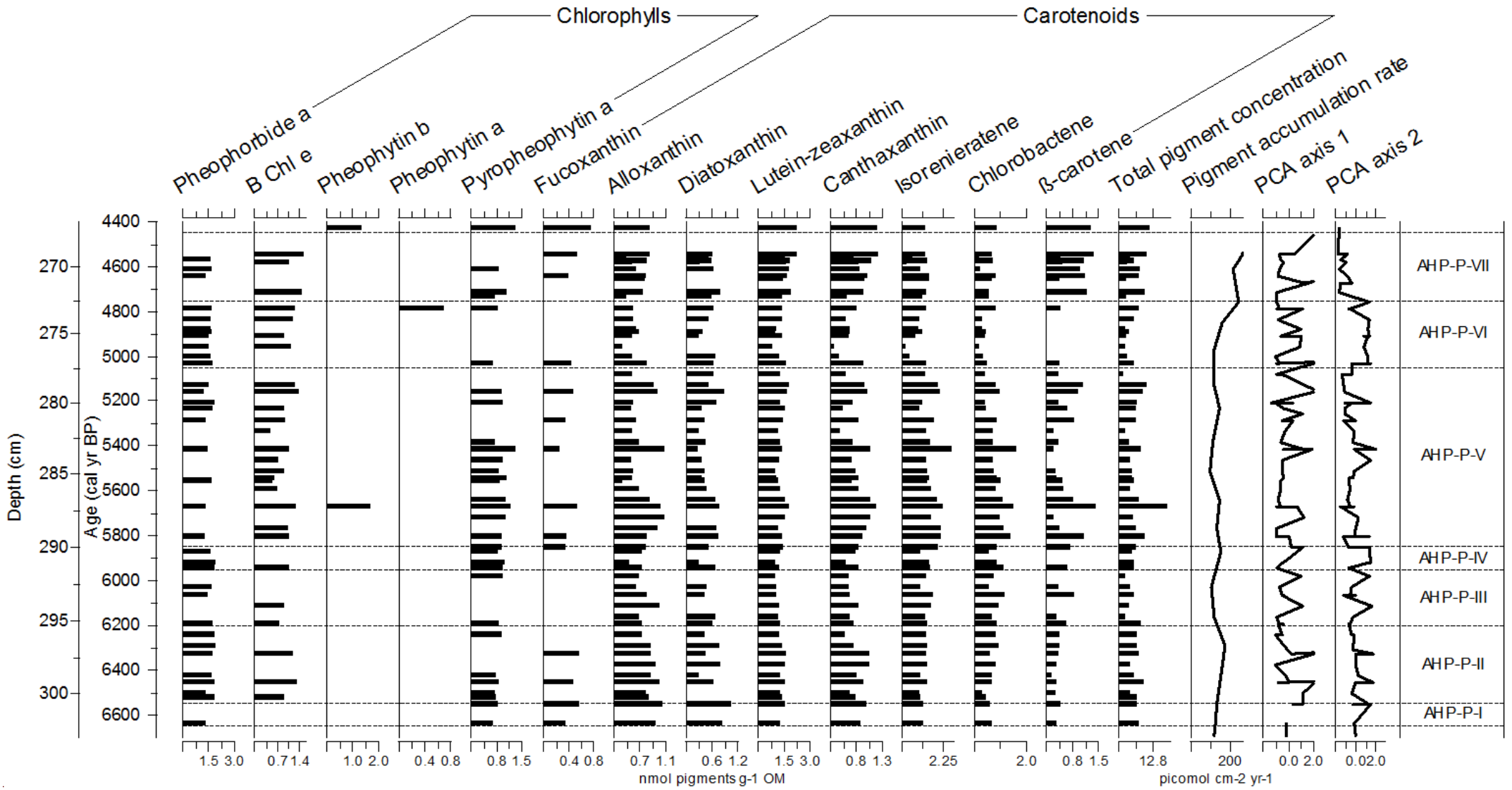

Figure 7.5 (b). Pigment concentration (nmol pigments g^{-1} OM) for the high-resolution section (302.0 – 267.0 cm) and associated metrics, arranged according to age (cal yr BP). Pigment accumulation rate is shown as picomol cm^{-2} yr^{-1}.

7.5.1 Zone AHP-P-I (302.0 – 300.75 cm, 6,650 – 6,550 cal yr BP) This zone is characterised by moderate total pigment concentrations ($\bar{x}$ = 118.4 nmol pigments g^{-1} OM) and dominance by carotenoid pigments. Isorenieratene and lutein-zeaxanthin are found in the greatest quantities (34.5 and 31.9 nmol pigments g^{-1} OM respectively) whilst other carotenoids are found in stable concentrations. Pyropheophytin *a* is also present in low concentrations ($\bar{x}$ = 4.6 nmol pigments g^{-1} OM).

7.5.2 Zone AHP-P-II (300.75 – 295.5 cm, 6,550 – 6,200 cal yr BP) This zone continues to maintain a steady total pigment concentration, though slightly higher than the underlying zone ($\bar{x}$ = 149.8 nmol pigments g^{-1} OM). Carotenoid concentrations fluctuate, with some showing slight increases towards the mid-zone (alloxanthin, diatoxanthin and canthaxanthin). β-carotene in contrast, disappears intermittently from the record, as does fucoxanthin which is not found past 297.5 cm. Pyropheophytin *a* also disappears at 298.5 cm but is present again at 296.0 cm. Pheophorbide *a* and bacteriochlorophyll *e* appear intermittently in moderate concentrations ($\bar{x}$ = 49.2 and 9.6 nmol pigments g^{-1} OM respectively). Accumulation rate is stable, averaging 129.8 pmol cm^2 yr^{-1}.

7.5.3 Zone AHP-P-III (295.5 – 291.5 cm, 6,200 – 5,950 cal yr BP) This zone sees total pigment concentration decline from 182.7 to 14.4 nmol pigments g^{-1} OM (295.0 – 292.0 cm). Carotenoid pigments continue to vary but overall concentrations are fairly stable. β-carotene and diatoxanthin are not present at 294.0 cm and fucoxanthin is absent throughout. Pheophorbide *a* and bacteriochlorophyll *e* continue to appear irregularly ($\bar{x}$ = 40.6 and 7.6 nmol pigments g^{-1} OM respectively). Pyropheophytin *a* is found at the base and top of the zone only ($\bar{x}$ = 7.4 nmol pigments g^{-1} OM).

7.5.4 Zone AHP-P-IV (291.5 – 290.25 cm, 5,950 – 5,850 cal yr BP) This is the smallest zone in the high-resolution pigment record and is characterised by slightly increased total pigment concentrations ($\bar{x}$ = 178.7 nmol pigments g^{-1} OM). β-carotene is not present in the record and diatoxanthin disappears past 291.0 cm. Pheophorbide *a* and pyropheophytin *a* are both found in moderate concentrations ($\bar{x}$ = 44.6 and 7.9 nmol pigments g^{-1} OM respectively).

7.5.5 Zone AHP-P-V (290.25 – 277.75 cm, 5,850 – 5,050 cal yr BP) This zone sees an overall decline in total pigment concentration from 453.2 to 79.4 nmol pigments g^{-1} OM (287.5 – 283.5 cm). Accumulation rate is steady, ranging between 50.1 – 127.6 pmol cm^2 yr^{-1}. Carotenoids vary considerably in concentration throughout this zone and chlorophyll degradation products continue to appear intermittently.

Sub-zone AHP-P-V-A (290.25 – 283.5 cm, 5,850 – 5,450 cal yr BP) is characterised by relatively stable total pigment concentrations ($\overline{x}$ = 182.7 nmol pigments g^{-1} OM), with the exception of a single peak reaching 453.2 nmol pigments g^{-1} OM (287.5 cm). This is reflected by the carotenoids, all of which show increases at this depth, some as a gradual rise (lutein-zeaxanthin and canthaxanthin) and other as a significant peak (chlorobactene and β-carotene). Total pigment concentration then declines to 112.3 nmol pigments g^{-1} OM (283.5 cm), which is similarly reflected by carotenoid concentrations; β-carotene reaches a minimum of 0.7 nmol pigments g^{-1} OM (283.5 cm). Fucoxanthin is irregularly present in this sub-zone. Bacteriochlorophyll *e* and pyropheophytin *a* are found in stable concentrations ($\overline{x}$ = 5.7 and 6.7 nmol pigments g^{-1} OM respectively). Pheophorbide *a* occurs frequently whilst pheophytin *b* is only present at 287.5 cm.

Sub-zone AHP-P-V-B (283.5 – 277.75 cm, 5,450 – 5,050 cal yr BP) shows greater variability in total pigment concentration, ranging from 79.4 – 419.3 nmol pigments g^{-1} OM. The carotenoids similarly demonstrate significant variability in this sub-zone. Alloxanthin, canthaxanthin, isorenieratene and chlorobactene experience a peak in concentration at 283.0 cm (11.4 – 286.2 nmol pigments g^{-1} OM). Canthaxanthin and β-carotene exhibit smaller peaks at 281.5 cm. Alloxanthin, canthaxanthin, isorenieratene, chlorobactene and β-carotene peak again between 279.0 – 278.5 cm. Diatoxanthin in contrast peaks at 279.5 cm and then temporarily disappears from the record, whilst lutein-zeaxanthin shows a gradual increase in pigment concentration throughout the sub-zone. Fucoxanthin continues to appear irregularly. Pheophorbide *a*, bacteriochlorophyll *e* and pyropheophytin *a* are present in moderate to high concentration at regular intervals ($\overline{x}$ = 43.3, 9.2 and 9.3 nmol pigments g^{-1} OM respectively).

7.5.6 Zone AHP-P-VI (277.75 – 272.75 cm, 5,050 – 4,750 cal yr BP) This zone is characterised by low total pigment concentrations at the base of the zone (70.8 nmol pigments g^{-1} OM, 277.0 cm) after which an increase occurs, reaching 158.5 nmol pigments g^{-1} OM (273.5 cm). Diatoxanthin, canthaxanthin, lutein-zeaxanthin and isorenieratene follow this same general trend. Alloxanthin in contrast peaks earlier (3.8 nmol pigments g^{-1} OM, 275.0 – 274.5 cm), before declining slightly. Chlorobactene maintains a relatively stable abundance ($\bar{x}$ = 5.9 nmol pigments g^{-1} OM) with the exception of a large peak at 273.5 cm (12.7 nmol pigments g^{-1} OM), when β-carotene is present. Pheophorbide *a* appears in moderate abundances, as does bacteriochlorophyll *e* ($\bar{x}$ = 44.6 and 13.1 nmol pigments g^{-1} OM respectively), though intermittently.

7.5.7 Zone AHP-P-VII (272.75 – 267.0 cm, 4,750 – 4,450 cal yr BP) This zone features a very low total pigment concentration at the base of the zone, after which it immediately increases (100.7 – 248.4 nmol pigments g^{-1} OM). The carotenoid pigments demonstrate this same initial peak at the base of the zone and then fluctuate in abundance; canthaxanthin ranges between 3.4 – 16.6 nmol pigments g^{-1} OM and chlorobactene between 2.2 – 13.3 nmol pigments g^{-1} OM. Highest concentrations for most carotenoids occur at the top of the zone. Fucoxanthin is present at 182.5 cm and 179.5 – 178.0 cm. Pheophorbide *a* occurs in a steady abundance towards the mid-zone ($\bar{x}$ = 42.2 nmol pigments g^{-1} OM), whilst bacteriochlorophyll *e* and pyropheophytin *a* are found sporadically. Accumulation rate increases, averaging 264.2 pmol cm^2 yr^{-1}.

7.6 Linear Ordination: Principal Components Analysis (PCA)

PCA analysis of the high-resolution pigment dataset shows that the first axis accounts for 41.3 % of variance and cumulatively with the second axis for 62.5 % (Table 7.2). The cumulative variance explained by the four axes is 85.6 %. A PCA plot of the pigment species and samples is shown in Figure 7.6. As found in the complete pigment record (Chapter 6, 6.7), axis 1 shows a clear division between sedimentary pigments derived from macrofaunal grazing and those derived directly from the breakdown of phytoplankton groups. Low PCA scores correspond to zones containing an abundance of the grazing indicator, pheophorbide *a* (zones AHP-P-IV and AHP-P-VI), whilst higher scores reflect zones containing high concentrations of

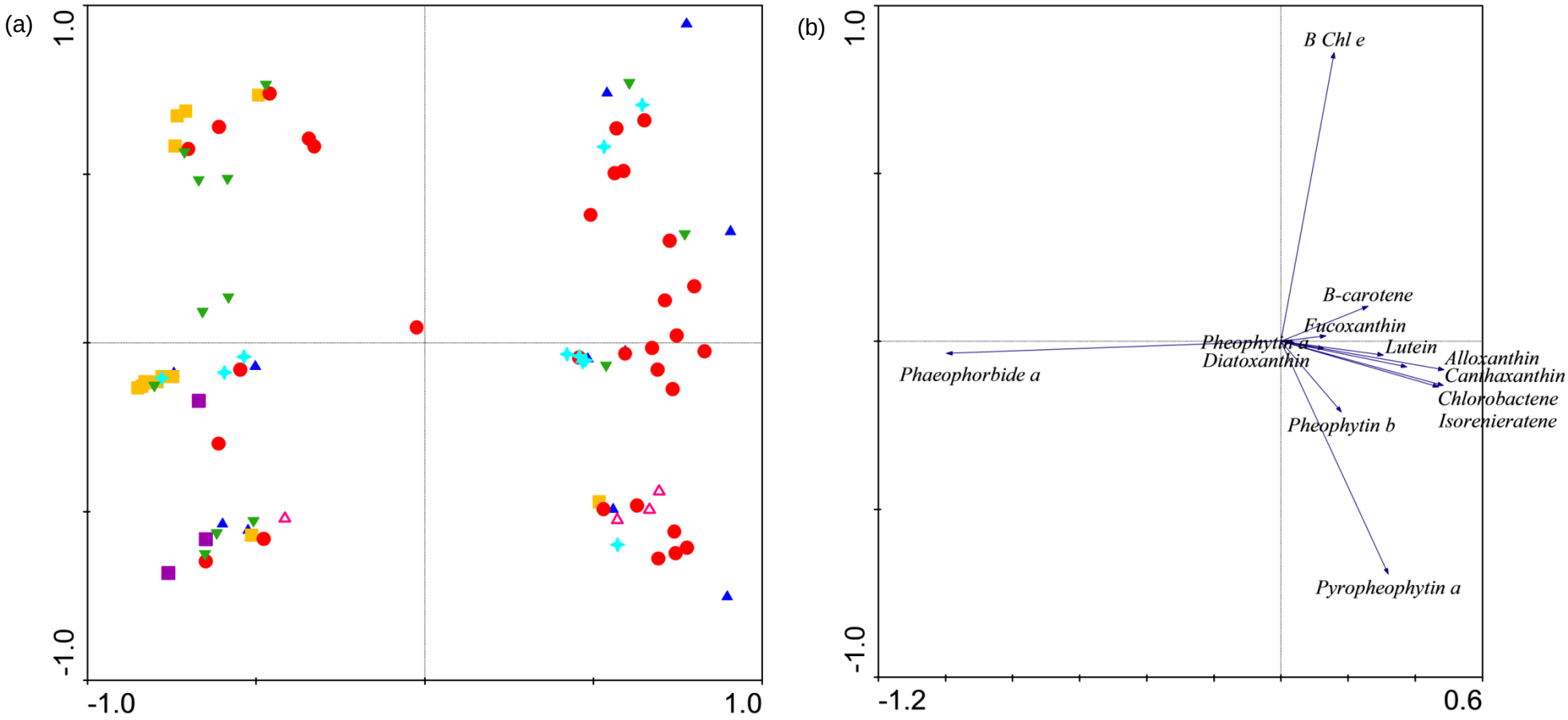

Figure 7.6. PCA results for the high-resolution sedimentary pigment dataset showing (a) samples according to zone (AHP-P-I – pink triangle, AHP-P-II – green triangle, AHP-P-III – cyan star, AHP-P-IV – purple square, AHP-P-V – red circle, AHP-P-VI – yellow square, AHP-P-VII – blue triangle), and (b) sedimentary pigments.

Table 7.2. Summary of PCA results for the high-resolution Lake Hayq pigment dataset (302.0 – 267.0 cm).

Dataset	No. of samples	No. of species	Total variance	Axis	1	2	3	4
High-resolution pigments	83	13	1	Eigen values	0.413	0.212	0.152	0.079
				Cumulative % variance of species data	41.3	62.5	77.7	85.6
Carotenoids only	83	8	1	Eigen values	0.431	0.333	0.166	0.045
				Cumulative % variance of species data	43.1	76.5	93.1	97.6

pigments derived from the degradation of cyanobacteria and other algae (alloxanthin, canthaxanthin, zone AHP-P-V). This reflects the changing size of the zooplankton population. Axis 2 separates bacteriochlorophyll *e* (zone AHP-P-VII) from pyropheophytin *a* (zone AHP-P-IV), which may reflect changes between periods of meromixis and greater mixing.

As for the complete pigment record in Chapter 6, PCA analysis was repeated to include only carotenoid pigments, as chlorophylls have been intermittently preserved. Axis 1 and 2 cumulatively account for 43.1 % and 76.5 % of variance, whilst the addition of axis 3 and 4 increase cumulative variance to 97.6 % (Table 7.2). A PCA plot of the pigment species and samples split into the major zones identified in section 7.5 is shown in Figure 7.7. Axis 1 separates fucoxanthin and diatoxanthin. High PCA scores correspond to zones containing fucoxanthin (zones AHP-P-I – II and AHP-P-V – VII), whilst low PCA scores reflect zones containing higher concentrations of diatoxanthin (AHP-P-III – IV). This most likely reflects the lability of fucoxanthin in the sediment record.

Axis 2 shows a division between zones dominated by green sulfur bacteria and more common pigments found in most plants and algae. Low PCA correspond to zones

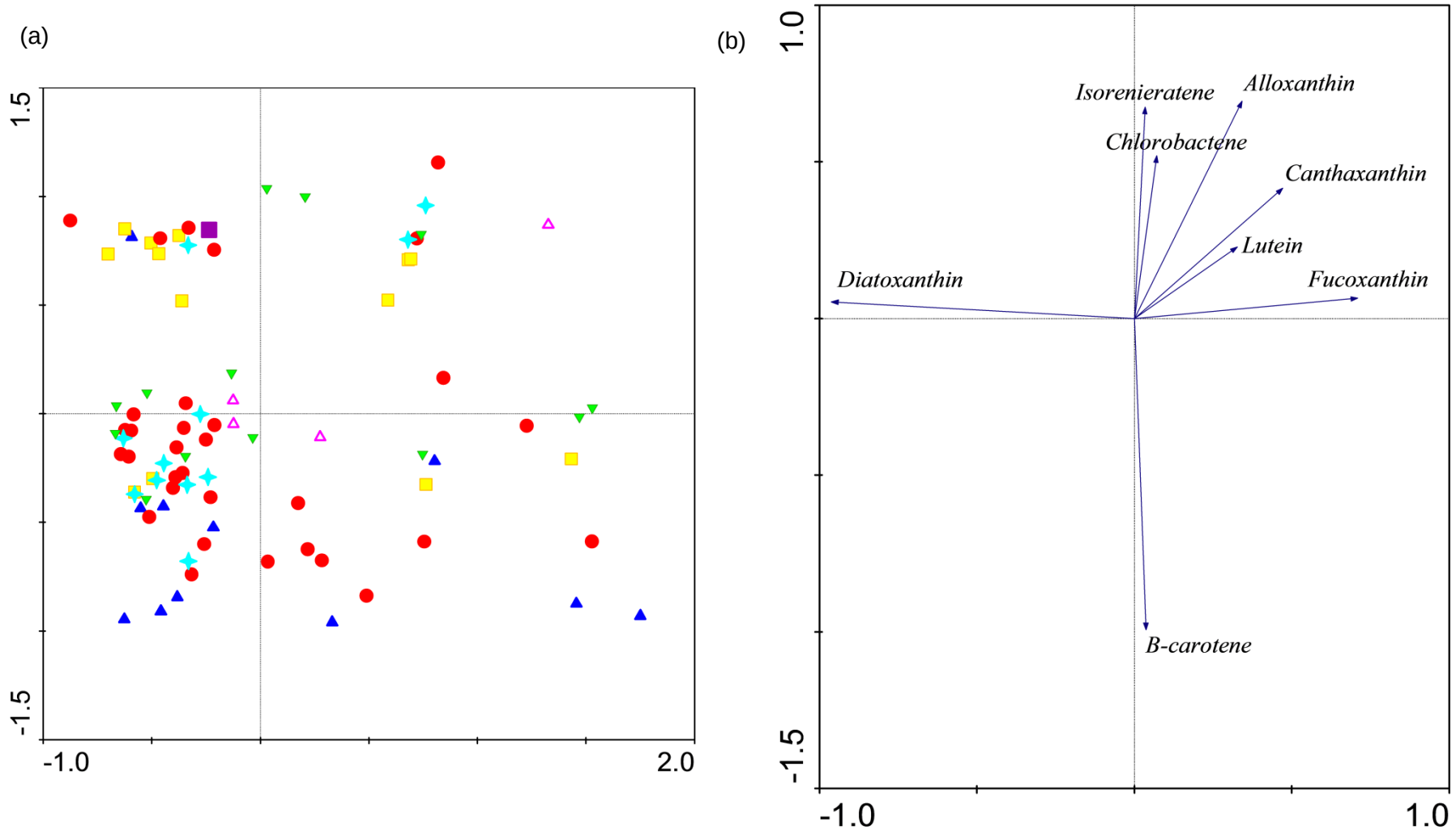

Figure 7.7. PCA results for the high-resolution carotenoid dataset only showing (a) samples according to zone (AHP-P-I – pink triangle, AHP-P-II – green triangle, AHP-P-III – cyan star, AHP-P-IV – purple square, AHP-P-V – red circle, AHP-P-VI – yellow square, AHP-P-VII – blue triangle), and (b) sedimentary pigments.

containing high concentrations of β-carotene (zones AHP-P-V and AHP-P-VII), whilst higher PCA scores are associated with zones containing the derivatives of green sulfur bacteria, isorenieratene and chlorobactene (zones AHP-P-II – III and AHP-P-V. This reflects changes in lake depth, habitat availability, mixing regime and light intensity.

7.7 Interpretation and Synthesis of the High-Resolution Palaeolimnological Record

The independent proxy records analysed from the high-resolution section of core Hayk-01-2010 are now interpreted in terms of limnetic and environmental changes that have taken place in the Lake Hayq basin between 6,650 – 4,450 cal yr BP. It is important to consider this high-resolution study in the context of the complete sediment proxy records (Chapter 6, 6.9); it has previously been interpreted as the start of a gradual shallowing phase (Hayq-VII, Hayq-VIII and Hayq-IX), eventually leading to a late-Holocene lowstand from 3,950 – 2,200 cal yr BP. Figure 7.8 provides a summary of the major shifts in the proxy records; the record is divided into six major zones based on significant shifts in the palaeoenvironmental data. The ecology of dominant taxa is discussed in detail in Chapter 6 but is used to inform interpretation here.

7.7.1 Hayq-AHP-I (302.0 – 299.0 cm, 6,650 – 6,450 cal yr BP) The diatom assemblage of this zone indicates that Lake Hayq was relatively deep, fresh and turbulent (evidenced by diatom-inferred conductivity [Table 6.4]), given the dominance of the planktonic *Aulacoseira granulata* var. *angustissima* and, to a lesser extent, *Ulnaria delicatissima*. Lake depth, as well as area and volume, may have been similar to the lakes' current state; in the most recent 100 cal yr BP, Lake Hayq has been dominated by *Aulacoseira* taxa of equal measure to this mid-Holocene period, and maximum lake level varied between 81.0 – 88.8 m (1939 – 2000). Potentially lake depth at this time, having declined from a possible highstand of ~ 120 m during the early Holocene, may have been between a maximum depth of ~ 80 – 90 m, with a surface area of > ~ 23 km². Lake Hayq was most likely hydrologically closed at this time but may have still received some overflow from Lake Hardibo.

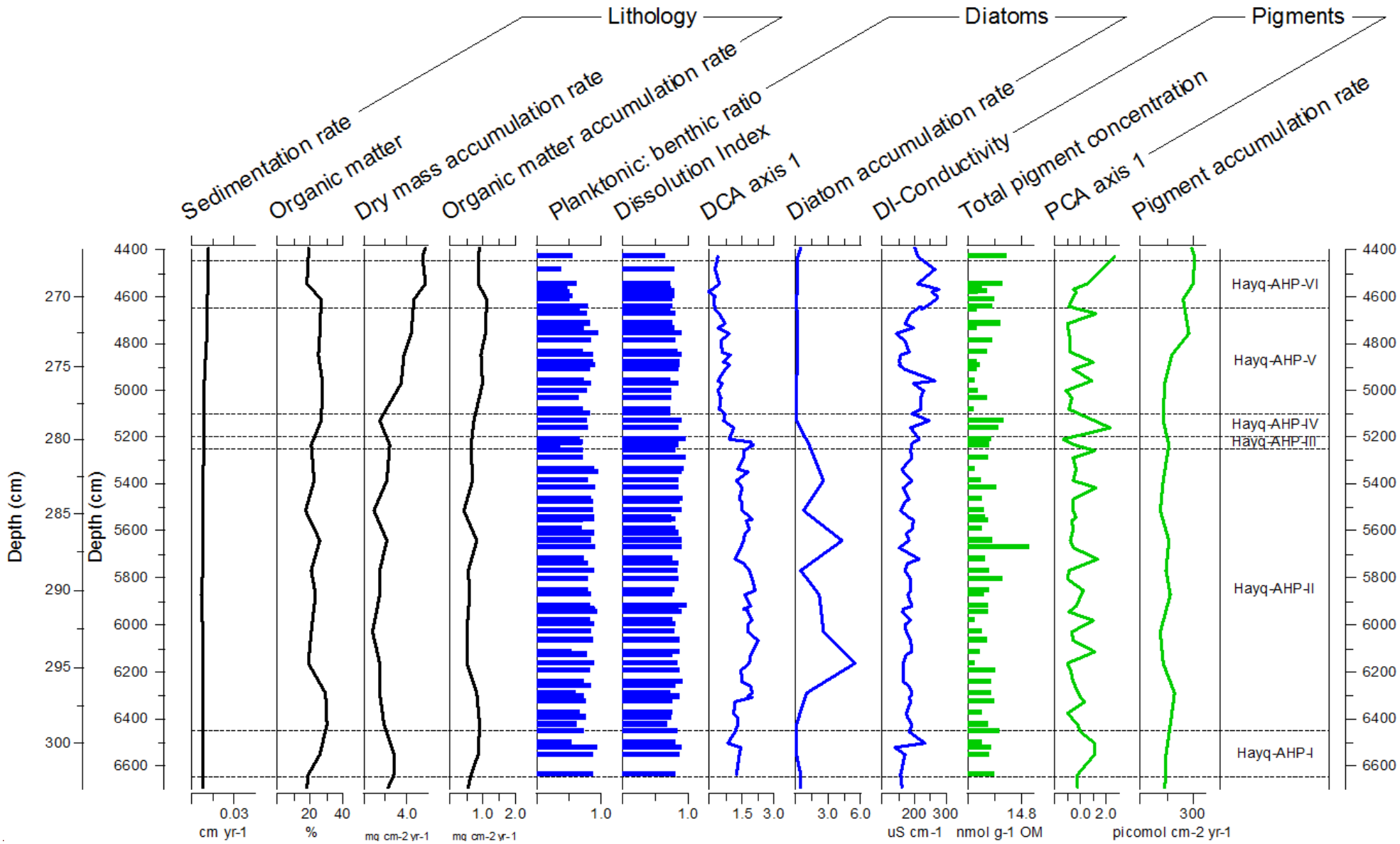

Figure 7.8. Summary diatom and pigment diagram showing major compositional changes in the high-resolution section (302.0 –

267.0 cm) of Hayk-01-2010. Sedimentation accumulation rate is expressed as cm yr^{-1}, organic matter content as a percentage of the total wet weight of the sediment, and dry mass and organic matter accumulation rates as mg cm^{-2} yr^{-1}. Diatom accumulation rate is expressed as million valves cm^{-2} yr^{-1} and diatom-inferred (DI) conductivity as µS cm^{-1}. Pigment concentration is shown as nmol pigments g^{-1} OM and accumulation rate as picomol cm^{-2} yr^{-1}. PCA scores refer to carotenoid pigments only.

Ulnaria ulna var. *ulna* is also present in this zone, signalling a high Si: P ratio, as well as submerged macrophytes (also indicated by the minor presence of *Gomphonema parvulum*) in the littoral zone and marsh, swamp-like area left around the shoreline as the water level recedes (Kilham et al. 1986; Gasse 1987).

The presence of green sulfur bacteria confirms meromictic conditions in the lake. Cryptophytes, dinoflagellates (an additional indicator of stratified conditions), green algae, euglenophytes and colonial cyanobacteria are also present, as well as a steady zooplankton population (Hurley and Armstrong 1990). Pigment accumulation rate indicates this was a relatively productive period, most likely a mesotrophic-eutrophic state, and preservation was very good. The geochemical data at this time does not indicate any significant change in climate, although a decline in lithogenic silica is evident.

7.7.2 Hayq-AHP-II (299.0 – 280.6 cm, 6,450 – 5,250 cal yr BP) Evidence of decadal to centennial changes in lake level are found in the zone, given the abrupt shifts in the diatom assemblage. *Aulacoseira granulata* var. *angustissima* fluctuates regularly throughout this zone, alternating dominance with *Fragilaria radians*. Both taxa have high Si: P requirements so it is unlikely that major changes in nutrient availability caused the large swings in abundance (further evidenced by the near continuous presence of *Ulnaria ulna* var. *ulna* also). As previously discussed, Gasse (1986) identifies *Fragilaria radians* as an important component of the bottom mud in small, shallow lakes (though it is generally considered to be a facultatively planktonic species, rather than benthic). As such, its sudden increase in abundance at the start of the zone and frequent dominance, alongside declines in *Aulacoseira granulata* var. *angustissima*, are likely an indication of a decrease in water level (including associated changes in turbidity and light availability in the water column) and a greater availability of shallow water habitats in the benthic areas in response to greater aridity. This is further evidenced by spikes in diatom-inferred conductivity which occurs simultaneously with peaks in *Fragilaria radians*. However, these spikes are minor in comparison to the complete diatom-inferred conductivity record, varying by < 100 µS cm^{-1}, and the lake never becomes subsaline (Table 6.4). Increases in *Ulnaria delicatissima* towards the top of the zone may similarly indicate intensifying aridity, as despite being generally considered planktonic, it too is known to occur on

the bottom mud of shallow lakes (Gasse 1986). As the climate became wetter again and lake level rises, *Aulacoseira granulata* var. *angustissima* resumes dominance and *Fragilaria radians* declines. The frequency at which the taxa dominate is irregular; *Aulacoseira granulata* var. *angustissima* peaks every ~ 80 – 270 years (1.3 – 4.0 cm), whilst *Fragilaria radians* dominates every ~ 50 – 320 years (0.7 – 5.0 cm). The alternations between the two occur at ~ 40 – 180 year intervals. If Lake Hardibo had assumedly been experiencing the same changes in climate, given its proximity to Lake Hayq, the variability in overflow Lake Hayq had been receiving would have most likely amplified the changes in lake level. Given the recent changes in water level at Lake Hayq documented during the 20th century, it is possible that lake depth may have fluctuated by ~ 7 m or more during this time.

Despite these periodic declines in water level, the continued presence of green sulfur bacteria indicates that Lake Hayq was still meromictic. Therefore lake depth never declined to such an extent that the waterbody was completely mixed. The surrounding topography and bathymetry of the lake may have also reduced wind fetch; the gradual decline in lake level since the early to mid-Holocene may have exposed the steep shelving margins of the lake creating protection against wind exposure. Chrysophytes, cryptophytes, dinoflagellates, as well as zooplankton populations are still present throughout this zone, generally increasing in concentration during periods of higher water level. The abundance of colonial cyanobacteria, which are often found amongst the benthic algae of lakes, provides further support for episodes of lake level decline, and its presence may account for periodic occurrences of the obligate nitrogen heterotroph *Nitzschia subcommunis (*Kalff 2003). Total pigment and diatom concentration and accumulation rates both peak between ~ 5,780 – 5,700 cal yr BP (288.8 – 287.5 cm) indicating optimal conditions for productivity in the lake during this period. Following this peak, diatom concentration remains consistently low throughout the remainder of the high-resolution sediment record.

The changing climate is evidenced further by the geochemical data, which indicates a shift towards aridity at ~ 5.8 cal kyr BP (~ 289.0 cm). The incoherent: coherent backscatter intensity ratio and biogenic silica both decline from the bottom to the top of the zone, signalling lower productivity (supported by the steeply declining diatom

accumulation rate; Fig. 6.19) and preservation at the lake, associated with drying conditions. Increased mechanical weathering towards the top of the zone similarly indicates aridity, as does increasing concentrations of calcium (as enhanced evaporitic conditions allow for enhanced preservation), potassium (eroded from exposed rock formations with sparse vegetation cover) and titanium (indicating enhanced erosion and transportation of silt and fine sand) (Burnett et al. 2011; Brown 2012; Foerster et al. 2012).

7.7.3 Hayq-AHP-III (280.6 – 280.13 cm, 5,250 – 5,200 cal yr BP) This zone is characterised by a peak in *Fragilaria radians*, alongside a decline in *Aulacoseira granulata* var. *angustissima*, which indicates a fall in lake level and therefore arid conditions. Diatom-inferred conductivity exhibits a slight increase in this zone, but the lake remained fresh. Aridity is further indicated by reduced concentrations of cryptophytes, dinoflagellates, colonial cyanobacteria as well as green sulfur bacteria. This suggests that meromictic conditions may have temporarily been disturbed or weakened, potentially a result of declining lake level which made the water column more susceptible to mixing by wind, although complete overturn did not occur.

7.7.4 Hayq-AHP-IV (280.13 – 278.5 cm, 5,200 – 5,100 cal yr BP) The abrupt decline of *Fragilaria radians*, synchronous with the increase of *Ulnaria delicatissima* in this zone, indicates a second phase of lake level decline and heightened aridity at Lake Hayq. Although associated with planktonic taxa, in Figure 7.4 (b), *Ulnaria delicatissima* has a slightly lower DCA axis 1 score than *Fragilaria radians*, which may indicate that it is found in marginally shallower waters. As such, its occurrence in the diatom record is interpreted as another, more substantial fall in lake level, amplified by the steep shelving nature of the lake, and an increase in the availability of benthic habitat. This is evidenced further by the temporary disappearance of *Aulacoseira granulata* var. *angustissima* from the sediment record, as well as increasing abundances of *Gomphonema parvulum* and *Gomphonema pumilum*. The taxa present indicate that Lake Hayq remained alkaline (pH of 7.4 – 7.8 [Gasse 1986]) and, along with diatom-inferred conductivity, fresh.

Despite a decline in lake depth, total pigment concentration increases in this zone (pigment accumulation rate remains stable), as phytoplankton such as green algae

and colonial cyanobacteria favour benthic habitats. A rise in green sulfur bacteria suggests that meromictic conditions reestablished and/or intensified, potentially a result of a decrease in wind-driven mixing allowing the water to become stratified again (which would further support the decrease of *Aulacoseira granulata* var. *angustissima*). Based on the phytoplankton present, the lake was most likely still in a mesotrophic-eutrophic condition.

Geochemical data in this zone supports a further shift towards aridity; a minor decrease in the incoherent: coherent backscatter intensity ratio and an increase in calcium concentration signals increasingly dry, evaporitic conditions at the core site (Burnett et al. 2011).

7.7.5 Hayq-AHP-V (278.5 – 270.9 cm, 5,100 – 4,650 cal yr BP) The start of a significant period of declining water level and surface area at Lake Hayq, driven by increasing aridity, occurs in this zone. The increase in the periphytic *Gomphonema parvulum* and *Gomphonema pumilum* at the start of the zone indicates increasing availability of shallow water habitats and submerged macrophytes (Cocquyt 1998; Barker et al. 2003). Most likely as the lake level declined, shallow, swamp-marsh areas became established on the steep lake shelves as they became exposed. Overflow from Lake Hardibo most likely ceased at this time, increasing water residence time at the lake as it remained hydrologically closed.

Green sulfur bacteria also decline, indicating the breakdown of meromixis driven by the shallowing conditions, which would have resulted in mixing throughout the water column and possibly some sediment disturbance (Parkin and Brock 1980; Chen et al. 2001). Light conditions would have also declined in the water column as a consequence, leading to lower diatom accumulation. These conditions (along with declining lake level), may have further contributed to the decline of *Aulacoseira granulata* var. *angustissima* at this time, as well as providing a greater diversity of benthic habitats in the lake margins, triggering an increase in species diversity. The collective diatom assemblage indicates Lake Hayq was still fresh (also indicated by diatom-inferred conductivity) and had a low to medium alkalinity (pH 7.2 – 7.8) (Gasse 1986). Total pigment concentration and diatom accumulation rate indicates that productivity declined at this time. Most green and blue algae and plants as well

as cryptophytes and euglenophytes saw declining concentrations as a result of shallowing habitats, as well as reduced nutrient availability.

However, shallowing was not a continual process and was temporarily interrupted between ~ 4,900 – 4,750 cal yr BP (275.25 – 272.25 cm), most likely due to a short-lived wet period. The abundance of *Aulacoseira granulata* var. *angustissima* increases during this period, indicating a rise in lake level, whilst the abundance of *Gomphonema* taxa and species diversity decline, signalling a reduction the availability of benthic substrates. Diatom-inferred conductivity also declines slightly during this time as a result of lake deepening. Zooplankton populations were rejuvenated during this period in response to lake deepening, which would have increased lake area and therefore created a greater diversity of both littoral and pelagic habitats (Kalff 2003).

Shallowing resumed after ~ 4,750 cal yr BP, evidenced by increases in the abundance of *Gomphonema parvulum* and *Gomphonema pumilum*, synchronous with the decline of *Aulacoseira granulata* var. *angustissima*, as well as increased species diversity and diatom-inferred conductivity. Many photosynthetic pigments, as well as total pigment concentration, increase at this time despite the shallow conditions. The availability of benthic habitats would have favoured colonies of green algae and cyanobacteria.

The geochemical data generally agree with the diatom and pigment record. The greatest shift towards aridity occurred at ~ 5.0 cal kyr BP (~277.0 cm), indicated by increased concentrations of potassium, calcium, titanium as well as mechanical weathering at the core sight. After this peak in aridity, elemental profiles return to values similar to those of Hayq-AHP-IV, Hayq-AHP-III and the top of Hayq-AHP-II, rather than signalling a direct shift to wetter conditions. Aridity increases again towards the top of the zone (~ 271.5 cm, ~ 4.7 cal kyr BP).

7.7.6 Hayq-AHP-VI (270.9 – 267.0 cm, 4,650 – 4,450 cal yr BP) The diatom assemblage in this zone indicates another significant decline in lake level as *Gomphonema parvulum* and *Gomphonema pumilum* see considerable increases in abundance and *Aulacoseira granulata* var. *angustissima* experiences a rapid decline

and begins to disappear from the sediment record. Lake Hayq would have been approaching its (potential) Holocene lowstand depth of ~ 30 m or less at this time, as the decline in water depth revealed a shallow, less steeply shelving morphometry, with a surface area of < ~ 16 km² (Demlie et al. 2007). Aerophilous taxa were also observed in this zone, suggesting that parts of the basin were being exposed and sediment re-worked. Diatom-inferred conductivity increases slightly, reaching maximum values for this high-resolution time period (though Lake Hayq remained fresh), as does species diversity, suggesting a greater availability and range of benthic habitats. Photosynthetic pigment concentrations do not show a significant shift at this time, although accumulation rate increases slightly.

The geochemical data indicates gradually increasing aridity (rather than an abrupt shift), evidenced by a low incoherent: coherent backscatter intensity ratio (suggesting poor productivity and preservation), as well as increasing concentrations of potassium, silicon and titanium (Burnett et al. 2011; Brown 2012; Foerster et al. 2012). The calcium profile does indicate a peak in aridity centred at ~ 270.0 cm, suggesting enhanced evaporitic conditions (Burnett et al. 2011).

7.8 Summary of the High-Resolution Palaeolimnological Record

The interpretations of the limnetic and environmental changes inferred from the available date are summarised below.

Hayq-AHP-I (302.0 – 299.0 cm, 6,650 – 6,450 cal yr BP)

- A deep (~ 80 – 90 m, > ~ 23 km² surface area), fresh, alkaline lake.
- Hydrologically closed but connected to Lake Hardibo by overflow.
- Meromictic conditions allowing for green sulfur bacteria to dominate in the anoxic bottom waters.
- Presence of cryptophytes, dinoflagellates, colonial cyanobacteria and zooplankton indicate mesotrophic-eutrophic conditions.

Hayq-AHP-II (299.0 – 280.6 cm, 6,450 – 5,250 cal yr BP)

- Beginning of climate instability, causing fluctuations in lake depth.
- Diverse phytoplankton assemblage.

- Peak diatom and pigment concentrations (5,772 – 5,690 cal yr BP) followed by decline.
- Peaks in diatom-inferred conductivity but still a fresh water lake.
- Shift towards aridity at ~ 5.8 cal kyr BP.

Hayq-AHP-III (280.6 – 280.13 cm, 5,250 – 5,200 cal yr BP)

- Reduced lake level in response to aridity, amplified by lake morphometry.
- Reduced phytoplankton.
- Weakened meromixis.

Hayq-AHP-IV (280.13 – 278.5 cm, 5,200 – 5,100 cal yr BP)

- Further decline in lake level due to arid conditions and lake morphometry.
- Still a fresh, alkaline lake.
- Meromictic conditions reestablished.

Hayq-AHP-V (278.5 – 270.9 cm, 5,100 – 4,650 cal yr BP)

- Significant period of lake level decline, interrupted briefly from ~ 4,900 – 4,750 cal yr BP by a wet period.
- Hydrologically closed but no longer receiving overflow from Lake Hardibo.
- Less turbulent, intensive light conditions in water column and reduced nutrient availability.
- Increased availability of benthic habitats, causing increased diatom species diversity.
- Declining phytoplankton productivity.

Hayq-AHP-VI (270.9 – 267.0 cm, 4,650 – 4,450 cal yr BP)

- Further decline in lake level, marking the start of Lake Hayq's Holocene lowstand (3,950 – 2,200 cal yr BP).
- Lake depth potentially approaching ~ 30 m, with a surface area of < ~ 16 km^2.

Chapter 8
Discussion.

8.1 Introduction

In this discussion, the palaeolimnological results presented in Chapters 6 and 7 are synthesised and considered with reference to the research aim, questions and hypotheses outlined in Chapter 1. The results are examined in the context of other Ethiopian, East African and intertropical African palaeoclimatic and palaeoenvironmental records from the late Pleistocene and Holocene.

8.2 Late Quaternary Palaeolimnology and Environmental Change at Lake Hayq

8.2.1 The Late Pleistocene

The palaeolimnological record strongly suggests that Lake Hayq was experiencing a lowstand in response to extremely arid conditions, which began prior to ~ 15.6 cal kyr BP. The stiff, compacted sediment, low water content, minimum sedimentation rate and poor diatom preservation at the base of Hayk-01-2010 implies a very low water level at the core site that was, at times, exposed, given the presence of aerophilous diatoms. The sporadic occurrence of other benthic and planktonic diatom taxa and phytoplankton indicate alternating periods of longer, dry, saline conditions and short flood events, which may have reworked the sediments at the core site between ~ 15.6 – 15.1 cal kyr BP (Fig. 8.1).

As the preceding conditions of this arid event at Lake Hayq are unknown, it cannot be confirmed what the trajectory of change may have been and as such, hypothesis 1 cannot be accepted with certainty. However, lowstand events in other East African lakes, as well as the desiccation of the River Nile, around this time period have been linked to Heinrich Event 1 (see Chapter 3, 3.4.1). In Ethiopia, Lake Tana dried out some time after 18.7 kyr BP and remained closed until 15.7 kyr BP when a *Cyperus* swamp, fed by seasonal inflows, developed at the centre of the lake basin (Marshall 2006; Fig. 7.2 and 7.3). Lamb et al. (2007a) used a simple hydrological model to reconstruct the rainfall necessary to form the shallow water sediments found at the base of the central deep water core, 03TL3, at Lake Tana; rainfall was at the most, just 40 % of modern precipitation values. Lake Ashenge may also have been

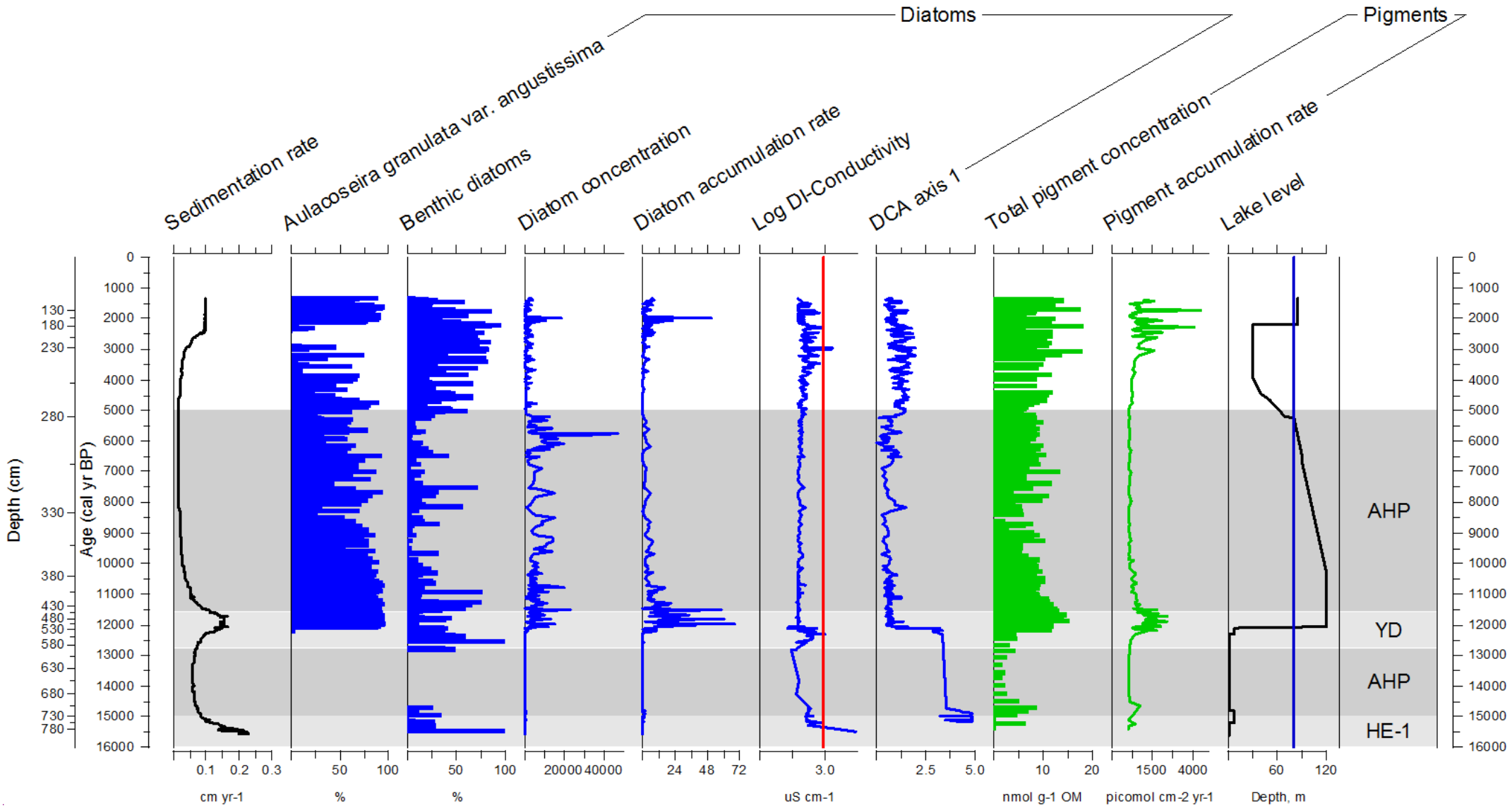

Figure 8.1. Summary diagram of stratigraphic data from Lake Hayq. Sediment accumulation rate is expressed as cm yr^{-1}. Diatom data are shown as a percentage (%), concentration as x 10^5 g^{-1}, accumulation rate as x 10^6 valves cm^{-2} yr^{-1} and log diatom-inferred

(DI) conductivity as μS cm^{-1}. Conductivity recorded in 1969 (920 μS cm^{-1}) is indicated by the red line (Baxter and Golobitsh 1970). Total pigment concentration is shown as nmol pigments g^{-1} OM and accumulation rate as picomol cm^2 yr^{-1}. A simple lake level curve, representing maximum depth, is shown based on the collective interpretation of the available proxies. Maximum lake level in 2000 (81.0 m; Lamb et al. 2007b) is indicated by the blue line. Key time periods identified in Chapter 3 are indicated: HE-1 – Heinrich Event 1, AHP – African Humid Period and YD – Younger Dryas.

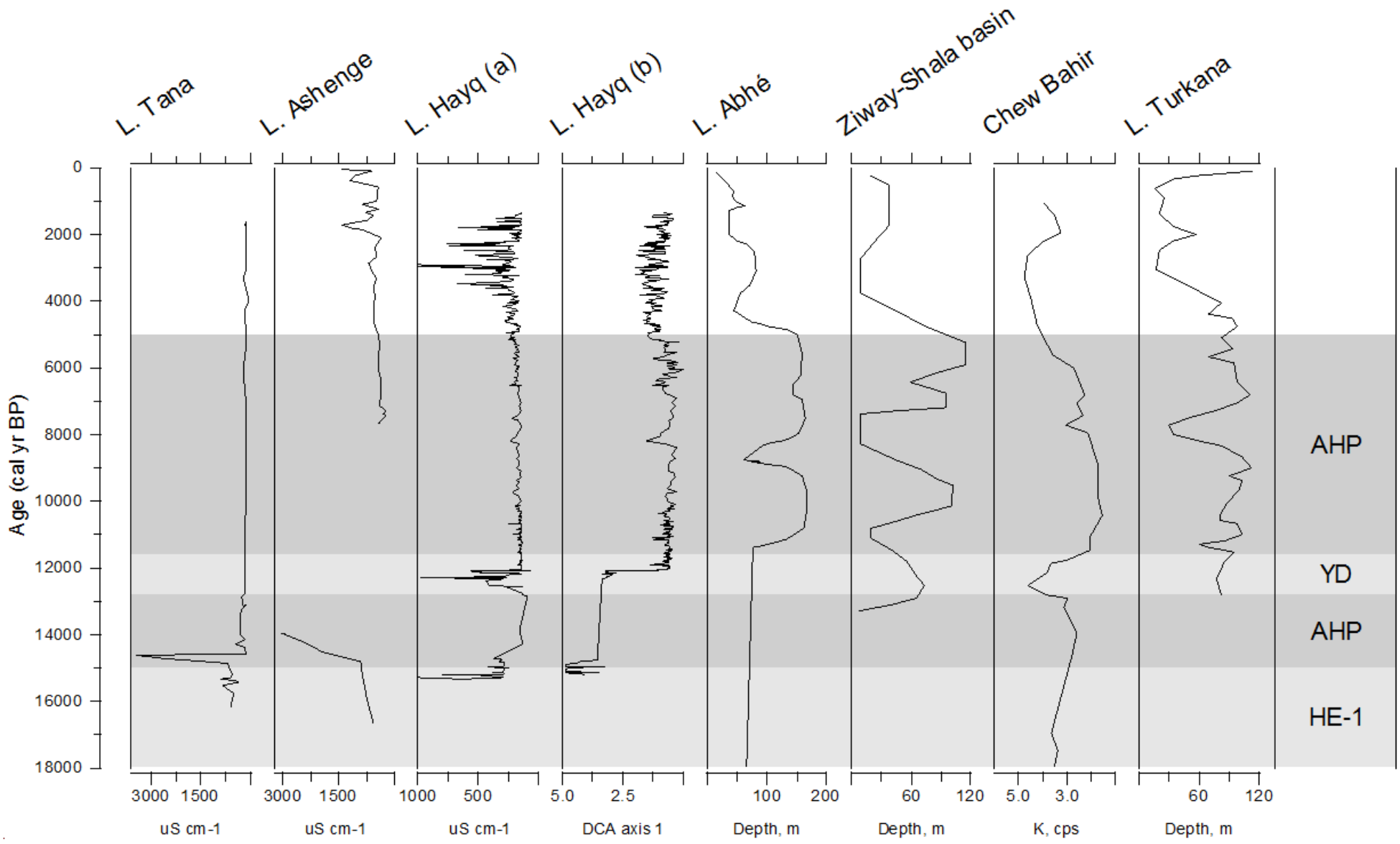

Figure 8.2. Comparison of the onset and termination of Ethiopian lake levels arranged in an *approximate* north to south order (see

Figure 3.1 [b] for location map). Lakes Tana (Marshall 2006), Ashenge (Marshall et al. 2009) and Hayq (a) are shown as diatom-inferred conductivity (µS cm^{-1}). Lake Hayq (b) is shown as DCA axis 1. Lakes Abhé (Gasse and Street 1978), the Ziway-Shala basin (Gillespie et al. 1983) and Turkana (Johnson 1996) are shown as lake level (m) and Chew Bahir (Foerster et al. 2012) as potassium (K, cps) content. Key time periods identified in Chapter 3 are indicated: HE-1 – Heinrich Event 1, AHP – African Humid Period and YD – Younger Dryas. The axes for Lakes Tana, Ashenge, Hayq and Chew Bahir have been reversed to show the comparative shallow (dry) to deep (wet) lake trend from left to right.

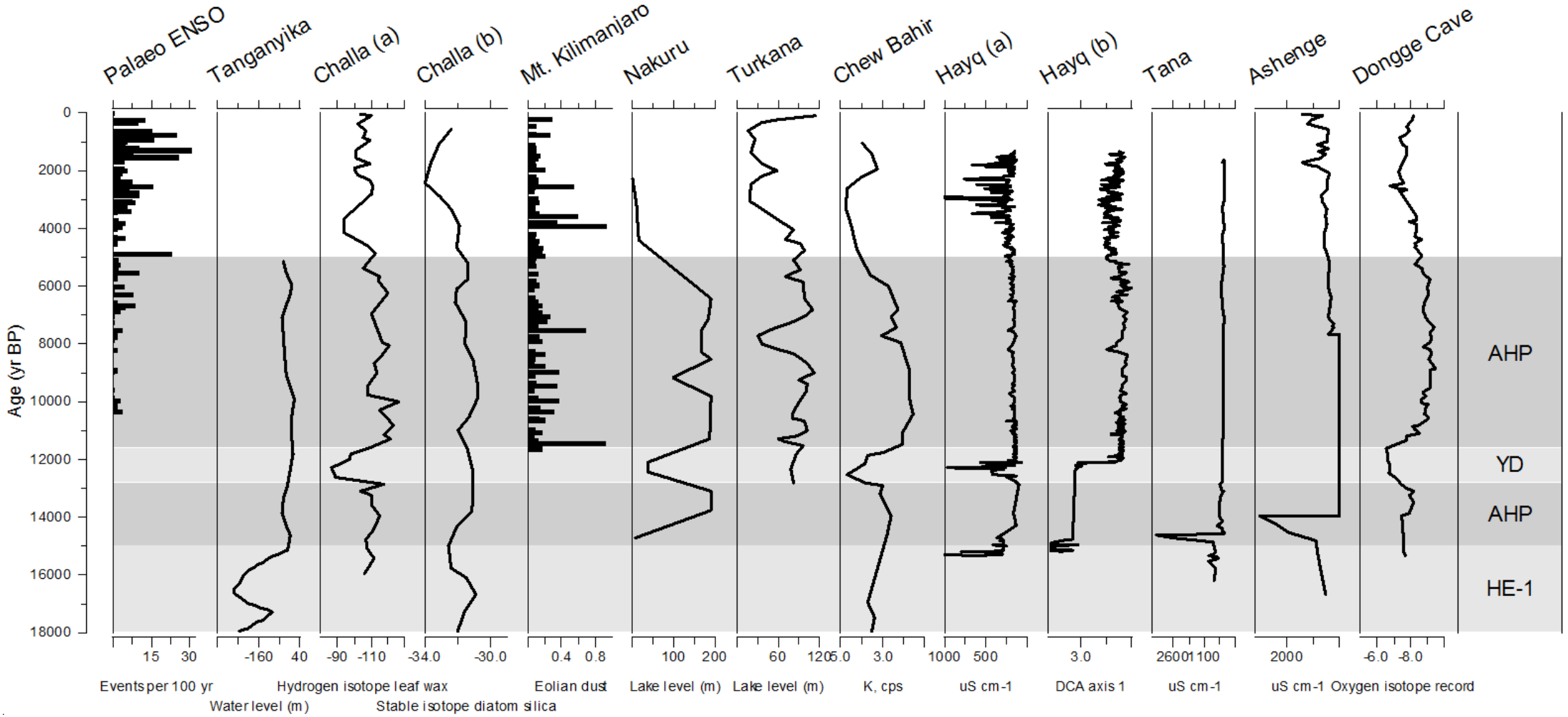

Figure 8.3. Comparison of the onset and termination of East African lake levels and other palaeo-records, arranged in an *approximate* south to north order (see Figure 3.1 [a] and [b] for location map). The paleo-ENSO record from Laguna Pallcacocha, southern Ecuador, is shown as events per century (Moy et al. 2002). Lakes Tanganyika (*approximate* height above present lake level; Gasse et al. 1989), Nakuru (Richardson and Dussinger 1986) and Turkana (Johnson et al. 1991; Brown and Fuller 2008) are

shown as lake level (m). Lake Challa is shown as (a) δ*D* leaf wax (Tierney et al. 2011) and (b) as a 10 sample running mean of stable carbon isotope composition of organic carbon contained within diatom silica ($\delta^{13}C_{diatom}$) (Barker et al. 2013). Mt. Kilimanjaro is shown as the eolian dust record (NIF3 dust 10^5; Thompson et al. 2002) and Chew Bahir as potassium (K, cps) content (Foerster et al. 2012). Lakes Hayq (a), Tana (Marshall 2006) and Ashenge (Marshall et al. 2009) are shown as diatom-inferred conductivity (µS cm^{-1}). Lake Hayq (b) is shown as DCA axis 1. The Dongge cave record, China, is shown as oxygen-isotope values (Dykoski et al. 2005). Key time periods identified in Chapter 3 are indicated: HE-1 – Heinrich Event 1, AHP – African Humid Period and YD – Younger Dryas. Note the reversed axes for Lakes Challa, Chew Bahir, Hayq, Tana, Ashenge and the Dongge Cave record to show the shallow/dry to deep/wet trend between sites from left to right.

exposed between 17.2 – 16.2 kyr BP, evidenced by a relatively slow accumulation rate, compacted sediments and presence of aerophilous and other lake marginal diatom taxa (Marshall et al. 2009). Both of these arid episodes occurred synchronous with the timing of Heinrich Event 1.

The cooling in the North Atlantic as a result of ice-rafting during Heinrich Event 1 would have caused meridional repositioning of the Intertropical Convergence Zone (ITCZ) southward, by up to 10 latitudinal degrees. However, given the far reaching nature of Heinrich Event 1, Stager et al. (2011) argue that the mega-drought conditions were not caused by displacement of the ITCZ alone. Whilst the northern tropics would have undoubtedly received less rainfall due to a more southerly position of the ITCZ, the equatorial regions should have continued to receive rainfall once or twice annually. Drying has been documented at Lake Challa, where $\delta^{13}C_{diatom}$ values (average of – 31.3 ‰ from 25.0 – 15.8 kyr BP) indicated a low precipitation-evaporation balance (P/E), causing soils to become desiccated and reduce biogenic carbon transport to the lake (Fig. 8.3; Barker et al. 2013). Extreme aridity is also found in records from Lake Bosumtwi, Ghana (Peck et al. 2004), the Niger-Sanaga and Congo watersheds (Weijers et al. 2007; Weldeab et al. 2007), as well as in oxygen isotope records from stalagmites in northern Borneo (Partin et al. 2007), a feat that would have only occurred with an extreme, and unlikely, shift of the ITCZ southwards by twenty or more latitudinal degrees (Stager et al. 2011).

Instead it is more likely that in addition to the southwards displacement of the ITCZ, there was a reduction in convection and/or moisture content of the regional rainfall systems. This would have resulted in the droughts observed with or without the shift in position. Denton et al. (2010) suggest weakening of the tropical Hadley cell's southern limb during Heinrich Event 1 as a possible cause of drought across equatorial and Southern Africa. Lower sea surface temperatures (SST) in the south-east Atlantic, along the West African coast, may have also reduced tropical rainfall by reducing the evaporative moisture content of the ITCZ, causing the summer monsoons to fail (Mulitza et al. 2008). Stronger upwelling from the Southern Ocean may have cooled the western margins of the Indian Ocean, deflecting cool, eastward flowing water towards the equator, resulting in aridity across East Africa (Stager et al. 2011). SST may have been cooled further in the northern Indian Ocean by winter

monsoon winds moving southward over land masses that were being cooled by conditions in the Mediterranean and North Atlantic (Denton et al. 2010; Stager et al. 2011).

Whatever the cause, the combined effect of Heinrich Event 1 synchronous with a systemic weakening of the Afro-Asian rainfall systems would have resulted in the intense and widely distributed drought conditions observed across East Africa and is most likely the cause for the aridity observed at Lake Hayq between ~ 15.6 – 15.2 cal kyr BP. However, it should be noted that the occurrence of an 'extreme and widespread' mega-drought at this time, as suggested by Stager et al. (2011), is debated. There is doubt as to whether data sets have been appropriately interpreted and synthesized in an attempt to follow the current 'fashion' of using extreme climate events to explain the drivers of ancestral human behaviour and Paleolithic cultures in Africa (Thomas et al. 2012).

8.2.2 The African Humid Period

An abrupt (~ 100 years) shift towards wetter, more humid conditions is documented at Lake Hayq from ~ 15.2 – 15.1 cal kyr BP, evidenced by lithological changes and the geochemical data record. This shift resulted in an increase in water depth at the core site, and a lake began to develop between ~ 15.1 – 14.8 cal kyr BP, dominated by pioneer diatom taxa associated with lake colonisation.

This transition coincides with the timing of rapid refilling at other tropical lake sites across Ethiopia and East Africa caused by the first phase of monsoon reactivation associated with the onset of the African Humid Period at ~ 15.0 kyr BP. The rejuvenation of the African-Indian monsoonal circulation has been attributed to an increase in Northern Hemisphere summer insolation based on general circulation modelling (Prell and Kutzbach 1987; Adkins et al. 2006). However, given the evidence for an orbitally-forced African Humid Period, the spatial and temporal pattern for the onset and intensity of the wetter, warmer conditions is debated, as the event appear to be synchronous and abrupt at some sites and asynchronous and gradual at others (Fig 8.4) (Costa et al. 2014). Climate models are likewise

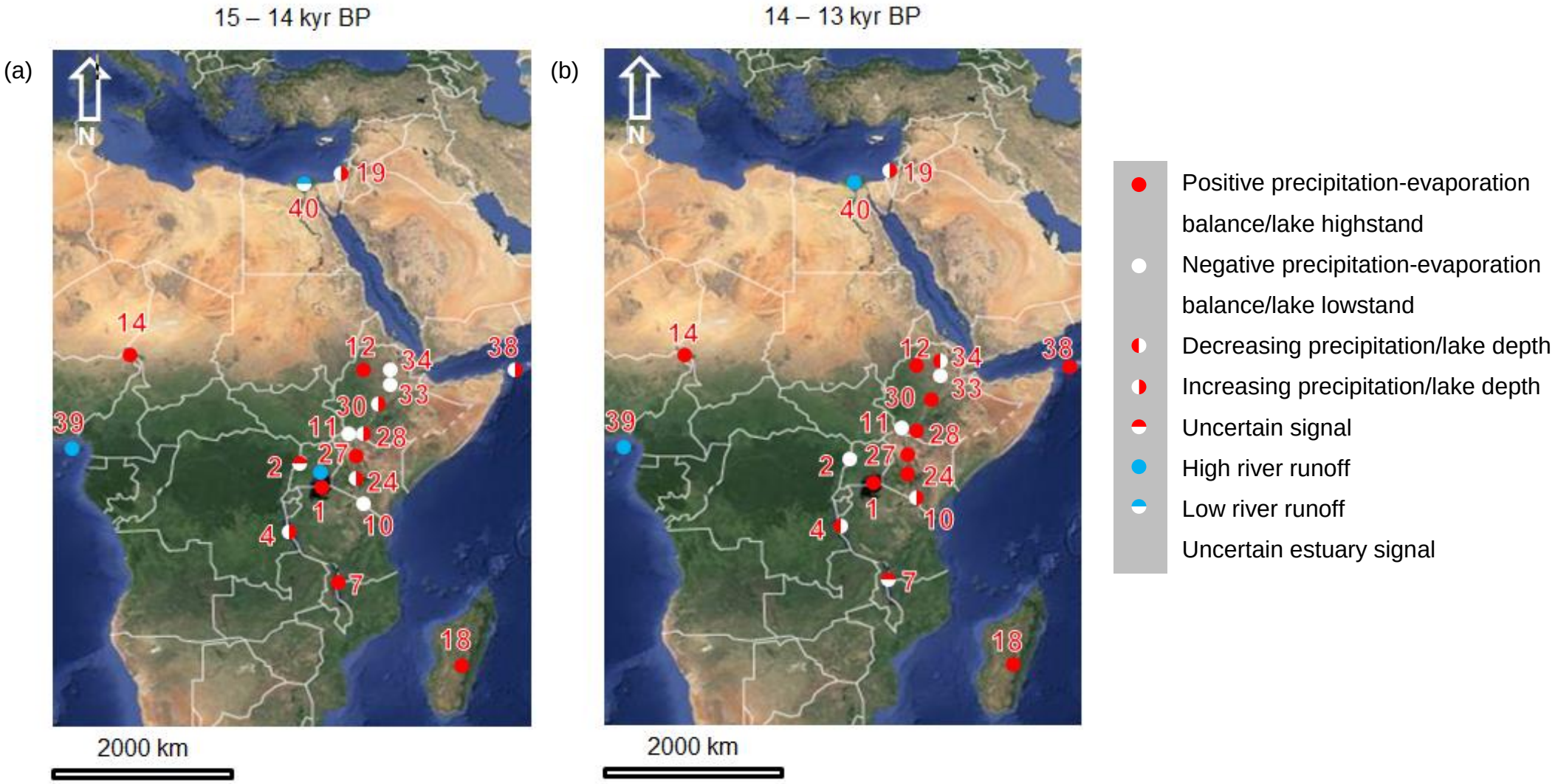

Figure 8.4. Site map of records showing average hydrological conditions between (a) 15 – 14 kyr BP and (b) 14 – 13 kyr BP (Google Maps 2015). See Figure 3.1 for location map and Table 8.1 for authorities.

inconclusive, suggesting a gradual transition in East Africa, an abrupt transition in West Africa or abrupt vegetation collapse followed by a gradual decline in precipitation (Liu et al. 2007; Hély et al. 2009). However, this is perhaps not unsurprising given the behaviour of varying air masses and seasonal changes occurring over such a large geographical area. Therefore, other bio-geophysical mechanisms must have influenced the expression of the climate. For example, Adkins et al. (2006) suggest that vegetation cover may amplify a rainfall response through evapotranspiration, as higher soil moisture can enhance the water vapour flux and latent heating of the atmosphere. Responses may also have been affected by SST in the Indian Ocean, Red Sea, Arabian Sea and eastern Mediterranean, which altered feedbacks between the monsoon systems, coastal upwelling intensity, migration of the tropical rain belts and Congo Air Boundary, as well as convergence zones over Africa (Adkins et al. 2006; Tierney et al. 2008; Loomis et al. 2015).

At Lake Ashenge an early return of monsoon circulation in the Ethiopian highlands is documented between ~ 16.2 – 15.2 kyr BP, causing lake level to rise following the Heinrich Event 1 lowstand (Fig. 8.2; Marshall 2006; Marshall et al. 2009). The diatom record is dominated (> 50 %) by *Cyclotella ocellata* during this period, as found at Lake Hayq. Diatom-inferred conductivity at Lake Ashenge is lower than the modern lake (~ 1600 µS cm^{-1}) and was probably even lower than estimated given the underrepresentation of *Cyclotella ocellata* in the European Diatom Database (EDDI) African training set (Fig. 8.5; Marshall et al. 2009; see Chapter 4, 4.6.4). At Lake Tana, magnetic and geochemical data from core 03TL3 indicate abrupt lake deepening and flooding at 15.3 – 15.2 kyr BP following Heinrich Event 1 and freshwater conditions resumed (Fig. 8.2; Marshall et al. 2011; Loomis et al. 2015). Previously, this rapid (~ 100 years) increase in water depth between 15.3 – 15.2 kyr BP had been reported to have happened at 14.7 kyr BP by Lamb et al. (2007a). However, more recent dating of bulk sediment samples, as well as plant and charred material, by Marshall et al. (2011) shows the increase in water level caused Lake Tana to overflow into the Blue Nile, occurring at the same time as refilling at Lakes Victoria and Albert, the sources of the White Nile (Talbot and Lærdal 2000; Williams et al. 2006; Williams 2009). This suggests that Blue Nile overflow preceded that of the White Nile, most likely due to the shallower depth of Lake Tana in comparison to

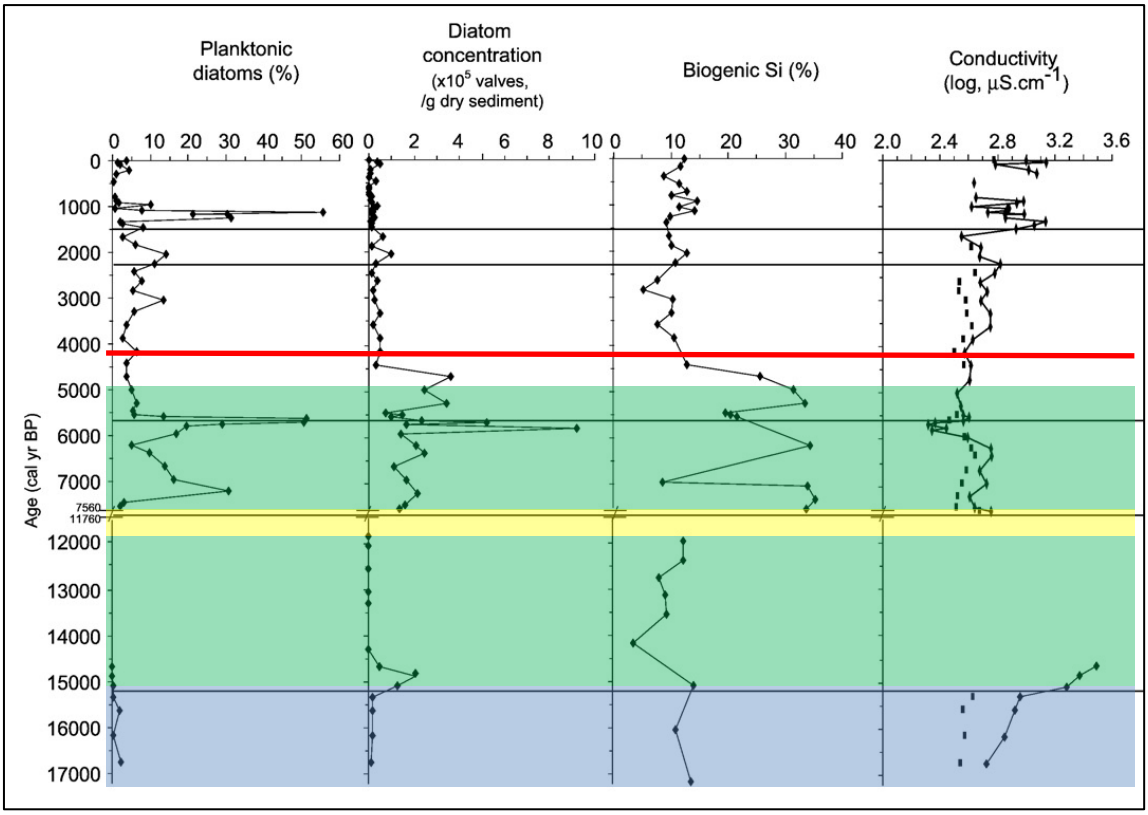

Figure 8.5. Summary diagram of stratigraphic data from Lake Ashenge. Squares on the diatom-inferred conductivity plot indicate values where *Cyclotella ocellata* was excluded from the transfer function procedure. Key time periods are identified: LGM – blue, AHP – green and the 4.2 event – red line. The hiatus in the sediment record is shown in yellow (adapted from Marshall et al. 2009).

Lake Victoria, causing it to overflow faster (Marshall et al. 2011). As a result, flow in the main River Nile reestablished between 14.7 – 14.5 kyr BP (Talbot and Lærdal 2000; Williams et al. 2006; Williams 2009; Box et al. 2011).

Elsewhere in East Africa, lake deepening in response to the onset of the African Humid Period has been found in the Ziway-Shala basin (14.5 kyr BP; Grove et al. 1975), Lake Turkana (14.0 kyr BP; Morrissey and Scholz 2014), Chew Bahir (Fig. 8.2; 14.5 kyr BP; Foerster et al. 2012), palaeo-lake Suguta (14.8 kyr BP; Garcin et al. 2009) and at Lakes Magadi (Roberts et al. 1993), Manyara (Barker et al. 2004), Nakuru (Fig 8.3; Richardson and Dussinger 1986), Challa (Fig. 8.3; Tierney et al. 2011; Barker et al. 2013) and Tanganyika (Fig 8.3; Gasse et al. 1989; Costa et al. 2014) around 15.0 kyr BP (Fig. 8.4a). Refilling was not a rapid, linear process at all sites however, and some lakes such as Lakes Ashenge and Tanganyika show oscillations in lake level during this time (Fig. 8.4).

Therefore, it would appear the shift to wet, humid conditions at Lake Hayq is a result of the onset of the African Humid Period in the north Ethiopian highlands, and as such, hypothesis 2 may be accepted. Discrepancies in the timing of the start of the African Humid Period reflect local manifestations of variability in precipitation amount, water vapour transport and convection over East Africa caused by shifts in the position of major convergence zones such as the Congo Air Boundary, which in turn are affected by SST variability in the Atlantic and Indian Oceans, the Red Sea and Mediterranean (Nicholson 2000; Tierney et al. 2011; Costa et al. 2014). As such, Costa et al. (2014) propose a time-transgressive change in atmospheric circulation caused by a north-south migration of the tropical rain belts and an east-west migration of the Congo Air Boundary. This would account for the gradual onset of the African Humid Period across lakes in Ethiopia, beginning at Lake Ashenge (~ 16.2 kyr BP; Marshall 2006; Marshall et al. 2009) and Lake Hayq and ending at Chew Bahir and Lake Turkana (14.5 – 14.0 kyr BP; Foerster et al. 2012).

It is important to consider however, that some discrepancies in the timing of the start of the African Humid Period, as well as other climatic events, may have arisen from chronological issues (see Chapter 3, 3.2). For example, terrestrial macrofossils were not sufficiently present in the Lake Ashenge core 03AL3/2 and so radiocarbon dating

was performed on bulk sediment samples, despite being less accurate (Marshall et al. 2009). The same applies to this study of Lake Hayq and Done Ella.

Sedimentation may likewise affect the chronology in lakes which were desiccated in response to aridity, truncating or destroying the climate record in the sediments accumulating at the bottom of them (Verschuren 1999a); an issue also affecting the Lake Ashenge sediment record (Marshall et al. 2009). It is important to consider these issues when interpreting any palaeo-record obtained from a lake site and when making comparisons between sites.

8.2.3 The Deglacial Transition: Evidence of Regional Climatic Heterogeneity

Following apparent lake colonisation between ~ 15.1 – 14.8 cal kyr BP, the diatom and pigment data indicate that Lake Hayq suddenly became shallower again between ~ 14.7 – 12.3 cal kyr BP, presumably in response to evaporative concentration caused by a return to arid conditions (Figs. 8.1 and 8.4). This contrasts to the majority of other tropical lake sites across Ethiopia and East Africa, which continued to refill and reached highstands following the beginning of the African Humid Period around ~ 15.0 kyr BP (Fig. 8.4b). Refilling around this time is documented at the Ziway-Shala basin (Fig. 8.2; Grove et al. 1975; Gillespie et al. 1983; Chalié and Gasse 2002a), Chew Bahir (Fig. 8.2; Foerster et al. 2012), Lakes Victoria (Johnson et al. 1996; Beuning et al. 1997; Talbot and Lærdal 2000), Magadi (Roberts et al. 1993), Manyara (Barker et al. 2004), Malawi (Gasse et al. 2002; Johnson et al. 2004), Rukwa (Barker et al. 2002) and palaeo-Lake Suguta (Garcin et al. 2009). These lakes then demonstrate a shift to aridity between 12.8 – 11.6 kyr BP in response to the high-latitude European Younger Dryas Stadial (see Chapter 3, 3.4.4; Fig. 8.6a).

The Younger Dryas has been identified in numerous records across Europe and its signal is well-constrained in the GRIP and GISP2 ice cores from central Greenland, indicating rapid Northern Hemisphere cooling between ~ 12.8 – 11.6 kyr BP (Alley 2000). The drying documented at Lake Hayq during the deglacial transition precedes

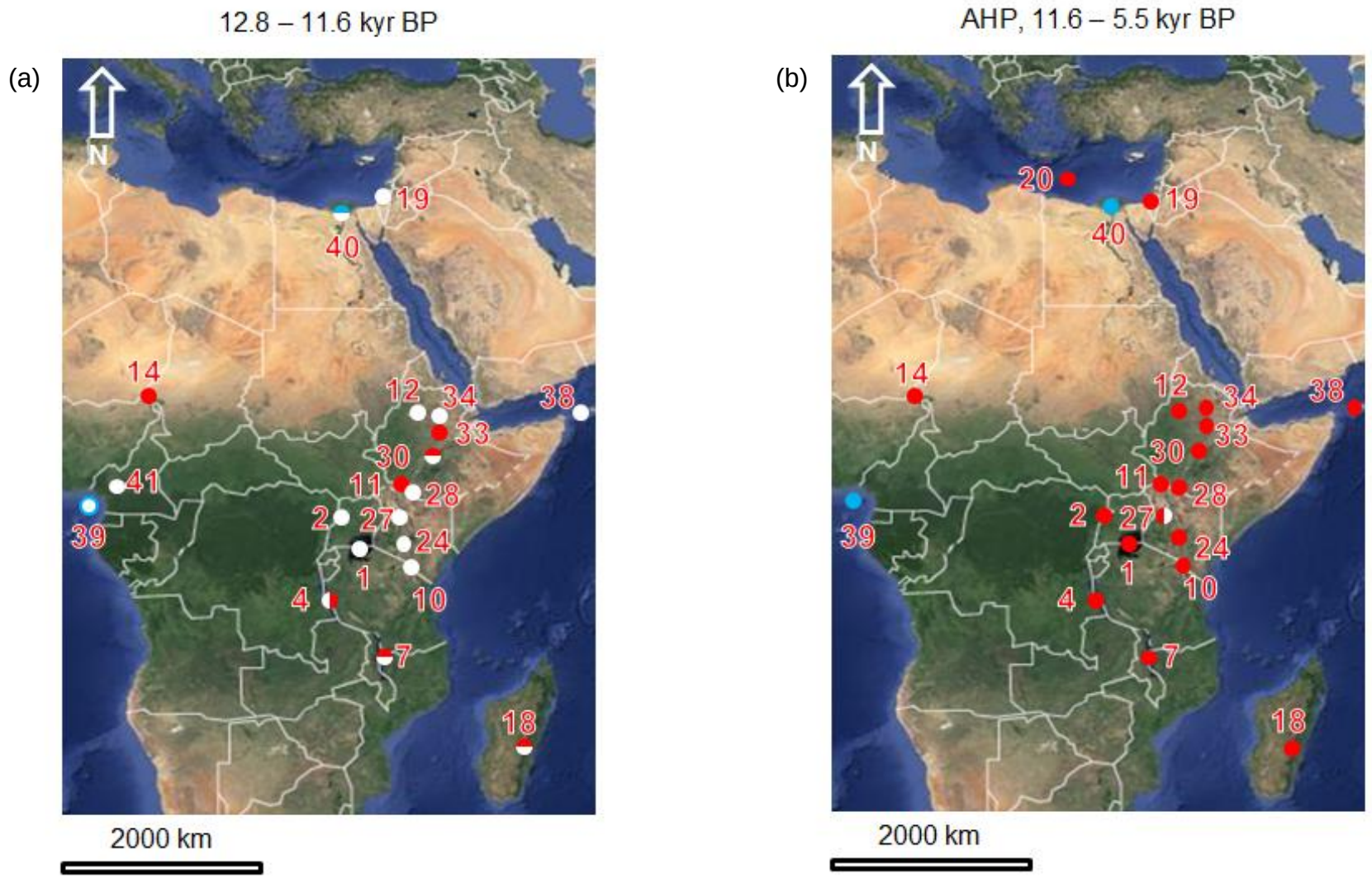

Figure 8.6. Site map of records showing average hydrological conditions between (a) 12.8 – 11.6 kyr BP and (b) 11.6 – 5.5 kyr BP (Google Maps 2015). See Figure 3.1 for location map and Table 8.1 for authorities. See Figure 8.4 for key.

the Younger Dryas by ~ 1.9 cal kyr BP, at a time when the Greenland ice core $\delta^{18}O$ records indicate step-wise cooling in the Northern Hemisphere. During the Younger Dryas proper, Lake Hayq began refilling and rapidly deepened, in stark contrast to other lake and palaeo-sites across subtropical Africa and the Mediterranean. Therefore hypothesis 1 may be rejected (Fig. 8.6a).

Early onset aridity has been documented at other subtropical African sites during this deglacial transition however. For example, in the Sahelian belt, monsoon reactivation occurred in two stages at 15.0 – 14.5 kyr BP and 11.5 – 11.0 kyr BP, sandwiching drier conditions, which precedes the Younger Dryas by 1.7 kyr (Gasse 2000). Off the coast of south-west Africa, marine core GeoBio1023 records aridity between 14.4 – 12.5 kyr BP, a period thought to have been more arid than any other time since the Last Glacial Maximum (Shi et al. 1998). This resulted in the expansion of desert/semi-desert vegetation, particularly *Tribulus* and Chenopodiaceae between 13°S and 21°S, covering the northern Namib Desert, the Angola-northern Namibian highlands and the north-western Kalahari (Shi et al. 1998).

Lake Ashenge experienced drying ~ 900 years prior to the start of the Younger Dryas (Fig 8.4b) (Marshall et al. 2009). At 14.2 kyr BP, low calcite content, increased organic matter and negative $\delta^{18}O$ and $\delta^{13}C$ values indicate an increase in surface water input, which caused Lake Ashenge to deepen. This was interrupted at 13.6 kyr BP, evidenced by maximum $\delta^{18}O$ and $\delta^{13}C$ values of authigenic carbonates and enhanced aragonite precipitation, signaling a highly negative water balance and lake shallowing. This lasted until at least ~ 11.8 kyr BP when a hiatus in the sediment record occurred (Marshall et al. 2009).

At Lake Albert, Berke et al. (2014) used the TEX_{86} temperature proxy, $\delta^{13}C_{wax}$ and δD analysis to reconstruct the climatic expression (evidenced by temperature, precipitation and vegetation change) of the deglacial transition prior to the Younger Dryas. Between 13.8 – 11.5 kyr BP, significant aridity and cooling (~ 3 °C) occurred at Lake Albert causing a decline in lake level and a prominent increase in grass pollen (Fig. 8.4b) (Berke et al. 2014). Cooling is also documented at Lakes Tanganyika (~ 1 °C) (Tierney et al. 2008) and Malawi (~ 2 °C) (Powers et al. 2005)

between 13.8 – 13.6 kyr BP, resulting in reduced lake levels (Fig. 8.4b). These lakes reached minimum temperatures by ~ 13.4 kyr BP, whilst Lake Albert continued cooling until 12.9 kyr BP (Berke et al. 2014). Lake Victoria (Berke et al. 2012) and the Congo Basin (Weijers et al. 2007) saw a break in warming between ~ 14.0 – 11.5 kyr BP, whilst Lake Challa experienced a gradual increase in temperature and a comparable shift in its δ*D* record as Lake Albert between 14.0 – 13.0 kyr BP and during the Younger Dryas (Tierney et al. 2011; Sinninghe Damste et al. 2012).

The cooling and drying documented at Lakes Albert, Challa and Tanganyika, as well as Lakes Ashenge and Hayq prior to the Younger Dryas, indicate a complex pattern of spatial and temporal heterogeneity (Fig. 8.4b), which coincides with step-wise cooling in Greenland and the warm, wet Bølling-Allerød interstadial (~ 14.7 – 12.8 kyr BP), as well as the Antarctic Climatic Reversal cold interval in the Southern Hemisphere (ACR, ~ 14.8 – 12.0 kyr BP) (Jouzel et al. 1995; Alley and Clark 1999). Beal et al. (2011) suggest that at this time, the ACR may have impacted the Agulhas current (the western boundary current in the south-western Indian Ocean off the coast of Southern Africa) by reducing the exchange of water between the Indian and Atlantic Oceans around Africa. This may have subsequently weakened the Atlantic Meridional Overturning Circulation (AMOC) (Shakun and Carlson 2010). Reconstructions of the AMOC using $^{231}Pa/^{230Th}$, temperature proxies and $\delta^{13}C$ values of benthic foraminifera indicate reduced circulation strength in the AMOC at ~ 14.0 kyr BP (Vidal et al. 1997; McManus et al. 2004; Ritz et al. 2013). Although this reduction is not as significant as at the Younger Dryas, it may have been sufficient enough to cause anomalies in Indian Ocean SST and consequently weakened the Indian Ocean monsoon. Berke et al. (2014) conclude this disturbance to the monsoon system triggered the cooling and drying observed at subtropical African lake sites as the ITCZ migrated southwards.

The aridity observed at Lake Hayq beginning at ~ 14.7 cal kyr BP coincides with the proposed changes to the Indian Ocean monsoon system caused by the ACR and disturbance to the AMOC. It is likely that the drying observed reflects a manifestation of the changes to the monsoon alongside local, site-specific mechanisms affecting moisture delivery. These manifestations occurred during a period of complex climate change that remains poorly constrained in East African palaeo-records. For example,

Berke et al. (2014) attribute patterns of rainfall delivery in the Rift Valley (Lakes Albert and Tanganyika) and coastal regions (Lake Challa) to a zonal gradient of SST in the Indian Ocean, although this is not well understood. Orography may similarly affected regional hydroclimates (see Chapter 2). As such, the aridity at Lake Hayq and other East African lakes during this deglacial period prior to the Younger Dryas, highlights the complex spatial and temporal pattern of heterogeneous climate expression and the importance of regional drivers, as well as the role of global teleconnections such as the links between conditions in the North Atlantic Ocean and monsoon circulation in the Indian Ocean.

8.2.4 Resumption of the African Humid Period

Following the end of the Younger Dryas at ~ 11.6 kyr BP, monsoon circulation over East Africa resumed, seeing a return of increased seasonality in regional rainfall. A continuous record of the Asian monsoon (one of three major air streams modulating monsoon circulation over Africa; see Chapter 2, 2.2) over the last 16.0 kyr BP is available from $\delta^{18}O$ measurements of stalagmite calcite taken from Dongge Cave in south China (Dykoski et al. 2005). A dramatic decrease in $\delta^{18}O$ occurred at 11.5 kyr BP lasting until the mid-Holocene, signalling a period of intense monsoon activity (Fig. 8.3; Dykoski et al. 2005). Ice accumulation is also documented at Mt. Kilimanjaro from 11.65 kyr BP, indicating that the monsoon was once again active, promoting ice cap growth (Fig. 8.3; Thompson et al. 2002).

At Lake Hayq, a rise in lake level is interpreted as the reactivation of the monsoon system. Organic, carbonate and water content all increase in the sediment and geochemical data indicators (chemical weathering, biogenic silica and grain size) show a shift towards increased precipitation and humidity as evaporative conditions declined. The diatom data indicates Lake Hayq was recolonised by pioneer taxa between ~ 12.3 – 12.1 cal kyr BP following this climatic shift, and experienced fluctuations in nutrient availability as the lake became established. Between ~ 12.0 – 10.0 cal kyr BP water levels rose significantly, potentially reaching maximum depth, given the dominance of *Aulacoseira granulata* var. *angustissima* and low diatom-inferred conductivity (Fig. 7.1). This most likely reflects peak intensity (a stable maximum), or ‘optimum’ humid conditions at Lake Hayq. It is possible that Lake Hayq became connected to Lake Hardibo during this time via a now permanently dry

palaeochannel and was receiving overflow, which in conjunction with wetter, humid condition would have caused a rapid increase in lake depth and seen the lake expand up to three times its' modern surface area (Ghinassi et al. 2012). Lake Hayq may have then begun overflowing into the Wazi River, eventually reaching the Afar Depression, creating an open hydrological system (Fig. 8.7, H1) (Ayenew 2009). If so, this highlights the significance of local, site-specific feedbacks, including lake and catchment bathymetry, morphology and connectivity, for affecting the regional expression and timing of high-magnitude climate events, paced by precessional cycling. As this refilling at Lake Hayq precedes the end of the Younger Dryas Stadial by approximately 700 years, hypothesis 3 must be rejected.

From ~ 10.0 – 5.2 cal kyr BP, Lake Hayq remained deep, fresh and productive, with symbiotic relationships forming between diatoms and pigments, and meromictic conditions (Fig. 8.1). There is evidence of a gradually declining lake level over time, as benthic and facultatively planktonic diatom taxa gradually increase in abundance and the lake most likely became hydrologically closed as outflow ceased (Fig. 8.7, H2). Potentially it may have still received some overflow from Lake Hardibo. Overall, the lake remained deep in response to a positive water balance.

Other lakes across Ethiopia also experienced dramatic refilling at the beginning of the Holocene, following the termination of the Younger Dryas proper (12.8 – 11.6 kyr BP; Alley 2000), synchronous with the rejuvenation of the monsoon system (Fig. 8.6b). At Lake Tana (as well as Lake Victoria) the hydrogen isotope record from leaf waxes (δD_{wax}) indicates that peak intensity of the African Humid Period occurred between ~ 11.5 – 8.5 kyr BP (Costa et al. 2014). Lake level increased and diatom-inferred conductivity indicates the lake was fresh (Fig. 8.2; Marshall 2006; Marshall et al. 2011). At Lake Ashenge, despite a hiatus in the sediment record (sediments were probably removed either by aeolian deflation during a lowstand, and/or following a lowstand when the lake refilled [Marshall et al. 2009]), water level had also risen substantially by 7.6 kyr BP in response to resumption of the African Humid Period (Marshall et al. 2009). Potentially, the lake was overflowing at its southern

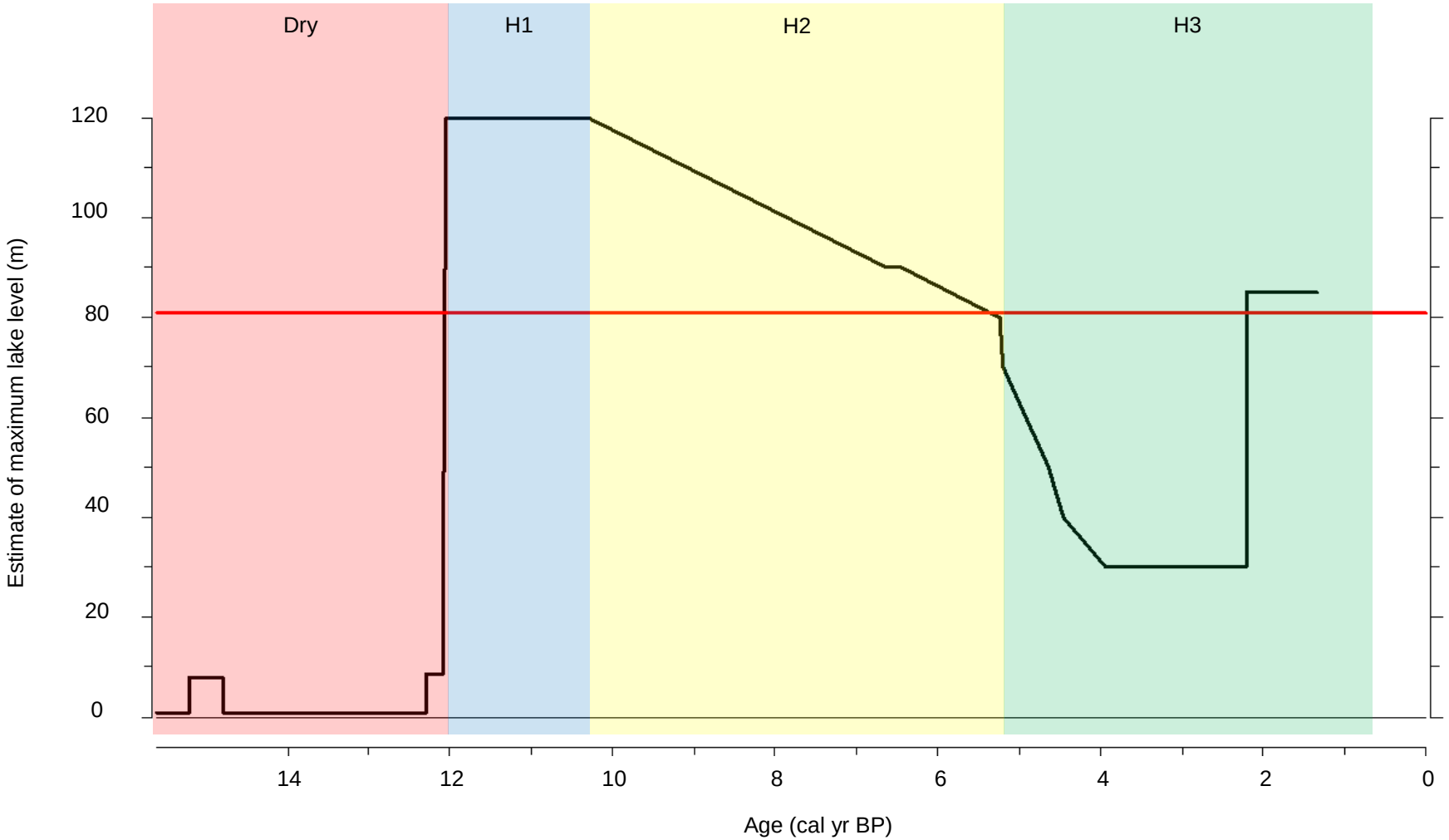

Fig. 8.7. A simple maximum lake level curve (based on the collective interpretation of the available proxies) against time, showing changes in the hydrological functioning and connectivity of Lake Hayq. Maximum lake level in 2000 (81.0 m; Lamb et al. 2007b) is indicated by the red line. H1 – Lake Hayq was an open system, receiving overflow from Lake Hardibo and overflowing itself during a highstand; H2 – Lake Hayq was closed (there was no out flow) but potentially received some overflow from Lake Hardibo; H3 – Lake Hayq was a closed system and did not receive inflow from Lake Hardibo.

shore, requiring a water level rise of 12 m (above present depth), resulting in the filling of the southern basin, creating a major waterbody comprised of two smaller basins (Marshall et al. 2009). As at Lake Hayq, biological productivity at Lake Ashenge was also high during this time and diatom-inferred conductivity indicate a fresh lake and therefore, positive water balance (Fig. 8.5; Marshall et al. 2009). Foerster et al. (2012) and Costa et al. (2014) suggest that the extreme humidity experienced in northern Ethiopia during this time, which caused lake levels to rise so dramatically, was a result of an eastward shift in the Congo Air Boundary due to a deepening of the atmospheric low over India, which enhanced the pressure gradient between India and Asia. In combination with rising SST, this resulted in continuous moisture availability.

Elsewhere in Ethiopia, the water level at the Ziway-Shala basin also rose significantly, resulting in the formation of a macro-lake, which overflowed twice in the early to mid-Holocene (Nilsson 1940; Gillespie et al. 1983; Umer et al. 2004) and subsequently resulted in Lake Abhé also reaching its maximum extent between 9.4 – 8.3 kyr BP (Fig. 8.2; Butzer et al. 1972; Fontes et al. 1973; Gasse and Van Campo 1994; Umer et al. 2004; Benvenuti et al. 2013). At Chew Bahir, the potassium record indicates the monsoon returned in two phases; the first at 11.8 kyr BP and then a second, abrupt return (~ 200 years) to full humid conditions at 11.6 kyr BP (Fig. 8.2; Foerster at al. 2012). Potentially this same phenomenon also occurred at Lake Hayq, although slightly earlier given the lakes more northerly position, at ~ 12.3 cal kyr BP when it was dominated by pioneer diatom taxa, and then more abruptly at ~ 12.0 cal kyr BP, when maximum lake level occurred. At Lake Turkana water level between 13.0 – 11.5 kyr BP reached elevations of ~ 440 – 410 m above sea level (as palaeo-lake Suguta overflowed into it) and began overflowing into the White Nile basin (Fig. 8.2; Garcin et al. 2012). Morrissey and Scholz (2014) likewise argue that the consistent nature of the sediment record from cores 4P, 14P, and 46P, indicate a high, stable water level at Lake Turkana between ~ 12.5 – 5.0 kyr BP.

Regionally, other Ethiopian and East African lakes exhibit similar signals to Lake Hayq as highstands occurred between 13.0 – 5.0 kyr BP in response to the resumption of the African Humid Period (Fig. 8.6b) (Barker et al. 2002; Lærdal et al. 2002; Bergner et al. 2003; Stager et al. 2003; Barker et al. 2004; Damsté et al. 2011;

Konecky et al. 2011; Junginger et al. 2013). Lakes Tanganyika and Nakuru both document highstands in the early Holocene (Fig. 8.3; Richardson and Dussinger 1986; Gasse et al. 1989). At Lake Challa, peaks in $\delta^{13}C_{diatom}$ and δD_{wax} similarly indicate the most positive water balance occurred at ~ 11.5 – 9.8 kyr BP, after which the lake level and aquatic productivity remained high (Fig. 8.3; Tierney et al. 2011; Barker et al. 2013). Increasingly wet and humid conditions are also documented at sites in North Africa (Giraudi et al. 2012) and the Mediterranean (Bar-Matthews and Ayalon 1997; Bar-Matthews et al. 2000) at the start of the Holocene, including the formation of the eastern Mediterranean sapropels (Rossignol-Strick 1985; Rholing and Hilgen 1991; see Chapter 3, 3.5.1).

There does not appear to be any significant change or variability in the palaeolimnological record at Lake Hayq in response to the 8.2 event (see Chapter 3, 3.5.2), despite a high-resolution diatom study being undertaken. Therefore hypothesis 4 is rejected. Potentially, with improved dating, an arid episode pertaining to the 8.2 event may become identifiable and constrained. It is evident though from the current state of the sediment record that even if the arid interval were to be identified, it did not have such an extreme effect on the lake system as other arid events such as Heinrich Event 1 or the Younger Dryas Stadial. Alternatively, the reason for no 8.2 event signal being identified in the Lake Hayq sediment is because, as previously discussed in Chapter 3 (3.5.2), the 8.2 event is not an abrupt occurrence caused by catastrophic melt water outburst, but is instead a fluctuation in a long-term background climatic anomaly (Rohling and Palike 2005). Unlike European sites, most lakes across subtropical Africa, incuding Lake Hayq, do not exhibit a clear climatic response to the 8.2 event and no distinct signal is preserved in the palaeo-records (Fig. 8.8). Where a fluctuation is observable in a palaeo-record around this time period (several hundred years either side of 8.2 kyr BP, within the margin of dating errors), it more likely reflects long-term changes in East African climate rather than an abrupt event. For example, Marshall et al. (2011) argues that the decline in rainfall at Lake Tana from ~ 8.5 kyr BP onwards is due to the gradual migration of the tropical rain belts southward, which saw rainfall become more variable and seasonal. This has also been identified by Stager et al. (2003) in a

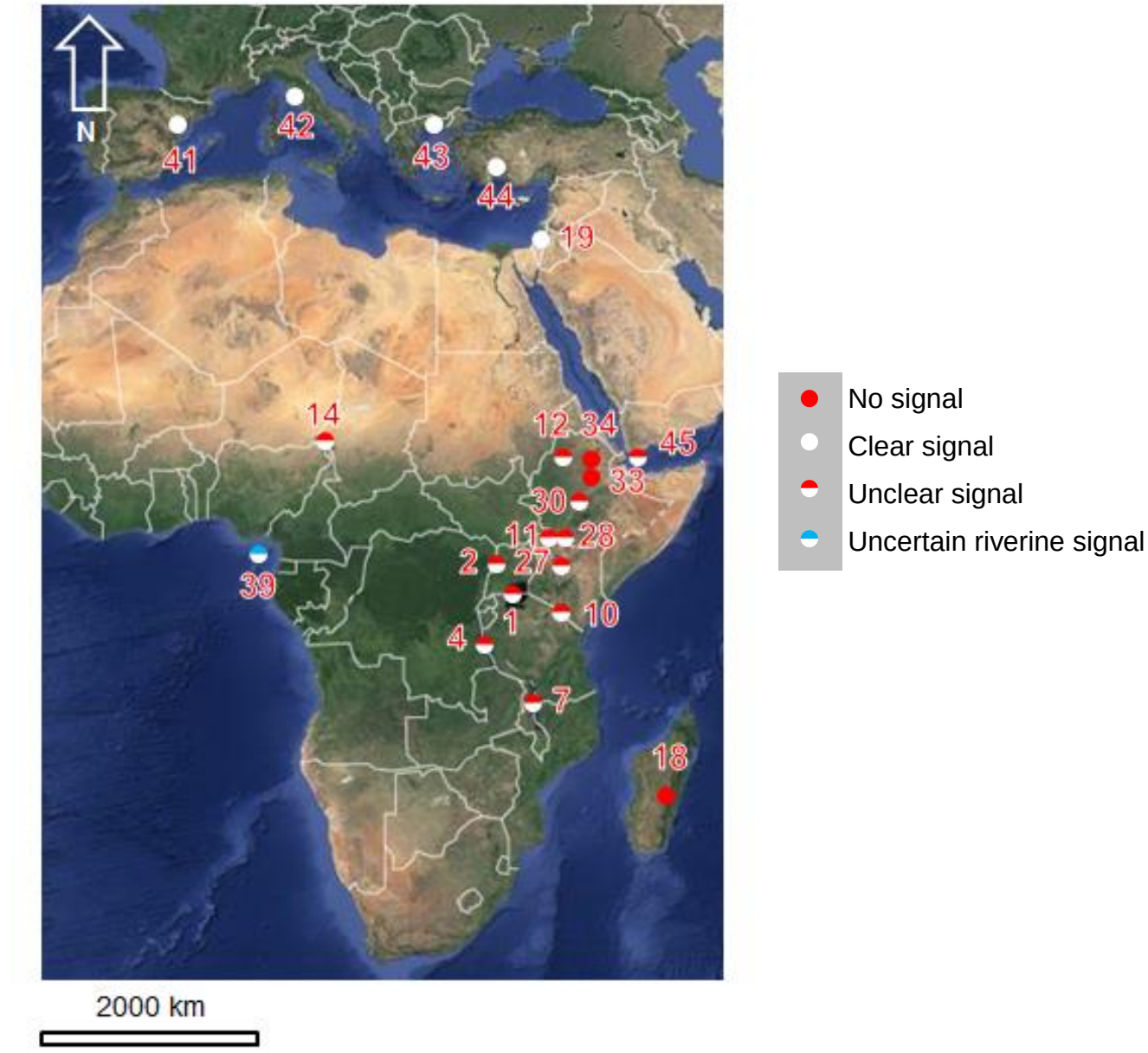

Figure 8.8. Site map of records showing average hydrological conditions at 8.2 kyr BP (Google Maps 2015). See Figure 3.1 for location map and Table 8.1 for authorities.

study of the White Nile, as well as the Nile Delta (Revel et al. 2010) and from a marine core extracted off the coast of Somalia (Jung et al. 2004). This would account for the long-term decline in water level observed at Lake Hayq from the early to mid-Holocene, rather than an abrupt shift centred at 8.2 kyr BP.

8.2.5 Termination of the African Humid Period

The high-resolution study of the termination of the African Humid Period indicates that in the build-up to the end of wet, humid conditions (~ 6.4 – 5.2 cal kyr BP), oscillations occurred in the diatom record; switches in dominance occurred between *Aulacoseira granulata* var. *angustissima* and *Fragilaria radians* every ~ 40 – 180 cal years, most likely reflecting periods of lake level rise and decline. These changes in water depth and, by association, lake volume and area will have subsequently affected (to varying degrees) the light and mixing regime (including wind fetch) of the lake, as well nutrient ratios.

These oscillations potentially signal climate instability leading up to the cessation of the African Humid Period. 'Flickering' in systems may occur before a critical transition or tipping point; systems switch back and forth between alternative states in the build-up to large external impacts, which can be interpreted as an early warning of substantial changes or disturbance to the system (Brock and Carpenter 2010; Dakos et al. 2012; Wang et al. 2012; Dakos et al. 2013). Wang et al. (2012) argue that such a phenomenon has occurred at Lake Erhai, China, where 'flickering' in the diatom assemblage and other water quality indicators signalled a regime shift in the lakes trophic state. Carstensen et al. (2013) have refuted the findings of Wang et al. (2012) however, arguing that the phenomenon may instead be a result of data processing rather than a true signal of system change (Wang et al. [2013] replied stating that the results of their findings should not be overturned). At Lake Hayq, the switches in the diatom assemblage may be verified as a true diatom signal, rather than an error in data analysis, given the use of replicate counting, which identifies the range of natural variability (see Chapter 4, 4.4.3.3.2; Fig. 4.6). As such, the changing states between a deeper and shallower lake may, potentially, reflect 'flickering' as a result of climate instability caused by the build-up to the termination of the African Humid Period.

However, the high-resolution record is not long enough to state definitively whether the fluctuations (or 'flickering') in the diatom assemblage and lake level are a result of a climatic tipping point, or are long-term cycles in response to century scale climate variability. During the Holocene, temporary weakening of the south-west Indian Ocean summer monsoon occurred in response to reduced northward heat transport in the North Atlantic (Gupta et al. 2003). As a result, precipitation regimes across North and tropical Africa experienced greater seasonality (Lamb et al. 1995; Stager and Mayewski 1997). At Lake Victoria rapid (three to four decades) switches between *Aulacoseira* and *Nitzschia* dominated assemblages occurred between 7.2 – 2.2 kyr BP due to greater rainfall variability and lake mixing (Stager et al. 1997). Given the comparable depths at Lakes Victoria and Hayq (average and maximum depths: 40 m and 80 m at L. Victoria, 37.4 m and 81.0 m at L. Hayq; Stager et al. 2002; Lamb et al. 2007b), potentially the shifts in diatom assemblage at Lake Hayq are a result of the same phenomenon; enhanced seasonality due to temporary weakening of the monsoon circulation. Therefore, without a longer record, spanning at least the early to mid-Holocene, at the same decadal to centennial resolution, it is difficult to determine whether the shifts between *Aulacoseira granulata* var. *angustissima* and *Fragilaria radians* are a threshold response to the termination of the African Humid Period or due to century-scale climate variability.

The geochemical data indicate a shift towards aridity occurred at ~ 5.8 cal kyr but it is not until ~ 5.2 – 5.1 cal kyr BP that the first changes are observed in the diatom and pigment record, comprised of two small declines in water depth, which saw productivity decrease and meromixis weakened (Fig. 8.1). The next, more significant change occurred at ~ 5.1 cal kyr BP when a major increase in benthic diatom taxa indicates an abundance of shallow water habitats, synchronous with the disappearance of *Aulacoseira granulata* var. *angustissima*. A short-lived wet period is documented in the diatom and pigment records between ~ 4.9 – 4.7 cal kyr BP, which temporarily rejuvenated lake productivity, but intense aridity is indicated again at ~ 4.6 cal kyr BP, when further increases in benthic and aerophilous taxa occurred.

Based on the palaeo-records, it appears that Lake Hayq experienced a relatively quick termination of the African Humid Period, superimposed on a long-term decline in lake depth. Between ~ 10.0 – 6.4 cal kyr BP a gradual decline in lake depth is

inferred from the diatom data, most likely due to the gradual migration of the rain belts southward (although geochemical data do not indicate a major shift in climate) but it is not until ~ 5.2 cal kyr BP that the first significant changes in the diatoms and phytoplankton are observed, in response to an increasingly arid, evaporative climate which resulted in a negative water balance. The lake would have remained closed and overflow from Lake Hardibo would have ended (Fig. 8.7, H3). Therefore, it is (tentatively) interpreted that the African Humid Period termination, in terms of diatom and pigment response, was relatively abrupt, spanning ~ 600 cal years between ~ 5.2 – 4.6 cal kyr BP (hypothesis 5 is accepted). The geochemical data in the high-resolution section suggests a longer termination beginning at ~ 5.8 cal kyr BP but when compared to the complete XRF record, the shifts towards aridity are minor. In comparison to other terminations within the Horn of Africa, the theoretical duration of the termination period from the Gulf of Aden record ranges from 280 – 490 years, slightly less than that observed at Lake Hayq (~ 600 yr), but overall the termination may be described as relatively abrupt, lasting several centuries rather than millennia.

Tierney and deMenocal (2013) suggest the average timing of the termination of the African Humid Period in the Horn of Africa and East Africa is 4,960 ± 70 yr BP, based on records from Lakes Tanganyika and Challa and the Gulf of Aden. In West Africa, termination is placed at 4,900 ± 400 yr BP by Tierney and deMenocal (2013), although deMenocal et al. (2000) suggest it occurred earlier at 5,440 ± 30 yr BP. At Lake Chad, Armitage et al. (2015) argue that lake level fell abruptly in response to aridity at 5.0 kyr BP. Based on these average terminations, the Lake Hayq record is broadly synchronous with regional records and closest to that of Lake Turkana, which is placed at 5,270 ± 300 yr BP (Tierney and deMenocal 2013). This reflects the north to south progression of the end of the African Humid Period as monsoon rains were progressively reduced with latitude in response to decreasing summer insolation, as well as the southward migration of the tropical rain belts (deMenocal 2015; Shanahan et al. 2015).

However, despite this latitudinal decline in precipitation, lake system responses to the termination do not mirror this north to south trend. The earliest recorded responses are identified at Qunf cave, Oman (Fleitmann et al. 2007) and Lake Victoria (Stager et al. 1997), whilst the latest signal are found in proxy records from

the River Nile (Williams 2009), Lake Chad (Armitage et al. 2015), Lake Tritrivakely (Gasse and Van Campo 1998) and the Gulf of Aden (Tierney and deMenocal 2013) (Fig. 8.9 and Table 8.1). Therefore, there is no discernible geographic pattern in terms of climatic response to the termination of the African Humid Period across the continent. The termination at Lake Hayq is neither significantly early nor late in comparison to other records from Ethiopia, the Horn of Africa or subtropical Africa, but in combination with these other records, emphasises the heterogeneous pattern of regional response to this climatic event across the African continent.

Variability in the timing and length of termination between sites, resulting in such a heterogeneous pattern, is most likely in response to local, non-linear mechanisms. The CLIMBER2 climate and biosphere model[15] found that abrupt responses to gradual insolation forcing during the termination of the African Humid Period were attributed to positive feedbacks caused by vegetation cover, surface albedo, soil moisture and precipitation. For example, declining precipitation would reduce vegetation cover, raising surface albedo and reducing the efficiency of the initial radiation forcing of the monsoon (Claussen et al. 1999; deMenocal et al. 2000). Reduced vegetation density would also affect catchment runoff, as well as sediment and nutrient supply to the lake. In contrast, atmosphere only, coupled ocean-atmosphere simulations without responsive vegetation, exhibited a smooth climatic response to the gradual orbital forcing (Claussen et al. 1999; deMenocal et al. 2000). However, Tierney and deMenocal (2013) suggest there was no great regional shift observed in vegetation across the Horn of Africa, and so the full extent of a vegetation-driven feedback is potentially unlikely in the most arid areas of East Africa (deMenocal 2015; Shanahan et al. 2015); Lake Hayq has a subhumid climate though, and so potentially the effect of vegetation feedbacks on local climate is greater than anticipated.

[15] A zonally averaged, coupled ocean-atmosphere model with an equilibrium vegetative subsystem (Claussen et al. 1999).

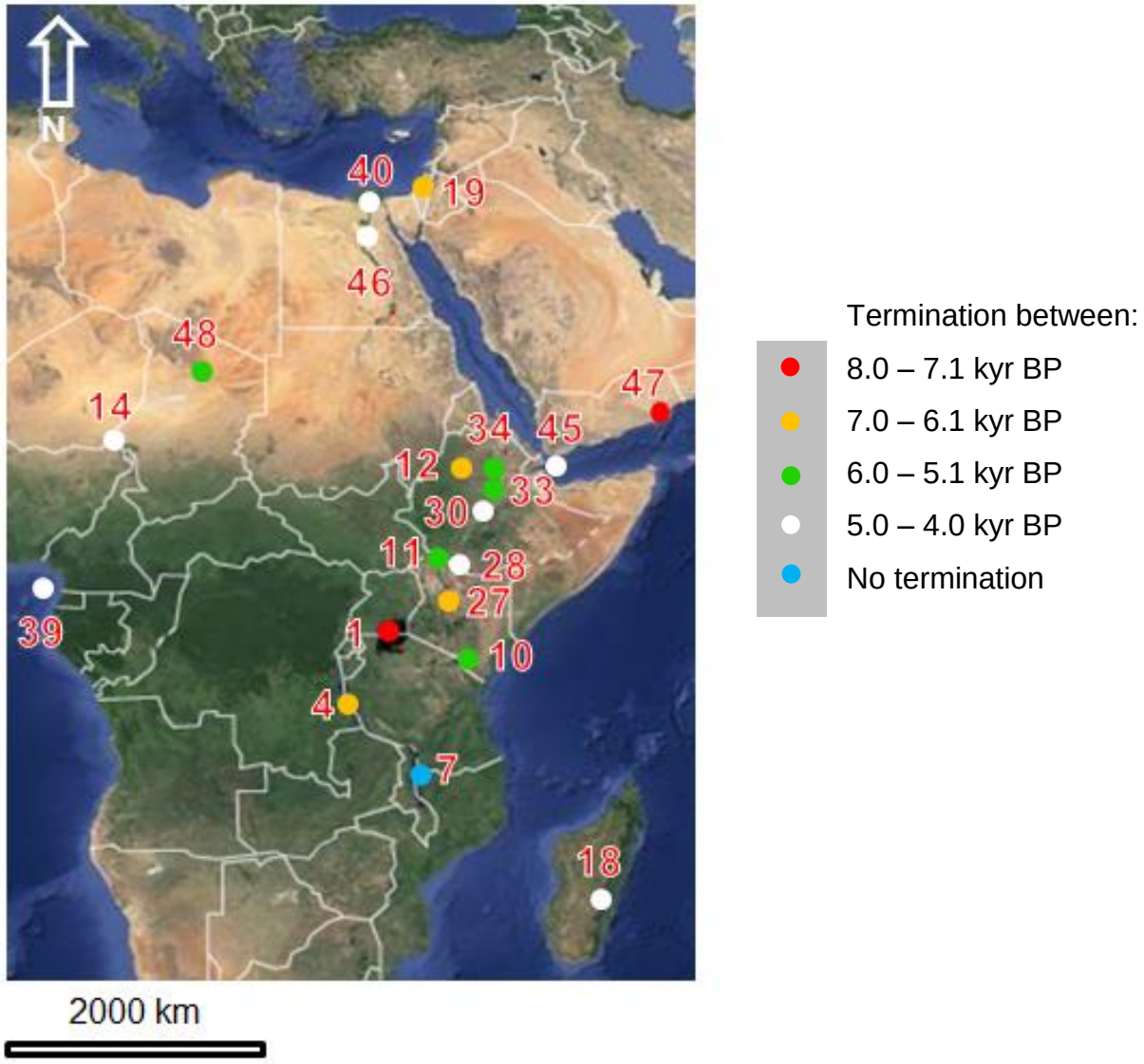

Figure 8.9. Site map of records showing the timing of the start of the African Humid Period termination between 8.0 – 4.0 kyr BP (Google Maps 2015). See Figure 3.1 for location map and Table 8.1 for authorities.

Table 8.1. Palaeo-records from Africa, the Mediterranean and Europe (arranged in an *approximate* north to south order) and their approximate termination of the African Humid Period.

Site	Country/ Location	Map ID	Authority	Approximate termination of the AHP
Ebro desert	Spain	41	Davis and Stevenson (2007)	N/A
Lake Accessa	Italy	42	Peyron et al. (2011)	N/A
Tenaghi Philippon	Greece	43	Peyron et al. (2011)	N/A
Antalaya	Turkey	44	Weninger et al. (2006)	N/A
Soreq cave	Israel	19	Bar-Matthews et al. (1997)	7.0
River Nile	Egypt	40	Williams (2009)	4.3
Saqqara necropolis	Egypt	46	Welc and Marks (2014)	5.0
Qunf cave	Oman	47	Fleitmann et al. (2007)	7.8
Lake Yoa	Chad	48	Kröpelin et al. (2008)	5.6
Lake Chad	Chad	14	Armitage et al. (2015)	5.0
Socotra Island	Yemen	38	Shakun et al. (2007)	-
Lake Ashenge	Ethiopia	34	Marshall et al. (2009)	5.6
Lake Tana	Ethiopia	12	Marshall et al. (2011)	6.3
Lake Hayq	Ethiopia	33	This study	5.2
Gulf of Aden	Arabian Sea	45	Tierney and deMenocal (2013)	5.0
Ziway-Shala basin	Ethiopia	30	Benvenuti et al. (2002)	5.0
Lake Turkana	Keyna	11	Morrissey and Scholz (2014)	5.2
Chew Bahir	Ethiopia	28	Foerster et al. (2012)	5.0
paleo- Lake Suguta	Keyna	27	Junginger et al. (2013)	6.7
Lake Challa	Kenya	10	Barker et al. (2013)	5.5
Gulf of Guinea	West Africa	39	Armitage et al. (2015)	4.9
Lake Albert	Rift Lake	2	Berke et al. (2014)	-
Lake Victoria	Rift Lake	1	Stager et al. (1997)	7.2
Lake Tanganyika	Rift Lake	4	Tierney et al. (2010)	6.2
Lake Malawi	Rift Lake	7	Konecky et al. (2011)	Lake highstand from 6.2 - 3.0
Lake Tritrivakely	Madagascar	18	Gasse and Van Campo (1998)	4.0

A second positive feedback process is Indian Ocean surface temperature-moisture transport. Western Indian Ocean SSTs are close to the threshold boundary for deep convection (26 – 28 ºC) and so very small changes in temperature caused by the El Niño Southern Oscillation (ENSO), the Indian Ocean Dipole or multi-decadal oscillations, can alter Walker Circulation, inducing deep convection and heavy rainfall in East Africa (Tierney and deMenocal 2013). Therefore, abrupt shifts in East African climate may reflect convective feedback with seasonal dimensions; as the summer monsoon winds migrated southwards during the Holocene in response to orbital forcing, a critical SST threshold may have been crossed causing the sudden cessation of the deep convection in the Indian Ocean rainy season, resulting in regional aridity across the Horn of Africa (Tierney and deMenocal 2013).

In contrast to Lake Hayq, Lake Tana saw a long-term shift away from aridity as the African Humid Period came to an end. Between 6.3 – 4.1 kyr BP, a decline in the supply of titanomagnetite and lithogenic elements (titanium and zirconium) occurred, as well as an increase in the concentration of haematite. Marshall (2006) interprets this as a long-term reduction in rainfall and runoff, as well as increased aeolian dust supply and enhanced oxidation of iron minerals within non-waterlogged aerobic catchment soils. The differences in duration of termination between Lakes Hayq and Tana may, either completely or partially, be due to differences in lake basin morphometry (including the lake and surrounding catchment), which encompasses a multitude of physical, biological and chemical components and processes, including in recent centuries, anthropogenic activities (Table 8.2). Lake morphometry may buffer or amplify the impact of climate variability by increasing or decreasing the area on which climate variability is expressed. In contrast, at Lake Ashenge, a step-wise decline in productivity is observed from ~ 5.6 kyr BP, as well as an increase in diatom-inferred conductivity and stable isotope values, with $\delta^{18}O$ increasing by ~ 10 ‰ over two centuries, indicating intensified aridity (Fig. 8.2 and 8.4; Marshall 2006; Marshall et al. 2009). This indicates a relatively quick termination of the African Humid Period.

Given the proximity of Lakes Tana and Ashenge to Lake Hayq and their differing responses to the end of humid conditions in the mid-Holocene, this would indicate that positive feedback mechanisms (including the effect of morphological

differences) were operating at Lake Hayq, rather than a direct, linear response to gradual climatic forcing. The variability in timing, duration and expression of the termination of the African Humid Period between sites, highlights the significance of site specific, non-linear feedbacks on local (as opposed to regional) climate and environment responses. The results from Lake Hayq indicating an abrupt termination of the African Humid Period may provide a new benchmark for hydroclimatic and palaeoclimatic history in the underrepresented Horn of Africa.

Table 8.2. Morphological characteristics of Lakes Hayq, Tana and Ashenge (Marshall 2006; Lamb et al. 2007b; Ashenge 2009; Yesuf et al. 2013).

	Lake Hayq	**Lake Tana**	**Lake Ashenge**
Latitude	11º20'53''N	12°01'58"N	12°34'45"N
Longitude	39º42'32''E	37°18'23''E	39°30'05"E
Altitude (m)	1,950	1,775	2,440
Lake area (km²)	23.2	3,156.0	15.4
Lake volume (km³)	1.0	28.4	0.35
Maximum depth (m)	88.8 (1938)	14.0	23.0
	81.0 (2000)		
Mean depth (m)	37.4	9.0	14.0
Catchment area (km²)	65.0	16,500.0	82.0
Lake area/Catchment area	0.35	0.19	0.18

8.2.6 The Late Holocene and Other Records from Lake Hayq

The termination of the African Humid Period culminated in a late Holocene lowstand at Lake Hayq from ~ 3.9 – 2.2 cal kyr BP. The lake became subsaline at times in response to a negative water balance and benthic diatoms dominated the assemblage indicating an availability of shallow water habitats, as well as increases in the abundance of benthic algae (Fig. 8.1). The lake most likely became a closed system at this time, following the gradual decline of overflow from Lake Hardibo after the early Holocene highstand. Unlike other records from Ethiopia and East Africa, there is no evidence of the 4.2 event at Lake Hayq (see Chapter 3, 3.5.4); no observable change in the diatom, pigment or geochemical data occurred around this time period. Ghinassi et al. (2012) suggest that a lowstand identified by stratigraphical and geomorphological analyses at Lake Hayq prior to 3.25 kyr BP was probably due to the 4.2 event but more likely this is due to the lowstand beginning at ~ 3.9 cal kyr BP, or the termination of the African Humid Period.

Potentially the effects of the 4.2 drought event may have been supressed by natural feedback mechanisms (vegetation cover, soil moisture) in the basin resulting in minimal impact. Alternatively, the event is the final cessation of the African Humid Period, rather than a separate short-term drought. The highstand identified by Ghinassi et al. (2012) between 3.25 – 3.0 cal kyr BP is not identified in the diatom, pigment or geochemical records.

The record from Lake Ashenge is most similar to Lake Hayq during this time, although many lakes across Ethiopia and East Africa experienced lowstands following the end of humid conditions in the mid-Holocene (Fig. 8.2 and 8.3). After the termination of the African Humid Period, water level at Lake Ashenge continued to fall in response to increasing aridity (Marshall et al. 2009). Diatom productivity declined from 5.6 kyr BP onwards, as did the abundance of planktonic diatoms. Between 2.2 – 2.3 kyr BP, a further decrease in water level occurred at Lake Ashenge, evidenced by the dominance of benthic diatom taxa and changing $\delta^{18}O$ and $\delta^{13}C$ values, which indicate increased evaporative concentration.

Both Lake Hayq and Lake Ashenge saw an increase in lake depth and wetter conditions at ~ 2.2 cal kyr BP, evidenced by the rise of planktonic diatoms in both records (Fig. 8.2). This contrasts to the more southerly Lake Challa, where the $\delta^{13}C_{diatom}$ record became strongly depleted at 2.0 kyr BP, indicating that aquatic productivity has declined, suggesting a shift towards aridity (Fig. 8.3; Barker et al. 2013). At Lake Hayq, this wet period lasted until at least ~ 1.3 cal kyr BP, when the core Hayk-01-2010 ends, and is most likely the same highstand identified in the Uarababo and Ankarka River districts from 2.6 – 0.95 kyr BP (Ghinassi et al. 2012). This is in agreement with the oxygen isotope record from 2.35 – 1.36 kyr BP when $\delta^{18}O$ values were relatively uniform, ranging from + 3.8 – + 4.8 ‰. This indicates climatic conditions were stable although slightly wetter than present (in May 2002 $\delta^{18}O$ was + 8.7 ‰ ± 0.1 ‰; Lamb et al. 2007b). This interpretation does require caution however due to low sample resolution and possible sediment disturbance (Lamb et al. 2007b).

The wet period at Lake Hayq between ~ 2.2 – 1.3 cal kyr BP provides additional support to the hypothesis put forward by Butzer (1981) of an extended growing

season in northern Ethiopia. Butzer (1981) proposes that a northward extension of the ITCZ allowed for a strongly bi-modal rainfall season to develop over Tigray, which enabled greater food production in the region to support a growing population. This allowed the Aksumite Empire to rise to power. Evidence of this wet period has also been found at Lake Ashenge (Marshall et al. 2009), from infilled valley deposits in the Tigray region (Machado et al. 1998), as well as Aksum itself, in stable hydrogen isotopic ratios (δ*D*) of land plant-derived fatty acids (Terwilliger et al. 2013). There is tentative evidence of a drop in water level at Lake Hayq at ~ 1.5 cal kyr BP, as both total pigment concentration and *Aulacoseira granulata* var. *angustissima* decline, synchronous with an increase in benthic taxa (Fig. 8.1). This may coincide with a similar shift observed at Lake Ashenge at 1.5 kyr BP, which signals a move towards aridity (Marshall 2006). This lends further support to Butzer's (1981) theory that a shift in climate back towards drier conditions in northern Ethiopia occurred, as the climate reverted back to its previous (and present) state of a unimodal rainfall regime. This would have reduced the capacity of the Aksumite Kingdom to grow food for its population, which in combination with other factors such as political instability and environmental degradation, ultimately led to its collapse (Butzer 1981; Fattovich 1987; 1990; 2010). However, as at Lake Ashenge, the shift towards aridity at Lake Hayq occurred ~ 250 cal years earlier than suggested by Butzer (1981), who argues a change in climate during the 8th century was disastrous for Aksumite agricultural productivity. The shift at Lake Hayq was also short-lived and by ~ 1.3 cal kyr BP, the lake level was high again (Fig. 8.1). Therefore, whilst there is no evidence of a permanent shift towards aridity at this time, the climate in northern Ethiopia was potentially becoming less stable, which may have contributed to the demise of the Kingdom of Aksum.

Potentially, a possible mechanism for the relatively quick shifts in aridity-humidity at Lake Hayq during the late Holocene (as indicated by the large shifts in the abundance of *Aulacoseira granulata* var. *angustissima* and benthic diatom taxa, as well as diatom-inferred conductivity and pigment accumulation rate; Fig. 8.1), may reflect an enhanced, higher frequency ENSO regime caused by cooling of the Pacific tropical deep waters (Sun 2000; Moy et al. 2002; Foerster et al. 2012; Fig. 8.3). In particular, a period of heightened ENSO periodicities centred at 1.6 cal kyr BP and

1.3 cal kyr BP may account for the variability seen in the Lake Hayq record (Moy et al. 2002).

As Hayk-01-2010 ends at ~ 1.3 cal kyr, late Holocene climate at Lake Hayq is based on interpretations from HYK99-1 (Lamb et al. 2007b). Effective precipitation increased from 1.3 kyr BP, peaking at 1.24 kyr BP (average $\delta^{18}O$ of - 0.9 ‰), after which rainfall rapidly declined and peak aridity occurred at 1.15 kyr BP (average $\delta^{18}O$ of + 6.2 ‰). From 1.15 – 0.75 kyr BP there was significant interdecadal variability but conditions were on average similar to, if not slightly more humid, than present. A decrease in lake level occurred during this time from 950 – 650 yr BP, which lowered the shoreline by at least 8 – 9 m (Ghinassi et al. 2012).

Ghinassi et al. (2012) document a highstand at Lake Hayq beginning at 650 yr BP which caused the lake level to rise by 9 – 10 m. Effective precipitation likewise increased to a maximum value at 650 yr BP (average $\delta^{18}O$ of - 4.0 ‰). This period of low oxygen and carbon isotopes coincides with an unlaminated section of core containing peak diatom concentration and abundant microfossil remains of the green alga, *Pediastrum* (Lamb et al. 2007b). These features indicate that the bottom waters of Lake Hayq were most likely oxygenated at this time due to frequent overturn; meromixis at Lake Hayq had ended. Increased rainfall would have reduced salinity and lowered lake surface temperatures, thus aiding mixing during this time and enhancing productivity in the epilimnion (Lamb et al. 2007b). The lake highstand lasted until 160 yr BP, just after the driest conditions of the last two millennia were recorded (200 yr BP, average $\delta^{18}O$ of + 6.9 ‰).

8.2.7 Vegetation Change and Anthropogenic Impacts at Lake Hayq

Prior to 2.5 kyr BP the highlands surrounding Lake Hayq were covered in a coniferous forest dominated by *Podocarpus falcatus* and *Juniperus procera* (similar to the Afromontane forest of central Ethiopia today). The occurrence of *Poaceae* pollen also suggests an open forest and/or littoral grasses (Darbyshire et al. 2003). At 2.45 kyr BP the pollen record indicates the *Podocarpus-Juniperus* forest declined rapidly and was replaced by disturbed, secondary bushland vegetation containing common ruderal taxa such as *Rumex* species and the pioneer shrub, *Dodonaea angustifolia*. The peak in the charcoal record indicates the change was driven by

people using fire to clear the forest, most likely to make room for agriculture and for animal grazing (Darbyshire et al. 2003). Ducrotoy (2013) likewise attributed the decrease in Afromontane taxa at 2.4 kyr BP to the onset of pastoral and arable agriculture, using a core taken from the western edge of Lake Hayq. Whilst both these cores overlap temporally with Hayk-01-2010, there is no discernible signal in the palaeolimnological records obtained in this research to suggest anthropogenic impact to the lake, such as the leaching of nutrients from the catchment to lake following deforestation; hypothesis 8 may be accepted. Potentially the effect of human activity may have been supressed in the palaeo-record by the changes in climate, which had a more significant and pronounced effect on the lake. The human population at 2.45 kyr BP would have been significantly smaller in comparison to the current population (in 2007 ~ 12,640 people lived in the town of Hayq; CSA 2007b) and so impacts on the lake, in comparison to the catchment, may not be so immediate as activities such as deforestation and burning. Cultural eutrophication for example is a recent phenomenon caused by the widespread use of industrial fertilisers, and whilst this would be identifiable in modern limnological records, it would not have been an issue in the late Holocene.

By 750 yr BP, the *Podocarpus-Juniperus* had almost completely disappeared from the region (Darbyshire et al. 2003). Between 750 – 550 yr BP, *Dodonaea* and *Rumex* declined, alongside an increase in Poaceae. The conversion of the secondary bushland to grassland was most likely in response to livestock grazing, as well as increased burning to clear land (Darbyshire et al. 2003). Higher abundances of Cyperaceae pollen also suggest the lake may have declined in water level, which allowed sedges to increase in the littoral zone. The appearance of *Pediastrum duplex* signals a change in lake trophic status, although this is the opposite of what would be expected from soil erosion associated with anthropogenic vegetation degradation (Darbyshire et al. 2003).

The period 550 – 250 yr BP saw an increase in the extent of *Juniperus* dominated by dry Afromontane forest. This increase was broadly synchronous across East Africa and most likely signals a regional increase in rainfall, or a local reduction in human impact. Whilst it is believed the *Juniperus* forest was the natural vegetation of the northern Ethiopian highlands it appears to actually have been a relatively recent

development. In the last three centuries Cupressaceae, *Olea* and *Celtis* all declined, signalling a second phase of deforestation and soil erosion most likely due to an increase in agricultural activity and human population density (Darbyshire et al. 2003). Soil erosion consequently increased, although fire may have been a less significant tool used in anthropogenic vegetation change.

8.3 Implications for Future Climate Research

This new record from Lake Hayq adds to a growing body of research, which is improving the fundamental knowledge and understanding of the climatically sensitive and vulnerable region of northern Ethiopia. The use of palaeo-data is well recognised as an important and valuable tool in future climate prediction, as the records and proxies provide data on the climate and environment beyond the timescale of the modern instrumental records (Henderson et al. 2009). Palaeo-data provides a reference against which future climate projections can be tested, refined and evaluated (Henderson et al. 2009).

This record from Lake Hayq identifies historical changes in the climate, environment and lake system during the late Pleistocene and Holocene. In particular, this record highlights the role of global teleconnections in influencing regional East African climate and how site-specific feedback dynamics can affect the local expression of climate over varying timescales within the same geographical region. As such, this information has the potential to fill research gaps identified in the Intergovernmental Panel on Climate Change's (IPCC) fifth assessment report (AR5) (Niang et al. 2014). Regional climate data are imperative for downscaling General Circulation Models (GCM) in order to identify the influence of topography and hydrology and the regional impacts (Niang et al. 2014). This will also inform how long-term changes affect critical ecosystems such as lakes and the highlands, and how this in turn feeds back into the regional climate system (Niang et al. 2014).

Importantly for the climatically vulnerable and drought prone north of Ethiopia, is how future climate change will affect local hydrology, water quality and access, as well as the impact on food security and human well-being (Niang et al. 2014). At Lake Hayq, identifying the range of lake level rise and decline in response to natural climate variability is vital for informing future predictions of how the lake may respond to more or less precipitation or evaporation, and how this will affect other systems. The

ability to manage future access to water is vital to the population of Ethiopia; small scale farmers and pastoralists in particular, are likely to shoulder the majority of negative impacts of climate change such as changing weather regimes, including potentially less precipitation.

Managing access to water for agriculture and livestock is not only fundamental to maintaining life in northern Ethiopia but it may also improve adaptive capacity and reduce vulnerability of other susceptible economic and cultural sectors of Ethiopia. For example, if farmers do not have to move their herds to better grazing grounds, they are less likely to remove their children from school to help, which will improve education and literacy rates across the country (Oxfam 2010). Women are often disproportionately affected by climate change as they will stay at home with the children when the men move away to find new grazing grounds or other means of survival. Women will often eat last and have limited access to their own wealth whilst the men are away and so are more likely to succumb to the hardships of climate change. Improved capacity to adapt will prevent the gender gap from widening any further (Oxfam 2010). Therefore, the ability to predict how access to water in the future may change is vital for not only improving the adaptive capacity of the immediate dependant sectors such as agriculture, but also for reducing the vulnerability of Ethiopian culture, society and the economy, which in turn, has the potential to buffer the detrimental impacts of climate change.

Perhaps most importantly in terms of future climate change modelling is the ability to predict how fast the climate and lake system may respond, which will inform the timescale for response and adaptation. At Lake Hayq, the high-resolution study of the termination of the African Humid Period provides a reference for how quickly the lake system may respond to natural climate variability on a multi-decadal scale, which has the potential to be amplified or supressed under anthropogenic climate change. This may inform current research initiatives such as Future Climate for Africa (FCFA), a five year international project funded by the UK`s Department for International Development (DFID) and the Natural Environment Research Council (NERC) (http://futureclimateafrica.org/). The research aims to improve understanding of climate variability and change across sub-Saharan Africa, including East Africa, with the intention of advancing prediction of climate variability and change on 5 to 40

year timescales to improve the capacity for long-term decision making. The ability to identify such short-term changes in a lake system is essential for informing such work and increasing the resilience and adaptability of the local and wider region. The high-resolution study from Lake Hayq may also offer insight into how systems respond in the build-up to a climatic shift through observable 'flickering' (although this is only speculative in the observations), which has the potential to serve as a warning signal in future climate observations.

8.4 Methodological Considerations

The proxies used in this study have provided a quantitative and qualitative record of the palaeolimnology of Lake Hayq since the late Pleistocene. Significant changes have been identified in the biological, geochemical, lithological and elemental proxies, which with the use of quantitative analyses, have been interpreted in terms of limnological variability in response to climate change. This has provided a comprehensive, detailed record of the changes in climate and environment in the Lake Hayk basin over the past ~ 15.6 cal kyr BP.

It is evident however, that different proxies have diverging responses to climatic variability. It has been a common feature of the elemental profiles to indicate a climatic transition of different magnitude, duration and timing to the diatom and pigment records. For example, the wet period between ~ 2,900 – 2,550 cal yr BP indicated by the elemental records is not found in the diatom record. Similarly, the elemental record suggests the termination of the African Humid Period began approximately 600 cal years earlier than changes observed in the diatom and pigment data. Such discrepancies between proxies has already been identified as an issue affecting East African palaeolimnology (see Chapter 3, 3.6; Johnson et al. 2004; Konecky et al. 2011; Garcin et al. 2012; Junginger et al. 2013; Forman et al. 2014). In this research, emphasis has been placed on diatoms given their power as an ecological indicator (see Chapter 4, 4.4.3), as well as their widespread usage across East Africa, which has assisted making comparisons between sites. By using a multi-proxy approach, combining biological, geochemical, lithological and elemental proxies, from both the lake and catchment, strength is given to interpretations made by independently confirming the climatic sensitivity of the Lake Hayq basin. Whilst it is not possible to solve the discrepancies between proxies –

diatom and elemental proxies will continue to respond differently given their fundamental variability – by combining multiple proxies, it is possible to gain a comprehensive understanding of how the entire lake system, including its' catchment, was operating and functioning at different times.

The development of the diatom-inferred conductivity model to include European sites containing *Cyclotella ocellata*, has attempted to improve the robustness and predictive capacity (based purely on the statistical output) of the conductivity reconstruction at Lake Hayq by compensating for the inherent bias caused by this taxon in the African training set (Chapter 4, 4.6.4). The model could be improved by incorporating more analogues from the European combined TP training set to increase the conductivity gradient coverage further. It appears though the model has improved the reconstruction sufficiently enough to indicate low conductivity during *Cyclotella ocellata* dominated time periods, as expected, given the modern day distribution and ecological tolerances of the taxon. An alternative would have been to exclude *Cyclotella ocellata* from the transfer function. Experiments by Chalié and Gasse (2002b) and Marshall et al. (2009) (Fig. 8.5) indicate a high degree of similarity between including and excluding the taxon from a transfer function when calculating diatom-inferred conductivity, despite its underrepresentation in the modern day training set. However, it was deemed worthwhile by the author to attempt to improve the predictive capacity of the transfer function given the overwhelming dominance and significance of the taxon in sections of the sediment record, rather than accept the inherent bias. Three-dimensional modelling of Lake Hayq's morphometry may strengthen the diatom-based interpretations by enabling a conceptual understanding of how diatom habitat areas respond to climatic driven changes in lake depth and area, particularly given the lakes steeply shelving form (Stone and Fritz 2004).

This research has been affected by methodological and technical constraints. Core 7B for example, could not be scanned by the Itrax® core scanner due to the machine requiring maintenance abroad. Furthermore, the sediment record is incomplete (the most recent ~ 1.3 cal kyr BP are missing from the record) and so a continuous record of change throughout the Holocene is not available from the core. The core HYK99-1 collected by Lamb et al. (2007b) does cover this missing time period,

although stable oxygen and carbon isotope analysis is the primary proxy used, which is not directly comparable to the Hayk-01-2010 proxies (diatoms are also analysed in HYK99-1 but interpretation may require caution [see 8.4.1]). Despite these limitations, every effort has been made to produce an accurate and precise reconstruction of the environmental and climatic changes that have occurred over the past ~ 15.6 cal kyr BP. For example, replicate counting of diatom samples were used to identify within sample variability (average of 2.82 %) and error, which was found to vary between taxa. Within sample variability was not found to affect the abundance of taxa or interpretation of the diatom record, including the high-resolution section across the termination of the African Humid Period.

At the time of writing, four additional sediment samples were awaiting chronological analysis using luminescence dating at Aberystwyth University by Dr Helen Roberts. Fine grained (4 – 11 μm in diameter), polymineral material will be used for dating in order to improve the chronology of the core between 311.0 – 206.5 cm (~ 7.2 – 2.5 cal kyr BP), a section of sediment originally believed to pertain to the 4.2 event. These additional dates will increase confidence in the chronological model for Hayk-01-2010 further. As previously discussed (see Chapter 3, 3.2) bulk dating of organic sediment is problematic, given the potential to be affected by various sources of error. Caution should be used when interpreting the timing of events presented in this thesis; Blaauw et al. (2011) estimate age offsets of 200 – 450 years for dating of bulk organic carbon samples from Lake Challa. Potentially, the dates obtained in this study at Lake Hayq may be affected in a similar way. Luminescence dating of additional samples therefore, will improve the current age-depth model.

8.4.1 The Diatom Record from HYK99-1 The dominant planktonic taxa identified in core HYK99-1 was *Aulacoseira ambigua* (~ 10 – 100 %), except in the uppermost sample where it was absent (Lamb et al. 2007b). *Aulacoseira granulata* was found in low abundances (< 15 %) throughout the sediment core. Whilst the two taxa are known to occur simultaneously within the same lake system (Stager et al. 1997; 2003), it seems highly unlikely that such a rapid, significant switch between dominance would have occurred without evidence of it also being observed in Hayk-01-2010, given the ~ 1000 year overlap between the two cores. *Aulacoseira ambigua* was only identified in Hayk-01-2010 in five samples, all older than the overlapping section, where it accounted for 0.3 – 1.9 % of valves.

The identification of *Aulacoseira granulata* var. *angustissima* in Hayk-01-2010 was verified by colleagues at Loughborough University. Separation spines were evident, clearly distinguishing *Aulacoseira granulata* var. *angustissima* from *Aulacoseira ambigua* (see Plate I). Efforts were made to obtain the original diatom slides prepared from HYK99-1 but they were unavailable. Therefore, whilst it is not possible to verify the identification of the *Aulacoseira* taxon in HYK99-1, it can be confidently stated that *Aulacoseira granulata* var. *angustissima* was present in Hayk-01-2010.

8.4.2 Defining Abrupt Climate Change One arising issue from the current literature is how to define a climatic transition in terms of its abruptness. The US National Research Council (NRC) formally define abrupt climate change as,

'…when the climate system is forced to cross some threshold, triggering a transition to a new state at a rate determined by the climate system itself and faster than the cause. The cause may be chaotic and thus undetectably small' (NRC 2002:14).

This definition is mostly applied in terms of the effect of abrupt climate change on society, human perturbations and anthropogenic forcing and does not include the intricate responses by lake systems to climate and environmental changes (Hulme 2003; Lenton et al. 2008). Defining a climatic transition beyond the need for human consideration differs, being based largely on various proxy records from a multitude of sources, all with varying responses over different time periods. For example, until recently the formal subdivision of the Holocene had not been agreed upon and inconsistencies across the literature caused confusion and limited direct comparisons between records (Walker et al. 2012).

In African palaeoclimate research, the termination of the African Humid Period in terms of its rapidity is open to interpretation, based on the range of data from various proxy records. The termination is loosely described as either gradual, taking several millennia, or abrupt, taking place within several centuries (deMenocal et al. 2000; Fleitmann et al. 2003; Asrat et al. 2007; Kropelin et al. 2008; Tierney and deMenocal 2013). The question arises though, at what point does abrupt become gradual? Would 900 – 950 years duration for example, be a gradual or abrupt transition?

Tierney and deMenocal (2015) describe the average duration for termination, based on hydrogen isotopic composition of leaf waxes (δD_{wax}), as 280 – 490 years in terms of being abrupt, whereas deMenocal et al. (2000) describe geological evidence documenting the termination over one millennia from 6.0 – 5.0 kyr BP as 'relatively abrupt' (deMenocal et al. 2000: 348). This contradicts the vague termination and leads to a further question; how many millennia constitute gradual? This lack of clarity is evidently open to interpretation in the literature; Marshall (2006) describes the transition from the African Humid Period towards Holocene aridity at Lake Ashenge as 'not so abrupt' (Marshall 2006: 231), but Marshall et al. (2009) describe the same transition as abrupt (for the purpose of comparison to Lake Hayq, the more recent interpretation of an abrupt termination at Lake Ashenge is cited [Marshall et al. 2011]). Interpretation is therefore, clearly based on human perception of time, which is not always quantitative, and how the rate of change for different proxy records is perceived.

Formally defining what is meant by an abrupt change in terms of duration of termination of the African Humid Period may be useful in order to ensure consistency of interpretations. This may improve understanding of regional and continental hydroclimate, as well as by how much the effect of non-linear feedbacks (vegetation cover, soil moisture and albedo) can speed up or slow down a response.

8.5 Conclusion

The palaeolimnological record indicates that Lake Hayq is a climatically sensitive waterbody, which has responded to climatic and environmental variability during the course of the late Pleistocene and Holocene. Evidence of changes in the physical lake morphometry (lake depth and surface area) is apparent, as are changes in the biological, lithological and chemical properties of the waterbody. Regionally, Lake Hayq appears to have been affected by many of the same high-latitude, glacial-interglacial dynamics and sub-millennial shifts in climate found in other palaeolimnological records from across East Africa and the wider study region. Tentative evidence of Heinrich Event 1 and the onset and termination of the African Humid Period are found in the Lake Hayq records. However, there is no evidence of

a hydrological response to the Younger Dryas Stadial at Lake Hayq and in contrast to other subtropical African waterbodies, the lake is at a highstand during this time. Differences in the timing and expression of response to these climatic events have not been synchronous between Lake Hayq and other lakes (beyond any dating errors), indicating regional climatic heterogeneity; hypothesis 7 is rejected as a result. Positive feedback mechanisms have been postulated as possible causes for the variability observed between sites. The data obtained from Lake Hayq have the potential to inform future climate change modelling and prediction by identifying the natural range of lake response to such variability. This is of critical importance to the climatically sensitive and vulnerable north of Ethiopia.

Chapter 9
Conclusion.

9.1 Introduction

This thesis has aimed to present a high-resolution, detailed paleolimnological reconstruction of changes to the environment and climate of the north-central Ethiopian highlands since the late Pleistocene, by applying a multi-proxy approach to a continuous sediment record (Hayk-01-2010) from Lake Hayq. Based on the biological, geochemical, lithological and elemental proxies and analyses used, quantitative palaeolimnological evidence has been obtained from the sediment, which has been successfully used to infer changes in the lake system. These records have not only provided reliable evidence of local changes to the environment and climate, but have allowed for wider comparison to records from Ethiopia, the Horn of Africa and East Africa during the late Pleistocene, identifying how long- and short-term climate trends have been expressed at different sites since the Last Glacial Maximum.

9.2 The Palaeolimnology of Lake Hayq

The palaeolimnological evidence suggests that Lake Hayq was experiencing a lowstand in response to extremely arid conditions, which began prior to ~ 15.6 cal kyr BP and lasted until ~15.1 cal kyr BP. This lowstand coincides with the timing of Heinrich Event 1 (~ 18.0 – 15.0 kyr BP) in the North Atlantic, as well as a mega-drought in East Africa, which saw the displacement of the Intertropical Convergence Zone (ITCZ) southwards and weakening of the Afro-Asian rainfall systems (Verschuren et al. 2009; Marshall et al. 2011; Stager et al. 2011; Barker et al. 2013). Lakes across East Africa document a fall in water level at this time and in some cases became desiccated (Stager et al. 1986; Talbot and Livingstone 1989; Lamb et al. 2007a; Marshall et al. 2009; Barker et al. 2013). It is most likely that this is the cause of the Lake Hayq lowstand.

More humid, wetter conditions occurred between ~ 15.1 – 14.8 cal kyr BP, which saw a lake begin to develop at the core site, dominated by pioneer diatom taxa. This positive shift towards a wetter climate is interpreted as the reactivation of the African-

Indian monsoon system, attributed to an increase in Northern Hemisphere summer insolation; this marks this start of the African Humid Period at Lake Hayq (Prell and Kutzbach 1987; Adkins et al. 2006). However, the wet, humid conditions appear to have been cut short as a shift back towards aridity is documented in the palaeolimnological records between ~ 14.7 – 12.3 cal kyr BP. This contrasts to the majority of other tropical lake sites across Ethiopia and East Africa, which continued refilling during this time (Gasse 2000). The aridity at Lake Hayq is interpreted as a manifestation of changes to the Indian Ocean monsoon system caused by variability in the Atlantic Meridional Overturning Circulation, combined with site-specific mechanisms, which affected the delivery of monsoon precipitation to Lake Hayq (Berke et al. 2014).

The African Humid Period resumed at Lake Hayq at ~ 12.3 cal kyr BP. The palaeolimnological record indicates that the lake was recolonised by pioneer diatom taxa as the water level began to increase at the core site, and saw fluctuations in nutrient availability as the lake system established and opened. Lake level maximum was reached between ~ 12.0 – 10.0 cal kyr BP, after which Lake Hayq remained fresh, deep, productive and meromictic. There is evidence of a gradually declining lake level with time as the rain belts migrated southward, but overall the conditions identified at Lake Hayq during the early to mid-Holocene are synchronous with records from across East and North Africa and the Mediterranean (Rholing and Hilgen 1991; Rossignol-Strick 1985; Bar-Matthews et al. 2000; Gasse 2000). No evidence of the sub-millennial 8.2 event is found in the Lake Hayq palaeolimnology.

A high-resolution study of the termination of the African Humid Period indicates that Lake Hayq experienced a (tentatively interpreted) abrupt end to wet conditions between ~ 5.2 – 4.6 cal kyr BP, based on the diatom and pigment records, which saw several drops in lake level before the full onset of aridity. In the build-up to this shift in climate, there is potential evidence of climatic ‘flickering’, as the lake system switched back and forth between alternative states. This serves potentially as an early warning for a disturbance to the system (Brock and Carpenter 2010; Dakos et al. 2012; Wang et al. 2012; Dakos et al. 2013). In combination with other records from across Africa and the Mediterranean, the Lake Hayq record indicates that there was no distinct geographic trend in the timing of the termination of the African Humid

Period, highlighting the heterogeneous pattern of regional response to this climatic event. The termination at Lake Hayq was neither early nor late in comparison to other records from Ethiopia, the Horn of Africa or subtropical Africa,

The termination of the African Humid Period culminated in a late Holocene lowstand at Lake Hayq from ~ 3.9 – 2.2 cal kyr BP. There is no palaeolimnological evidence of the 4.2 event. At ~ 2.2 cal kyr BP a return to wetter conditions occurred at Lake Hayq, evidenced by the dominance of planktonic diatom taxa at the core site, which lasted until at least ~ 1.3 cal kyr BP. The Lake Hayq record is most similar to Lake Ashenge at this time and provides additional support for Butzer's (1981) hypothesis of an extended growing season in northern Ethiopia caused by a northward extension of the ITCZ. There is palaeolimnological evidence of climate variability during this time however, and the lake most likely experienced short-term rises and declines, as well as changes in volume and surface area, in response to variability in the precipitation-evaporation ratio. The Lake Hayq record does not provide any discernible evidence for anthropogenic impact to the catchment.

The Hayk-01-2010 sediment record ends at ~ 1350 cal yr BP. Other records from the late Holocene at Lake Hayq are available, which provide an overview of climatic and environmental changes, including vegetation change, as well as anthropogenic activity (Darbyshire et al. 2003; Lamb et al. 2007b; Ghinassi et al. 2012).

9.3 An Evaluation of Lake Hayq's Climatic Sensitivity

The palaeolimnological records obtained from Lake Hayq using a multi-proxy approach have successfully provided high-resolution evidence of millennial to multi-decadal variability in the lake. Changes identified in the lake system since ~ 15.6 cal kyr BP includes variability in nutrient availability, productivity and trophic state, stratification and overturn, catchment weathering and erosion, preservation and most importantly in terms of identifying climatic signals, changing lake level (and by association volume and surface area, as well as changes in catchment size) and conductivity. These changes in the palaeolimnology since the late Pleistocene indicate that the climate signal at Lake Hayq has been expressed indirectly through changes in lake hydrology and associated catchment processes and can be used to

infer variability in the local environment and climate of the north-central Ethiopian highlands; hypothesis 6 is accepted.

At the millennial scale, the palaeolimnological records indicate that the local climate at Lake Hayq has been sensitive to high-latitude glacial conditions and paced over thousands of years by variations in insolation caused by changes in Earth's orbital precession (Milankovitch cycles) (Gasse 2000; Trauth et al. 2003). Hydrological changes have been driven by ocean surface temperature conditions and ocean-atmosphere and ocean-land interactions, which caused variability in ocean heat transport into and away from the tropics, affecting precipitation deliver to the African continent (Gasse 2000). As such, Lake Hayq experienced the same transitions from arid to humid and humid to arid as experienced by other lake sites across East Africa since the Last Glacial Maximum, including high-magnitude events such as Heinrich Event 1 (~ 18.0 – 15.0 kyr BP), the onset and termination of the African Humid Period (~ 15.0 – 5.0 kyr BP) and the Younger Dryas Stadial (~ 12.8 – 11.6 kyr BP).

Though broadly synchronous, there are discrepancies in the precise timing and expression of climatic events and comparison of the Lake Hayq sedimentary record to other sites from the region shows variability in the nature of climate shifts. Minor discrepancies may be attributed to chronological issues between sites which, as demonstrated, has been an issue affecting the chronology of this record (see Chapter 4, 4.5) and that of Done Ella (Verschuren 2003). Beyond this, response to climatic change reflects the inherent climatic sensitivity of individual lake basins. Lake Hayq is a closed lake, making it sensitive to changes in the precipitation-evaporation ratio (see Table 4.1 for Lake Hayq's water balance estimates). It most likely acted as an open system during the early Holocene however, receiving overflow and overflowing itself. Morphometric differences in the lake and its' basin, including inflow, outflow and the role of groundwater, will also affect a sites ability to record a climatic change in its sediment, as well as its ability to buffer or amplify the effects of such shifts (Burrough and Thomas 2009; Olaka et al. 2010). Such differences are the likely cause of discrepancies between the Lake Hayq, Tana and Ashenge records, despite their proximity to one another, as well as discrepancies between Lake Hayq and other sites across Ethiopia and East Africa.

The role of local, non-linear mechanisms has been highlighted in this study as another crucial aspect affecting a lakes' climate sensitivity. Positive feedbacks caused by vegetation cover in particular, surface albedo, soil moisture and precipitation have been shown to reduce/enhance the efficiency of the initial radiation forcing of the monsoon beyond the response threshold by orbital forcing alone (Claussen et al. 1999; deMenocal et al. 2000). Understanding the role of these mechanisms is vital for identifying the full nature of climate change and the comprehensive impact this has on the system.

The ability of a proxy to adequately respond to climatic-hydrological change and be preserved in the sediment is another issue affecting climate sensitivity. Responses are often complex and not always directly related to climate or hydrology (Verschuren 2003). Even if a response does occur, post-depositional processes and preservation may modify or remove the signal from the sedimentary archive. For example, diatoms and photosynthetic pigments were affected by preservation during the late Pleistocene (~ 15.5 – 15.1 cal kyr BP and ~ 14.8 – 12.3 cal kyr BP) but climate data was still obtained from the elemental responses. This highlights the advantages and significance of using a multi-proxy approach for not only gaining more data, but for independently confirming and verifying a climate signal when discrepancies between proxies occur.

Further work to expand this investigation would be useful at Lake Hardibo, the source of potential overflow into Lake Hayq. Identifying if and when overflow occurred and ceased would improve the reliability of inferences made in this thesis by improving current understanding of Lake Hayq's climatic sensitivity. Increasing the sample time resolution during the early to mid-Holocene would also be beneficial for improving understanding of how lake sensitivity is expressed in the build-up to a significant climatic shift by identifying whether the climate 'flickering' observed is a true signal of change. Utilising a wider range of proxies, such as pollen analysis, stable isotope analysis and branched glycerol dialkyl glycerol tetraether (brGDGT) paleotemperature reconstructions, would invariably expand the data available from which interpretations may be made, and provide additional independent verification of limnological and climatic changes. However, introducing a greater number of proxies may also increase the discrepancies between records when responses

diverge. Sediment cores collected closer to the shoreline may constrain lake level changes and potentially improve dating with the presence of terrestrial macrofossils that have not been destroyed by transportation processes to the deeper lake.

9.4 Final Comments

In conclusion, Lake Hayq is a climatically sensitive lake, which has experienced significant long-term (millennial scale) changes, most significantly in lake depth, over the last ~ 15.6 – 1.3 cal kyr BP. These changes have been driven by high-latitude glacial conditions, paced by variability in orbital precession. As a result, Lake Hayq demonstrated the same general shifts between aridity and humidity as identified in other lake records from across East Africa, including Heinrich Event 1 and the onset and termination of the African Humid Period. There are discrepancies between the records however, caused by site-specific variability in lake sensitivity and positive feedback processes, which have altered the spatial and temporal delivery of precipitation to the tropics. The Lake Hayq palaeo-record therefore indicates that response to climatic events were regionally heterogeneous.

The information obtained from Lake Hayq is important in identifying the natural range of sensitivity and response to climate change for the site. The information gained will improve current understanding and knowledge of the climatically sensitive and vulnerable northern Ethiopia, which will be vital for future regional climate prediction and modelling, as well as preparation for the populations that may be potentially affected. The sedimentary archive may also provide an environmental context for important ethnographic-archaeological research in the region. As such, the Lake Hayq palaeo-record may help bridge knowledge gaps in the currently underrepresented, climatically vulnerable north of Ethiopia.

References.

Aaby, B. and Berglund, B.E. (1986) Characterization of peat and lake deposits, in B.E. Berglund (ed.) *Handbook of Holocene Palaeoecology and Palaeohydrology*. Great Britain: John Wiley and Sons. pp. 231–246.

Aaby, B. and Digerfeldt, G. (1986) Sampling techniques for lakes and bogs, in B.E. Berglund (ed.) *Handbook of Holocene Palaeoecology and Palaeohydrology*. Great Britain: John Wiley and Sons. pp. 181–194.

Adamson, D.A., Gasse, F., Street, F.A. and Williams, M.A.J. (1980) Late Quaternary history of the Nile. *Nature*, 228, 50–55.

Adkins, J., deMenocal, P. and Eshel, G. (2006) The “African humid period” and the record of marine upwelling from excess ^{230}Th in Ocean Drilling Program Hole 658C. *Paleoceanography*, 21, 1–14, PA4203, DOI: 10.1029/2005PA001200.

AlgaeBase (2015) AlgaeBase website. Available at: http://www.algaebase.org/ [Access date: 06/03/2015].

Alley, R.B. (2000) The Younger Dryas cold interval as viewed from central Greenland. *Quaternary Science Reviews*, 19, 213–266.

Alley, R.B. and Clark, P.U. (1999) The deglaciation of the Northern Hemisphere: a global perspective. *AREPS*, 27, 149–182.

Anderson, N.J. (2000) Diatoms, temperature and climate change. *European Journal of Phycology*, 35, 307–314.

Anfray, F. (1968) Aspects de l'archéologie éthiopienne. *Journal of African History*, 9, 345–366.

Anfray, F. (1990) *Les anciens éthiopiens*. Paris: Colin.

Anyah, R.O. and Qiu, W. (2012) Characteristic 20th and 21st century precipitation and temperature patterns and changes over the Greater Horn of Africa. *International Journal of Climatology*, 32, 347–363.

Armitage, S.C., Bristow, C.S. and Drake, N.A. (2015) West African monsoon dynamics inferred from abrupt fluctuations of Lake Mega-Chad. *Proceedings of the National Academy of Sciences*, 112, 8543–8548.

Arthur, J.W. (2002) Pottery use-alteration as an indicator of socioeconomic status: an ethnoarchaeological study of the Gamo of Ethiopia. *Journal of Archaeological Method and Theory*, 9, 331–355.

Arthur, J.W. (2003) Brewing beer: status, wealth and ceramic use alteration among the Gamo of south-western Ethiopia. *World Archaeology*, 34, 516–528.

Asante, M.K. (2009) Gamo religion, in M.K. Asante and A. Mazama (eds.) *Encyclopaedia of African Religion*. USA: SAGE Publications. pp. 281–282.

Ashley, G.M., Ndiema, E.K., Spencer, J.Q.G., Harris, J.W.K. and Kiura, P.W. (2011) Paleoenvironmental context of archaeological sites, implications for subsistence strategies under Holocene climate change, northern Kenya. *Geoarchaeology*, 26, 809–837.

Ashton, P.J. (2002) Avoiding conflicts over Africa's water resources. *Ambio*, 31, 236–242.

Asmare, G. (2005) *Groundwater flow modelling of the Hayq-Ardibo lakes catchment*. MSc thesis. Addis Ababa University.

Asrat, A., Baker, A., Umer, M., Moss, J., Leng, M., Van Calsteren, P. and Smith, C. (2007) A high-resolution multi-proxy stalagmite record from Mechara, southeastern Ethiopia: palaeohydrological implications for speleothem palaeoclimate reconstruction. *Journal of Quaternary Science*, 22, 53–63.

Augustinus, P., Bleakley, N., Deng, Y., Shane, P. and Cochran, U. (2008) Rapid change in early Holocene environments inferred from Lake Pupuke, Auckland City, New Zealand. *Journal of Quaternary Science*, 23, 435–447.

Ayenew, T. (1998) *The hydrogeological system of the Lake District basin, Central Main Ethiopian Rift*. PhD thesis. Free University of Amsterdam.

Ayenew, T. (2007) Water management problems in the Ethiopian rift: Challenges for development. *Journal of African Earth Sciences*, 48, 222–236.

Ayenew, T. (2009) *Natural lakes of Ethiopia*. Ethiopia: Addis Ababa University Press.

Ayenew, T. and Demlie, M. (2004) Bathymetric survey and estimation of the water balance of Lake Ardibo, Northern Ethiopia. *SINET: Ethiopian Journal of Science*, 27, 61–68.

Barber, D.C., Dyke, A., Hillarie-Marcel, C., Jennings, A.E., Andrews, J.T., Kerwin, M.W., Bilodeau, G., McNeely, R., Southon, J., Morehead, M.D. and Gagnon, J.M. (1999) Forcing of the cold event of 8,200 years ago by catastrophic drainage of Laurentide lakes. *Nature*, 400, 344–348.

Bard, K.A., Coltorti, M., Di Blasi, M.C., Dramis, F. and Fattovich, R. (2000) The environmental history of Tigray (Northern Ethiopia) during the Holocene: A preliminary outline. *The African Archaeological Review*, 17, 65–86.

Bard, E., Rostek, F. and Sonzogni, C. (1997) Interhemispheric synchrony of the last deglaciation inferred from alkenone palaeothermometry. *Nature*, 385, 707–710.

Bard, E., Rostek, F., Turon, J.L. and Gendreau, S. (2000) Hydrological impact of Heinrich events in the subtropical northeast Atlantic. *Science*, 289, 1321–1324.

Barker, P.A. (1992) Differential diatom dissolution in Late Quaternary sediments from Lake Manyara, Tanzania: an experimental approach. *Journal of Paleolimnology*, 7, 235–251.

Barker, P.A., Fontes, J.C., Gasse, F. and Druart, J.C. (1994) Experimental dissolution of diatom silica in concentrated salt solutions and implications for paleoenvironmental reconstruction. *Limnology and Oceanography*, 39, 99–110.

Barker, P.A. and Gasse, F. (2003) New evidence for a reduced water balance in East Africa during the Last Glacial Maximum: implication for model-data compassion. *Quaternary Science Reviews*, 22, 823–837.

Barker, P.A., Hurrell, E.R., Leng, M.J., Plessen, B., Wolff, C., Conley, D.J., Keppens, E., Milne, I., Cumming, B.F., Laird, K.R., Kendrick, C.P., Wynn, P.M. and Verschuren, D. (2013) Carbon cycling within an East African lake revealed by the carbon isotope composition of diatom silica: a 25-ka record from Lake Challa, Mt. Kilimanjaro*. Quaternary Science Reviews*, 66, 55–63.

Barker, P.A., Hurrell, E.R., Leng, M.J., Wolff, C., Cocquyt, C., Sloane, H.J. and Verschuren, D. (2011) Seasonality in equatorial climate over the last 25 k.y. revealed by oxygen isotope records from Mount Kilimanjaro. *Geology*, 39, 1111–1114.

Barker, P.A., Roberts, N., Lamb, H.F., van der Kaars, S. and Benkaddour, A. (1994) Interpretation of Holocene lake-level change from diatom assemblages in Lake Sidi Ali, Middle Atlas, Morocco. *Journal of Paleolimnology*, 12, 223–234.

Barker, P.A., Street-Perrott, F.A., Leng, M.J., Greenwood, P.B., Swain, D.L., Perrott, R.A., Telford, R.J. and Ficken, K.J. (2001) A 14,000-year oxygen isotope record from diatom silica in two Alpine lakes on Mt. Kenya. *Science*, 292, 2307–2310.

Barker, P.A., Telford, R., Gasse, F. and Thevenon, F. (2002) Late Pleistocene and Holocene palaeohydrology of Lake Rukwa, Tanzania, inferred from diatom analysis. *Palaeogeography, Palaeoclimatology, Palaeoecology*, 187, 295–305.

Barker, P.A., Telford, R., Merdaci, O., Williamson, D., Taieb, M., Vincens, A. and Gibert, E. (2000) The sensitivity of a Tanzanian crater lake to catastrophic tephra input and four millennia of climate change. *The Holocene*, 10, 303–310.

Barker, P.A., Talbot, M.R., Street-Perrott, F.A., Marret, F., Scourse, J. and Odada, E.O. (2004) Late Quaternary climatic variability in intertropical Africa, in R.W. Battarbee, F. Gasse and C.E. Stickley (eds.) *Past Climate Variability through Europe and Africa*. Dordrecht: Springer. pp. 117–138.

Barker, P.A., Williamson, D., Gasse, F. and Gilbert, E. (2003) Climatic and volcanic forcing revealed in a 50,000-year record from Lake Massoko, Tanzania. *Quaternary Research*, 60, 368–376.

Bar-Matthews, M. and Ayalon, A. (1997) Late Quaternary paleoclimate in the Eastern Mediterranean region from stable isotope analysis of speleothems at Soreq Cave, Israel. *Quaternary Research*, 47, 155–168.

Bar-Matthews, M., Ayalon, A. and Kaufman, A. (2000) Timing and hydrological conditions of Sapropel events in the Eastern Mediterranean, as evident from speleothems, Soreq cave, Israel. *Chemical Geology*, 169, 145–156.

Bastow, R.F. (1960) The diatom flora of the Sudan (concerning the irrigation ditches around Khartom). *The Journal of the Queckett Microscopical Club*, 4, 236–246.

Battarbee, R.W. (1986) Diatom analysis, in B.E. Berglund (ed.) *Handbook of Holocene palaeoecology and palaeohydrology*. Great Britain: John Wiley and Sons. pp. 527–570.

Battarbee, R.W. (1991) Palaeolimnology and climate change, in B. Frenzel and A. Pons (eds.) *Evaluation of Climate Proxy Data in Relation to the European Holocene*. Stuttgart: Gustav Fischer Verlag. pp. 149–157.

Battarbee, R.W. (2000) Palaeolimnological approaches to climate change, with special regard to the biological record. *Quaternary Science Reviews*, 19, 107–124.

Battarbee, R.W, Charles, D.F., Bigler, C., Cumming, B.F. and Renberg, I. (2010) Diatoms as indicators of surface water acidity, in J.P. Smol and E.F. Stoermer (eds.) *The Diatoms: Applications for Environmental and Earth Sciences Second Edition*. New York: Cambridge University Press. pp. 98–121.

Battarbee, R.W., Grytnes, J.A., Thompson, R., Appleby, P.G., Catalan, J., Korhola, A., Birks, H.J.B., Heegaard, E. and Lami, A. (2002) Comparing palaeolimnological and instrumental evidence of climate change for remote mountain lakes over the last 200 years. *Journal of Paleolimnology*, 28, 161–179.

Battarbee, R.W., Jones, V.J., Flower, R.J., Cameron, N.G., Bennion, H., Carvalho, L. and Juggins, S. (2001) Diatoms, in J.P. Smol, H.J.B. Birks and W.M. Last (eds.) *Tracking Environmental Change Using Lake Sediments. Volume 3: Terrestrial, Algal, and Siliceous Indicators*. The Netherlands: Kluwer Academic Publishers. pp. 155–202.

Battarbee, R.W. and Kneen, M.J. (1982) The use of electronically counted microspheres in absolute diatom analysis. *Limnology and Oceanography*, 27, 184–188.

Battarbee, R.W., Mackay, A.W., Jewson, D., Ryves, D.B. and Strum, M. (2005) Differential dissolution of Lake Baikal diatoms: Correction factors and implications for palaeoclimatic reconstruction. *Global and Planetary Change*, 46, 75–86.

Baxter, R.M. and Golobitsch, D.L. (1970) A note on the limnology of Lake Hayq, Ethiopia. *Limnology and Oceanography*, 15, 144–148.

BBC (2000) 'Flashback 1984: Portrait of a famine', 6th April 2000. BBC website. Available at: http://news.bbc.co.uk/1/hi/world/africa/703958.stm [Access date: 08/10/2015].

BBC (2013) ‘Egyptian warning over Ethiopian Nile dam’, 10th June 2013. BBC website. Available at: http://www.bbc.co.uk/news/world-africa-22850124 [Access date: 08/10/2015].

Beadle, L.C. (1981) *The inland waters of tropical Africa. An introduction to tropical limnology*. USA: Longman Group.

Beal, L.M., De Ruijter, W.P.M., Biastoch, A. and Zahn, R. (2011) On the role of the Agulhas system in ocean circulation and climate. *Nature*, 472, 429–436.

Bell, B. (1971) The Dark Ages in ancient history: The first dark age in Egypt. *American Journal of Archaeology*, 75, 1–25.

Ben Khelifa, L. (1989) *Diatomees continentales at paleomillieux du Sud-Tunisien aux Quaternaire superieur*. PhD thesis. Université Paris–Sud.

Bennett, K.D. (1995 – 2007) *psimpoll* and *pscomb* programs for plotting and analysis. Available at: http://www.chrono.qub.ac.uk/psimpoll/psimpoll.html [Access date: 08/10/2015].

Bennett, K.D. (1996) Determination of the number of zones in a biostratigraphical sequence. *New Phytologist*, 132, 155–170.

Benvenuti, M., Bonini, M., Tassi, F., Corti, G., Sani, F., Agostini, A., Manetti, P. and Vaselli, O. (2013) Holocene lacustrine fluctuations and deep CO_2 degassing in the northeastern Lake Langano Basin (Main Ethiopian Rift). *Journal of African Earth Sciences*, 77, 1–10.

Benvenuti, M., Carnicelli, S., Belluomini, G., Dainelli, N., Di Grazia, S., Ferrari, G.A., Iasio, C., Sagri, M., Ventra, D., Atnafu, B. and Kebede, S. (2002) The Ziway-Shala lake basin (main Ethiopian rift, Ethiopia): a revision of basin evolution with special reference to the Late Quaternary. *Journal of African Earth Sciences,* 35, 247–269.

Berger, A.L. (1978) Long-term variations of daily insolation and Quaternary climatic changes. *Journal of Atmospheric Science*, 35, 2362–2367.

Bergner, A.G.N., Trauth, M.H. and Bookhagen, B. (2003) Paleoprecipitation estimates for the Lake Naivasha basin (Kenya) during the last 175 k.y. using a lake-balance model. *Global and Planetary Letters*, 36, 117–136.

Berke, M.A., Johnson, T.C., Werne, J.P., Grice, K., Schouten, S. and Sinninghe Damsté, J.S. (2012b) Molecular records of climate variability and vegetation response since the Late Pleistocene in the Lake Victoria basin, East Africa. *Quaternary Science Reviews*, 55, 59–74.

Berke, M.A., Johnson, T.C., Werne, J.P., Livingstone, D., Grice, K., Schouten, S. and Sinninghe Damsté, J.S. (2014) Characterization of the last deglacial transition in tropical East Africa: Insights from Lake Albert. *Palaeogeography, Palaeoclimatology, Palaeoecology*, 409, 1–8.

Berke, M.A., Johnson, T.C., Werne, J.P., Schouten, S. and Sinninghe Damsté, J.S. (2012a) A mid-Holocene thermal maximum at the end of the African Humid Period. *Earth and Planetary Science Letters*, 351–352, 95–104.

Berrang-Ford, L., Ford, J.D. and Paterson, J. (2011) Are we adapting to climate change? *Global Environmental Change*, 21, 25–33.

Beuning, K.R.M., Kelts, K. and Stager, J.C. (1998) Abrupt climatic changes associated with the arid Younger Dryas interval in Africa, in J.T. Lehman (ed.) *Environmental Change and Response in East African Lakes*. The Netherlands: Kluwer Academic Publishers. pp. 147–156.

Beuning, K.R.M., Talbot, M. and Kelts, K. (1997) A revised 30,000-year palaeoclimatic and palaeohydrologic history of Lake Albert, East Africa. *Palaeogeography, Palaeoclimatology, Palaeoecology*, 136, 259–279.

Beyene, T., Lettenmaier, D.P. and Kabat, P. (2010) Hydrologic impacts of climate change on the Nile River Basin: Implications of the 2007 IPCC scenarios. *Climatic Change*, 100, 433–461.

Bidle, K.D. and Azam, F. (1999) Accelerated dissolution of diatom silica by marine bacterial assemblages. *Nature*, 397, 508–512.

Bidle, K.D., Brzezinski, M.A., Long, R.A., Jones, J.L. and Azam, F. (2003) Diminished efficiency in the oceanic silica pump caused by bacteria-mediated silica dissolution. *Limnology and Oceanography*, 48, 1855–1868.

Bidle, K.D., Manganelli, M. and Azam, F. (2002) Regulation of oceanic silicon and carbon preservation by temperature control on bacteria. *Science*, 298, 1980–1984.

Birks, H.J.B. (1998) Numerical tools in paleolimnology – progress, potentialities, and problems. *Journal of Paleolimnology*, 20, 307–332.

Birks, H.J.B. and Gordon, A.D. (1985) *Numerical Methods in Quaternary Pollen Analysis*. London: Academic Press.

Birks, H.J.B., Line, J.M., Juggins, S., Stevenson, A.C. and ter Braak, C.J.F. (1990) Diatoms and pH reconstruction. *Philosophical Transactions of the Royal Society of London B*, 327, 263–278.

Björck, S., Bennike, O., Possnert, G., Wohlfarth, B. and Digerfeldt, G. (1998) A high-resolution ^{14}C dated sediment sequence from southwest Sweden: age comparisons between different components of the sediment. *Journal of Quaternary Science*, 13, 85–89.

Björk, S. and Wohlfarth, B. (2001) ^{14}C Chronostratigraphic techniques in palaeolimnology, in W.M. Last and J.P. Smol (eds.) *Tracking Environmental Change Using Lake Sediments. Volume 1: Basin Analysis, Coring, and Chronological Techniques*. The Netherlands: Kluwer Academic Publishers. pp. 205–260.

Blaauw, M. (2010) Methods and code for 'classical' age-modelling of radiocarbon sequences. *Quaternary Geochronology*, 5, 512–518.

Blaauw, M., van Geel, B., Kristen, I., Plessen, B., Lyaruu, A., Engstrom, D.R., van der Plicht, J. and Verschuren, D. (2011) High-resolution 14C dating of a 25,000-year lake-sediment record from equatorial East Africa. *Quaternary Science Reviews*, 30, 3043–3059.

Blais, J.M and Kalff, J. (1995) The influence of lake morphometry on sediment focusing. *Limnology and Oceancgraphy*, 40, 582–588.

Blanchet, C.L., Tjallingii, R., Frank, M., Lorenzen, J., Reitz, A., Brown, K., Feseker, T. and Bruckmann, W. (2013) High- and low-latitude forcing of the Nile River regime during the Holocene inferred from laminated sediments of the Nile deep-sea fan. *Earth and Planetary Science Letters*, 364, 98–110.

Blunier, T., Chappellaz, J., Schwander, J., Dallenbach, A., Stauffer, B., Stocker, T.F., Raynaud, D., Jouzel, J., Clausen, H.B., Hammer, C.U. and Johnsen, S.J. (1998) Asynchrony of Antarctic and Greenland climate change during the last glacial period. *Nature*, 394, 739–743.

Boës, X., Rydberg, J., Martinez-Cortizas, A., Bindler, R. and Renberg, I. (2011) Evaluation of conservative lithogenic elements (Ti, Zr, Al, and Rb) to study anthropogenic element enrichments in lake sediments. *Journal of Paleolimnology*, 46, 75–87.

Boko, M., Niang, I., Nyong, A., Vogel, C., Githeko, A., Medany, M., Osman-Elasha, M., Tabo, R. and Yanda, P. (2007) Africa, in M.L. Parry, O.F. Canziani, J.P. Palutikof, P.J. van der Linden and C.E. Hanson (eds.) *Climate Change 2007: Impacts, Adaptation and Vulnerability. Contribution of Working Group II to the Fourth Assessment Report of the Intergovernmental Panel on Climate Change.* Cambridge: Cambridge University Press. pp. 433–467.

Bonnefille, R., Riollet, G., Buchet, G., Icole, M., Lafont, R. and Arnold, M. (1995) Glacial/interglacial record from tropical Africa, high-resolution pollen and carbon data at Rusaka, Burundi. *Quaternary Science Reviews*, 14, 917–936.

Bonnefille, R. and Umer, M. (1994) Pollen inferred climatic fluctuations in Ethiopia during the last 3000 years. *Palaeogeography, Palaeoclimatology, Palaeoecology*, 109, 331–343.

Booth, R.K., Jackson, S.T., Forman, S.L., Kutzbach, J.E., Bettis III, E.A., Kreigs, J. and Wright, D.K. (2005) A severe centennial-scale drought in mid-continental North America 4200 years ago and apparent global linkages. *The Holocene*, 15, 321–328.

Borchardt, S. and Trauth, M.H. (2012) Remotely-sensed evapotranspiration estimates for an improved hydrological modelling of the early Holocene mega-lake Suguta, northern Kenya Rift. *Palaeogeography, Palaeoclimatology, Palaeoecology*, 361, 14–20.

Box, M.R., Krom, M.D., Cliff, R.A., Bar-Matthews, M., Almogi-Labin, A., Ayalon, A. and Paterne, M. (2011) Response of the Nile and its catchment to millennial-scale climate change since the LGM from Sr isotopes and major elements of East Mediterranean sediments. *Quaternary Science Reviews*, 30, 431–442.

Boyle, J.F. (2001) Inorganic Geochemical Methods in Palaeolimnology, in W.M. Last and J.P. Smol (eds.) *Tracking Environmental Change Using Lake Sediments. Volume 2: Physical and Geochemical Methods*. The Netherlands: Kluwer Academic Publishers. pp. 83–142.

Bradshaw, E.G., Anderson, N.J., Jensen, J.P. and Jeppesen, E. (2002) Phosphorous dynamics in Danish lakes and the implications for diatom ecology and palaeoecology. *Freshwater Biology*, 47, 1963–1975.

Brandt, S.A., Fisher, E.C., Hildebrand, E.A., Vogelsang, R., Ambrose, S.H., Lesur, J. and Wang, H. (2012) Early MIS 3 occupation of Mochena Borago rockshelter, southwest Ethiopian highlands: implications for Late Pleistocene archaeology, paleoenvironments and modern human dispersals. *Quaternary International*, 274, 38–54.

Brandt, S.A., Spring, A., Heibsch, C., McCabe, J.T., Tabogie, E., Diro, M., Wolde-Michael, G., Yntiso, G., Shigeta, M. and Tesfaye, S. (1997) *The 'tree against hunger', enset-based agricultural systems in Ethiopia*. Washington: American Association for the Advancement of Science with Awassa Agricultural Research Center, Kyoto University Center for African Area Studies and University of Florida.

Brock, W.A. and Carpenter, S.R. (2010) Interacting regime shifts in ecosystems: implication for early warnings. *Ecological Monographs*, 80, 353–367.

Broecker, W.S. (1998) Paleocean circulation during the last deglaciation: a bipolar seesaw? *Paleoceanography*, 13, 119–121.

Brooks, K., Scholz, C.A., King, J.W., Peck, J., Overpeck, J.T., Russell, J.M. and Amoako, P.Y.O. (2005) Late-Quaternary lowstands of lake Bosumtwi, Ghana: evidence from high-resolution seismic-reflection and sediment-core data. *Palaeogeography, Palaeoclimatology, Palaeoecology,* 216, 235–249.

Brown, S.R. (1968) Bacterial carotenoids from freshwater sediments. *Limnology and Oceanography*, 13, 233–241.

Brown, E.T. (2011) Lake Malawi's response to "megadrought" terminations: Sedimentary records of flooding, weathering and erosion. *Palaeogeography, Palaeoclimatology, Palaeoecology*, 303, 120–125.

Brown, S.R. and Colman, B. (1963) Oscillaxanthin in lake sediments. *Limnology and Oceanography*, 8, 352–353.

Brown, J., Collins, M., Tudhope, A.W. and Toniazzo, T. (2008) Modelling mid-Holocene tropical climate and ENSO variability: towards constraining predictions of future change with palaeo-data. *Climate Dynamics*, 30, 19–36.

Brown, E.T. and Fuller, C.H. (2008) Stratigraphy and tephra of the Kibish formation, southwestern Ethiopia. *Journal of Human Evolution*, 55, 366–403.

Brugam, R.B., Mckeever, K. and Kolesa, L. (1998) A diatom-inferred water depth reconstruction for an Upper Peninsula, Michigan, lake. *Journal of Paleolimnology*, 20, 267–276.

Bunting, L., Leavitt, P.R., Gibson, C.E., McGee, E.J. and Hall, V.A. (2007) Degradation of water quality in Lough Neagh, Northern Ireland, by diffuse nitrogen flux from a phosphorus-rich catchment. *Limnology and Oceanography*, 52, 354–369.

Burnett, A.P., Soreghan, M.J., Scholz, C.A. and Brown, E.T. (2011) Tropical East African climate change and its relation to global climate: A record from Lake Tanganyika, Tropical East Africa, over the past 90+ kyr. *Palaeogeography Palaeoclimatology Palaeoecology*, 303, 155–167.

Burrough, S.L. and Thomas, D.S.G. (2009) Geomorphological contributions to paleolimnology on the African continent. *Geomorphology*, 103, 285–298.

Bush, A.G.B. and Philander, S.G.H (1998) The role of ocean-atmosphere interactions in tropical cooling during the Last Glacial Maximum. *Science*, 279, 1341–1344.

Butzer, K.W. (1980) The Holocene lake plains of north Rudolph, East Africa. *Physical Geography*, 1, 42–58.

Butzer, K.W. (1981) Rise and Fall of Axum, Ethiopia: A geo-archaeological interpretation. *American Antiquity*, 46, 471–495.

Butzer, K.W., Isaac, G.L., Richardson, J.L. and Washbourn-Kamau, C. (1972) Radiocarbon dating of East African lake levels. *Science*, 175, 1069–1076.

Carstensen, J., Telford, R.J. and Birks, H.J.B. (2013) Diatom flickering prior to regime shift. *Nature*, 498, E11–E12.

Casson, L. (1989) *The Periplus Maris Erythraei: Text With Introduction, Translation, and Commentary.* USA: Princeton University Press.

Castañeda, I.S., Werne, J.P. and Johnson, T.C. (2009) Influence of climate change on algal community structure and primary productivity of Lake Malawi (East Africa) from the Last Glacial Maximum to present. *Limnology and Oceanography*, 54, 2431–2447.

Chalié, F. (1995) Paléoclimats du bassin Tanganyika Sud au cours des 25 derniers milleans. Reconstruction quantitative per le traitement statistique des données polliniques. *Comptes Redus del' Académie des Sciences, Paris, Série 2,* 320, 205–208.

Chalié, F. and Gasse, F. (2002a) A 13,500 year diatom record from the tropical East African Rift Lake Abiyata (Ethiopia). *Palaeogeography, Palaeoclimatology, Palaeoecology,* 187, 259–284.

Chalié, F. and Gasse, F. (2002b) Late Glacial-Holocene diatom record of water chemistry and lake level change from the tropical East African Rift Lake Abiyata (Ethiopia). *Palaeogeography, Palaeoclimatology, Palaeoecology,* 187, 259–283.

Chen, N., Bianchi, T.S., McKee, B.A. and Bland, J.M. (2001) Historical trends of hypoxia on the Louisiana shelf: application of pigments as biomarkers. *Organic Geochemistry*, 32, 543–561.

Cheng, H., Fleitmann, D., Edwards, R.L., Wang, X., Cruz, F.W., Auler, A.S., Mangini, A., Wang, Y., Kong, X., Burns, S.J. and Matter, A. (2009) Timing and structure of the 8.2 kyr B.P. event inferred from δ18O records of stalagmites from China, Oman and Brazil. *Geology*, 37, 1007–1010.

Cheung, W.H., Senay, G.B. and Singh, A. (2008) Trends and spatial distribution of annual and seasonal rainfall in Ethiopia. *International Journal of Climatology*, 28, 1723–1734.

Cholnoky, B.J. (1964) Die Diatomeenflora einiger Gewässer der Ruwenzori-Genirge in Zentralafrika. *Nova Hedwigia*, 8, 55–101.

Christensen, J.H., Hewitson, B., Busuioc, A., Chen, A., Gao, X., Held, I., Jones, R., Koli, R.K., Kwon, W.T., Laprise, R., Rueda, V.M., Mearns, L., Menéndez, C.G., Räisänen, J., Rinke, A., Sarr, A. and Whetton, P. (2007) Regional climate projections, in S. Solomon, D. Qin, M. Manning, Z. Chen, M. Marquis, K.B. Averyt, M. Tignor and H.L. Miller (eds.) *Climate Change 2007: The Physical Science Basis. Contribution of Working Group I to the Fourth Assessment Report of the Intergovernmental Panel on Climate Change*. Cambridge: Cambridge University Press. pp. 847–940.

Ciais, P., Petit, J.R., Jouzel, J., Lorius, C., Barkov, N.I., Lipenkov, V. and Nicolaiev, V. (1992) Evidence for an early Holocene climatic optimum in the Antarctic deep ice-core record. *Climate Dynamics*, 6, 169–177.

Ciampalini, R., Billi, P., Ferrari, G., Borselli, L. and Follian, S. (2012) Soil erosion induced by land use changes as determined by plough marks and field evidence in the Aksum area (Ethiopia). *Agriculture, Ecosystems and Environment*, 146, 197–208.

Clark, P.U. and Mix, A.C. (2002) Ice sheets and sea level of last Glacial Maximum. *Quaternary Science Reviews*, 21, 1–7.

Claussen, M., Brovkin, V., Ganopolski, A., Kubatzki, C. and Petoukhov, V. (2003) Climate change in northern Africa: the past is not the future. *Climatic Change*, 57, 99–118.

Claussen, M., Kubatzki, C., Brovkin, V., Ganopolski, A., Hoelzmann, P. and Pachur, H.J. (1999). Simulation of an abrupt change in Saharan vegetation in the mid-Holocene. *Geophysical Research Letters*, 26, 2037–2040.

Clay, J.W. and Holcomb, B.K. (1986) *Politics and the Ethiopian famine 1984–1985*. USA: Cultural Survival, Inc.

Clement, A.C., Hall, A. and Broccoli, A.J. (2004) The importance of precessional signals in the tropical climate. *Climate Dynamics*, 22, 327–341.

Cocquyt, C. (1998) *Diatoms from the Northern Basin of Lake Tanganyika*. Bibliotecha Diatomologica Band 39. Berlin: J. Cramer in der Gebrüder Borntraeger Verlagsbuchhandlung.

Cole, G.A. (1975) *Textbook of limnology*. USA: The C. V. Mosby Company.

Comenetz, J. and Caviedes, C.N. (2002) Climate variability, political crises, and historical population displacements in Ethiopia. *Environmental Hazards*, 4, 113–127.

Conley, D.J. (1988) Biogenic silica as an estimate of siliceous microfossil abundance in Great Lakes sediments. *Biogeochemistry*, 161–179.

Conway, D., Mould, C. and Bewket, W. (2004) Over one century of rainfall and temperature observations in Addis Ababa, Ethiopia. *International Journal of Climatology*, 24, 77–91.

Conway, D. and Schipper, E.L.F. (2011) Adaptation to climate change in Africa: Challenges and opportunities identified from Ethiopia. *Global Environmental Change,* 21, 227–237.

Cook, A.H. (1945) Algal pigments and their significance. *Biological Reviews*, 20, 115–132.

Costa, K., Russell, J., Konecky, B. and Lamb, H.F. (2014) Isotopic reconstruction of the African Humid Period and Congo Air Boundary migration at Lake Tana, Ethiopia. *Quaternary Science Reviews*, 83, 58–67.

Cremer, H., Heiri, O., Wagner, B. and Wagner-Cremer, F. (2007) Abrupt climatic warming in East Antarctica during the early Holocene. *Quaternary Science Reviews*, 26, 2012–2018.

Cremer, H. and Wagner, B. (2003) The diatom flora in the ultra-oligotrophic Lake El'gygytgyn, Chukotka. *Polar Biology*, 26, 105–114.

Croudace, I.W., Rindby, A. and Rothwell, R.G. (2006) ITRAX: description and evaluation of a new X-ray core scanner, in R.G. Rothwell (ed.) *New techniques in sediment core analysis*. *Geology Society, London, Special Publications*, 267, 51–63.

CSA (2007a) Population and Housing Census Report–Country – 2007. Ethiopian Central Statistics Agency (CSA) website. Available at:

http://www.csa.gov.et/newcsaweb/images/documents/surveys/Population%20and%20Housing%20census/ETH–pop–2007/survey0/data/Doc/Reports/National_Statistical.pdf [Access date: 08/10/2015].

CSA (2007b) Population and Housing Census 2007 Report, Amhara, Part I: Population Size and Characteristics. International Household Survey Network website. Available at: http://catalog.ihsn.org/index.php/catalog/3583 [Access date: 08/10/2015].

Cuddington, K. and Leavitt, P.R. (1999) An individual-based model of pigment flux in lakes: Implications for organic biogeochemistry and paleoecology. *Canadian Journal of Fisheries and Aquatic Sciences*, 56, 1964–1977.

Cullen, H.M., deMenocal, P.B., Hemming, S., Hemming, G., Brown, F.H., Guilderson, T. and Sirocko, F. (2000) Climate change and the collapse of the Akkadian empire: evidence from the deep sea. *Geology*, 28, 379–382.

Cumming, B.J. and Smol, J.P. (1993) Development of diatom-based models for paleoclimatic research from lakes in British Colombia (Canada). *Hydrobiologia*, 269/270, 179–196.

Cwynar, L.C., Rees, A.B.H., Pedersen, C.R. and Engels, S. (2012) Depth distribution of chironomids and an evaluation of site-specific and regional lake-depth inference models: a good model gone bad? *Journal of Paleolimnology*, 48, 517–533.

Cyr, H. (1998) How does the vertical distribution of chlorophyll vary in littoral sediments of small lakes? *Freshwater Biology*, 39, 25–40.

Dahl, K.A., Broccoli, A.J. and Stouffer, R.J. (2005) Assessing the role of North Atlantic freshwater forcing in millennial scale climate variability: a tropical Atlantic perspective. *Climate Dynamics*, 24, 325–346.

Dakos, V., Carpenter, S.R., Brock, W.A., Ellison, A.M., Guttal, V., Ives, A.R., Kéfi, S., Livina, V., Seekell, D.A., van Nes, E.H. and Scheffer, M. (2012) Methods for detecting early warnings of critical transitions in time series illustrated using simulated ecological data. *PloS one*, 7, e41010, DOI: 10.1371/journal.pone.0041010.

Dakos, V., van Nes, E.H. and Scheffer, M. (2013) Flickering as an early warning signal. *Theoretical Ecology*, 6, 309–317.

Damnati, B. (2000) Holocene lake records in the Northern Hemisphere of Africa. *Journal of African Earth Sciences*, 31, 253–262.

Damsté, J.S.S., Verschuren, D., Ossebaar, J., Blokker, J., van Houten, R., van de Meer, M.T.J., Plessen, B. and Schouten, S. (2011) A 25,000-year record of climate-induced changes in lowland vegetation of eastern equatorial Africa revealed by the stable carbon-isotopic composition of fossil plant leaf waxes. *Earth and Planetary Science Letters*, 302, 236–246.

Darbyshire, I., Lamb, H.F. and Umer, M. (2003) Forest clearance and regrowth in northern Ethiopia during the last 3000 years. *The Holocene*, 13, 537–546.

DARES (2004) Enumeration of diatom slides. DARES (Diatom Assessment of River Ecological Status). Available at: http://craticula.ncl.ac.uk/DARES/methods/DARES_Protocol_Diatom_Counting.pdf [Access date: 08/10/2015].

Das, S.K., Routh, J., Roychoudhury, A.N. (2009) Biomarker evidence of macrophyte and plankton community changes in Zeekoevlei, a shallow lake in South Africa. *Journal of Paleolimnology*, 41, 507–521.

Davis, S.J., Metcalfe, S.E., Caballero, M.E. and Juggins, S. (2002) Developing diatom-based transfer functions for Central Mexican lakes. *Hydrobiologia*, 467, 199–213.

Davis, B.A.S. and Stevenson, A.C. (2007) The 8.2 ka event and Early–Mid Holocene forests, fires and flooding in the Central Ebro Desert, NE Spain. *Quaternary Science Reviews*, 13–14, 1695–1712.

Davis, M.E. and Thompson, L.G. (2006) An Andean ice-core record of a Middle Holocene mega-drought in North Africa and Asia. *Annals of Glaciology*, 43, 34–41.

Dean, W. (1974) Determination of carbonate and organic matter in calcareous sediments and sedimentary rocks by loss on ignition: comparison with other methods. *Journal of Sedimentary Petrology*, 44, 242–248.

Dean, W. (1997) Rates, timing, and cyclicity of Holocene eolian activity in north-central United States: evidence from varved lake sediments. *Geology*, 25, 331–334.

De Cort, G., Bessems, I., Keppens, E., Mees, F., Cumming, B. and Verschuren, D. (2013) Late-Holocene and recent hydroclimatic variability in the central Kenya Rift Valley: The sediment record of hypersaline lakes Bogoria, Nakuru and Elementeita. *Palaeogeography, Palaeoclimatology, Palaeoecology*, 388, 69–80.

Degefu, W. (1987) Some aspects of meteorological drought in Ethiopia, in M.H. Glantz (ed.) *Drought and hunger in Africa*. Cambridge: Cambridge University Press. pp. 23–36.

Demelie, M. (2000) *Hydrology, hydrogeology and hydrochemistry of the lakes system Hayq-Ardibo, Northern Ethiopia*. MSc thesis. Addis Ababa University.

Demelie, M., Ayenew, T. and Wohnlich, S. (2007) Comprehensive hydrological and hydrogeological study of topographically closed lakes in highland Ethiopia: The case of Hayq and Ardibo. *Journal of Hydrology*, 339, 145–158.

deMenocal, P.B. (2001) Cultural responses to climate change during the Late Holocene. *Science*, 292, 667–673.

deMenocal, P.B. (2015) Palaeoclimate: End of the African Humid Period. *Nature Geoscience*, 8, 86–87.

deMenocal, P.B., Ortiz, J., Guilderson, T., Adkins, J., Sarnthein, M., Baker, L. and Yarusinsky, M. (2000) Abrupt onset and termination of the African Humid Period: rapid climate responses to gradual insolation forcing. *Quaternary Science Reviews*, 19, 347–361.

Denton, G.H., Anderson, R.F., Toggweiler, J.R., Edwards, R.L., Schaefer, J.M. and Putnam, A.E. (2010) The Last Glacial Termination. *Science*, 328, 1652–1656.

De Rijk, S., Hayes, A. and Rohling, E.J. (1999) Eastern Mediterranean sapropel S1 interruption: an expression of the onset of climatic deterioration around 7 ka BP. *Marine Geology*, 153, 337–343.

Descy, J.P., Hardy, M.A., Sténuite, S., Pirlot, S., Leporcq, B., Kimirei, I., Sekadende, B., Mwaitega, S.R. and Sinyenza, D. (2005) Phytoplankton pigments and community composition in Lake Tanganyika. *Freshwater Biology*, 50, 668–684.

DiatCode (2015) UCL Environmental Change Research Centre, Department of Geography website. Available at: http://www.ecrc.ucl.ac.uk/?q=databases/diatcode [Access date: 08/10/2015].

Drysdale, R., Zanchetta, G., Hellstrom, J., Maas, R., Fallick, A., Pickett, M., Cartwright, I. and Piccini, L. (2006) Late Holocene drought responsible for the collapse of Old World civilizations is recorded in an Italian cave flowstone. *Geology*, 34, 101–104.

Ducrotoy, H. (2013) *A palaeoecological and biomolecular investigation of early agriculture in Ethiopia, with particular reference to Sorghum bicolor domestication*. PhD thesis. Aberystwyth University.

Durand, A. (1982) Oscillations of Lake Chad over the past 50,000 years: New data and new hypothesis*. Palaeogeography, Palaeoclimatology, Palaeoecology*, 39, 37–53.

Dykoski, C.A., Edwards, R.L., Cheng, H., Yuan, D., Cai, Y., Zhang, M., Lin, Y., Qing, J., An, Z. and Revenaugh, J. (2005) A high-resolution, absolute dated Holocene and deglacial Asian monsoon record from Dongge Cave, China. *Earth and Planetary Science Letters*, 233, 71–86.

EDDI (2015a) East African Dataset, European Diatom Database website. Available at: http://craticula.ncl.ac.uk/Eddi/jsp/datasetdesc.jsp?DatasetId=AfricaE [Access date: 08/10/2015].

EDDI (2015b) Combined TP dataset, List of samples for: Cyclotella ocellata (agg.) (XXG991). Available at: http://craticula.ncl.ac.uk/Eddi/jsp/taxonlist.jsp?DatasetId=TP&TaxonId=XXG991&TaxId=TP [Access date: 08/10/2015].

Edmunds, W.M., Fellman, E. and Baba Goni, I. (1999) Environmental change, lakes and groundwater in the Sahel of Northern Nigeria. *Journal of the Geological Society, London*, 156, 345–355.

Elizabeth, K., Getachew, T., Taylor, W.D. and Zinabu, G.M. (1992) Eutrophication of Lake Hayq in the Ethiopian Highlands. *Journal of Plankton Research*, 14, 1473–1482.

Elshamy, M.E., Seierstad, I.A. and Sorteberg, A. (2009) Impacts of climate change on Blue Nile flows using bias-corrected GCM scenarios. *Hydrology and Earth System Sciences*, 13, 551–565.

Eltahir, E.A. (1996) El Niño and the natural variability in the flow of the Nile River. *Water Resources*, 32, 131–137.

Eriksen, S.H., Brown, K. and Kelly, P.M. (2005) The dynamics of vulnerability: locating coping strategies in Kenya and Tanzania. *The Geographical Journal*, 171, 287–305.

Farmer, G. (1988) Seasonal forecasting of the Kenya coast short rains, 1901 – 84. *Journal of Climatology*, 8, 489–497.

Fattovich, R. (1987) Some remarks on the origins of the Aksumite Stelae. *Annales d'Ethiopie*, 14, 43–69.

Fattovich, R. (1990) The peopling of the northern Ethiopian-Sudanese borderland between 7000 and 1000 BP: A preliminary model. *Nubica*, 1, 3–45.

Fattovich, R. (2008) *Kings farmers: The urban development of Aksum, Ethiopia: ca. 500 BC-AD 1500 (PSAE Research Series, 4)*. Boston: Boston University, African Studies Center.

Fattovich, R. (2010) The development of ancient states in the northern Horn of Africa, c. 3000 BC–AD 1000: An archaeological outline. *Journal of World Prehistory*, 23, 145–175.

Fetahi, T., Mengistou, S. and Schagerl, M. (2011a) Zooplankton community structure and ecology of the tropical-highland Lake Hayq, Ethiopia. *Limnologica*, 41, 389–397.

Fetahi, T., Schagerl, M., Mengistou, S. and Libralato, S. (2011b) Food web structure and trophic interactions of the tropical highland lake Hayq, Ethiopia. *Ecological Modelling*, 222, 804–813.

Finneran, N. (2007) *The archaeology of Ethiopia*. London: Routledge.

Finney, B.P., Scholz, C.A., Johnson, T.C. and Trumbore, S. (1996) Late Quaternary lake-level changes of Lake Malawi, in T.C. Johnson and E.O. Odada (eds.) *The Limnology, Climatology and Paleoclimatology of the East African Lakes*. The Netherlands: Gordon and Breach Publishers. pp. 495–508.

Fleitmann, D., Burns, S.J., Mangini, A., Mudelsee, M., Kramers, J., Villa, I., Neff, U., Al-Subbary, A.A., Buettner, A., Hippler, D. and Matter, A. (2007) Holocene ITCZ and Indian monsoon dynamic recorded in stalagmites from Oman and Yemen (Socotra). *Quaternary Science Reviews*, 26, 170–188.

Fleitmann, D., Burns, S.J., Mudelsee, M., Neff, U., Kramers, J., Mangini, A. and Matter, A. (2003) Holocene forcing of the Indian monsoon recorded in a stalagmite from Southern Oman. *Science*, 300, 1737–1739.

Flower, R.J. (1993) Diatom preservation: experiments and observations on dissolution and breakage in modern and fossil material. *Hydrobiologia*, 269/270, 473–484.

Flower, R.J. and Likhoshway, Y. (1993) An investigation of diatom preservation in Lake Baikal, in M.A. Grachev (ed.), *Fifth Workshop on Diatom Algae*. Irkutsk: Russian Botanical Society.

Foerster, V., Junginger, A., Langkamp, O., Gebru, T., Asrat, A., Umer, M., Lamb, F.H., Wennrich, V., Rethemeyer, J., Nowaczyk, N., Trauth, M.H. and Schaebtz, F. (2012) Climatic change recorded in the sediments of the Chew Bahir basin, southern Ethiopia, during the last 45,000 years. *Quaternary International*, 274, 25–37.

Fogg, G.E. and Belcher, J.H. (1961) Pigments from the bottom deposits of an English lake. *New Phytologist*, 60, 129–138.

Fontes, J.C., Moussie, C., Pouchan, P. and Weidmann, M. (1973) Phases humides au Pleistocene superieur et a l'Holocene dans le Sud de TAfar (TFAI). *Comptes rendus de l'Académie des Sciences*, 277, 1973–1976.

Fontugne, M.R., Arnold, M., Labeyrie, L., Paterne, M., Calvert, S.E. and Duplessy, J.C. (1994) Palaeoenvironment, sapropel chronology and Nile River discharge during the last 20,000 years as indicated by deep sea sediment records in the Eastern Mediterranean. *Radiocarbon*, 34, 75–88.

Forman, S.L., Wright, D.K. and Bloszies, C. (2014) Variations in water level for Lake Turkana in the past 8500 years near Mt. Porr, Kenya and the transition from the African Humid Period to Holocene aridity. *Quaternary Science Reviews*, 97, 84–101.

Forti, A. (1909 – 1910) Contribuzioni diatomologische. X–Diatomacee quaternaire e subfossili d'acqua dolce raccolte in Ethiopia dal doti. *Atti del Reale Istituto veneto di scienze, lettere ed arti*, 69, 1273–1303.

Fox, D.L. (1944) Biochemical fossils. *Science*, 10, 111–113.

Friis, I., Demissewm, S. and van Breugel, P. (2011) *Atlas of the Potential vegetation of Ethiopia*. Ethiopia: Addis Ababa University Press, Shama Books.

Friis, I. and Ryding, O. (eds.) (2001) *Biodiversity Research in the Horn of Africa Region: Proceedings of the Third International Symposium on the Flora of Ethiopia*

and Eritrea at the Carlsberg Academy, Copenhagen, August 25–27, 1999. Denmark: Det Kongelige Danske Videnskabernes Selskab. Biologiske Skrifter.

Fritz, S.C., Cumming, B.F., Gasse, F. and Laird, K. (2010) Diatoms as indicators of hydrological and climate change in saline lakes, in J.P. Smol and E.F. Stoermer (eds.) *The Diatoms: Applications for the Environmental and Earth Sciences Second Edition*. New York: Cambridge University Press. pp. 186–208.

Fritz, S.C., Juggins, S. and Battarbee, R.W. (1993) Diatom assemblages and ionic characterization of lakes of the Great Northern Plains, North America: a tool for reconstructing past salinity and climate fluctuations. *Canadian Journal of Fisheries and Aquatic Sciences*, 50, 1844–1856.

Funk, C., Dettinger, M.D., Michaelsen, J.C., Verdin, J.P., Brown, M.E., Barlow, M. and Hoell, A. (2008) Warming of the Indian Ocean threatens eastern and southern African food security but could be mitigated by agricultural development. P*roceedings of the National Academy of Sciences of the United States of America*, 105, 11081–11086.

Funk, C., Eilerts, G., Verdin, J., Rowland, J. and Marshall, M. (2011) A climate trend analysis of Sudan. *U.S. Geological Survey Fact Sheet*, 2011–3072, 6. Available at: http://pubs.usgs.gov/fs/2011/3072/pdf/FS2011-3072.pdf [Access date: 08/10/2015].

Funk, C., Michaelsen, J. and Marshall, M. (2012) Mapping recent decadal climate variations in precipitation and temperature across Eastern Africa and the Sahel, in B.D. Wardlow, M.C. Anderson and J.P. Verdin (eds.) *Remote Sensing of Drought: Innovative Monitoring Approaches.* USA: CRC Press. pp. 331–358.

Ganopolski, A., Rahmstorf, S., Petoukhov, V. and Claussen, M. (1998) Simulation of modern and glacial climates with a coupled global model of intermediate complexity. *Nature*, 391, 351–356.

Garcin, Y., Junginger, A., Melnick, D., Olago, D.O., Strecker, M.R. and Trauth, M.H. (2009) Late Pleistocene-Holocene rise and collapse of Lake Suguta, northern Kenya Rift. *Quaternary Science Reviews*, 28, 911–925.

Garcin, Y., Melnick, D., Strecker, M.R., Olago, D.O. and Tiercelin, J.J. (2012) East African mid-Holocene wet-dry transition recorded in palaeo-shorelines of Lake Turkana, northern Kenya Rift. *Earth and Planetary Science Letters,* 331–332, 322–334.

Garcin, Y., Vincens, A., Williamson, D., Buchet, G. and Guiot, B. (2007) Abrupt resumption of the African Monsoon at the Younger Dryas–Holocene climatic transition. *Quaternary Science Reviews*, 26, 690–704.

Garcin, Y., Williamson, D., Taieb, M., Vincens, A., Mathe, P.E. and Majule, A. (2006) Centennial to millennial changes in maar-lake deposition during the last 45,000 years in tropical Southern Africa (Lake Masoko, Tanzania)*. Palaeogeography, Palaeoclimatology, Palaeoecology*, 239, 334–354.

Gasse, F. (1975) *L'évolution des lacs de l'Afar Central (Ethiopie et T.F.A.I.) du Plio-Pléistocène à l'actuel: reconstitution des paléomilieux lacustres à partir de l'étude des diatomées*. DSc thesis. Université de Paris.

Gasse, F. (1977) Evolution of Lake Abhé (Ethiopia and T.F.A.I.) from 70,000 B.P. *Nature,* 2, 42–45.

Gasse, F. (1980) *Les diatomées lacustres plio-pléistocènes du Gadeb (Éthiopie): sytematique, paleoecologie, biostratigraphie*. Revue Algologique, Mémoire hors-série no 3.

Gasse, F. (1986) *East African diatoms; Taxonomy, ecological distribution*. Bibliotheca Diatomologica 11. Berlin: J. Cramer in der Gebrüder Borntraeger Verlagsbuchhandlung.

Gasse, F. (1987) Diatoms for reconstructing palaeoenvironments and paleohydrology in tropical semi-arid zones. Example of some lakes from Niger since 12000 BP. *Hydrobiologia*, 154, 127–163.

Gasse, F. (2000) Hydrological changes in the African tropics since the last Glacial Maximum. *Quaternary Science Reviews*, 19, 189–211.

Gasse, F. (2006) Climate and hydrological changes in tropical Africa during the past million years. *Comptes Rendus Palevol*, 5, 35–43.

Gasse, F., Barker, P., Gell, P.A., Fritz, S.C. and Chalié, F. (1997) Diatom-inferred salinity in palaeolakes: An indirect tracer of climate change. *Quaternary Science Reviews*, 16, 547–563.

Gasse, F., Barker, P. and Johnson, T.C. (2002) A 24,000 yr diatom record from the northern basin of Lake Malawi, in E.O. Odada and D.O. Olago (eds.) *The East African Great Lakes: Limnology, Palaeolimnology and Biodiversity*. The Netherlands: Kluwer Academic Publishers. pp. 393–414.

Gasse, F., Juggins, S. and Ben Khelifa, L. (1995) Diatom-based transfer function for inferring past hydrochemical characteristics of African lakes. *Palaeogeography, Palaeoclimatology, Palaeoecology*, 117, 31–54.

Gasse, F., Lédée, V., Massault, M. and Fontes, J.C. (1989) Water-level fluctuations of Lake Tanganyika in phase with oceanic changes during the last glaciation and deglaciation. *Nature*, 342, 57–59.

Gasse, F., Rognon, P. and Street, F.A. (1980) Quaternary history of the Afar and Ethiopian Rift Lakes, in M.A.J. Williams and H. Faure (eds.) *The Sahara and the Nile: Quaternary environments and prehistoric occupation in northern Africa*. Rotterdam: Balkema. pp. 161–200.

Gasse, F. and Street, F.A. (1978) Late Quaternary lake-level fluctuations and environments of the northern Rift valley and Afar region (Ethiopia and Djibouti). *Palaeogeography, Palaeoclimatology, Palaeoecology*, 24, 279–295.

Gasse, F., Talling, J.F. and Kilham, P. (1983) Diatom assemblages in East Africa: classification, distribution and ecology. *Review Hydrobiology Tropical*, 116, 3–34.

Gasse, F. and Van Campo, E. (1994) Abrupt post-glacial climate events in West Asia and North Africa monsoon domains. *Earth and Planetary Science Letters*, 126, 435–456.

Gasse, F. and Van Campo, E. (1998) A 40,000-yr pollen and diatom record from Lake Tritrivakely, Madagascar, the southern tropics. *Quaternary Research*, 49, 299–311.

Getnet, M., Hengsdijk, H. and van Ittersum, M. (2014) Disentangling the impacts of climate change, land use change and irrigation on the central Rift Valley water system of Ethiopia. *Agricultural Water Management*, 137, 104–115.

Gherardi, J.M., Labeyrie, L., McManus, J.F., Francois, R., Skinner, L.C. and Cortijo, E. (2005) Evidence from the Northeastern Atlantic basin for variability in the rate of the meridional overturning circulation through the last deglaciation*. Earth and Planetary Science Letters*, 240, 710–723.

Ghinassi, M., D'Oriano, F., Benvenuti, M., Awramik, S., Bartolini, C., Fedi, M., Ferrari, G., Papini, M., Sagri, M. and Talbot, M. (2012) Shoreline fluctuations of Lake Hayq (northern Ethiopia) during the last 3500 years: Geomorphological, sedimentary and isotope records. *Palaeogeography, Palaeoclimatology, Palaeoecology*, 365–366, 209–226.

Gibbons, A. (2009) *Ardipithecus ramidus*. *Science*, 326, 1598–1599.

Gibbons, A. (2013) How a fickle climate made us human. *Science*, 341, 474–479.

Gibson, C.E., Wang, G. and Foy, R.H. (2000) Silica and diatom growth in Lough Neagh: The importance of internal cycling. *Freshwater Biology*, 45, 285–293.

Gillespie, R., Street-Perrott, F.A. and Switzur, R. (1983) Post-glacial arid episodes in Ethiopia have implications for climate prediction. *Nature,* 306, 680–683.

Giraudi, C., Mercuri, A.M. and Esu, D. (2012) Holocene palaeoclimate in the northern Sahara margin (Jefara Plain, northwest Libya). *The Holocene*, 23, 339–353.

Gómez, N., Riera, J.L. and Sabater, S. (1995) Ecology and morphological variability of *Aulacoseira granulata* (Bacillariophyceae) in Spanish reservoirs. *Journal of Plankton Research*, 17, 1–16.

Google Earth 7.1.2.2041 (2013a) *The Horn of Africa, 8°59'54.58''N, 42°12'55.09''E, 880 m altitude*. Available at: http://www.google.com/intl/en_uk/earth/ [Access date: 08/10/2015].

Google Earth 7.1.2.2041 (2013b) *Lake Hayq, Ethiopia, 11°20'53''N, 39°42'32''E, 1950 m altitude*. Available at: http://www.google.com/intl/en_uk/earth/ [Access date: 08/10/2014].

Google Earth 7.1.2.2041 (2013c) *Done Ella, Ethiopia, 6°15'41.39"N, 37°39'52.80"E, 2001 m altitude*. Available at: http://www.google.com/intl/en_uk/earth/ [Access date: 08/10/2015].

Google Earth 7.1.2.2041 (2013d) *Done Ella's location in the Main Ethiopian Rift, 6°15'41.39"N, 37°39'52.80"E, 2001 m altitude*. Available at: http://www.google.com/intl/en_uk/earth/ [Access date: 08/10/2015].

Google Maps (2015) *Continental Africa*. Available at: https://www.google.co.uk/maps/@3.9519411,26.3671879,11485228m/data=!3m1!1e3?hl=en [Access date: 08/10/2015].

Goudie, A.S., Viles, H.A. and Pentecost, A. (1993) The late-Holocene tufa decline in Europe. *The Holocene*, 3, 181–186.

Grachev, A.M. and Severinghaus, J.P. (2005) A revised + 10 ± 4 ºC magnitude of the abrupt change in Greenland temperature at the Younger Dryas termination using published GISP2 gas isotope data and air thermal diffusion constants. *Quaternary Science Reviews*, 24, 513–519.

Grove, A.T., Street, F.A. and Goudie, A.S. (1975) Former lake levels and climatic change in the Rift Valley of southern Ethiopia. *The Geographical Journal*, 141, 177-194.

Guilizzoni, P., Lami, A. and Marchetto, A. (1992) Plant pigment ratios from lake-sediments as indicators of recent acidification in alpine lakes. *Limnology and Oceanography*, 37, 1565–1569.

Guillard, R.R.L. and Kilham, P. (1977) The ecology of marine planktonic diatoms, in D. Werner (ed.) *The Biology of Diatoms: Botanical Monographs*. Oxford: Blackwell Scientific Publications. pp. 372–469.

Gupta, A.K., Anderson, D. and Overpeck, J. (2003) Abrupt changes in the Asian southwest monsoon during the Holocene and their links to the North Atlantic. *Nature*, 421, 354–357.

Gupta, A.K., Sarkar, S., De, S., Clemens, S.C. and Velu, A. (2010) Mid–Brunhes strengthening of the Indian Ocean Dipole caused increased equatorial East African and decreased Australasian rainfall. *Geophysical Research Letters,* 37, L06706. DOI: 10.1029/2009GL042225.

Haberyan, K.A. (1985) The role of copepod fecal pellets in the deposition of diatoms in Lake Tanganyika. *Limnology and Oceanography*, 30, 1010–1023.

Haberyan, K.A. (1987) Fossil diatoms and the paleolimnology of Lake Rukwa, Tanzania. *Freshwater Biology*, 17, 429–436.

Haberyan, K.A. (1990) The misrepresentation of the planktonic diatom assemblage in traps and sediments: Southern Lake Malawi, Africa. *Journal of Paleolimnology*, 3, 35–44.

Haile, T. (1988) Causes and characters of drought in Ethiopia. *Ethiopian Journal of Agricultural Sciences*, 10, 85–97.

Hailemichael, M., Aronson, J.L., Savin, S., Tevesz, M.J.S. and Carter, J.G. (2002) $\delta^{18}O$ in mollusc shells from Pliocene Lake Hadar and modern Ethiopian lakes: implications for history of the Ethiopian monsoon. *Palaeogeography, Palaeoclimatology, Palaeoecology*, 186, 81–99.

Håkanson, L. and Jansson, M. (1983) *Principles of Lake Sedimentology*. Berlin: Springer.

Halfman, J.D., Jacobson, D.F., Cannella, C.M., Haberyan, K.A. and Finney, B.P. (1992) Fossil diatoms and the mid to late Holocene palaeolimnology of Lake Turkana, Kenya: a reconnaissance study. *Journal of Paleolimnology*, 7, 23–35.

Halfman, J.D., Jacobson, D.F. and Finney, B.P. (1994) New AMS dates, stratigraphic correlations and decadal climatic cycles for the past 4 ka at Lake Turkana, Kenya. *Palaeogeography, Palaeoclimatology, Palaeoecology*, 111, 83–98.

Hall, R.I., Leavitt, P.R., Quinlan, R., Dixit, A.S. and Smol, J.P. (1999) Effects of agriculture, urbanization and climate on water quality in the northern Great Plains. *Limnology and Oceanography*, 43, 739–756.

Hamilton, A.C. (1982) *Environmental history of East Africa. A study of the Quaternary.* London: Academic Press.

Hamilton, A.C. and Taylor, D. (1991) History of climate and forests in tropical Africa during the last 8 million years. *Climatic Change*, 19, 65–78.

Hammer, U.T. (1986) *Saline Lake Ecosystems of the World (Monographiae Biologicae)*. Dordrecht: Dr. W. Junk Publishers.

Hartmann, J., Ebi, K., McConnell, L., Chan, N. and Weyant, J.P. (2002) Climate suitability: for stable malaria transmission in Zimbabwe under different climate change scenarios. *Global Change and Human Health*, 3, 42–54.

Harvey, T.J. (1976) The paleolimnology of Lake Mobutu Sese Seko. Uganda-Zaire: the last 28,000 years. PhD thesis. Duke University, Durham.

Hassan, F.A. (1981) Historical Nile floods and their implications for climatic change. *Science*, 212, 1142–1145.

Hassan, F.A. (1997) Nile floods and political disorder in Early Egypt, in H.N. Dalfes, G. Kukla and H. Weiss (eds.) *Third Millennium BC Climate Change and Old World Collapse. NATO ASI Series. Series 1. Vol.1*. Berlin: Springer-Verlag. pp. 1–24.

Hassan, F.A. (2007) Extreme Nile floods and famines in Medieval Egypt (AD 930–1500) and their climatic implications. *Quaternary International*, 173–174, 101–112.

Hecky, R.E. and Kilham, P. (1973) Diatoms in alkaline, saline lakes: Ecology and geochemical implications. *Limnology and Oceanography*, 18, 53–71.

Hecky, R.E. and Kling, H.J. (1981) The phytoplankton and protozooplankton of the euphotic zone of Lake Tanganyika: Species composition, biomass, chlorophyll content, and spatio-temporal distribution. *Limnology and Oceanography*, 26, 548–564.

Heinrich, H. (1988) Origin and consequences of cyclic ice rafting in the northeast Atlantic Ocean during the past 130,000 years. *Quaternary Research*, 29, 142–152.

Hély, C., Braconnot, P., Watrin, J. and Zheng, W. (2009) Climate and vegetation: simulating the African humid period. *Comptes Rendus Geoscience*, 341, 671–688.

Hemming, S.R. (2004) Heinrich events: massive late Pleistocene detritus layers of the North Atlantic and their global climate imprint. *Reviews of Geophysics*, 42, RG1005, DOI: 10.1029/2003RG000128.

Henderson, G., Collins, M., Hall, I., Lockwood, M., Palike, H., Rickaby, R., Schmidt, G., Turney, C. and Wolff, E. (2009) *Improving Future Climate Prediction Using Palaeoclimate Data*. A community White Paper for consideration by the Natural Environment Research Council (NERC). An outcome of The Leverhulme Climate Symposium 2008 – Earth's Climate: Past, Present and Future. Oxford: The Leverhulme Trust. Available at: http://www.earth.ox.ac.uk/~gideonh/reports/PaleoClimateWhitePaper.pdf [Access date: 08/10/2015].

Hill, M.O. (1973) Diversity and evenness: a unifying notation and its consequences. *Ecology*, 54, 427–432.

Hillier, D. and Dempsey, B. (2012) *A Dangerous Delay: The cost of late response to early warnings in the 2011 drought in the Horn of Africa*. Oxford: Oxfam and Save the Children. Available at: https://www.oxfam.org/sites/www.oxfam.org/files/bp-dangerous-delay-horn-africa-drought-180112-en.pdf [Access date: 08/10/2015].

Hilton, J. (1985) A conceptual framework for predicting the occurrence of sediment focusing and sediment redistribution in small lakes. *Limnology and Oceanography*, 30, 1131–1143.

Hodgson, D.A., Tyler, P. and Vyvermanm W. (1996) The palaeolimnology of Lake Fidler, a meromictic lake in south-west Tasmania and the significance of recent human impact. *Journal of Paleolimnology*, 18, 313–333.

Hodgson, D.A., Wright, S.W., Tyler, P.A. and Davies, N. (1998) Analysis of fossil pigments from algae and bacteria in meromictic Lake Fidler, Tasmania, and its application to lake management. *Journal of Paleolimnology*, 19, 1–22.

Holmgren, K., Karlen, W. and Shaw, P. (1995) Paleoclimatic significance of the stable isotopic composition and petrology of a late Pleistocene stalagmite from Botswana. *Quaternary Research*, 43, 320–328.

Holmgren, K., Lee-Thorp, J.A., Cooper, G.R.J., Lundblad, K., Partridge, T.C., Scott, L., Sithaldeen, R., Talma, A.S. and Tyson, P.D. (2003) Persistent millennial-scale climatic variability over the past 25,000 years in Southern Africa. *Quaternary Science Reviews*, 22, 2311–2326.

Hua, Y., Yingqian, X., Zhenxia, L., Berné, S., Huang, C.H. and Jia, G. (2008) Evidence for the 8,200 a BP cooling event in the middle Okinawa Trough. *Geo-Marine Letters*, 28, 131–136.

Huang, C.C., Pang, J., Zha, X., Su, H. and Jia, Y. (2011) Extraordinary floods related to the climate event at 4200 a BP on the Qishuihe River, middle reaches of the Yellow River, China. *Quaternary Science Reviews*, 30, 460–468.

Huang, C.C., Pang, J.L., Zha, X., Su, H., Jia, Y. and Zhu, Y. (2007) Impact of monsoonal climatic change on Holocene overbank flooding along the Sushui River within the Middle Reaches of the Yellow River, China. *Quaternary Science Reviews*, 26, 2247–2264.

Hughes, P.D.M., Mauquoy, D., Barber, K.E. and Langdon, P.G. (2000) Mire development pathways and palaeoclimatic records from a full Holocene peat archive at Walton Moss, Cumbria, England. *The Holocene*, 10, 465–479.

Hulme, M. (2003) Abrupt climate change: can society cope? *Philosophical Transactions of the Royal Society A*, 361, 2001–2019.

Hulme, M., Doherty, R.M., Ngara, T., New, M.G. and Lister, D. (2001) African climate change: 1900–2100. *Climate Research*, 17, 145–168.

Hurley, J.P. and Armstrong, D.E. (1990) Fluxes and transformations of aquatic pigments in Lake Mendota, Wisconsin. *Limnology and Oceanography*, 35, 384–398.

Hustedt, F. (1922) Zellplanzen Ostafrikas, gesammelt auf der akademischen Studienfahrt 1910 von Bruno Schröder. VI-Bacillariales. *Hedwigia*, 63, 117–173.

Hustedt, F. (1949) Süßwasser-Diatomeen aus dem Albert-National park in Belgisch–Kongo. Exploratie van het National Albert.

Jeffrey, S.W., Mantoura, R.F.C. and Wright, S.W. (eds.) (1997) *Phytoplankton Pigments in Oceanography: Guidelines to Modern Methods*. California: UNESCO Publishing.

Jeffrey, S.W., Wright, S.W. and Zapata, M. (1999) Recent advances in HPLC pigment analysis of phytoplankton. *Marine and Freshwater Research*, 50, 879–896.

Johnsen, S.J., Claused, H.B., Dansgaard, W., Fuhrer, K., Gundestrup, N., Hammer, C.U., Iversen, P., Jouzel, J., Stauffer, B. and Steffensen, J.P. (1992) Irregular glacial interstadials recorded in a new Greenland ice core. *Nature*, 359, 311–313.

Johnsen, S.J., Dansgaard, W., Calusen, H.B. and Langway Jr., C.C. (1972) Oxygen isotope profiles through Antarctic and Greenland ice sheets. *Nature*, 235, 429–434.

Johnson, T.C. (1996) Sedimentary processes and signals of past climatic change in the large lakes of the East African Rift Valley, in T.C. Johnson and E.O. Odada (eds.) *The Limnology, Climatology and Paleoclimatology of the East African Lakes*. The Netherlands: Gordon and Breach Publishers. pp. 367–412.

Johnson, T.C., Brown, E.T. and McManus, J. (2004) Diatom productivity in Northern Lake Malawi during the past 25,000 years: Implications for the position of the Intertropical Convergence Zone at millennial and shorter time scales, in R.W. Battarbee, F. Gasse and C.E. Stickley (eds.) *Past Climate Variability through Europe and Africa*. The Netherlands: Springer. pp. 93–116.

Johnson, T. C., Brown, E.T., McManus, J., Barry, S., Barker, P. and Gasse, F. (2002) A high-resolution paleoclimate record spanning the past 25,000 years in southern East Africa. *Science*, 296, 113–132.

Johnson, T.C., Halfman, J.D. and Showers, W.J. (1991) Paleoclimate of the past 4000 years at Lake Turkana, Kenya, based on the isotopic composition of authigenic calcite. *Palaeogeography, Palaeoclimatology, Palaeoecology*, 85, 189–198.

Johnson, T.C., Kelts, K. and Odada, E. (2000) The Holocene history of Lake Victoria. *Ambio*, 29, 2–11.

Johnson, T.C., Scholz, C.A., Talbot, M.R., Kelts, K., Ricketts, R.D., Ngobi, G., Beuning, K., Ssemmanda, I. and McGill, J.W. (1996) Late Pleistocene desiccation of Lake Victoria rapid evolution of cichlid fishes. *Science*, 272, 1091–1093.

Jolly, D., Harrison, S.P., Damnati, B. and Bonnefille, R. (1998) Simulated climate and biomes of Africa during the late Quaternary: comparison with pollen and lake status data. *Quaternary Science Reviews*, 17, 629–657.

Jones, P.D., Osborn, T.J. and Briffa, K.R. (2001) The evolution of climate over the last millennium. *Science*, 292, 662–667.

Jouzel, J., Lorius, C., Petit, J.R., Genthon, C., Barkov, N.I., Kotlyakov, V.M. and Pretrov, V.M. (1987) Vostok ice core: a continuous isotope temperature record over the last climatic cycle (160,000 years). *Nature*, 329, 403–408.

Jouzel, J., Vaikmae, R., Petit, J.R., Martin, M., Duclos, Y., Stievenard, M., Lorius, C., Toots, M., Melieres, M.A., Burckle, L.H., Barkov, N.I. and Kotlyakov, V.M. (1995) The two-step shape and timing of the last deglaciation in Antarctica. *Climate Dynamics*, 11, 151–161.

Juggins, S. (2007) *C2 Version 1.5 User guide. Software for ecological and palaeoecological data analysis and visualisation*. Newcastle University, Newcastle upon Tyne, UK. pp. 73.

Juggins, S. (2013) Quantitative reconstructions in palaeolimnology: new paradigm or sick science? *Quaternary Science Reviews*, 64, 20–32.

Julius, M.L. and Theriot, E.C. (2010) The diatoms: a primer, in J.P. Smol and E.F. Stoermer (eds.) *The Diatoms: Applications for the Environmental and Earth Sciences Second Edition*. New York: Cambridge University Press. pp. 8–22.

Jung, S., Davis, D.R., Janssen, G.M. and Kroon, D. (2004) Stepwise Holecene aridification in the NE Africa deduced from dust-borne radiogenic isotope records. *Earth and Planetary Science Letters*, 221, 27–47.

Junginger, A., Roller, S., Olaka, L.A. and Trauth, M.H. (2013) The effects of solar irradiation changes on the migration of the Congo Air Boundary and water levels of paleo-Lake Suguta, Northern Kenya Rift, during the African Humid Period (15–5 ka BP). *Palaeogeography, Palaeoclimatology, Palaeoecology*, 396, 1–16.

Junginger, A. and Trauth, M.H. (2013) Hydrological constraints of paleo-Lake Suguta in the Northern Kenya Rift during the African Humid period (15– 5 ka BP). *Global and Planetary Science*, 111, 174–188.

Kaland, P.E., Krzywinski, K. and Stabell, B. (1984) Radiocarbon-dating of transitions between marine and lacustrine sediments and their relation to the development of lakes. *Boreas*, 13, 243–258.

Kalff, J. (2003) *Limnology Inland Water Ecosystems*. USA: Pearson Education Ltd.

Kameri-Mbote, P. (2007) *Water, Conflict, and Cooperation: Lessons from the Nile River Basin*. No. 4 in the Navigating Peace series, Woodrow Wilson for International Scholars, Environmental Change and Security Programme. Available at: http://www.wilsoncenter.org/sites/default/files/NavigatingPeaceIssuePKM.pdf [Access date: 08/10/2015].

Karim, A.G.A. (1975) Studies on the freshwater algae of the Sudan. II - The distribution of the Bacillariophyceae of Wadi Galol, Jebel Mana. *Hydrobiologia*, 47, 31–42.

Keller, E.J. (1992) Drought, war, and the politics of famine in Ethiopia and Eritrea. *Journal of Modern African Studies*, 30, 609–624.

Kendall, R.L. (1969) An ecological history of the Lake Victoria basin. *Ecological Monographs,* 39, 121–176.

Kiage, L.M. and Liu, K. (2006) Late Quaternary palaeoenvironmental changes in East Africa: a review of multiproxy evidence palynology, lake sediments, and associated records. *Progress in Physical Geography*, 30, 633–658.

Kilham, P. (1971) A hypothesis concerning silica and the planktonic freshwater diatoms. *Limnology and Oceanography*, 16, 10–18.

Kilham, P. and Kilham, S.S. (1990) Endless summer: internal loading processes dominate nutrient cycling in tropical lakes. *Freshwater Biology*, 23, 379–389.

Kilham, P., Kilham, S.S. and Hecky, R.E. (1986) Hypothesized resource relationships among African planktonic diatoms. *Limnology and Oceanography*, 31, 1169–1181.

Kim, J. and Guha-Sapir, D. (2012) Famines in Africa: is early warning early enough? *Global Health Action*, 5, 1–3.

Kingston, J.D., Deino, A.L., Edgar, R.K. and Hill, A. (2007) Astronomically forced climate change in the Kenya Rift Valley 2.7 – 2.55 Ma: implications for the evolution of early hominin ecosystems. *Journal of Human Evolution*, 53, 487–503.

Kingston, D.G. and Taylor, R.G. (2010) Sources of uncertainty in climate change impacts on river discharge and groundwater in a headwater catchment of the Upper Nile Basin, Uganda. *Hydrology and Earth System Sciences*, 14, 1297–1308.

King'uyu, S.M., Ogallo, L.A. and Anyamba, E.K. (2000) Recent trends of minimum and maximum surface temperatures over Eastern Africa. *Journal of Climate*, 13, 2876–2886.

Konecky, B.L., Russel, J.M., Huang, Y., Vuille, M., Cohen, L. and Street-Perrott, F.A. (2014) Impact of monsoons, temperature, and CO_2 on the rainfall and ecosystems of Mt. Kenya during the Common Era. *Palaeogeography, Palaeoclimatology, Palaeoecology*, 396, 17–25.

Konecky, B.L., Russell, J.M., Johnson, T.C., Brown, E.T., Berke, M.A., Werne, J.P. and Huang, Y. (2011) Atmospheric circulation patterns during the late Pleistocene climate changes at Lake Malawi, Africa. *Earth and Planetary Science Letters*, 312, 318–326.

Kopalova, K., Kociolek, J.P., Lowe, R.L., Zidarova, R. and Van de Vijver, B. (2015) Five new species of the genus *Humidophila* (Bacillariophyta) from the Maritime Antarctic Region. *Diatom Research*, 30, 117–131.

Krammer, K. and Lange-Bertalot, H. (1988) *Süßwasserflora von Mitteleuropa, 2/2 Bacillariophyceae, 2. Teil: Bacillariaceae, Epithemiaceae, Surirellaceae.* New York: Gustav Fischer Verlag, 596 pp.

Krammer, K. and Lange-Bertalot, H. (1991a) *Süßwasserflora von Mitteleuropa, 2/3 Bacillariophyceae, 3. Teil: Centrales, Fragilariaceae, Eunotiaceae.* Berlin: Gustav Fischer Verlag, 576 pp.

Krammer, K. and Lange-Bertalot, H. (1991b) *Süßwasserflora von Mitteleuropa, 2/4 Bacillariophyceae, 4. Teil: Achnanthaceae Kritische Ergansungen zu Achnanthes s.l, Navicula s.str., Gomphonema.* Berlin: Gustav Fischer Verlag, 437 pp.

Krammer, K. and Lange-Bertalot, H. (1999) *Süßwasserflora von Mitteleuropa, 2/1 Bacillariophyceae, 1. Teil: Naviculaceae*. New York: Gustav Fischer Verlag, 876 pp.

Kropelin, S., Verschuren, D., Lezine, A.M., Eggermont, H., Cocquyt, C., Francus, P., Cazet, J.P., Fagot, M., Rumes, B., Russell, J.M., Darius, F., Conley, D.J., Schuster,

M., von Suchodoletz, H. and Engstrom, D.R. (2008) Climate-driven ecosystem succession in the Sahara: the past 6000 years. *Science,* 320, 765–768.

Kruger, A.C. and Shongwe, S. (2004) Temperature trends in South Africa: 1960–2003. *International Journal of Climatology*, 24, 1929–1945.

Kuper, R. and Kröpelin, S. (2006) Climate-Controlled Holocene Occupation in the Sahara: Motor of Africa's Evolution. *Science*, 313, 803–807.

Kutzbach, J.E., Guetter, P.J., Behling, P.J. and Delin, R. (1993) Simulated climatic changes: results of the COHMAP climate-model experiments, in H.E. Wright, J.E. Kutzbach, T. Webb III, W.R. Ruddiman, F.A. Street-Perrott, P.J. Bartlein (eds.) *Global Climates Since the Last Glacial Maximum*. Minneapolis: University of Minnesota Press. pp. 5–11.

Kutzbach, J.E. and Street-Perrott, F.A. (1985) Milankovitch forcing of fluctuations in the level of tropical lakes from 18 to 0 kyr BP. *Nature,* 317, 130–134.

Kylander, M.E., Ampel, L., Wohlfarth, B. and Veres, D. (2011) High-resolution X-ray fluorescence core scanning analysis of Les Echets (France) sedimentary sequence: new insights from chemical proxies. *Journal of Quaternary Science*, 26, 109–117.

Lærdal, T., Talbot, M.R. and Russell, J.M. (2002) Late Quaternary sedimentation and climates in the Lakes Edward and George area, Uganda-Congo, in E.O. Odada and D.O. Olago (eds.) *The East African Great Lakes: Limnology, Palaeolimnology and Biodiversity*. The Netherlands: Kluwer Academic Publishers. pp. 429–470.

Lamb, H.F., Bates, C.R., Coombes, P.V., Marshall, M.H., Umer, M., Davies, S.J. and Dejen, E. (2007a) Late Pleistocene desiccation of Lake Tana, source of the Blue Nile. *Quaternary Science Reviews,* 26, 287–299.

Lamb, H.F., Leng, M.J., Telford, R.J., Ayenew, T. and Umer, M. (2007b) Oxygen and carbon isotope composition of authigenic carbonate from an Ethiopian lake: a climate record of the last 2000 years. *The Holocene*, 17, 515–524.

Lamb, H.F., Gasse, F., Benkaddour, A., El Hamouti, N., van der Kaars, S., Perkins, W.T., Pearce, N.J. and Roberts, C.N. (1995) Relation between century-scale Holocene arid intervals in tropical and temperate zones. *Nature*, 373, 134–137.

Lamb, A.L., Leng, M.J., Lamb, H.F., Telford, R.J. and Umer, M.U. (2002a) Climatic and non-climatic effects on the $\delta^{18}O$ and $\delta^{13}C$ composition of Lake Awassa, Ethiopia, during the last 6.5 ka. *Quaternary Science Reviews*, 21, 2199–2211.

Lamb, H.F., Kebede, S., Leng, M., Ricketts, D., Telford, R. and Mohammed, M. (2002b) Origin and isotopic composition of aragonite laminae in an Ethiopian crater lake, in E.O. Odada and D.O. Olago (eds.) *The East African Great lakes: Limnology, Palaeolimnology and Biodiversity*. The Netherlands: Kluwer Academic Publishers. pp. 471–508.

Lamb, A.L., Leng, M.J., Lamb, H.F. and Mohammed, M.U. (2000) A 9000-yr oxygen and carbon isotope record of hydrological change in a small crater lake. *The Holocene*, 10, 167–177.

Lamb, A.L., Leng, M.J., Sloane, H.J. and Telford, R.J. (2005) A comparison of the palaeoclimate signals from diatom oxygen isotope ratios and carbonate oxygen isotope ratios from a low latitude crater lake. *Palaeogeography, Palaeoclimatology, Palaeoecology*, 223, 290–302.

Lami, A., Guilizzoni, P. and Masaferro, J. (1991) Record of fossil pigments in an alpine lake (L. Tovel, N. Italy). *Memorie dell'Istituto Italiano di Idrobiologia*, 49, 117–126.

Last, G. (2009) The geology and soils of Ethiopia and Eritrea, in J. Ash and J. Atkins (eds.) *Birds of Ethiopia and Eritrea: An atlas of distribution*. London: Christopher Helm. pp. 25–26.

Leavitt, P.R. (1993) A review of factors that regulate carotenoid and chlorophyll deposition and fossil pigment abundance. *Journal of Paleolimnology*, 9, 109–127.

Leavitt, P.R. and Brown, S.R. (1988) Effects of grazing by *Daphnia* on algal carotenoids: Implications for paleolimnology. *Journal of Paleolimnology*, 1, 201–213.

Leavitt, P.R. and Carpenter, S.R. (1989) Effects of sediment mixing and benthic algal production on fossil pigment stratigraphies. *Journal of Paleolimnology*, 2, 147–158.

Leavitt, P.R., Findlay, D.L., Hall, R.I. and Smol, J.P. (1999) Algal responses to dissolved organic carbon loss and pH decline during whole-lake acidification: Evidence from paleolimnology. *Limnology and Oceanography*, 44, 757–773.

Leavitt, P.R. and Hodgson, D.A. (2001) Sedimentary Pigments, in J.P. Smol, H.J.B. Birks and W.M. Last (eds.) *Tracking Environmental Change Using Lake Sediments. Volume 3: Terrestrial, Algal, and Siliceous Indicators*. The Netherlands: Kluwer Academic Publishers. pp. 295–325.

Leavitt, P.R., Hann, B.J., Smol, J.P., Zeeb, B.A., Christie, C.C., Wolfe, B. and Kling, H.J. (1994c) Paleolimnological analysis of whole-lake experiments: An overview of results from Experimental Lakes Area Lake 227. *Canadian Journal of Fisheries and Aquatic Sciences*, 51, 2322–2332.

Leavitt, P.R., Sanford, P.R., Carpenter, S.R. and Kitchell, J.F. (1994a) An annual fossil record of production, planktivory and piscivory during whole-lake experiments. *Journal of Paleolimnology*, 11, 133–149.

Leavitt, P.R., Schindler, D.E., Paul, A.J., Hardie, A.K. and Schindler, D.W. (1994b) Fossil pigment records of phytoplankton in trout-stocked alpine lakes. *Canadian Journal of Fisheries and Aquatic Sciences*, 51, 2411–2423.

Leavitt, P.R., Vinebrooke, R.D., Donald, D.B., Smol, J.P. and Schindler, D.W. (1997) Past ultraviolet radiation environments in lakes derived from fossil pigments. *Nature*, 388, 457–459.

Lebel, T., Delclaux, F., Le Barbe, L. and Polcher, J. (2000) From GCM scales to hydrological scales: rainfall variability in West Africa. *Stochastic Environmental Research and Risk Assessment*, 14, 275–295.

Lee-Thorp, J.A., Holmgren, K., Lauritzen, S.E., Linge, H., Moberg, A., Partridge, T.C., Stevenson, C. and Tyson, P.D. (2001) Rapid climate shifts in the southern African interior throughout the mid- to late Holocene. *Geophysical Research Letters*, 28, 4507–4510.

Legesse, D., Gasse, F., Radakovitch, O., Vallet-Coulomb, C., Bonnefille, R., Verschuren, D. Gibert, E. and Barker, P. (2002) Environmental changes in a tropical lake (Lake Abiyata, Ethiopia) during recent centuries. *Palaeogeography, Palaeoclimatology, Palaeoecology*, 187, 233–258.

Legesse, D., Vallet-Coulomb, C. and Gasse, F. (2003) Hydrological response of a catchment to climate and land use changes in Tropical Africa: case study South Central Ethiopia. *Journal of Hydrology*, 275, 67–85.

Leng, M.J., Lamb, A.L., Lamb, H.F. and Telford, R.J. (1999) Palaeoclimatic implications of isotopic data from modern and early Holocene shells of the freshwater snail *Melanoides tuberculata*, from lakes in the Ethiopian Rift Valley. *Journal of Paleolimnology*, 21, 97–106.

Lenton, T.M., Held, H., Kriegler, E., Hall, J.W., Lucht, W., Rahmstorf, S. and Schellnhuber, H.J. (2008) Tipping elements in the Earth's climate system. *Proceedings of the National Academy of Sciences of the United States of America*, 105, 1786–1993.

Lewin, J.C. (1961) The dissolution of silica from diatom walls. *Geochimica et Cosmochimica Acta*, 21, 182–198.

Lezine, A.M., Duplessy, J.C. and Cazet, J.P. (2005) West African monsoon variability during the last deglaciation and the Holocene: Evidence from freshwater algae, pollen and isotope data from core KW31, Gulf of Guinea. *Palaeogeography, Palaeoclimatology, Palaeoecology*, 219, 225–237.

Liu, Z., Wang, Y., Gallimore, R., Gasse, F., Johnson, T., deMenocal, P., Adkins, J., Notaro, M., Prentice, I.C., Kutzbach, J., Jacob, R., Behling, P., Wang, L. and Ong, E. (2007) Simulating the transient evolution and abrupt change of Northern Africa atmosphere-ocean-terrestrial ecosystem in the Holocene. *Quaternary Science Reviews*, 26, 1818–1837.

Loomis, S.E., Russell, J.M. and Lamb, H.F. (2015) Northeast African temperature variability since the Late Pleistocene. *Palaeogeography, Palaeoclimatology, Palaeoecology*, 423, 80–90.

Lotter, A.F., Birks, H.J.B., Hofmann, W. and Marchetto, A. (1997) Modern diatom, cladocera, chironomid and chrysophyte cyst assemblages as quantitative indicators for the reconstruction of past environmental conditions in the Alps. I. Climate. *Journal of Paleolimnology*, 18, 395–420.

Lowe, J.J., Walker, M.J.C., Scott, E.M., Harkness, D.D., Bryant, C.L. and Davies, S.M. (2004) A coherent high-precision radiocarbon chronology for the Late-glacial sequence at Sluggan Bog, Co. Antrim, Northern Ireland. *Journal of Quaternary Science*, 19, 147–158.

Lowenstern, J.B., Janik, C.J., Fournier, R.O., Tesfai, T., Duffield, W.A., Clynne, M.A., Smith, J.G., Woldegiorgis, L., Weldemariam, K. and Kahsai, G. (1999) A geochemical reconnaissance of the Alid volcanic center and geothermal system, Danakil depression, Eritrea. *Geothermics*, 28, 161–187.

Machado, M.J., Perez-Gonzalez, A. and Benito, G. (1998) Paleoenvironmental changes during the Last 4000 yr in the Tigray, northern Ethiopia. *Quaternary Research*, 49, 312–321.

Magadza, C.H.D. (2010) Environmental state of Lake Kariba and Zambezi River Valley: Lessons learned and not learned. *Lakes and Reservoirs: Research and Management*, 15, 167–192.

Magri, D. and Parra, I. (2002) Late Quaternary western Mediterranean pollen records and African winds. *Earth and Planetary Science Letters*, 200, 401–408.

Maley, J. (1992) The African rain forest vegetation and palaeoenvironments during the Late Quaternary. *Climate Change* 19, 79–98.

Maley, J. (2000) Last Glacial Maximum lacustrine and fluviatile formations in the Tibesti and other Saharan mountains, and large-scale climatic teleconnections linked to the activity of the Subtropical Jet Stream. *Global and Planetary Change*, 26, 121–136.

Maley, J. and Brenac, P. (1998) Vegetation dynamics, palaeoenvironments and climate changes in the forests of western Cameroon during the last 28,000 years BP. *Review of Palaeobotany and Palynology*, 99, 157–187.

Mann, D.G. and Droop, J.M. (1996) Biodiversity, biogeography and conservation of diatoms. *Hydrobiologia*, 336, 19–32.

Manning, K. and Timpson, A. (2014) The demographic response to Holocene climate change in the Sahara. *Quaternary Science Reviews*, 101, 28–35.

Marciniak, B. and Khursevich, G. (2002) Comparison of diatom successions from Mazovian (Poland) and Alexandrian (Belarus) lacustrine inter glacial deposits. *Geological Quarterly*, 46, 59–68.

Marshall, M.H. (2006) *Late Pleistocene and Holocene palaeolimnology of Lakes Tana and Ashenge, northern Ethiopia*. PhD thesis. University of Wales.

Marshall, M.H., Lamb, H.F., Davies, S.J., Leng, M.J., Kubsa, Z., Umer, M. and Bryant, C. (2009) Climatic change in northern Ethiopia during the past 17,000 years: A diatom and stable isotope record from Lake Ashenge. *Palaeogeography, Palaeoclimatology, Palaeoecology,* 279, 114–127.

Marshall, M.H., Lamb, H.F., Huws, D., Davies, S.J., Bates, R., Bloemendal, J., Boyle, J., Leng, M.J., Umer, M. and Bryant, C. (2011) Late Pleistocene and Holocene drought events at Lake Tana, source of the Blue Nile. *Global and Planetary Change*, 78, 147–161.

Martinson, D.G., Pisias, N., Hays, J.D., Imbrie, J., Moore, T.C. Jr. and Shackleton, N.J. (1987) Age dating and the orbital theory of the ice ages: development of a high-resolution 0 to 300,000-year chronostratigraphy. *Quaternary Research*, 27, 1–29.

Maslin, M.A. and Christensen, B. (2007) Tectonics, orbital forcing, global climate change, and human evolution in Africa: introduction to the African paleoclimate special volume. *Journal of Human Evolution*, 53, 443–464.

Mayewski, P.A., Rohling, E.E., Stager, J.C., Karlén, W., Maasch, K.A., Meeker, L.D., Meyerson, E.A., Gasse, F., van Kreveld, S., Holmgren, K., Lee-Thorp, J., Rosqvist, G., Rack, F., Staubwasser, M., Schneider, R.R. and Steig, E.J. (2004) Holocene climate variability. *Quaternary Research*, 62, 243–255.

McGowan, S. (2013) Pigment Studies, in S.A. Elias (ed.) *The Encyclopedia of Quaternary Science*, 3. Amsterdam: Elsevier. pp. 326–338.

McGowan, S., Leavitt, P.R., Hall, R.I. Anderson, N.J., Jeppesen, E. and Odgaard, B.V. (2005) Controls of Algal Abundance and Community Composition During Ecosystem State Change. *Ecology*, 86, 2200–2211.

McIntyre, A., Ruddiman, W.F., Karlin, K. and Mix, A.C. (1989) Surface water response of the equatorial Atlantic Ocean to orbital forcing. *Paleoceanography*, 4, 19–55.

McManus, J.F., Francois, R., Gherardi, J.M., Keigwin, L.D. and Brown-Leger, S. (2004) Collapse and rapid resumption of Atlantic meridional circulation linked to deglacial climate changes. *Nature*, 428, 834–837.

McMinn, A. (1995) Comparison of diatom preservation between oxic and anoxic basins in Ellis Fjord, Antarctica. *Diatom Research*, 10, 145–151.

McSweeney, C. and Lizcano, G. (2012) Ethiopia, United Nations Development Programme (UNDP) climate change country profiles. School of Geography and the Environment, University of Oxford website. Available at: http://www.geog.ox.ac.uk/research/climate/projects/undp-cp/ [Access date: 08/10/2015].

Melack, J.M. (1981) Photosynthetic activity of phytoplankton in tropical African soda lakes. *Hydrobiologia*, 81, 71–85.

Mercuri, A.M., Sadori, L. and Uzquiano Ollero, P. (2011) Mediterranean and north-African cultural adaptations to mid-Holocene environmental and climatic change. *The Holocene*, 21, 189–206.

Metwally, A.A., Scott, L., Neumann, F.H., Bamford, M.K. and Oberhänsli, H. (2014) Holocene palynology and palaeoenvironments in the Savanna Biome at Tswaing Crater, central South Africa. *Palaeogeography, Palaeoclimatology, Palaeoecology*, 402, 125–135.

Meze-Hausken, E. (2004) Contrasting climate variability and meteorological drought with perceived drought and climate change in northern Ethiopia. *Climate Research*, 27, 19–31.

Michels, J.W. (2005) *Changing settlement patterns in the Aksum-Yeha Region of Ethiopia: 700 BC–AD 850*. Oxford: BAR International Series.

Mills, K. (2009) *Ugandan Crater Lakes Limnology, Palaeolimnology and Palaeoenvironmental history*. PhD thesis. Loughborough University.

Mills, K. and Ryves, D.B. (2012) Diatom-based models for inferring past water chemistry in western Ugandan crater lakes. *Journal of Paleolimnology*, 48, 383–399.

Moernaut, J., Verschuren, D., Charlet, F., Kristen, I., Fagot, M. and De Batist, M. (2010) The seismic-stratigraphic record of lake-level fluctuations in Lake Challa: Hydrological stability and change in equatorial East Africa over the last 140 kyr. *Earth and Planetary Science Letters*, 290, 214–223.

Moeyersons, J., Nyssen, J., Poesen, J., Deckers, J. and Haile, M. (2006) Age and backfill/overfill stratigraphy of two tufa dams, Tigray Highlands, Ethiopia: evidence for Late Pleistocene and Holocene wet conditions. *Palaeogeography, Palaeoclimatology, Palaeoecology*, 230, 165–181.

Mohammed, U. and Bonnefille, R. (1998) A Late Glacial to Late Holocene pollen record from a high land peat at Tamsaa, Bale Mountains, South Ethiopia. *Global and Planetary Change,* 16–17, 121–129.

Mohammed, U., Bonnefille, R. and Kebede, S. (2002) Pigment analysis of short cores from the Central Ethiopian Rift Valley lakes, in E.O. Odada and D.O. Olago (eds.) *The East African Great Lakes: Limnology, Palaeolimnology and Biodiversity*. The Netherlands: Kluwer Academic Publishers. pp. 471–485.

Moise, A.F. and Hudson, D.A. (2008) Probabilistic predictions of climate change for Australia and southern Africa using the reliability ensemble average of IPCC CMIP3 model simulations. *Journal of Geophysical Research D: Atmospheres,* 113, D15113, DOI: 10.1029/2007JD009250.

Morrissey, A. and Scholz, C.A. (2014) Paleohydrology of Lake Turkana and its influence on the Nile River System. *Palaeogeography, Palaeoclimatology, Palaeoecology*, 403, 88–100.

Moss, B. (1968) Studies on the Degradation of Chlorophyll *a* and Carotenoids in Freshwater. *New Phytologist*, 67, 49–59.

Moy, C.M., Seltzer, G.O., Rodbell, D.T. and Anderson, D.M. (2002) Variability of El Niño/Southern Oscillation activity at millennial timescales during the Holocene epoch. *Nature*, 420, 162–165.

Mulitza, S., Prange, M., Stutt, J.B., Zabel, M., von Dobeneck, T., Itambi, A.C., Nizou, J., Schulz, M. and Wefer, G. (2008) Sahel megadroughts triggered by glacial slowdowns of Atlantic meridional overturning. *Paleoceanography*, 23, PA4206, DOI: 10.1029/2008PA001637.

Müller, O. (1903) Bacillariaceen aus dem Nyassalande und einigen benachbarten Gebiet. *Engler's Botanischen Jahrbuch für Systematik Pflanzenges und Pflanzengeographie*, 34, 9–38.

Müller, O. (1904) Bacillariaceen aus dem Nyassalande und einigen benachbarten Gebiet. *Engler's Botanischen Jahrbuch für Systematik Pflanzenges und Pflanzengeographie*, 34, 255–301.

Müller, O. (1905) Bacillariaceen aus dem Nyassalande und einigen benachbarten Gebiet. *Engler's Botanischen Jahrbuch für Systematik Pflanzenges und Pflanzengeographie*, 36, 137–206.

Müller, O. (1910) Bacillariaceen aus dem Nyassalande und einigen benachbarten Gebiet. *Engler's Botanischen Jahrbuch für Systematik Pflanzenges und Pflanzengeographie*, 45, 69–122.

National Meteorology Agency (2014) Climate of city: Arba Minch. Ethiopia's National Meteorology Agency website. Available at: http://www.ethiomet.gov.et/climates/climate_of_city/2467/Arba%20Minch [Access date: 08/10/2014].

National Research Council (2002) *Abrupt climate change: inevitable surprises*. Washington DC, USA: National Academy of Science.

Ndiema, K.E., Dillan, C.D., Braun, D.R., Harris, J.W.K. and Kiura, P.W. (2011) Transport and subsistence patterns at the transition to pastoralism, Koobi Fora, Kenya. *Archaeometry*, 53, 1085–1098.

Niang, I., Ruppel, O.C., Abdrabo, M.A., Essel, A., Lennard, C., Padgham, J. and Urquhart, P. (2014) Africa, in V.R. Barros, C.B. Field, D.J. Dokken, M.D. Mastrandrea, K.J. Mach, T.E. Bilir, M. Chatterjee, K.L. Ebi, Y.O. Estrada, R.C. Genova, B. Girma, E.S. Kissel, A.N. Levy, S. MacCracken, P.R. Mastrandrea and L.L. White (eds.) *Climate Change 2014: Impacts, Adaptation, and Vulnerability. Part B: Regional Aspects. Contribution of Working Group II to the Fifth Assessment Report of the Intergovernmental Panel on Climate Change*. Cambridge, UK and New York, USA: Cambridge University Press. pp. 1199–1265.

Nicholls, N. (1988) El Niño-Southern Oscillation and rainfall variability. *Journal of*

Climate, 1, 418–421.

Nicholls, N. and Wong, K. (1990) Dependence of rainfall variability on mean rainfall, latitude, and the Southern Oscillation. *Journal of Climate*, 3, 163–170.

Nicholson, S.E. (1982) Pleistocene and Holocene climates in Africa. *Nature*, 296, 779.

Nicholson, S.E. (1986) The spatial coherence of African rainfall anomalies: interhemispheric teleconnections*. Journal of Applied Meteorology and Climatology*, 25, 1365–1381.

Nicholson, S.E. (1996) A review of climate dynamics and climate variability in Eastern Africa, in T.C. Johnson, E.O. Odada (eds.) *The Limnology, Climatology and Paleoclimatology of the East African Lakes*. Amsterdam: Gordon and Breach. pp. 25–56.

Nicholson, S.E. (2000) The nature of rainfall variability over Africa on time scales of decades to millennia. *Global Planetary Change*, 26, 137–158.

Nicholson, S.E. (2014) Spatial teleconnections in African rainfall: A comparison of 19th and 20th century patterns. *The Holocene*, 1–9.

Nicholson, S.E. and Entekhabi, D. (1986) The quasi-periodic behaviour of rainfall variability in Africa and its relationship to the Southern Oscillation. *Journal of Climate and Applied Meteorology*, 34, 311–348.

Nicholson, S.E., Nash, D.J., Chase, B.M., Grab, S.W., Shanahan, T.M., Verschuren, D., Asrat, A., Lezine, A.M. and Umer, M. (2013) Temperature variability over Africa during the last 2000 years. *The Holocene*, 23, 1085–1094.

Nicholson, S.E. and Selato, J.C. (2000) The Influence of La Niña on African Rainfall. *International Journal of Climatology*, 20, 1761–1776.

Nicholson, S.E. and Yin, X. (2002) Mesoscale patters of rainfall, cloudiness and evaporation over the Great Lakes of East Africa, in E.O. Odada and D.O. Olago (eds.) *The East African Great Lakes: Limnology, Palaeolimnology and Biodiversity*. The Netherlands: Kluwer Academic Publishers. pp. 93–119.

Nilsson, E. (1940) Ancient changes of climate in British East Africa and Abyssinia. A study of ancient lakes and glaciers. *Geografiska Annaler Series A*, 22, 1–78.

Öberg, H., Andersen, T.J., Westerberg, L.O., Risberg, J. and Holmgren, K. (2012) A diatom record of recent environmental change in Lake Duluti, northern Tanzania. *Journal of Paleolimnology*, 48, 401–416.

Ogallo, L. (1987) Relationships between seasonal rainfall in East Africa and the Southern Oscillation. *Journal of Climatology*, 7, 1–13.

Olaka, L.A., Odada, E.O., Trauth, M.H., Olago, D.M. (2010) The sensitivity of East African rift lakes to climate fluctuations. *Journal of Paleolimnology*, 44, 629–644.

Olmstead, J. (1973) Agricultural land and social stratification in the Gamu Highland of Southern Ethiopia, in H. Marcus (ed.) *Proceedings of the First United States Conference on Ethiopian Studies*. USA: African Studies Centre, Michigan State University. pp. 223–233.

Olsson, I. (1986) Radiometric dating, in B.E. Berglund (ed.) *Handbook of Holocene Palaeoecology and Palaeohydrology*. Great Britain: John Wiley and Sons. pp. 273–297.

Olsson, I. (1991) Accuracy and precision in sediment chronology. *Hydrobiologia*, 214, 25–34.

Osmaston, H.A. and Harrison, S.P. (2005) The Late Quaternary glaciation of Africa: A regional synthesis. *Quaternary International*, 138–139, 32–54.

Ostrovsky, I. and Yacobi, Y.Z. (1999) Organic matter and pigments in surface sediments: Possible mechanisms of their horizontal distributions in a stratified lake. *Canadian Journal of Fisheries and Aquatic Sciences*, 56, 1001–1010.

Owen, R.B., Barthelme, J.W., Renaut, R.W. and Vincens, A. (1982) Paleolimnology and archaeology of Holocene deposits north-east of Lake Turkana, Kenya. *Nature*, 298, 523–529.

Owen, R.B. and Crossley, R. (1989) Recent sedimentation in lakes Chilwa and Chiuta, Malawi. *Palaeoecology of Africa*, 20, 109–117.

Owen, R.B., Lee, R.K.L. and Renaut, R. (2012) Early Pleistocene lacustrine sedimentation and diatom stratigraphy at Munya wa Gicheru, southern Kenya Rift Valley. *Palaeogeography, Palaeoclimatology, Palaeoecology*, 331–332, 60–74.

Oxfam (2010) 'The rain doesn't come on time anymore: Poverty, vulnerability, and climate variability in Ethiopia', 22nd April 2010. Oxfam website. Available at: https://www.oxfam.org/en/research/rain-doesnt-come-time-anymore [Access date: 08/10/2015].

Pankhurst, R. (1966) The Great Ethiopian Famine of 1888 – 1892: A new assessment. Part 1. *Journal of the History of Medicine and Allied Sciences*, 21, 95–124.

Pankhurst, R. (1985) *The history of famine and epidemics in Ethiopia prior to the twentieth century*. Addis Ababa: Relief and Rehabilitation Commission.

Pankhurst, R. (1992) The history of deforestation and afforestation in Ethiopia prior to World War I, in J.T. Hinne and B. Finne (eds.) *Proceedings of the Sixth Michigan State University Conference of Northeast Africa*. USA: Michigan State University Press. pp. 275–286.

Parkin, T.B. and Brock, T.D. (1980) The Effects of Light Quality on the Growth of Phototrophic Bacteria in Lakes. *Archives of Microbiology*, 125, 19–27.

Parkin, T.B. and Brock, T.D. (1981) The role of phototrophic bacteria in the sulfur cycle of a meromictic lake. *Limnology and Oceanography*, 26, 880–890.

Partin, J.W., Cobb, K.M., Adkins, J.F., Clark, B and Fernandez, D.P. (2007) Millennial-scale trends in west Pacific warm pool hydrology since the Last Glacial Maximum. *Nature*, 449, 452–455.

Partridge, T.C., deMenocal, P.B., Lorentz, S.A., Paiker, M.J. and Vogel, J.C. (1997) Orbital forcing of climate over South Africa: a 200 000-year rainfall record from the Pretoria Saltpan. *Quaternary Science Reviews*, 16, 1–9.

Patrick, R. and Reimer C.W. (1966) *The Diatoms of the United States Exclusive of Alaska and Hawaii, Volume 1*. USA: Monographs of the Academy of Natural Sciences of Philadelphia 13.

Peck, J.A., Green, R.R., Shanahan, T., King, J.W., Overpeck, J.T. and Scholz, C.A. (2004) A magnetic mineral record of Late Quaternary tropical climate variability from Lake Bosumtwi, Ghana. *Palaeogeography, Palaeoclimatology, Palaeoecology*, 215, 37–57.

Peyron, O., Goring, S., Dormoy, I., Kotthoff, U., Pross, J., de Beaulieu, J.L., Drescher-Schneider, R., Vannière, B. and Magny, M. (2011) Holocene seasonality changes in the central Mediterranean region reconstructed from the pollen sequences of Lake Accesa (Italy) and Tenaghi Philippon (Greece). *The Holocene*, 21, 131–146.

Peyron, O., Jolly, D., Bonnefille, R. and Vincens, A. (2000) Climate of East Africa 6000 ^{14}C yr BP as inferred from pollen data. *Quaternary Research*, 54, 90–101.

Pfander, H. and Riesen, R. (1995) High-performance liquid chromatography, in G. Briton, S. Liaaen-Jensen and H. Pfander (eds.) *Carotenoids. Vol 1A. Isolation and Analysis*. Boston: Birkhäuser. pp. 145–190.

Phillips, J. (1997) Punt and Aksum: Egypt and the Horn of Africa. *The Journal of African History*, 38, 423–457.

Pienitz, R., Smol, J.P. and Birks, H.J.B. (1995) Assessment of freshwater diatoms as quantitative indicators of past climate change in the Yukon and Northwest Territories, Canada. *Journal of Paleolimnology*, 13, 21–49.

Powers, L.A., Johnson, T.C., Werne, J.P., Castaneda, I.S., Hopmans, E.C., Sinninghe Damsté, J.S. and Schouten, S. (2005) Large temperature variability in the southern African tropics since the Last Glacial Maximum. *Geophysical Research Letters*, 32, 1–4.

Powers, L.A., Johnson, T.C., Werne, J.P., Castaneda, I.S., Hopmans, E.C., Sinninghe Damsté, J.S. and Schouten, S. (2011) Organic geochemical records of

environmental variability in Lake Malawi during the last 700 years, Part I: The TEX86 temperature record. *Palaeogeography, Palaeoclimatology, Palaeoecology*, 303, 133–139.

Prasad, S. and Enzel, Y. (2006) Holocene paleoclimates of India. *Quaternary Research*, 66, 442–453.

Prell, W.L. and Kutzbach, J.E. (1987) Monsoon variability over the past 150,000 years. *Journal of Geophysical Research*, 92, 8411–8425.

Rasmussen, S.O., Vinther, B.M., Clausen, H.B. and Andersen, K.K. (2007) Early Holocene climate oscillations recorded in three Greenland ice cores. *Quaternary Science Reviews*, 26, 1907–1914.

Ray, N. and Adams, J.M. (2001) A GIS-based vegetation map of the world at the Last Glacial Maximum (25,000–15,000 BP). *Internet Archaeology*, 11, 1–44.

Reader, J. (1998) *Africa: A Biography of the Continent*. London: Penguin Books.

Reed, J.M. (1998a) A diatom-conductivity transfer function for Spanish salt lakes. *Journal of Paleolimnology*, 19, 399–416.

Reed, J.M. (1998b) Diatom preservation in the recent sediment record of Spanish saline lakes: implications for palaeoclimate study. *Journal of Paleolimnology*, 19, 129–137.

Reimer, P.J., Bard, E., Bayliss, A., Beck, J.W., Blackwell, P.G., Ramsey, C.B., Brown, D.M., Buck, C.E., Edwards, R.L., Friedrich, M., Grootes, P.M., Guilderson, T.P., Haflidason, H., Hajdas, I., Hatté, C., Heaton, T.J., Hogg, A.G., Hughen, K.A., Kaiser, K.F., Kromer, B., Manning, S.W., Reimer, R.W., Richards, D.A., Scott, E.M., Southon, J.R., Turney, C.S.M. and van der Plicht, J. (2013) Selection and treatment of data for radiocarbon calibration: an update to the international calibration (INTCAL) criteria. *Radiocarbon*, 55, 1923–1945.

Renberg, I. (1990) A procedure for preparing large sets of diatom slides for sediment cores. *Journal of Paleolimnology*, 4, 87–90.

Renssen, H., Mairesse, A., Goosse, H., Mathiot, P., Heiri, O., Roche, D.M., Nisancioglu, K.H. and Valdes, P.J. (2015) Multiple causes of the Younger Dryas cold period. *Nature Geoscience*, 8, 946–949.

Reuss, N., Conley, D.J. and Bianchi, T.S. (2005) Preservation conditions and the use of sediment pigments as a tool for recent ecological reconstruction in four Northern European estuaries. *Marine Chemistry*, 95, 283–302.

Revel, M., Ducassou, E., Grousset, F.E., Bernasconi, S.M., Migeon, S., Revillon, S., Mascle, J., Murat, A., Zaragosi, S. and Bosch, D. (2010) 100,000 years of African monsoon variability recorded in sediments of the Nile margin. *Quaternary Science Reviews*, 29, 1342–1362.

Ricci, L. (1984) L'expansion de l'Arabie mèridionale, in S. Chelod (ed.) *L'Arabie du Sud: Histoire et Civilisation, I*. Paris: Maisonneuve et Larose. pp. 249–257.

Richardson, J.L. (1968) Diatoms and lake typology in East and Central Africa. *Internationale Revue der gesamten Hydrobiologie*, 53, 299–338.

Richardson, J.L. (1969) Characteristic planktonic diatoms of the lakes of tropical Africa. (Addendum to: Diatoms and lake typology in East and Central Africa). *Internationale Revue der gesamten Hydrobiologie*, 54, 175–176.

Richardson, J.L. and Dussinger, R.A. (1986) Paleolimnology of mid-elevation lakes in the Kenya Rift Valley. *Hydrobiologia*, 143, 167–174.

Richardson, J.L., Harvey, T.J. and Holdschip, S.A. (1978) Diatom in the history of shallow East African lakes. *Polskie Archiwum Hydrbiologii*, 25, 341–353.

Ricketts, R.D. and Johnson, T.C. (1996) Climate change in the Turkana basin as deduced from a 4000 year long δO^{18} record. *Earth and Planetary Science Letters*, 142, 7–17.

Ritz, S.P., Stocker, T.F., Grimalt, J.O.,Menviel, L. and Timmermann, A. (2013) Estimated strength of the Atlantic overturning circulation during the last deglaciation. *Nature Geoscience*, 6, 208–212.

Robbins, L.H. (1972) Archaeology in the Turkana district, Kenya. *Science*, 176, 359–366.

Roberts, N. and Barker, P. (1993) Landscape stability and biogeomorphic response to past and future climatic shifts in intertropical Africa, in D.S.G. Thomas and R.J. Allison (eds.) *Landscape sensitivity (British Geomorphological Research Group Symposia Series*. Chichester: Wiley. pp. 65–82.

Roberts, N., Taieb, M., Barker, P., Damnati, B., Icole, M. and Williamson, D. (1993) Timing of the Younger Dryas event in East Africa from lake-level changes. *Nature,* 366, 146–148.

Rognon, P. and Coudé-Gaussen G. (1996) Paleoclimates off Northwest Africa (28°–35°N) about 18,000 yr B.P. based on continental eolian deposits. *Quaternary Research*, 46, 118–126.

Rohling, E.J. and Hilgen, F.J. (1991) The eastern Mediterranean climate at times of sapropel formation: a review. *Geologie en Mijnbouw*, 70, 253–264.

Rohling, E.J. and Palike, H. (2005) Centennial-scale climate cooling with a sudden cold event around 8,200 years ago. *Nature*, 434, 975–979.

Ropelewski, C.F. and Halpert, M.S. (1987) Global and regional scale precipitation and temperature patterns associated with El Niño/Southern Oscillation. *Monthly Weather Review*, 115, 1606–1626.

Rossignol-Strick, M. (1985) Mediterranean Quaternary sapropels, an immediate response of the African monsoon to variation of insolation. *Palaeogeography, Palaeoclimatology, Palaeoecology*, 49, 237–263.

Round, F.E. (1964) The diatom sequence in lake deposits, some problems of interpretation. *Verhandlungen Internationale Vereinigung für Theoretische und angewandte Limnologie*, 15, 1012–1020.

Roy, S., Llewellyn, C.A., Egeland, E.S. and Johnsen, G. (eds.) (2011) *Phytoplankton pigments characterization, chemotaxonomy and applications in oceanography*. Cambridge: Cambridge University Press.

Rühlemann, C., Mulitza, S., Muller, P.J., Wefer, G. and Zahn, R. (1999) Warming of the tropical Atlantic Ocean and slowdown of thermohaline circulation during the last deglaciation. *Nature*, 402, 511–514.

Russell, J.M., Eggermont, H., Taylor, R. and Verschuren, D. (2009) Paleolimnological records of recent glacier recession in the Rwenzori Mountains, Uganda-D.R. Congo. *Journal of Paleolimnology*, 41, 253–271.

Russell, J.M. and Johnson, T.C. (2005) A high-resolution geochemical record from Lake Edward, Uganda-Congo, and the timing and causes of tropical African drought during the late Holocene. *Quaternary Science Reviews*, 24, 1375–1389.

Russell, J.M., Johnson, T.C., Kelts, K.R., Lærdal, T. and Talbot, M.R. (2003) An 11,000-year lithostratigraphic and paleohydrologic record from Equatorial Africa: Lake Edward, Uganda-Congo. *Palaeogeography, Palaeoclimatology, Palaeoecology*, 193, 25–49.

Russell, J.M., Verschuren, D. and Eggermont, H. (2007) Spatial complexity of 'Little Ice Age' climate in East Africa: sedimentary records from two crater lake basins in western Uganda. *The Holocene*, 17, 183–193.

Ryves, D.B., Battarbee, R.W., Juggins, S., Fritz, S.C. and Anderson, N.J. (2006) Physical and chemical predictors of diatom dissolution in freshwater and saline lake sediments in North America and West Greenland. *Limnology and Oceanography*, 51, 1355–1368.

Ryves, D.B., Juggins, S., Fritz, S.C. and Battarbee, R.W. (2001) Experimental diatom dissolution and the quantification of microfossil preservation in sediments. *Palaeogeography, Palaeoclimatology, Palaeoecology*, 172, 99–113.

Ryves, D.B., Mills, K., Bennike, O., Brodersen, K.P., Lamb, A.L., Leng, M.J., Russell, J.M. and Ssemmanda, I. (2011) Environmental change over the last millennium recorded in two contrasting crater lakes in western Uganda, eastern Africa (Lakes Kasenda and Wandakara). *Quaternary Science Reviews*, 30, 555–569.

Sagri, M., Bartolini, C., Billi, P., Ferrari, G., Benvenuti, M., Carnicelli, S. and Barbano, F. (2008) Latest Pleistocene and Holocene river network evolution in the Ethiopian Lakes region. *Geomorphology*, 94, 79–97.

Said, R. (1993) *The Blue Nile*. Oxford: Elsevier.

Sarmento, H., Isumbisho, M. and Descy, J.P. (2006) Phytoplankton ecology of Lake Kivu (eastern Africa). *Journal of Plankton Research*, 28, 815–829.

Sayer, C.D. (2001) Problems with the application of diatom-total phosphorous transfer functions: examples from a shallow English lake. *Freshwater Biology*, 46, 743–757.

Schnurrenberger, D., Russell, J. and Kelts, K. (2003) Classification of lacustrine sediments based on sedimentary components. *Journal of Paleolimnology,* 29, 141–154.

Scholz, C.A. and Finney, B.P. (1994) Late Quaternary sequence stratigraphy of Lake Malawi (Nyasa), Africa. *Sedimentology*, 41, 163–179.

Scholz, C.A., King, J.W., Ellis, G.S., Swart, P.K., Stager, J.C. and Colman, S.M. (2003) Paleolimnology of Lake Tanganyika, East Africa, over the past 100 kyr; lake basins as archives of continental tectonics and paleoclimate. *Journal of Paleolimnology,* 30, 139–150.

Schreck, C.J. and Semazzi, F.H.M. (2004) Variability of the recent climate of eastern Africa. *International Journal of Climatology*, 24, 681–701.

Scott, L. (1996) Palynology of hyrax middens: 2000 years of palaeoenvironmental history in Namibia. *Quaternary International*, 33, 73–79.

Scott, L. (1999) Vegetation history and climate in the Savanna biome South Africa since 190,000 ka: A comparison of pollen data from the Tswaing Crater (the Pretoria Saltpan) and Wonderkrater. *Quaternary International*, 57–58, 215–223.

Scott, L., Holmgren, K., Talma, A.S., Woodborne, S. and Vogel, J.C. (2003) Age interpretation of the Wonderkrater spring sediments and vegetation change in the Savanna Biome, Limpopo province, South Africa: research letter. *South African Journal of Science*, 99, 484–488.

Scott, L. and Thackeray, J.F. (1987) Multivariate analysis of Late Pleistocene and Holocene pollen spectra from Wonderkrater, Transvaal, South Africa. *South African Journal of Science*, 83, 93–98.

Scussolini, P. Vegas-Vilarrúbia, T., Rull, V., Corella, J.P., Valero-Garcés, B. and Gomà, J. (2011) Middle and late Holocene climate change and human impact inferred from diatoms, algae and aquatic macrophyte pollen in sediments from Lake Montcortès (NE Iberian Peninsula). *Journal of Paleolimnology*, 46, 369–385.

Servant-Vildary, S. (1978) *Etude des diatomées at paléolimnologie du bassin Tchadien au Cénozoique Supérieur*. Paris: OSTROM (Travaux et Documents de l'ORSTOM). pp. 346.

Servant, M. and Servant-Vildary, S. (1980) L'environnement quaternaire du bassin du Tchad, in M.A.J. Williams and H. Faure (eds.) *The Sahara and the Nile*. Rotterdam: Balkema. pp. 133–162.

Shakun, J.D., Burns, S.J., Fleitmann, D., Kramers, J., Matter, A. and Al-Subary, A. (2007) A high-resolution, absolute-dated deglacial speleothem record of Indian Ocean climate from Socotra Island, Yemen. *Earth and Planetary Science Letters*, 259, 442–456.

Shakun, J.D. and Carlson, A.E. (2010) A global perspective on Last Glacial Maximum to Holocene climate change. *Quaternary Science Reviews*, 29, 1–16.

Shanahan, T.M., McKay, N.P., Hughen, K.A., Overpeck, J.T., Otto-Bliesner, B., Heil, C.W., King, J., Scholz, C.A. and Peck, J. (2015) The time-transgressive termination of the African Humid Period. *Nature Geoscience*, 8, 140–144.

Shanahan, T.M., Overpeck, J.T., Sharp, W.E., Scholz, C.A. and Arko, J.A. (2006) Simulating the response of a closed-basin lake to recent climate changes in tropical West Africa (Lake Bosumtwi, Ghana). *Hydrological Processes*, 21, 1678–1691.

Shi, N., Dupont, L.M., Beug, H.J. and Schneider, R. (1998) Vegetation and climate changes during the last 21 000 years in S.W. Africa based on a marine pollen record. *Veget Hist Archaeobot*, 7, 127–140.

Shongwe, M.E., van Oldenborgh, G.J., van den Hurk, B. and van Aalst, M. (2011) Projected changes in mean and extreme precipitation in Africa under global warming. Part II: East Africa. *Journal of Climate*, 24, 3718–3733.

Sinninghe Damsté, J.S., Verschuren, D., Ossebaar, J., Blokker, J., van Houten, R., van de Meer, M.T.J., Plessen, B. and Schouten, S. (2011) A 25,000-year record of climate-induced changes in lowland vegetation of eastern equatorial Africa revealed by the stable carbon-isotopic composition of fossil plant leaf waxes. *Earth and Planetary Science Letters*, 302, 236–246.

Siraj, A.S., Santo-Vega, M., Bouma, M.J., Yadeta, D., Ruiz Carrascal, D. and Pascual, M. (2014) Altitudinal Changes in Malaria Incidence in Highlands of Ethiopia and Colombia. *Science*, 343, 1154–1158.

Slota Jr., P.J., Jull, A.J.T., Linick, T.W and Toolin, L.J. (1987) Preparation of small samples for ^{14}C accelerator targets by catalytic reduction of CO. *Radiocarbon*, 29, 303–306.

Soviet military (1984) Map of Lake Hayq and the surrounding area, 1:100,000. Ethiopia.

Ssemmanda, I. and Vincens, A. (2002) Vegetation changes and their climatic implications for the Lake Victoria region during the late Holocene, in E.O. Odada and D.O. Olago (eds.) *The East African Great Lakes: Limnology, Palaeolimnology and Biodiversity*. The Netherlands: Kluwer Academic Publishers. pp. 509–523.

Stager, J.C. (1998) Ancient analogues for recent environmental changes at Lake Victoria, East Africa, in J.T. Lehman (ed.) *Environmental Change and Response in East African Lakes*. The Netherlands: Kluwer Academic Publishers. pp. 37–46.

Stager, J.C., Cocquyt, C., Bonnefille, R., Weyhenmeyer, C. and Bowerman, N. (2009) A late Holocene paleoclimatic history of Lake Tanganyika, East Africa. *Quaternary Research*, 72, 47–56.

Stager, J.C., Cumming, B.F. and Meeker, L.D. (1997) A high-resolution 11 400-yr diatom record from Lake Victoria, East Africa. *Quaternary Research*, 47, 81– 89.

Stager, J.C., Cumming, B.F. and Meeker, L.D. (2003) A 10,000-year high-resolution diatom record from Pilkington Bay, Lake Victoria, East Africa. *Quaternary Research*, 59, 172–181.

Stager, J.C. and Johnson, T.C. (2000) A 12,400 ^{14}C year offshore diatom record from east central Lake Victoria, East Africa. *Journal of Paleolimnology*, 23, 373–383.

Stager, J.C. and Mayewski, P.A. (1997) Abrupt early to mid-Holocene climatic transition registered at the Equator and the Poles. *Science*, 276, 1834–1836.

Stager, J.C., Mayewski, P.A. and Meeker, L.D. (2002) Cooling cycles, Heinrich event 1, and the desiccation of Lake Victoria. *Palaeogeography, Palaeoclimatology, Palaeoecology*, 183, 169–178.

Stager, J.C., Ryves, D.B., Chase, B.M. and Pausata, F.S.R. (2011) Catastrophic drought in the Afro-Asian monsoon region during Heinrich Event 1. *Science*, 331, 1299–1302.

Stager, J.C., Ryves, D.B., King, C., Madson, J., Hazzard, M., Neumann, F. and Maud, R. (2013) Late Holocene precipitation variability in the summer rainfall region of South Africa. *Quaternary Science Reviews*, 67, 105–120.

Stager, J.C., Reinthal, P.N. and Livingstone, D.A. (1986) A 25,000 year history of Lake Victoria, East Africa and some comments on its significance for the evolution of cichlid fishes. *Freshwater Biology*, 16, 15–19.

Stager, J.C., Westwood, J., Grzesik, D. and Cumming, B.F. (2005) A 5500-year environmental history of Lake Nabugabo, Uganda. *Palaeogeography, Palaeoclimatology, Palaeoecology*, 218, 347–353.

Stanley, J.D., Krom, M.D., Cliff, R.A. and Woodward, J.C. (2003) Short contribution: Nile flow failure at the end of the Old Kingdom, Egypt: strontium isotopic and petrologic evidence. *Geoarchaeology*, 18, 395–402.

Stock, R. (2004) *Africa South of the Sahara, 2nd edition: A Geographical Interpretation*. New York: The Guilford Press.

Stoermer, E.F. and Yang, J.J. (1970) *Distribution and relative abundance of dominant planktonic diatoms in Lake Michigan*. Great Lake Research Division, 16,

University of Michigan, Ann Arbor, M.I., pp. 64.

Stone, J.R. and Fritz, S.C. (2004) Three-dimensional modeling of lacustrine diatom habitat areas: Improving paleolimnological interpretation of planktic: benthic ratios. *Limnology and Oceanography*, 49, 1540–1548.

Street, F.A. (1979a) *Late Quaternary lakes in the Ziway-Shala basin, southern Ethiopia*. PhD thesis. Cambridge University.

Street, F.A. (1979b) Late Quaternary precipitation estimates for the Ziway-Shala basin, southern Ethiopia. *Palaeoecology of Africa*, 11, 135–143.

Street, F.A. (1980) The relative importance of climate and local hyrdrogeological factors in influencing lake-level fluctuations. *Palaeoecology of Africa*, 12, 137–158.

Street, F.A. and Grove, A.T. (1976) Environmental and climatic implications of Late Quaternary lake-level fluctuations in Africa. *Nature,* 261, 385–390.

Street, F.A. and Grove, A.T. (1979) Global maps of lake-level fluctuations since 30,000 years BP. *Quaternary Research*, 12, 83–118.

Street-Perrott, F.A., Barker, P.A., Swain, D.L., Ficken, K.J., Wooller, M.J., Olago, D.O. and Huang, Y. (2007) Late Quaternary changes in ecosystems and carbon cycling on Mt. Kenya, East Africa: a landscape-ecological perspective based on multi-proxy lake-sediment influxes. *Quaternary Science Reviews*, 26, 1838–1860.

Street-Perrott, F.A. and Harrison, S.P. (1985) Lake level and climate reconstructions, in A.D. Hecht (ed.) *Paleoclimate Analysis and Modelling*. New York: John Wiley and Sons. pp. 291–340.

Street-Perrott, F.A. and Perrott, R.A. (1990) Abrupt climate fluctuations in the tropics: the influence of Atlantic Ocean circulation. *Nature*, 343, 607–612.

Stuiver, M. and Polach, H.A. (1977) Discussion: reporting of ^{14}C data. *Radiocarbon*, 19, 355–363.

Stuiver, M. and Reimer, P.J. (1986) A computer program for radiocarbon age calibration. *Radiocarbon*, 28, 1022–1030.

Stuiver, M. and Reimer, P.J. (1993) Extended 14C database and revised CALIB radiocarbon calibration program. *Radiocarbon*, 35, 215–230.

Sulas, F., Madella, M. and French, C. (2009) State formation and water resources management in the Horn of Africa: the Aksumite Kingdom of the northern Ethiopian highlands. *World Archaeology*, 41, 2–15.

Sun, D. (2000) Global climate change and El Niño: a theoretical framework, in H.F. Diaz and V. Markgraf (eds.) *El Niño and Southern Oscillation*. Cambridge: Cambridge University Press. pp. 443–463.

Talbot, M.R. and Johannessen, T. (1992) A high-resolution palaeoclimate record of the last 27,000 years in Tropical West Africa from the carbon and nitrogen isotopic composition of lacustrine organic matter. *Earth and Planetary Science Letters,* 110, 23–37.

Talbot, M.R. and Livingstone, D.A. (1989) Hydrogen index and carbon isotopes of lacustrine organic matter as lake level indicators. *Palaeogeography, Palaeoclimatology, Palaeoecology*, 70, 121–137.

Talbot, M.R. and Lærdal, T. (2000) The late Pleistocene-Holocene palaeolimnology of Lake Victoria, East Africa, based upon elemental and isotopic analyses of sedimentary organic matter. *Journal of Paleolimnology*, 23, 141–164.

Talling, J.F. (1963) Origin of stratification in an African rift lake. *Limnology and Oceanography*, 8, 68–78.

Talling, J.F. (1965) The photosynthetic activity of phytoplankton in East African lakes. *Internationale Revue gesamten Hydrobiologie*, 50, 1–32.

Talling, J.F. (1966) The annual cycle of stratification and phytoplankton growth in Lake Victoria (East Africa). *Internationale Revue gesamten Hydrobiologie und Hydrographie*, 51, 545–621.

Talling, J.F. and Talling, I.B. (1965) The chemical composition of African lake waters. *Internationale Revue der gesamten Hydrobiologie und Hydrographie*, 50, 421–463.

Talma, A.S. and Vogel, J.C. (1992) Late Quaternary paleotemperatures derived from a speleothem from Cango Caves, Cape Province, South Africa. *Quaternary Research*, 37, 203–213.

Tattersall, I. (2003) Out of Africa again…and again? *Nature*, 13, 38–45.

Taye, M.T., Ntegeka, V., Ogiramoi, N.P. and Willems, P. (2011) Assessment of climate change impact on hydrological extremes in two source regions of the Nile River Basin. *Hydrology and Earth System Sciences*, 15, 209–222.

Taylor, K.C., Mayewski, P.A., Alley, R.B., Brook, E.J., Gow, A.J., Grootes, P.M., Meese, D.A., Saltzman, E.S., Severinghaus, J.P., Twickler, M.S., White, J.W.C., Whitlow, S. and Zielinski, G.A. (1997) The Holocene Younger Dryas transition recorded at Summit, Greenland. *Science*, 278, 825–827.

Telford, R.J. and Birks, H.J.B. (2011) Effect of uneven sampling along an environmental gradient on transfer-function performance. *Journal of Paleolimnology*, 46, 99–106.

Telford, R.J. and Lamb, H.F. (1999) Ground water mediated response to Holocene climate change recorded by diatom stratigraphy of an Ethiopian crater lake. *Quaternary Research*, 52, 63–75.

Telford, R.J., Lamb, H.F. and Mohammed, M.U. (1999) Diatom-derived palaeoconductivity estimates for Lake Awassa, Ethiopia: evidence for pulsed inflows of saline groundwater? *Journal of Paleolimnology*, 21, 409–421.

ter Braak, C.J.F. and Šmilauer, P. (2002) *CANOCO reference manual and CanoDraw for Windows user's guide: software for canonical community ordination (version 4.5)*. New York, USA: Microcomputer Power. pp. 1–352.

Terwilliger, V.J., Eshetu, Z., Disnar, J.R., Jacob, J., Adderley, W.P., Huang, Y., Alexandra, M. and Fogel, M.L. (2013) Environmental changes and the rise and fall of civilizations in the northern Horn of Africa: An approach combining δ*D* analyses of land-plant derived fatty acids with multiple proxies in soil. *Geochimica et Cosmochimica Acta*, 111, 140–161.

Thomas, D.S.G., Burrough, S.L. and Parker, A.G. (2012) Extreme events as drivers of early human behaviour in Africa? The case for variability, not catastrophic drought. *Journal of Quaternary Science*, 27, 7–12.

Thomas, C.D., Cameron, A., Green, R.E., Bakkenes, M., Beaumont, L.J., Collingham, Y.C., Erasmus, B.F.N., de Siqueira, M.F., Grainger, A., Hannah, L., Hughes, L., Huntley, B., van Jaarsveld, A.S., Midgley, G.F., Miles, L., Ortega-Huerta, M.A., Peterson, A.T., Phillips, O.L. and Williams, S.E. (2004) Extinction from climate change. *Nature*, 427, 145–148.

Thomas, M.F. and Thorp, M.B. (1995) Geomorphic response to rapid climatic and hydrologic change during the Late Pleistocene and Early Holocene in the humid and subhumid tropics. *Quaternary Science Reviews*, 14, 193–207.

Thompson, L.G., Mosley-Thompson, E., Davis, M.E., Henderson, K.A., Brecher, H.H., Zagorodnov, V.S., Mashiotta, T.A., Lin, P.N., Mikhalenko, V.N., Hardy, D.R. and Beer, J. (2002) Kilimanjaro ice core records: Evidence of Holocene climate change in tropical Africa. *Science*, 298, 589–593.

Thornton, P.K., Jones, P.G., Alagarswamy, G. and Andresen, J. (2009) Spatial variation of crop yield response to climate change in East Africa. *Global Environmental Change*, 19, 54–65.

Tierney, J.E. and deMenocal, P.B. (2013) Abrupt shifts in Horn of Africa hydroclimate since the Last Glacial Maximum. *Science*, 342, 843–846.

Tierney, J.E., Russell, J.M. and Huang, Y. (2010) A molecular perspective on Late Quaternary climate and vegetation change in the Lake Tanganyika basin, East Africa. *Quaternary Science Reviews*, 29, 787–800.

Tierney, J.E., Russell, J.M., Huang, Y., Sinninghe Damsté, J.S., Hopmans, E.C. and Cohen, A.S. (2008) Northern Hemisphere controls on tropical southeast African climate during the past 60,000 years. *Science*, 322, 252–255.

Tierney, J.E., Russell, J.M., Sinninghe Damsté, J.S., Huang, Y. and Verschuren, D. (2011) Late Quaternary behaviour of the East African monsoon and the importance of the Congo Air Boundary. *Quaternary Science Reviews*, 30, 798–807.

Tierney, J.E., Smerdon, J.E., Anchukaitis, K.J. and Seager, R. (2013) Multidecadal variability in East African hydroclimate controlled by the Indian Ocean. *Nature*, 493, 389–392.

Tiki, W., Oba, G. and Tvedt, T. (2011) Human stewardship or ruining cultural landscapes of the ancient *Tula* wells, southern Ethiopia. *The Geographical Journal*, 177, 62–78.

Törnqvist, T.E., De Jong, A.F.M., Oosterbaan, W.A. and Van der Borg, K. (1992) Accurate dating of organic deposits by AMS ^{14}C measurement of macrofossils. *Radiocarbon*, 34, 566–577.

Touzeau, A., Blichert-Toft, J., Amiot, R., Fourel, F., Martineau, F., Cockitt, J., Hall, K., Flandrois, J.P. and Lecuyer, C. (2013) Egyptian mummies record increasing aridity in the Nile valley from 5500 to 1500 yr before present. *Earth and Planetary Science Letters*, 375, 92–100.

Trauth, M.H., Deino, A., Bergner, A.G.N., and Strecker, M.R. (2003) East African climate change and orbital forcing during the last 175 kyr BP. *Earth and Planetary Science Letters*, 206, 297–313.

Trauth, M.H., Maslin, M.A., Deino, A.L., Junginger, A., Lesoloyia, M., Odada, E.O., Olago, D.O., Olaka, L.A., Strecker, M.R. and Tiedemann, R. (2010) Human evolution in a variable environment: the amplifier lakes of Eastern Africa. *Quaternary Science Reviews*, 29, 2981–2988.

Tripathi, R.P. and Singh, H.P. (1993) *Soil erosion and conservation*. New Delhi: Wiley Eastern Limited.

Truc, L., Chevalier, M., Favier, C., Cheddadi, R., Meadows, M.E., Scott, L., Carr, A.S., Smith, G.F. and Chase, B.M. (2013) Quantification of climate change for the last 20,000 years from Wonderkrater, South Africa: implications for the long-term dynamics of the Intertropical Convergence Zone. *Palaeogeography, Palaeoclimatology, Palaeoecology*, 386, 575–587.

Tucker, M.E. and Wright, V.P. (1990) Carbonate depositional systems I: Marine shallow-water and lacustrine carbonates, in M.E. Tucker and V.P. Wright (eds.) *Carbonate Sedimentology*. Oxford: Blackwell Scientific Publications. pp. 101–227.

Tumbare, M.J. (2008) Managing Lake Kariba sustainably: Threats and challenges. *Management of Environmental Quality*, 19, 731–739.

Umer, M., Lamb, H.F., Bonnefille, R., Lezine, A.M., Tierceline, J.J., Gibert, E., Cazet, J.P. and Watrin, J. (2007) Late Pleistocene and Holocene vegetation history of the Bale Mountains, Ethiopia. *Quaternary Science Reviews,* 26, 2229–2246.

Umer, M., Legesse, D., Gasse, F., Bonnefille, R., Lamb, H.F., Leng, M.L. and Lamb, A.L. (2004) Late Quaternary climate changes in the Horn of Africa, in R.W. Battarbee, F. Gasse and C.E. Stickley (eds.) *Past Climate Variability through Europe and Africa*. The Netherlands: Springer. pp. 159–180.

Vallentyne, J.R. (1954) Biochemical limnology. *Science*, 119, 605–606.

Valsecchi, V., Chase, B.M., Slingsby, J.A., Carr, A.S., Quick, L.J., Meadows, M.E., Cheddadi, R. and Reimer, P.J. (2013) A high-resolution 15,600-year pollen and microcharcoal record from the Cederberg Mountains, South Africa. *Palaeogeography, Palaeoclimatology, Palaeoecology*, 387, 6–16.

Van de Giessen, E. (2011) *Horn of Africa Environmental Security Assessment*. A report by the Institute for Environmental Security and the Programme on Environmental Security for Poverty Alleviation. The Netherlands: Institute for Environmental Security.

Verburg, P. and Hecky, R.E. (2009) The physics of the warming of Lake Tanganyika by climate change. *Limnology and Oceanography*, 54, 2418–2430.

Verschuren, D. (1999a) Sedimentation controls on the preservation and time resolution of climate-proxy records from shallow fluctuating lakes. *Quaternary Science Reviews*, 18, 821–837.

Verschuren, D. (1999b) Influence of depth and mixing regime on sedimentation in a small, fluctuating tropical soda lake. *Limnology and Oceanography*, 44, 1103–1113.

Verschuren, D. (2001) Reconstructing fluctuations of a shallow East African lake during the past 1800 yrs from sediment stratigraphy in a submerged crater basin. *Journal of Paleolimnology*, 25, 297–311.

Verschuren, D. (2003) Lake-based climate reconstruction in Africa: progress and challenges. *Hydrobiologia*, 500, 315–300.

Verschuren, D., Cocquyt, C., Tibby, J., Roberts, C.N. and Leavitt, P.R. (1999) Long-term dynamics of algal and invertebrate communities in a small, fluctuating tropical soda lake. *Limnology and Oceanography*, 44, 1216–1231.

Verschuren, D., Edgington, D.N., Kling, H.J. and Johnson, T.C. (1998) Silica depletion in Lake Victoria: sedimentary signals at offshore stations. *Journal of Great Lakes Research*, 24, 118–130.

Verschuren, D., Laird, K.R. and Cumming, B.F. (2000) Rainfall and drought in equatorial east Africa during the past 1,100 years. *Nature*, 403, 410–414.

Verschuren, D., Sinninghe Damsté, J.S., Moernout, J., Kristen, I., Blaauw, M., Fagot, M., Haug, G.H. and CHALLACEA project members (2009) Half-precessional dynamics of monsoon rainfall near the east African equator. *Nature*, 462, 637–641.

Vidal, L., Labeyrie, L., Cortijo, E., Arnold, M., Duplessy, J.C., Michel, E., Becque, S. and van Weering, T.C.E. (1997) Evidence for changes in the North Atlantic Deep Water linked to meltwater surges during the Heinrich events. *Earth and Planetary Science Letters*, 146, 13–27.

Vincens, A., Buchet, G., Williamson, D. and Taieb, M. (2005) A 23,000 yr pollen record from Lake Rukwa (8°S, SW Tanzania): New data on vegetation dynamics and climate in Central Eastern Africa. *Review of Palaeobotany and Palynology*, 137, 147–162.

Vincent, L.A., Aguilar, E., Saindou, M., Hassane, A.F., Jumaux, G., Roy, D., Booneeady, P., Virasami, R., Randriamarolaza, L.Y.A., Faniriantsoa, F.R., Amelie, V., Seeward, H. and Montfraix, B. (2011) Observed trends in indices of daily and extreme temperature and precipitation for the countries of the western Indian Ocean, 1961– 2008. *Journal of Geophysical Research D: Atmospheres,* 116, D10108, DOI: 10.1029/2010JD015303.

Vinebrooke, R.D., Dixit, S.S., Graham, M.D., Gunn, J.M., Chen, Y.W. and Belzile, N. (2002) Whole-lake algal responses to a century of acidic industrial deposition on the Canadian Shield. *Canadian Journal of Fisheries and Aquatic Sciences*, 59, 483–493.

Vinebrooke, R.D., Hall, R.I., Leavitt, P.R. and Cumming, B.F. (1998) Fossil pigments as indicators of phototrophic response to salinity and climatic change in lakes of western Canada. *Canadian Journal of Fisheries and Aquatic Sciences*, 55, 668–681.

Vizy, E.K. and Cook, K.H. (2012) Mid-twenty-first-century changes in extreme events over northern and tropical Africa. *Journal of Climate*, 25, 5748–5767.

Von Deimling, T.S., Held, H., Ganopolski, A. and Rahmstorf, S. (2008) Are paleo-proxy data helpful for constraining future climate change? *PAGES News*, 16, 20–21.

Waelbroeck, C., Duplessy, J.C., Michel, E., Labeyrie, L., Paillard, D. and Duprat, J. (2001) The timing of the last deglaciation in North Atlantic climates. *Nature*, 412, 724–727.

Walker, M.J.C., Berkelhammer, M., Björk, S., Cwynar, L.C., Fisher, D.A., Long, A.J., Lowe, J.J., Newnham, R.M., Rasmussen, S.O. and Weiss, H. (2012) Discussion Paper Formal subdivision of the Holocene Series/Epoch: a Discussion Paper by a Working Group of INTIMATE (Integration of ice–core, marine and terrestrial records) and the Subcommission on Quaternary Stratigraphy (International Commission on Stratigraphy). *Journal of Quaternary Science*, 27, 649–659.

Wang, Y. and Amundson, R. (1996) Radiocarbon dating of soil organic matter. *Quaternary Research*, 45, 282–288.

Wang, Y., Cheng, H., Edwards, R.L., He, Y., Kong, X., An, Z., Wu, J., Kelly, M.J., Dykoski, C.A. and Li, X. (2005) The Holocene Asian monsoon: links to solar changes and North Atlantic climate. *Science*, 308, 854–857.

Wang, R., Dearing, J.A., Langdon, P.G., Zhang, E., Yang, X., Dakos, V. and Scheffer, M. (2012) Flickering gives early warning signals of a critical transition to a eutrophic lake state. *Nature*, 492, 419–422.

Wang, R., Dearing, J.A., Langdon, P.G., Zhang, E., Yang, X., Dakos, V. and Scheffer, M. (2013) Replying to J. Carstensen, R. J. Telford & H. J. B. Birks *Nature* 498. *Nature*, 498, E12–E1.

Weckström, J., Korhola, A. and Blom, T. (1997a) The relationship between diatoms and water temperature in thirty subarctic Fennoscandian lakes. *Arctic and Alpine Research*, 29, 75–92.

Weckström, J., Korhola, A. and Blom, T. (1997b) Diatoms as quantitative indicators of pH and water temperature in subarctic Fennoscandian lakes. *Hydrobiologia*, 347, 171–184.

Weedman, K.J. (2000) *An Ethnoarchaeological study of stone scrapers among the Gamo people of Southern Ethiopia*. PhD thesis. University of Florida.

Weedman, K.J. (2006) An Ethnoarchaeological Study of Hafting and Stone Tool Diversity among the Gamo of Ethiopia. *Journal of Archaeological Method and Theory*, 13, 188–237.

Weedman Arthur, K., Arthur, J.W., Curtis, M.C., Lakew, B. and Lesur-Gebremariam, J. (2009) Historical archaeology in the highlands of southern Ethiopia: Preliminary findings. *Nyame Akuma*, 72, 3–11.

Weijers, J.W.H., Schefuß, E., Schouten, S. and Sinninghe Damsté, J.S. (2007) Coupled thermal and hydrological evolution of tropical Africa over the last deglaciation. *Science*, 315, 1701–1704.

Welc, F. and Marks, L. (2014) Climate change at the end of the Old Kingdom in Egypt around 4200 BP: New geoarchaeological evidence*. Quaternary International*, 324, 124–133.

Weldeab, S., Lea, D.W., Schneider, R.R. and Andersen, N. (2007) 155,000 years of West African monsoon and ocean thermal evolution. *Science*, 316, 1303–1307.

Weltje, G.J. and Tjallingii, R. (2008) Calibration of XRF core scanners for quantitative geochemical logging of sediment cores: Theory and application. *Earth and Planetary Science Letters*, 274, 423–438.

Weninger, B., Alram-Stern, E., Bauer, E., Clare, L., Danzeglocke, U., Jöris, O., Kubatzki, C., Rollefson, G., Todorova, H. and van Andel, T. (2006) Climate forcing due to the 8200 cal yr BP event observed at Early Neolithic sites in the eastern Mediterranean. *Quaternary Research*, 66, 401–420.

White, F. (1983) *The vegetation of Africa*. *A descriptive memoir to accompany the UNESCO/AETFAT/UNSO vegetation map of Africa.* Paris: UNESCO.

Wigger, K.M. (1998) Ethiopia: A Dichotomy of Despair and Hope. *Tulsa Journal of Comparative and International Law*, 5, 389–411.

Wilhite, D.A. (1993) The enigma of drought, in D.A. Whilhite (ed.) *Drought Assessment, Management, and Planning: Theory and Case Studies*. New York: Kluwer Academic Publishers. pp. 3–15.

Wilhite, D.A., Hayes, M.J. and Svoboda, M.D. (2013) Drought. *Encyclopedia of Environmetrics*, 2, DOI: 10.1002/9780470057339.vnn046.

Williams, W.D. (1967) The Chemical Characteristics of Lentic Surface Waters in Australia: A Review, in A.H. Weatherley (ed.) *Australian Inland Waters and Their Fauna*. Canberra: Australia National University Press. pp. 18–77.

Williams, M.A.J. (2009) Late Pleistocene and Holocene environments in the Nile basin. *Global and Planetary Change*, 69, 1–15.

Williams, D.M. (2011) *Synedra*, *Ulnaria*: definitions and descriptions – a partial resolution. *Diatom Research*, 26, 149–153.

Williams, M.A.J. and Adamson, D. (1980) Late Quaternary depositional history of the Blue and White Nile rivers in central Sudan, in M.A.J. Williams and H. Faure (eds.) *The Sahara and the Nile. Quaternary Environments and Prehistoric Occupation in Northern Africa.* Rotterdam: Balkema. pp. 281–304.

Williams, M.A.J., Adamson, D., Cock, B. and McEvedy, R. (2000) Late Quaternary environments in the White Nile region, Sudan. *Global and Planetary Change*, 26, 305–316.

Williams, A.P. and Funk, C. (2011) A westward extension of the warm pool leads to a westward extension of the Walker circulation, drying eastern Africa. *Climate Dynamics,* 37, 2417–2435.

Williams, A.P., Funk, C., Michaelsen, J., Rauscher, S.A., Robertson, I., Wils, T.H.G., Koprowski, M., Eshetu, Z. and Loader, N.J. (2012) Recent summer precipitation trends in the Greater Horn of Africa and the emerging role of Indian Ocean sea surface temperature. *Climate Dynamics,* 39, 2307–2328.

Williams, M.A.J., Talbot, M., Aharon, P., Abdlsalaam, Y., Williams, F. and Inge Brendeland, K. (2006) Abrupt return of the summer monsoon 15,000 years ago: new supporting evidence from the lower White Nile valley and Lake Albert. *Quaternary Science Reviews,* 25, 2651–2665.

Williamson, D., Jelinowska, A., Kissel, C., Tucholka, P., Gibert, E., Gasse, F., Massault, M., Taieb, M., Van Campo, E. and Wieckowski, K. (1998) Mineral-magnetic proxies of erosion/oxidation cycles in tropical maar-lake sediments (Lake Tritrivakely, Madagascar) paleoenvironmental implications. *Earth and Planetary Science Letters*, 155, 205–219.

Wolde-Mariam, M. (1986) *Rural Vulnerability to Famine in Ethiopia 1958–1977*.

London: Intermediate Technology Publications.

Wolin, J.A. and Stone, J.R. (2010) Diatoms as indicators of water-level change in freshwater lakes, in J.P. Smol and E.F. Stoermer (eds.) *The Diatoms: Applications for the Environmental and Earth Sciences Second Edition*. New York: Cambridge University Press. pp. 174–185.

World Bank (2014) Countries. World Bank website. Available at: http://www.worldbank.org/en/country [Access date: 08/10/2015].

Wright, D.K. (2011) Frontier animal husbandry in the Northeast and East Africa Neolithic: a multiproxy palaeoenvironmental and paleodemographic study. *Journal of Anthropological Research*, 67, 213–244.

Yacobi, Y.Z., Eckert, W., Trüper, H.G. and Berman, T. (1990) High Performance Liquid Chromatography detection of phototrophic bacterial pigments in aquatic environments. *Microbial Ecology*, 19, 127–136.

Yesuf, H.M., Alamirew, T., Melesse, A.M. and Assen, M. (2013) Bathymetric study of Lake Hayq, Ethiopia. *Lakes and Reservoirs: Research and Management*, 18, 155–165.

You, Q., Wang, Q. and Kociolek, J.P. (2015) New *Gomphonema* Ehrenberg (Bacillariophyceae: Gomphonemataceae) species from Xinjiang Provinence, China. *Diatom Research*, 30, 1–12.

Zanon, V. (1941) Diatomee dei Laghi Galla (A.O.I). Atti della reale Accademia d'Italia. *Memorie della classe de Scienze Fisiche, Matematische e Naturali*, 5, 1–60.

Appendix 1

Troels-Smith Lithological Description.

Key:

Ld - limus detrituosus, common lake mud.

Lso - limus siliceous organogenes, siliceous remains of plants or animals.

Lc - limus calcareous, compacted calcium carbonate.

As - argrilla steatodes, clay < 0.002 mm in size.

Ag - argrilla granosa, silt > 0.002 mm and < 0.06 mm in size.

Ga - grana arenosa, fine sand.

Gs - grana suburralia, coarse sand.

Gg - grana glareosa, small to medium gravel.

Subdrive 1A

Depth (cm)	Description
0.0 – 4.5	Oasis, top 4.5 cm sediment missing.
4.5 – 7.0	Dark brown gyttja containing almost pure white laminations. Y2.5 2.5/1 (black), strf 2, diffuse lim. Dg+, Ld1, Lso1, Ag 2.
7.0 – 10.0	Dark brown gyttja containing pulpy laminations (dark yellow-brown). Y2.5 2.5/1, strf 1, diffuse lim. Ld1, Lso1, Ag 2.
10.0 – 18.0	Darker brown gyttja, homogenous in texture without laminations. Traces of larger particles, possibly sand, and black organic material. Y2.5 2.5/1, strf 0, gradual lim. Dg++, Ld2, Ag2, Gs+.
18.0 – 20.0	Dark brown gyttja containing pulpy laminations up to 2.5 mm thick. Y2.5 2.5/1, strf 3, gradual lim. Dg, Ld1, Lso1, Ag2, Ga+.
20.0 – 31.0	Dark brown gyttja containing thin, straight laminations up to 1.0 mm thick. Y2.5 2.5/1, strf 3, gradual lim. Dg, Ld1, Lso1, Ag2, Ga+.
31.0 – 33.0	Dark brown gyttja containing pulpy laminations. Y2.5 2.5/1, strf 3, gradual lim. Dg, Ld1, Lso1, Ag2, Ga+.

33.0 – 38.0	Sediment deformed but traces of thin laminations. Y2.5 2.5/1, strf 3, gradual lim. Dg, Ld1, Lso1, Ag2, Ga+.
38.0 – 39.0	Dark brown gyttja containing pulpy straight laminations 1.5 mm thick. Y2.5 2.5/1, strf 3, gradual lim. Dg, Ld1, Lso1, Ag2, Ga+.
39.0 – 61.0	Dark brown gyttja containing straight laminations (dark yellow) < 1.0 mm thick, spaced < 1.0 mm – 2.0 cm apart. Y2.5 2.5/1, strf 4, gradual lim. Dg+, Ld1, Lso1, Ag2.
61.0 – 69.0	Dark brown gyttja containing traces of laminations. Y2.5 2.5/1, strf 1, gradual lim. Dg+, Ld1, Lso1, Ag2, Ga+.
69.0 – 74.0	Dark brown gyttja containing pulpy laminations 1.0 mm thick and unevenly spaced. Y2.5 2.5/1, strf 2, sharp lim. Ld1, Lso1, Ag2.
74.0 – 87.0	Very dark brown-black gyttja containing pulpy laminations (brown-yellow) 1.0 mm thick and unevenly spaced. Y2.5 2.5/1, strf 2, sharp lim. Ld1, Lso1, Ag2.
87.0 – 91.5	Dark brown gyttja containing pulpy laminations (dark brown-yellow) up to 7.0 mm thick in places. Y2.5 2.5/1, strf 3, sharp lim. Ld1, Lso1, Ag2.
91.5 – 100.0	Dark brown gyttja containing very thin (< 1.0 mm) laminations unevenly spaced. Y2.5 2.5/1, strf 1, sharp lim. Ld1, Lso1, Ag2.

Gaps/broken sediment at 27.0 – 28.0, 28.5 – 29.5 and 35.0 – 37.0 cm.

Subdrive 1B

Depth (cm)	Description
0.0 – 11.5	Dark brown-black gyttja with thin (< 1.0 mm), straight laminations (brown-yellow). Y2.5 2.5/1 (black), strf 2, gradual lim. Dg+, Ag2, Ld1, Lso1.
11.5 – 15.0	Dark brown-black gyttja with pulpy laminations 2.0 mm thick and unevenly spaced. Y2.5 2.5/1, strf 3, gradual lim. Ag2, Ld1, Lso1.
15.0 – 20.0	Lighter brown-black gyttja with thin (1.0 mm), straight laminations (light brown) spaced at 2.0 mm intervals. Y2.5 3/1 (very dark grey), strf 3, sharp lim. Ag2, Ld1, Lso1.
20.0 – 25.0	Dark brown-black gyttja containing a pulp matrix of laminations (light brown to dirty yellow) up to 5.0 mm thick in places. Y2.5 2.5/1, strf 4, sharp lim. Ag1, Ld1, Lso2.
25.0 – 30.0	Dark brown-black gyttja with thin (1.0 mm) laminations evenly spaced (1.0 mm). Y2.5 2.5/1, strf 3, gradual lim. Ag2, Ld1, Lso1.
30.0 – 34.5	Darker brown-black sediment. Faint, thin laminations, unevenly spaced. Y2.5 2.5/1, strf 1, gradual lim. Ag2, Ld2, Lso++.
34.5 – 42.0	Brown-black gyttja with thick (> 1.0 mm), pulpy laminations (dirty yellow). Y2.5 3/1, strf 4, sharp lim. Ag2, Ld1, Lso1, but more

	laminations than gyttja.
42.0 – 53.5	Brown-black gyttja with faint laminations. Y2.5 2.5/1, strf 1, diffuse lim. Ag2, Ld2, Lso++.
53.5 – 70.0	Black gyttja with very, very faint laminations. Y2.5 2.5/1, strf 1, diffuse lim. Ag2, Ld2, Lso++.
70 – 87.0	Very black gyttja. Y2.5 2.5/1, strf 0, diffuse lim. Ag2, Ld2.

Gaps in sediment at 36.0 – 38.0, 39.0 – 40.0, 43.0 – 43.5 and 56.0 – 56.5 cm.

Subdrive 2A

Depth (cm)	Description
0.0 – 6.5	Oasis, top 6.5 cm sediment missing.
6.5 – 18.0	Light brown gyttja with faint traces of laminations. Y2.5 3/2 (very dark greyish-brown), strf 1, gradual lim. Ag2, Ld2, Lso+, Dg+.
18.0 – 21.0	Brown gyttja with pulpy laminations up to 5.0 mm in thickness. Y2.5 2.3/1 (very dark grey), strf 4, sharp lim. Ag2, Ld1, Lso1 (Ld 25 %, Lso 75 %).
21.0 – 25.5	Dark brown gyttja with traces of laminations. Y2.5 3/1, strf 1, very gradual lim. Ag2, Ld2, Lso+.
25.5 – 28.0	Dark brown gyttja with pulpy laminations (brown-grey) up to 8.0 mm in thickness in places. Y2.5 3/1, strf 4, sharp lim. Ag2, Ld1, Lso1 (Ld 75 %, Lso 25 %).
28.0 – 34.5	Dark brown gyttja homogenous in colour and texture. Y2.5 3/1, strf 0, very diffuse lim. Ag2, Ld2.
34.5 – 44.0	Black gyttja homogenous in colour and texture. Y2.5 2.5/1, strf 0, very gradual lim. Ag2, Ld2, Dg+.
44.0 – 60.5	Black gyttja containing a matrix of pulpy laminations (grey). Y2.5 2.5/1, strf 2/3, gradual lim. Ag2, Ld1, Lso1 (Ld 75 %, Lso 25 %), Dg+.
60.5 – 66.0	Black gyttja homogenous in colour and texture. Y2.5 2.5/1 (black), strf 0, diffuse lim. Ag2, Ld2.
66.0 – 77.0	Black-brown gyttja homogenous in colour and texture. Y2.5 2.5/1, strf 0, gradual lim. Ag2, Ld2, Lso+.
77.0 – 94.0	Black-brown gyttja with matrix of laminations. Y2.5 2.5/1, strf 2, very gradual lim. Ag2, Ld2, Lso1 (Ld 75 %, Lso 25 %).
94.0 – 95.5	Black-brown gyttja. Y2.5 2.5/1, strf 0, very gradual lim. Ag2, Ld2, Lso+.
95.5 – 100.0	Black-brown gyttja containing a matrix of pulpy (grey) laminations. Y2.5 2.5/1, strf 4, very gradual lim. Ag2, Ld1, Lso1.

Subdrive 2B

Depth (cm)	Description
0.0 – 11.5	Dark brown-green gyttja containing pulpy matrix of laminations (dirty brown-yellow). Y2.5 2.5/1 (black), gradual lim, strf 4. Ag2, Ld1, Lso1.
11.5 – 15.0	Dark brown gyttja containing traces of pulpy laminations. Y2.5 2.5/1, gradual lim, strf 2. Ag2, Ld2, Lso++.
15.0 – 19.0	Very dark brown gyttja with traces of thin laminations. Y2.5 2.5/1, gradual lim, strf 1. Ag2, Ld2, Lso+.
19.0 – 21.5	Dark brown gyttja with traces of thin laminations. Y2.5 2.5/1, gradual lim, strf 2. Ag2, Ld2, Lso1 (Ld 75 %, Lso 25 %).
21.5 – 24.0	Very dark brown gyttja homogenous in colour and texture. Y2.5 2.5/1, gradual lim, strf 1. Ag2, Ld2.
24.0 – 26.0	Black gyttja containing traces of a pulpy lamination matrix. Y2.5 2.5/1, gradual lim, strf 2. Ag2, Ld2, Lso++.
26.0 – 29.0	Dark brown gyttja containing traces of a pulpy lamination matrix. Y2.5 2.5/1, gradual lim, strf 2. Ag2, Ld2, Lso++.
29.0 – 31.0	Dark brown gyttja containing very thick (1.5 cm) laminations (dark grey). Y2.5 2.5/1, strf 3, gradual lim. Ag2, Ld1, Lso1.
31.0 – 32.5	Brown-black gyttja, homogenous in colour and texture. Y2.5 2.5/1, strf 0, gradual lim. Ag2, Ld2.
32.5 – 34.0	Brown-black gyttja containing thin (< 1.0 mm), straight, evenly spaced laminations. Y2.5 2.5/1, strf 3, very gradual lim. Ag2, Ld1, Lso1.
34.0 – 36.0	Brown-black gyttja, homogenous in colour and texture. Y2.5 2.5/1, strf 0, gradual lim. Ag2, Ld2.
36.0 – 36.5	Brown-black gyttja containing thin (< 1.0 mm), straight, evenly spaced laminations. Y2.5 2.5/1, strf 3, very gradual lim. Ag2, Ld1, Lso1.
36.5 – 42.0	Black gyttja homogenous in colour and texture. Y2.5 2.5/1, strf 1, gradual lim. Ag2, Ld2, Lso+.
42.0 – 47.0	Dark brown gyttja containing a pulpy matrix of laminations (grey). Y2.5 2.5/1, strf 1, very gradual lim. Ag2, Ld1, Lso1.

Subdrive 3A

Depth (cm)	Description
0.0 – 16.5	Oasis, top 16.5 cm sediment missing.
16.5 – 29 .0	Brown gyttja with subtle stratification- light brown and dark brown laminations, 1.0 mm in thickness, < 1.0 mm spacing. Y2.5 3/1 (very dark grey), strf 4, sharp lim. Ld2, Ag2.
29.0 – 30.0	Brown gyttja containing a matrix of pulpy laminations (dark grey in colour). Y2.5 3/1, strf 3, sharp lim. Ag2, Ld2, Lso++.
30.0 – 33.5	Brown gyttja homogenous in colour and texture. Y2.5 3/1, strf 0, very gradual lim. Ag2, Ld2, Dg+.

33.5 – 34.5	Brown gyttja containing a matrix of pulpy laminations (dark grey in colour). Y2.5 3/1, strf 4, diffuse lim. Ag2, Ld2, Lso++.
34.5 – 55.0	Dark brown-black gyttja homogenous in colour and texture. Y2.5 2.5/1 (black), strf 0, diffuse lim. Ag2, Ld2.
55.0 – 81.0	Black gyttja homogenous in colour and texture. Y2.5 2.5/1, strf 0, very gradual lim. Ag2, Ld2.
81.0 – 83.0	Black gyttja containing traces of pulpy laminations (grey). Y2.5 2.5/1, strf 1-2, very gradual lim. Ag2, Ld2, Lso++.
83.5 – 88.0	Black gyttja containing pulpy laminations (grey), unevenly distributed and disjointed. Y2.5 2.5/1, strf 4, very gradual lim. Ag2, Ld1, Lso1.
88.0 – 92.5	Black gyttja homogenous in colour and texture. Y2.5 2.5/1, strf 0, very gradual lim. Ag2, Ld2.
92.5 – 100.0	Black gyttja containing traces of laminations (grey). Most prominent laminations from 96.0 – 98.0 cm in a left-down to right-up position. Y2.5 2.5/1, strf 2, very gradual lim. Ag2, Ld1, Lso1.

Subdrive 3B

Depth (cm)	Description
0.0 – 8.0	Brown-grey gyttja with some thin laminations (black to light grey in colour). Y2.5 2.5/1 (black), strf 1, very sharp lim. Ag2, Ld2.
8.0 – 16.0	Gap in sediment.
16.0 – 24.0	Brown-black gyttja containing pulpy laminations (dirty-yellow in colour). Laminations are not uniform in width, spacing or directionality. Y2.5 2.5/1, strf 4, very gradual lim. Ag2, Ld1, Lso1.
24.0 – 24.5	A thick (0.5 mm) pulpy lamination intermixed with black gyttja. Y2.5 2.5/1, strf 4, very sharp lim. Ag2, Ld1, Lso1 (Ld 33 %, Lso 66 %).
24.5 – 33.5	Brown-black gyttja containing pulpy laminations (dirty yellow). Laminations are not uniform in width, spacing or directionality. The thickest lamination occurs at 31.0 cm (2.0 – 3.0 mm). Y2.5 2.5/1, strf 4, very gradual lim. Ag2, Ld1, Lso1.
33.5 – 50.5	Black gyttja homogenous in colour and texture. A single, straight grey-brown lamination, 3.0 mm thick occurs at 49.5 cm. Y2.5 2.5/1, strf 1, very sharp lim. Ag2, Ld2, Lso+.

Subdrive 4A

Depth (cm)	Description
0.0 – 11.0	Oasis, top 11.0 cm sediment missing.
11.0 – 19.0	Brown gyttja containing a pulpy matrix (dirty yellow). Y2.5 3/1 (very dark grey), strf 3, sharp lim. Ag2, Ld1, Lso1.

19.0 – 24.5	Dark brown gyttja containing very thin (< 1.0 mm), evenly spaced, light laminations. Y2.5 3/1, strf 4, sharp lim. Ag2, Ld1, Lso1.
24.5 – 27.5	Dark brown gyttja with very pulpy laminations, up to 6.0 mm in thickness (dirty yellow). Y2.5 3/1, strf 4, sharp lim. Ag2, Ld1, Lso1.
27.5 – 33.5	Dark brown gyttja containing very thin (<1.0 mm), unevenly spaced, light laminations. Y2.5 3/1, strf 3, very gradual lim. Ag2, Ld1, Lso1.
33.5 – 36.5	Dark brown gyttja with very pulpy laminations, up to 1.0 cm in thickness (dirty yellow). Y2.5 3/1, strf 4, sharp lim. Ag2, Ld1, Lso1.
36.5 – 49.0	Very dark brown-black gyttja containing traces of light laminations. Y2.5 2.5/1 (black), strf 1, diffuse lim. Ag2, Ld2, Lso+.
49.0 – 64.0	Black gyttja, homogenous in colour and texture. Y2.5 2.5/1, strf 0, very gradual lim. Ag2, Ld2.
64.0 – 81.0	Black gyttja containing an uneven, matrix of laminations (dirty white). Y2.5 2.5/1, strf 2, very gradual lim. Ag2, Ld1, Lso1.
81.0 – 85.0	Black gyttja, homogenous in colour and texture. Y2.5 2.5/1, strf 0, diffuse lim. Ag2, Ld1, Lso+.
85.0 – 100.0	Black-brown gyttja containing traces of a pulpy lamination matrix. Y2.5 2.5/1, strf 2, diffuse lim. Ag2, Ld1, Lso1 (Ld 66 %, Lso 33 %).

Subdrive 4B

Depth (cm)	Description
0.0 – 2.0	Dark brown gyttja. Y2.5 2.5/1 (black), strf 1, very gradual lim. Ag2, Ld2, Lso+.
2.0 – 4.0	Brown-grey gyttja containing a pulpy lamination matrix (yellow-brown). Y2.5 2.5/1, strf 4, very gradual lim. Ag2, Ld1, Lso1.
4.0 – 15.0	Brown-black gyttja containing traces of pulpy laminations. Y2.5 2.5/1, strf 1, diffuse lim. Ag2, Ld2, Lso++.
15.0 – 21.5	Brown-grey gyttja containing a pulpy lamination matrix (yellow-brown). Y2.5 2.5/1, strf 3, very gradual lim. Ag2, Ld1, Lso1.
21.5 – 27.5	Brown-black gyttja containing traces of pulpy laminations. Y2.5 2.5/1, strf 1, diffuse lim. Ag2, Ld2, Lso++.
27.5 – 30.5	Brown-grey gyttja containing a pulpy lamination matrix (yellow-brown). Y2.5 2.5/1, strf 3, very gradual lim. Ag2, Ld1, Lso1.
30.5 – 33.0	Brown-black gyttja containing traces of pulpy laminations. Y2.5 2.5/1, strf 1, very gradual lim. Ag2, Ld2, Lso+.
33.0 – 44.0	Brown-grey gyttja containing a pulpy lamination matrix (yellow-brown). Y10 3/1 (very dark grey), strf 3, very gradual lim, Ag2, Ld1, Lso1.
44.0 – 71.0	Light brown-grey gyttja containing traces of pulpy laminations. One distinct lamination at 57.0 cm, 3.0 mm thick. Y10 3/1, strf 1, diffuse lim. Ag2, Ld2, Lso+.
71.0 – 90.0	Brown-grey gyttja containing unevenly spaced laminations (white-grey). Y10 3/1, strf 2, diffuse lim. Ag2, Ld2, Lso++.

Subdrive 5A

Depth (cm)	Description
0.0 – 3.5	Oasis, top 3.5 cm missing.
3.5 – 8.0	Brown-grey gyttja containing traces of a pulpy lamination matrix. Y2.5 3/1 (very dark grey), strf 1, gradual lim. Ag2, Ld2, Lso++.
8.0 – 8.5	Pulpy lamination (dirty yellow). Y2.5 3/1, strf 3, gradual lim. Ag2, Ld1, Lso1 (Ld 33 %, Lso 66 %).
8.5 – 20.0	Brown-grey gyttja with some light laminations, unevenly spaces, < 1.0 mm thick. Y2.5 2.5/1 (black), strf 2, gradual lim. Ag2, Ld2, Lso++.
20.0 – 20.5	Pulpy lamination (dirty yellow). Y2.5 3/1, strf 3, gradual lim. Ag2, Ld1, Lso1 (Ld 33 %, Lso 66 %).
20.5 – 31.0	Brown-grey gyttja with some light laminations, unevenly spaces, < 1.0 mm thick. Y2.5 2.5/1 (black), strf 2, gradual lim. Ag2, Ld2, Lso++.
31.0 – 31.5	Pulpy lamination (dirty yellow). Y2.5 3/1, strf 3, gradual lim. Ag2, Ld1, Lso1 (Ld 33 %, Lso 66 %).
31.5 – 38.5	Brown gyttja, homogenous in colour and texture. Y2.5 2.5/1, strf 1. very gradual lim. Ag2, Ld2.
38.5 – 39.0	Pulpy lamination (dirty yellow). Y2.5 3/1, strf 3, gradual lim. Ag2, Ld1, Lso1 (Ld 33 %, Lso 66 %).
39.0 – 69.0	Brown-grey gyttja with some light laminations, unevenly spaces, < 1.0 mm thick. Y2.5 2.5/1 (black), strf 2, diffuse lim. Ag2, Ld2, Lso++.
69.0 – 88.0	Brown-grey gyttja with some more pronounced light laminations than the previous section. Laminations are light in colour, spaced evenly (1.0 mm apart) and are < 1.0 mm in thickness. Also some pulpy laminations intermixed. Y2.5 3/1, strf 4, diffuse lim. Ag2, Ld1, Lso1.

Subdrive 5B

Depth (cm)	Description
0.0 – 9.0	Dark brown gyttja containing laminations. Laminations are faint in places, unevenly spaced and uneven in width (< 1.0 mm – 2.0 mm). Some laminations resemble the pulpy lamination matrix. Y10 3/1 (very dark grey), strf 3, very gradual lim. Ag2, Ld2, Lso++.
9.0 – 20.0	Dark brown gyttja containing light coloured laminations (< 1.0 mm thick), fairly evenly spaced. Y10 3/1, strf 3, diffuse lim. Ag2, Ld2, Lso++.
20.0 – 30.0	Dark brown gyttja containing laminations. Laminations are faint in places, unevenly spaced and uneven in width (< 1.0 mm – 2.0 mm). Some laminations resemble the pulpy lamination matrix. Y10 3/1 (very dark grey), strf 3, diffuse lim. Ag2, Ld2, Lso++.
30.0 – 47.0	Dark brown gyttja with distinct, alternating light and black laminations, < 1.0 mm thick, fairly evenly spaced. Y10 3/1, strf 4, diffuse lim. Ag2, Ld1, Lso1.
47.0 – 60.0	Dark brown gyttja containing laminations. Laminations are faint in places, unevenly spaced and uneven in width (< 1.0 mm – 2.0 mm).

	Some laminations resemble the pulpy lamination matrix. Y10 3/1 (very dark grey), strf 3, very gradual lim. Ag2, Ld1, Lso1.
60.0 – 64.0	Dark brown gyttja with distinct, alternating light and black laminations, < 1.0 mm thick, fairly evenly spaced. Y10 3/1, strf 4, diffuse lim. Ag2, Ld1, Lso1.
64.0 – 67.0	Dark brown gyttja with faint light laminations, < 1.0 mm thick, fairly evenly spaced. Y10 3/1, strf 4, diffuse lim. Ag2, Ld1, Lso1.

Drive 6

Depth (cm)	Description
0.0 – 9.0	Oasis, top 9.0 cm missing.
9.0 – 25.0	Black-brown gyttja, homogenous in colour and texture. Y2.5 2.5/1 (black), strf 0, gradual lim. Ag2, Ld2.
25.0 – 31.0	Black-brown gyttja containing grana. Y2.5 2.5/1, strf 0, very gradual lim. Ag1, Ld2, Ga1.
31.0 – 33.0	Black-brown gyttja with white laminations < 1.0 mm thick, spaced < 1.0 mm apart. Laminations are not continuous through the sediment section, but broken in places and faint in colour. Y2.5 3/1 (very dark grey), strf 3, gradual lim. Ag1, Ld1, Lso1, Ga1.
33.0 – 38.5	Black-grey gyttja homogenous in colour and texture. Y2.5 3/1, strf 0, sharp lim. Ag2, Ld2.
38.5 – 41.0	Black-grey gyttja with white laminations < 1.0 mm thick, spaced < 1.0 mm apart. Laminations are very distinct in the gyttja as well as continuous through the sediment section. Y2.5 3/1, strf 4, very sharp lim. Ag2, Ld1, Lso1.
41.0 – 58.0	Brown-grey gyttja homogenous in colour and texture. Y2.5 3/1, strf 0, diffuse lim. Ag2, Ld2.
58.0 – 91.5	Light brown-grey gyttja homogenous in colour and texture. Y2.5 4/1 (dark grey), strf 0, very gradual lim. Ag2, Ld2, Lso+.
91.5 – 94.0	Grey gyttja homogenous in colour and texture. Y2.5 5/1 (grey), strf 0, very gradual lim. Ag2, Ld2.
94.0 – 99.0	Light brown-grey gyttja homogenous in colour and texture. Y2.5 4/1 (dark grey), strf 0, very gradual lim. Ag2, Ld2, Lso+.

Subdrive 7A

Depth (cm)	Description
0.0 – 7.0	Oasis, top 7.0 cm missing.
7.0 – 12.0	Dark brown-grey gyttja, homogenous in colour and texture. Y2.5 3/1 (very dark grey), strf 0, very gradual lim. Ld2, Ag2.
12.0 – 15.0	Slightly lighter brown-grey gyttja homogenous in colour and texture. Y2.5 3/1, strf 0, very gradual lim. Ld2, Ag2.

15.0 – 16.0	Dark brown-grey gyttja, homogenous in colour and texture. Y2.5 3/1 (very dark grey), strf 0, very gradual lim. Ld2, Ag2.
16.0 – 23.5	Marbled gyttja containing the dark brown-grey and slightly lighter brown-grey colours. Y2.5 3/1, strf 0, very gradual lim, Ld2, Ag2, Ga+.
23.5 – 26.5	Grey gyttja containing traces of white laminations < 1.0 mm thick. Y2.5 3/1, strf 1, very gradual lim. Ld2, Ag2, Lc+, Ga+.
26.5 – 36.0	Light grey-brown gyttja, homogenous in texture with some small patches of dark grey gyttja intermixed. Y2.5 4/1 (dark grey), strf 0, very gradual lim. Ld2, Ag2, Lc+, Ga+.
36.0 – 40.0	Dark grey gyttja homogenous in colour and texture. Y2.5 3/1, strf 0, very gradual lim. Ld2, Ag2.
40.0 – 42.0	Light grey-brown gyttja, homogenous in colour and texture. Y2.5 4/1, strf 0, gradual lim. Ld2, Ag2.
42.0 – 49.0	Dark grey-brown gyttja homogenous in colour and texture. Y2.5 3/1, strf 0, diffuse lim. Ld2, Ag2.
49.0 – 53.5	Black-grey gyttja homogenous in colour and texture. Y2.5 2.5/1 (black), strf 0, diffuse lim. Ld2, Ag2, Ga+.
53.5 – 58.0	Medium grey-brown gyttja with slight marbling of colour, homogenous in texture. Y2.5 3/1, strf 0, gradual lim. Ld2, Ag2.
58.0 – 59.5	Light grey-brown gyttja homogenous in colour and texture. Y2.5 4/1, strf 0, gradual lim. Ld2, Ag2, Ga+.
59.5 – 60.5	Medium grey-brown gyttja, homogenous in colour and texture. Y2.5 3/1, strf 0, gradual lim. Ld2, Ag2.
60.5 – 62.0	Light grey-brown gyttja homogenous in colour and texture. Y2.5 4/1, strf 0, gradual lim. Ld2, Ag2, Ga+.
62.0 – 71.5	Medium to dark grey-brown gyttja with slight marbling of colour, homogenous in texture. Y2.5 3/1, strf 0, diffuse lim. Ld2, Ag2.
71.5 – 76.0	Grey gyttja homogenous in colour and texture. Y2.5 4/1, strf 0, very gradual lim. Ld2, Ag2.
76.0 – 78.0	Light grey gyttja homogenous in colour and texture. Y2.5 5/2 (greyish brown), strf 0, very gradual lim. Ld2, Ag2, Ga+.
78.0 – 79.5	Grey gyttja homogenous in colour and texture. Y2.5 4/1, strf 0, very gradual lim. Ld2, Ag2.
79.5 – 82.5	Light grey gyttja homogenous in colour and texture. Y2.5 5/2, strf 0, very gradual lim. Ld2, Ag2.
82.5 – 85.0	Medium to dark grey-brown gyttja, homogenous in colour and texture. Y2.5 3/1, strf 0, very gradual lim. Ld2, Ag2, Ga+.
85.0 – 92.0	Light grey gyttja homogenous in colour and texture. Y2.5 5/2, strf 0, very gradual lim. Ld2, Ag2.
92.0 – 93.0	Slightly darker grey gyttja homogenous in texture. Y2.5 3/1, strf 0, gradual lim. Ld2, Ag2.
93.0 – 94.0	Black-grey gyttja with slight marbling of colour. Y2.5 2.5/1, strf 0, sharp lim. Ld2, Ag2.
94.0 – 96.0	Brown- grey gyttja homogenous in colour and texture. Y2.5 3/1, strf 0, sharp lim. Ld2, Ag2.
96.0 – 100.0	Light grey gyttja homogenous in colour and texture. Y2.5 5/2, strf 0, very gradual lim. Ld2, Ag2.

Subdrive 7B

Depth (cm)	Description
41.0 – 48.5	Dark grey gyttja homogenous in colour and texture. Y2.5 3.1 (very dark grey), strf 0, gradual lim. Ag2, Ld2.
48.5 – 50.0	Medium-grey gyttja homogenous in colour and texture. Y2.5 4/1, strf 0, gradual lim. Ag2, Ld2.
50.0 – 61.0	Black-grey gyttja homogenous in colour and texture. Y2.5 3/1, strf 1, very gradual lim. Ag2, Ld2, Lc+.
61.0 – 74.5	Black-grey gyttja homogenous in colour and texture. Y2.5 3/1, strf 0, sharp lim. Ag2, Ld2.
74.5 – 75.5	Grey gyttja. Y2.5 4/1, strf 1, gradual lim. Ag2, Ld2, Lc++.
75.5 – 77.5	Black-grey gyttja homogenous in colour and texture. Y2.5 3/1, strf 0, diffuse lim. Ag2, Ld2.
77.5 – 81.5	Light grey gyttja. Y2.5 5/1 (grey), strf 1, diffuse lim. Ag2, Ld2, Lc++.

Subdrive 8A

Depth (cm)	Description
0.0 – 10.5	Oasis, top 10.5 cm missing.
10.5 – 16.5	Black-grey gyttja homogenous in colour and texture. Y2.5 3/1 (very dark grey), strf 0, very gradual lim. Ag2, Ld2.
16.5 – 21.0	Grey gyttja containing traces of limus calcareous laminations. The most distinct lamination occurs at 17.4 cm, is 1.0 mm thick and fairly straight. Y2.5 4/1 (dark grey), strf 1, diffuse lim. Ag2, Ld2, Lc++.
21.0 – 25.5	Light grey gyttja containing traces of limus calcareous. Y2.5 5/1 (grey), strf 0, very gradual lim. Ag2, Ld2, Lc+.
25.5 – 26.0	Dark grey gyttja homogenous in colour and texture. Y2.5 3.1, strf 0, gradual lim. Ag2, Ld2.
26.0 – 32.0	Dark grey gyttja containing white limus calcareous. The limus is not in regular laminations but irregular in spacing and varying in distinctiveness. Y2.5 3/1, strf 2, gradual lim. Ag2, Ld1, Lc1.

Subdrive 8B

Depth (cm)	Description
0.0 – 3.0	Grey gyttja. Y2.5 3/1 (very dark grey), strf 0, very gradual lim. Ag2, Ld2.

3.0 – 8.5	Grey gyttja intermixed with mustard coloured grana. Y2.5 5/4 (light olive brown), strf 0, gradual lim. Ag2, Ld1, Gs1.
8.5 – 20.0	Grey-brown gyttja homogenous in colour and texture. Y2.5 3/1, strf 0, diffuse lim. Ag2, Ld2.
20.0 – 23.0	Grey-brown gyttja containing traces of mustard coloured grana. Y2.5 3.1, strf 0, diffuse lim. Ag2, Ld2, Gs+.
23.0 – 58.5	Grey-brown gyttja homogenous in colour and texture. Y2.5 3/1, strf 0, gradual lim. Ag2, Ld2.
58.5 – 83.0	Black, sticky clay. Y2.5 2.5/1 (black), strf 0, gradual lim. Ld2, As2, Ga+.
Core deformed (slumped) in the middle section, 23.0 – 52.0 cm.	

Drive 9

Depth (cm)	Description
0.0 – 25.5	Black clay homogenous in colour and texture. Y2.5 2.5/1 (black), strf 0, sharp lim. Ld2, As2.
25.5 – 27.5	Black, crumbly clay with a clear break in the sediment sequence, separating it from the next section. Y2.5 2.5/1, strf 0, sharp lim. Ld2, As2, Ga++.
27.5 – 32.5	Black, crumbly clay. Y2.5 2.5/1, strf 0, very gradual lim. Ld2, As2.
32.5 – 44.0	Black clay homogenous in colour and texture. Y2.5 2.5/1, strf 0, very gradual lim. Ld2, As2.
44.0 – 47.0	Black clay homogenous in colour and texture, containing small gravel. Y2.5 2.5/1, strf 0, very gradual lim. Ld1, As2, Lg1.

Appendix 2

Photographs of Sediment Cores.

Subdrive 1A, 95.5 cm long, 89.0 – 184.5 cm depth.

Subdrive1B, 87.0 cm long, 184.5 – 271.5 cm depth.

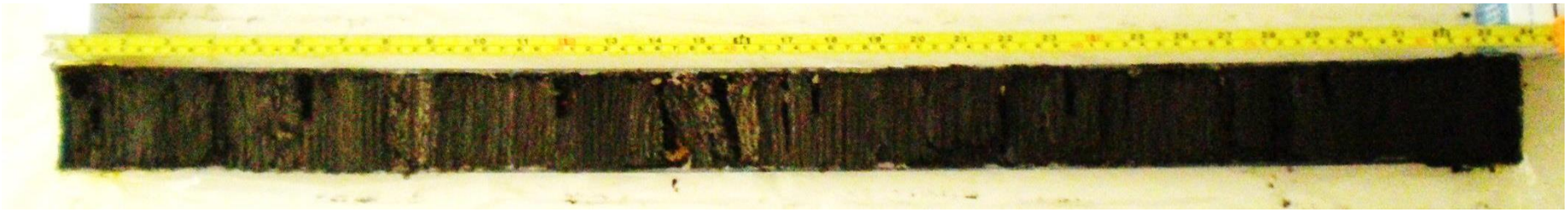

Subdrive 2A, 93.5 cm long, 247.5 – 341.0 cm depth.

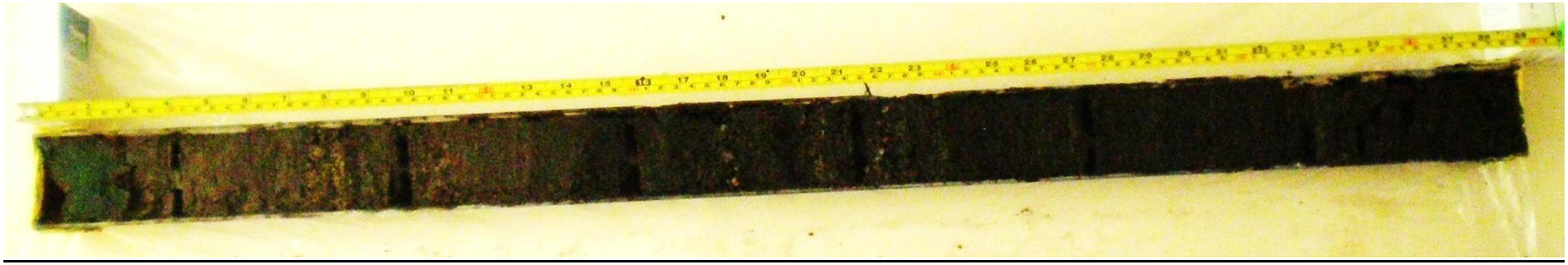

Subdrive 2B, 47.0 cm long, 341.0 – 388.0 cm depth.

Subdrive 3A, 83.5 cm long, 236.5 – 320.0 cm depth.

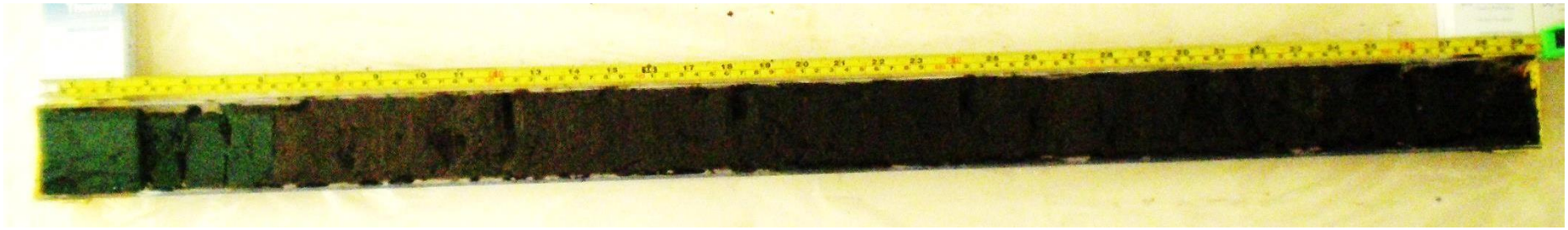

Subdrive 3B, 50.5 cm long, 320.0 – 370.5 cm depth.

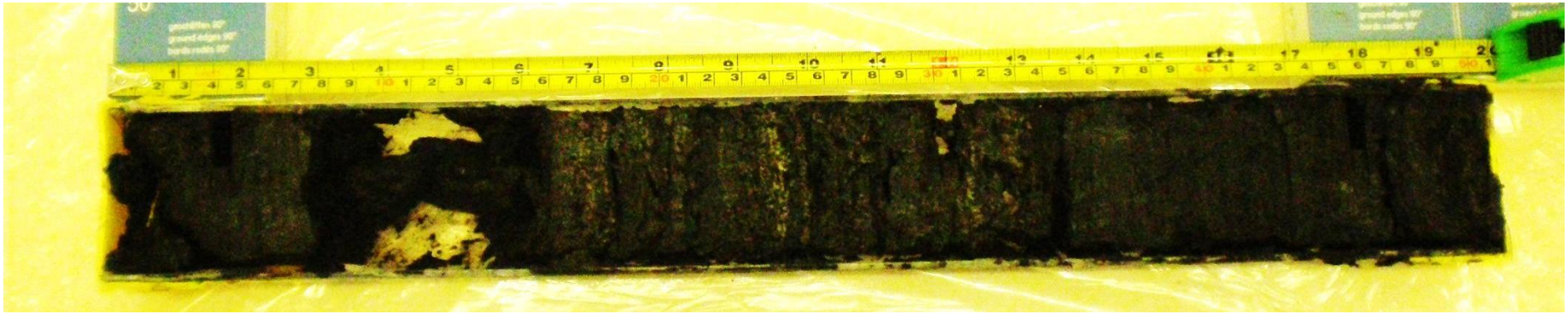

Subdrive 4A, 89.0 cm long, 226.5 – 315.5 cm depth.

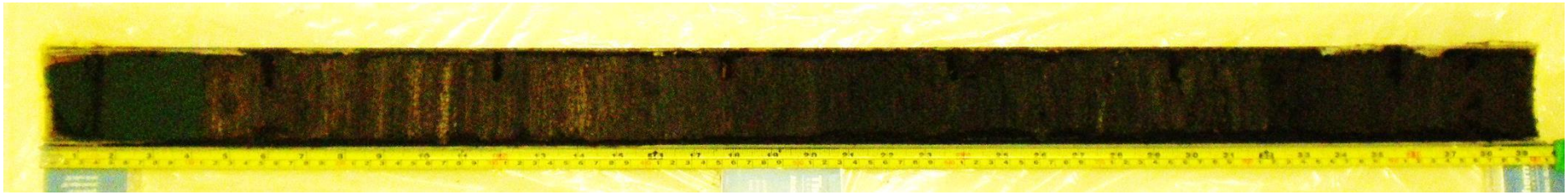

Subdrive 4B, 90.0 cm long, 315.5 – 405.5 cm depth.

Subdrive 5A, 84.5 cm long, 369.0 – 453.5 cm depth.

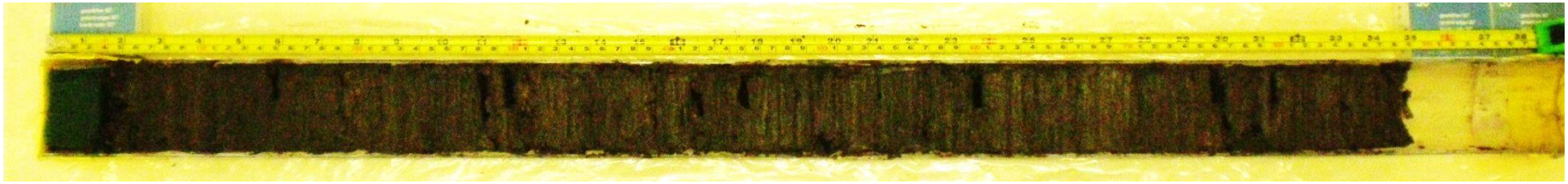

Subdrive 5B, 67.0 cm long, 453.5 – 520.5 cm depth.

Drive 6, 90.0 cm long, 522.5 – 612.5 cm depth.

Subdrive 7A, 93.0 cm long, 572.5 – 665.5 cm depth.

Subdrive 7B, 81.5 cm long, 665.5 – 747.0 cm depth.

Subdrive 8A, 21.5 cm, 723.5 – 745.0 cm depth.

Subdrive 8B, 77.0 cm, 745.0 – 828.0 cm depth.

Drive 9, 47.0 cm, 773.0 – 820.0 cm long.

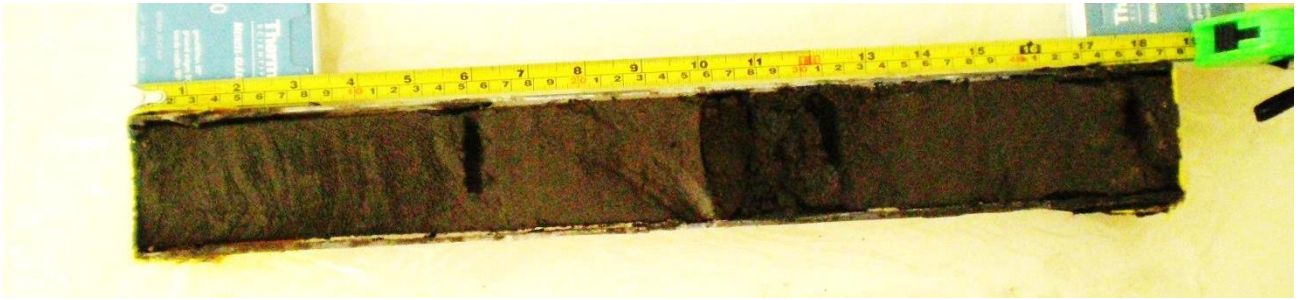

Appendix 3.

Taxonomic Authorities for Diatom Taxa Identified.

Code	Name Used in Thesis	Other Name	Authority	Year
AC047A	*Achnanthes lemmermannii*	*Achnanthes lemmermannii*	Hustedt	1933
AC9964	*Achnanthes minutissima* var. *scotica*	*Achnanthes minutissima* var. *scotica*	(Carter) Lange-Bertalot	1989
AC9999	*Achnanthes* sp.	*Achnanthes* sp.		
AC184A	*Achnanthes ziegleri*	*Achnanthes ziegleri*	Lange-Bertalot	1991
XXC987	*Achnanthidium affine*	*Achnanthes minutissima* var. *affinis*	(Grunow) Lange-Bertalot in Lange-Bertalot & Krammer	1989
AC008A	*Achnanthidium exiguum*	*Achnanthes exigua*	Grunow	1880
AC065A	*Achnanthidium exilis*	*Achnanthes exilis*	Kützing	1833
AC149A	*Achnanthidium kranzii*	*Achnanthes kranzii*	Lange-Bertalot & Krammer	1989
AC013A	*Achnanthidium minutissimum*	*Achnanthes minutissima*	Kützing	1833
AC037A	*Achnanthidium pyrenaicum*	*Achnanthes biasolettiana*	Kützing (Grunow)	1880
AM011A	*Amphora copulata*	*Amphora libyca*	Ehrenberg	1844
AM065A	*Amphora holsatica*	*Amphora holsatica*	Hustedt	1930
AM013A	*Amphora inariensis*	*Amphora inariensis*	Krammer	1980
AM084A	*Amphora montana*	*Amphora montana*	Krasske	1932
AM001A	*Amphora ovalis*	*Amphora ovalis*	Kützing	1844
AM012A	*Amphora pediculus*	*Amphora pediculus*	(Kützing) Grunow ex A. Schmidt	1875
AM9999	*Amphora* sp.	*Amphora* sp.		
AM008A	*Amphora thumensis*	*Amphora thumensis*	(Mayer) Krieger	1929
AM004A	*Amphora veneta*	*Amphora veneta*	Kützing	1844
AN9999	*Anomoeoneis* sp.	*Anomoeoneis* sp.		
AN009A	*Anomoeoneis sphaerophora*	*Anomoeoneis sphaerophora*	(Kützing) Pfitzer	1871
AU002A	*Aulacoseira ambigua*	*Aulacoseira ambigua*	(Grunow in Van Heurck) Simonsen	1979
AU003D	*Aulacoseira granulata* var. *angustissima*	*Aulacoseira granulata* var. *angustissima*	(O. Müller) Simonsen	1979
BA001A	*Bacillaria paradoxa*	*Bacillaria paradoxa*	Gmelin in Linnaeus	1788

CA002A	*Caloneis bacillum*	*Caloneis bacillum*	(Grunow) Cleve	1894
HAYQ01	*Caloneis branderii*	*Caloneis branderii*	(Hustedt) Krammer	1985
CA035A	*Caloneis lauta*	*Caloneis lauta*	Carter & Bailey-Watts	1981
CA048A	*Caloneis molaris*	*Caloneis molaris*	(Grunow) Krammer	1985
CP007A	*Campylodiscus bicostatus*	*Campylodiscus bicostatus*	W. Smith in Roper	1854
CP9999	*Campylodiscus* sp.	*Campylodiscus* sp.		
CO010A	*Cocconeis disculus*	*Cocconeis disculus*	(Schumman) Cleve	1896
CO006A	*Cocconeis neodiminuta*	*Cocconeis neodiminuta*	Pantocsek	1902
CO001B	*Cocconeis placentula* var. *euglypta*	*Cocconeis placentula* var. *euglypta*	(Ehrenberg) Grunow	1884
CO001D	*Cocconeis placentula* var. *klinoraphis*	*Cocconeis placentula* var. *klinoraphis*	Geitler	1927
CO001C	*Cocconeis placentula* var. *lineata*	*Cocconeis placentula* var. *lineata*	(Ehrenberg) Van Heurck	1885
CO001A	*Cocconeis placentula* var. *placentula*	*Cocconeis placentula* var. *placentula*	Ehrenberg	1838
CO001E	*Cocconeis pseudolineata*	*Cocconeis placentula* var. *pseudolineata*	Geitler	1927
CO9999	*Cocconeis* sp.	*Cocconeis* sp.		
NA056A	*Craticula cuspidata*	*Navicula cuspidata*	(Kützing) Kützing	1844
NA022A	*Craticula halophila*	*Navicula halophila*	(Grunow ex Van Heurck) Cleve	1894
NA752A	*Craticula riparia*	*Navicula riparia*	Hustedt	1942
CC002A	*Cyclostephanos invisitatus*	*Cyclostephanos invisitatus*	Theriot, Stoermer & Hakansson	1987
CC003A	*Cyclostephanos tholiformis*	*Cyclostephanos tholiformis*	Stoermer, Hakansson & Theriot	1987
CY010A	*Cyclotella comensis*	*Cyclotella comensis*	Grunow in Van Heurck	1882
CY059A	*Cyclotella cyclopuncta*	*Cyclotella cyclopuncta*	Hakansson & Carter	1990
CY003A	*Cyclotella meneghiniana*	*Cyclotella meneghiniana*	Kützing	1844
CY009A	*Cyclotella ocellata*	*Cyclotella ocellata*	Pantocsek	1902
CY055A	*Cyclotella schummani*	*Cyclotella schummani*	(Grunow) Hakansson	1990
CY9999	*Cyclotella* sp.	*Cyclotella* sp.		
CM022A	*Cymbella affinis*	*Cymbella affinis*	Kützing	1844
CM006A	*Cymbella cistula*	*Cymbella cistula*	(Ehrenbergin Hempr. & Ehrenberg) Kirchner	1878
CM007A	*Cymbella cymbiformis*	*Cymbella cymbiformis*	Agardh	1830
CM018A	*Cymbella gracilis*	*Cymbella gracilis*	(Rabenhorst) Cleve	1894
HAYQ03	*Cymbella hungarcia*	*Cymbella hungarcia*	Grunow	

CM086A	*Cymbella leptoceros*	*Cymbella leptoceros*	(Ehrenberg) Kützing	1844
CM023A	*Cymbella pusilla*	*Cymbella pusilla*	Grunow ex A. Schmidt	1875
HAYQ04	*Cymbella socialis*	*Cymbella socialis*		
CM9999	*Cymbella* sp.	*Cymbella* sp.		
HAYQ05	*Cymbella subalpina*	*Cymbella subalpina*	Hustedt	1942
CM109A	*Cymbella tumidula*	*Cymbella tumidula*	Grunow	1875
CM002A	*Cymbella turgida f. angulata*	*Cymbella turgida f. angulata*	Gregory	1856
CM002A	*Cymbella turgidula*	*Cymbella turgidula*	Grunow	1875
CM001B	*Cymbella ventricosa*	*Cymbella ventricosa*	Kützing	1844
DP009A	*Diploneis elliptica*	*Diploneis elliptica*	(Kützing) Cleve	1894
DP067A	*Diploneis modica*	*Diploneis modica*	Hustedt	1945
DP005A	*Diploneis smithii*	*Diploneis smithii*	(Brébisson ex W. Smith) Cleve	1894
DP9999	*Diploneis* sp.	*Diploneis* sp.		
CY004A	*Discostella stelligera*	*Cyclotella stelligera*	(Cleve & Grunow in Cleve) Van Heurck	1882
EL001A	*Ellerbeckia arenaria*	*Ellerbeckia arenaria*	(Moore ex Ralfs) R.M. Crawford	1988
CM024A	*Encyonema muelleri*	*Cymbella muelleri*	Hustedt	1937
CM010A	*Encyonema perpusillum*	*Cymbella perpusilla*	A. Cleve	1895
CM045A	*Encyonema prostrata*	*Cymbella prostrata*	Berkeley	1880
CM103A	*Encyonema silesiacum*	*Cymbella silesiaca*	Bleisch ex Rabenhorst	1864
CM049A	*Encyonopsis falaisensis*	*Cymbella falaisensis*	(Grunow) Krammer & Lange-Bertalot	1985
CM004A	*Encyonopsis microcephala*	*Cymbella microcephala*	Grunow in Van Heurck	1880
EP007A	*Epithemia adnata*	*Epithemia adnata*	(Kützing) Rabenhorst	1853
EP021A	*Epithemia smithii*	*Epithemia smithii*	Carruthers	1864
EP001A	*Epithemia sorex*	*Epithemia sorex*	Kützing	1844
EP9999	*Epithemia* sp.	*Epithemia* sp.		
EP004A	*Epithemia turgida*	*Epithemia turgida*	(Ehrenberg) Kützing	1844
EU009A	*Eunotia exigua*	*Eunotia exigua*	(Brébisson ex Kützing) Rabenhorst	1864
EU110A	*Eunotia minor*	*Eunotia minor*	(Kützing) Grunow in Van Heurck	1881
EU111A	*Eunotia soleirolii*	*Eunotia soleirolii*	(Kützing) Rabenhorst	1864
EU9999	*Eunotia* sp.	*Eunotia* sp.		
EU021A	*Eunotia sudetica*	*Eunotia sudetica*	O. Müller	1898

NA452A	*Fallacia insociabilis*	*Navicula insociabilis*	Krasske	1932
NA010A	*Fallacia pygmaea*	*Navicula pygmaea*	Kützing	1849
NA676A	*Fallacia tenera*	*Navicula tenera*	Hustedt	1937
NA617A	*Fistulifera saprophila*	*Navicula saprophila*	Lange-Bertalot & Bonik	1976
FR026A	*Fragilaria bidens*	*Fragilaria bidens*	Heiberg	1863
FR009A	*Fragilaria capucina*	*Fragilaria capucina*	Desmazières	1825
FR009L	*Fragilaria capucina* var. *amphicephala*	*Fragilaria capucina* var. *amphicephala*	(Grunow) Lange-Bertalot	1991
HAYQ06	*Fragilaria fonticola*	*Fragilaria fonticola*	Hustedt	1995
SY014A	*Fragilaria goulardii*	*Fragilaria goulardii*	(Brébisson ex Grunow) Lange-Bertalot	1880
FR045A	*Fragilaria parasitica*	*Fragilaria parasitica*	(W. Smith) Grunow in Van Heurck	1881
FR059A	*Fragilaria radians*	*Fragilaria radians*	(Kützing) Williams & Round	1987
FR9999	*Fragilaria* sp.	*Fragilaria* sp.		
SY016A	*Fragilaria vaucheriae*	*Fragilaria capucina* var. *vaucheriae*	(Kützing) Lange-Bertalot	1980
NA317A	*Geissleria decussis*	*Navicula decussis*	Østrup	1910
HAYQ16	*Geissleria dolomitica*	*Navicula dolomitica*	W. Bock	1970
NA433C	*Geissleria paludosa*	*Navicula ignota* var. *palustris*	(Hustedt) J.W.G. Lund	1946
NA128A	*Geissleria schoenfeldii*	*Navicula schoenfeldii*	Hustedt	1930
GO001A	*Gomphoneis olivaceum*	*Gomphonema olivaceum*	(Hornemann) Brébisson	1838
GO003A	*Gomphonem angustatum*	*Gomphonem angustatum*	(Kützing) Rabenhorst	1864
GO006A	*Gomphonema acuminatum*	*Gomphonema acuminatum*	Ehrenberg	1832
GO020A	*Gomphonema affine*	*Gomphonema affine*	Kützing	1844
HAYQ09	*Gomphonema amoenum*	*Gomphonema amoenum*	Lange-Bertalot	1985
GO073A	*Gomphonema angustum*	*Gomphonema angustum*	Agardh	1831
HAYQ10	*Gomphonema anjae*	*Gomphonema anjae*	Ludwig & Schnittler	1996
HAYQ11	*Gomphonema aquaemineralis*	*Gomphonema aquaemineralis*	Ludwig & Schnittler	1997
GO019A	*Gomphonema augur*	*Gomphonema augur*	Ehrenberg	1840
HAYQ08	*Gomphonema augur* var. *turris*	*Gomphonema augur* var. *turris*	Lange-Bertalot in Krammer & Lange-Bertalot	1985
GO029A	*Gomphonema clavatum*	*Gomphonema clavatum*	Reichardt	1999
GO024A	*Gomphonema clevei*	*Gomphonema clevei*	Fricke in A. Schmidt	1902
HAYQ12	*Gomphonema contraturris*	*Gomphonema contraturris*	Lange-Bertalot & Reichardt in Lange-Bertalot	1993
HAYQ13	*Gomphonema exigua*	*Gomphonema exigua*	Kützing	1844

GO004A	*Gomphonema gracile*	*Gomphonema gracile*	Ehrenberg	1838
GO074A	*Gomphonema hebridense*	*Gomphonema hebridense*	Gregory	1854
GO043A	*Gomphonema insigne*	*Gomphonema insigne*	Gregory	1856
GO050A	*Gomphonema minutum*	*Gomphonema minutum*	(Agardh) Agardh	1831
HAYQ15	*Gomphonema parallelistriatum*	*Gomphonema parallelistriatum*	Lange-Bertalot & Reichardt	1993
GO013A	*Gomphonema parvulum*	*Gomphonema parvulum*	Lange-Bertalot & Reichardt	1993
GO013C	*Gomphonema parvulum* var. *exilissimum*	*Gomphonema parvulum* var. *exilissimum*	Grunow in Van Heurck	1880
GO055A	*Gomphonema pseudoaugur*	*Gomphonema pseudoaugur*	Lange-Bertalot	1979
GO080A	*Gomphonema pumilum*	*Gomphonema pumilum*	(Grunow) Reichardt & Lange-Bertalot	1991
GO058A	*Gomphonema rhombicum*	*Gomphonema rhombicum*	Fricke in A. Schmidt	1904
GO9999	*Gomphonema* sp.	*Gomphonema* sp.		
GO011A	*Gomphonema subclavatum*	*Gomphonema subclavatum*	(Grunow in Schneider) Grunow in Van Heurck	1880
GO023A	*Gomphonema truncatum*	*Gomphonema truncatum*	Ehrenberg	1832
GOM0118A	*Gomphonema utae*	*Gomphonema utae*	Lange-Bertalot & Reichardt in Reichardt	1999
GO025H	*Gomphonema vibrio*	*Gomphonema vibrio*	Ehrenberg	1843
GY9999	*Gyrosigma* sp.	*Gyrosigma* sp.		
HA001B	*Hantzschia amphioxys*	*Hantzschia amphioxys*	(Ehrenberg) Grunow	1877
AC018A	*Karayevia laterostrata*	*Achnanthes laterostrata*	Hustedt	1933
AC032A	*Lemnicola hungarica*	*Achnanthes hungarcia*	(Grunow) Grunow in Cleve & Grunow	1880
NA025A	*Luticola mutica*	*Navicula mutica*	Kützing	1844
NA529A	*Luticola nivalis*	*Navicula nivalis*	Ehrenberg	1853
NA025J	*Luticola ventricosa*	*Navicula mutica* var. *ventricosa*	(Kützing) Cleve & Grunow	1880
MA009A	*Mastogloia baltica*	*Mastogloia baltica*	Grunow in van Heurck	1880
NA084A	*Mayamaea atomus*	*Navicula atomus*	(Kützing) Grunow	1860
NA037A	*Navicula angusta*	*Navicula angusta*	Grunow	1860
NA745A	*Navicula capitatoradiata*	*Navicula capitatoradiata*	Germain	1981
NA051A	*Navicula cari*	*Navicula cari*	Ehrenberg	1836
NA171A	*Navicula constrans*	*Navicula constrans*	Hustedt in Lange-Bertalot	1980
NA007A	*Navicula cryptocephala*	*Navicula cryptocephala*	Kützing	1844
NA003A	*Navicula cryptotenella*	*Navicula radiosa*	Kützing	1844

NA751A	*Navicula cryptotonella*	*Navicula cryptotonella*	Lange-Bertalot	1985
NA060A	*Navicula digitoradiata*	*Navicula digitoradiata*	Gregory	1861
NA415A	*Navicula harderi*	*Navicula harderi*	Hustedt in Brendemuhl	1948
NA004A	*Navicula hungarcia*	*Navicula hungarcia*	Grunow	1860
NA757A	*Navicula libonensis*	*Navicula libonensis*	Schoeman	1970
NA748A	*Navicula lucinensis*	*Navicula lucinensis*	Hustedt	1950
NA030A	*Navicula menisculus*	*Navicula menisculus*	Schumman	1867
NA042A	*Navicula minima*	*Navicula minima*	Grunow in Van Heurck	1880
NA123A	*Navicula modica*	*Navicula modica*	Hustedt	1945
NA024A	*Navicula oblonga*	*Navicula oblonga*	(Kützing) Kützing	1844
NA555A	*Navicula paramutica*	*Navicula paramutica*	Bock	1963
NA562E	*Navicula peregrina*	*Navicula peregrina*	(Ehrenberg) Kützing	1844
NA589A	*Navicula pseudotuscula*	*Navicula pseudotuscula*	Hustedt	1943
NA590A	*Navicula pseudoventralis*	*Navicula pseudoventralis*	Hustedt	1953
XXC957	*Navicula pupula* var. *nyassenis*	*Navicula pupula* var. *nyassenis*	(O. Müller) Lange-Bertalot	
NA008A	*Navicula rhynchocephala*	*Navicula rhynchocephala*	Kützing	1844
NA090A	*Navicula rotunda*	*Navicula rotunda*	Hustedt	1945
NA035A	*Navicula salinarum*	*Navicula salinarum*	(Grunow in Van Heurck) Cleve	1896
NA110A	*Navicula schadei*	*Navicula schadei*	Krasske	1929
NA764A	*Navicula schroterii*	*Navicula schroterii*	Meister	1932
NA9999	*Navicula* sp.	*Navicula* sp.		
NA134A	*Navicula subminiscula*	*Navicula subminuscula*	Manguin	1942
NA114A	*Navicula subrotundata*	*Navicula subrotundata*	Hustedt	1945
NA743A	*Navicula subrynchocephala*	*Navicula subrynchocephala*	Hustedt	1935
NA063A	*Navicula trivialis*	*Navicula trivalis*	Lange-Bertalot	1980
NA144A	*Navicula utermoehlii*	*Navicula utermoehlii*	Hustedt	1943
NA054A	*Navicula veneta*	*Navicula veneta*	Kützing	1844
NA027E	*Navicula viridulacalcis*	*Navicula viridula* var. *linearis*	Hustedt	1937
NA168A	*Navicula vitabunda*	*Navicula vitabunda*	Hustedt	1930
NE036A	*Neidium ampliatum*	*Neidium ampliatum*	(Ehrenberg) Krammer in Krammer & Lange-Bertalot	1985

NE007A	*Neidium dubium*	*Neidium dubium*	(Ehrenberg) Cleve	1894
NE002A	*Neidium productum*	*Neidium productum*	(W.Smith) Cleve	1894
NE9999	*Neidium* sp.	*Neidium* sp.		
AF_3904	*Nitzschia adapta*	*Nitzschia adapta*	Stoermer, Kreis & Andresen	1999
NI014A	*Nitzschia amphibia* var. *amphibia*	*Nitzschia amphibia* var. *amphibia*	Grunow	1862
HAYQ17	*Nitzschia amphibia* var. *frauenfeldii*	*Nitzschia amphibia* var. *frauenfeldii*	O. Müller	1895
NI210A	*Nitzschia bacilliformis*	*Nitzschia bacilliformis*	Hustedt	1922
NI073A	*Nitzschia brevissima*	*Nitzschia brevissima*	Grunow in Van Heurck	1881
NI010A	*Nitzschia communis*	*Nitzschia communis*	Rabenhorst	1860
NI082A	*Nitzschia confinis*	*Nitzschia confinis*	Hustedt	1949
HAYQ18	*Nitzschia consummata*	*Nitzschia consummata*	Hustedt	
AF_4053	*Nitzschia elliptica*	*Nitzschia elliptica*	Hustedt	
AF_3918	*Nitzschia epiphytica*	*Nitzschia epiphytica*	O. Müller	1905
AF_3919	*Nitzschia epiphyticoides*	*Nitzschia epiphyticoides*	Hustedt	1949
NI002A	*Nitzschia fonticola*	*Nitzschia fonticola*	Grunow in Van Heurck	1881
NI212A	*Nitzschia fossilis*	*Nitzschia fossilis*	(Grunow) Grunow in Van Heurck	1881
NI008A	*Nitzschia frustulum*	*Nitzschia frustulum*	(Kützing) Grunow in Cleve & Grunow	1880
AF_3936	*Nitzschia goetzeana*	*Nitzschia goetzeana*	Hustedt	1921
NI209A	*Nitzschia incognita*	*Nitzschia incognita*	Legler & Krasske	1940
NI043A	*Nitzschia inconspicua*	*Nitzschia inconspicua*	Grunow	1862
NI044A	*Nitzschia intermedia*	*Nitzschia intermedia*	Hantzsch ex Cleve & Grunow	1880
NI121A	*Nitzschia kützingingioides*	*Nitzschia Kützingingioides*	Hustedt	1959
HAYQ19	*Nitzschia lanceolata*	*Nitzschia lanceolata*	W. Smith	1853
NI221A	*Nitzschia lancettula*	*Nitzschia lancettula*	O. Müller	1905
NI031A	*Nitzschia linearis*	*Nitzschia linearis*	W. Smith	1853
AF_4045	*Nitzschia nyassensis*	*Nitzschia nyassensis*	O. Müller	1905
NI009A	*Nitzschia palea*	*Nitzschia palea*	(Kützing) W. Smith	1856
NI033A	*Nitzschia paleacea*	*Nitzschia paleacea*	(Grunow in Cleve & Grunow) Grunow in Van Heurck	1881
NI005A	*Nitzschia perminuta*	*Nitzschia perminuta*	(Grunow) M. Peragallo	1903
NI004A	*Nitzschia punctata*	*Nitzschia punctata*	(W. Smith) Grunow	1878

NI152A	*Nitzschia pusilla*	*Nitzschia pusilla*	Grunow	1862
NI025A	*Nitzschia recta*	*Nitzschia recta*	Hantzsch	1861
HAYQ20	*Nitzschia rostellata*	*Nitzschia rostellata*	Hustedt	1923
NI164B	*Nitzschia sinuata* var. *delognei*	*Nitzschia sinuata* var. *delognei*	(Grunow in Van Heurck) Lange-Bertalot	1980
NI166A	*Nitzschia sociabilis*	*Nitzschia sociabilis*	Hustedt	1957
NI206A	*Nitzschia solita*	*Nitzschia solita*	Hustedt	1953
NI9999	*Nitzschia* sp.	*Nitzschia* sp.		
AF_4027	*Nitzschia spiculum*	*Nitzschia spiculum*	Hustedt	
NI205A	*Nitzschia stompsii*	*Nitzschia stompsii*	Cholnoky	1963
AF_4030	*Nitzschia subcommunis*	*Nitzschia subcommunis*	Hustedt	1949
HAYQ21	*Nitzschia subrostrata*	*Nitzschia subrostrata*	Hustedt	1942
NI183A	*Nitzschia thermalis*	*Nitzschia thermalis*	Hilse in Rabenhorst	1862
NI047A	*Nitzschia tropica*	*Nitzschia tropica*	Hustedt	1949
NI186A	*Nitzschia valdecostata*	*Nitzschia valdecostata*	Lange-Bertalot & Simonsen	1978
NI038A	*Nitzschia valdestriata*	*Nitzschia valdestriata*	Aleem & Hustedt	1951
HAYQ23	*Nitzschia vanoyei*	*Nitzschia vanoyei*	Cholnoky	
NA067A	*Parlibellus crucicula*	*Navicula crucicula*	(W. Smith) Donkin	1871
PI012A	*Pinnularia borealis*	*Pinnularia borealis*	Ehrenberg	1843
PI012D	*Pinnularia borealis* var. *rectangularis*	*Pinnularia borealis* var. *rectangularis*	Carlson	1913
PI011A	*Pinnularia microstauron*	*Pinnularia microstauron*	(Ehrenberg) Cleve	1891
PI011G	*Pinnularia microstauron* var. *brebissonii*	*Pinnularia microstauron* var. *brebissonii*	(Kützing) Ant. Mayer	1913
PI161A	*Pinnularia subrostrata*	*Pinnularia subrostrata*	(A. Cleve) Cleve-Euler	1955
HAYQ24	*Pinnularia superdivergentissima*	*Pinnularia superdivergentissima*	Chaumont & Germain	1976
NA050A	*Placoneis clementis*	*Navicula clementis*	Grunow	1882
NA057A	*Placoneis elginensis*	*Navicula elginensis*	Gregory	1861
NA065A	*Placoneis gastrum*	*Navicula gastrum*	(Ehrenberg) Kützing	1844
AC016A	*Planothidium delicatulum*	*Achnanthes delicatula*	Kützing (Grunow)	1880
AC158A	*Planothidium granum*	*Achnanthes grana*	Hohn & Hellerman	1963
AC001A	*Planothidium lanceolatum*	*Achnanthes lanceolatata*	(Brébisson) Grunow in Cleve & Grunow	1880
NI083A	*Psammodictyon constrictum*	*Nitzschia constricta*	(Gregory) Grunow	1880
AC163A	*Psammothidium helveticum*	*Achnanthes helvetica*	(Hustedt) Lange-Bertalot in Lange-Bertalot &	1989

			Krammer	
AC044A	*Psammothidium levanderi*	*Achnanthes levanderi*	Hustedt	1933
AC119A	*Psammothidium sacculum*	*Achnanthes saccula*	J.R. Carter in J.R. Carter & Watts	1981
AC161A	*Psammothidium ventralis*	*Achnanthes ventralis*	(Krasske) Lange-Bertalot	1989
FR006A	*Pseudostaurosira brevistriata*	*Fragilaria brevistrata*	Grunow in Van Heurck	1885
RC002A	*Rhoicosphenia abbreviata*	*Rhoicosphenia abbreviata*	(C.Agardh) Lange-Bertalot	1980
RH010A	*Rhopalodia acuminata*	*Rhopalodia acuminata*	Krammer	1987
RH009A	*Rhopalodia brebissonii*	*Rhopalodia brebissonii*	Krammer	1987
RH001A	*Rhopalodia gibba*	*Rhopalodia gibba*	(Ehrenberg) O. Müller	1895
RH9999	*Rhopalodia* sp.	*Rhopalodia* sp.		
AF_4614	*Rhopalodia vermicularis*	*Rhopalodia vermicularis*	O. Müller	1895
AC105A	*Rossithidium petersennii*	*Achnanthes petersenii*	Hustedt	1937
AC035A	*Rossithidium pusillum*	*Achnanthes pusilla*	Grunow in Cleve & Grunow	1880
NA429A	*Sellaphora hustedtii*	*Navicula Hustedtii*	Krasske	1923
NA014A	*Sellaphora pupula*	*Navicula pupula* var. *pupula*	Kützing	1844
NA014D	*Sellaphora pupula* var. *mutata*	*Navicula pupula* var. *mutata*	(Krasske) Hustedt	1930
NA005A	*Sellaphora seminulum*	*Navicula seminulum*	Grunow	1860
FR064A	*Stauroforma exiguiformis*	*Fragilaria exigua*	Grunow in Cleve & Moller	1878
SA001A	*Stauroneis anceps*	*Stauroneis anceps*	Ehrenberg	1843
SA9999	*Stauroneis* sp.	*Stauroneis* sp.		
FR002A	*Staurosira construens*	*Fragilaria construens f. construens*	(Ehrenberg) Grunow	1862
FR002C	*Staurosira construens* var. *venter*	*Fragilaria construens f. venter*	(Ehrenberg) Grunow in Van Heurck	1881
FR018A	*Staurosira elliptica*	*Fragilaria elliptica*	Schumman	1867
FR011A	*Staurosirella lapponica*	*Fragilaria lapponica*	Grunow in Van Heurck	1881
FR014A	*Staurosirella leptostauron*	*Fragilaria leptostauron*	(Ehrenberg) Hustedt	1931
FR001A	*Staurosirella pinnata*	*Fragilaria pinnata* var. *pinnata*	Ehrenberg	1843
ST014A	*Stephanodiscus medius*	*Stephanodiscus medius*	Hakansson	1986
ST010A	*Stephanodiscus parvus*	*Stephanodiscus parvus*	Stoermer & Hakansson	1984
ST019A	*Stephanodiscus rotula*	*Stephanodiscus rotula*	(Kützing) Hendey	1964
ST9999	*Stephanodiscus* sp.	*Stephanodiscus* sp.		
ST001A	*Stephanodiscus tenuis*	*Stephanodiscus hantzschii*	Grunow in Cleve & Grunow	1880

SU001A	*Surirella angusta*	*Surirella angusta*	Kützing	1844
SU024B	*Surirella capronii*	*Surirella capronii*	Brébisson ex Kitton	1869
SU9999	*Surirella* sp.	*Surirella* sp.		
FR057A	*Tabularia fasciculata*	*Fragilaria fasciculata*	(Agardh) Lange-Bertalot sensu lato	1980
NI200A	*Tryblionella compressa*	*Nitzschia compressa*	(Bailey) Boyer	1916
NI017A	*Tryblionella gracilis*	*Nitzschia gracilis*	Hantzsch	1860
SY003A	*Ulnaria acus*	*Fragilaria acus*	Kützing	1844
SY011A	*Ulnaria delicatissima*	*Fragilaria delicatissima*	W. Smith	1853
SY001F	*Ulnaria ulna* var. *aequalis*	*Fragilaria ulna* var. *aequalis*	(Kützing) Pankow, Haendel & Richter	1991
SY001H	*Ulnaria ulna* var. *biceps*	*Fragilaria ulna* var. *biceps*	(Kützing) Compère	1991
HAYQ07	*Ulnaria ulna* var. *claviceps*	*Fragilaria ulna* var. *claviceps*	Hustedt	1937
SY001A	*Ulnaria ulna* var. *ulna*	*Fragilaria ulna* var. *ulna*	(Nitzsch) Ehrenberg	1836

Plate I.

1. *Aulacoseira granulata* var. *angustissima* (1A 30.5 cm, absolute depth 119.5 cm).

2. *Aulacoseira granulata* var. *angustissima* (1A 30.5 cm, absolute depth 119.5 cm). The separation spine is indicated.

3. *Aulacoseira granulata* var. *angustissima* (4A 69.0 cm, absolute depth 295.5 cm).

4. *Aulacoseira granulata* var. *angustissima* (4B 168.0 cm, absolute depth 394.5 cm). The separation spine is indicated.

5. *Aulacoseira granulata* var. *angustissima* (4B 168.0 cm, absolute depth 394.5 cm).

6. *Aulacoseira granulata* var. *angustissima* (5B 140.5 cm, absolute depth 509.5 cm).

Plate I.

1

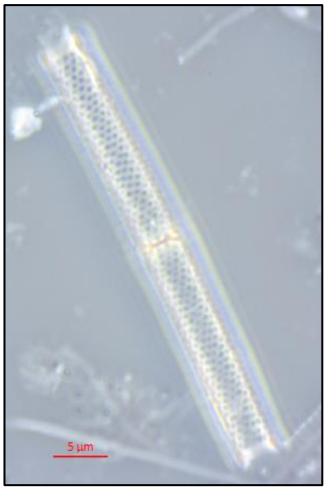

2

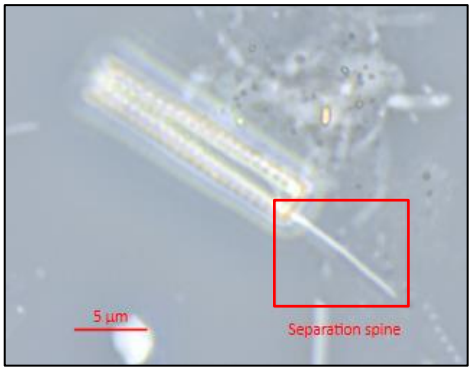

3

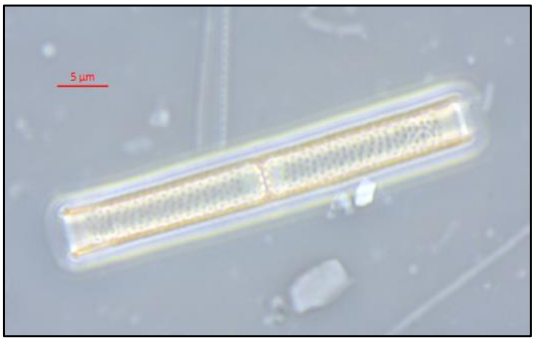

4

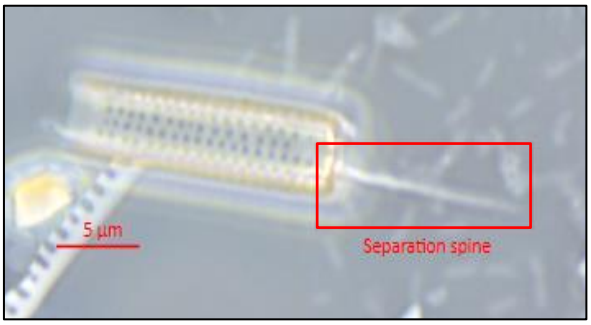

5

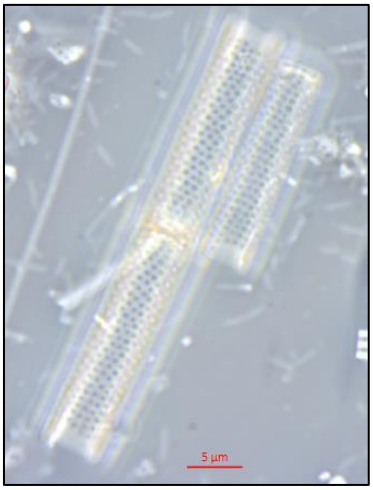

6

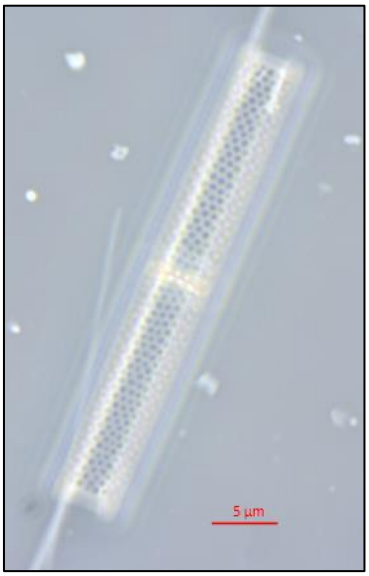

Plate II.

Cyclotella species dissolution at Lake Hayq.

Valve dissolution was assessed during counting using a binary system with valves marked as either ‘0’ for visibly dissolved or ‘1’ being non-dissolved or ‘pristine’. However, significant differences in the degree of dissolution can be observed in the photographs.

1. *Cyclotella cyclopuncta* (1B 110.5 cm, absolute depth 199.5 cm). Pristine valve.

2. *Cyclotella cyclopuncta* (7B 145.0 cm, absolute depth 716.5 cm). Near pristine valve.

3. *Cyclotella ocellata* (7B 163.0 cm, absolute depth 734.5 cm). Extremely degraded valve.

4. *Cyclotella ocellata* (7B 148.0 cm, absolute depth 719.5 cm). Extremely degraded valve.

5. *Cyclotella ocellata* (7B 145.0 cm, absolute depth 716.5 cm). Extremely degraded valve.

6. *Cyclotella ocellata* (7B 163.0 cm, absolute depth 734.5 cm). Extremely degraded valve.

7. *Stephanodiscus parvus* (6 3.0 cm, absolute depth 524.5 cm). Degraded valve. No pristine valves were found during counting.

8. *Stephanodiscus parvus* (6 5.0 cm, absolute depth 526.5 cm). Extremely degraded valve.

9. Two *Stephanodiscus parvus* valves (6 5.0 cm, absolute depth 526.5 cm). Extremely degraded valves.

Plate II.

1 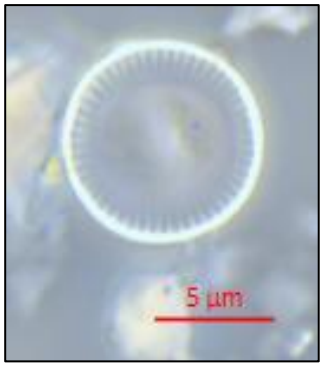

2 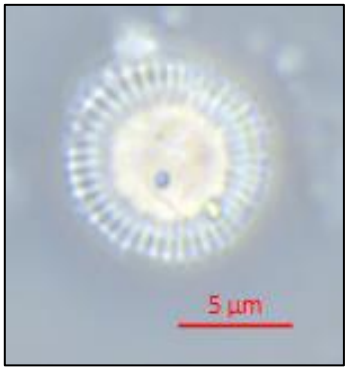

3 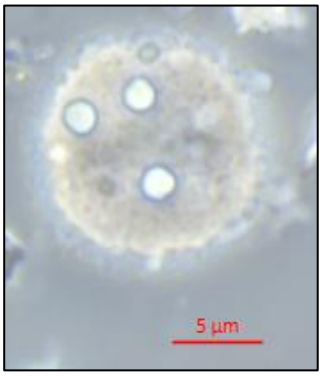

4 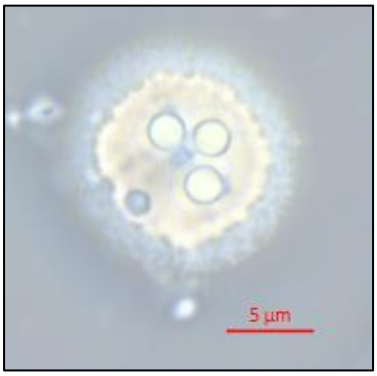

5 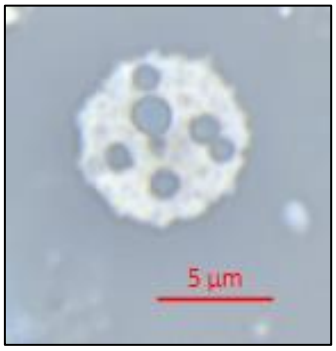

6 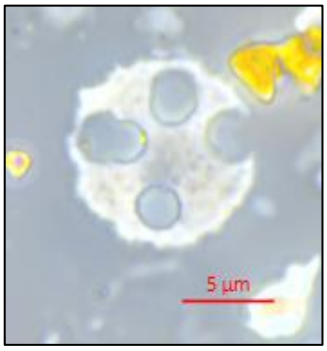

7 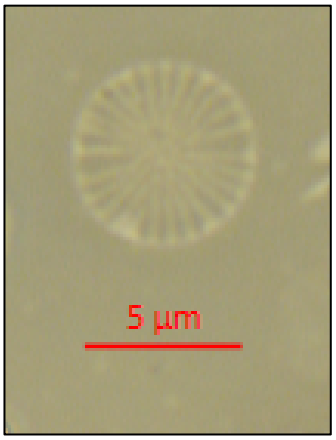

8 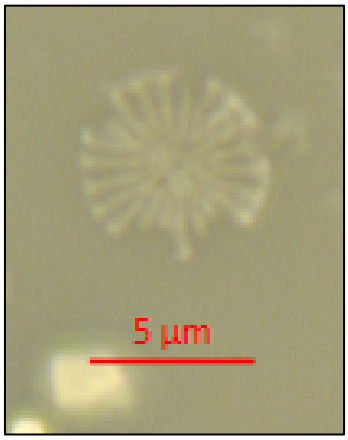

9 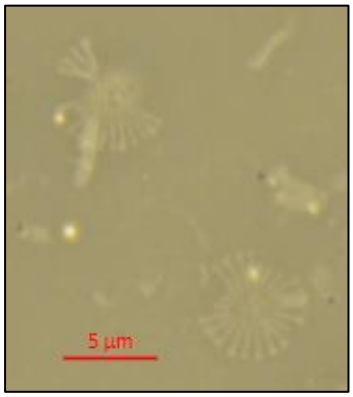

Plate III.

1. *Ulnaria acus* (1B 127.5 cm, absolute depth 216.5 cm).

2. *Ulnaria acus* (1B 127.5 cm, absolute depth 216.5 cm).

3. *Fragilaria radians* (4A 53.5 cm, absolute depth 280.0 cm).

4. *Fragilaria radians* (4A 53.5 cm, absolute depth 280.0 cm).

5. *Fragilaria radians* (4A 53.5 cm, absolute depth 280.0 cm).

Plate III.

1

2

3

4

5

Plate IV.

1. *Ulnaria delicatissima* (1B 117.5 cm, absolute depth 206.5 cm).

2. Central area of *Ulnaria delicatissima* (1B 117.5 cm, absolute depth 206.5 cm).

3. *Ulnaria* var. *ulna* (1A 74.5 cm, absolute depth 163.5 cm). The rimoportula is indicated.

4. Central area of *Ulnaria* var. *ulna* (1A 90.5 cm, absolute depth 179.5 cm).

5. *Ulnaria* var. *ulna* (1B 167.5 cm, absolute depth 256.5 cm). The rimoportula is indicated.

Plate IV.

1

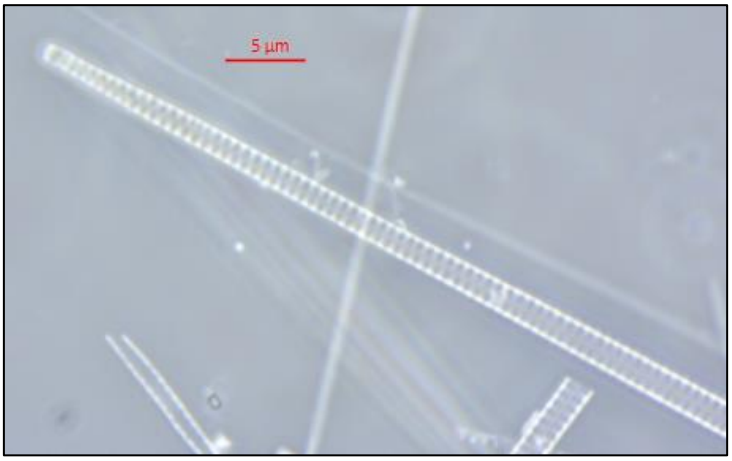

2

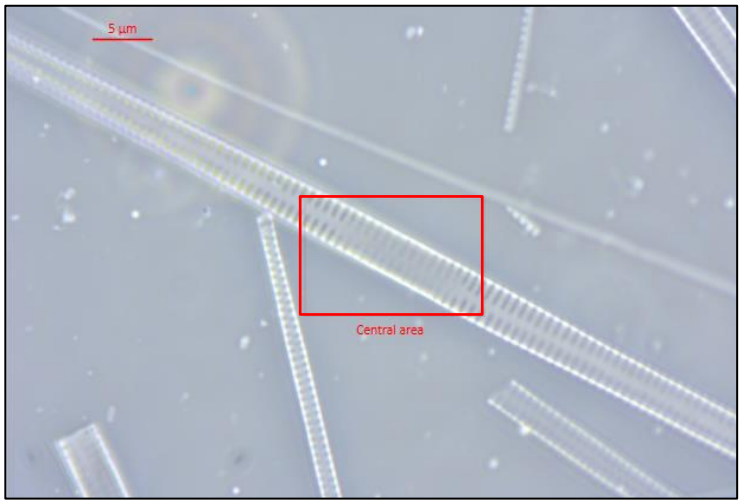

3

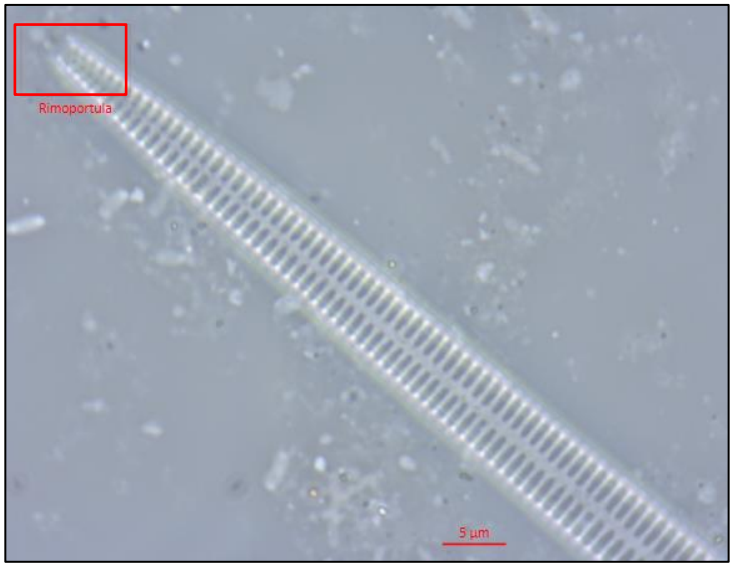

4

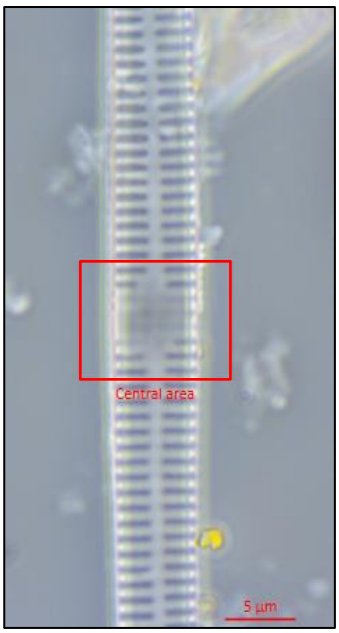

5

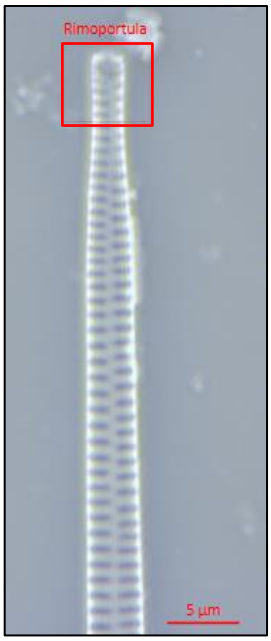

Plate V.

1. *Pseudostaurosira brevistriata* (6 15.0 cm, absolute depth 536.5 cm).

2. *Staurosirella pinnata* (6 9.0 cm, absolute depth 530.5 cm).

3. *Gomphonema parvulum* (4A 69.0 cm, absolute depth 295.5 cm).

4. *Gomphonema affine* (4A 19.0 cm, absolute depth 245.5 cm).

5. *Amphora copulata* (6 15.0 cm, absolute depth 536.5 cm)..

6. *Nitzschia fonticola* (6 7.0 cm, absolute depth 528.5 cm).

7. *Gomphonema pumilum* (4A 43.0 cm, absolute depth 269.5 cm).

8. *Cymbella muelleri* (1B 110.5 cm, absolute depth 199.5 cm).

9. *Amphora pediculus* (6 7.0 cm, absolute depth 528.5 cm).

10. *Fragilaria vaucheriae* (1B 145.5 cm, absolute depth 234.5 cm).

Plate V.

1

2

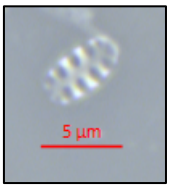

3

4

5

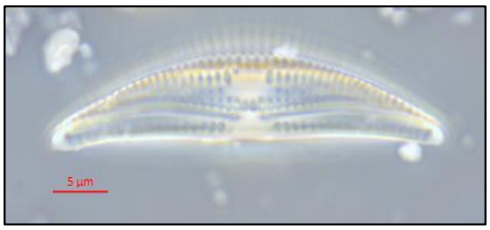

6

7

8

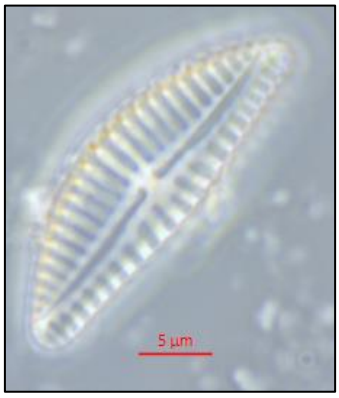

9

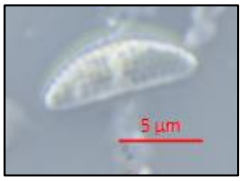

10

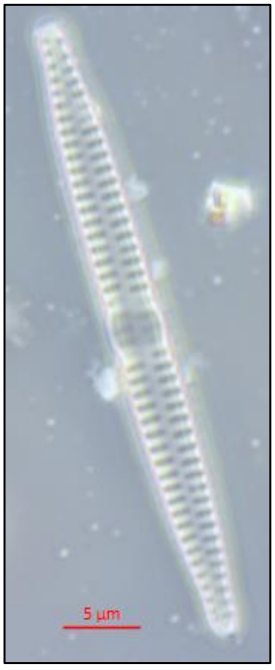

Plate VI.

1. *Sellaphora pupula* (4A 19.0 cm, absolute depth 245.5 cm).

2. *Nitzschia lancettula* (6 7.75 cm, absolute depth 529.25 cm).

3. *Nitzschia epiphytica* (6 15.0 cm, absolute depth 536.5 cm).

4. *Navicula cryptotenella* (1B 140.5 cm, absolute depth 229.5 cm). A microsphere is indicated.

5. *Nitzschia subcommunis* (5B 112.5 cm, absolute depth 481.5 cm).

6. *Nitzschia amphibia var. amphibia* (1B 110.5 cm, absolute depth 199.5 cm).

7. *Hantzschia amphioxys* (6 7.75 cm, absolute depth 529.25 cm).

1

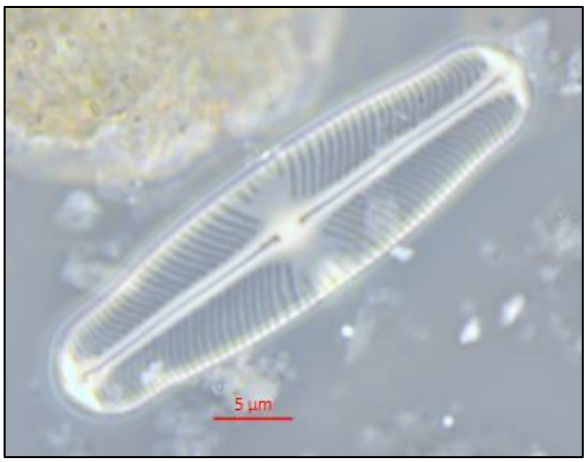

2

3

4

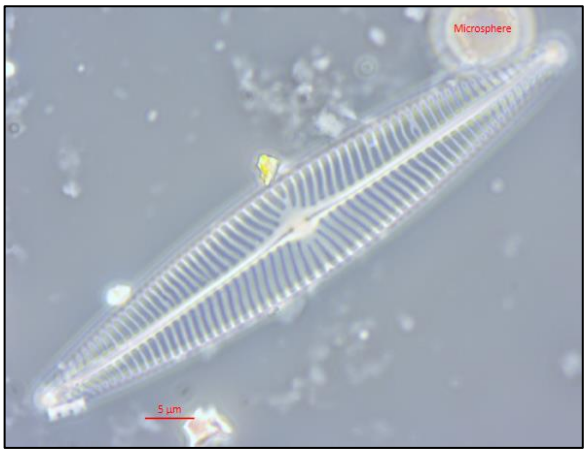

5

6

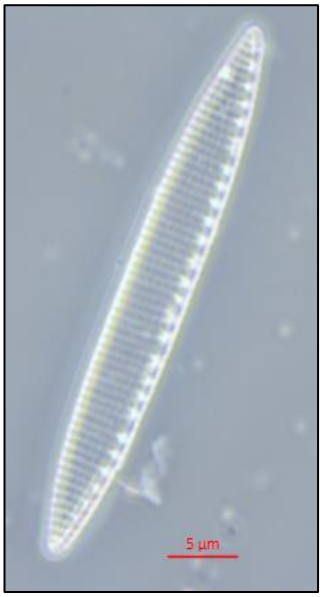

7